Advances in Science, Technology & Engineering Systems Journal

Editorial

In this compilation of research papers, we present 31 accepted research papers of a diverse array covering topics ranging from educational practices to cybersecurity, from robotics to healthcare. These papers reflect the commitment of researchers to advancing knowledge and addressing contemporary challenges. Each contribution offers a unique perspective, employing various methodologies and technologies to delve into specific domains. Let's explore the each paper of this stimulating collection.

The integration of Information and Communication Technologies (ICTs) in education is explored in this paper, emphasizing the importance of considering the perceptions of students and teachers. Drawing on the technology acceptance model (TAM2), the study provides insights into how these perceptions influence the intentional and behavioral use of ICTs in educational practices [1].

Addressing the evolving landscape of cybersecurity, this paper introduces an effective method for detecting stepping-stone intrusions using packet crossover ratios. The proposed approach not only enhances ease of implementation but also demonstrates efficiency through well-designed network experiments [2].

Focusing on database applications, this paper introduces algorithms for optimal allocation and deallocation of multi-tiered persistent storage devices. Leveraging extended Petri nets, the study highlights the linearization of data flows to generate optimal storage plans, showcasing improvements in performance compared to random allocation strategies [3].

Swarm robotics is explored in the context of collective movement for tasks like transportation and observation. The paper introduces a leader-follower-controlled method that calculates direction and distance potentials, allowing a robot swarm to maintain formations with different densities while on the move [4].

This paper delves into the realm of education and technology, presenting StereoMV, a software for stereometry training. It explores different 3D visualization types and modes, emphasizing the importance of 3D technology in strengthening students' interest and spatial thinking [5].

Exploring the vulnerabilities in WiFi-based IoT devices, this paper extends previous work by employing time series monitored WiFi data frames and advanced machine learning algorithms. The study reveals the potential for high-accuracy profiling of IoT devices, emphasizing the need for robust security measures [6].

In the realm of unmanned aerial vehicles, this paper focuses on electrical drive systems for high-speed multicopters. Introducing sensorless control methods based on field-oriented control, the study showcases innovative approaches for rotor position estimation, verified through simulation and experiments [7].

Recognizing the significance of emotion in human interaction, this paper addresses emotion detection in Bangla speech data. Employing ensemble machine learning methods, the study achieves notable accuracy in emotion detection, crucial for scenarios where video interaction is limited [8].

Exploring the potential of quantum computers in enhancing information system security, this paper introduces basic concepts of quantum computing. The study discusses applications in image

processing security and introduces the prospect of multilevel systems, showcasing the exponential gains in data processing time [9].

This paper focuses on telemedicine, presenting a cloud platform for teleconsultation and telemonitoring. Embracing a workflow management system, the study adopts international healthcare standards and emphasizes an integrated clinical workflow management approach, showcasing advancements in telemedicine [10].

Addressing inventory control challenges, this paper discusses the redesign and improvement of raw material inventory control processes. Utilizing Oracle APEX, the study demonstrates positive outcomes, including increased productivity, elimination of manual tasks, and improved response times in the textile industry [11].

This innovative paper combines CubeSat technology with AI frameworks for crowd management during large-scale events. The proposed system, integrating aerial imaging and wearable devices, demonstrates accuracy in managing crowds and notifying ground controllers of potential issues, offering a comprehensive solution [12].

Building on hardware prefetching techniques, this paper introduces an extension to improve prefetch coverage. The study proposes a refined metric for measuring the net contribution of a prefetcher, showcasing significant IPC speedup improvements over existing methods [13].

In the realm of information security, this paper presents a security prototype aimed at mitigating risks, vulnerabilities, and threats. Through a deductive and exploratory research approach, the study introduces prototypes that effectively control raw data, ensuring data integrity in both public and private companies [14].

Exploring the application of process mining in healthcare, this paper conducts a systematic literature review and presents a case study on medical teleconsultation. The study highlights the potential of process mining in improving healthcare processes, even in the challenging context of identifying relevant log files [15].

In "Natural Tsunami Wave Amplitude Reduction by Straits – Seto Inland Sea", the authors shed light on the protection of coastal populations and infrastructure in the Seto Inland Sea, Japan. Utilizing numerical modelling, the study explores the influence of strait width and tsunami wave period on wave amplitude reduction, providing crucial information for tsunami safety regulations [16].

In the realm of 5G telecommunication, "Designing the MIMO SDR-based Antenna Array for 5G Telecommunication" introduces a new 2×2 MIMO testbed, emphasizing the importance of flexibility and real-time processing in the implementation of multiple-input–multiple-output systems. The study employs USRP B210 and microstrip antennas to achieve high-quality service and coverage in the rapidly evolving landscape of 5G technology [17].

Shifting focus to healthcare, "A Structuration View of the South African National Health Insurance Readiness" investigates the challenges faced by the implementation of the National Health Insurance in South Africa. Employing structuration theory, the study identifies factors influencing the project, emphasizing the empirical nature of the findings [18].

For bird enthusiasts, "Birds Images Prediction with Watson Visual Recognition Services from IBM-Cloud and Conventional Neural Network" presents the "Birds Images Predictor" application. Comparing the performance of a convolutional neural network with IBM's visual recognition service, the study highlights advantages such as higher training image volume, better color distinction, and a remarkable 99% prediction accuracy with the latter [19].

The impact of information technology on Brazilian higher education during the Covid-19 pandemic is explored in "A Review of the Role of Information Technology in Brazilian Higher Educational Institutions during Covid-19 Pandemic". The study, based on reports from 66 institutions, underscores the role of information systems in enabling rapid responses to the crisis, maintaining academic routines, and ensuring student satisfaction [20].

"Estimating Subjective Appetite based on Cerebral Blood Flow" delves into the development and validation of a biological food preference task. By observing changes in cerebral blood flow related to subjective evaluations of various food states, the study uncovers potential correlations between neural responses and subjective preferences [21].

In the realm of medical research, "Ensemble Extreme Learning Algorithms for Alzheimer's Disease Detection" addresses the critical need for early detection of Alzheimer's disease. The study utilizes Ensemble Extreme Learning Models on the OASIS dataset, exploring various models and comparing their performance for Alzheimer's detection [22].

Turning our attention to environmental concerns, "Emerging Trends in Green Best Practices and the Impact on Government Policy" examines 'green' companies' practices. The study recommends that U.S. government agencies formalize and release sustainability policies, setting quantifiable goals to bridge the gap between industry and government practices in achieving sustainable objectives [23].

In the cybersecurity domain, "Operating Systems Vulnerability – An Examination of Windows 10, macOS, and Ubuntu from 2015 to 2021" investigates vulnerabilities in three operating systems. The study reveals varying vulnerability scores, attributing differences to the popularity of the operating systems and their susceptibility to attacks [24].

Addressing challenges in renewable energy systems, "Design and Analysis of a Virtual Synchronous Generator Control Scheme to Augment FRT Capability of PMSG-Based Wind Turbine" proposes an advanced control method for wind turbines. The study introduces a Virtual Synchronous Generator-based inverter controller to enhance fault ride-through competence and frequency stability [25].

For data warehouses, "Consideration of Ambiguity in the Analysis Phase of Data Warehouses" adopts fuzzy logic to account for ambiguity in the analysis phase. The study explores the context-dependent definition of membership functions, presenting an extensible solution enriched with natural language terms [26].

In the context of smart agriculture, "Interference-Aware Nodes Deployment of a LoRa-Based Architecture for Smart Agriculture in the Southern Region of Senegal" addresses the use of IoT in agriculture. The study proposes a network architecture using Low-Power, Wide Area Networks (LPWANs) for water irrigation techniques in Casamance, emphasizing the optimal choice of technology and sensor deployment [27].

Optimizing tsunami warning systems is the focus of "Optimizing Sensors Locations for Tsunami Warning System". The study proposes an algorithm to balance the number of sensors and the time needed to determine tsunami wave parameters. The findings suggest different optimal sensor positions based on minimizing detection time or maximizing the time to approach the nearest coast after recovering wave parameters at the source [28].

In the field of age estimation, "Transfer and Ensemble Learning in Real-time Accurate Age and Age-group Estimation" employs deep learning techniques for accurate age and age group prediction from facial images. The study introduces a hierarchical aggregation model, showcasing promising results in predicting age and age group in real-time situations [29].

Lastly, the importance of mobility intelligence in urban planning is highlighted in "Mobility Intelligence: Machine Learning Methods for Received Signal Strength Indicator-based Passive Outdoor Localization". The study compares traditional methods and machine learning approaches for RSSI-based passive outdoor localization, showcasing the superiority of machine learning methods in providing accurate results [30].

In "Technical Aspects and Social Science Expertise to Support Safe and Secure Handling of Autonomous Railway Systems", the authors delve into the growing realm of autonomous vehicles, specifically focusing on autonomous railway systems. The study takes a multilevel approach, combining Failure Mode, Effects and Criticality Analysis (FMECA) with sociological and technical aspects to ensure safe operations and effective human-machine interactions in the context of autonomous railway systems. By integrating both technical components and sociological considerations, the paper aims to enhance trust in digital solutions and Cyber-Physical Systems (CPS), contributing valuable insights for the future development and safe deployment of autonomous railway systems [31].

In summary, this collection of papers offers a comprehensive exploration of diverse topics, ranging from natural disasters and technology implementation to healthcare, environmental sustainability, and artificial intelligence. Each article contributes valuable insights, advancing knowledge in its respective domain. As we navigate the complexities of our rapidly evolving world, these research findings provide a foundation for informed decision-making and further exploration of critical issues.

References:

[1]   A. Pearce, "The Perceptions of Students and Teachers When using ICTs for Educational Practices Matter: A Systematic Review," Advances in Science, Technology and Engineering Systems Journal, **7**(6), 1–12, 2022, doi:10.25046/aj070601.

[2]   L. Wang, J. Yang, A. Lee, P.-J. Wan, "Matching TCP Packets to Detect Stepping-Stone Intrusion using Packet Crossover," Advances in Science, Technology and Engineering Systems Journal, **7**(6), 13–19, 2022, doi:10.25046/aj070602.

[3]   N.N. Noon, J.R. Getta, T. Xia, "Optimization of Query Processing on Multi-tiered Persistent Storage," Advances in Science, Technology and Engineering Systems Journal, **7**(6), 20–30, 2022, doi:10.25046/aj070603.

[4]   K. Yamagishi, T. Suzuki, "Regular Tessellation-Based Collective Movement for a Robot Swarm with Varying Densities, Scales, and Shapes," Advances in Science, Technology and Engineering Systems Journal, **7**(6), 31–38, 2022, doi:10.25046/aj070604.

[5]   P. Lebamovski, "Advantages of 3D Technology in Stereometry Training," Advances in Science, Technology and Engineering Systems Journal, **7**(6), 39–48, 2022, doi:10.25046/aj070605.

[6] I.A. Alharbi, A.J. Almalki, M. Alyami, C. Zou, Y. Solihin, "Profiling Attack on WiFi-based IoT Devices using an Eavesdropping of an Encrypted Data Frames," Advances in Science, Technology and Engineering Systems Journal, **7**(6), 49–57, 2022, doi:10.25046/aj070606.

[7] C. Zhao, W. Kong, F. Percacci, P. Gnos, "Field Oriented Control and Commutation Based on Sensorless Methods for High-Speed Electrical Motors of Unmanned Multicopters," Advances in Science, Technology and Engineering Systems Journal, **7**(6), 58–69, 2022, doi:10.25046/aj070607.

[8] R.D.G. Ayon, Md.S. Rabbi, U. Habiba, M. Hasana, "Bangla Speech Emotion Detection using Machine Learning Ensemble Methods," Advances in Science, Technology and Engineering Systems Journal, **7**(6), 70–76, 2022, doi:10.25046/aj070608.

[9] T. Nouioua, A.H. Belbachir, "The Security of Information Systems and Image Processing Supported by the Quantum Computer: A review," Advances in Science, Technology and Engineering Systems Journal, **7**(6), 77–86, 2022, doi:10.25046/aj070609.

[10] G. Mitrano, A. Caforio, T. Calogiuri, C. Colucci, L. Mainetti, R. Paiano, C. Pascarelli, "A Cloud Telemedicine Platform Based On Workflow Management System: A Review Of An Italian Case Study," Advances in Science, Technology and Engineering Systems Journal, **7**(6), 87–102, 2022, doi:10.25046/aj070610.

[11] J.A.D. Delgado, J. Sulla-Torres, "Redesign and Improvement in the Management of the Raw Material Inventory Control Process with Oracle APEX," Advances in Science, Technology and Engineering Systems Journal, **7**(6), 103–113, 2022, doi:10.25046/aj070611.

[12] F.A. Almalki, A.M. Mutawi, I.A. Turkistani, L.K. Alqurashi, M.T. Fattah, M.T. Almogher, R.S. Aldaher, R.A. Wali, W.M. Almalki, Y.M. Almubayed, "Developing CubeSat and AI Framework for Crowd Management Case of Short-Term Large-Scale Events," Advances in Science, Technology and Engineering Systems Journal, **7**(6), 114–125, 2022, doi:10.25046/aj070612.

[13] J. So, M. Lu, "Extended Buffer-referred Prefetching to Leverage Prefetch Coverage," Advances in Science, Technology and Engineering Systems Journal, **7**(6), 126–138, 2022, doi:10.25046/aj070613.

[14] S.M.T. Toapanta, R.H.D.P. Durango, L.E.M. Gallegos, E.Z.G. Díaz, Y.J.M. Quintana, J.N.M. Jimenez, Ma.R.M. Arellano, J.A.O. Trejo, "Prototype to Mitigate the Risks, Vulnerabilities and Threats of Information to Ensure Data Integrity," Advances in Science, Technology and Engineering Systems Journal, **7**(6), 139–150, 2022, doi:10.25046/aj070614.

[15] F. Striani, C. Colucci, A. Corallo, R. Paiano, C. Pascarelli, "Process Mining in Healthcare: A Systematic Literature Review and A Case Study," Advances in Science, Technology and Engineering Systems Journal, **7**(6), 151–160, 2022, doi:10.25046/aj070615.

[16] M. Lavrentiev, A. Marchuk, K. Oblaukhov, M. Shadrin, "Natural Tsunami Wave Amplitude Reduction by Straits – Seto Inland Sea," Advances in Science, Technology and Engineering Systems Journal, **7**(6), 161–166, 2022, doi:10.25046/aj070616.

[17] M. Drissi, N. Benjelloun, P. Descamps, A. Gharsallah, "Designing the MIMO SDR-based Antenna Array for 5G Telecommunication," Advances in Science, Technology and Engineering Systems Journal, **7**(6), 167–171, 2022, doi:10.25046/aj070617.

[18] N. Tungela, T. Iyamu, "A Structuration View of the South African National Health Insurance Readiness," Advances in Science, Technology and Engineering Systems Journal, **7**(6), 174–180, 2022, doi:10.25046/aj070618.

[19] F.-Z. Elbouni, A. EL Ouaazizi, "Birds Images Prediction with Watson Visual Recognition Services from IBM-Cloud and Conventional Neural Network," Advances in Science, Technology and Engineering Systems Journal, **7**(6), 181–188, 2022, doi:10.25046/aj070619.

[20] L.C.D. Saldanha, "A Review of the Role of Information Technology in Brazilian Higher Educational Institutions during Covid-19 Pandemic," Advances in Science, Technology and Engineering Systems Journal, **7**(6), 189–194, 2022, doi:10.25046/aj070620.

[21] L. Kecheng, H. Qikun, H. Ning, F. Tsutomu, "Estimating Subjective Appetite based on Cerebral Blood Flow," Advances in Science, Technology and Engineering Systems Journal, **7**(6), 195–203, 2022, doi:10.25046/aj070621.

[22] V. H R, S. Shukla, V. krishna A, "Ensemble Extreme Learning Algorithms for Alzheimer's Disease Detection," Advances in Science, Technology and Engineering Systems Journal, **7**(6), 204–211, 2022, doi:10.25046/aj070622.

[23] E. Holt, C. Corrado, "Emerging Trends in Green Best Practices and the Impact on Government Policy," Advances in Science, Technology and Engineering Systems Journal, **7**(6), 212–221, 2022, doi:10.25046/aj070623.

[24] J. Softić, Z. Vejzović, "Operating Systems Vulnerability – An Examination of Windows 10, macOS, and Ubuntu from 2015 to 2021," Advances in Science, Technology and Engineering Systems Journal, **7**(6), 230–235, 2022, doi:10.25046/aj070625.

[25] H.J. Prema, Md.R. Hazari, M.A. Mannan, Md.A. Rahman, "Design and Analysis of a Virtual Synchronous Generator Control Scheme to Augment FRT Capability of PMSG-Based Wind Turbine," Advances in Science, Technology and Engineering Systems Journal, **7**(6), 236–243, 2022, doi:10.25046/aj070626.

[26] D. Hammouche, K. Atif, "Consideration of Ambiguity in the Analysis Phase of Data Warehouses," Advances in Science, Technology and Engineering Systems Journal, **7**(6), 244–247, 2022, doi:10.25046/aj070627.

[27] E.H.M. Ndoye, O. Diallo, N. Hakem, E.N. Cabral, "Interference-Aware Nodes Deployment of a LoRa-Based Architecture for Smart Agriculture in the Southern Region of Senegal," Advances in Science, Technology and Engineering Systems Journal, **7**(6), 248–255, 2022, doi:10.25046/aj070628.

[28] M. Lavrentiev, D. Kuzakov, A. Marchuk, "Optimizing Sensors Locations for Tsunami Warning System," Advances in Science, Technology and Engineering Systems Journal, **7**(6), 256–261, 2022, doi:10.25046/aj070629.

[29] A.-T. Mai, D.-H. Nguyen, T.-T. Dang, "Transfer and Ensemble Learning in Real-time Accurate Age and Age-group Estimation," Advances in Science, Technology and Engineering Systems Journal, **7**(6), 262–268, 2022, doi:10.25046/aj070630.

[30] F. Bao, S. Mazokha, J.O. Hallstrom, "Mobility Intelligence: Machine Learning Methods for Received Signal Strength Indicator-based Passive Outdoor Localization," Advances in Science, Technology and Engineering Systems Journal, **7**(6), 269–282, 2022, doi:10.25046/aj070631.

[31] C. Gnauer, A. Prochazka, E. Szalai, A. Fraunschiel, "Technical Aspects and Social Science Expertise to Support Safe and Secure Handling of Autonomous Railway Systems," Advances in Science, Technology and Engineering Systems Journal, **7**(6), 283–294, 2022, doi:10.25046/aj070632.

Editor-in-chief

Prof. Passerini Kazmersk

ADVANCES IN SCIENCE, TECHNOLOGY AND ENGINEERING SYSTEMS JOURNAL

CONTENTS

ASTES

The Perceptions of Students and Teachers When using ICTs for Educational Practices Matter: *A Systematic Review*

Angela Pearce*

College of Doctoral Studies, Grand Canyon University, Phoenix, AZ, City, 85061, United States

A R T I C L E I N F O	A B S T R A C T
	Before succumbing to the 2019 Coronavirus pandemic, information and communication technologies (ICTs) have sustained a ubiquitous presence in human lives and society. ICTs have changed the standards and dynamics of educational practices (EPs). Many academic institutions had already integrated technological-based pedagogical instructions into their educational practices but, in various cases, faced challenges of failing to consider the perceptions of chief users, students, teachers, and subjective norms. This paper is an extension of work originally presented at the 2022 11th International Conference on Education and Information Technology (ICEIT). This paper aims to demonstrate and provide future directions regarding the effects of ICTs and how such usage proliferates and disharmonizes learning and teaching experiences and academic achievement. The expanded version of the technology acceptance model (TAM2) is the theoretical foundation for this research. TAM2 provides insight into how the perceptions of students and teachers matter when adopting and using ICTs in educational practices. Depending on these perceptions of perceived ease of use and usefulness, using ICTs in educational practices can impact intentional and behavioral use, currently and futuristically. Subjective norms also influence individuals' perceptions and willingness to use ICTs for educational practices. Limitations, strengths, and future recommendations and directions are discussed.

1. Introduction

This paper is an extension of work originally presented at the 2022 11th International Conference on Education and Information Technology (ICEIT) [1]. The purpose of this paper is to demonstrate the effects of ICTs and how such usage proliferates and disharmonizes learning and teaching experiences and academic achievement. There is a need for this study, especially as research [1] suggested social networking sites (SNSs) have stated a claim in educational practices while losing the battle to the 2019 coronavirus pandemic and onward situations. It was suggested that future researchers take a student-center approach and to study teachers' and students' perceptions regarding the use of ICTs for education-based involvements [1].

Although the 2019 coronavirus and its variants are still omnipresent, onward situations remain inevitable. Outside of SNSs, information and communication technologies (ICTs) hold great promise in educational practices (EPs) [2], [3]. Education remains to be a significant factor in human connections and

relationships and has become instrumental in increasing access to various opportunities [4]. It is at the heart of what, how, where, and when individuals learn and teach [5]. ICTs play a leading role in academic achievement and future endeavors, especially as it has become a considerable agent for changes in EP [5]. However, when deciding to place ICTs in educational institutions, many decision-makers and policymakers failed to consider students' and teachers' perceptions. This paper suggests that while ICTs for EPs are both beneficial and detrimental, these outcomes are influenced by students' and teachers' perceptions of acceptance and adoption, which affects their attitudes toward technology and intentional and behavioral use.

As the primary stakeholders in education, students', and teachers' perceptions of ICTs for EPs matter. Other factors that matter when using ICTs for EPs are subjects, types of digital apparatuses, the persons using the devices, and geographical locations [2], [6]. Material access, digital skills, technology literacy, and equality also matter [7], [8]. Many academic institutions have already embraced and implemented technology in their institutions. Much of this resulted from the inexplicable

onset of the covid pandemic, forcing schools to use technology, thus accelerating the adoption and usage levels of ICTs for EPs. This implementation has resulted in a mega shift and has become revolutionary for improving the qualities and efficiencies of EPs [9].

In the 21st century, technology pedagogy and content knowledge (TPACK) is a requirement that teachers must encompass when engaging in new learning environments [10]. This requirement assists teachers restructure educational practices, thus minimizing the today versus the future learning and teaching gaps that currently exist [11]. The Organisation for Economic Co-Operation and Development (OECD) suggested that students and teachers could benefit from using innovative ICTs [3], primarily as teachers are critical assets to the qualities of EPs [12]. However, these benefits will result from how well the frontliners are trained and prepared to use the technologies provided, especially as ICTs have become the lifeline for EPs [2] and will continue to be post-pandemic and while facing onward situations. The benefits will also result from how accessible and easy ICTs are to use and navigate and their usefulness to students' and teachers' educational experiences and academic outcomes.

Governmental entities play a significant role in ensuring quality education [13]. Yet, digital and educational gaps between communities exist, which influence students' and teachers' intentional use of ICTs for EPs [14], [15]. It is essential to provide equal access to physical materials and resources to students and teachers regardless of their geographical location. It is equally crucial to equip classrooms with quality ICTs, maintain the facilities, keep the systems up to date, provide technical support, and train teachers and students to use them effectively and efficiently [9], [14], and [16]. For students and teachers to fully participate in EPs, they must be granted access to quality equipment and broadband connections [11], particularly as ICTs for EPs have become mandatory, not necessarily voluntary. They must not be subjected to digital divides or geographical disparities where they lack access to the necessary materials and resources to successfully engage in educational practices [8], [14], and [17], and [18]. The quality of training in ICTs for EPs is significant and can substantially affect learning and teaching experiences [3], [11], and [14]. Technology training can help students and teachers overcome their reluctance to learn and use ICTs for EPs [10]. Furthermore, it will enable them to perceive ICTs for EPs as easy to use and useful [10], resulting in intentional and behavioral use and positive attitudes.

Significant findings in some studies [10], [19] suggested that teachers' acceptance and self-efficacy were associated with behavioral and intentional use of technology. Teachers are a significant asset in the educational field [11]. So, when teachers feel they lack proper training, feel unprepared, and are forced to use ICTs in EPs, it reduces teaching quality [3], [14]. It also diminishes the chances of accepting, adopting, intentional use, and contributing to negative attitudes toward ICTs for EPs. Studies [6], [9] showed evidence that ICTs could improve students' academic achievement, particularly in science, but not necessarily for practicing skills, math, and reading. Students reportedly had higher academic achievement when teachers used ICTs for EPs than teachers who did not [2]. For the types of ICTs, the system functionality should meet the standards to increase

acceptance and adoption [13], which means being easy to use and navigate, which leads to usefulness and intentional use. Digital content should be attractive and interactive, encompassing audio, video, and animated simulations related to the learning content [6], [13]. Several scholars demonstrated positive effects of using visual content in learning environments [5], [20], and [21]. These visual and auditory aids were said to capture learners' attention, make learning more engaging and cooperative, and improve academic experiences [20], especially in the attempt to boost language proficiency [5], [21]. Additionally, response time should be fast and consistent in ways that cultivate users' interest [13], whereas working from slow and outdated systems can result in lower use and nonuse.

ICTs have shifted societal and life dynamics, where the influences are felt in schools [11], [22]. Now more than ever, ICTs have gained a leading role in EPs for knowledge acquisition and academic achievement [1], [14], and [16]. It has reshaped education into more flexible and efficient learning in developing nations, providing optimal learning, and teaching experiences [13], [16], and [22]. In OECD countries, the use of ICTs for EPs has increased significantly and has become an amalgamation into traditional education to provide cost-effective education [6], [13]. There are positive and negative associations of using ICTs in OECD countries to look up ideas and information [9]. However, the usage of ICTs in EPs in non-OECD countries remains marginal, as the effects may be less pronounced due to low levels of effective teaching [9].

There continues to be controversy and mixed views about how beneficial ICTs are in EPs and how it influences students' performance and academic success [4], [6]. It remains questionable whether introducing ICTs in EPs guarantees the acceptance and continued use or whether the material being taught, and the digital infrastructures are ample enough to implement in academic institutions [13]. In a study, [6] illustrated the differences of opinions in studies investigating the use of ICTs for EPs. Something researchers term the *null* effect [9]. Some advantages were related to improving students' academic outcomes by placing a wealth of information at their fingertips and more comprehensive resources [9].

Positive associations have been linked to using ICTs to look up information and explore new ideas that are otherwise unavailable in traditional settings [9]. They provide students and teachers with flexibility and autonomy, thus improving their attitudes and experiences toward usage [6]. Using ICTs in EPs can foster digital competencies required to reap the benefits that innovative technologies ICTs offer [3]. ICTs in EPs can optimize learning and teaching experiences and increase well-being [16], [23].

Furthermore, using ICTs for EPs could increase social presence, collaboration, and cooperation and promote active, diverse, and inclusive learning environments [1], [24]. Multiple studies [6], [11], and [25] argued that using ICTs can allow teachers to augment their teaching materials by making them more attractive and engaging, thus improving academic outcomes. Information and communication technologies can support teachers in assessing students' progress and levels of engagement at a group and individual level, monitor their

behaviors, and provide instant feedback or get assistance from teachers and other students [1], [16], and [25]. It also provides the means to form quality student- teacher dyads, increase communication, cooperation, and collaborative efforts, and boost social enrichment and academic and personal well-being [1], [11], [16], and [23]. When ICT activities fail to improve students learning experiences, it takes away from other activities that could potentially harvest students' academic outcomes [9]. It also removes their willingness to engage and accept ICTs for EPs.

While ICTs are instrumental in EPs, research has suggested that ICT use cannot determine whether students have learned what was taught, as good grades do not predict academic success [26]. In contrast, research suggested that ICT use can influence students' academic achievement, where specific environmental and family dynamics and using ICTs passively and recreationally resulted in low grades and markings [27]. ICTs in EPs can distract students from learning [1], [6], [16], and [17]. Placing an abundance of information at students' fingertips can result in cognitive and information overloads and technoference, thus negatively affecting their ability to process information [1]. Furthermore, ICTs can result in social disengagement, exclusion, or diminished human interactions [1], [6], and [14]. Studies have suggested that students are less creative when using ICTs for EPs and can be easily targeted for cyberbullying [1], [6], and [16].

A significant barrier associated with using ICTs for EPs is that many school districts and students, mainly those in rural and undeveloped areas, face the triple digital divide of not having physical, skill, and usage accessibility [14], [16], [17], [28], and [29]. Also, they cannot afford the required ICTs or home broadband connectivities to engage in EPs, which contributes to poor academic achievement, reduced social presence, attrition or dropout [14], [16]. More importantly, persons residing in rural communities face geographical disparities of lacking quality broadband and internet connections [14], [17], [23], and [30].

Using ICTs for EPs is also faced with endogeneity problems- unobservable characteristics that can dramatically impact students' and teachers' willingness to accept and intentionally use ICTs for EPs [6]. Many ICT interactions are done in private and unobservable settings. Moreover, individuals use technology to engage in activities other than for EPs. Therefore, it would be difficult to determine how often students and teachers intentionally engage in ICTs for EPs. It may also be nuanced to suggest that technology acceptance results from using it for EPs, whereas technologies offer many activities that could facilitate acceptance and intentional and behavioral use.

This study extends work originally presented at the 2022 11th International Conference on Education and Information Technology (ICEIT), where a study [1] suggested that social networking sites (SNSs) have stated a claim in educational practices while losing the battle to the 2019 Coronavirus pandemic and onward situations. This study examines the use of ICTs for EPs. The technology acceptance model (TAM2) is used to ground this research [31]. Adopting elements from this model will show how students' and teachers' perceptions matter when decisions are made to implement and use ICTs for EPs. Many of these perceptions result from perceived ease of use, usefulness, attitudes toward technology, and social influences, which may

lead to intentional and behavioral use. Although technology holds a dominating presence in human lives and society, and many students already use ICTs for reasons other than for academic achievement, using ICTs for EPs may not directly affect their intentional use. Limitations and future recommendations are discussed.

2. Theoretical Foundation

2.1. Technology Acceptance Model - 2

The technology acceptance model- TAM2 created in 2000 is an expansion of the 1989 technology acceptance model (TAM) and is used to guide this paper. Figure 1 displays the TAM2 model. It expands the model by incorporating the perceptions of students and teachers, information and communication technologies (ICTs), and educational practices (EPs) related to perceived ease of use (PEOU), perceived usefulness (PU), intentional use (IU) or behavioral use (BU), and social influences (SI). Since ICTs dominate most human lives and society and now play a significant role in communication methods, socialization, knowledge acquisition, and academic success, students' and teachers' perceptions matter when deciding to use ICTs for EPs. Additionally, the information provided below defines the concepts of TAM2 and its external variables and demonstrates their association with ICTs and EPs.
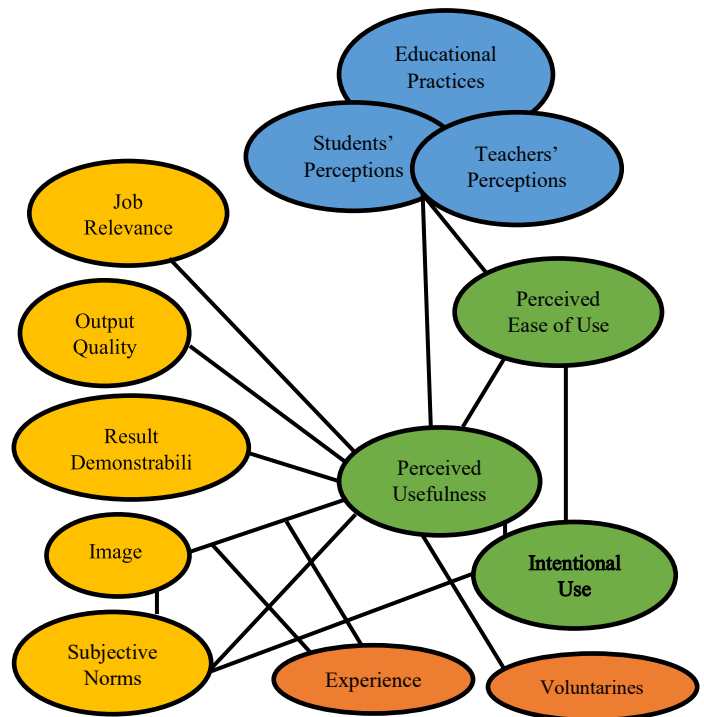
Figure 1: Technology Acceptance Model-2 and teachers' and students' perceptions of information and communication technologies for educational practices.

TAM stemmed from the theory of reasoned action (TRA) and the Theory of Planned Behavior (TPB) [32]. The TRA comprised three pillars, attitudes, subjective norms, and behavioral intentions, and focuses on two groups of variables: subjective norms and attitudes [33], [34]. TRA was designed to explain human behavior. It is also based on the premise that intention is

the primary determinant of an individual's actions and behavior [35]. As such, behavior is a direct function of intention [35].

As an extension of TRA, the central factors of TPB are individuals' intention to perform a given behavior [36]. These intentions are assumed to capture motivational factors that influence behavior, how hard a person is willing to try, and their effort in performing the behavior. The stronger the intention to engage in a specific behavior, the more likely it will be performed [35]. TPB comprises attitude toward the behavior, subjective norms, and perceived behavioral control (actual behavior) [32], [36].

The TAM model explains the behavior, attitudes, and intentions to use and adopt technology [37], [38], [39], and [40]. Constructs of TAM encompass various components, such as perceived ease of use (PEOU), perceived usefulness (PU), attitudes toward use (ATU), behavioral intentions to use (BIU), and actual use (AU) [39], [40]. PEOU is hypothesized to strongly influence PU, which directly impacts the ATU of various technologies [38], [41]. However, PEOU indirectly affects ATU [38]. Subsequently, BIU is influenced by AU [41]. Additionally, intentionality predicts users' willingness to adopt and use ICTs [39], [42]. These intentions are also influenced by an individual's attitudes [42]. The TAM model has been proven to be robust, the most influential, and has been widely applied to various regions examining technology acceptance and usage [13], [31], and [42]. Similarly, it is the most popular theory applied to research investigating students' behaviors and using and accepting ICTs for EPs [43], [44]. When individuals perceive ICTs as easy to use, useful, and beneficial, it increases their willingness to adopt, adapt, and accept technology [1]. More importantly, they develop positive attitudes toward technologies, resulting in continued and intentional use [39].

Due to the significant progress made over the past few decades in explaining and predicting users' acceptance and adoption of ICTs, the TAM model was expanded, constructing TAM2 [31]. The expansion aimed to determine how intentional use changes when individuals gain experience using ICTs [31]. While TAM rejected subjective norms due to their insignificant impact on usage, the TAM2 model incorporates these social aspects [40]. TAM2 theoretical constructs spanned from social influences (i.e., subjective norms, voluntariness, and image) and cognitive instrumental processes (i.e., job relevance and output quality) [31], [45]. The extension identifies and theorizes the social and cognitive influences that expand and determine usage perceptions [31], [45]. Job relevance, output quality, result demonstrability, and perceived ease of use capture to influences of cognitive instrument processes on perceived usefulness [45]. Social and cognitive influences are the most influential aspects that may result in students' and teachers' willingness to adopt ICTs for EPs. For example, when examining social influences or forces, many students are teachers face geographical disparities resulting from a lack of accessibility to physical materials and resources. Geographical disparities are also a result of poor broadband connectivity and internet access or no connections at all. Demographic disparities result from residing in rural rather than urban communities [14], [23]. Another contributing factor is financial stability, determining whether students, teachers, or other educational stakeholders can afford the essential ICTs needed to increase academic experiences and performances.

TAM2 also measures adoption behavior [31], [38], and [39]. Reputable researchers [35] suggested that behavior is a function of intentions. However, intentional behaviors are attributes of attitudes and beliefs [41]. Frequently, behaviors and attitudes are not factored into adopting and accepting ICTs for EPs. Moreover, this framework focuses on three interrelated social forces which impact an individual's decision to adopt, reject, or intentionally use innovative systems [31]. When students and teachers lack access to vital resources, digital skills, or the wherewithal to acquire quality equipment and internet connections, these social normalcies make the decisions for them.

2.2. TAM2 Concepts Defined

TAM has been used in various studies examining individuals' technology acceptance and usage.

- **Perceived Ease of Use**. Perceived ease of use (PEOU) is a cognitive instrumental process that determines perceived usefulness and refers to the degree to which individuals believe that using new and innovative ICTs is free of effort or effortless [31], [39], [41], and [46]. It is also defined by the degree to which usage lacks mental and physical effort [38]. Job and academic performances increase when little effort is put into using ICTs. [31]. PEOU is defined as the degree to which students believe using ICTs for EP is effortless and will simplify the learning process [5]. Therefore, PEOU is associated with students and teachers perceiving ICTs for EPs as easy to use, navigate, effortless, and user- friendly. When technologies are not user-friendly and users lack the necessary training, support, and technical knowledge, they are less inclined to adapt and accept ICTs for EPs [47]. Perceived knowledge about technology integration of ICTs for EPs directly influenced PEOU [48]. PEOU directly affects PU for both teachers and students [48]. Furthermore, when individuals find technology easy to use, they may find it useful, resulting in intentional usage and positive attitudes towards technology.

- **Perceived Usefulness.** Perceived usefulness (PU) is based on individuals believing that ICTs will improve their job performance [39], [41]. PU is the degree to which students and teachers perceive that using ICTs for EPs will enhance their performance in various ways [5]. Researchers [39], [48] posited that PEOU influences PU. That means using ICTs will assist individuals in performing or completing a task they set out to do. Several studies proved that PU strongly predicts intentional use [5], [20], and [38]. Therefore, the perceived usefulness of ICTs for educational practices is associated with students and teachers finding ICTs to be valuable tools that will assist them in effectively and efficiently completing specific educational tasks, inside and outside the academic settings. Even when students and teachers find ICTs for EPs useful, this does not necessarily contribute to their intentional use.

- **Intentional Use.** PEOU and PU are strong determinants of intentional use [31], [39]. However, intentional use can change over time with experience [31]. Attitudes toward

technology influence intended use [5], [48]. Several studies have demonstrated a positive effect that PEOU and PU can have on usage intentions [15]. Furthermore, researchers have suggested that system quality and trust in systems and institutions are critical factors affecting acceptance and adoption and users' satisfaction and intentional use [47], [49]. The program or content and the learning and teaching tools also influence the intention to use ICTs in EPs [5]. Therefore, it is essential to understand better which strategies influence the acceptance and adoption of ICTs for EPs [47]. Scholars have suggested fundamental ways to effectively implement innovative ICTs into EPs to improve learning and teaching experiences [11].

- *Behavioral Use.* The actual use of ICTs is a behavior [49]. Behavioral or actual use of ICTs for EPs is significantly associated with technology acceptance [5]. Intentional use of ICTs is influenced by an individual's attitude toward technology [49], [50]. Attitudes toward technologies are related to behavioral use [41]. The quality of services, satisfaction, trust in systems, and knowledge sharing were significant predictors of usage behaviors of ICTs for EPs [47]. When individuals set out to act, they do so without limitations or coercion [41]. This means peers or other social norms do not influence behavioral use. Therefore, it can be suggested that when teachers and students perceive ICTs for EPs to be easy to use and useful, they develop positive attitudes toward technologies, ultimately leading to intentional and behavioral use.

2.3. External Variables of TAM2 Defined

- *Image.* Image is a social process that refers to an individual's perception that using and accepting innovators will enhance their social status [31]. TAM2 is a supposition to subjective norms in that image is enhanced when individuals of a prominent group believe they can perform specific behaviors and that performing those behaviors will strengthen their standing and status within that group [31]. Therefore, image is students' and teachers' perceptions that innovative technologies will enhance their learning and teaching experiences or academic stance or status. Additionally, the image component can be seen as a significant contributor to increasing knowledge acquisition and academic achievement (students) and job performance (teachers), which others will recognize in ways that would increase their academic and professional status.

- *Job Relevance.* Job relevance is a cognitive instrumental process that determines perceived usefulness and refers to individuals' perceptions that ICTs are suitable for their job [31], [46]. The job relevance variable of TAM2 is a function of importance within one's job and using ICTs will support a person in completing specific tasks [31]. ICTs are advantageous when they enhance performance and assist in achieving functions [39]. Therefore, when ICTs can perform certain functions within the scope of educational practices, whereby enhancing academic experiences, the systems are categorized as being relevant to the job. Moreover, job

relevance will ultimately lead to positive attitudes toward technology and continued usage.

- *Output Quality.* Just like most things, output quality is a result of input quality. Like job relevance, output quality is a cognitive instrumental process that predicts perceived usefulness. It refers to individuals perceiving ICTs as good enough to perform specific functions; however, it is also based on whether the tasks performed by ICTs fit the desired goal [31], [46]. ICT users are the ones that consider how well systems perform, thus determining their output quality [31]. An information system (IS) model suggests system and information qualities impact user satisfaction [49]. Therefore, system and information quality may result from output quality. When students and teachers find that the output of ICTs for EPs is of quality, it may increase their likeliness to develop positive attitudes, wherein increasing intentional and behavioral use. While output quality is significantly related to input quality and the quality of the machines and software, it may also depend on the quality of internet and broadband connections. How teachers and students interact with ICTs for EPs can also establish output quality.

- *Result Demonstrability.* Result demonstrability (RD) is a cognitive instrumental process that determines perceived usefulness and is based on physical results and being able to attribute ICT use to increase performance [31], [46]. RD tangible results are positively associated with perceived usefulness [31]. Moreover, individuals will develop positive perceptions about how useful ICTs are when outcomes are of quality and noticeable [31]. Therefore, when ICTs are used in EPs, and the physical results can be attributed to increased performance academically, this demonstrates RD. Furthermore, all elements that have led to intentional and behavioral use may result in RD.

- *Subjective Norms.* Subjective norms (SNs) are social processes that refer to individuals perceiving social influences or social forces as the reason for performing a behavior or not [31], [36]. External variables and others influence many individuals' behaviors and actions. Internalization is based on individuals taking on the perceptions of others they see as crucial in their lives [46]. Furthermore, SNs are when inferior persons believe superior others approve or disapprove of specific behaviors. These beliefs of the inferior persons will result in them internalizing the perceptions of the majority figure in which they base their decisions on whether to engage in certain behaviors or believe that ICTs are useful [31], [36]. TAM2 reflects three interconnected social strengths that play a critical role in individuals' willingness to adopt or reject innovative ICTs when given the opportunity [31]. These social dynamics are subjective norms, voluntariness, and image [31]. Because subjective norms focus on social experiences and influences, these social dynamisms can relate to facilitating conditions, environmental factors, affordability, and accessibility. The usefulness of ICTs can be based on the perceptions of others and internalized processes [31], [36]. However, when individuals set out to perform specific behaviors, they do so

without limitations or coercion, as peers or other subjective norms do not influence their behaviors [41].

- *Voluntariness.* According to the TAM2 model, voluntariness is associated with subjective norms and intention to use. Voluntariness is a social process that refers to how technology adopters and adapters perceive their decisions to adopt new and innovative technologies as voluntary and not mandatory; freedom to choose [31], [46], and [51]. Moreover, it represents an individual's state to act or behave in a specific manner [51]. The use of ICTs voluntariness is significantly associated with TAM elements that lead to intentional and behavioral use [46]. Therefore, when using ICTs for educational practices, the voluntariness aspect refers to how teachers and students use digital devices of their own volition; usage is not mandatory or forced, and users do not take on the perceptions of essential others or social influences. Individuals who take the initiative to learn new and innovative technologies increase their experience and confidence levels in navigating the various functions [46] related to job relevance and evaluating the output quality.

There are two primary factors associated with actual or intentional use [51]. These factors are ease of use (technological contacts) when using ICTs in mandatory environments (low voluntariness) and 2) organization facilitating conditions (implementation context) and voluntary environment (high voluntariness) [51]. Demonstrating such relationships, when teachers and students find ICTs easy to use and usage or adoption is mandatory, it contributes to low voluntariness, which indicates that they were forced to use ICTs and were not provided with a choice [51]. Some students and teachers are exposed to specific organizational and facilitating conditions where ICTs are readily implemented. However, when using ICTs is mandatory, they are free to use or not use ICTs for educational practices, thus demonstrating high voluntariness in ICT use [51]. In sum, facilitating conditions predicted voluntariness and the actual use of ICTs in EPs [51].

3. Methodology and Study's Focus

This paper is an extension of work originally presented at the 2022 11th International Conference on Education and Information Technology (ICEIT) [1].

A researcher [1] suggested that social networking sites (SNSs) have stated a claim in educational practices while losing the battle to the 2019 coronavirus pandemic and onward situations. This study focuses on previous literature on accepting and adopting information and communication technologies (ICTs) in educational practices (EPs). ICTs have stated a claim in EPs and become a facilitating factor in academic engagements and success. However, when making decisions to implement ICTs in educational institutions, decision-makers and policymakers fail to consider the perceptions of students and teachers. This research seeks to understand the perceptions of students and teachers regarding the usefulness of ICTs for EPs as they relate to social influences and intentional use. The questions addressed in this research are:

1. What factors influence a student's perception of using ICTs in EPs that results in intentional use?

2. What factors influence a teacher's perception of using ICTs in EPs that results in intentional use?

4. Students' Perceptions of ICTs for EPs

Several dynamics influence students' perceptions of ICTs for EPs. Students are more likely to continually and intentionally use educational-based infrastructures through individual acceptance and personal willingness to using ICTs in EPs [5], [16], and [52]. In an article, a scholar [1] suggested various intricacies of using technology for learning. Some intrinsic factors include beliefs and attitudes toward ICTs [31], [39] cognitive abilities, learning styles [21], ICT literacy and competence [5], [52], and [53], academic intellect, motivation [5], [54], and gender [54], [55]. Moreover, previous experience, learning content and subject, and grade level [54] also contributed to students' perceptions of using ICTs in EPs.

While internal and self-motivating factors influence students' perceptions of using ICTs in EPs, students' willingness to use ICT and EPs depend on their learning styles [21]. More importantly, external, and contextual factors also shape their perceptions. These underlying forces are associated with social and peer influences, access to quality equipment, internet connections, training, academic settings, and learning environments [5], [23], and [52]. Many students feel they could use ICTs for EPs, especially as technology has become a significant part of their lives [54]. Children who started using technologies at younger ages demonstrated higher competence with using ICTs for EPs than those who began using technology later [56], resulting in positive perceptions of using ICTs in EPs and suggesting that ICT competency matters. Contrastingly, students from low socioeconomic and poor households who did not have previous exposure to ICTs performed at lower academic rates than students with prior ICT exposure and experiences [20]. However, this is not to suggest that students with later or no exposure to various technologies will develop negative perceptions about using ICTs, but that more experienced users were less confident in using ICTs for EPs than students with less experience [54]. Relatively, those students in lower grade levels were more satisfied with using ICTs in EPs than those in higher grade levels [54].

When considering gender differences, researchers [54], [55] revealed that male students were more confident in using ICTs in EPs than females. This finding could be based on some students' having equitable access and independently making decisions regarding the use of technology. Nonetheless, females may be less inclined to use technology because they perceive ICT usage as a male-centric activity [54].

Geographically, students in Portugal and Ukraine favored using ICTs for EPs compared to United Arab Emirate (UAE) students [57]. Students in all three countries, Portugal, Ukraine, and UAE, reported favorable perceptions and attitudes toward using ICTs in EPs [57]. This is because it allowed them to manage their time, work independently, and at their own pace and from their desired learning environments [57]. While some students in the United States found that educational-based technologies were too restrictive, their perceptions were based on teachers' knowledge, skills, and abilities (KSAs) to use ICTs for course instructions effectively and efficiently. American students' perceptions also resulted in whether teachers could assist in resolving technical issues [58].

Additionally, the learning environments, whether teachers cared about students' academic success, and whether students experienced a disconnect or disassociation between in-class and out-of-the-classroom settings also influenced their perceptions of how beneficial ICTs were for engaging in EPs [58]. In the United States and France, the quality, satisfaction, and loyalty of services provided to students through e-learning played a significant role in students constructing their perceptions of using ICTs in EPs [59], [60]. The quality of educational technologies that can assist with optimal learning experiences and successful outcomes also influenced students' perceptions of using ICTs in EPs [61].

With innovative technologies holding a ubiquitous presence in human lives and society, it is essential to account for how students use ICTs in everyday life and how such usage differs from educational purposes [53]. This is mainly because some students reported that educational-based technologies and digital infrastructures are too restrictive [58], particularly as they have unlimited access and usage of everyday technologies outside academia. While a few studies [53], [57], and [62] reported that past and previous experiences synchronously and asynchronously impact students' perceptions of using ICTs in EPs, others [52] suggested that this is not the case. Instead, some researchers [52] advocated that past experiences are not predictors of a student's willingness to accept ICTs for EPs simply because students' ICT usages and engagements differ from one context to the next.

Scholars [53] proclaimed that Chinese students' perceptions of using ICTs were based on past experiences, as they spent numerous hours on their devices which increased their comfort levels with using ICTs for EPs. Because of technology's flexibility and convenience, students in India developed positive perceptions of using ICTs in EPs [62]. Indonesian students' perceptions resulted from ICTs providing them with the capability to improve their motivation to learn, level of independence, understanding of the topics being taught, time management skills, self-discipline, and interactions. Information and communication technologies (ICTs) also increased their exposure to vital resources that would have been otherwise inaccessible without technology [52]. Some researchers [62], found that students preferred to use their smartphones, pre-recorded instructions, and take online quizzes [62]. Also, in an analysis based in India and South Korea, researchers [63] found that students' perceptions of using ICTs in EPs were influenced by classroom and social interactions, motivation, course structures and layout, instructors' knowledge, and facilitation [57]. Not long ago, Turkish students' perceptions of using ICTs resulted in their basis and motivation to learn [54].

Studies in several countries demonstrated students' positive perceptions and attitudes toward using ICTs in EPs [52], [53], [54], [57], [62], and [63] and how using ICTs are attractive but can be both beneficial and detrimental [1], [14], [16], and [23]. However, Canadian students demonstrated negative perceptions of ICTs in EPs due to cognitive overload, poor communication and interactions between students and teachers, technical issues, and inability to follow and navigate course structures [64], [65]. Using ICTs in EPs is not always beneficial, whereas some students, experienced and inexperienced, will face challenges and complexities related to cybersecurity, hacks, viruses, cyberbullying, and internet instability and outages. When using ICTs in EPs, some students face concerns about interacting with teachers and peers [57]. Some of these issues are associated with technical problems. However, technological disruptions and complexities were not always significant factors influencing a student's perception of using ICTs in EPs [52], [57]. Skills or digital literacy, time management, language, behavior, motivation, and their objectives and goals to learn were [52], [54], [57], and [66].

Digital knowledge and skills were primary determinants of a student's willingness to participate fully and accept ICTs in EPs [52], [66]. Students are not motivated to learn, accept, or use technology if they lack the necessary confidence to use ICTs for EPs [55]. This can result in students' fear of learning and unwillingness to engage or position themselves in novel situations due to negative technological experiences [55]. It can also increase attrition, enrollment, and academic disengagement rates [1], [23]. Some students' motivation to use ICTs in EPs deals with their ability to strategically communicate and interact with other students and teachers [52]. For novice language learners, systematic communication practices are essential, especially as they need to develop their language skills and competencies [5], [21], and [57] or have a desire for academic success [61]. Students that developed positive perceptions toward ICTs for EPs were those who found ICTs to be useful and easy to use [52]. The usefulness aspect allowed them to improve their understanding and academic competencies in a specific subject [52]. It also provided them the means to study independently and increased self-discipline and motivation to learn [52], [54]. Those who developed negative perceptions and attitudes toward ICTs found that the digital infrastructures and platforms were not designed to meet students' specific needs, presented navigation complexities, were not user-friendly, and produced cognitive overloads [65].

As some students continually face digital divides, such as access to physical materials and resources and geographical disparities [1], [14], [16], [18], [23], and [30], other students have access and can afford ICTs [57]. Academicians [1], [23], and [67], illustrated some advantages and disadvantages of using ICTs in EPs, a significant benefit of using ICTs in EPs is that students can actively, authentically, and cooperatively engage in the learning process, which ultimately resulted in them developing a positive perception of using ICTs in EPs. Overall, students' positive perceptions of using ICTs in EPs outweighed negative perceptions, but this may not be the same when considering teachers' perceptions.

5. Teachers' Perceptions of ICTs for EPs

Teachers' perceptions of using ICTs in EPs matter, especially as they are responsible for integrating technology into their classrooms, curricula, and pedagogies [68]. While there are several advantages and disadvantages of using ICTs in EPs [1], teachers' positive or negative perceptions or attitudes toward ICTs result from how easy and useful they use them in EPs [69]. When teachers perceive ICTs as useful and easy to use, they develop positive attitudes toward technology, which increases their intentional use [15]. Factors that motivated teachers to use ICTs in EPs resulted from self-efficacy, educational values, impact on teaching, and the quality of training in ICTs to be used in EPs [68].

Furthermore, educationalists accepted educational-based technologies because they provided them with the flexibility to deliver instructions [1], [70], and [71]. ICTs assist teachers with obtaining information easily and swiftly and make teaching and learning more interesting [72]. While ICTs offer significant benefits in teaching practices, teachers' gender [71] and the subjects they teach [73] played an essential role in their willingness to adopt and use ICTs in EPs. Furthermore, based on their own experiences, many teachers will form their individual attitudes and beliefs about how valuable and effective ICTs are when used for educational purposes.

Endogenous and exogenous factors influenced teachers' perceptions of using ICTs in EPs [74]. Endogenous factors were based on nonmanipulative conditions, while exogenous factors were manipulative and changeable [74]. Teachers and school levels are both endogenous and exogenous dynamics [74]. However, when considering the use of digital pedagogies and instructions, the digital platforms must not only be understandable and available to teachers and within the academic milieu, but students must be able to comprehend the material they are being taught through digital instructions.

Some teachers are apprehensive about using ICTs in EPs when they lack the training to use technological infrastructures, platforms, software, and hardware effectively and efficiently. There are two sides to teachers' perceptions of using ICTs in EPs, whereas some teachers had positive attitudes toward technologies and felt that ICTs were beneficial in teaching practices [72]. However, some teachers had opposing views and felt there was no value or benefit in using ICTs in EPs where language learning is concerned [72]. Despite such trepidations, academics [68], [72] advocated that those teachers who taught in Indonesia's rural school districts felt using ICTs in EPs was beneficial. Teachers found that using ICTs in EPs effectively increased students' motivation to learn, fostered positive attitudes toward ICTs, and made learning and teaching activities more exciting and enjoyable [68]. Additionally, teachers found that using ICTs in EPs helped students better understand how various technologies affected their lives. Regardless, teachers perceived ICTs in EPs to improve teaching performances and assisted them with developing new teaching skills [68].

In the West Indies, teachers' perceptions of ICTs significantly influenced how beneficial ICTs were in EPs [74]. These considerations were based on cooperation, job satisfaction, and self-confidence [74]. For Malaysian teachers, evidence showed that these teachers faced various challenges in integrating and using ICTs in EPs [69]. They found that using ICTs was helpful in ways that increased their job performance and productivity and allowed them to work more quickly and effectively. A teacher's perception of using ICTs heavily dealt with them finding that the provided digital infrastructures were straightforward, understandable, and easy to remember and control [69]. In Sweden, teachers had positive perceptions of using ICTs in EPs and used the digital platforms for various reasons [71]. Teachers

felt that ICTs provided them with the flexibility needed in the time and space and allowed them to provide students with online instructions and readily available assignments [71]. Palestinian teachers perceived ICTs to positively influence their teaching and educational practices [24]. In Ethiopia, some researchers [75] found a positive relationship between teachers' perceptions toward ICTs in teaching and learning practices, especially when they were encouraged to do so and received the necessary support. Although using ICTs in EPs increased the quality of courses and productivity and allowed teachers to prepare and deliver course material for students more efficiently, most teachers did not use ICTs as a teaching tool [75]. Significant barriers to using ICTs in EP were that teachers lacked the necessary technical knowledge and experienced substantial shortages of resources and materials [75].

In East African countries, students and teachers continually face digital transformation challenges of not having access to various technologies, physical materials, and resources. African countries, among other developed and undeveloped countries, incessantly lack vital resources for teaching and learning, resulting in educators' and pupils weakened digital knowledge and technology fluencies [12], [76]. Sub-Saharan African teachers who actively use ICTs in EPs are those who acquired equipment and training at their own expense [77]. While students are excited to use ICTs in EPs, teachers are open to such usability provided they receive the appropriate training and support needed to operate the devices effectively and efficiently [77]. Human, physical, technical, system, and policy environmental readiness' are some significant caveats that African countries face [77].

Insofar, there are several barriers that impact Indian teachers' perceptions of using ICTs in EPs [78]. Moreover, researchers found that while a large portion of teachers was ready and willing to use ICTs in EPs, many teachers were not [78]. Teachers with unfavorable attitudes toward ICTs in EPs felt that using technology was not beneficial to the teaching practices [78]. For example, several studies demonstrated challenges teachers faced when implementing ICTs into EPs. Challenging encounters were adequate training, teacher and technical competencies, accessibility and broadband/internet connectivity issues, lack of technical support, quality of equipment, updated software, and inability or time constraints to shift from formal/traditional teaching paradigms to informal teaching practices [68], [69], [71], [72], [75], and [78]. Some academic investigators [75] conjectured that equipping teachers' and academic institutions with ICTs are not enough to successfully integrate ICTs into EPs. Teachers and students must receive adequate training so that the ICTs for EPs afforded for learning and teaching can easily be understood.

6. Research Strengths, Implications, and Future Recommendations

This study demonstrates various strengths and limitations regarding the perceptions of students and teachers as they relate to their willingness to accept and intentionally use information

and communication technologies in educational practices. Furthermore, this study provides recommendations that future researchers could conduct to expand this study or add to existing bodies of literature regarding the use of ICTs in EPs. Strengths, limitations, and future recommendations are as follows:

6.1. Research Strengths

Some significant strengths of this research are that it illustrates how students and teachers are the primary stakeholders and frontliners when using ICTs in EPs. Yet, decision-makers and policymakers fail to consider their perceptions of how valuable ICTs are in EPs, especially regarding job relevance, output quality, result demonstrability, perceived ease of use, and all cognitive instrumental processes that contribute to perceived usefulness [46]. Another strong point is that the information presented is timely and relevant, mainly because ICTs have stated a claim not only in human lives, but in EPs and have become essential in educational practices. Students' and teachers' perceptions matter. This research demonstrates how using ICTs provides flexibility in teaching and learning practices and how they can increase the potential of academic experiences and achievement given that students and teachers are provided with adequate training and vital resources and equipment. Most importantly, this study demonstrates how teachers' and students' perceptions of using ICTs in EPs matter, as they are not harvested based on opinion but real-world circumstances and actualities.

6.2. Study Limitations

This study comes with limitations. A limitation associated with this study is that it is based on previous literature. At the same time, this study demonstrated the perceptions of students and teachers and how their perspectives matter when making decisions to integrate information and communication technologies into educational practices. However, examining specific learning management systems (LMS) and digital platforms while considering students' and teachers' perspectives jointly and individually may yield precise results. Comparing students and teachings in rural school districts versus urban academic settings may produce other meaningful outcomes, those that are distinct from what is revealed in this study.

6.3. Future Recommendations

Although this study provides evidence to show how students' and teachers' perceptions matter when using ICTs in EPs, it is suggested that future researchers examine students' and teachers' educational experiences as they relate to using ICTs in EPs while taking a diverse approach. A qualitative or quantitative approach that produces robust information can help understand how ICTs influence EPs among students and teachers. Future researchers should consider various demographics, socioeconomic status (SES), environmental and social influences, age, culture, geographical positions, and accessibility when trying to understand the perceptions of students and teachers as they relate to their intentional use of ICTs in educational practices. All

educational stakeholders must realize that students and their learning styles are not homogenous and should be viewed differently. Researchers should also note that teachers and their teaching styles are heterogeneous, as these aspects should be considered when examining the perceptions of students and teachers and their willingness to using ICTs in EPs, where technology acceptance paradigms are concerned.

7. Conclusion

The main objective of this paper was to expand the previous work presented at the 2022 11th International Conference on Education and Information Technology (ICEIT) [1]. This study [1] suggested that social networking sites (SNSs) have stated a claim in educational practices while losing the battle to the 2019 coronavirus pandemic and onward situations. However, when making critical decisions on whether to implement technologies into educational practices, the perceptions of students and teachers matter, but in frequent cases, they are not always considered. Therefore, this paper addressed two pressing questions a) what factors influence students' perceptions when using ICTs in EPs that result in intentional use, and b) what factors influence teachers' perceptions when using ICTs in EPs that result in intentional use. Understanding these factors and knowing what it takes to implement ICTs into EPs successfully, primary stakeholders will start to value the perceptions of students and teachers and not just focus on the affordability and geographical aspects.

While many governmental entities and policymakers encourage school districts to implement technologies into their learning and teaching practices, they do not bring students and teachers to the forefront to acknowledge what is doable. Instead, they take it upon themselves to purchase and decide whether to implement technology into schools, leaving students and teachers in the background. Yet, students and teachers are the primary users.

There are numerous advantages and disadvantages of using ICTs in EPs. Meanwhile, various endogenic and exogenic factors influence the perceptions of students and teachers about using and accepting educational-based digital infrastructures and platforms that will result in intentional use. However, to increase intended use, it is imperative that frontline users, such as school districts, students, and teachers, be provided with the necessary resources. The properties include funding, adequate training, access to quality equipment, software, internet connections, technical support, and unending support from primary decision-makers and educational and governmental stakeholders. Policymakers must pay attention to endogenous and exogenous factors and value students' and teachers' perceptions when deciding whether to implement ICTs in EPs [74]. Otherwise, it can result in students and teachers developing negative attitudes toward technology use in educational practices. These negative attitudes can stem from teachers and students facing the challenge of not being heard or receiving adequate training or resources.

As ICTs have stated a claim in educational practices, the perceptions of students and teachers matter. Their perceptions go beyond the scope of elements described in the technology acceptance model regarding ease of use and perceived usefulness and spill over into the extended model-TAM2. Teachers and students must receive essential materials and resources to successfully integrate digitally-based pedagogical instructions into their learning and teaching curricula and reap the full benefits technologies offer. Training will increase students' and teachers' confidence levels, comfortability in use, and knowledge acquisition. Studies have suggested that using ICTs in EPs can optimize learning and teaching experiences, mainly when training is provided. However, the training process cannot be a one-time thing, as training must be ongoing, as hardware and software packages and licenses are updated and supported frequently. Teachers' and students' perceptions are valuable assets in discovering the practicality of how beneficial and easy ICTs are to use EPs. Given that, this study suggests that primary decision-makers account for teachers' and students' perceptions when deciding what technologies are implemented into learning and teaching practices. In short, teachers and students are the frontliners when using ICTs in EPs, as their perceptions are not a matter of opinion but a matter of fact.

Conflict of Interest

The authors declare no conflict of interest.

References

[1] A. Pearce, "Socially networking sites stating claim in educational practices while losing the battle to COVID-2019 and onward situations", in 2022 11th International Conference on Education and Information Technology (ICEIT), IEEE, 105-111, 2022, doi:10.1109/ICEIT54416.2022.9690736.

[2] J. Bryant, F. Child, E. Dorn, S. Hall, New Global Data Reveal Education Technology's Impact on Learning, McKinsey & Company, 2020.

[3] Organization of Economic Co-operation and Development (OECD), "ICT Resources in School Education: What Do We Know from OECD Work?," OECD, 2020, https://www.oecd.org/officialdocuments/publicdisplaydocumentpdf/?cote=EDU/EDPC/SR/RD(2020)2&docLanguage=En

[4] The World Bank, Understanding Poverty / Education Overview, World Bank Group, 2022. https://www.worldbank.org/en/topic/education/overview

[5] Wiyaka, J. Mujiyanto, D. Rukmini, "Students' perceptions on the usefulness of ICT-based language program," English Language Teaching, 11(2), 53-60, 2018, doi:10.5539/elt.v11n2p53.

[6] M. Fernández-Gutiérrez, G. Gimenez, J. Calero, "Is the use of ICT in education leading to higher student outcomes? Analysis from the Spanish autonomous communities", Computers & Education, 157, 1-15, 2020, doi:10.1016/j.compedu.2020.103969.

[7] J. Adhikari, A. Mathrani, C. Scogings, "Bring your own devices classroom: Exploring the issue of digital divide in the teaching and learning contexts," Interactive Technology and Smart Education, 13(4), 323-343, 2016, doi:10.1108/ITSE-04-2016-0007.

[8] J. A. G. M. van Dijk, "The evolution of the digital divide – The digital divide turns to inequality of skills and usage," in Digital Enlightenment Yearbook 2012, IOS Press, 57-78, 2012.

[9] O. Falck, C. Mang, L. Woessmann, "Virtually no effect? Different uses of classroom computers and their effect on student achievement", Oxford Bulletin of Economics and Statistics, 80(1), 1-38, 2018, doi:10.1111/obes.12192.

[10] Y. J. Joo, S. Park, E. Lim, "Factors influencing preservice teachers' intention to use technology: TPACK, teacher self-efficacy, and technology acceptance model," Educational Technology & Society, 21(3), 48-59, 2018.

[11] L. Ratheeswari, "Information communication technology in education," Journal of Applied and Advanced Research, 3(S1), S45-S47, 2018, doi:10.21839/jaar.2018.v3iS1.169.

[12] S. Kommers, M. van der Zijde, A. Elfferich, E. Thravalou, Digitalisation of education in East Africa: Needs, experiences, and opportunities for the future, Nuffic, 2021. https://www.nuffic.nl/sites/default/files/2021-09/digitalisation-of-education-in-east-africa-needs-experiences-and-opportunities-for-the-future.pdf

[13] F. Kanwal, M. Rehman, "Factors affecting e-learning adoption in developing countries-empirical evidence from Pakistan's higher education sector," in 2017 IEEE Access, 5, 10968-10978, 2017, doi:10.1109/ACCESS.2017.2714379.

[14] A. Pearce, "The digital gap still exists, generationally, rurally, and academically," in 2020 12th International Conference on Education, Technology, and Computers (ICETC), ACM, 215-222, 2020 doi:10.1145/3436756.3437048.

[15] F. Weng, R-J. Yang, H-J. Ho, H-M. Su, "A TAM-based study of the attitudes towards use intention of multimedia among school teachers," Applied System Innovation, 1(3), 1-9, 2018, doi:10.3390/asi1030036.

[16] A. Pearce, "Optimal learning using technology: Amplifying students collaboration and social networking," in 2021 PUPIL: International Conference of Teaching, Education, and Learning (ICTEL), 5(2), 19-32, 2021, doi:10.20319/pijtel.2021.52.1932.

[17] B. Warf, "Teaching digital divides," Journal of Geography, 118(2), 77-87, 2019, doi:10.1080/00221341.2018.1518990.

[18] A. J. van Deursen, J. A. van Dijk, "The first-level digital divide shifts from inequities and physical access to inequities in material access," New Media & Society, 21(2), 354-375, 2019, doi:10.1177/1461444818797082.

[19] R. Sherer, F. Siddiq, J. Tondeur, "All the same or different? Revisiting measures of teachers' technology acceptance", Computers & Education, 143, 1-17, 2020, doi:10.1016/j.compedu.2019.103656.

[20] E. T. Maziriri, P. Gapa, T. Chuchu, "Students perceptions toward the use of Youtube as an educational tool for learning and tutorials," International Journal of Instructions, 13(2), 119-138, 2020, doi:10.29333/iji.2020.1329a.

[21] G. Sakkir, S. Dollah, J. Ahmad, "Students' perceptions toward using Youtube in EFL classrooms," Journal of Applied Sciences, Engineering, Technology, and Education, 2(1), 1-10, 2020, doi:10.35877/454RI.asci2125.

[22] Y. Jung, J. Lee, "Learning engagement and persistence in massive open online courses (MOOCs)," Computers & Education, 122, 9-22, 2018, doi:101016/j.compedu.2018.02.013.

[23] A. Pearce, "Achieving academic satisfaction through the use of education-based technologies: Strengthening students personal well-being while facing online learning mandates and digital disparities," London Journals Press, 21(5), 19-36, 2021, doi:10.34257/LJRHSSVOL21IS5PG21.

[24] H. Qaddumi, B. Bartram, A. L. Qashmar, "Elevating the impact of ICT on teaching and learning: A study of Palestinian students' and teachers' perceptions," Education and Information Technologies, 26, 1865-1876, 2021, doi:10.1007/s10639-020-10339-5.

[25] S. K. D'Mello, "Improving student engagement in and with digital learning technologies," in OECD Digital Education Outlook 2021: Pushing the Frontier with Artificial Intelligence, Blockchain and Robots, Paris, OECD Publishing, 67-92, 2021.

[26] A. Yli-Jyrä, "Optimal learning experiences in language technology education," ResearchGate, 1-14, 2014.

[27] S. Simões, T. Oliveira, C. Nunes, "Influence of computers on students' academic achievement," Heliyon, 8(1), 1-13, 2022, doi:10.1016/j.heliyon.2022.e09004.

[28] J. A. G. M. van Dijk, "Digital divide research, achievements and shortcomings," Poetics, 34(4-5), 221-235, 2006, doi:10.1016/j.poetic.2006.05.004

[29] J. A. G. M. van Dijk, "Digital divide: Impact of access," The International Encyclopedia of Media Effects, 1-11, 2017, doi:10.1002/9781118783764.wbieme0043.

[30] C. G. Reddick, R. Enriquez, R. J. Harris, B. Sharma, "Determinants of broadband access and affordability: An analysis of a community survey on the digital divide," Cities, 106, 1-12, 2020, doi:10.1016/j.cities.2020.102904.

[31] V. Venkatesh, F. D. Davis, "A theoretical extension of the technology acceptance model: Four longitudinal field studies," Management Sciences, 46(2), 186-204, 2000, doi:10.1287/mnsc.46.2.186.11926.

[32] I. Ajzen, "From intentions to actions: A theory of planned behavior," in Action Control: SSSP Springer Series in Social Psychology, Springer, 11-39, 1985.

[33] M. Fishbein, I. Ajzen, Belief, attitude, intention, and behavior: An introduction to theory and research, Addison-Wesley, 1975.

[34] B. Salgues, Health Industrialization. ISTE Press Ltd, 2016.

[35] G. D. Sideridis, A. Kaissidis, S. Padeliadu, "Comparison of the theories of reasoned action and planned behavior," British Journal of Educational Psychology, 68, 563-580, 1998.

[36] I. Ajzen, "The Theory of Planned Behavior," Organizational Behavior and Human Decision Processes, **50**(2), 179-211, 1991, doi:10.1016/0749-5978(91)90020-T.

[37] F. Abdullah, R. Ward, E. Ahmed, "Investigating the influences of the most commonly used external variables of TAM on students' perceived ease of use (PEOU) and perceived usefulness (PU) of e-portfolios," Computers in Human Behavior, **63**, 75-90, 2016, doi:10.1016/j.chb.2016.05.014.

[38] H. Ahmad, A. Basden, "Non-disciplinary use of information system and the technology acceptance model," University of Salford Manchester, 2008.

[39] F. D. Davis, "Perceived Usefulness, Perceived Ease of Use, and User Acceptance of Information Technology," MIS Quarterly, **13**(3), 319-340, 1989.

[40] P. Legris, J. Ingham, P. Collerette, "Why Do People Use Information Technology? A Critical Review of the Technology Acceptance Model," Information & Management, **40**(3), 191-204, 2003, doi:10.1016/S0378-7206(01)00143-4.

[41] S. R. Sakarji. K. B. M. Nor, M. M. Razali, N. Talib, N. Ahmad, W. A. A. W. M. Saferdin, "Investigating Students Acceptance of E-Learning Using Technology Acceptance Model Among Diploma in Office Management and Technology Students at Uitm Melaka," Journal of Information System and Technology Management, **4**(13), 13-26, 2019, doi:10.35631/JISTM.413002.

[42] P. Reddy, K. Chaudhary, B. Sharma, R. Chand, "The two perfect scores for technology acceptance," Education and Information Technologies, **26**, 1505-1526, 2021, doi:10.1007/s10639-020-10320-2.

[43] J. Henderson, N. B. Milman, "The technology acceptance model: Considerations for online educators," Distance Learning, **17**(3), 104-107, 2021.

[44] B. Šumak, M. Heričko, M. Pušnik, "A meta-analysis of e-learning technology acceptance: The role of user types and e-learning technology types," Computers in Human Behavior, **27**, 2067-2077, 2011, doi:10.1016/j.chb.2011.08.005.

[45] V. Venkatesh, H. Bala, "Technology acceptance model 3 and a research agenda on intervention," Decision Sciences, **39**(2), 273-315, 2008, doi:10.1111/j.1540-5915.2008.00192.x.

[46] M. Kaur, "Integration of ICT in education issues and challenges," in New Paradigm in Business and Education,. National Press Associates, 75-80, 2020.

[47] S. A. Salloum, M. Al-Emran, K. Shaalan, A. Tarhini, "Factors affecting the E-learning acceptance: A case study from UAE," Education and Information Technologies, **24**, 509-530, 2019, doi:10.1007/s10639-018-9786-3.

[48] P. Luik, M. Taimalu, "Predicting the intention to use technology in education among student teachers: A path analysis," Education Sciences, **11**, 1-14, 2021, doi:103390/educsci11090564.

[49] W. H. Deleon, E. R. McLean, "The Deleon and McLean model of information systems success: A ten-year update," Journal of Management Information Systems, **19**(4), 9-30. 2003, doi:10.1080/07421222.2003.11045748.

[50] S. R. Joseph, "Students' perspectives on ICTs acceptance and use in higher educational institutions of Botswana: Limkokwing University," International Journal of Engineering & Scientific Research, **3**(1), 185-198, 2015.

[51] B. Brevell, V. Arkorful, "LMS-enabled blended learning utilization in distance tertiary education: establishing the relationships among facilitating conditions, voluntariness of use and use behavior," International Journal of Educational Technology in Higher Education, **17**(6), 1-16, 2020, doi:10.1186/s41239-020—183-9.

[52] L. Vitoria, M. Mislinawati, N. Nurmasyitah, "Students' perceptions on the implementation of e-learning: Helpful or unhelpful?," Journal of Physics: Conference Series, **1088**(1), 1-6, 2018, doi:10.1088/1742-6596/1088/1/012058.

[53] A. Popovici, C. Mironov, "Students' perceptions of using learning technologies," Procedia-Social and Behavioral Sciences, **180**, 1514-1519, 2015, doi:10.1016/j.sbspro.2015.02.300.

[54] M. Kahveci, "Students perceptions to use technology for learning: Measurement integrity of the modified Fennema-Sherman Attitudes Scales," TOJET: The Turkish Online Journal of Educational Technology, **9**(1), 188-201, 2010.

[55] H. K. Yau, L. F. Cheng, "Gender differences of confidence in using technology for learning," The Journal of Teaching Studies, **38**(2), 74-79, 2012.

[56] L. Juhaňák, J. Zounek, K. Záleská, O. Bárta, K. Vlčková, "The relationship between the age at first computer use and students' perceived competence and autonomy in ICT usage: A mediation analysis," Computers & Education, **141**, 1-11, 2019, doi:10.1016/j.compedu.2019.103614.

[57] P. Fidalgo, J. Thormann, O. Kulyk, J. A. Lencastre, "Students' perceptions on distance education: A multinational study," International Journal of Educational Technology in Higher Education, **17**(18), 1-18, 2020, doi:10.1186/s41239-020-00194-2.

[58] J. Stefl-Mabry, M. Radlick, W. Doane, "Can you hear me now? Student voice: High school & middle school students' perceptions of teachers, ICT and learning", International Journal of Education and Development using ICT, **6**(4), 64-82, 2010.

[59] S. Ivanaj, G-B. Nganmini, A. Antoine, "Measure e-learners' perceptions of service quality," Journal of Organizational and End User Computing (JOEUC), **31**(2), 83-104, 2019, doi:10.4018/JOEUC.2019040105.

[60] L. Pham, S. Williamson, R. Berry, "Student perceptions of e-learning service quality, e-satisfaction, and e-loyalty," International Journal of Enterprise Information Systems (IJEIS), **14**(3), 19-40, 2018, doi:10.4018/IJEIS.2018070102.

[61] D. Petko, A. Cantieni, D. Prasse, "Perceived quality of educational technology matters: A secondary analysis of students' ICT use, ICT-related attitudes, and PISA 2012 test scores", Journal of Educational Computing Research, **54**(8), 1070-1091, 2017, dio:10.1177/0735633116649373.

[62] T. Muthuprasad, S. Aiswarya, K. S. Aditya, G. K. Jha, "Students' perception and preference for online education in India during COVID-19 pandemic," Social Sciences & Humanities Open, **3**(1), 1-11, 2021, doi:10.1016/j.ssaho.2020.100101.

[63] H. Baber, "Social interactions and effectiveness of the online learning-A moderating role of maintaining social distance during the pandemic COVID-19," Asian Education and Development Studies, **11**(1), 159-171, 2021, doi:10.1108/AEDS-09-2020-0209.

[64] A. Pearce, "Socially-oriented technologies attractability influence on individuals academically and neurologically," in 2020 12th International Conference on Education, Technology, and Computers (ICETC), ACM, 165-171, 2020, doi:10.1145/3436756.3437040.

[65] C. Conrad, Q. Deng, I. Caron, O. Shkurska, P. Skerrett, B. Sundararajan, "How student perceptions about online learning difficulty influenced their satisfaction during Canada's Covid-19 response", British Journal of Educational Technology, **53**(1), 534-557, 2022, doi:10.1111/bjet.13206.

[66] N. Selwyn, O. Husen, "The educational benefits of technology competence: an investigation of students' perceptions" Evaluation & Research in Education, **23**(2), 137-141, 2010, doi:10.1080/09500790.2010.483515.

[67] R. Faizi, R. Chiheb, A. E. Afia, "Students' perceptions toward using Web 2.0 technologies in education", International Journal of Emerging Technologies in Learning (IJET), **10**, 32-36, 2015, doi:10.3991/ijet.v10i6.4858.

[68] M. Mahdum, H. Hadriana, M. Safriyanti, " Exploring teachers perceptions and motivations to ICT use in learning activities in Indonesia," Journal of Information Technology Education: Research, **18**, 293-317, 2019, doi:10.28945/4366.

[69] S. Ghavifekr, T. Kunjappan, L. Ramasamy, A. Anthony, "Teaching and learning with ICT tools: Issues and challenges from teachers' perceptions," Malaysian Online Journal of Educational Technology (MOJET), **4**(2), 38-58, 2016.

[70] S. Amir, M. S. Kamal, M. D. T. Shahria, L. Iftekhar, "Undergraduate engineering courses: A case study of emergency remote teaching amid large digital divide," 2020 IEEE International Conference on Teaching, Assessment, and Learning for Engineering (TALE), 235-242, 2020, doi:10.1109/TALE48869.2020.9368316.

[71] J. O. Lindberg, A. D. Olofsson, G. Fransson, "Contrasting views: Student and teacher perceptions in ICT in education," The Proceedings of the International Conference on Information and Communication Technologies in Education (ICICTE), 1-10, 2016.

[72] C. V. Katemba, "Teachers' perceptions in implementing technologies in language teaching and learning," Acuity: Journal of English Language Pedagogy, Literature, and Culture, **5**(2), 38-51, 2020.

[73] Z. Walker, H. H. Kho, D. Tan, N. Lim, "Practicum teachers' use of mobile technology as measured by the technology acceptance model, Asia Pacific Journal of Education, **40**(2), 230-246, 2020, doi:10.1080/02188791.2019.1671808.

[74] S. Li, S. Yamaguchi, J-i. Takada, "Understanding factors affecting primary school teachers' use of ICT for student-centered education in Magnolia," International Journal of Education and Development using Information and Communication Technology (IJEDICT), **14**(1), 103-117, 2018.

[75] M. A. Gebremedhin, A. Fenta, "Assessing teachers' perceptions of integrating ICT in teaching-learning process: The case of Adwa College," Journal of Education and Practice, **6**(4), 114-124, 2015.

[76] J-P. Niyigena, Q. Jiang, D. Ziou, R-S. Shaw, A. S. M. T. Hasan, "Modeling the measurements of the determinants of ICT fluency and evolution of digital divide among students in developing countries—East Africa case study," Applied Sciences, **10**(1), 1-27, 2020, doi:10.3390/app10072613.

[77] M. Burns, M. I. Santally, R. Halkhoree, K. R. Sungkur, B. Juggurnath, Y. B. Rajabalee, "Information and communication technologies in secondary education in Sub-Saharan Africa: Policies, Practices, Trends, and Recommendations," 2019, https://www.edu-links.org/sites/default/files/media/file/ICT-in-Secondary-Education.pdf

[78] C. Singhavi, P. Basargekar, "Barriers perceived by teachers for use of information and communication technology (ICT) in the classroom in Maharashtra, India," International Journal of Education and Development using Information and Communication Technology (IJEDICT), **15**(2), 62-78, 2019.

ASTES

Matching TCP Packets to Detect Stepping-Stone Intrusion using Packet Crossover

Lixin Wang[*,1], Jianhua Yang[1], Austin Lee[1], Peng-Jun Wan[2]

[1]TSYS School of Computer Science, Columbus State University, Columbus, GA 31907, USA

[2]Department of Computer Science, Illinois Institute of Technology, Chicago, IL, USA

A R T I C L E   I N F O

A B S T R A C T

Hackers on the Internet often send attacking commands through compromised hosts, called stepping-stones, for the purpose to be hidden behind a long interactive communication session. In a stepping-stone attack, an intruder uses a chain of stepping-stones as relay machines and remotely login these machines using a remote login program such as SSH (secure shell). A great number of detection methods for SSI have been proposed since 1995. Many of these existing detection approaches are either not easy to implement, or not efficient as a great number of packets have to be monitored and analyzed. Some of these detection methods for SSI are even not effective as their capabilities to detect SSI are very limited. In this paper, we propose an effective detection method for SSI by using packet crossover. Packet crossover ratios can be easily computed, and thus our proposed detection method for SSI cannot only be easily implemented, but also efficient. Well-designed network experiments are conducted and the effectiveness of the developed SSID algorithm is verified through the experiments.

1. Introduction

Today hackers usually send attacking commands through compromised hosts in order to be hidden behind a long interactive communication session. These compromised hosts involved in attacks are referred to as stepping-stone ones. While launching a stepping-stone intrusion (SSI) attack, the intruder operates on a local host and sends attacking packets that will be relayed through the intermediate stepping-stones before they reach the final target system.

The TCP protocol was designed in a way that every interactive TCP connection between the attacker host and the final target is independent of one another, even though they are relayed connections. Therefore, the target machine is only able to get information from the last stepping-stone host in the connection chain. That is, it is notoriously hard for the final victim host to obtain information about the geographic region of the origin of the intrusion.

Figure 1 shows a sample of a connection chain that can be exploit to send attacking commands with an SSI. Host 0 in the figure serves as the intruder machine, Host N the final victim machine, and Host 1, Host 2, . . . , Host i-1, Host i, Host i+1, . . . , and Host N -1 serve as the stepping stones for the attack. The purpose of SSI detection (SSID) is to determine whether a host in a network is employed as a stepping-stone one for an attack. In the process of SSID, any intermediate machine within the chain could be chosen as the sensor. A packet sniffing program such as TCPdump or Wireshark must be available on a sensor host. In this figure, Host i is employed as the sensor.

Next, we introduce some important concepts that are needed design detection algorithms for SSI. An incoming connection to Host i is defined to be a connection from Host i-1 to Host i. An outgoing connection from Host i is defined to be a connection from Host i to Host i+1. There is possibly an intrusion if an incoming connection of the sensor matches with one of its outgoing connections.
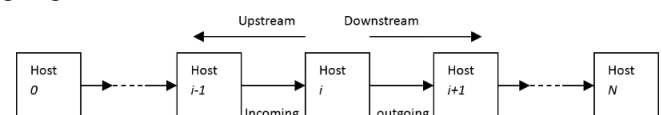

Figure 1. A sample connection chain

*Corresponding Author: Lixin Wang, 4225 University Ave., Columbus, GA 31907, USA. Contact No: 001-706-507-8190. Email: Wang_Lixin@ColumbusState.edu

A great number of methods for SSID have been proposed since the first seminar work [1] in 1995. These detection approaches for SSI can be divided into two different types. Compare the incoming connections to a machine with its outgoing connections, and then make a decision to determine whether there is an intrusion based on the comparison. This type of SSI detection approach is referred to as host-based detection [1]-[6]. It is well-known that stepping-stone hosts can be used by some applications to access a remote server legally. Therefore, high false-positive errors could be generated by using host-based detection methods for SSI.

In order to reduce the false-positive errors produced by host-based detection approaches, another category of detection methods was developed to overcome the challenge by counting the number of stepping-stone machines contained in a connection, which is called the length of the connection chain. This category of SSID methods is called connection-chain based or network-based detection [7]-[11], [14], [15]. Typically, there is no need to remotely access a sever via more than three stepping-stones as a lot of unnecessary network traffic will be produced and make the data communication much slower. The threshold number here is three as applications only uses one or two stepping-stone machines to access a remote server legitimately [12], [13].

Many of these existing detection approaches are either not easy to implement, or not efficient as a lot of packets have to be monitored and processed. Some of these SSID methods are even not effective as their detection capabilities for SSI are very limited. There is a need to propose an innovative detection algorithm for SSI that can be easily implemented without having to monitor a lot of TCP packets. Thus, such an algorithm for SSID is efficient in terms of processing time. In this paper, we propose an effective detection method for SSI by using packet crossover ratios. Packet crossover ratios can be easily computed, and thus our proposed detection method for SSI cannot only be easily implemented, but also efficient.

In [16], the authors used the idea of packet crossovers to identify a "long" connection chain. However, this paper made two assumptions (1) there exist packet crossovers in a long connection chain, and (2) a shorter connection chain produces less packet crossovers and a longer connection chain generates more packet crossovers. The conclusion made in [16] was based on these two assumptions. In this paper, we verify the following important statements through network experiments: if the packet crossover ratio of an incoming connection of a sensor host is almost equal to that of an outgoing connection of the sensor, then these two connections are relayed ones, and vice versa.

The remaining of this paper is organized as follows. A literature review for existing approaches for SSID is discussed in section 2. Preliminary knowledge needed in this paper is presented in section 3. In Section 4, an innovative algorithm to match TCP packets using packet crossover is proposed. In Section 5, we design and conduct network experiments to verify the

correctness of Proposition 1 described in Section 4. Section 6 gives a conclusion and future research direction for this paper.

2. Literature Reviews

Let us begin our reviews with the existing host-based detection methods that have been proposed for SSI since 1995. The content thumbprint approach to detect SSI was proposed in [1]. This method determines whether a communication session is an intrusion by comparing the content of the packets from the outgoing connection of the sensor host with that of the packets from its incoming connection. It is highly possible that the session is an intrusion if there is a relayed pair between them. However, this approach cannot be used to detect SSI for computer networks with encrypted traffic. To overcome the drawback of this method, a time-thumbprint based approach for SSID was developed in [2]. This approach utilized the timestamps of the monitored packets. This approach for SSID can be used for networks with encrypted traffic as packet timestamps are not encrypted. An example of encrypted traffic is to login to a remote server using SSH.

If the network traffic is encrypted, it is much harder to detect SSI, and even more difficult if a communication session is manipulated by attackers using hacking tools. The packet counting method proposed in [5] was to address such a challenge in detecting SSI through counting the number of packets in both the incoming and outgoing connections. The methods proposed in this paper were to identify stepping-stone connections when the traffic is encrypted and the packet timestamps are jittered. This method also allows an attacker to inject certain amount of meaningless chaff packets into an attacking stream. However, in order for this method to work effectively, both the amount of chaffed meaningless packets and the percentage of the packets with jittered timestamps must be small. Therefore, the capability of the detection approach proposed in [5] is very limited to handle session manipulation by hackers.

Next, we provide a literature review on network-based approaches for SSID that estimate a connection-chain length. In 2002, the authors of [7] developed the 1st network-based approach for SSID to estimate the length of a connection chain. Yung's method calculated the ratio between the Send-Echo RTT and of Send-Ack RTT. The RTTs of an Echo and a Send packet stand for the length of the connection chain from the sensor to the final victim host. On the other hand, an RTT for a Send packet and an Ack packet can only stand for the length from the sensor to its next adjacent machine in the downstream connection sub-chain. Therefore, a high false-negative error was generated by Yung's method in [7] because of the adoption of the acknowledgement packets. The issues of the method proposed in [7] was addressed in the work [8], which is the 2nd network-based approach for SSID proposed in 2004. The detection algorithm proposed in [8] uses the step-function approach to calculate the length of a connection chain in a local area network (LAN). An improvement of the approach in [8] over Yung's one in [7] is that the authors of [8] changed the way to set up the connection chain so that every Send packet can be possibly matched with a corresponding Echo packet.

In a LAN, the step-function method for SSID worked well and reduced both the false positive error and the false negative error, compared to Yung's method proposed in [7]. However, a major drawback of the detection method proposed in [8] is that this method only worked well within a LAN, but wasn't working in the Internet environment. With the context of the Internet, a conservative and greedy packet matching algorithm for SSID was proposed [14]. However, this method in [14] only very few Send packets can be matched with corresponding Echo packets. Therefore, the method in [14] did not work effectively either in the Internet environment.

To address this issue, a clustering and partitioning data mining detection approach for SSI was proposed in [9]. In [9], the packet RTTs were computed by utilizing the clustering and partitioning data mining approach. The packet matching method proposed in this paper is accurate as it went through all the possible Echo packets for every Send packet to be matched. A major issue of the detection method in [9] is that we have to monitor a great number of TCP packets. Therefore, in terms of packet processing time, the detection method proposed in [9] is not efficient.

One of our earlier works [10] addressed the issue of the SSID method proposed in [9] and developed a detection approach via mining network traffic by utilizing the *k*-Means clustering data mining algorithm. This k-Means based approach proposed in [10] does not need to capture and analyze a huge number of packets, and thus it is more efficient than MMD based approach proposed in [9]. But because of the use of the k-Means clustering, the length of a connection chain must be pre-determined for this approach, which makes its performance and capability very limited for SSID. Also, this *k*-Means based detection approach is ineffectively if large fluctuations of the TCP packets exist.

In a recent work [11], we developed an effective network-based SSID approach by calculating the packet crossover ratios. This packet-crossover based method is easy to implement as we can easily compute the packet crossover ratios. With a modification of the k-Means clustering algorithm, [12] proposed an improved algorithm for SSID based detection approach developed in [10] by eliminating some of the packet RTT outliers. However, this paper did not provide any technical analysis regarding whether or not the SSID method is resistant to session manipulations by intruders. Another algorithm proposed for removing packet-RTT outliers is the work [13]. This outlier detection algorithm in [13] can be used to design new approaches to detect SSI. A major drawback of the outlier detection algorithm in [13] it that the accuracy of discovering the RTT outliers is low.

3. Preliminaries

Let us introduce the preliminaries that are needed for our detection algorithm design for SSID in this section.

3.1. Definitions of Send/Echo Packets

Refer to [11] for the definitions of an Echo and a Send packets. For example, when a command is entered on a terminal window in a host running Linux, such as "cd", we assume that the command "cd" is delivered to the remote server in two separate TCP packets: one holding the letter "c" and the other holding the letter "d". Both of these packets are Send ones. When the letter "c" is entered on the user's machine, the packet holding "c" will be delivered to the remote server. Once this packet is received and processed at the server, an Echo packet is sent back to the user, the letter "c" displays on the command line of the user's screen. In such a scenario, the Send packet "c" and the Echo packet "p" are matched. Similarly, a Send packet holding "d" and its corresponding Echo packet holding "d" are also matched.

3.2. Packet Crossover

Packet crossover occurs when a newly Send packet meets an Echo packet of a previous Send packet along the connection chain between a client host and a server host (see Fig. 2). In Fig. 2, we have a connection chain starting from the client (Host 1), to Host 2, then to Host 3, and finally to the server (Host 4), where Host 2 and Host 3 are the stepping-stones in this chain. The red packets S1, S2 and are Send packets, and the green packets E1, E2, and E3 are their Echo packets, respectively. First let us assume that packet crossover is observed at Host 1. In this case, the sequence of these six packets is S1, S2, E1, S3, E2, and E3. Therefore, there are two occurrences of packet crossovers in this case. Now let us observe packet crossover at Host 2. The Send and Echo packets from the connection between Host 2 and Host 3 are monitored. The sequence of these six packets observed at Host 2 is S1, E1, S2, S3, E2, and E3. Thus, only one occurrence of packet crossover is observed in this case.
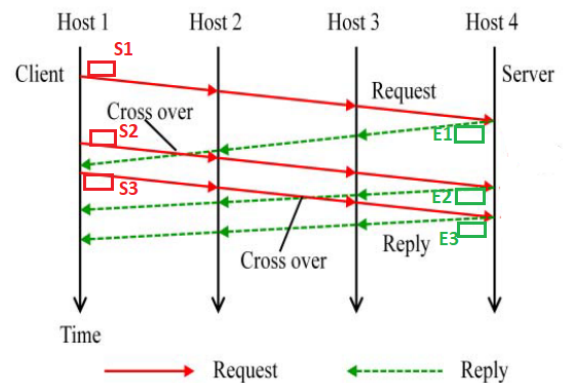
Figure 2: A sample of packet crossover in a connection chain of four hosts.

3.3. The Distribution of Packets' RTTs in a Connection Chain

It is well-known that the number of connections in a connection chain can be represented by utilizing the packet round-trip times computed using the Send packets with their matched Echo packets.

It is well-known that the packet RTTs computed from the TCP packets captured from a connection chain from the attacker host to a target host obey Poisson distribution. This statement was verified in the seminar work [2]. This discovery has been used in the design of SSID methods in the literature. The results of a well-designed network experiment conducted by the authors of [2] is shown in Figure 3. This figure shows that the packet RTTs follow

Poisson distribution. In this figure, the RTT values in micro-second are displayed on the X-axis, and the chances of the occurrences of RTT values are displayed on the Y-axis. In their network setup, the connection chain has a length of four. That is, the chain contains four connections with five machines in total. In their network experiment, μ stands for the mean of all the RTT values. From their observation, μ = 138,500. Since the packet RTTs follow Poison distribution, clearly, most values in the RTTs are very close to the value of μ (see Fig. 3).
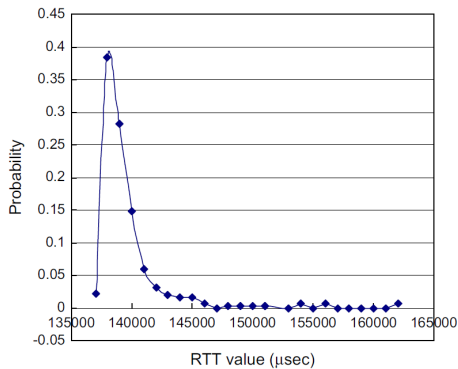
Figure 3: The Packets' RTTs Obey Poisson Distribution

4. Matching TCP Packets Using Packet Crossover

In this section, we first present a proposition that will be used to design our algorithm for SSID. Then we describe an effective algorithm to determine whether a host is used as a stepping-stone by utilizing packet crossover.

First, we present a proposition that will be verified through well-designed network experiments in Section 5. Our detection algorithm design for SSID using packet crossover is based on this proposition.

Proposition 1: If the packet crossover ratio of an incoming connection of a sensor host is almost equal to that of an outgoing connection of the sensor, then these two connections are relayed ones. If the two packet crossover ratios are not close to each other, then these two connections are not relayed.

Next, we describe our proposed host-based detection algorithm for SSI using packet crossover:

1). Pick a host of a network as the sensor host.

2). Adopt Algorithm 1 (Compute Packet Crossover Ratio) in [11] to calculate the packet crossover ratio for every **incoming** connection to the above sensor host.

3). Adopt Algorithm 1 (Compute Packet Crossover Ratio) in [11] to calculate the packet crossover ratio for every **outgoing** connection from the above sensor host.

4). If any of the packet crossover ratios calculated for an incoming connection at Step 2) is almost the same as one of the packet crossover ratios calculated for an outgoing connection at Step 3), then it is highly suspicious that these two connections are relayed ones, and the sensor host is used as a stepping-stone.

5). If none of the packet crossover ratios calculated at Step 2) for incoming connections is close to any of the packet crossover ratios

calculated for outgoing connections at Step 3), then it is almost sure that the sensor is not used as a stepping-stone.

The correctness of our above detection algorithm for SSI is clearly asserted according to Proposition 1.

5. Network Experiments

In this section, we design network experiments to verify the correctness of Proposition 1 described in Section 3 by comparing the packet crossover ratios of incoming and outgoing connections. Relayed pairs will typically result in almost equal packet crossover ratios. On the other hand, non-relayed pairs will typically result in dissimilar packet crossover ratios.

To set up our experimental environment, we created two distinct connection chains that shared the same sensor host H3 (see Fig. 4 below). The first connection chain consisted of one local host and four geographically dispersed Amazon AWS servers; all the hosts in the experiment ran Ubuntu Linux operating system. We created a long connection chain by using Secure Shell (SSH) to sequentially connect to each host in the connection chain from the attacker host H1 to the victim host H5 (see Fig. 4). In other words, a single terminal appearing on the attacker host H1 was used to create the entire connection chain by using sequential remote SSH access. From our local PC H1 in Georgia, USA with IP address 168.27.2.105, we remotely accessed host H2 (the first stepping-stone host in the chain), located in Northern Virginia, USA with public IP address 54.226.83.33. We then extended the connection chain by using H2 as a stepping-stone to remotely access the host H3 (our sensor host), located in Northern California, USA with public IP address 54.215.55.31. We then extended the connection chain again by using H3 as a stepping-stone to remotely access host H4 (the last stepping-stone in the chain), located in Tokyo, Japan with public IP address 3.115.8.190. We then extended the connection chain for the final time by using H4 as a stepping-stone to remotely access host H5, located in Central Canada with public IP address 3.99.215.22.

After the first connection chain was established, both the incoming and outgoing connections of the sensor host will be monitored and the packets will be captured using tcpDump at the sensor host (labeled respectively i1 and o1 on in Fig. 4) at H3, the sensor. All data are captured at H3 in this entire network experiment. We entered the following standard Linux commands for about three minutes into a terminal at the attacker host (H1) and captured all packets from the indicated connections at H3:

```
ls
mkdir test
ls
cd test
cd ..
rmdir test
ls
pwd
touch test.txt
```

ls
rm test.txt

We captured ten datasets in total, with each data set comprising two files at the sensor host. After capturing the data, we ran our Packet Crossover Ratio algorithm to calculate the packet crossover ratio observed at H3 from both the incoming and outgoing connections.

We then created a second SSH connection chain that consisted of two local hosts and three geographically dispersed Amazon AWS servers, with each host again running Ubuntu Linux operating system. The sensor host H3 is the only common host shared by these two connection chains. From our local PC H6 in Georgia, USA with IP address 168.27.2.103, we remotely accessed host H7, which had an IP address of 168.27.2.106 and was co-located on the same LAN with our local PC in Georgia. We then extended the connection chain by using H7 as a stepping-stone to remotely access the host H3 (the same sensor host that was used for the first connection chain), located in Northern California, USA with public IP address 54.215.55.31. We then extended the connection chain again by using H3 as a stepping-stone to remotely access host H8 (the last stepping-stone in the chain), located in Frankfurt, Germany with public IP address 3.121.98.162. We then extended the connection chain for the final time by using H8 as a stepping-stone to remotely access host H9, located in London, England with public IP address 18.133.230.186.

After the second connection chain was established, we used tcpDump to capture both the incoming and outgoing connections (labeled i2 and o2 on in Fig. 4) at H3, the sensor. We entered the following standard Linux commands for about three minutes into a terminal at the attacker host (H1) and captured all packets from the indicated connections in the chain:

whoami
uname
groups *username*
who
lscpu
hwclock –verbose
sudo lshw
whatis -h
whatis -l netstat
man netstat (with ten seconds of scrolling)
netstat
help
ifconfig -a
ping google.com
traceroute google.com
sudo cat /etc/shadow
history
!lastCommand

We captured ten datasets in total, with each data set comprising two files at the sensor host. After capturing the data, we ran our Packet Crossover Ratio algorithm to calculate the packet

crossover ratio observed in both the incoming and outgoing connections.
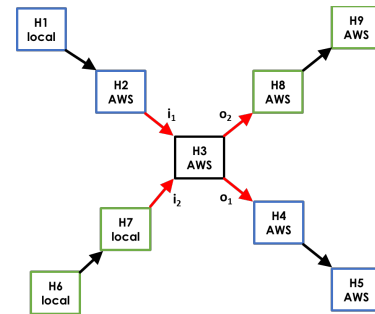
Figure 4: The experimental network setup. Depicts two distinct connection chains passing through the same sensor host H3. C=chain, i=incoming connection, o=outgoing connection, red arrows=connection captured from H3.

We then attempted to use the captured packet crossover ratios to match incoming and outgoing connections. Based on our previous research, we knew that the packet crossover ratios captured at a given sensor for the incoming and outgoing connections of a relayed pair should be close to 1. Therefore, we expected to see a matching of close to 1 for i1 and o1, as well as i2 and o2. Moreover, we expected to see a matching not close to 1 for non-relayed connection pairs such as i1 and o2. In Table 1, CR stands for Crossover Ratio, i1 for incoming connection 1, and o1 for outgoing connection 1. This table compares the CR of i1 to its respective outgoing connection. CR's of relayed pairs should be very similar. Therefore, the incoming connection's CR divided by the outgoing connection's CR should and does equal approx. 1.

Table 1: CR's of relayed pairs i1 and o1 close to 1

Matching Relayed Pair: i1/o1			
Dataset	i1 CR	o1 CR	i1/o1
1	0.3554	0.3554	1
2	0.5202	0.5202	1
3	0.3889	0.3879	0.9974
4	0.3864	0.3864	1
5	0.3431	0.3431	1
6	0.4898	0.4898	1
7	0.2879	0.2879	1
8	0.3279	0.3279	1
9	0.3725	0.3781	1.0150
10	0.3509	0.3509	1

Table 2: CR's of relayed pairs i2 and o2 close to 1

Matching Relayed Pair: i2/o2			
Dataset	i2 CR	o2 CR	i2/o2
1	1.7576	1.7452	0.9930
2	1.7615	1.7626	1.0006
3	1.9298	1.9240	0.9970
4	1.8020	1.8045	1.0013
5	1.8190	1.8212	1.0012
6	1.8362	1.8384	1.0012
7	1.8635	1.8656	1.0011
8	1.8563	1.8483	0.9957
9	1.7700	1.7683	0.9990
10	1.9382	1.9403	1.0011

In Table 2, i2 stands for incoming connection 2, and o2 for outgoing connection 2. This table compares the CR of i2 to its respective outgoing connection o2. CR's of relayed pairs should be very similar. Therefore, the incoming connection's CR divided by the outgoing connection's CR is approx. equal to 1.

Tables 1 and 2 depict a matching between relayed connections, where the packet crossover ratio of a given incoming connection is compared to the packet crossover ratio of its respective outgoing connection. Relayed pairs will typically result in almost equal packet crossover ratios. Therefore, the quotient of the packet crossover ratio of a given incoming connection divided by the packet crossover ratio of its respective outgoing connection should be approximately 1. All ten datasets for both connection chains demonstrate this general rule, with the quotients for connection chains 1 and 2 ranging from 0.9974 to 1.0150 and 0.9930 to 1.0013, respectively.

In Table 3, i1 stands for incoming connection 1, and o2 for outgoing connection 2. This table compares the CR of i1 to the CR of o2. Since these connections do not form a relayed pair, their crossover ratios should not be very similar. Therefore, the incoming connection's CR divided by the outgoing connection's CR should not approximate to 1.

In Table 4, i2 stands for incoming connection 2, and o1 for outgoing connection 1. This table compares the CR of i2 to the CR of o1. Since these connections do not form a relayed pair, their crossover ratios should not be very similar. Therefore, the incoming connection's CR divided by the outgoing connection's CR should not approximate to 1.

Table 3: CR's of non-relayed pairs i1 and o2

Matching Non-relayed Pair: i1/o2			
Dataset	i1 CR	o2 CR	i1/o2
1	0.3554	1.7452	4.9111
2	0.5202	1.7626	3.3882
3	0.3889	1.9240	4.9475
4	0.3864	1.8045	4.6703
5	0.3431	1.8212	5.3086
6	0.4898	1.8384	3.7536
7	0.2879	1.8656	6.4797
8	0.3279	1.8483	5.6366
9	0.3725	1.7683	4.7473
10	0.3509	1.9403	5.5299

Table 4: CR's of non-relayed pairs o1 and i2.

Matching Non-relayed Pair: i2/o1			
Dataset	i2 CR	o1 CR	i2/o1
1	1.7576	0.3554	0.2022
2	1.7615	0.5202	0.2953
3	1.9298	0.3879	0.2010
4	1.8020	0.3864	0.2144
5	1.8190	0.3431	0.1886
6	1.8362	0.4898	0.2667
7	1.8635	0.2879	0.1545
8	1.8563	0.3279	0.1767
9	1.7700	0.3781	0.2136
10	1.9382	0.3509	0.1810

Tables 3 and 4 depict a matching between non-relayed connections, where the packet crossover ratio of a given incoming connection is compared to the packet crossover ratio of another unrelated outgoing connection. Non-relayed pairs will typically

result in dissimilar packet crossover ratios. Therefore, the quotient of the packet crossover ratio of a given incoming connection divided by the packet crossover ratio of an unrelated outgoing connection should typically not be close to 1. All ten datasets demonstrate this general rule, with the quotients for i1/o2 and i2/o1 ranging from 3.3882 to 6.4797 and 0.1545 to 0.2953, respectively.

We can clearly see that matched connection pairs are very similar, and non-matched pairs are dissimilar. With a true-positive threshold of 0.99-1.02, 100% of the matched pairs would be recognized as a relayed pair. Furthermore, 100% of the non-relayed pairs would be identified correctly.

6. Conclusion

Many known SSID methods are either not easy to implement, or not efficient as a large number of packets have to be monitored and analyzed. Some of them are even not effective as their capabilities to detect SSI are very limited. In this paper, we proposed an effective SSID method by using packet crossover ratios. Packet crossover ratios can be easily computed, and thus the SSID method developed in this paper cannot only be easily implemented, but also efficient in terms of packet processing time. Through well-designed network experiments, we verified that for a given sensor, if an outgoing connection and an incoming connection are detected to be relayed with each other, then the packet crossover ratios obtained from these two connections should be very close, and vice versa.

As for future research direction, one may revise and improve our proposed detection method for SSI so that it will be resistant to session manipulation by intruders using hacking techniques such as chaff-perturbation of meaningless packets or time jittering.

Conflict of Interest

The authors declare no conflict of interest.

Acknowledgment

References

[1] S. Staniford-Chen, and L. T. Heberlein, "Holding Intruders Accountable on the Internet," Proc. IEEE Symposium on Security and Privacy, Oakland, CA, 39-49, 1995, DOI: 10.1109/SECPRI.1995.398921.

[2] Y. Zhang, and V. Paxson, "Detecting Stepping-Stones," Proc. of the 9th USENIX Security Symposium, Denver, CO, 67-81, August 2000, doi: https://dl.acm.org/doi/10.5555/1251306.1251319.

[3] D. Donoho, A. Flesia, U. Shankar, V. Paxson, J. Coit, and S. Staniford, "Multiscale stepping-stone detection: Detecting pairs of jittered interactive streams by exploiting maximum tolerable delay," in 5th International Symposium on Recent Advances in Intrusion Detection, Lecture Notes in Computer Science, 2516, 2002, DOI:10.1007/3-540-36084-0_2.

[4] T. He and L. Tong, "Detecting Stepping-stone Traffic in Chaff: Fundamental Limits and Robust Algorithms," the 9th International Symposium on Recent Advances in Intrusion Detection (RAID 2006), April 2006.

[5] T. He, L. Tong, "Detecting encrypted stepping-stone connections," In: Proceedings of IEEE Transaction on signal processing, 55(5), 1612-1623, 2007, DOI: 10.1109/TSP.2006.890881.

[6] A. Blum, D. Song, And S. Venkataraman, "Detection of Interactive Stepping-Stones: Algorithms and Confidence Bounds", Proceedings of International Symposium on Recent Advance in Intrusion Detection (RAID), Sophia Antipolis, France, 20-35, September 2004, DOI:10.1007/978-3-540-30143-1_14.

[7] K. H. Yung, "Detecting Long Connecting Chains of Interactive Terminal Sessions," Proc. of International Symposium on Recent Advance in Intrusion Detection (RAID), Zurich, Switzerland, 1-16, October 2002, https://doi.org/10.1007/3-540-36084-0_1.

[8] J. Yang, S.-H. S. Huang, "A Real-Time Algorithm to Detect Long Connection Chains of Interactive Terminal Sessions," Proceedings of 3rd ACM International Conference on Information Security (Infosecu'04), Shanghai, China, 198-203, November 2004, DOI:10.1145/1046290.1046312; Corpus ID: 18061584.

[9] J. Yang, and S. S.-H. Huang, "Mining TCP/IP Packets to Detect Stepping-Stone Intrusion", Journal of Computers and Security, Elsevier Ltd., 26, 479-484, December 2007, doi:10.1016/j.cose.2007.07.001.

[10] L. Wang, J. Yang, X. Xu, and P.-J. Wan, "Mining Network Traffic with the k-Means Clustering Algorithm for Stepping-stone Intrusion Detection", Wireless Communications and Mobile Computing, 2021, Article ID 6632671, 2021, https://doi.org/10.1155/2021/6632671.

[11] L. Wang, J. Yang, and A. Lee, "An Effective Approach for Stepping-Stone Intrusion Detection Using Packet Crossover," the 23rd World Conference on Information Security Applications (WISA), August 24-26, 2022, DOI: 10.26599/TST.2021.9010041.

[12] L. Wang, J. Yang, M. Workman, and P.-J. Wan, "Effective algorithms to detect stepping-stone intrusion by removing outliers of packet RTTs," Tsinghua Science and. Technology. 2021(27), 432-442, https://doi.org/10.26599/tst.2021.90100432-4421.

[13] O. Alghushairy, R. Alsini, X. Ma, and T. Soule, "Improving the Efficiency of Genetic-Based Incremental Local Outlier Factor Algorithm for Network Intrusion Detection," Advances in Artificial Intelligence and Applied Cognitive Computing. In Transactions on Computational Science and Computational Intelligence; Arabnia, H.R., Ferens, K., Fuente, D., Kozerenko, E.B., Olivas, J.A., Tinetti, F.G., Eds.; Springer, Cham: New York, NY, USA. 1, 1011–1027, 2021, http://dx.doi.org/10.1007/978-3-030-70296-0_81.

[14] J. Yang, S.–H. S. Huang, "Matching TCP Packets and Its Application to the Detection of Long Connection Chains," Proceedings of 19th IEEE International Conference on Advanced Information Networking and Applications (AINA 2005), Taipei, Taiwan, China, 1005-1010, March 2005, 10.1109/AINA.2005.240.

[15] J. Yang, B. Lee, and S.S.-H Huang, "Monitoring Network Traffic to Detect Stepping-Stone Intrusion," the Proceedings of 22nd IEEE International Conference on Advanced Information Networking and Applications (AINA 2008), Okinawa, Japan, 56-61, March 2008, DOI: 10.1109/WAINA.2008.30.

[16] S. S.-H Huang, H. Zhang, and M. Phay, "Detecting Stepping-stone intruders by identifying crossover packets in SSH connections", the Proceedings of 30th IEEE International Conference on Advanced Information Networking and Applications, Fukuoka, Japan, 1043-1050, March 2016, DOI: 10.1109/AINA.2016.132.

Optimization of Query Processing on Multi-tiered Persistent Storage

Nan Noon Noon[*], Janusz R. Getta, Tianbing Xia

School of Computing & Information Technology, University of Wollongong, Wollongong, 2500, Australia

A R T I C L E I N F O	A B S T R A C T
	The efficient processing of database applications on computing systems with multi-tiered persistent storage devices needs specialized algorithms to create optimal persistent storage management plans. A correct allocation and deallocation of multi-tiered persistent storage may significantly improve the overall performance of data processing. This paper describes the new algorithms that create allocation and deallocation plans for computing systems with multi-tiered persistent storage devices. One of the main contributions of this paper is an extension and application of a notation of Petri nets to describe the data flows in multi-tiered persistent storage. This work assumes a pipelined data processing model and uses a formalism of extended Petri nets to describe the data flows between the tiers of persistent storage. The algorithms presented in the paper perform linearization of the extended Petri nets to generate the optimal persistent storage allocation/deallocation plans. The paper describes the experiments that validate the data allocation/deallocation plans for multi-tiered persistent storage and shows the improvements in performance compared with the random data allocation/deallocation plans.

1. Introduction

In the last decade, we have observed the fast-growing consumption of persistent storage used to implement operational and analytical databases [1]. While the databases become larger, the total number of database applications also continuously increases and the applications themselves, especially the analytical ones, become more sophisticated and advanced than before [2]. Such trends increase the pressure on hardware resources for data processing, particularly on high-capacity and fast persistent storage devices.

Usually, the financial constraints invalidate the *single-step replacements* of all available persistent storage devices with better ones. Instead, a typical strategy is based on the continuous and systematic replacements of persistent storage devices with only a few at a time. Also, from an economic point of view, it is not worth investing significant funds in faster and larger persistent storage devices when only some of the available data is frequently processed. In reality, only some data sets are accessed more frequently than others. Financial and data processing requirements lead to the simultaneous utilization of persistent storage devices of different speeds and capacities. Therefore, data is distributed over many different storage devices with various capacity and speed characteristics [3]. This leads to a logical model of the *multi-tiered organization of persistent storage* [4, 5]. The lower *tiers (levels)*

consist of higher capacity and slower persistent storage devices than the lower capacity and faster devices at the higher levels.

Several research works have been already performed on the automatic allocation of storage resources over multi-tiered persistent storage devices and multi-tier caches. For example, in one of the solutions, persistent storage can be allocated over several cache tiers and in different arrangements [6]. Another research work shows how to distribute data on disk storage in the multi-tier hybrid storage system (MTHS) [7].

A number of approaches schedule the allocation of resources over multi-tiered persistent devices based on future predicted workloads. The algorithms for an optimal allocation of persistent storage on multi-tiered devices in environments where future workloads can be predicted have been proposed in [8, 9]. These algorithms arrange data according to an expected workload and contribute to the automated performance tuning of database applications. Most of the existing research outcomes show that performance tuning with the predicted database workloads improves performance during processing time and reduces database administration time [10].

A logical model of multi-tiered persistent storage consists of several *tiers (levels)* of persistent storage visible as a single persistent storage container. The processing speeds at the same tier are alike. Each tier is divided into several *partitions*, where each partition is a logical view of a physical persistent storage device

[*]Corresponding Author: Nan Noon Noon Email: nnn326@uowmail.edu.au

that implements a particular tier. Such a view is compatible with the organization of persistent storage within cloud systems. Nowadays, data can be stored on several remote devices. It contributes to the changes in the working style where the employees can work from home or distance. Therefore, storage on the cloud is required to provide access to data online anywhere, anytime over an internet connection. In addition, cloud storage for organizations must be shared by many users. Therefore, partitioning of persistent storage is required so that users can access storage simultaneously. Also, the efficient management of storage allocation on multi-tiered persistent storage with partitions is an essential factor for the performance of cloud systems.

The illustration of multi-tiered persistent storage with partitions is shown in Figure 1. Typically, the higher tiers of persistent storage have lower capacities and faster access times than the lower tiers. In a physical model, a sample *multi-tiered persistent storage* consists of the physical persistent storage devices available on the market, such as NVMe, SSD, and HDD [3].

Efficient processing of data stored at *multi-tiered persistent storage* is an interesting problem. When processed, data can "flow" from lower tiers to free space at the higher tiers to speed-up access to such data in the future. Scheduling the data transfers between the tiers require the allocation/deallocation of data based on the speed and capacities of the tiers. Thus, making the correct scheduling decisions automatically and within a short period of time becomes a critical factor for the overall performance of data processing.

Because of its limited capacity, it is impossible to store all data at the topmost and the fastest tier. Therefore, we must prepare for a compromise between the capacity, speed, and price of available *multi-tiered persistent storage*. Such compromise leads to all data being distributed over many tiers of multi-tiered persistent storage.
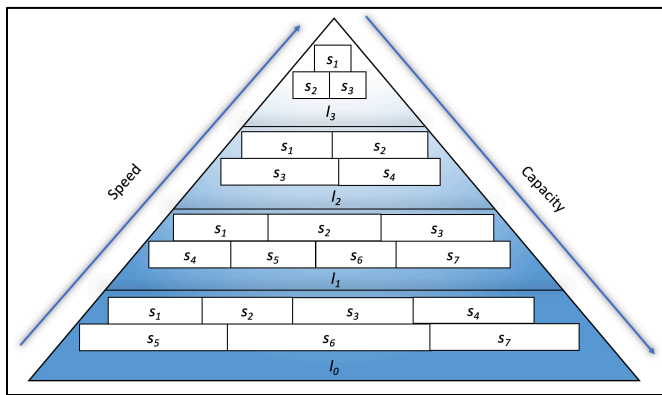

Figure 1: Illustration of multi-tiered persistent storage with four tiers divided into partitions

The main research objective of this work is to speed up data processing in environments where all data is located at *multi-tiered persistent storage*. We assume that data processing is organized as a collection of pipelines where the outputs from one operation are the inputs to the next operation in a pipeline. A strategy to speed up the data processing in a pipeline is to write the outputs of each operation to the highest available persistent tiers. The benefits of such a strategy are twofold. First, data is written faster at the higher tiers than at the lower ones. Second, the following operation in a

pipeline reads input data more quickly from the higher tiers. An essential factor in such a strategy is an optimal release of persistent storage allocated at the higher tiers to store temporary data.

Another problem addressed in the paper is the lower-level optimization of query processing on *multi-tiered persistent storage*. The present query optimizers do not consider an efficient implementation of higher-level operations on data located at *multi-tiered persistent storage*. However, it is possible to significantly improve performance by implementing higher-level operations in ways consistent with the characteristics of available persistent storage. Our second research objective is to generate more efficient data processing plans for predicted and unpredicted database workloads through the optimal implementation of elementary operations on data located at *multi-tiered persistent storage*.

The contributions of the paper are the following. First, the paper shows how to extend and apply a notation of Petri nets to describe the data flows in multi-tiered persistent storage. Second, the paper presents the algorithms that find optimal query processing plans through the linearization of Petri nets. Third, the paper analyses the results of experiments to show that query processing plans generated by the new algorithms efficiently use the properties of *multi-tiered persistent storage*.

This paper is an extension of work originally presented in [11]. The paper is organized in the following way. Section 2 extends a notation of Petri nets to describe data flow in query processing. Sections 3 and 4 present the algorithms for the automatic allocation of storage available on multi-tiered persistent storage devices. Section 5 describes an experiment, and Section 6 summarizes the paper.

2. Basic Concepts

In this work, we consider a scenario where a database application submits an SQL query to a relational database server. Then, a typical query optimizer finds an optimal query processing plan. Such a plan includes the list of operations organized as a directed bipartite graph. Then, to discover the data flows between the elementary operations, a plan is transformed into an extended Petri Net [12]. Finally, a graphical notation of Petri Nets represents the flow of data when processing a query.

The original Petri net model includes two types of elements: places and transactions. Places are denoted as circles, and transactions are denoted as vertical rectangles. Zero or more tokens, denoted as small black circles, can be located in the places. Arcs are connected between places and transactions—the illustration of Petri Net is shown in Figure 2.

An *Extended Petri Net* is quadruple $<B, E, A, W>$ where B and E are disjoint sets of *places* and *transitions*. *Places* are visualized as circles, and *transitions* are visualized as rectangles or bars. *Arcs* $A \subseteq (B \times E) \cup (E \times B)$ connect the *places* and *transitions*. A *place* may contain a finite number of tokens visualized as black circles, or it can be empty. A *transition fires* depending on the number of tokens connected at the input place. When an input place has no token, a *transition* is at a waiting state.

In our case, sets of places, B, are interpreted as input/output data sets, and the sets of transitions, E, are interpreted as operations on data sets (see Figure3 below).
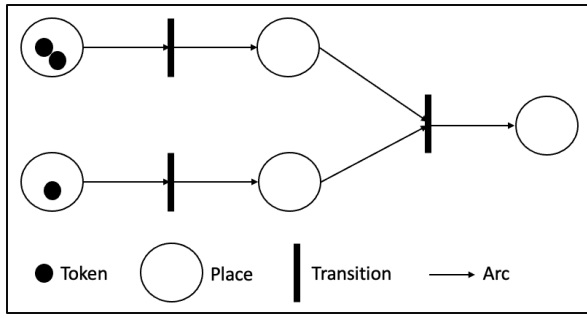
Figure 2: An original sample structure of a Petri net

Arcs, A, determine the input and output data sets of the operations. A weight function $W: A \rightarrow N^+$ determines the estimated total number of data blocks read and written by each operation. See the numbers attached to the *arcs* in Figure3. The *root nodes* are the *places* (data sets) in B that do not have the arcs from the *transitions* (operations) E. The root nodes represent the input data sets located in a database. An operation can have more than one input and output data set. Likewise, more than one operation can share input and output data sets.

There are two types of persistent storage data sets B: *permanent* or *temporary*. Both types of data sets are stored in *multi-tiered storage*. A temporary data set can be removed from the *storage* when it is no longer needed.
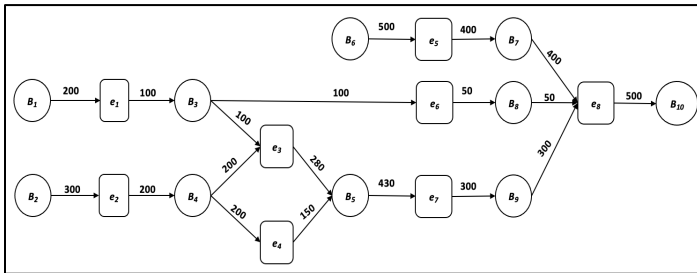

Figure 3: Data processing and data flows represented as an extended Petri net

Let $E = \{e_i, ..., e_j\}$ be a set of operations obtained for a query Q processing plan created by a database query optimizer. Each operation e_i is represented by a pair $e_i = (\{B_i, ..., B_m\}, \{B_{(m+1)}, ..., B_n\})$, where $\{B_i, ..., B_m\}$ are the input data sets and $\{B_{(m+1)}, ..., B_n\}$ are the output data sets of an operation e_i in E. Some of the input and output data sets processed by an operation e_i are permanent, and some of them are temporary.

This paper focuses on managing the multi-tiered persistent storage efficiently for each input/output data sets of each operation and generates the best allocation plan, called a processing plan, for each query. A list of persistent storage tiers is denoted as a sequence $L = <l_0, ..., l_n>$. We have $n+1$ tiers where l_0 denotes the lowest tier, called a base tier or a backup tier. The highest tier is denoted by l_n. Each tier l_i for $i = 0 \ldots n$ is described as a triple (r_i, w_i, $<s_{i_1}, ..., s_{i_n}>$) where r_i is a read speed per data block at tier l_i, w_i is a write speed per data block at tier l_i, and $<s_{i_1}, ..., s_{i_n}>$ is a sequence of partitions arranged from smallest available storage to largest available storage, where s_{i_j} is an amount of free space available in partition j at tier l_i. The read and write speed per data block is measured in the standardized time units that can be converted into real-time units when a specific hardware implementation of a persistent storage tier is considered.

The processing plan is denoted as $P = <D_{i_j}, ..., D_{n_k}>$, where D_{j_i} is a set of plans for an operation e_i, where e_i is in E_{s_j}. Each plan is a pair and is denoted as (B_i, s_{n_i}) and B_i is the total number of input/output data blocks located in partition i in tier l_n (index of s_{n_j}). If $l_j = l_0$, then the data blocks are located at the lowest tier in the *multi-tiered storage*.

After the output result of the operation e_i is allocated, unnecessary temporary input storage of operation e_i needs to be removed from multi-tiered persistent storage according to the persistent storage release plan. The persistent storage release plan is denoted as a sequence of pairs $\delta = < (e_i, (B_k, ..., B_h)), ..., (e_j, (B_x, ..., B_y))>$, where each pair $(e_i, (B_k, ..., B_h)$ is a group of data sets $(B_k, ..., B_h)$ that can be released after the results of an operation e_i are saved.

Then, the total processing time to read (B_i, s_{ij}) data blocks located at partition j in tier l_i is $T_{B_i} = B_i * r_i$. Formula (1) given below determines the total processing time T_r to read the data blocks for each input data set $D_i = \{(B_1, s_{n_j}), ..., (B_m, s_{k_n})\}$.

$$T_r = \mathrm{Max}\left(T_{B_1} + \cdots + T_{B_m} \right) \quad (1)$$

Similarly, formula (2) determines the total processing time T_w to write the data blocks for each output data set $D_j = \{(B_{(m+1)}, s_{i_j}), ..., (B_n, s_{k_{l_r}})\}$.

$$T_w = \mathrm{Max}\left(T_{B_{(m+1)}} + \cdots + T_{B_n} \right) \quad (2)$$

Let an *Extended Petri Net <B, E, A, W>* represent a query processing plan. Then, whenever it is possible, the output data sets of the operations $E = \{e_i, ..., e_k\}$ are written to the tiers located above the tiers of their input data sets. In other words, whenever possible, each operation tries to *push up* the results of its processing towards the partition at the higher tiers of persistent storage.

The benefits of such a strategy are as follows. First, it is faster to write the output data sets at a higher tier than at a lower tier. Second, the data sets written at a higher tier can be read faster by the next operation in a pipeline of a query processing plan. Therefore, the benefits include the time we gain from writing output data sets to the higher tiers and from reading the same data sets by the other operations.

3. Resource Allocation for a Single Query

This section describes the algorithms that convert a query processing plan obtained from the execution of EXPLAIN PLAN statement for a single query into an Extended Petri Net and serialize the operations of the Net in order to minimize the amounts of persistent storage required for query processing.

3.1. Creation of Extended Petri Net

We consider a query Q expressed as a SELECT statement and submitted for processing by a relational database server operating on *multi-tiered persistent storage*. A query Q is *ad-hoc* processed by the system in the following way. First, a query optimizer transforms the query into the best query processing plan. SQL statement EXPLAIN PLAN can be used to list a plan found by a

query optimizer. Next, the implementations of extended relational algebra operations such as selection, projection, join, anti-join, sorting, grouping, and aggregate functions are embedded into the query processing plan. Then, the plan is converted into an *Extended Petri Net*.

Operation $e_j \in E$ where e_j is member of query Q. Each operation has the estimated amounts of input data to be read from persistent storage and the estimated output amounts of data to be saved in persistent storage. Algorithm 1 below transforms a query Q into an *Extended Petri Net*.

The algorithm obtains a query processing plan from the results of the `EXPLAIN PLAN` statement. From there, we get a set of operations $E = \{e_i, ..., e_m\}$. A query processing plan provides information about the input data sets read by the operations and the output data sets written by the operations. The permanent and temporary data sets read and written by the operations in E form a set of places B in *Extended Petri Net*. The arcs leading from the input data sets to the operations and the arcs leading from the operations to the output data sets create a set of arcs A. A query processing plan provides information about the amounts of storage read and written by the operations. Such values contribute to the weight values w_j attached to each arc and are represented by a pair (a_j, w_j) in W. A weight value w_j attached to an arc between the input data set and an operation represents the total number of data blocks read by the operation. A weight value w_j attached to an arc between the operation and output data set represents the total number of data blocks written by the operation.

Algorithm 1: Create Extended Petri Net according to input a query q

---

Input: a query Q
Result: an extended Petri Net $<B, E, A, W>$

(1) Get a query processing plan through the application of `EXPLAIN PLAN` statement.
(2) Get operations from a query processing plan with the estimated amounts of input and output storage required by each operation. Then, create a set of operations E where e_i is an operation.
(3) **while** *Iterate over E* **do**
  - Let the current operation be e_i.
  - Let $B_i, ..., B_m$ be the input data sets and let $B_{(m+1)}, ..., B_n$ be the output data sets of an operation e_i.
  - Append to A the arcs $a_1, ..., a_m$ linking $B_{i-1}, ..., B_{i-m}$ and operation node.
  - Next, label the arcs with the values $w_{i_1}, ..., w_{i_m}$ representing the total number of input data blocks read by an operation e_i and append the pairs *to a weight function W*.
  - Append to A the arcs $a_{m+1}, ..., a_n$ linking an operation node e_i and the nodes $\{B_{(m+1)}, ..., B_n\}$. Then, label the arcs with values representing the total number of output data blocks written by an operation e_i and append the pairs $(a_1, w_{i_1}), ..., (a_m, w_{i_m})$ to a weight function W.

end

3.2. Serialization of Extended Petri Net

Preparation of an Extended Petri Net $<B, E, A, W>$ for processing requires serialization of its operations in a set E. Serialization arranges a set of operations E into a sequence of operations E_s. There exist many ways that the operations in E can be serialized in the implementations of more complex queries. If the operations in E can be serialized in more than one way, then we try to find a serialization that requires smaller amounts of persistent storage for its processing. Algorithm 2 finds a serialization of operations in E that tries to minimize the total amounts of persistent storage allocated during query processing. As a simple example, consider an Extended Petri Net given in Figure 3. The operations e_1 and e_2 write 100 and 200 units of persistent storage. Then, 100 units of persistent storage are released after the processing of operations e_3 and e_6, and 200 units of persistent storage are released after the processing of operations e_3 and e_4. Since the processing of e_3 and e_4 releases more storage, we assign e_3 and e_4 before e_6 in the serialization.

A *root operation* in E is an operation such that at least one of its input arguments is a permanent data set that belongs to the contents of a database. A *top persistent storage data* set in B is a data set that contains the final results of query processing and such that is not read by any other operation in E. It is possible that a query may output more than one top persistent storage data set. A *top operation* is an operation that writes only to the top persistent storage data sets.

Algorithm 2 traverses the arrows in A backward from the *top operations* to the *root operations* and generates a sequence of operations E_s from a set of operations E.

At the very beginning, a sequence of operations E_s is empty, and none of the persistent storage data sets in B is marked as released. In the first step, the algorithm finds the *top operations* and inserts such operations into a set of candidate operations E_c.

For each operation in E_c, the algorithm computes profit using formula (4). To compute profit, the algorithm deducts the total amounts of persistent storage allocated by an operation from the total amounts of persistent storage released by an operation. For example, assume that the current operation is e_i. To find the amounts of persistent storage released by an operation e_i, we perform the summation of the amounts of storage in all input data sets of operation e_i not marked as released yet. It is denoted by $\sum_{j=1}^{n} B_j$. To find the profits from the processing of an operation e_i, we deduct from the released amounts the amounts of persistent storage included in the output data sets of the operation and denoted as $\sum_{k=(n+1)}^{m} B_k$ in formula (3) below.

$$p(e_i) = \sum_{j=1}^{n} B_j - \sum_{k=(n+1)}^{m} B_k \qquad (3)$$

The profits are computed for each operation in E_c. The algorithm selects an operation with the smallest profit. If more than one operation has the smallest profit, then the algorithm randomly chooses one of them. Let a selected operation be e_i. The algorithm removes e_i from E_c, appends it in front of E_s, and marks all data sets read by e_i as released. Next, the algorithm finds the operations that write only to data sets marked as released by e_i, such that data sets released by e_i are read only by the operation already in E_s. An

objective is to find the operations that can be appended to E_c in a correct order of processing determined by a set of arcs A. Then, the algorithm appends those selected operations to a set of candidate operations E_c and the profits for each operation in E_c are computed again. An operation with the lowest profits is appended in front of E_c. The algorithm repeats the procedure until all operations in E are appended in front of E_s.

Algorithm 2: Generating Sequence of Operations E_s

Input: An *Extended Petri Net <B, E, A, W>* from Algorithm 1.
Result: A sequences of operations E_s for query Q.

(1) Create empty sequence E_s = <> for Q, create empty candidate operation sets $E_c = \varnothing$,
(2) Use a *Petri Net <B, E, A, W>* and get the top operation(s) from *Petri Net* that is connected to the top container/container that stored the final result and put those operation(s) into a set of operations $E_c = \{e_i, ..., e_k\}$.
(3) **while** E_c *not empty* **do**
  if E_c *contains more than one operation* **then**
    - Use formula (3) to compute the estimated profit for each operation in E_c.
    - Get all the operations with the smallest profit and randomly select one of the operations with the smallest profit.
  end
  - Let selected operation be e_i.
  - Append e_i in front of E_s and remove it from E_c.
  - Mark all data sets read by e_i as released.
  - Find all operations that write only to the data sets marked as released and save them in a set E_w.
  - Remove from E_w the operation that writes to data sets read by the other operations not in E_s.
  - Append the operations from E_w to E_c.
end
(4) End algorithm and return the result E_s.

Example1: The example explains a sample trace of Algorithm 2 when applied to an Extended Petri Net given in Figure3. In the first step, E_c contains only one operation e_8 connected to top data set B_{11}. Therefore, e_8 has the lowest profit in E_c. We append it in front of E_s = <e_8> and we remove it from E_c. The data sets B_5, B_6, and B_7 read only by e_8 are marked as released. The operations writing only to the data sets B_8, B_9, and B_{10} are e_5, e_6, e_7. None of the data sets B_8, B_9, and B_{10} are read by an operation that is not in E_s. Hence the operations e_5, e_6, e_7 can be added to $E_c = \{e_5, e_6, e_7\}$. The estimated profits for each operation computed with a formula (3) are the following: $p(e_5) = (0 - 400) = -400$, $p(e_6) = (100 - 50) = 50$ and $p(e_7) = (430 - 300) = 70$. According to those results, e_5 is picked, appended in front of E_s = <e_5, e_8>, and removed from $E_c = \{e_6, e_7\}$. A data set B_7 is an input data set, and it cannot be marked as released. As no new data sets are released, E_c remains the same. Next, an operation e_6 which has the second smallest profit, is taken from E_c. It is appended in front of E_s = <e_6, e_5, e_8> and is removed from $E_c = \{e_7\}$. A data set B_3 read by e_6 is marked as released. A data set B_3 is marked as written by operation e_1 and later it is read by e_3. In this case, e_1 cannot be appended to E_c because a data set B_3 is read by e_3 that is not assigned to E_s yet. Next, e_7 is taken from E_c, it is appended in front of E_s = <e_7, e_6, e_5, e_8>, and is removed

from E_c. A data set B_5 read by e_7 is marked as released. A data set B_5 is written by the operations e_3 and e_4. Both operations are appended to $E_c = \{e_3, e_4\}$. The computations of the profits provide: $p(e_3) = 0 - 280 = -280$ and $p(e_4) = 0 - 150 = -150$. According to the results, e_3 is appended in front of E_s = <e_3, e_7, e_6, e_5, e_8> and it is removed from $E_c = \{e_4\}$. The data sets B_3 and B_4 read by e_3 are marked as released. The operations e_1 and e_2 are written to data sets B_3 and B_4. An operation e_1 can be appended into E_c because e_6 that read B_3 is already assigned in E_s. An operation e_2 cannot be appended into $E_c = \{e_1, e_4\}$ because e_4 that reads a data set B_4 is not in E_s yet. The computations of the profits provide: $p(e_1) = 0 - 100 = -100$ and $p(e_4) = 200 - 150 = 50$. According to the results, e_1 is appended in front of E_s = <$e_1, e_3, e_7, e_6, e_5, e_8$> and is removed from $E_c = \{e_4\}$. Operation e_1 reads an input data set, therefore, no new operations can be added to E_c. Next, operation e_4 is append to E_s = <$e_4, e_1, e_3, e_7, e_6, e_5, e_8$> and is removed from E_c. A data set B_4 read by e_4 is marked as released and operation e_2 is appended to E_c. Finally, operation e_2 is appended in front of E_s = <$e_2, e_4, e_1, e_3, e_7, e_6, e_5, e_8$>. Operation e_2 reads from an input data set and because of that, no more operations can be assigned to E_c. The final sequence of operations E_s = <$e_2, e_4, e_1, e_3, e_7, e_6, e_5, e_8$> is generated at the end.

3.3 Estimation of Storage Requirements and Generation of Persistent Storage Release Plan

A sequence of operation E_s obtained from the linearization of an Extended Petri Net with Algorithm 2 is used to estimate the requirements on the amounts of persistent storage needed for the processing of the sequence. Algorithm 3 estimates the persistent storage requirements while processing the operations in E_s. The output of Algorithm 3 is the estimated processing time T for E_s using the read/write speed of single-tier, the maximum required storage V to process E_s, and a sequence of the persistent storage release plans δ = <$(e_i, (B_k, ..., B_h))$, ..., $(e_j, (B_x, ..., B_y))$>.

Algorithm 3 uses a sequence of operations E_s and information about reading speed per data block r_n and writing speed per data block w_n parameters unchanged and extracted from a single tier in multi-tiered persistent storage. Typically, the algorithm is processed with the read/write parameters of the highest tier. First, the algorithm sets V = 0, which stores the maximum storage required to be allocated in the multi-tiered persistent storage, and T = 0, which stores the estimated processing time for E_s. Next, the algorithm iterates over E_s in step (2) in Algorithm 3 and lets the current operation be e_i. First, the total read storage V_r is computed by summing all input storage for e_i and the total write storage V_w is computed by summing all output storage for e_i. After that, the current temporary storage $V_{temp} = V_{temp} + V_w$ is updated, where V_{temp} stores the temporary storage required to process until the current operation. Next, the algorithm compares V_{temp} with V. If V_{temp} is larger than V, then V = V_{temp} is updated. Next, the algorithm computes the estimated total processing time t_i for current operation e_i using the following equation.

$$T(e_i) = (V_r * r_n) + (V_w * w_n) \tag{4}$$

Then, the algorithm updates the total processing time until operation e_i by summing $T = T + T(e_i)$.

Next, the algorithm gets the storage released by operation e_i, denoted as a pair $(e_i, (B_x, ..., B_y))$. The detailed procedure is shown

from step (2)(vi) to step (2)(viii) in the algorithm. After this, the storage is appended into the persistent storage release plan δ.

If e_i is the member of δ then the algorithm needs to release data blocks after the output data blocks of e_i are allocated. Next, the algorithm needs to update $V_{temp} = V_{temp}$ - *the total number of release storage by e_i.*

Algorithm 3 iterates those procedures above for each operation from the input sequence E_{s_i}. Finally, Algorithm 3 will generate V, T, and $\delta = <(e_i, (B_k, ..., B_h)), ..., (e_j, (B_x, ..., B_y))>$.

Algorithm 3: Estimate the total storage required, estimate the execution time, and create a persistent storage release plan.

Input: A sequence of operations $E_s = <e_i, ..., e_k>$ obtained from Algorithm 2 and information about the reading speed per data block r_n and the writing speed per data block w_n of a single tier in multi-tiered persistent storage.
Result: The maximum storage V and the estimated processing time T required to process E_s and a sequence of the persistent storage release plan $\delta = <(e_i, (B_k, ..., B_h)), ..., (e_j, (B_x, ..., B_y))>$.

(1) Set $V = V_{temp} = T = 0$, $E_{temp} = \{\}$ and $\delta = <>$
(2) **while** *iterate over E_{s_i}* **do**
  (i) Let current operation be $e_i = (\{B_j, ..., B_k\}, \{B_m, ..., B_n\})$ where $\{B_j, ..., B_k\}$ is the input set of the number of data blocks and $\{B_m, ..., B_n\}$ is the output set of the number of data blocks.
  (ii) Next, get the total reading (V_r) and writing (V_w) data blocks for e_i.
  (iii) Next, use the values of V_r, V_w, r_n, w_n to compute $T(e_i)$ by using a formula (4). Update $T = T + T(e_i)$.
  (iv) Update $V_{temp} = V_{temp} + V_w$.
  (v) **if** $V_{temp} > V$ **then** $V = V_{temp}$.
  (vi) Get all the input storage read only by e_i and get all the input storage connected to both e_i and other operations in E_{temp} and create a group of data sets $(B_x, ..., B_y)$.
  (vii) Next, remove a data set from $(B_x, ..., B_y)$ if the data set is the input argument of root operations in E_s.
  (viii) Create a pair $(e_i, (B_x, ..., B_y))$ and append it into δ.
  if $e_i \in \delta$ **then**
    | - Add the storage requirements of $(B_x, ..., B_y)$ to get the total number of data blocks R_i released by e_i.
    | - Update $V_{temp} = V_{temp} - R_i$.
  end
end
(3) Return V, T and $\delta = <(e_i, (B_k, ..., B_h)), ..., (e_j, (B_x, ..., B_y))>$.

Example 2: A sample trace of Algorithm 3 is performed on a sequence of operations $E_s = <e_2, e_4, e_1, e_3, e_7, e_6, e_5, e_8>$ from Example 1 together with the reading and writing speed per data block from the highest tier $l_3 = (0.05, 0.055, <500, 300, 100>)$. As it has been mentioned before, the reading and writing speed per data block is measured in the standardized time units.

At the very beginning, we set $V = V_{temp} = T = 0$, and $\delta = <>$. Next, we iterate over E_s, and let the current operation be e_2. It reads $V_r = 300$ data blocks and writes $V_w = 200$ data blocks. Next, we compute $t_2 = (300*0.05) + (200*0.055) = 26$ and update $T = T + t_2 = 26$. Then, we set $V_{temp} = V = 200$. A persistent storage release

plan δ remains empty because e_2 is the first operation in the sequence E_s.

In the next iteration, the current operation is e_4. We compute $t_4 = (200*0.05) + (150*0.055) = 18.25$ and update $T = 26 + 18.25 = 44.25$ and $V_{temp} = 200 + 150 = 350$. Due to V_{temp} being larger than V, we increase $V = 350$. The operation does not release storage and there is no need to update δ.

In the next iteration e_1 is the current operation. $T = 59.75$, $V_{temp} = 350 + 100 = 450$ and $V = 450$.

In the next iteration e_3 is the current operation. $T = 90.15$, $V_{temp} = 450 + 280 = 730$ and $V = 730$. This time, e_3 released 200 data blocks, therefore, we need to update $\delta = <(e_3, (B_4)>$. Total number of data blocks released by e_3 is 200. Therefore, we update $V_{temp} = 730 - 200 = 530$.

In the next iteration, e_7 is the current operation. $T = 128.15$ and $V_{temp} = 530 + 300 = 830$ and $V = 830$. This time we release storage B_5 and update $\delta = <(e_3, (B_4)), (e_7, (B_5)) >$ and $V_{temp} = 830 - 430 = 400$.

In the next iteration, e_6 is the current operation. $T = 135.9$ and $V_{temp} = 400 + 50 = 450$ and $V = 830$. The storage released by e_6 is B_3 and update $\delta = <(e_3, (B_4)), (e_7, (B_5)), (e_6, (B_3)) >$ and $V_{temp} = 450 - 100 = 350$.

In the next iteration, e_5 is the current operation. The algorithm computes $T = 182.9$ and $V_{temp} = 350 + 400 = 750$ and $V = 830$. An operation e_5 does not release any storage.

The last operation from the sequence E_s is e_8. The algorithm computes $T = 247.9$ and $V_{temp} = 750 + 500 = 1250$ and $V = 1250$. This operation releases three storages, B_8, B_9, and B_{10}. The updated storage released plan is $\delta = <(e_3, (B_4)), (e_7, (B_5)), (e_6, (B_3)), (e_8, (B_7, B_8, B_9))>$.

Finally, Algorithm 3 returns $T = 247.9$ of time units, $V = 1250$ data blocks and $\delta = <(e_3, (B_{i4})), (e_7, (B_5)), (e_6, (B_3)), (e_8, (B_7, B_8, B_9))>$ for a sequence of operations E_s.

4. Resource Allocation for a Group of Queries

Algorithm 4 takes on input a set of query processing plans $\mathcal{E} = \{E_{s_1}, ..., E_{s_n}\}$ created by Algorithm 2, a set of estimated processing times $\mathcal{T} = \{T_1, ..., T_n\}$, a set of maximum storage requirements for each processing plan $\mathcal{V} = \{V_1, ..., V_n\}$, a set of deallocation plans $\mathcal{D} = \{\delta_1, ..., \delta_n\}$ from the Algorithm 3, and a sequence of persistent storage tiers $L = <l_0, ..., l_n>$. The output of the algorithm is a sequence of storage allocation plans P.

First, the algorithm gets the estimated processing time T and the estimated highest allocation storage V for processing plans from $\mathcal{E}$. Next, the algorithm collects the candidate operations from $\mathcal{E}$, where a candidate operation is the first operation from each sequence, and puts them into a set of candidate operations E_c. Next, the algorithm picks one operation from E_c in the following way. First, the algorithm picks the operations from the sequences with the smallest volume, V. If more than one operation is found, then from the operations found so far, the algorithm picks the operations from the sequences with the shortest time, T. If again more than one operation is found, then the algorithm uses formula (3) to compute a profit for each operation and picks the operations with

the highest profit. Again, if more than one operation is still found, then the algorithm randomly picks one operation. Let selected in this way, the candidate operation be $e_i = (\{B_i, \ldots, B_j\}, \{B_k, \ldots, B_h\})$, and the total number of data blocks in output data sets of the operation be V_w.

Algorithm 4 passes the information about L, V_w, and P to Algorithm 4.1 to find the best partition and generate the updated storage allocation plan P. Next, Algorithm 4 must update L with information about temporary storage to be released after the processing of e_i. To do so, Algorithm 4 passes a deallocation plan δ_i for E_{s_i}, a sequence of tiers L, and the operation e_i to Algorithm 4.2 to update information about available storage in L.

Finally, an operation e_i is removed from E_{s_i}. The algorithm repeats the steps above for each operation from each sequence until all sequences are empty. The algorithm returns the final storage allocation plan P.

Algorithm 4: Generating storage allocation plans

Input: A set of processing plans $\mathcal{E} = \{E_{s_1}, \ldots, E_{s_n}\}$ from algorithm 2, deallocation plan δ, the maximum storage V, and the estimated processing time T for each sequence from Algorithm 3. A sequence of tiers $L = <l_0, \ldots, l_n>$ where each tier l_i is described as triple $(r_i, w_i, <s_{i_j}, \ldots, s_{i_i}>)$.
Result: A sequence of allocation plans $P = <D_{i_j}, \ldots, D_{n_k}>$.

(1) Create empty sequence of allocation plans $P = <>$.
(2) **While** *until all sequences in $\mathcal{E}$ are empty* **do**
  - Create an empty set of candidate operations $E_c = \{\}$.
  - Get the first operations from the sequences with the smallest volume V and put them into E_c.
  if *more than one operation is found in E_c* **then**
    - Keep the operations from the sequence $E_{s_1}, \ldots, E_{s_n}$ with the smallest estimated processing time T and remove the rest of the operations from E_c.
  else if *more than one operation is found in E_c* **then**
    - Keep the operations with the highest profit using formula (3) and remove the rest of the operations from E_c.
  else if *more than one operation is found in E_c* **then**
    - Select one operation randomly and make E_c empty.
  end
  - Let the selected operation be $e_i = \{B_i, \ldots, B_j\}, \{B_k, \ldots, B_h\}$ from E_{s_j} and its input storage be $\{B_i, \ldots, B_j\}$ and its output storage be $\{B_k, \ldots, B_h\}$.
  - Let the number of total output storage be V_w.
  - Use the information of L, V_w, and P to find the best partition using Algorithm 4.1 and get the result of updated plan P from algorithm 4.1.
  - Pass the information about a deallocation plan δ_j, a state of multi-tiered persistent storage L, and the operation e_i to Algorithm 4.2 to update L with information about temporary storage released by e_i.
  - Remove e_i from E_{s_j}.
  - Update estimated processing time T and V for E_{s_j}.
end
(3) Return the sequence of multi-tiered storage allocation plans $P = <D_{i_j}, \ldots, D_{n_k}>$.

Algorithm 4.1 finds the best partition using the information in L, V_w, P and e_i provided by Algorithm 4.

Let e_i be a member of E_{s_j}, and a set of allocation plans for e_i is denoted D_{j_i}. First, the algorithm needs to find the best partition located at the highest possible tier in order to achieve the best processing time. Next, the algorithm finds a partition that can accommodate the storage V_w where V_w is the total output storage required to store the temporary/permanent result of e_i. The input storage $\{B_i, \ldots, B_j\}$ is already assigned to one of the partitions on L. Therefore, the algorithm needs to find the best storage allocation for V_w only.

Next, the algorithm iterates over the tiers in L. Let the current tier be $(r_n, w_n, <s_{n_j}, \ldots, s_{n_i}>)$. The algorithm needs to check whether the required storage V_w can be allocated entirely in one partition or over more partitions. When the amount of storage available at one of the partitions in the highest tier is larger or equal to V_w, the algorithm creates an allocation plan (B_i, s_{n_j}) where $B_i = V_w$ and appends that plan to D_{j_i}. But sometimes, the amounts of storage available at all partitions in the highest tier are smaller than the required storage V_w. In that case, the algorithm splits storage V_w into multiple storages $V_w', \ldots, V_w''$. Some storage is to be allocated at the faster tier, and some may be at the lower tier. For that case, the algorithm splits V_w to allocate more than one partition and creates allocation plans $(B_i, s_{n_j}), \ldots, (B_j, s_{n_k})$. Next, the algorithm appends all those plans into D_{j_i}. Finally, the allocation plan D_{j_i} is appended to P and returned to Algorithm 4.

Algorithm 4.1: Finding the best partition and generating a plan for storage allocations

Input: A multi-tiered persistent storage $L = <l_0, \ldots, l_n>$, storage requirements V_w of an operation e_i, a sequence of storage allocation plans P.
Result: The updated sequence of storage allocation plans P.

(1) Let the amounts of temporary storage $V_{temp} = 0$ and let an initial storage allocation plan D_{j_i} for the operation e_i be empty.
(2) **while** *iterate over L in reverse order* **do**
  (i) Let current tier be $l_i = (r_i, w_i, <s_{i_j}, \ldots, s_{i_n}>)$ and let $<s_{i_j}, \ldots, s_{i_n}>$ be a sequence of partitions in l_i arranged from the smallest to the largest partition.
  (ii) Iterate over partitions $<s_{i_j}, \ldots, s_{i_n}>$ and choose a partition s_{i_k} such that its size is equal or larger than V_w.
  (iii) **if** *size of s_{i_k} is larger or equal to V_w* **then**
    - Create a pair (B_i, s_{n_j}) where $B_i = V_w$ and append it into D_{j_i}.
    - Update $s_{i_k} = s_{i_k} - V_w$ and $V_w = V_{temp}$.
    - Sort a sequence of partitions arranged from smallest available storage to largest available storage.
  else if *all storage in current set is smaller than V_w* **then**
    - Update $V_{temp} = V_w$.
    while *iterate over partition in reverse order and until V_{temp} = 0 or all available storage become zero* **do**
      - Let the current storage in a set be s_{i_k}.
      - Split storage into two parts: V_w, where $V_{temp} = V_{temp} - s_{n_i}$ and $V_w = s_{i_k}$

- Create a pair (B_i, s_{i_k}) where $B_i = V_w$ and append it into D_{j_i}.
- Update $s_{i_i} = 0$, and $V_w = V_{temp}$.
- Sort a sequence of partitions arranged from smallest available storage to largest available storage.
end
end
end
(3) Append $D_{j_i} = \{(B_i, s_{n_i}), \ldots, (B_j, s_{m_k})\}$ into P.
(4) Return P.

Algorithm 4.2 releases persistent storage no longer needed by an operation e_i. An input to the algorithm is a deallocation plan δ_i, a sequence of tier $L = <(r_n, w_i, <s_{n_i}, \ldots, s_{n_i}>), \ldots, (r_0, w_0, <s_{n_0}, \ldots, s_{n_j}>)>$, and the operation e_i passed from Algorithm 4.

Algorithm 4.2 checks whether e_i releases any persistent storage. If e_i is a member of the deallocation plan δ_i, then the algorithm needs to update L according to the deallocation plan, such as removing the storage released by e_i from the occupied storage. If e_i is not a member of the deallocation plan, then the algorithm does not need to update L.

Algorithm 4.2: Deallocation the storage

Input: A deallocation plan δ_i, a multi-tiered persistent storage $L = <l_0, \ldots, l_n>$, and the operation e_i.
Result: The updated multi-tiered persistent storage $L = <l_0, \ldots, l_n>$.

(1) **if** $e_i \in \delta_i$ **then**
- Get the storage released by e_i like $(B_x, \ldots, B_y)$.
while *iterate over* $(B_x, \ldots, B_y)$ **do**
- Let current storage be B_i and the location of B_i be (B_i, s_{h_i}) where storage B_i is located at partition i from tier l_h.
- Remove a storage B_i from partition i in level l_h and update $s_{h_i} = s_{h_i} + B_i$.
- Let s_{h_i} is belong to the sequence $<s_{h_x}, \ldots, s_{h_y}>$.
- Sort a sequence of partitions $<s_{h_x}, \ldots, s_{h_y}>$ arranged from smallest available storage to largest available storage.
end
end
(2) Return the updated $L = <l_0, \ldots, l_n>$.

Algorithm 5 computes the total processing time T_f for the allocation plan P created by Algorithm 4. First, the algorithm iterates over plan P. Let the current set of plans be $D_{j_i} = \{(B_i, s_{n_i}), \ldots, (B_j, s_{i_k})\}$ where D_{j_i} is a set of plans for the operation e_i in sequence E_{s_j}. Next, the algorithm iterates over D_{j_i}. Let the current pair be (B_i, s_{n_i}). Then, the algorithm computes the processing time for that pair. If B_i is a member of input data blocks for e_i, then compute $T_f = T_f + (B_i * r_n)$ where r_n is a reading speed per data block. If B_i is the member of output data blocks for e_i, then compute $T_f = T_f + (B_i * w_n)$ where w_n is a writing speed per data block. Next, the algorithm checks whether e_i is the last operation in the sequence E_{s_j} or not. If e_i is the last operation, then the algorithm needs to compute the reading time for final storage such as $T_f = T_f + (V_w * r_n)$, where V_w is the total data blocks written by operation

e_i. Finally, the algorithm returns the total execution time for plan P.

Algorithm 5: Final estimated processing time for allocation plan

---

Input: A sequence of allocation plans $P = <D_{i_j}, \ldots, D_{n_k}>$.
Result: Total estimated processing time T_f for allocation plan P.

(1) Let total processing time for sequences be $T_{f=0}$.
(2) **while** *iterate over* P **do**
- Set total writing data block be $V_w = 0$.
- Let the current plan be $D_{j_i} = \{(B_i, s_{n_i}), \ldots, (B_j, s_{i_k})\}$ for operation $e_i = \{B_i, \ldots, B_j\}, \{B_k, \ldots, B_h\}$ from E_{s_j}.
while *iterate over* D_{j_i} **then**
- Let current pair be (B_i, s_{n_i}) where B_i is a total number of data blocks allocated at a tier n in a partition i (s_{n_i}).
if B_i *is member of input storage* $\{B_i, \ldots, B_j\}$ **then**
- $T_f = T_f + (B_i * r_n)$
else
- $T_f = T_f + (B_i * w_n)$
end
end
if e_i *is the last operation from* E_{s_j} **then**
- Read the final result and release the storage.
- Update $T_f = T_f + (V_w * r_n)$.
end
end
(3) Return total processing time for allocation plan T_f.

Example 3: In this example, we use a multi-tiered persistent storage with 3 tiers. We assume that the highest tier l_2 has 3 partitions, the lower one l_1 has 2 partitions, and the bottom tier l_0 has 3 partitions. The parameters of the tiers are listed below.

$L = <l_0, l_1, l_2>$

- $l_0 = (0.2, 0.21, <200, 500, 1000>)$

- $l_1 = (0.1, 0.105, <100, 200>)$

- $l_2 = (0.05, 0.055, <40, 50>)$

Next, we use a set of sequences $\mathcal{E} = \{E_{s_1}, E_{s_2}, E_{s_3}\}$. A sequence E_{s_1} consists of the following 3 operations $E_{s_1} = <e_1, e_2, e_3>$ where

- $e_1 = (\{50, 50\}, \{100\})$

- $e_2 = (\{100\}, \{50\})$

- $e_3 = (\{50\}, \{20\})$

The total estimated processing time for E_{s_1} is $T_2 = 37.85$ and $V_1 = 150$.

The sequence E_{s_2} consists of one operation, $E_{s_2} = <e_1>$ where

- $e_1 = (\{150\}, \{100\})$

The total estimated processing time for E_{s_2} is $T_2 = 40.50$ and $V_2 = 100$.

The last sequence E_{s_3} consists of 4 operations $E_{s_3} = <e_1, e_3, e_2, e_4,>$ where

- $e_1 = (\{50\}, \{40, 40\})$

- $e_2 = (\{40\}, \{20\})$

- $e_3 = (\{40\}, \{10\})$

- $e_4 = (\{30\}, \{10\})$

The total estimated processing time for E_{s_3} is $T_3 = 22.60$ and $V_3 = 110$.

Following step (2) of Algorithm 4, we picked an operation e_1 from sequence E_{s_2}, because V_2 is the smallest volume, and put it into $E_c = \{e_1\}$. Since we have only one candidate operation, it is passed to Algorithm 4.1 to find the storage allocations for the outputs of operation e_1. According to Algorithm 4.1, the best storage is s_{2_3} and therefore, we created a plan like $(100, s_{2_3})$. We then appended the plan into $P = <(100, s_{2_3})>$. Next, Algorithm 4 released storage if e_1 needs to release some storage. According to Algorithm 4.2, e_1 does not need to release any storage. We repeated the above procedure and finally get the plan P for $\mathcal{E}$ where $P = <\{(40, s_{2_1}), (50, s_{2_2}), (10, s_{1_1})\}, \{(40, s_{2_1}), (40, s_{2_2})\}, \{(10, s_{2_1}), (10, s_{1_1})\}, \{(10, s_{2_1})\}, \{(10, s_{2_1})\}, \{(40, s_{2_1}), (50, s_{2_2}), (10, s_{1_1})\}, \{(50, s_{1_1})\}, \{(20, s_{2_1})\}>$.

Next, we compute the processing time for a sequence of plan P by using the algorithm 5. The total processing time T_f for $\mathcal{E}$ is 112.55 time units. With random allocation, the total processing time for $\mathcal{E}$ become 143.45 time units. Without multi-tiered persistent storage with partitions, the total execution time for $\mathcal{E}$ is 219.90 time units.

5. Example/Experiment

Different types of persistent storage devices such as SSD, HDD, and NVMe can be used to create a multi-tiered persistent storage system. In the experiment, we picked a sample multi-tiered persistent storage L that consists of 4 tiers $<l_0, l_1, l_2, l_3>$, where l_3 is the fastest tier such as NVMe and l_0 is the slowest tier, such as HDD and l_2 and l_1 are faster and slower SSDs. Each tier is divided into two partitions of different sizes. Table 1 shows the read and write speed per data block expressed in standardized time units and the total number of data blocks available at each partition.

Table 1: Read/Write Speed with Available Size for Multi-tiered Storage Devices

Level of Devices	Reading Speed	Writing Speed	Partition 1	Partition 2
l_0	$0.15 * 10^3$	$0.155 * 10^3$	1000	2000
l_1	$0.1 * 10^3$	$0.105 * 10^3$	500	600
l_2	$0.08 * 10^3$	$0.085 * 10^3$	150	200
l_3	$0.05 * 10^3$	$0.055 * 10^3$	50	100

In the experiment, we applied Algorithm 1 to convert eight query processing plans into the Extended Petri Nets. Next, we used Algorithm 2 to find the optimal sequences of operations for each Petri Net. Next, Algorithm 3 was used to get the deallocation plans δ, the maximum volumes V, and the estimated execution times T required for each sequence of operations found by Algorithm 2. The values for each sequence are the following.

$E_{s_1} = <e_1, e_3, e_2, e_4, e_5, e_6, e_7, e_8, e_9>$

$V_1 = 150, T_1 = 110.70$

Table 2: Operations With Input and Output Data sets For E_{s_1}

Operation	Input data set	Output data set

e_1	300	100
e_2	200	50
e_3	100	50
e_4	50	20
e_5	50, 20	50
e_6	50	20, 20
e_7	20	10
e_8	20	10
e_9	10, 10	10

$E_{s_2} = <e_2, e_5, e_1, e_4, e_7, e_9, e_3, e_6, e_8, e_{11}, e_{10}, e_{12}>$

$V_2 = 300, T_2 = 108.35$

Table 3: Operations with Input and Output Data sets For E_{s_2}

Operation	Input data set	Output data set
e_1	100	50
e_2	100	70
e_3	100	60
e_4	50	30
e_5	70	30
e_6	60	40
e_7	30, 30	50
e_8	40	20
e_9	50	30
e_{10}	20	10
e_{11}	30	20
e_{12}	20, 10	20

$E_{s_3} = <e_1, e_3, e_2, e_4, e_7, e_5, e_8, e_6, e_{11}, e_{10}, e_9, e_{12}, e_{13}, e_{14}, e_{15}>$

$V_3 = 300, T_3 = 147.40$

Table 4: Operations with Input and Output Data sets For E_{s_3}

Operation	Input data set	Output data set
e_1	500	400
e_2	600	300
e_3	400	100, 50
e_4	300	200, 50
e_5	100	30
e_6	50	30
e_7	200	100
e_8	50	10
e_9	30	20
e_{10}	30	10
e_{11}	100, 10	60
e_{12}	20	10
e_{13}	60	50
e_{14}	50	40
e_{15}	10, 10, 40	50

$E_{s_4} = <e_1, e_2, e_4, e_3, e_5 >$

$V_4 = 250, T_4 = 100.70$

Table 5: Operations with Input and Output Data sets For E_{s_4}

Operation	Input data set	Output data set
e_1	80	70
e_2	70	30, 30
e_3	30	20
e_4	30	10
e_5	20, 10	20

$E_{s_5} = <e_1, e_3, e_5, e_2, e_4, e_6, e_7, e_9, e_8, e_{10} >$

$V_5 = 200, T_5 = 93.50$

Table 6: Operations with Input and Output Data sets For E_{s_5}

Operation	Input data set	Output data set
e_1	300	100

e_2	100	50
e_3	200	100
e_4	50	30
e_5	100	50
e_6	30	20
e_7	100	50
e_8	50	30
e_9	20, 50	40
e_{10}	30, 40	50

$E_{s_6} = <e_1, e_2, e_3>$

$V_6 = 150, \qquad T_6 = 37.85$

Table 7: Operations with Input and Output Data sets For E_{s_6}

Operation	Input data set	Output data set
e_1	50, 50	100
e_2	100	50
e_3	50	20

$E_{s_7} = < e_1>$

$V_7 = 100, T_7 = 40.50$

Table 8: Operations with Input and Output Data sets For E_{s_7}

Operation	Input data set	Output data set
e_1	150	100

$E_{s_8} = < e_1, e_3, e_2, e_4, >$

$V_8 = 110, T_8 = 22.60$

Table 9: Operations with Input and Output Data sets For E_{s_8}

Operation	Input data set	Output data set
e_1	50	40, 40
e_2	40	20
e_3	40	10
e_4	20, 10	10

Next, we used Algorithm 4 to decide on an order of concurrent processing of operations from the sequences in $\mathcal{E}$. Algorithms 4.1 and 4.2 were used within Algorithm 4 to find the best allocation of partitions and to generate a persistent storage allocation plan. The details of the plan are listed in the Appendix. After that, we used Algorithm 5 to simulate the processing of the plan to get the total estimated execution time T_f, see Table X.

In the second experiment, we used the same set of sequences of operations $\mathcal{E}$, and whenever more than one operation could be selected for processing, we randomly picked an operation. The total execution time for the second experiment is given in Table X.

In the third experiment, we used only a single tier of persistent storage, and like before, whenever more than one operation could be selected for processing, we randomly picked an operation. The final results of all experiments are summarized in a Table X.

Table 10: Summary of Experimental Results

Experiment	Method	Total execution time-units
Experiment 1	Using allocation plan over multi-tiered persistend storage that proposed in this work.	857
Experiment 2	Using random allocation plan over multi-tiered persistend storage.	1,068.35
Experiment 3	Using allocation plan without multi-tiered persistend storage.	1,466.95

By comparing those three results, one can find that the execution plan for experiment 1 achieves better performance and faster execution time than experiment 2 and experiment 3.

6. Summary and Future Work

This paper presents the algorithms that optimize the allocations of persistent storage over a multi-tiered persistent storage device when concurrently processing a number of database queries. The first algorithm converts a single query processing plan obtained from a database system into an Extended Petri Net. An Extended Petri Net represents many different sequences of database operations that can be used for the implementation of a query processing plan. The second algorithm finds in an Extended Petri Net a sequence of operations that optimizes storage allocation in multi-tiered persistent storage when a query is processed. The third algorithm estimates the maximum amount of persistent storage and processing time needed when a sequence of operations found by Algorithm 2 is processed.

In the second part of the paper, we considered the optimal allocation of multi-tiered persistent storage when concurrently processing a set of queries. We assumed that the first three algorithms are used for individual optimization of storage allocation plans for each query in a set. The fourth algorithm optimizes the allocation of multi-tiered persistent storage when a set of sequences of operations obtained from the first three algorithms is concurrently processed. The algorithm creates a persistent storage allocation and releases a plan according to the available size and speed of the devices implementing multi-tiered persistent storage.

The last algorithm processes a storage allocation plan created by the previous algorithm and returns the estimated processing time. To validate the proposed algorithms, we conducted several experiments that compared the efficiency of processing plans created by the algorithms with the random execution plans and execution plans without multi-tiered persistent storage. According to the outcomes of experiments, the storage allocation plans obtained from our algorithms consistently achieved better processing time than the other allocation plans.

Several interesting problems remain to be solved. An optimal allocation of persistent storage in the partitions of multi-tiered storage contributes to a dilemma of spreading a large allocation over smaller allocations at many higher-level partitions versus a single allocation at a lower partition.

Another interesting question is related to a correct choice of a level at which storage is allocated depending on the stage of query processing. It is almost always such that the initial stages of query processing operate on the large amounts of storage later reduced to the smaller results. It indicates that the early stages of query processing should be prioritized through storage allocations at higher levels of multi-tiered storage. It means that the parameters of multi-tiered storage allocation may depend on the phases of query processing with faster storage available at early stages.

The next interesting problem are the alternative multi-tiered storage allocation strategies. In one of the alternative approaches, after the serialization of Extended Petri Nets representing individual queries, it is possible to combine the sequence of operations into one large Extended Petri Net and apply serialization again. Yet another idea is to combine the Extended

Petri Nets of individual queries into one Net and try to eliminate multiple accesses to common data containers.

The next stimulating problem is what to do when the predictions on the amounts of data read and/or written to multi-tiered persistent storage do not match the reality. A solution for these cases may require ad-hoc resource allocations and dynamic modifications of existing plans.

It is also possible that a set of queries can be dynamically changed during the processing. For example, a database application can be aborted, or it can fail. Then, the management of persistent storage also needs to be dynamically changed. A solution to such a problem would require the generation of a plan with the options where certain tasks are likely to increase or decrease their processing time.

Conflict of Interest

The authors declare no conflict of interest.

Acknowledgment

References

[1] Data Storage Trends in 2020 and Beyond, https://www.spiceworks.com/marketing/reports/storage-trends-in-2020-and-beyond/ (accessed on 30 April 2021)

[2] U. Sivarajah, M. M. Kamal, Z. Irani, V. Weerakkody, "Critical Analysis of Big Data Challenges and Analytical methods". In Journal of Business Research, **70**, 263--286, 2017.

[3] S. wang, Z. Lu, Q. Cao, H. Jiang, J. Yao, Y. Dong, P. Yang, C. Xie, "Exploration and Exploitation for Buffer-controlled HDD-Writes for SSD-HDD Hybrid Storage Server", ACM Trans. Storage 18, 1, Article 6, February 2022.

[4] Apache Ignite Multi-tier Storage, https://ignite.apache.org/arch/multi-tier-storage.html (accessed on 30 April 2021)Trans. Roy. Soc. London, A247, 529–551, April 1955.

[5] Tiered Storage, https://searchstorage.techtarget.com/definition/tiered-storage (accessed on 30 April, 2021).

[6] E. Tyler, B. Pranav, W. Avani, Z. Erez, "Desperately Seeking Optimal Multi-Tier Cach Configurations", In 12th USENIX Workshop on Hot Topics in Storage and File System (HotStorage 20), 2020.

[7] H. Shi, R. V. Arumugam, C. H. Foh, K. K. Khaing, "Optimal disk storage allocation for multi-tier storage system", Digest APMRC, Singapore, 2012, 1-7.

[8] N.N. Noon, "Automated performance tuning of database systems", Master of Philosophy in Computer Science thesis, School of Computer Science and Software Engineering, University of Wollongong, 2017.

[9] N.N. Noon, J.R. Getta, "Optimisation of query processing with multilevel storage", Lecture Notes in Computer Science, 9622 691-700. Da Nang, Vietnam Proceedings of the 8th Asian Conference, ACIIDS 2016.

[10] B. Raza, A. Sher, S. Afzal, A. Malik, A. Anjum, Adeel, Y. Jaya Kumar, "Autonomic workload performance tuning in large-scale data repositories", Knowledge and Information Systems. 61. DOI: 10.1007/s10115-018-1272-0.

[11] N.N. Noon, J.R. Getta, T. Xia, "Optimization Query Processing for Multi-tiered Persistent Storage", IEEE 4th International Conference on Computer and Communication Engineering Technology (CCET), 2021, 131-135, doi: 10.1109/CCET52649.2021.9544285.

[12] R. Wolfgang, "Understanding Petri Nets: Modeling Techniques, Analysis Methods, Case Studies", Springer Publishing Company, Incorporated, 2013.

APPENDIX

A processing plan for the experiments described in a section 6 of the paper is the following sequence P of the individual plans.

$P = <D_{7_1}, D_{8_1}, D_{8_3}, D_{8_2}, D_{8_4}, D_{6_1}, D_{6_2}, D_{6_3}, D_{1_1}, D_{1_3}, D_{1_2}, D_{1_4}, D_{1_5}, D_{1_6}, D_{1_7}, D_{1_8}, D_{1_9}, D_{5_1}, D_{5_3}, D_{5_5}, D_{5_2}, D_{5_4}, D_{5_6}, D_{5_9}, D_{5_8}, D_{5_{10}}, D_{4_1}, D_{4_2}, D_{4_4}, D_{4_3}, D_{4_5}, D_{2_2}, D_{2_5}, D_{2_1}, D_{2_4}, D_{2_7}, D_{2_9}, D_{2_3}, D_{2_6}, D_{2_8}, D_{2_{11}}, D_{2_{10}}, D_{2_{12}}, D_{3_1}, D_{3_3}, D_{3_2}, D_{3_4}, D_{3_7}, D_{3_5}, D_{3_8}, D_{3_6}, D_{3_{11}}, D_{3_{10}}, D_{3_9}, D_{3_{12}}, D_{3_{13}}, D_{3_{14}}, D_{3_{15}}>$

Each plan D_{i_j} is the following set of pairs:

$D_{7_1} = \{(50, s_{3_1}), (100, s_{3_2})\}$, $D_{8_1} = \{(40, s_{3_1}), (10, s_{3_1}), (30, s_{3_2})\}$

$D_{8_3} = \{(20, s_{3_2})\}$, $D_{8_2} = \{(10, s_{3_1})\}$, $D_{8_4} = \{(10, s_{3_1})\}$

$D_{6_1} = \{(100, s_{3_2})\}$, $D_{6_2} = \{(50, s_{3_1})\}$, $D_{6_3} = \{(20, s_{3_2})\}$

$D_{1_1} = \{(100, s_{3_2})\}$, $D_{1_3} = \{(50, s_{3_1})\}$, $D_{1_2} = \{(50, s_{3_2})\}$, $D_{1_4} = \{(20, s_{3_2})\}$, $D_{1_5} = \{(50, s_{3_2})\}$, $D_{1_6} = \{(20, s_{3_1}), (20, s_{3_1})\}$, $D_{1_7} = \{(10, s_{3_1})\}$, $D_{1_8} = \{(10, s_{3_1})\}$, $D_{1_9} = \{(10, s_{3_1})\}$

$D_{5_1} = \{(50, s_{3_1}), (100, s_{3_2}), (50, s_{2_1})\}$, $D_{5_3} = \{(100, s_{2_1})\}$, $D_{5_5} = \{(50, s_{3_1})\}$, $D_{5_2} = \{(50, s_{3_2})\}$, $D_{5_4} = \{(30, s_{3_2})\}$, $D_{5_6} = \{(20, s_{3_2})\}$, $D_{5_7} = \{(50, s_{3_2})\}$, $D_{5_9} = \{(30, s_{3_2}), (10, s_{2_1})\}$, $D_{5_8} = \{(30, s_{3_2})\}$, $D_{5_{10}} = \{(50, s_{3_1})\}$

$D_{4_1} = \{(70, s_{3_2})\}$, $D_{4_2} = \{(30, s_{3_1}), (30, s_{3_2})\}$, $D_{4_4} = \{(10, s_{3_1})\}$, $D_{4_3} = \{(20, s_{3_1})\}$, $D_{4_5} = \{(20, s_{3_1})\}$

$D_{2_2} = \{(70, s_{3_2})\}$, $D_{2_5} = \{(30, s_{3_2})\}$, $D_{2_1} = \{(50, s_{3_1})\}$, $D_{2_4} = \{(30, s_{3_2})\}$, $D_{2_7} = \{(50, s_{3_1})\}$, $D_{2_9} = \{(30, s_{3_2})\}$, $D_{2_3} = \{(60, s_{3_2})\}$, $D_{2_6} = \{(40, s_{3_1})\}$, $D_{2_8} = \{(20, s_{3_2})\}$, $D_{2_{11}} = \{(20, s_{3_1})\}$, $D_{2_{10}} = \{(10, s_{3_1})\}$, $D_{2_{12}} = \{(20, s_{3_1})\}$

$D_{3_1} = \{(150, s_{2_1}), (100, s_{2_2}), (50, s_{3_1}), (100, s_{3_2})\}$, $D_{3_3} = \{(50, s_{1_1}), (100, s_{2_2})\}$, $D_{3_2} = \{(150, s_{2_1}), (50, s_{3_1}), (100, s_{3_2})\}$, $D_{3_4} = \{(150, s_{1_1}), (50, s_{2_2}), (50, s_{2_2})\}$, $D_{3_7} = \{(100, s_{3_2})\}$, $D_{3_5} = \{(30, s_{3_1})\}$, $D_{3_8} = \{(10, s_{3_1})\}$, $D_{3_6} = \{(20, s_{2_1}), (10, s_{3_1})\}$, $D_{3_{11}} = \{(60, s_{2_1})\}$, $D_{3_{10}} = \{(10, s_{3_1})\}$, $D_{3_9} = \{(20, s_{3_2})\}$, $D_{3_{12}} = \{(10, s_{3_1})\}$, $D_{3_{13}} = \{(50, s_{3_2})\}$, $D_{3_{14}} = \{(40, s_{3_1})\}$, $D_{3_{15}} = \{(50, s_{3_2})\}$

Regular Tessellation-Based Collective Movement for a Robot Swarm with Varying Densities, Scales, and Shapes

Kohei Yamagishi[*], Tsuyoshi Suzuki

Tokyo Denki University, Department of Information and communication Engineering, Adachi-ku, 120-8551, Japan

A R T I C L E I N F O	A B S T R A C T
	In complex swarm robotic applications that perform different tasks such as transportation and observation, robot swarms should construct and maintain a formation to adapt and move as a single large-scale robot. For example, transportation and observation tasks require unique robot swarms with either high densities to support the weight of the transported objects or low densities to avoid overlapping field of views and avoid obstructions. Previous literature has not focused on structure optimization because swarming provides a large-collective capability. This paper proposes a leader-follower-controlled collective movement method by calculating direction and distance potentials between robots based on geometric constraints, constricting robot positioning along radial gradients around the leader robot according to these potentials. This paper demonstrates a robot swarm applying the proposed method while maintaining formations with different densities while moving and evaluates the robot swarm structure-maintaining performance.

1. Introduction

Cooperation between multiple robots is one method to complete large-scale and parallel tasks that a single robot cannot solve alone. Swarm robotic systems achieve this cooperative capability without centralized control by implementing swarm intelligence. In this system, a swarm of robots behaves in an organized manner through robot interactions [1]. When robots must complete a complex task that requires object transportation and tracking, they must move in a group or swarm. Various methods have been studied to determine swarm behaviors suitable for the task. Heavy object transportation requires a high-density robot swarm to support the weight. In contrast, the transport of light objects requires a low-density robot swarm to reduce the number of operating robots. In addition, monitoring dynamic targets, such as a school of fish, requires a low-density robot swarm to expand and optimize the observation range. Swarm robotics requires adaptive swarm behaviors that control robots to achieve different densities and shapes.

Swarm behavior control for object transportation robots includes collective movements in which the robot swarm moves while maintaining either a pre-organized shape in a two-dimensional [2] or three-dimensional space [3], or a flock, in which robots move while changing their arrangement to adapt to the

velocities and positions of other robots [4, 5]. These approaches typically control the robots using local interactions based on inter-robot relative distances and orientations [6], global interactions based on a virtual leader robot [7], environmental geometry, and the positions of the robots [8]. Local interactions distribute control based on the states of neighboring robots; formations determined in this way must place robots at intervals in which they recognize their neighbors. Robots can build a dense hexagonal close-packed structure to ensure that they do not deform, split, or break formation, while at the same time prioritizing swarming [9] or area cover [10]. Global interactions, on the other hand, require centralized control to share arbitrary information. Formations constructed using this method can freely position the robots individually. The number of controllable robots in this global-control scheme then depends on the communication performance of the robots and the computational performance of the centralized control unit. Hence, distributed control based on local information is advantageous when controlling a large-scale robot swarm. However, the formations constructed under this control method cannot provide density and area coverage suitable for many cooperative tasks with different densities. Therefore, we consider a method for constructing and moving a large-scale robot swarm with different densities, scales, and shapes to perform cooperative tasks. Cooperation between multiple robots is one method to complete large-scale and parallel tasks that a single robot cannot solve alone. Swarm robotic systems achieve this cooperative

*Corresponding Author: Kohei Yamagishi, 5 Senju Asahi-cho, Adachi-ku, Tokyo, Japan 120-8551, k.yamagishi@nrl.c.dendai.ac.jp

capability without centralized control by implementing swarm intelligence. In this system, a swarm of robots behaves in an organized manner through robot interactions [1]. When robots must complete a complex task that requires object transportation and tracking, they must move in a group or swarm. Various methods have been studied to determine swarm behaviors suitable for the task. Heavy object transportation requires a high-density robot swarm to support the weight. In contrast, the transport of light objects requires a low-density robot swarm to reduce the number of operating robots. In addition, monitoring dynamic targets, such as a school of fish, requires a low-density robot swarm to expand and optimize the observation range. Swarm robotics requires adaptive swarm behaviors that control robots to achieve different densities and shapes.

Figure 1 shows two types of structures based on connections between neighboring robots: crystalline structures, which arrange robots in a regular tessellation [11], and amorphous structures, which place robots in an irregular pattern suited to a given condition [12]. Comparing the density of each crystalline structure when packed by circular robots, the hexagonal lattice is the highest, and the honeycomb lattice is the lowest, depending on the number of neighbors. In crystalline structures, robots can maintain their construction with only the relative angles and distances between them, making the formations match the constructed lattice. In contrast, an amorphous structure has irregular angles between neighboring robots. Therefore, the swarm shape can meet evolving environmental requirements. Amorphous swarms also prevent splitting by reinforcing high-load sections during transportation. However, owing to these properties, amorphous structures cannot build a shape with high density. This study focuses on crystalline robotic formations to stably control swarms with different densities.

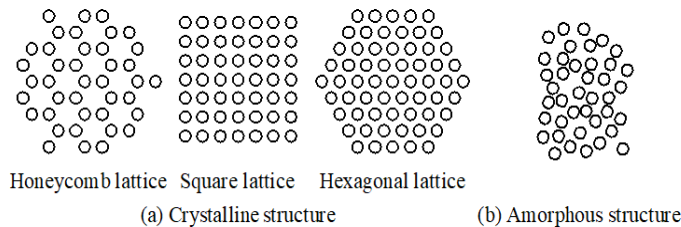(a) Crystalline structure   (b) Amorphous structure

Figure 1: Examples of crystalline and amorphous structures

Regular tessellations provide latticed structures with high density by arranging the robots according to geometric constraints. The study of modular robots in lattice structures has facilitated the development of self-organizing robots with angular joints between neighbors in honeycomb, square, and hexagonal lattices [13, 14, 15]. These robots can self-organize various swarm shapes by recursively communicating with their neighbors, and can behave rigidly as they are physically interconnected with neighboring robots. However, these modular robots cannot organize other lattice formations owing to the physical constraints of their joint assemblies. In this study, we design a virtual interaction to construct lattice-based swarm shapes without the physical restriction of joints, such as the joint limits of modular robots. In our previous study, we proposed a collective movement using a distance-based local interaction based on the Lennard-Jones potential, an intermolecular potential [16]. This potential converges into a hexagonal close-packed structure, as described

above. This study develops a group-forming model that adds an angular potential to this distance potential. For collective movement, the method introduces a leader-follower control, in which the robots orient with respect to a single leader robot in the group. Host systems and operators can then control the robot swarm by managing only the path of the leader. Therefore, the system does not require a large-capacity network to connect all robots. The above global-information-based approach can achieve collective movement without this physical leader by introducing a goal location and a virtual leader. For the host system to broadcast such information to the swarm, the system must either deploy an area network to communicate the information to all robots or equip them with a sensor device that can detect the direction of a physical goal, such as a light [17] or sound [18]. The robots then move autonomously toward the position indicated by the global information. Unfortunately, it is difficult for systems to manage the moving path of the whole swarm because the robots move autonomously. Therefore, this study considers the collective movement of a large-scale robot swarm using leader-follower control, controlling the swarm path in real-time by communicating with a single robot. We developed a collective movement method for a robot swarm with a density, scale, and shape suitable for cooperative tasks solved by robot swarms via teleoperation of a leader robot. This paper shows that a robot swarm applying the proposed method can move while maintaining various swarm shapes constructed with different densities.

The rest of this paper is structured as follows: Section 2 describes the configuration of the robot swarm and mathematical variables. Section 3 proposes a group-forming potential and collective movement method using leader-follower control. In Section 4, we discuss changing the robot swarm structures, and apply the changes during movements with different densities, sizes, and shapes. Finally, Section 5 summarizes the study.

2. Preliminaries

The robot swarm used in this study consists of two or more homogeneous mobile robots that may move within a linearly controllable speed v_{max} in all directions in a two-dimensional plane without any obstacles. The robot is equipped with both a distance sensor, such as light detection and ranging (LiDAR), to obtain the relative positions of surrounding neighbor robots and a local communication device, such as an infrared communicator, to exchange unique information with neighbors detected by the sensor. The position information is input to the proposed controller. As shown in Figure 2, the controller recognizes the neighbors to construct the lattice connected by the red lines among the communicable neighbors in all directions. The outer shape of the robots is circular with a diameter of σ [m] to prevent the occurrence of distance error due to robots measuring each other from all directions. All robots require a shared common reference direction to determine their neighboring angles and construct lattice structures; to provide this orientation, we initialize the robots with the same heading or synchronize directional information by averaging the data through local communication [19]. The i-th robot obtains the physical information of a neighbor robot with a distance-vector r_{ij}, composed of the distance $\|r_{ij}\|$ and the direction angle θ_{ij}, to the j-th neighboring robot.
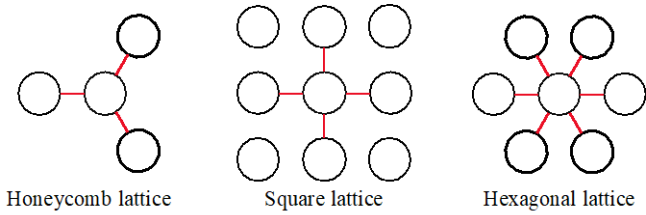
Figure 2: Neighbors that can communicate with the central robot in each latticed structure. The red line represents the connection with the neighboring robots equidistant from the central robot.

3. Multi-Robot Movement Control Method

3.1. Group-forming potential with latticed structures

Geometric swarm tessellations depend on the distance and angle between neighboring robots, treated as points. To maintain the structure of these points, distance and angle are used to compute and converge on a target structure. We propose a virtual potential-based interaction that depends on the relative position of neighboring robots to maintain cohesion.

Regarding the distance potential, we took inspiration from the interaction of molecules that organize molecular lattice structures. Among the various potential models that describe molecular bonds, the Lennard-Jones potential [20] is calculated with simple operations. With this potential, the repulsive and attractive forces diverge to infinity as the distance between molecules shrinks with an arbitrary maximum value determined by a coefficient past a certain distance depending on the molecular diameter. Considering the robot as a molecule, this study modifies the potential using the normalized coefficient adjusted to ensure that the maximum attractive force is one; the force on the relative distance, which is the first-order derivative of the Lennard-Jones potential, is expressed as follows:

$$f_i^D(r_{ij}) = \frac{169 \sqrt[6]{\frac{13}{7}}}{63 \cdot 2^{\frac{5}{6}}} \frac{1}{\|r_{ij}\|} \left(12 \left(\frac{\sigma}{\|r_{ij}\|} \right)^{12} - 6 \left(\frac{\sigma}{\|r_{ij}\|} \right)^6 \right) \hat{r}_{ij}. \quad (1)$$

The robot moves according to the calculated force, converging to a distance of $\|r_0\|$, where $f_i^{D\prime}(r_0) = 0$, depending on the diameter. The robots are controlled only by this potential move toward the balance distance between themselves and their neighbors, moving freely about a circle of radius $\|r_0\|$. Consequently, the robots organize into a close-packed hexagonal lattice structure. This study introduces an angular potential that converges in equally spaced directions, suitable for lattices with different densities. Robots constructing the lattice structure must place their neighbors in the angular intervals of $2\pi/3$, $\pi/2$, and $\pi/3$ [rad], divided by the number of connections in honeycomb, square, and hexagonal lattices, respectively, as shown in Figure 2. This study applies a simple angular potential model to converge robots into these lattices, as follows:

$$f_i^A(r_{ij}) = \sin(2L\theta_{ij}) R \left(\frac{\pi}{2} \right) \hat{r}_{ij} \quad (2)$$

where L is three, four, and six for honeycomb, square, and hexagonal lattices, respectively, matching the number of neighbors constructing the lattice structure. This model works normal to the

relative distance vector between each pair of robots and can modify the angular error between robots within $\pm\pi/4L$ [rad]. Thus, the robot moves to arrange its neighbors into angles matching the target lattice structure. By combining the distance and angular potentials, the robots converge into a lattice with their neighbors, as shown in Figure 3. The swarm organized by these robots maintains a latticed structure.
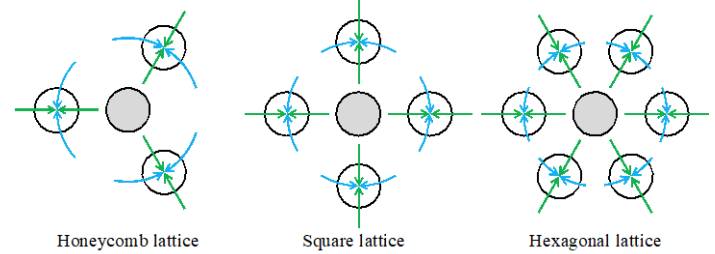
Figure 3: Positions of neighbors converged by the proposed angular and distance potentials

3.2. Collective movement using potential weights

The collective movement method in this study uses leader-follower control to ensure that the host system can manage the robot swarm similarly to the individual robots. Because the host system controls only the leader, as described above, we consider autonomous decentralized control for followers maintaining positional relationships with their neighbors. The proposed potential models rectify the positional errors caused by an organized latticed structure; if a robot swarm includes a leader, it can move while maintaining formation by adapting to structural changes caused by the leader's movement. Followers will react to structural changes caused by both the leader and each other, because this interaction affects all neighbors uniformly. Consequently, the approach using the proposed potential models creates a slow and inefficient collective movement for the robots', limiting formation speed.

We facilitate follower behavior during structural change caused by the leader's movement by weighting robot interactions. Interactions in the direction of the leader are weighted higher than interactions away from the leader. In a previous study [16], this approach was applied only to the distance potential. This study formulates a collective movement model for followers that introduces additional weights to the model potentials as follows:

$$v_i = \sum_j^{N_i} \begin{cases} P_r v_{max} \left(f_i^D(r_{ij}) + f_i^A(r_{ij}) \right) & ; l_i > l_j \\ P_w v_{max} \left(f_i^D(r_{ij}) + f_i^A(r_{ij}) \right) & ; l_i < l_j \\ v_{max} \left(f_i^D(r_{ij}) + f_i^A(r_{ij}) \right) & ; l_i = l_j \end{cases} \quad (3)$$

where N_i is the set of neighbors around the i-th robot. The robot applies a weight-adjusted potential to each neighbor, where P_r and P_w are the weights for neighbors closer to or farther from the leader, respectively. These weights are constrained by $P_r + P_w = 2$; $(P_r > P_w > 0)$ to ensure that the adjusted interactions provide the same interaction magnitude as the interactions without the new collective movement approach. Followers weigh their neighbors based on the distance between themselves and the leader. We introduce an ordering layer based on the lattice construction, which represents the routing metric to the leader as shown in Figure 4.

The leader is given a layer reference value of zero, and followers set their layer value, l_i, as $l_i = \min(l_j) + 1$ based on the layer value of their neighbors, l_j. The followers update this metric by repeating the calculation by each follower, and quickly produce a radial gradient around the leader. Consequently, each follower adjusts their potential weights according to this gradient to ensure that they more strongly perceive the structural change caused by the leader.

The movement of the leader is teleoperated through a host system to control the destination of the swarm. The leader's moving vector, related to a given moving command, is as follows:

$$v_i = P_l v_{max} f_c \qquad (4)$$

where P_l is an upper-speed limit coefficient for the leader designed as $P_r - 1$ to ensure that the leader's movement does not exceed the convergence force for the neighbors around the leader, as shown in (3). f_c is a velocity vector given via teleoperation that is less than one.

With these control methods, this study realizes the collective movement of a leader-follower robotic swarm while maintaining a lattice swarm shape. The proposed method can be implemented into any swarm shape with lattice construction.
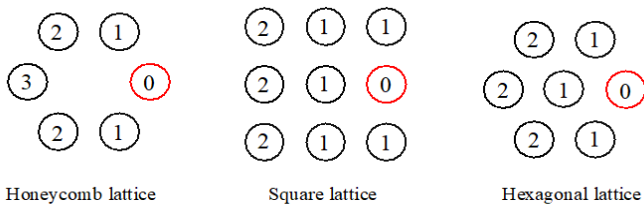

Figure 4: Calculated layer metric between the leader and followers according to the lattice structures

4. Verification of Collective Movement

Collective movement is an essential technology to support swarm robotic applications. Robot swarms can contribute to cost reduction and efficiency in their applications. In Section 1, we focus on transport and observation tasks using multiple robots, explaining the necessity for unique swarm densities, scales, and shapes. This section confirms that the proposed control method satisfies these goals. The proposed method can control an arbitrary number of robots via distributed control based on local measurements and information exchanged with neighbor robots. This study demonstrates that a robot swarm applying the proposed method can move collectively in all directions, and quantitatively evaluates the scalability of the method for any swarm size [21].

We developed numerical simulations for these evaluations using Java. The robot in this simulation is a moving object with a diameter of 0.25 m, moving with a speed limit of 0.5 m/s. The robot computes a velocity output via the proposed method at 2 ms intervals and simultaneously updates the communicated information. First, this paper evaluate the design and effectiveness (collective movement efficiency) of the parameters for the proposed method, P_r and P_w.

4.1. Collective movable speed relative to P_r–P_w ratio

The proposed collective movement performance depends on the design of P_r, P_w, and P_l. Therefore, we evaluate the maximum

value of the parameter P_l that can be set under the parameters P_r and P_w. Because collective movement must be able to move in all directions, the experiment uses an environment in which formations of each lattice structure with ten-layers filled moves on a circle with a diameter of 10 m.

Figure 5 plots the maximum P_l that did not change in the structure before and after movement, as P_l is increased by 0.01 from zero under each setting P_r and P_w condition. This property also shows the collective movement efficiency for each P_r–P_w ratio. Compared to the condition with $P_w = 1$, where P_r and P_w were not introduced, the introduction of the P_r–P_w ratio resulted in higher collective movement efficiency. This result also shows that the smaller P_w is, the higher movement efficiency.

We focus on the properties of the proposed method for hexagonal and honeycomb lattices. By introducing an angular potential, the proposed method can detect and adjust the structural changes caused by moving faster than the distance-potential-only collective movement method in the previous study [16]. As a result, the proposed method achieves high collective movement efficiency even for large values of P_w. On the other hand, this property of the square lattice did not improve significantly. This is because the square lattice formation moving in the vertical and horizontal directions has no angular potential action of the neighbors in that direction and less distance potential action for robots closer to the leader. Therefore, the followers could not maintain the connection with the neighbors in the vertical and horizontal movement directions, and the collective movement efficiency decreased.
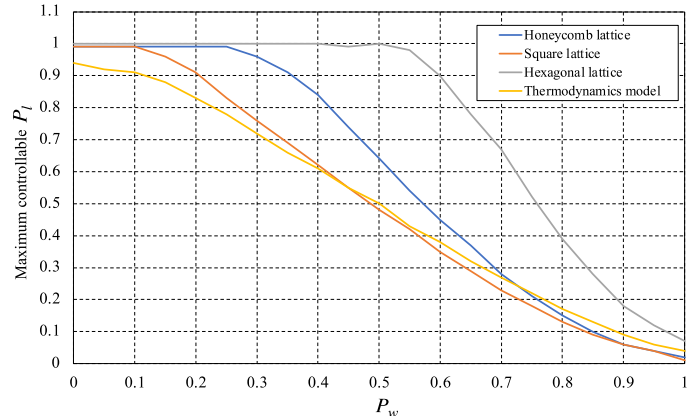
Figure 5: Maximum P_l that can be set according to the P_l–P_w ratio

The proposed collective migration requires the design of parameters, P_r, P_w, and P_l based on Figure 5. In subsequent experiments, P_l, P_r, and P_w are evaluated as 0.5, 1.55, and 0.45, respectively, to ensure that the collective movement efficiency is $P_l = 0.5$ for all lattices. These parameters are the balance values for the performance of swarm cohesion and collective movement speed, which have a trade-off relationship.

4.2. Demonstration of collective movement using various swarm shapes

This study focuses on cooperative transportation and sweep coverage using swarm robotics. These tasks require collective movement while maintaining a cohesive robot swarm in the shape

of the transported object around its center of gravity [22], or a robot swarm assembled in a row [23].
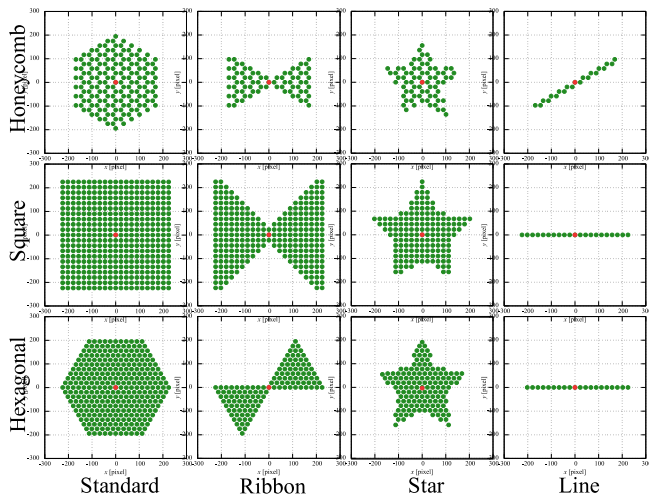
Figure 6: Formations with a scale of ten layers represented according to latticed structures

Therefore, we consider the characteristic formations in a ten-layer formation, as shown in Figure 6. The swarm shapes are as follows: standard formation, which builds a large-scale robot by

enlarging the lattice structure around the leader; ribbon formation, which connects two groups at the leader position to transport multiple objects simultaneously; star formation, which is an example of an arbitrary swarm shape represented by a latticed structure, and line formation, which provides an efficient sweep. We confirm that robots implementing the proposed method can move in all directions without breaking formation by demonstrating circular movement.

Figure 7 shows the trajectories of all robots during the movement using these formations. The leader of each formation moves counterclockwise. In all conditions, followers move alongside the remotely controlled leader. This means that while the robots move according to the proposed method, they maintain their positional relationships with each other in a latticed structure. Followers move while modifying the structural changes caused by the movement of robots in the inner layer. Thus, the standard and star formations, arranging the robots to fill the inner layer, transmit their changes to the outer followers from both directions. In contrast, the line and ribbon formations cannot react as strongly, because formations with reduced interconnectivity cannot transmit the information required for the proposed method fast enough to achieve perfect collective movement; this suggests that the proposed method works best when the followers and the leader are adjacent.

Figure 7: Movement trajectories of robots during collective movement in a circle using the formations shown in Figure 6. Each leader moves along the red arrow.

Figure 8: Movement trajectories of robots during collective movement in a straight line using standard formations for each lattice without the proposed angular potential

Subsequently, we confirm the structure-maintaining effect of the proposed method by comparing it with an existing collective movement method that can also maintain a high-density state. As already demonstrated, the proposed method organizes lattice structures using direction and distance potentials. In contrast, many existing collective movement methods control robots using interaction models without angular potentials. As a comparison, we employ a similar swarm behavior model for maintaining a high-density shape in an open space without obstacles that also applies the same Lennard-Jones potential and leader-follower control scheme as shown in our previous study [16]. We apply this existing method to a robot swarm initially arranged in a latticed structure and track their movement trajectories dur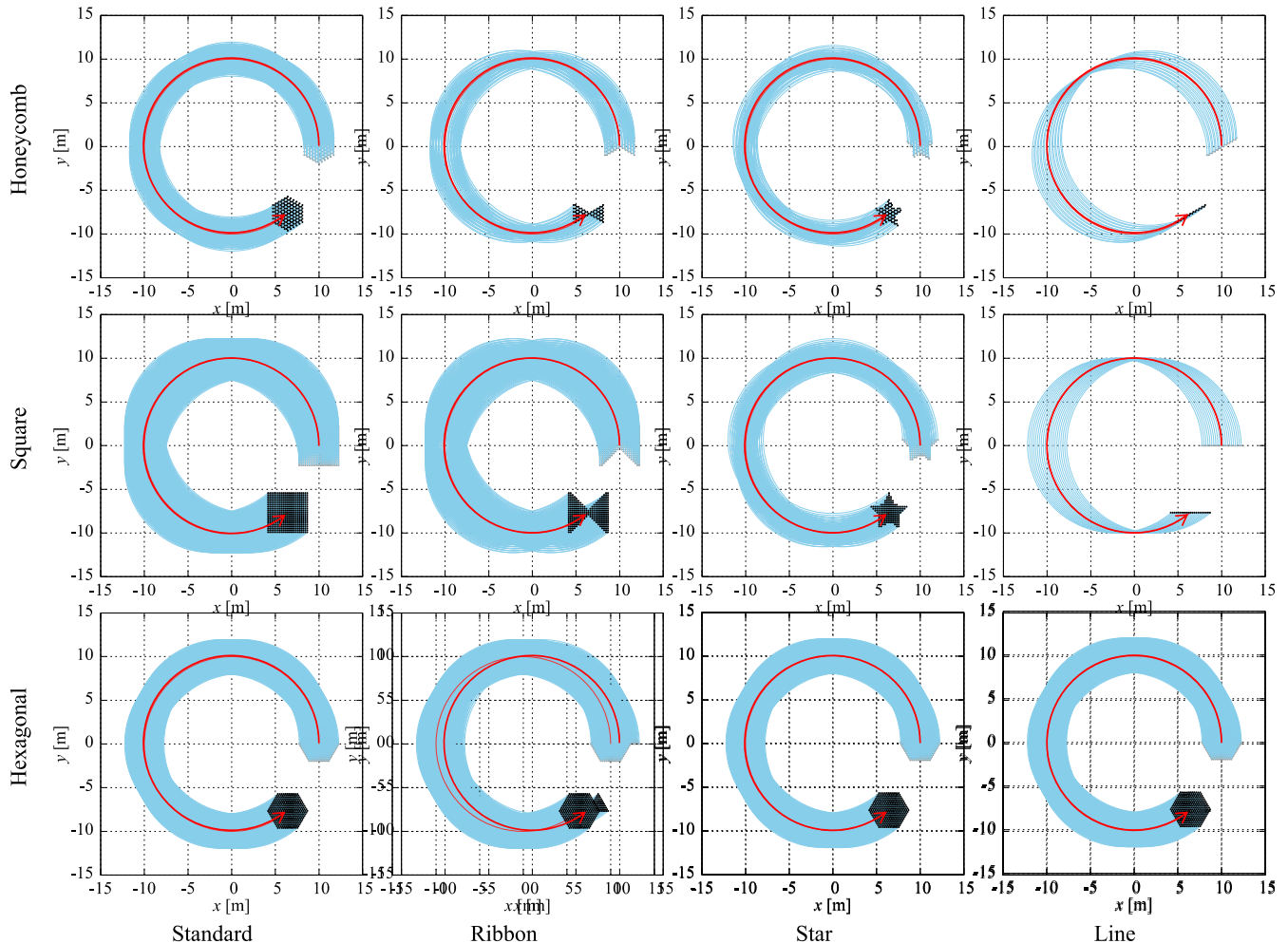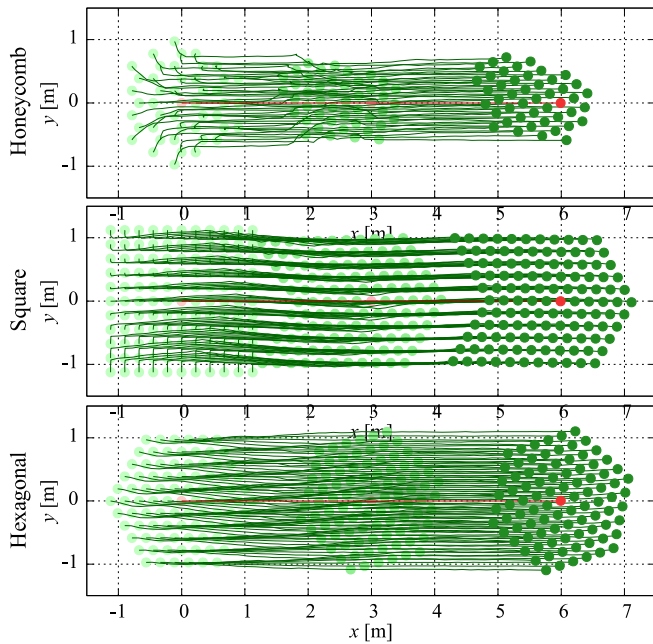ing collective movement. The robot swarm consists of a standard formation with five layers and moves in a straight 3 m line.

Figure 8 shows the movement trajectories of the robot swarm in standard formations with each lattice. The robot swarms arranged in honeycomb and square lattices devolved into a hexagonal lattice, while the robot swarm already arranged in a hexagonal lattice did not deform, as it was already in the highest-density state. These results mean that the angular potential applied in this paper maintains these regular latticed structures.

4.3. Evaluation of the scalability of the demonstrated formations

We demonstrated collective movement using robot swarms with a ten-layer swarm. We subsequently verify that the proposed method can provide scalable control by quantitatively evaluating the structural changes of the lattice structure during movement. To quantify structural change in the new potential, we combine the angle and distance errors between inter-neighbor positions during movement as follows:

$$
\begin{cases}
e_a & = \dfrac{\sum_i^N \sum_j^{N_i} \| \sin^{-1} \sin(L\theta_{ij} - l_i\pi)\|}{2LNN_i} \\
e_d & = \dfrac{\sum_i^N \sum_j^{N_i} \|r_{ij} - r_0\|}{2NN_i}
\end{cases}
\tag{5}
$$

where e_a is the angular error from the $l_i\pi$ direction, and e_d is the distance error from r_0, where $f^D(r_0) = 0$. These two metrics average values over all N robots in the swarm.

Figure 9 shows the average errors and their deviations during collective movement, with formation size varying in the demonstration from one to seventy layers. The overall result did not show any error divergence caused by lattice structure collapse, because these errors are both much smaller than the angles $\pi/12$, $\pi/16$, and $\pi/24$ [rad] that can be created by the angular potential for honeycomb, square, and hexagonal lattices, respectively, and the distance r_m [m], the radius with the greatest distance potential attraction where $f_i^{D\prime\prime}(r_m + r_0) = 0$. Where the number of robots is small, these values do not give accurate averages and are noisy. Thus, these series showed notably small values at small scales.

In line formations, robots have neighbors in chains for angular and distance comparisons regardless of the lattice type. That is, hexagonal, honeycomb, and hexagonal lattices all form a line. First, the distance errors changed with a similar magnitude regardless of the lattice structure used, because the proposed method applies the same distance potential to all latticed structures. In contrast, the angular errors were the largest for the honeycomb lattice and the smallest for the hexagonal lattice. This result means that the angular potential has a different performance depending on the lattice, as noted in the demonstration. The proposed angular potential has a convergence period based on the number of neighbors, L, to ensure that angular convergence occurs according to the angular properties of the lattice structures. Using this design, the convergence range of the angular potential is inversely proportional to L. Therefore, the angular potential of the honeycomb lattice has a wide convergence range while the hexagonal lattice has a narrow convergence range. To achieve the same shape-maintaining performance on all lattices, we should improve the angular potential to ensure that it works regardless of the lattice structure in question.

4.4. Limitations of the proposed method

In Figure 7 and 9, the entire robot swarm held formation. However, the swarm propagates local angular and distance errors to followers in subsequent layers. Therefore, the formation of the robot swarm should arrange the robots radially to ensure that the structural changes caused by the leader movement propagate quickly along the shortest possible route. The robot swarms used in this study, designed for practical applications, satisfy this requirement. To test the importance of radial error propagation, we consider collective movement under spiral formations that do not arrange robots radially. The followers in this formation were physically placed near the robots closer to the center. However, they only detect structural changes through neighbors in the spiral chain and ignore radial neighbors. Therefore, followers will have difficulty maintaining their shape owing to long delays when detecting structural changes in the formation. This study simulates the movement using spiral formations constructed with each lattice structure, as shown in Figure 10.

The robots arranged in a spiral pattern moved from left to right. Followers close to the leader maintained their structure, while followers on the outer periphery at higher layers experienced structure collapse. As expected, the proposed method could not maintain spiral formations in latticed structures. This limitation is unimportant for transportation and sweeping applications, because these applications rely on close packed lattice formations, rather than long-delay spiral formations. However, we will improve the proposed method to ensure robot swarms can be controlled with long delays in detecting structural changes, such as spiral formations for other applications.

under various formation sizes regardless of formation lattice and scale, reacting to the movement of the swarm leader. The host system can lead a scalable robot swarm from a single robot using the proposed method of leader-follower control. Therefore, the system can distribute control to multiple robot swarm systems in various use cases, such as parallel transportation and environmental exploration. This approach allows robotic swarm systems to obtain higher resolution and larger scales. This approach can contribute to the flexible operation of robot swarms while reducing economic cost.

Figure 9: Angle and distance deflections during collective movements in various formations and lattices
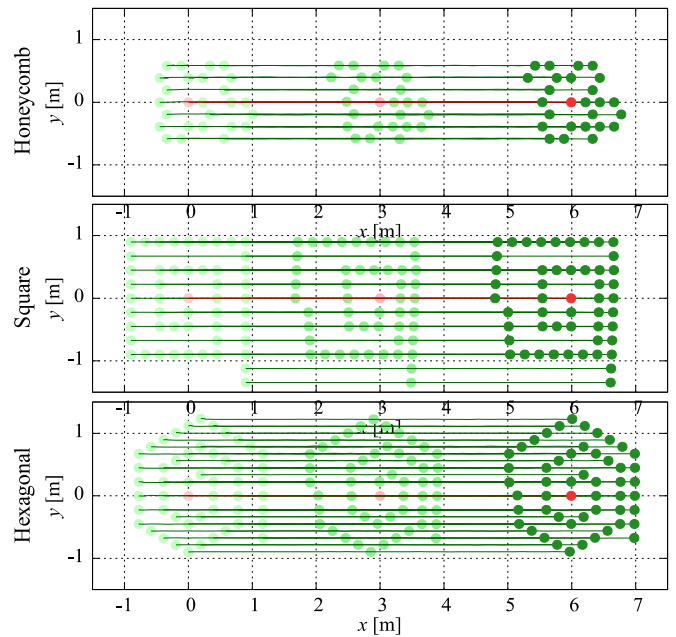
Figure 10: Movement trajectories of robots during collective movement in a straight line using spiral formations with long delays in the propagation of the movement information

5. Conclusion

Robotic cooperation and coordination is essential for a swarm robotic system when transporting long, large, heavy objects and observing over a wide area. Robots can efficiently complete these tasks by using a swarm with a suitable density for the task. Therefore, this paper proposed a structure-maintaining potential that can control swarm formations in regular tessellations and a collective movement method for a robot swarm using leader-follower control with a host system whereby an operator can handle the entire swarm as a single, large, and mobile robot. This study confirmed that the proposed method could maintain a structure with different densities during collective movement with four formations. The swarm control was evaluated and verified

In future work, we will develop autonomous collision avoidance and navigation for multiple robot swarms with different scales instead of multiple mobile robots in parallel distributed systems. We improve the proposed method to control even slow propagating formations of structural changes. In addition, the proposed method targets omnidirectional agents such as Omni-wheeled vehicles and multi-copters. Therefore, it does not consider nonlinear dynamics such as nonholonomic constraints. To implement this method on robots with various dynamics, we will develop a method that dynamically shares the direction of movement.

Acknowledgment

References

[1] M. Schranz, M. Umlauft, M. Sende, W. Elmenreich, "Swarm Robotic Behaviors and Current Applications," Frontiers in Robotics and AI, **7**, 2020, doi:10.3389/frobt.2020.00036.
[2] J. Wiech, V. A. Eremeyev, I. Giorgio, "Virtual spring damper method for nonholonomic robotic swarm self-organization and leader following,"

Continuum Mechanics and Thermodynamics, **30**(5), 1091–1102, 2018, doi: 10.1007/s00161-018-0664-4.

[3] Y. Kambayashi, H. Yajima, T. Shyoji, R. Oikawa, M. Takimoto, "Formation Control of Swarm Robots Using Mobile Agents," Vietnam Journal of Computer Science, **6**(2), 193–222, 2019, doi:10.1142/S2196888819500131.

[4] F. Dai, M. Chen, X. Wei, H. Wang, "Swarm Intelligence-Inspired Autonomous Flocking Control in UAV Networks," IEEE Access, **7**, 61786–61796, 2019, doi:10.1109/ACCESS.2019.2916004.

[5] J. Cheng, B. Wang, "Flocking Control of Mobile Robots with Obstacle Avoidance Based on Simulated Annealing Algorithm," Mathematical Problems in Engineering, **2020**, 2020, doi:10.1155/2020/7357464.

[6] A. Casteigts, J. Albert, S. Chaumette, A. Nayak, I. Stojmenovic, "Biconnecting a network of mobile robots using virtual angular forces," Computer Communications, **35**(9), 1038–1046, 2012, doi:10.1016/j.comcom.2011.09.008.

[7] T. Yan, X. Xu, Z. Li, E. Li, "Flocking of Multi-agent Systems with Un- known Nonlinear Dynamics and Heterogeneous Virtual Leader," International Journal of Control, Automation and Systems, **19**(9), 2931–2939, 2021, doi:10.1007/s12555-020-0578-3.

[8] A.D. Dang, H.M. La, T. Nguyen, J. Horn, "Formation control for autonomous robots with collision and obstacle avoidance using a rotational and repulsive force–based approach," International Journal of Advanced Robotic Systems, **16**(3), 2019, doi:10.1177/1729881419847897.

[9] A.M. Parrany, A. Alasty, "Introducing shell formation and a thermodynamics-inspired concept for swarm robotic systems," Robotics and Autonomous Systems, **148**, 2022, doi:10.1016/j.robot.2021.103939.

[10] Q. Wang, H. Zhang, "A Self-Organizing Area Coverage Method for Swarm Robots Based on Gradient and Grouping," Symmetry, **13**(4), 2021, doi:10.3390/sym13040680.

[11] A. Ekblaw, J. Paradiso, "Self-Assembling Space Habitats: TESSERAE design and mission architecture," in 2019 IEEE Aerospace Conference, 1–11, 2019, doi:10.1109/AERO.2019.8742122.

[12] P. Swissler, M. Rubenstein, "FireAnt3D: a 3D self-climbing robot towards non-latticed robotic self-assembly," in 2020 IEEE/RSJ International Conference on Intelligent Robots and Systems (IROS), 3340–3347, 2020, doi:10.1109/IROS45743.2020.9341116.

[13] Z. Yang, Z. Fu, G. Yu, J. Fei, H. Zheng, "A self-repairing approach for the M-Lattice modular robotic system using digital hormone model," Robotics and Autonomous Systems, **97**, 1–15, 2017, doi:10.1016/j.robot.2017. 08.001.

[14] J. W. Romanishin, K. Gilpin, D. Rus, "M-blocks: Momentum-driven, magnetic modular robots," in 2013 IEEE/RSJ International Conference on Intelligent Robots and Systems, 4288–4295, 2013, doi:10.1109/IROS.2013.6696971.

[15] A. V. Le, R. Parween, R. Elara Mohan, N. H. K. Nhan, R. Enjikalayil Abdulka- der, "Optimization Complete Area Coverage by Reconfigurable hTrihex Tiling Robot," Sensors, **20**(11), 2020, doi:10.3390/s20113170.

[16] K. Yamagishi, T. Suzuki, "Collective Movement Method for Swarm Robot based on a Thermodynamic Model," International Journal of Advanced Computer Science and Applications, **8**(11), 2017, doi:10.14569/IJACSA.2017. 081163.

[17] P. Bannur, P. Gujarathi, K. Jain, A. J. Kulkarni, "Application of Swarm Robotic System in a Dynamic Environment using Cohort Intelligence," Soft Computing Letters, **2**, 2020, doi:10.1016/j.socl.2020.100006.

[18] T. Kida, Y. Sueoka, H. Shigeyoshi, Y. Tsunoda, Y. Sugimoto, K. Osuka, "Verification of Acoustic-Wave-Oriented Simple State Estimation and Application to Swarm Navigation," Journal of Robotics and Mechatronics, **33**(1), 119–128, 2021, doi:10.20965/jrm.2021.p0119.

[19] A. Gutierrez, A. Campo, M. Dorigo, J. Donate, F. Monasterio-Huelin, L. Mag- dalena, "Open E-puck Range Bearing miniaturized board for local communication in swarm robotics," in 2009 IEEE International Conference on Robotics and Automation, 3111–3116, 2009, doi:10.1109/ROBOT.2009.5152456.

[20] N. Yu, A. A. Polycarpou, "Adhesive contact based on the Lennard–Jones po- tential: a correction to the value of the equilibrium distance as used in the potential," Journal of Colloid and Interface Science, **278**(2), 428–435, 2004, doi:10.1016/j.jcis.2004.06.029.

[21] M. K. Heinrich, M. D. Soorati, T. K. Kaiser, M. Wahby, H. Hamann, "Swarm robotics: Robustness, scalability, and self-X features in industrial applications," it - Information Technology, **61**(4), 159–167, 2019, doi:10.1515/itit-2019-0003.

[22] K. Huang, J. Chen, J. Oyekan, "Decentralised aerial swarm for adaptive and energy efficient transport of unknown loads," Swarm and Evolutionary Computation, **67**, 2021, doi:10.1016/j.swevo.2021.100957.

[23] A. S. Matveev, P. A. Konovalov, "Distributed reactive motion control for dense cooperative sweep coverage of corridor environments by swarms of non-holonomic robots," International Journal of Control, 1–14, 2021, doi:10.1080/00207179.2021.2005258.

Advantages of 3D Technology in Stereometry Training

Penio Lebamovski[*]

Bulgarian Academy of Sciences, Institute of Robotics, Sofia, 1000, Bulgaria

ARTICLE INFO

ABSTRACT

This paper presents a new software for stereometry training. Its name is StereoMV (Stereo Math Vision). It is results from a dissertation work on the topic "Stereoscopic Training System". It introduces virtual reality systems that are both immersive and non-immersive. The difference between them is in the equipment and the stereo effect they offer. A comparative analysis is performed between the virtual environments that are part of the software. 3D visualization is of four types: traditional, 3D active, 3D passive, and through immersive systems such as CAVE (Cave Automatic Virtual Environment) and HMD (Head Mounted Display). There are also four visualization modes in Java3D. Mixed Immediate Mode is used to implement stereoscopic projection using 3D active technology. Passive technology uses anaglyph glasses with a red and blue filter. Traditional visualization can be implemented from any computer. The system's most important function is exporting the objects in a file with the extension .obj. All this is thanks to a Java 3D library and a new boundary method involved in generating geometric objects, which sets the program apart from existing software solutions for training in the discipline of stereometry. The software can be used for stereo visualization of random 3D models from various scientific fields. Unlike planimetry in stereometry, a three-dimensional drawing would be much more difficult to understand, and that's why 3D technology comes to the rescue. This way, the student's interest will be strengthened, from where their spatial thinking will be further developed.

1. Introduction

"This paper is an extension of work originally presented in conference 2021 International Conference Automatics and informatics [1]".

One of the fastest-growing areas of the modern world is 3D technology, which in recent decades has found application in almost all spheres of society, including education. What until recently looked like science fiction is a reality today. The principle of 3D visual stereo is based on binocular parallax. One of the most important features of 3D technology is making the invisible/visible and the inaccessible/accessible. By means of it, new concepts are learned and higher levels of concentration are showed. The introduction of 3D systems in the education of the Republic of Bulgaria is currently hindered by many objective reasons, such as the lack of high-tech infrastructures and standards, as well as the insufficient awareness of potential consumers about the benefits of the new technology. These limitations can be overcome in the near future. Despite the constraints, experts predict the active introduction of 3D systems in secondary and higher education, and the first steps in this direction have been taken. The use of these systems in education will lead to a paradigm shift in how people view school and university education [2]. The application of this technological innovation in the education sector will improve how pupils and students will acquire new knowledge [3]. Three-dimensional modeling and animation of information will provide teachers with high-quality teaching materials and programs that will help students more easily absorb understand the material studied, increase their motivation and ability to learn large amounts of information.

Nowadays, solid knowledge is built faster through the so-called digital model, which can be realized through information technology and virtual reality devices [4] . The teacher's choice of appropriate software can become a potent tool in the learning process. In this way, students will be involved in the most innovative way possible to build knowledge. The proposed new software can participate in stereometry training. In contrast to planimetry, a problem arises related to understanding three-dimensional drawing. A large part of the students does not have well-developed spatial thinking. This problem can be solved by using appropriate 3D technology, such as (virtual, augmented, mixed reality, and 3D printing). It is assumed that the greater the immersion in virtual reality, the greater the interest in mathematics on the part of students.

The article aims are to present new software for teaching geometry in three-dimensional space. It is intended for middle and upper middle schools. Virtual environments that can visualize the software are both immersive and non-immersive. The system can export the shapes to a .obj file.

[*]Corresponding Author: Penio Dimitrov Lebamovski; p.lebamovski@abv.bg

2. 3D stereoscopic systems

Stereoscopic systems in a virtual environment are available with and without immersion. Each of them has specific characteristics that distinguish them from the others. Some systems require more money to invest in hardware but at the same time offer a very great experience. These are immersive systems such as CAVE and HMD. Non-immersive systems are desktop computers and can be 3D passive or active technology [5]. In one case, the active virtual environment is presented on a special stereo display, and 3D active (shooter) glasses are required. With passive technology, only a pair of anaglyph glasses is needed. Compared to other environments for VR, immersion is relatively less, but still, good experiences are offered. Their advantage is that they are relatively cheaper. And therefore, they are widely used. That is why they are suitable for application in education in the case of training in streometry.

3. Softwares for training in stereometry

After a study in European and Bulgarian education regarding the use of dynamic software in mathematics classes, it was found that the following programs have been used so far: Geogebra, Dalest, and Cabri3D. Thanks to these software solutions, students become engrossed in the presentation and study of mathematics material. The programs help the student to develop his spatial imagination and logical thinking and to accumulate new knowledge and skills. GeoGebra is an interactive program designed to learn and teach algebra, geometry, and statistics from elementary school to university. The program can work in many modes, such as a mode for 2D graphics i.e. planimetry, and a way for 3D graphics - stereometry, at the same time, there is also a mode for algebraic calculations related to the mentioned sections of geometry. The DALEST software project results from the joint work of five European universities: Cyprus, Great Britain, Portugal, Greece, and Bulgaria. The project aims to create dynamic 3D software for young people learning stereometry in middle school for young students. The CABRI 3D software system allows the construction of geometric figures in three-dimensional space and manipulations with them. The main functions of CABRI 3D and GEOGEBRA are constructing lines, surfaces, and 3D figures; translation, inversion, rotation, sections; polyhedra constructions, etc. Of the three considered software for training in the discipline of stereometry, only one of them has the possibility of implementing stereoscopy through anaglyph projection through passive 3D technology, and that is the GEOGEBRA program. The softwares uses trigonometry and the extrusion technique to construct geometric figures (polygons, prisms and pyramids) and rotational bodies. CABRI 3D and GEOGEBRA use an advanced traditional method, which is again based on trigonometry, to construct the geometric objects. An essential part of programming is regular polygons. On their basis, the complex polyhedra as prism and pyramid are constructed. As is well known, they are the basis of the geometry discipline in secondary school. The traditional way of creating them is based on trigonometry (sine, cosine, and radius). Several vertices and radius characterize them. This paper presents a new method for generating a regular polygon. It defines them by the number of vertices and the length of the side. The traditional way to create a polyhedra is by extruding a polygon defined by a radius. Here, extruding is the most used technique in 3D programming, and it is not appropriate to use when constructing geometric figures studied in mathematics. In this way, meaningful information about the vertices of the geometric body is lost. Therefore, thanks to the new method, the geometric objects are mathematically more accurate since they do not use the mentioned technique.

4. Extrude/sweep 2D graphics

One of the main techniques in 3D programming to create 3D models is extruding 2D and 3D graphics. Various arbitrary objects can be formed with it. It is usually applied to curves and polygons. The idea is that through a certain movement, such as (rotation, translation, and trajectory defined by an arbitrary curve) a complex geometric construction can be generated. Math software uses this technique in developing stereometric figures. A regular hexagonal prism generated by the traditional method is shown in Figure №1. The base is a polygon with 6 vertices and a radius equal to 2. The volume body is created by planar sectioning and setting a rule in the case of prism extrusion by translation. The diagram Figure №2 shows how the stereo system visualizes a regular polygon with new method without extrusion. First, it is necessary to enter input data, such as the number of vertices and side lengths. Here, the side length parameter is the same for each polygon. The values of parameter I vary between (3, 4, 5 and 6). Each shape is drawn using coordinate arrays. The values of the vertices are of type double. They were followed by visualization of the figure and calculating the perimeter and face.
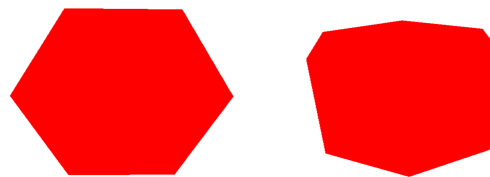
Figure 1: Traditional method and prism

5. Methods for stereoscopic visualization

The principle of 3D visual stereo is based on binocular parallax. The two images with parallax information are used, each of the images being seen by the corresponding eye, resulting in different incarnations. There are two methods to distinguish it [6]: First one with the help of display, and second one with stereo glasses.

6. 3D stereoscopic Display

3D stereoscopic displays are classified into two categories depending on the equipment:

1. Autostereoscopic, which does not require additional equipment to generate a 3D stereo image.
2. Stereoscopic displays: These are assisted by other devices.

In stereoscopic displays, the 3D image is obtained from two different images for the left and right eyes, respectively [7]. The two images are similar, with a slight offset from each other. The beginning was given in the 20s of the last century, mainly in films,

cinema halls, and television. Nowadays this technology already has a mass application, for example: in education and video games. Stereoscopic 3D technologies are divided into active (LC liquid crystal) and passive (anaglyph and polarizing). Anaglyph technology uses two color-filtered images and relatively inexpensive glasses. The colors that are commonly used are: red-cyan, red-green and blue-red. With this system, no additional equipment is needed. It is enough to have a pair of anaglyph glasses. The main disadvantage of anaglyph glasses is that a lot of colors can be lost. The active (shooter) system is a 3D stereoscopic technique that sends the left image to the left eye and the right image to the right eye, respectively [7]. One of the most used immersive 3D systems is the HMD (Head Mounted Display) virtual helmet [7]. This is a device that is mounted on head, with a small optical display in front of each eye. The virtual helmet is used in various virtual and augmented reality applications. It is easy to operate and can be installed on any platform. This system consists of two optical parts: an input and an output pair [7]. The first pair magnifies the image on the microdisplay, while the outer pair projects the color image to the viewer. II (integral imaging display) This type of display offers 3D imaging without needing additional glasses or tracking devices. In recent years II has attracted much attention from many researchers due to its full color moving 3D imaging full parallax, which sets II apart from other 3D display technologies [7]. Volumetric display is used and developed to present 3D volumetric or animated images in space. This technology is mostly used in military, medical, and academic applications.

Figure 2. Diagram of polygons: new method

7. 3D Technology

The stereoscopic vision techniques that are part of the proposed new software are: HMD, active glasses, passive glasses (anaglyph) and CAVE (Cave Automatic Virtual Environment). There are several options for visual stereo. The first one uses the so-called active glasses, which alternate between the eyes in sync with the monitor. Stereoscopic perception requires each eye to receive a separate view of the scene. The view should be at a different angle and by according to the position of the head. The distance between the eyes is called interocular distance. The second way to generate stereoscopic objects on stage is by having two serial and different monitors [8]. This is precisely the way the HMD is ready to work, as each eye has its monitor. Here again, each eye has a different view, but there is no switching between the eyes and the two monitors are constantly on [8]. The display with which the three-dimensional perception is visualized is of two types: head-mounted or room mounted [8, 9]. Most displays are single screens without head tracking. Such systems are the simplest forms of room-mounted displays. In the case of the HMD, the screens are attached to the head (i.e. when the head moves, the screens follow it). There are several options for visual stereo. The first uses the so-called Head tracking that allows head movement instead of the standard mouse, joystick, keys, and other controllers.

7.1. HMD vs Screen

The full view specification can be divided into two parts, namely the view position and the view volume [8, 9]. Here it is necessary to calculate two matrices depending on the specification. When using the HMD, the camera needs to depend on the movement of the head, so that when the user's head moves and rotates, the 3D view moves together with it. It is important that the relationship between the eyes and the screen don't mustn't change. Therefore, the projection matrix remains constant [9]. When using room-mounted, the movement of the head changes the projection matrix but does not control the camera. This is a problem when watching stereo. With room mounted it is not necessary to use head tracking unless we are in stereo mode. Appearance settings depend on the location and orientation of the eyes. If the user's head changes position, the view also changes [9]. Dynamically recalculating the projection matrix and the view matrix is a very annoying task. Java allows tracking and supports features for automatic head tracking [8]. Where the view is considered a camera. A projection matrix represents the section definition. A visual matrix represents the position of the view. The first of the matrices are defined in the coordinate system, where the eye is located at the beginning of the view to the negative direction of the application z-axis (applicate) and up to the ordinate. On the other hand, in the view/camera, the eye is located at the beginning, looking down at z and up at y.

7.2. 3D Active, Passive and Immersion Systems

Anaglyph technology does not require expensive equipment, unlike 3D active technology. Here the user must be equipped with only one pair of glasses. The colors most often used are red for the left eye and blue for the right [10]. This projection is most often used when viewing magazine photos. The idea is to filter the
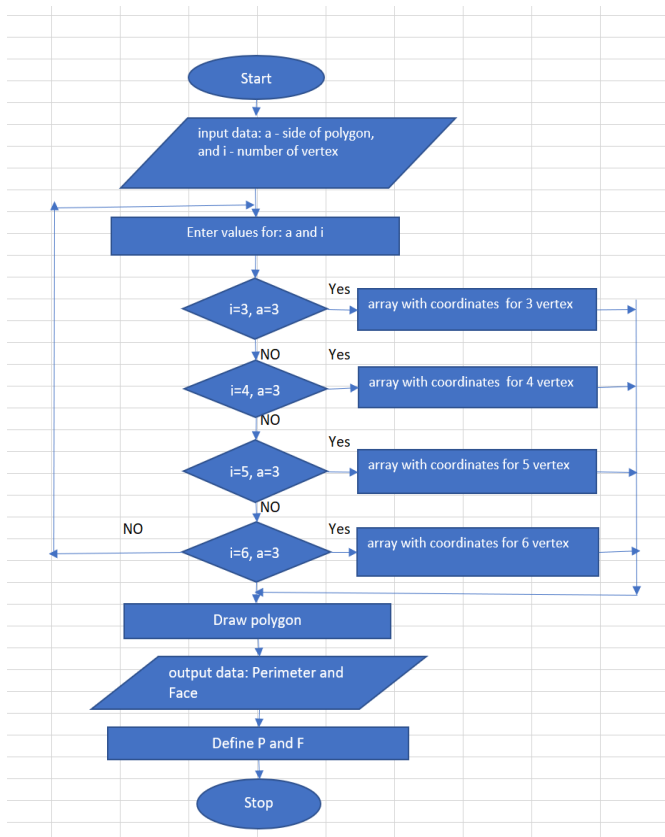
eye images based on color. The second technique requires two monitors for each eye to generate a stereo image. Here, as in the first technique, each eye must receive a certain image. The virtual reality helmet - HMD - works on such a principle. The difference between the two techniques is user interaction. How interactivity is carried out through the helmet is similar to non-immersive systems: through a mouse, joystick, keyboard, etc. The main feature that differs between the two systems when interacting is "Head Tracking" - a 6DoF device (six degrees of freedom) that offers 3D information in the form of location and orientation. In this way, a higher-level interaction is performed, offering a relatively more significant emotional effect on the part of the average user. The stereometry software proposed in this article can be implemented by immersive and non-immersive virtual reality devices, such as 3D active (shooter technology), 3D passive (anaglyph), and immersive systems (CAVE, HMD). With active technology, frames are alternated sequentially, first for one eye and then for the other [11]. The frequency of these frames is usually 120 Hz, 60 Hz per eye [11]. For the structure to be perceived by the viewer, special active glasses are used, which darken the glass of the eye which doesn't have to see the frame that was displayed. Here, darkening alternate first in one eye and then in the other. The use of a synchronization device is also required. One of the systems that offer the most excellent immersive effect is the CAVE system. In this 3D technology, the projectors are placed between the walls of a cube-shaped room. As with the active technique, the user must use glasses[5, 12].

8. Java stereoscopic mode

In Java3D, rendering modes are four in number **Table1**, and choosing a particular mode becomes very easy [9]. It is recommended that the programmer sticks to the first two modes.

8.1. Retained mode

This is the default rendering mode. The application remains in a continuous rendering state in this mode unless the method Canvas3D.stopRender of Java3D API (Application Programming Interface) is called. Also, in this mode, Java3D rendering will build a structure for handling geometry and operations related to 3D transformations[9].

8.2. Compiled Retained mode

Bitwise assignment in Java is one of the most confusing operations [9]. The following can be given as an example:

TransformGroup tg = new TransformGroup(); tg.setCapability(TransformGroup.ALLOW_TRANSFORM_WRITE); It should also be noted that there is a reference relationship between the classes: TransformGroup and Switch. These two classes can only be used in the first two modes and partially in the fourth mode. This is one of the main differences, which is not unimportant. The second mode gives Java the freedom to perform many optimisations. The most important of which are scene graphics compression and geometry grouping. This mode requires calling the compile() method of BranchGroup; this method optimizes the graph itself by grouping and sorting [9]. Another significant difference between the two modes is grouping, which is an advantage when there are many figures on the scene.

8.3. Immediate mode

Immediate mode - in this mode, applications intended for users have more freedom, which is at the expense of performance. This mode provides great flexibility, however rendering is at the lowest level when using it. A programmer using this mode only wants to take advantage of the geometry classes[9]. The first two modes (compression of geometry, grouping of geometry, and scene graph are more highly developed than the third.

8.4. Mixed mode

The fourth mode allows mixing the first two with the third mode. The mixed mode preserves the continuous rendering from the first two modes. For realization of the system is used this mode.

9. 3D printing and .OBJ file

3D printing, also known as additive manufacturing, creates three-dimensional solid objects corresponding to a given digital file. In this process, the object is created through successive layers of material until the 3D model itself is generated [13]. Each layer is a thinly sliced horizontal section of the object [13]. Before getting to the actual printing of the three-dimensional shape, it is necessary to go through the following steps.

1. Virtual design of the object, through a 3D modeling program (for a new object), through a 3D scanner (when an existing object needs to be copied) or, in this case, through the stereoscopic system.
2. The next step is to export to a .obj file
3. In the end, add to the printing device.

Table 1: Java 3D stereo Mode

Render stereo mode	Canvas3D	Stereo type
Retaind mode	*Canvas3D*	*Active3D*
Compiled – retained mode	*Canvas3D BranchGroup.compile()*	*Active3D*
Immediate mode	*Canvas3D.stopRenderer()*	*hybrid*
Mixed Immediate mode	*User Canvas3D: preRender(), postRender(), postSwap() and renderField()*	*Active3D*

Today, digitizing a real object into a 3D model becomes as easy as, for example, taking a photo. To prepare the .obj file for printing, the software slices the final model into hundreds of horizontal layers [13]. Next is uploading the 3D file to the printer; the object is created layer by layer [13]. The device makes the object by blending the layer. There are different types of technologies for working with 3D printing. One of the most used formats for storing polygon mesh information is the .obj format. One file can store data about indexed walls, normal vectors, and texture coordinates. The required data is stored in text format and

can be edited using a text editor, for example, Notepad. Each line contains the following characters: • "v" - vertices • "vn" – normal vector • "vt" – for texture • "f" – for the faces. Next comes the setting of specific values. Each of the sides is formed based on a triangle and a quadrilateral as shown on Figure 6 and Figure 7 . The row data for each wall contains a description of the vertices that make up the wall by specifying the vertices. Depending on the primitive being used.

10. Results

The software presented in this article, named StereoMV runs under Windows operating system. The object-oriented programming language Java, and more specifically, the Java3D library, was chosen as the means of implementation. The software interface uses JDK (Java Development Kit) version No. 8. This article presents 3D technologies that can be involved in teaching the discipline of stereometry, which is a branch of geometry in three-dimensional space. Besides the fact that technologies are divided into systems with and without immersion, they can be divided into two more groups: room-mounted and head-mounted. The main parameters of the stereoscopic system are:

• Software functionality

Two types of geometric figures are studied in the study of stereometry in secondary school:

1. Ribbed geometric figures – polygon, prism, cube, parallelepiped, and pyramid
2. Rotational bodies – cone, sphere, torus, and cylinder

The stereoscopic system can generate both types of geometric objects using the new boundary method for the first objects. For rotary bodies, the traditional extrusion method is used translational (cone and cylinder) and rotational (sphere and torus). The new program enables objects to be presented in three ways:

1. Transparent - makes it possible to understand the body's geometry, such as information about vertices, sides, angles, and polygons.
2. Solid – this presentation gives the finished look to figure
3. Mesh and solid body can be combined at the same time. It is possible to paint the walls of a polyhedra in different colors.

The program can perform algebraic calculations, such as finding faces, volumes, polygon side length, and more. This is made possible by a numerical calculation mode. Geometric objects can be viewed in different ways: 1. Traditional visualization 2. Full screen 3. Stereoscopic visualization (anaglyph, active, HMD, CAVE) 4. Mode for development of geometric objects

• Additional opportunity and contribution

Thanks to a new boundary method for generating geometric figures and a Java 3D library, it is possible to add additional features that are missing in stereometry software. For example, visualization can be given through virtual environment systems. StereoMV's most significant contribution is that it can convert geometric objects into a .obj file for printing or adding to an augmented or mixed reality device. The software enables arbitrary

3D models to be visualized through immersive and non-immersive virtual reality systems.

• Technical means for the realization of the stereo system

To operate with the system: VR systems are available with and without immersion. They differ in different ways from each other. For those whose stereo effect is relatively more minor, the following equipment is required: a special video card, such as NVIDIA QUADRO. Powered 3D monitor and glasses, as well as a projector. With passive technology, only a pair of anaglyph glasses are needed. Immersion systems require much more funds to invest in equipment, but simultaneously allow for great exciting experiences, unlike non-immersion systems.

• Objects for stereo visualization

The main Java3D API class that can be used to construct stereometric figures that are part of a stereo system is Shape3D, which defines the geometry and appearance of polyhedra and solids of rotation objects. In programming, these objects are called Java Nodes. A stereoscopic system can convert them to a .obj file. When developing the system in a program, it is necessary to have two methods: one creates the geometry, and the second the visualization.

• The stereoscopic system StereoMV

The core Java3D API class that enables stereo rendering via immersive and non-immersive systems is Canvas3D. It represents the canvas where objects from three-dimensional space are visualized. In Java3D, there are four modes for stereo visualization using active technology. The system uses Mixed Immediate Mode. The drawing of stereometry objects (edges and solids of rotation) are in Immediate mode, while static objects are in default mode, for example (app background, the three-dimensional coordinate system, the geometric network, axis and vertex labels. The createSceneGraph() method adds the objects that are part of the default mode. The geometric figures are in a class inheriting Canvas3D in which the mentioned four methods are added in Table №2.

• Appearance and mathematical description of geometric objects

In Java3D, several basic primitives can be used to construct complex geometric shapes, such as those from stereometry. When creating, for example, polyhedra such as a pyramid and a prism, it is necessary to traverse them in the same direction: clockwise or counter-clockwise.

LineArray – this array allows the creation of a mesh body by connecting a sequence of vertices. Here, the definition of a pair of vertices and topology is necessary.

TriangleArray – this array enables the construction of polygons that are formed by triangles. A sequence of triangles can generate any regular polygon. Here a sequence of three-vertex polygons is set, and the topology is defined.

QuadArray - objects are created using quadrilaterals. Arrays with four-vertex sequences and topology are defined.

In the results described in this article for constructing a quadrilateral prism - in this case is used all three types of primitives are used. The Appearance class from the Java3D API is used for object visualization. With its help, the following characteristics can be determined: color, type, and transparency of the considered primitives. The class using which the .obj file is generated is Geometryarray. It is possible to rebase the .obj file into a Shape3D object using the mentioned class. It is necessary to use an array of values of the vertices of the geometric figure. To generate a quadrilateral prism, the article uses only the information about the vertices and the primitive, which is used in the case of a triangle and a quadrilateral. The values are set using the COORDINATES parameter. If it is necessary to add more information to the creation of the .obj file, such as normal and texture ie "vn" and "vt" two more parameters -NORMALS and TEXTURE must be defined to the program code. Thanks to the normal, it is possible to color the objects with a specific color using a material. Here there are some crucial parameters, with the help of which the coloring is performed: ambient, emissive, specular, diffuse, and shininess. For the first four, the values range between 0 and 1. Based on these primitives, 3D geometric models (polygons, polygons, and surfaces based on curves) are constructed using a programming language or a 3D modeling program.

- Implementation of 3D active and passive technologies

For the realization of the 3D passive technology through the new stereoscopic system, it is necessary to do the following:

1. In the renderField() method, adding two identical geometric shapes with a slight deviation from each other. This is done as for the dynamically changing figures in Immediate Mode. Likewise, for static objects that are in retain() mode.

2. Next is setting the appearance for the two objects in blue and red, respectively

3. Finally, transparency is set, which varies between 0 and 1. The user can specify both the object's transparency and offset, representing the stereo effect. This will be done using a slider.

About 3D active Technology: In this technology, the two stereo images are created using the video card and the monitor. For this reason, a stereo effect cannot be defined here via an interface. It is set in advance by the stereo system developer, with values for the left and right eye, respectively: -0.01 and +0.01. It is possible to change the color of the system background through the interface. The background is white by default when the user is in traditional rendering mode. While in passive and active technology, the color is black. The goal is to make the objects stand out. Thanks to the Immediate Mode mode, it is possible to change the values of the parameters of the geometric figures using a text field, a slider, and keys. The proposed stereo system can generate, and at the same time visually present, both: java nodes in the case of polygons and polyhedra and files with the extension .obj. This way, arbitrary 3D models from various scientific fields can be visualized using immersive and non-immersive virtual

reality devices. In this way, an accurate and complete picture of the studied object would be acquired. The system can import and export 3D files. Figure № 8 shows a regular hexagonal prism generated using geometry software. The object is represented in three ways: (3D active, 3D passive, and 3D traditional) perspectives. Also presented is a three-dimensional heart model for stereo visualization, downloaded from the following site: https://www.blendswap.com. It is preferable when observing a 3D file that the background offered by a virtual reality system is black. The aim is to make the model stand out in this way.

The visualization mode used through 3D active technology to implement the stereoscopic system is MixedImmediate. Geometric shapes created using the new boundary method are in Immediate mode. They are called once in the renderField() method. A Table №2 shows the methods for the 3D active technology mode. The most important of the four methods is renderField() - in this method, the 3D geometric objects that will be visualized by 3D active stereo visualization are called. It calls each of the objects that will be in Immediate mode.

A pair of glasses is required to realize 3D passive technology through anaglyph projection. With color, filters are blue and red for the right and left eyes, respectively. Each eye needs to have its own display for implementation through immersive HMD (virtual helmet) technology. For this purpose, two objects of type Canvas3D are created. Unlike planimetry, where the drawing of the geometric figure drawn on a piece of paper or board matches 100% with its original. Drawing the bodies from stereometry makes it very difficult for students, especially those who do not have well-developed spatial thinking. The problem is that the drawing transferred to a board, or a piece of paper can hardly be understood. This is where 3D technology, including (virtual reality, augmented reality, mixed reality, and 3D printing) comes to the rescue. In this way, students' interest in mathematics would be strengthened, and their spatial imagination would be further developed. The stereoscopic system realizes two types of geometric objects, which are studied by stereometry.

1. Edged geometric objects (polygon, prism, and pyramid) as shown on Figure 4 and Figure 5
2. Cylindrical bodies (cylinder, cone, sphere, and torus)

The system enables the geometric object to be presented solid and wireframe. The second presentation will enable the student to understand the object's geometry. At the same time, the dense presentation will allow its finished look. There is also a combination option between the two expressions.

Two methods are used to generate the geometric objects that are part of the stereoscopic system (traditional and new author's boundary method). Both cases aim to generate a regular polygon, which is the basis for drawing the pyramid and prism. The traditional method is based on trigonometry using (radius, cosine, and sine). Characterizes the polygon with number of vertices and radius. The new method defines the polygon by the number of vertices and the side length [14, 15]. It is based on Isaac Newton's method of limits and Cavalieri's indivisibles. It uses only the relation of parallel segments. At the same time, it gives a more accurate result since it is not necessary to use the technique of extrusion and trigonometry involved in generating objects in programming and, in this case, in stereometry. The objects created

in this way allow visualization through an immersive and non-immersive system and their representation as a .obj file. To illustrate the method, a regular hexagon will be considered as an example Table 3 and Figure 3. The same rules apply to polygons with the number of vertices increasing to infinity. The ratio of the parallel segments AB:FC =1:2 is determined, the length of the side of the polygon is represented by the parameter **a**. The regular polygon is placed in the center of the coordinate axis. The value of the height of the trapezoid FCBA is of value **h**. The Pythagorean theorem can determine it for triangle BCH; therefore, BH = a/2*sqrt(3). The height value is involved at four vertices of the polygon in the case of 6 vertices (A,B,D,E), defining values along the "**y**" ordinate (1,2,4,5).

- Prism construction

For the parametric representation of a regular hexagonal prism, it is necessary to do the following. The base is set, a polygon with 6 vertices with the length of the base through the parameter a. The parameter **h** sets the height of the prism. The bottom base is placed in the center of the coordinate axis, from which it follows that the values along the Z axis will be equal to zero. Vertices define the base numbered 1 to 6. The top base has vertices 7 to 12. The height rises along the z-axis. Therefore the values will be different from 0. Additionally, two more parameters h1 and h2 will be added, respectively. With the help of this, an inclined prism can be constructed; if they have a value equal to zero, the prism will be straight. An inclined prism follows at values where one parameter is zero and the other non-zero on Table 4.

Table 2: Java Mixed mode methods

Mixed – mode methods	Pipeline
preRender()	Allow you to prepare any data structures for rendering
postRender()	After 3D rendering operation
postSwap()	Called once the rendered frame has been made visible to the user
renderField()	Useful in stereoscopic imaging.

- Right straight/oblique prism

The algorithm for building a correct straight/slanted prism is as follows:

1. A regular prism is selected from the object panel. The type of the two bases is chosen, which are regular polygons with 3 to 6 vertices.
2. A length value is set for the main edge, then the multiwall is raised along the y-axis to set the height.
3. The abscissa (or Z coordinate) value is checked. If the value is a non-zero number, the final result will be a slanted prism; otherwise, the prism is straight.

The primitives used to generate a regular polygon are a triangle, a quadrilateral, and a line for mesh representation. The .obj file information in the article is based on vertices and walls as shown on figures 6 & 7. The traditional way to color is by setting a material. Thanks to the new boundary method, it is possible to color the walls using the mathematical description of the objects using adjacent vertices expressed by the side length of the polygon and a suitable primitive. A disadvantage of the system is that when generating the .obj file, it is necessary to use a material, i.e., its body is set in one color.

Table 3: Regular polygon

№ vertex	X	Y	Z
1	-a/2	a/2*sqrt(3)	0
2	a/2	a/2*sqrt(3)	0
3	a	0	0
4	a/2	-a/2*sqrt(3)	0
5	-a/2	-a/2*sqrt(3)	0
6	-a	0	0
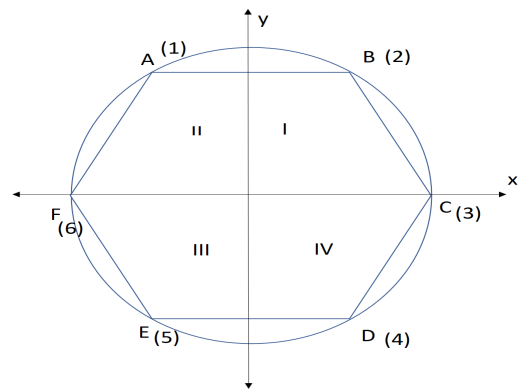
Figure 3: regular polygon with six vertex
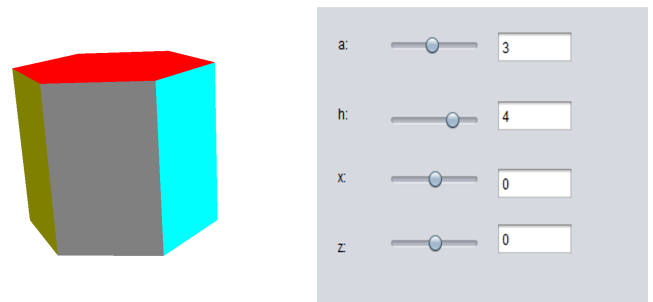
Figure 4: right regular prism
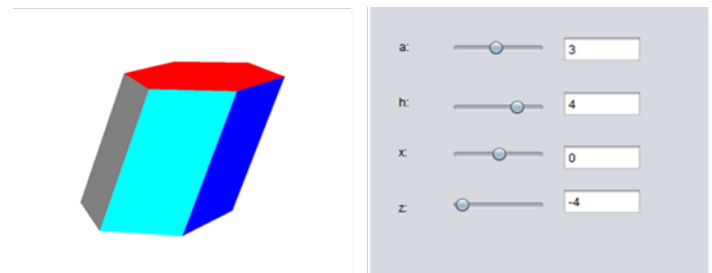
Figure 5: Tilted regular prism

45

```
# StereoMV
mtllib StereoMV.mtl

v 3 4 3
v 1 4 3
v 3 4 1
v 1 4 1
v 3 0 1
v 1 0 1
v 3 0 3
v 1 0 3
f 2 3 4
f 2 1 3
f 8 7 5
f 8 5 6
f 7 1 3
f 7 3 5
f 5 3 6
f 3 4 6
f 4 2 8
f 4 8 6
f 2 1 8
f 1 7 8
```
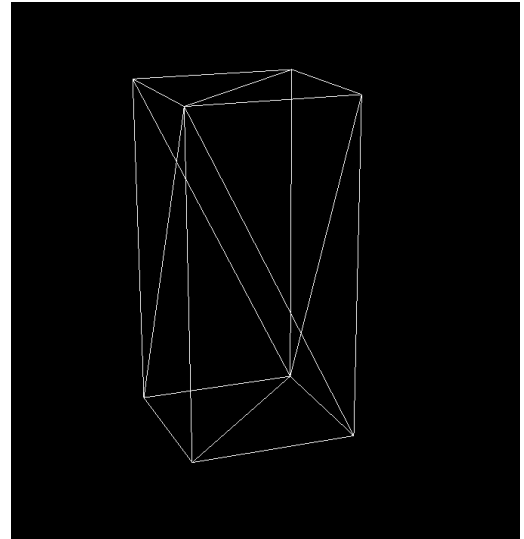
Figure 6: prism generated by primitive triangle

Table 4: Prism

Number of vertex	X	Y	Z
1	-a/2	a/2*sqrt(3)	0
2	a/2	a/2*sqrt(3)	0
3	a	0	0
4	a/2	-a/2*sqrt(3)	0
5	-a/2	- a/2*sqrt(3)	0
6	-a	0	0
7	-a/2-h1	a/2*sqrt(3)-h2	h
8	a/2-h1	a/2*sqrt(3)-h2	h
9	a-h1	0-h2	h
10	a/2-h1	- a/2*sqrt(3)-h2	h
11	-a/2-h1	- a/2*sqrt(3)-h2	h
12	-a-h1	0-h2	h

```
# StereoMV
mtllib StereoMV.mtl

v 3 4 3
v 1 4 3
v 3 4 1
v 1 4 1
v 3 0 1
v 1 0 1
v 3 0 3
v 1 0 3
f 1 3 4 2
f 7 8 6 5
f 1 7 5 3
f 2 4 6 8
f 2 8 7 1
f 3 5 6 4
```
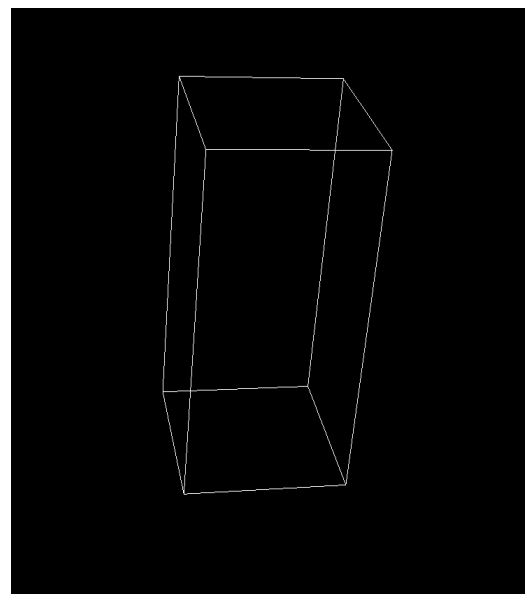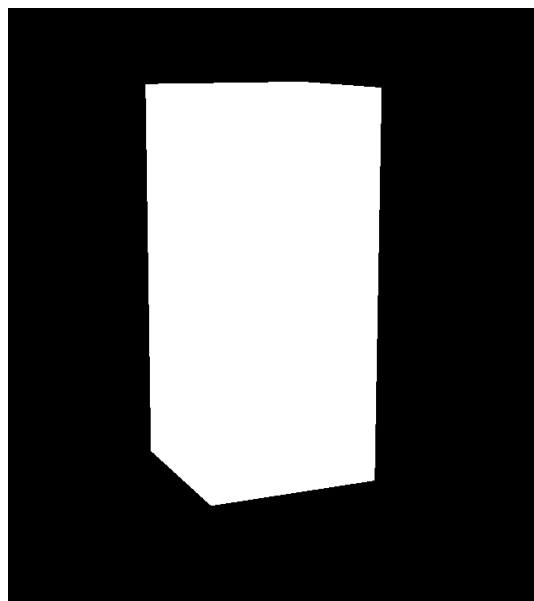
Figure 7: prism generated by primitive quad

(a)3D active   b) 3D traditional   c) 3D anaglyph
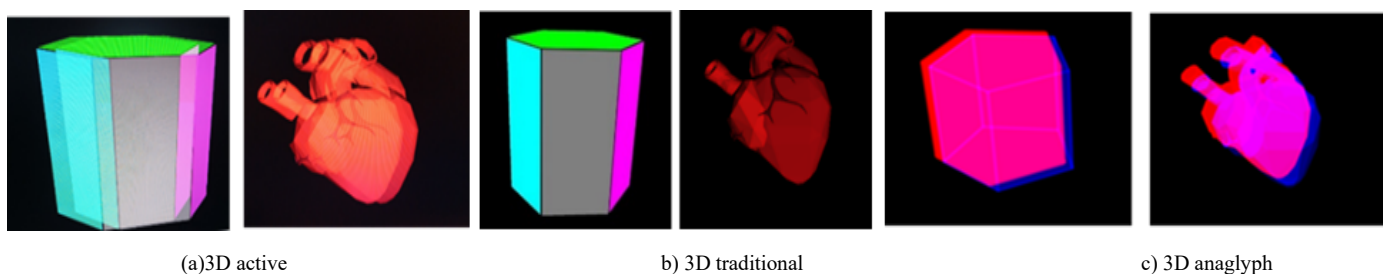
Figure 8: 3D   Visualization

Table 5: Comparative analysis between 3D technologies realized by the new stereoscopic system

Type of Technology	Type of system	Advantage	Disadvantage
3D active/ 3D projector	**Without immersion**	- The colors are preserved - Great stereo effect - Short program code - Applies to .obj and nodes - Easy connection to the stereo system	- The stereo cannot be adjusted - Requires expensive equipment - There may be incompatibility with the video card
3D passive	**Without immersion**	- Applies to .obj and nodes - The stereo can be adjusted with a slider - Does not require expensive equipment	- Does not retain primary colors (blue / red only) - Small stereo effect - Long program code - Difficult to connect to the system
HMD/CAVE	**With immersion**	- The colors are preserved - Very large immersion effect - Applies to .obj and nodes - Easy connection to the stereo system	- They are very expensive - Long program code

11. StereoMV The stereoscopic system

StereoMV is the result of a dissertation work on the topic "Stereoscopic training system". It was originally developed for a non-immersive VR system using 3D active technology. Currently, the system can be visualized by an immersive system – an example being an HMD. A CAVE and semi-submersible FishTank system is also possible in the future. Table №5 provides a comparative analysis of the Virtual Reality systems discussed in this article. So far, the software is not yet finished. But at the same time, it continues to be further developed. The system can be used to visualize trimer models with VR from different domains. It also includes another direction - in medicine—the idea of creating stressful situations through a virtual environment. A mathematical analysis of recordings using a Holter device will be performed [16]. As well as a comparison of the data between recordings made by immersion and non-immersion systems. The goal is to be able to change heart rate and, from there, compare RR intervals to those at rest.

12. Conclusion

As is known, stereometry is a part of Euclidean geometry. Geometric figures are in three-dimensional space. Many students do not have a well-developed imagination to understand three-dimensional geometric objects. For the solution to this serious problem, a new mathematical software called StereoMV is presented in this paper. It allows students to view things in virtual reality. The main contribution of the system is that it can export geometric figures in files with the extension .obj. Then the three-dimensional model can be added to an augmented reality device or printed on a printer. The other innovation is that virtual systems with and without immersion can visualize the system. This will pique the interest of students. Studying the discipline of stereometry will become interesting, valuable, and enjoyable. This article performs a comparative analysis of virtual environment systems. Each of them differs in a specific way from one another. Some require more equipment, and others are relatively cheaper and offer an excellent stereo effect. Prolonged observation on the computer monitor through 3D active glasses can cause discomfort. Autostereoscopic monitors that do not require additional hardware come to the rescue. The Java programming language is used to implement the StereoMV stereoscopic system. Mixed immediate mode for stereo visualization through 3D active technology. Anaglyph projection is used for 3D passive technology with right and left eye color filters (blue and red), respectively. At this stage of system development, the immersive virtual reality that can visualize the software is the HMD (virtual helmet) device via *head* tracking. The system can export the objects in the .obj file extension. To add to a virtual or augmented reality device. As well as for 3D printing.

References

[1] P. Lebamovski, "Analysis of 3D technologies for stereo visualization," in International Conference Automatics and Informatics, ICAI 2021 Proceedings, Varna: 206–209, 2021, doi:10.1109/ICAI52893.2021.9639534.

[2] Y. Lan, "Immersion, interaction and experience – oriented learning: Bringing Virtual reality into FL learning," Language Learning & Technology, **24**(1), 1–15, 2020.

[3] A. Yeh, R. Nason, "Toward a Semiotic Framework for Using Technology in Mathematics Education : The Case of Learning 3D Geometry," International Conference on Computers in Education Melbourne, Australia, 2004.

[4] M. Nikolova, P. Byalmarkova, R. Radoeva, "3D technologies as electronic educational resource 3D technologies as electronic educational resource," 2015(November).

[5] D. Minkovska, "Virtualna realnost – edin nov pogled kam savremennoto obuchenie," **56**(1), 64–72, 2013.

[6] J. Kang, B. Liu, "Application of 3D stereoscopic visualization technology in casting aspect," China Foundary, (August), 308–313, 2014.

[7] N. Kim, M. Erdenebat, "3D Display Technology," ©2013 Old City Publishing, Inc., June, 73–95, 2013.

[8] Y.Liang, H. Zhang, "Computer Graphics using Java 2D and 3D", Pearson Education, 2003.

[9] A.Terrazas, J. Ostuni, M. Barlow, "Java Media APIS: Cross-platform Imaging, Media, and Visualization", Sams, Indiana, 2002.

[10] K. Kerestes, "Making the anaglyph map," 2000.

[11] "3D Технологии - Pro Screens, Oct. 2022", [Online]. Available:http://www.proscreens.eu/bg/3d-technologies

[12] M.G.O. Brien, R.M. Levy, A. Orich, "Virtual immersion : The role of CAVE and PC technology," CALICO Journal, **26(2)**(January 2009).

[13] J.Q. Al-maliki, A.J.Q. Al-maliki, "The Processes and Technologies of 3D Printing," International Journal of Advances in Computer Science and Technology, **4**(10), 161-165, October 2015.

[14] P. Lebamovski, "THE EFFECT OF 3D TECHNOLOGIES IN STEREOMETRY TRAINING," CBU International Conference Proceedings, **202**, 68–74, 2021, doi:10.12955/pns.v2.155.

[15] P. Lebamovski, E. Petkov, "USAGE OF 3D TECHNOLOGIES IN STEREOMETRY TRAINING," CBU International Conference Proceedings, **202**, 139–146, 2020, doi:10.12955/pss.v1.61.

[16] E. Gospodinova, M. Gospodinov I. Domuschiev, N. Dey, A. Ashour, "Nonlinear analysis of heart rate variability in Type 2 diabetic patients," Fractal Geometry and Nonlinear Analysis in Medicine and Biology, **1**(4), 2016, doi:10.15761/fgnamb.1000123.

ASTES

Profiling Attack on WiFi-based IoT Devices using an Eavesdropping of an Encrypted Data Frames

Ibrahim Alwhbi Alharbi[*,1], Ali Jaber Almalki[2], Mnassar Alyami[1], Cliff Zou[1], Yan Solihin[1]

[1]*Department of Computer Science, University of Central Florida, Orlando, 32816, USA*

[2]*Department of Computer Science and Information Technology, University of Bisha, Bisha, 67714, Saudi Arabia*

A R T I C L E   I N F O

A B S T R A C T

The rapid advancement of the Internet of Things (IoT) is distinguished by heterogeneous technologies that provide cutting-edge services across a range of application domains. However, by eavesdropping on encrypted WiFi network traflc, attackers can infer private information such as the types and working status of IoT devices in a business or residential home. Moreover, since attackers do not need to join a WiFi network, such a privacy attack is very easy for attackers to conduct while at the same time invisible and leaving no trace to the network owner. In this paper, we extend our preliminary work originally presented at the CCNC'22 conference by using a new set of time series monitored WiFi data frames with extended machine learning algorithms. We instrument a testbed of 10 IoT devices and conduct a detailed evaluation using multiple machine learning techniques for fingerprinting, achieving high accuracy up to 95% in identifying what IoT devices exist and their working status. Compared with our previous work in , the new approach could achieve IoT device profiling much quicker while maintaining the same level of classification accuracy. Moreover, the experimental results show that outside intruders can significantly harm the IoT devices without joining a WiFi network and can launch the attack within a minimum time without leaving any detectable footprints.

1. Introduction

This paper is an extended version of the paper published in Alyami, Mnassar, Ibrahim Alharbi, Cliff Zou, Yan Solihin, and Karl Ackerman. "WiFi-based IoT Devices Profiling Attack based on Eavesdropping of Encrypted WiFi Traffic." In 2022 IEEE 19th Annual Consumer Communications & Networking Conference (CCNC), pp. 385-392. IEEE, 2022 [1].

The emerging smart infrastructures are integrated with the Internet of Things (IoT) devices and their applications to make daily life easier for individuals and improve the public environment [2]. To this end, IEEE 802.11 Wireless network (WiFi) is a significant development that helps connect a wide variety of IoT devices such as smartphones, smart TV, home automation, intelligent vehicles, surveillance cameras, health monitoring, and many more [3]. The increase in applications increases the attention of attackers that find the loopholes and gain maximum knowledge of users' private in- formation. The connected devices, digital systems, and sensors that play a vital role in people's daily life cause a significant threat of privacy leakage of private information [4]. For example, the

Mirai malware attack, which triggered distributed denial-of-service (DDoS), generates attacks on WiFi-connected IoT devices and ap- plications [5]. Additionally, worms in smart bulbs gave attackers access to all adjacent IoT lights that were compatible [6]. To this end, the infrastructure and IoT applications must incorporate pri- vacy protection during intelligent network design and development phases. Figure 1 shows an overview of IoT ecosystems and relevant scenarios.

Considering the aforementioned privacy threat, this paper focuses on the attacker's ability to fingerprint the IoT devices in the WiFi network. The existing work mostly assumes the attacker is inside the network where the attacker has to either join the network prior to fingerprinting or wiretap the network link of the WiFi network [7]-[9]. This assumption cannot be satisfied in the real world by most attackers as most WiFi networks have secured password protection, and very hard to impossible for attackers to have physical access to their WiFi routers/access points.

To this end, in this paper, we conduct a brief investigation of whether an outside attacker can identify a network's IoT devices without having a joined in a WiFi network. Compared to the entities in the network, the outsider attacker may face several

difficulties, i.e., the attack may be prevented from analyzing the plaintext of packet payload due to the WiFi data-link layer encryption. On the other hand, the outside attacker captures the fingerprint of the data packet, which would be noisy (especially when more nodes are present in the network). Moreover, the captured data cannot obtain the IP address or the port information; thus, it is difficult to assume whether the hypothesis is correct or not.
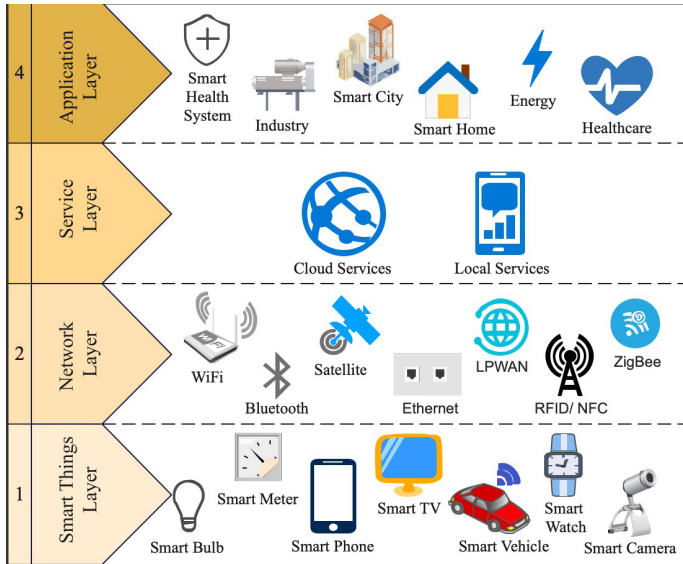

Figure 1: The overview of IoT ecosystem and applications scenarios.

However, if the hypothesis is correct, there could be major threats as follows:

- The attack is possible on all WiFi networks which are in close proximity to the attacker. So it is easy to attack those with weak passwords.

- The attacker only needs to drive or walk a short distance to begin analyzing traffic, where no specific preparations are required beforehand.

- The attack is usually untraceable because it leaves no traces. Thus it is undetectable neither for users nor for forensic investigators.

The hypothesis needs to be investigated in detail based on the above points.

To this end, we demonstrate that the outside attacker cannot only fingerprint the IoT devices, but it is a straightforward process that one can achieve depth information about the network devices. The significant contributions of the proposed research are summarized as follows:

- We conduct a detailed investigation and prove that finger-printing the IoT devices from the outside of the network eavesdropping is not only feasible, but it's a straightforward process.

- We consider nine real-world IoT devices and capture the out-of-network WiFi traffic in two modes, idle and active, using the sniffing tool capable of single-channel and multi-channel monitoring.

- We explore the time-series data and train a machine-learning algorithm to profile nine real-world IoT devices and present their prediction accuracy. The experimental results prove that the fingerprint can be possible by achieving high accuracy of up to 95%.

The rest of the paper is organized as follows: In section 2, we present a brief literature review that motivates us to conduct this research work. In section 3, we first define the problem statement and then present the threat model and assumptions of the proposed research. Section 4 briefly explains a detailed procedure for capturing WiFi traffic from outside the network. In section 5, we conduct data processing and analysis for profiling attacks based on machine learning. Section 6 shows the experimentation and proves that the hypothesis above is true. Finally, in section 7, we conclude the proposed research and define the future work.

2. Related Work

Thanks to the IEEE 802.11 protocol and the development of Wi- Fi-enabled devices, instant access to the internet is now possible everywhere near a public AP through a Wi-Fi connection [10]. Bil- lions of people's lives have been significantly impacted by this development throughout the world. However, when a massive num- ber of people are involved, there are higher chances of misuse or exploitation [11]. The general public can now be followed and profiled due to security vulnerabilities brought on by the ease of use of the 802.11 protocol suite and the number of open public Wi-Fi hotspots [12].

Since the early days of the internet, device identification has been one of the primary targets for classifying network traffic [13]. Several studies have been conducted on WiFi and ethernet, proving that various information can be extracted from IoT devices using traffic classification, such as the device type and the device's activi- ties [14]. The existing literature predicts that a collection of TCP/IP level packets would allow observation of network activity. Those techniques are used to extract the device's potential information. In [15], the authors claim the possibility of a single attribute signature for a variety of IoT devices by employing a port number. Moreover, the deep learning technique is used to perform device fingerprinting for flow volume features. However, this technique is not suitable for the network which is accessed from the outside adversary because the IP traffic is encapsulated in the upper layer that encrypts all significant network features such as cipher suites, protocol, and port number. To this end, we employ a unique collection of attributes that are straightforward to extract the features even from outside the net- work. In [16], the authors used hardware fingerprinting and extracts clock skew measurement. This major focus in this study is more on the hardware rather than the device-specific classification which is considered in the proposed research. In [7], the authors used traffic analysis of WiFi, Bluetooth, and ZigBee to identify the status of the devices and proposed a defensive strategy based on traffic spoofing. In order to gain the traces of WiFi, the authors use a rogue access point with tcpdump, which means the authors assume that all the adversaries are either a part of the network or the adversary already contains significant knowledge about the network. However, the proposed technique considered that the adversary doesn't have any prior knowledge, and the attack is conducted from the outside of the network. There are many other

studies that have been conducted with a focus on WiFi traffic analytics from the outside of the network where the traffic is analyzed using off-the-shelf monitoring devices [17]. However, to the best of our knowledge, none of the existing studies reports the missing rate using those off-the-shelf sniffers or the lost frames as a result of channel hopping eavesdropping [18].

On the other hand, several studies have been conducted on the defense mechanism for those traffic analysis attacks [19, 20]. How- ever, the primary focus of the existing literature is either on location anonymity or website fingerprinting. Moreover, the techniques such as padding or traffic morphing result in less accuracy of the classifier [21]. Besides, those methods cannot rely on time-based classifi- cation because of their limited capabilities for obfuscating traffic patterns.

In contrast to comparable work mentioned above, the proposed research presents an alleged privacy attack against WiFi-based de- vices that rely on WiFi traffic monitoring from outside the network. We proceed with a precise and practical proof-of-concept attack on the assumption of a realistic threat scenario. We also discuss a possible defense against those attacks.

3. Problem Statement, Threat Model, and Assumptions

In this section, we first define the problem statement that serves as a strong motivation for the proposed research. Afterward, we present the threat model that needs to be covered by the proposed study. Finally, we discuss the considered assumptions while conducting the proposed research.

3.1. Problem Statement

The TCP/IP paradigm is used for communicating devices on net- works. The IP address at the Network Layer and the MAC address at the Data Link Layer can be used to identify the devices on the network. Spoofing identities have been used to get around these identifying mechanisms and access restricted resources. Using WiFi traffic analysis, an attacker can "fingerprint" devices to determine private user behavior [22]. For instance, by continuously watching the camera's bitrate, the attacker could ascertain the movements of objects inside a building [23]. Moreover, the attacker can predict which vulnerabilities are available to exploit depending on the type of IoT devices in the network. However, extensive research has been conducted on fingerprinting the IoT devices using eavesdropping from the inside network [24]. This research performs a detailed investigation and proves that fingerprinting the IoT devices eaves- dropping from outside the network is not only possible but also a straightforward process. The developers of the IoT devices must need to consider some extra security constraints to overcome those privacy threats.

3.2. Threat Model

In the proposed research, we consider that the attacker aims to target the information of IoT devices using a targeted WiFi network. More- over, the attacker is also interested in the number and type of unique IoT devices, e.g., Laptop, Smart TV, Light Bulb, etc. Moreover, the attacker is also interested in getting the mode of those devices, such as idle or active. The attacker intends to gain maximum sensitive information by gathering the devices' data. For example, the device type may reveal potential vulnerabilities to software/hardware status. The number of devices

may reveal the customers in business, the number of employees, or the family size. The type and number both can reveal the status of socioeconomic.

Considering this as a potential threat model, we aim to perform a detailed investigation that fingerprinting the IoT devices eavesdrop- ping from outside the network is a straightforward process. This threat should be considered in the first place.

3.3. Assumptions

In the proposed research investigation, we assume that the attacker continuously observes the network traffic outside the network using the targeted WiFi or access point. We also believe that the attacker is physically in the signal range of the access point, so he can per- form eavesdropping using a sniffing tool and gather the nearby WiFi network traffic. We assume that the attacker can't join or break the network. To this end, in the proposed research investigation, we prove that fingerprinting the IoT devices from the outside of the network eavesdropping is possible. Moreover, the existing research focuses on the IoT devices operated at 2.4GHz; we consider the same. However, the proposed study can be applied to 5GHz as well.

4. Verification of Collective Movement

In this section, we first present the system architecture, and then we discuss how the attacker captures the network traffic from outside of the network. After that, we present the pre-processing of the captured data.

4.1. System Architecture

In the proposed investigation, we consider the system architecture illustrated in Figure 2 where the attacker uses to access the WiFi network. The system architecture consists of two stages, offline and online. The first stage (offline) is the attacker's profiling model training and building stage, where an attacker uses his computer and many IoT devices to conduct experiments in order to build the profiling model of each IoT device. On the other hand, the second stage (online) is the attacking stage, where the attacker monitors a WiFi network, trying to identify all IoT devices in the WiFi network based on monitored data and profiling models built in the offline stage. In the first stage (offline), the attacker configures maximum IoT devices which are connected to the nearby WiFi gateway. The attacker accesses the network traffic using a sniffing tool, where the traffic data would be labeled as the device name using the MAC address. The collected data is then pre-processed, where we re- moved the noise (e.g., network traffic gathered from nearby WiFi networks, data link layer broadcast frames, WiFi protocol beacon frames), and dumped the valuable features into a CSV file for apply- ing the machine learning techniques. In particular, we apply several machine learning algorithms and achieve accuracy up to 95% for device identification.

In the second stage (online), the attacker applies a sniffing tool and targets the victim's access point for a short period of, for ex- ample, 30 seconds, and stores the traces for pre-processing. To this point, we never require prior knowledge of the IoT devices for pre- processing, which we will explain in detail later in the follow- ing subsection. Precisely, we use standard and statistical filtering techniques to eliminate the noise from the data frames which do

not represent the patterns of data. After that, we use Python scripting to extract the features from pre-processed data. Finally, we were able to predict the type of devices and their activity.
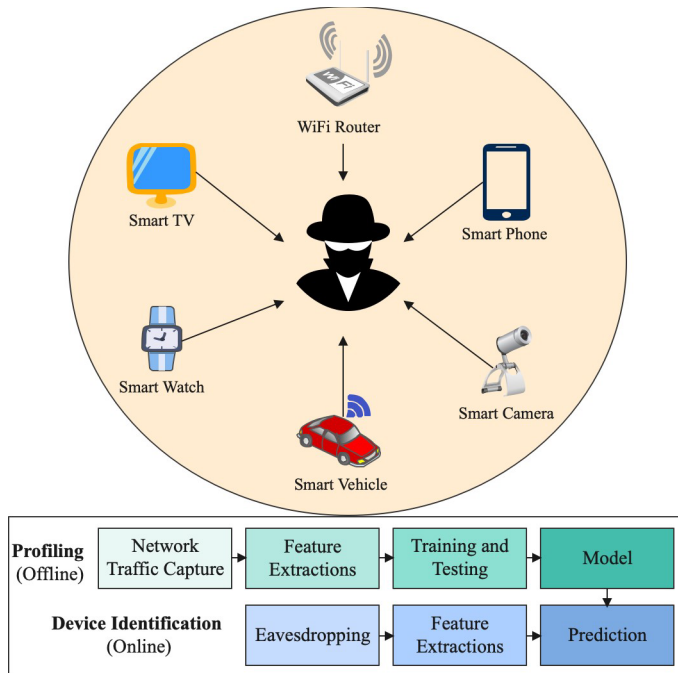

Figure 2: The attacker's perspective of profiling attack on the IoT devices

Table 1: Comparison of captures by out-of-network Airtool with the in-network Wireshark

Size Range of Packets/Frames	Wireshark	Airtool	
	#Packets	#Frames	#Data Frames
0-19	0	2428	0
20-39	0	5593	199
40-79	2441	0	0
80-159	260	2890	2883
160-319	108	239	239
320-639	173	194	190
640-1279	241	255	255
1280-2559	13574	13846	13846
Total	16797	25445	17612

4.2. Traflc Capturing From Outside of the WiFi Net- work

In order to capture the data frames from outside of the WiFi net- work, we first test to use the two most popular sniffing tools, Kismet and Airodump-ng. Kismet stores the network traces as SQLite3 database, whereas Ariodump-ng dump the traces into a capture file format such as pcap. The output of pcap is used to perform packet inspection as the output is in a compatible format, where the packet inspection can be done via a network analyzer such as Wireshark. We use those sniffing tools because of their capabil- ity to sniff raw 802.11 frames. Besides, both of them are able to monitor single-channel and multi-channel using frequency hop- ping. For the hardware, we use an external wireless adapter (Alfa AWUS036ACM) as the built-in WiFi cards don't serve our purpose because they are programmed to accept the data packets which are particularly addressed to the machine's interface card.

Once the captured traffic is analyzed, we observe that a signifi- cant proportion of captured packets contradicts the elephant-mouse internet traffic phenomenon [25]. The elephant flows of 1500 bytes

were unable to see for all the available devices, including the video packets captured from a Camera or a smart TV. The proposed in- vestigation shows that the aforementioned tools can only capture a limited range of packets in terms of their sizes. For example, they are able to capture the packet up to the frame size of 472 bytes; how- ever, this size is enough for particular applications such as signal intelligence. Due to such limitations of Kismet and Airodump-ng, we consider another sniffing tool called Airtool5. The Airtool snif- fer is a MAC's built-in sniffing tool that can passively sniff WiFi traffic and store the traces in a pcap format which can be further analyzed using Wireshark. We simultaneously run Wireshark on a different laptop connected to the network to record its own in- coming/outgoing network traffic to the AP in order to confirm the accuracy of the traffic caught by Airtool which is running on an out-of-network MacBook. The traffic between the second laptop connected to the network and the AP was considered for comparison of those two traces.

Because Airtool also records additional control and management frames at the data-link layer (most frames have sizes between 0 and 39), which are absent from Wireshark's in-network traffic captur- ing, we discovered that Airtool collects more frames than packets recorded by Wireshark, as shown in Table 1. Every frame that is collected by Airtool is translated into a WiFi data-link layer frame,

Whereas every frame that is captured by Wireshark is translated into an Ethernet II frame. As a result, for the same WiFi packet, the Wireshark capture is smaller than the Airtool interpretation of the data-link layer frame. This explains why the 2441 packets in the Wireshark capture that are between 40 and 79 bytes all show up in the Airtool capture's higher packet size range (80 to 159 bytes). Additionally, the comparison holds even after excluding all control and management frames from the Airtool capture (as seen in the last column), so there aren't any apparent missing packets according to Airtool. As a result, we employ Airtool as our testbed for evaluation.

4.3. Data Pre-Processing on Captured Data

Once the encrypted WiFi traffic data is captured using the Airtool software, the output in pcap format is analyzed using the Wireshark tool. In particular, the following steps are taken to analyze the captured data:

- We start with the traffic broadcasting in both directions to the MAC address of the WiFi network under investigation. This is required since Airtool could potentially monitor WiFi traffic from many neighboring APs. Only data frame types are kept since all other control, and management MAC-layer frames do not adequately depict the profiling data pattern.
- We export the pcap files into the csv files for the following steps number 3 and 4.
- We eliminate noisy frames that some MACs produced. Since they often only appeared as a single frame, these noise frames are simple to filter out. By just keeping traffic frames with bi- directional communication traffic, they are filtered away.
- To make dataset labeling easier, we swap out the MAC ad- dresses for the relevant device names and their operational status. This step is included only in the offline training stage.

- The dataset required for both offline training and performance testing is eventually obtained using a Python script that ex- tracts and calculates statistical characteristics.

5. Data Processing and Analysis

In the section, we first discuss the observable Data Fields, and then we discuss data analysis. Finally, we discuss device profiling on time-series data.
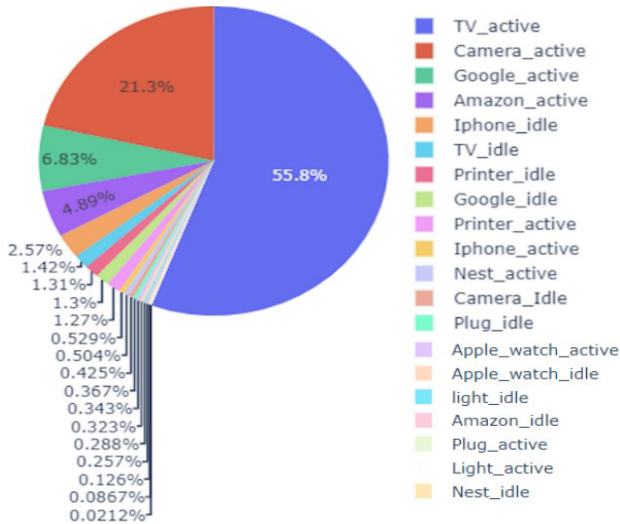

Figure 3: The total number of data packets captured with respect to the IoT device. Many devices' names show whether they are in active or in an idle state.

5.1. Useful Data from Network Monitoring

As we have discussed earlier, the process of out-of-network monitor- ing. Here, we present the observable data fields on a secured WiFi network where everything above the data-link layer is encrypted because of WiFi protocol WPA-PSK. Because of this encryption, the only observable data is the MAC-layer frame header, signal strength, and the observation timestamp. The frame header pro- vides the source and destination's MAC addresses, frame size, and frame type. However, the signal strength cannot be used as it has been affected by several factors such as neighboring WiFi net- works, deflection, absorption, and reflections of the surrounding objects. Therefore, in the proposed investigation, we neglect the signal strength and only use the MAC layer frame header.

5.2. Data Analysis

As discussed earlier, we consider 10 different IoT devices and col- lected their data through out-of-network monitoring. In Figure 3, we show the total percentage of captured data from each device. To provide insights into the monitored traffic, we measure the working and idle status of all the IoT devices. From Figure 3, we can observe that the number of received packets from TV is more than the other IoT devices such as the camera and Google. All of the other devices' captured data are comparatively way less than those three devices. Consequently, the camera and google both display different behavior with regard to packet sizes, as shown in Figure 4. Specifically, the camera and google both appear to send the majority of their packets at a fixed size of 170 bytes and 140 bytes, respectively, as shown in Figure 5. We will discuss this part in the following section.

As shown in Figure 3, we believe that the attacker can easily build the signature. Moreover, the attacker can also change the status of those IoT devices. As we can see in Figure 3, there is a huge difference between the active and idle states of the devices which means the AP initiated communication to send an off signal to those devices. On the other hand, due to the notable decline in flow when switching to the idle state, the working condition of other devices with better network capabilities and memory storage, such as iPhones, printers, and Amazon, is impressively noticeable. For instance, Amazon will only get a small number of packets when it is idle because the user is not searching the Internet. Similarly, we show a detailed transmission of data packets from each IoT device in Figure 4. In particular, we show the total number of packets sent from the access point to the IoT device, which is represented by 1, and the total number of packets sent from IoT devices to the access point, which is represented by 0. Moreover, the figure depicts both the total data captured in the active and idle states of all the devices.
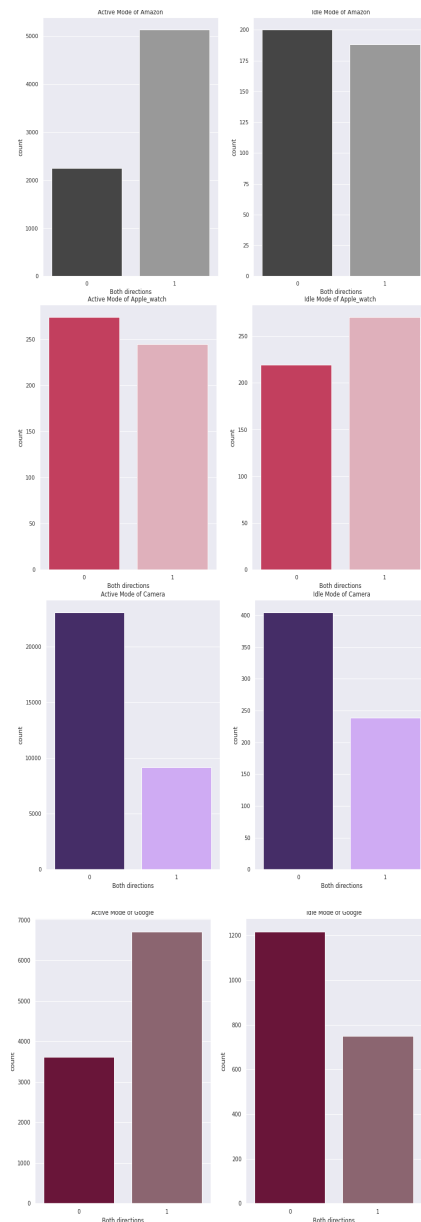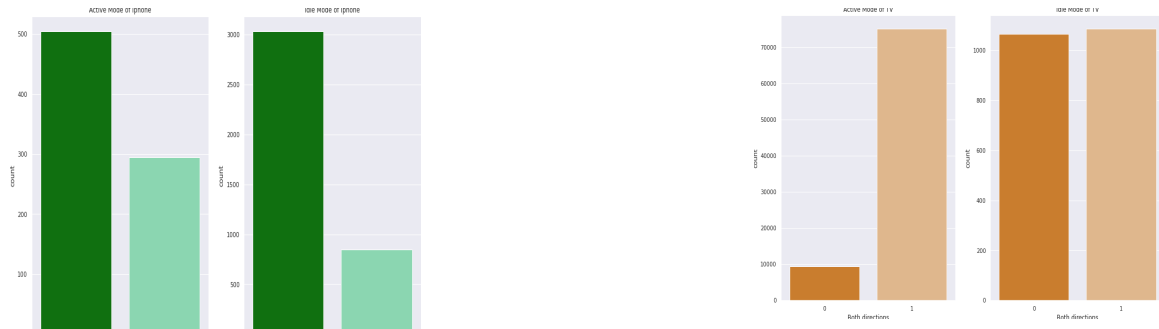
Figure 4: Total number of packet transmission from access point and IoT devices, respectively. In particular, the figure shows the total number of packets sent from the access point to the IoT device, which is represented by **1**, and the total number of packets sent from IoT devices to the access point, which is represented by **0**.

5.3. Machine Learning Techniques

In order to execute our investigation, we choose several classifi- cation methods, and a popular machine learning model XGBoost [26]. We consider XGBoost because of its superior performance, especially for the problems of network classification among other popular machine learning models. Because our data is captured in two different sequence sizes, so we consider precision, recall f-1 score, and support vector machine (SVM) as performance metrics to tackle the time series data.

5.4. Profiling on IoT Devices using Time-series Data

Processing time-series data is simple. The captured traces from the Data-link layer is converted into a string of three-feature items. The monitored frame is then converted into three nu- meric values: the size of packet P, the direction of packet X, and the arrival time Y, where 0 represents the transmitted pack- ets and 1 represents the received packets by an IoT device. Fol- lowing those numeric values, we can obtain the series of data such as $\{P0, X0, Y0\}$, $\{P1, X1, Y1\}$, ..., $\{Pn, Xn, Yn\}$. Figure 5 shows the heatmap of the correlations for each feature in the dataset, where 1 shows the maximum value, and 0 shows the minimum.
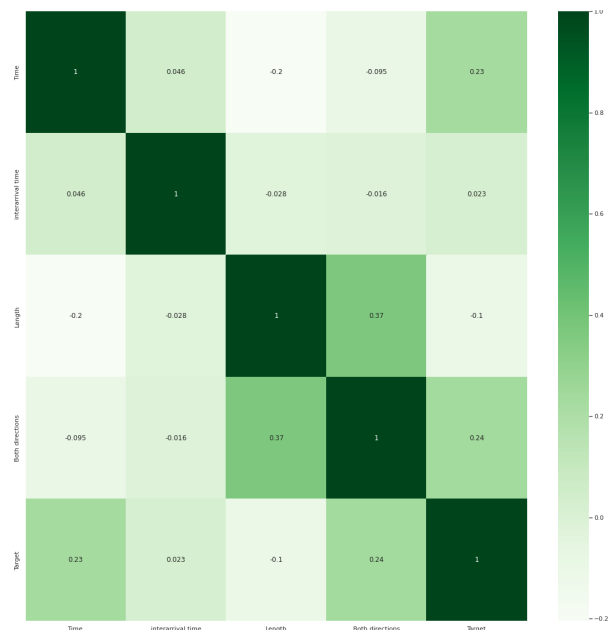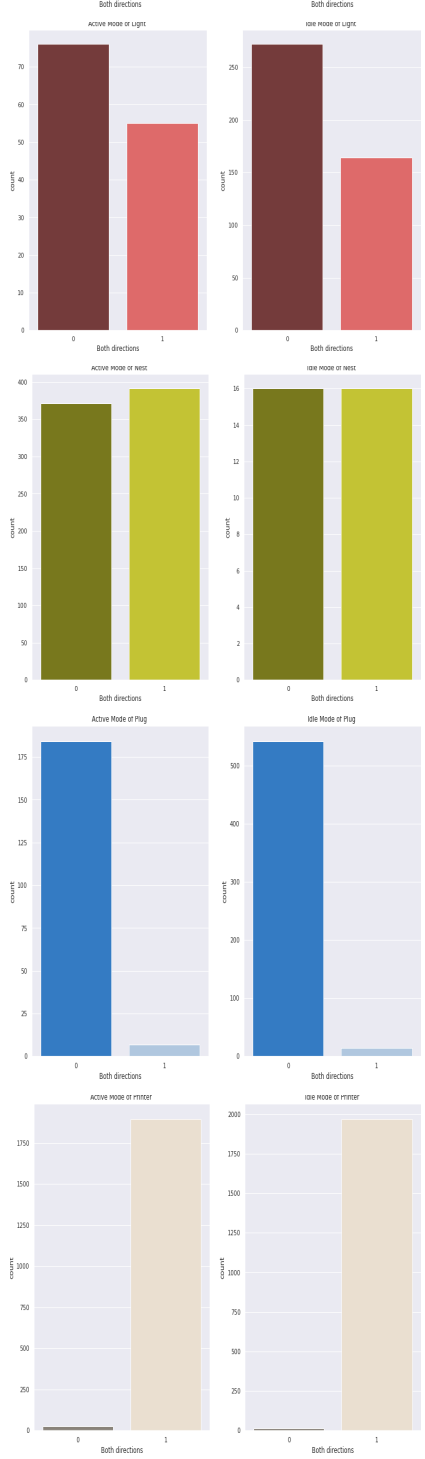
Figure 5: Correlation of features in a dataset

This method's main disadvantage is that it needs a lot of packets to supply all the data points needed for categorization or machine learning training. In our case, we are dealing with a heterogeneous system monitored inside a specific time window; certain devices (such as Smart TV) generate a large volume of data packets while others only produce very sparse packets (such as smart light bulb). For instance, if we compare how long it takes the light and TV to collect a 100-packet series, the TV just needs one second of visible data while the light needs approximately 30 minutes.

To overcome this challenge, we use a two-level categorization technique, starting with a traffic intensity threshold. Devices are divided into two groups in the first level according to whether there is a high or low volume of traffic. Then, in accordance with the volume of device traffic, we use an appropriate sequence size. Using ML algorithms, the second level determines the prediction proba- bility. A prediction is made if the probability rises above a certain threshold; else, the data is labeled as an "unknown" device. Once the dataset is created, we extracted the following features from the monitored traffic in each time window:
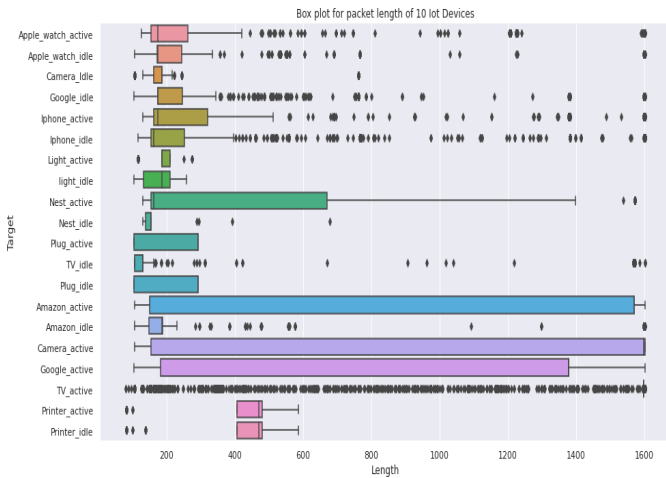
(a) Box plot for packet length frames of 10 IoT devices.
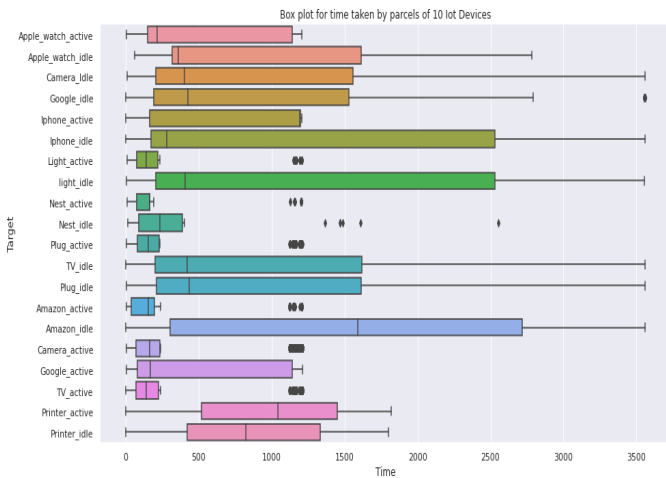
(b) Box plot for the time taken by packets of 10 IoT devices1.

Figure 6: Packet length and time-taken in transmission or reception of 10 IoT devices

- Packets transmitted and received by the access point to and from the IoT devices, respectively.

- The difference in inter-arrival time.

- Total number of bytes in the transmitted and received packets.

- Variance of sizes in transmitted and received packets.

- The average number of consecutively transmitted or received packets before seeing a received or transmitted packet, respectively.

6. Results and Discussion

In this section, we first present the testbed settings and the evaluation metrics. Afterward, we show the IoT devices' packets transmission and their reception in terms of packet length, and time. Finally, we show the evaluation results and prove that the outsider intruder can significantly harm the IoT devices without joining the WiFi network.

6.1. Testbed and Evaluation Metrics

With the help of a WiFi router, we built up a testbed with 10 distinct IoT devices. We use AirTool to capture the WiFi data frames be- tween all IoT devices and the WiFi router for an appropriate amount of time in order to collect enough data. Once the data is captured, we use a time-series format and randomly split the dataset into two groups, 20% for testing and 80% for training.

The following metrics are used to assess our classification mod- els: Precision, Recall, F1 Score, and Accuracy. Let's use the abbre- viation T to stand for true prediction, further subdivided into true positives and true negatives. The letters F stand for false prediction, which is further divided into false positives and false negatives. The following equations are used to measure the Precision, Recall, F1 Score, and Accuracy, respectively.

Figure 7: Packets transmission in both directions of each IoT device with respect to time.

- Variance of size distribution in transmitted and received pack- ets.

- Mode of transmitted and received packets.

$$Precision = \frac{TP}{TP + FP} \quad (1)$$

$$Recall = \frac{TP}{\quad} \quad (2)$$

$$TP + FN$$

$$F1 - Score = 2 \times \frac{Precision \times Recall}{Precision + Recall} \quad (3)$$

To access point and access point to IoT device) with respect to time. The line in the middle of the box shows the average length of the pack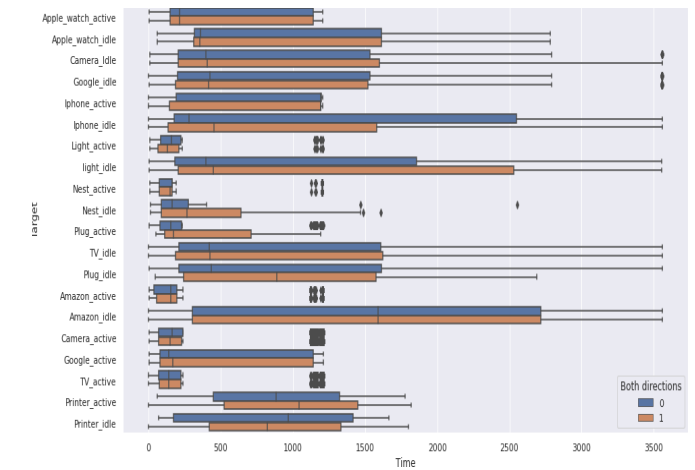et transmitted or received. In particular, 0 represents the packets transmitted from the IoT device to the access point, and 1 represents

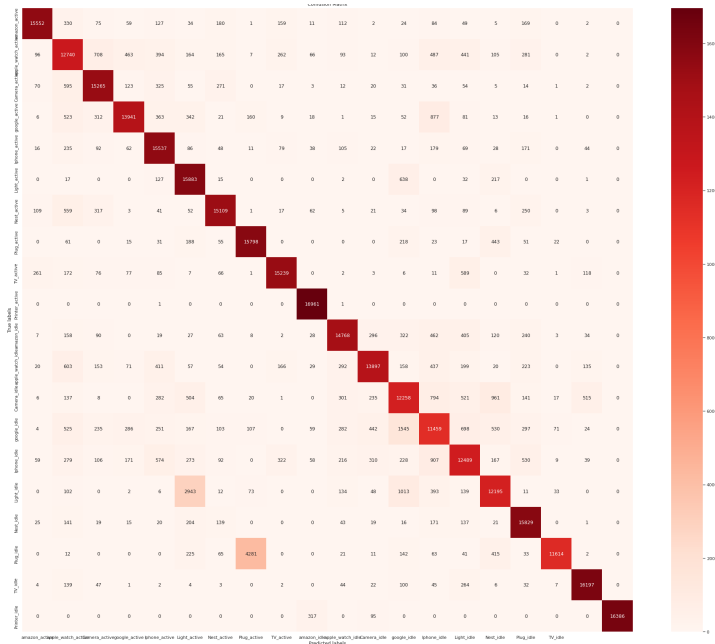$$Accuracy = T + N \qquad (4)$$

Figure 8: Predicted labels of each IoT device

6.2. Captured Data

Before going to the evaluation, we first show the captured data in terms of packet length and time. In Figure 6, we show the packet length and time taken in transmission or reception of 10 IoT devices, respectively. In particular, in Figure 6 (a), we show a box plot for the packet length of 10 IoT devices. The packet length of each device is captured in both active and idle states. Similarly, in Figure 6 (b), we show a box plot for the time taken by packets to transmit or receive by each IoT device in both active and idle states. To further show the significance of captured data, in Figure 7, we show the packet transmission in both directions (IoT device the packets transmitted from the access point to the IoT device. The above-mentioned box plots prove that a significant amount of data is captured in the proposed investigations, where an attacker can easily access the useful information of the IoT devices and can significantly harm the user. We also prove that the IoT devices can reveal the potential vulnerabilities to hardware/software status as the attacker can change the status of IoT devices.

Considering this as a potential achievement in our investigation, below we present the results of model accuracy, which can further support our claim.

	precision	recall	f1-score	support
1	0.98	0.91	0.95	1841
2	0.75	0.18	0.28	137
3	0.96	0.98	0.97	8025
4	0.85	0.94	0.89	2629
5	0.78	0.65	0.71	202
6	0.61	0.34	0.44	32
7	0.80	0.53	0.63	173
8	0.85	0.23	0.37	47
9	0.98	0.99	0.98	21158
10	0.95	1.00	0.97	483
11	0.87	0.72	0.79	92
12	0.88	0.71	0.79	119
13	0.70	0.51	0.59	162
14	0.77	0.49	0.60	495
15	0.78	0.66	0.72	937
16	0.78	0.63	0.69	105
17	0.00	0.00	0.00	8
18	0.76	0.89	0.82	132
19	0.85	0.94	0.89	538
20	1.00	0.95	0.97	479
accuracy			0.95	37794
macro avg	0.79	0.66	0.70	37794
weighted avg	0.95	0.95	0.95	37794

Figure 9: Machine learning model accuracy on Precision, Recall, and F1-Score.

6.3. Results

We chose a 30-minute time window size for evaluation. We believe that long-term observed traces can teach us more about time-series patterns than short-term ones, which call for much longer time ob- servations to carry out the attack. As we were facing a challenge in working with imbalanced data, for example, data captured from some devices are extremely high such as TV or Camera, whereas other devices are barely showing any record for example Nest, Light as shown in Figure 3. To balance such data, we use SMOTE anal- ysis to prove the significance of the results. Figure 8 shows the confusion matrix of prediction accuracy using a SMOTE analysis on the XGBoost model. The Figure shows that the IoT device "Printer active" captures maximum true labels, whereas the IoT device "google idle" captures minimum true labels.

Finally, we show the accuracy of all 10 IoT devices in each active and idle state with respect to Precision, Recall, and F1-Score. In order to provide a significance of the results, here we consider the captured data without balancing and show the result without modify- ing any values. In Figure 9, we show that the model achieves 95% of accuracy. We attribute this performance to the XGBoost model, as it performs significantly well over imbalanced classification datasets.

7. Discussion and Future Work

Our findings support the hypothesis that an outside-of-network at- tacker can successfully identify IoT devices without connecting to a WiFi network. The type of devices and their operating modes may be determined by characteristics like the number of packets, inter-arrival time, packet sizes, and distributions. The attack is straightforward to execute without leaving any traces or fingerprints.

The profiling attack causes serious privacy issues. A potential attacker could drive close to a business to evaluate the volume of economic activity, the socioeconomic background of the clients, expected revenues, revenue trends, or even find possible weak tar- gets for future attacks. It can provide environmental awareness that

can be utilized to track mobile devices in more complicated circum- stances (e.g., cars, drones, phones, etc.). For instance, a swarm of drones can be deployed over a sizable area to classify, identify, and monitor the movement of signal-emitting devices in the covered area. This might show how gadgets communicate with one another and show where each device travels.

As we have proved that the experimental testbed is reliable and has significant importance in the real-world, the implementation in real-world scenarios is of utmost importance to secure the privacy of the individual. To this end, we aim to further extend the proposed implementation in real-world scenarios, where we would be able to show the further importance of such attacks.

8. Conclusion

This paper investigates a privacy leakage from an out-of-network eavesdropper on encrypted WiFi traffic. To this end, we consider 10 IoT devices and capture their data from outside the network without joining the WiFi network. During the investigation, we prove that IoT device eavesdropping is not only possible but also a straightforward process. To this end, we exploit the WiFi frame timing and header information and conduct a detailed evaluation using a machine learning technique for inferring and fingerprinting which IoT device exists in the network and what working status each device is. The models we found had exceptional high accu- racy, they are most likely approaching the point where subsequent improvement becomes more difficult and might even come with the loss of generalizeability [27]. Our evaluation achieves high accuracy, up to 95%, in identifying the devices and their working status. The experimental results show that outside intruders can significantly harm the IoT devices without joining a WiFi network and can launch the attack within a minimum time without leaving any detectable footprints.

References

[1] M. Alyami, I. Alharbi, C. Zou, Y. Solihin, K. Ackerman, "WiFi-based IoT Devices Profiling Attack based on Eavesdropping of Encrypted WiFi Traffic," in 2022 IEEE 19th Annual Consumer Communications & Networking Confer- ence (CCNC), 385–392, IEEE, 2022, doi:10.1109/CCNC49033.2022.9700674.

[2] P. Dudhe, N. Kadam, R. Hushangabade, M. Deshmukh, "Internet of Things (IOT): An overview and its applications," in 2017 International conference on energy, communication, data analytics and soft computing (ICECDS), 2650– 2653, 2017, doi:10.1109/ICECDS.2017.8389935.

[3] G. R. Hiertz, D. Denteneer, L. Stibor, Y. Zang, X. P. Costa, B. Walke, "The IEEE 802.11 universe," IEEE Communications Magazine, **48**(1), 62–70, 2010, doi:10.1109/MCOM.2010.5394032.

[4] K. Boeckl, K. Boeckl, M. Fagan, W. Fisher, N. Lefkovitz, K. N. Megas,E. Nadeau, D. G. O'Rourke, B. Piccarreta, K. Scarfone, Considerations for managing Internet of Things (IoT) cybersecurity and privacy risks, US De- partment of Commerce, National Institute of Standards and Technology, 2019.

[5] K. Vengatesan, A. Kumar, M. Parthibhan, A. Singhal, R. Rajesh, "Analysis of Mirai botnet malware issues and its prediction methods in internet of things," in International conference on Computer Networks, Big data and IoT, 120–126, Springer, 2018, doi:10.1007/978-3-030-24643-3 13.

[6] E. Ronen, A. Shamir, "Extended functionality attacks on IoT devices: The case of smart lights," in 2016 IEEE European Symposium on Security and Privacy (EuroS&P), 3–12, IEEE, 2016, doi:10.1109/EuroSP.2016.13.

[7] A. Acar, H. Fereidooni, T. Abera, A. K. Sikder, M. Miettinen, H. Aksu, M. Conti, A.-R. Sadeghi, S. Uluagac, "Peek-a-boo: I see your smart home activities, even encrypted!" in Proceedings of the 13th ACM Conference on Security and Privacy in Wireless and Mobile Networks, 207–218, doi: 10.1145/3395351.3399421.

[8] S. Aneja, N. Aneja, M. S. Islam, "IoT device fingerprint using deep learning," in 2018 IEEE international conference on internet of things and intelligence

system (IOTAIS), 174–179, IEEE, 2018, doi: 10.1109/IOTAIS.2018.8600824

[9] N. Apthorpe, D. Reisman, S. Sundaresan, A. Narayanan, N. Feamster, "Spying on the smart home: Privacy attacks and defenses on encrypted iot traffic," arXiv preprint arXiv:1708.05044, 2017.

[10] M. W. Nadeem, H. G. Goh, M. Hussain, M. Hussain, M. A. Khan, et al., "Internet of Things for Green Building Management: A Survey," in Role of IoT in Green Energy Systems, 156–170, IGI Global, 2021.

[11] F. Meneghello, M. Calore, D. Zucchetto, M. Polese, A. Zanella, "IoT: Internet of threats? A survey of practical security vulnerabilities in real IoT devices," IEEE Internet of Things Journal, **6**(5), 8182–8201, 2019, doi: 10.1109/JIOT.2019.2935189

[12] A. Sujanani, S. Pai, "802.11 Frame-level Network IDS for Public Wireless Networks," in ICT Systems and Sustainability, 453–461, Springer, 2021.

[13] O. Salman, I. H. Elhajj, A. Chehab, A. Kayssi, "A machine learning based framework for IoT device identification and abnormal traffic detection," Trans- actions on Emerging Telecommunications Technologies, **33**(3), e3743, 2022, doi:10.1002/ett.3743.

[14] J. S. Atkinson, J. E. Mitchell, M. Rio, G. Matich, "Your WiFi is leaking: What do your mobile apps gossip about you?" Future Generation Computer Systems, 80, 546–557, 2018, doi:10.1016/j.future.2016.05.030.

[15] A. Sivanathan, H. H. Gharakheili, F. Loi, A. Radford, C. Wijenayake, A. Vish- wanath, V. Sivaraman, "Classifying IoT devices in smart environments using network traffic characteristics," IEEE Transactions on Mobile Computing, **18**(8), 1745–1759, 2018, doi:10.1109/TMC.2018.2866249.

[16] I. Sanchez-Rola, I. Santos, D. Balzarotti, "Clock around the clock: Time-based device fingerprinting," in Proceedings of the 2018 ACM SIGSAC Conference on Computer and Communications Security, 1502–1514, 2018, doi: 10.1145/3243734.3243796.

[17] R. VanSickle, T. Abegaz, B. Payne, "Effectiveness of tools in identifying rogue access points on a wireless network," 2019.

[18] P. Serrano, M. Zink, J. Kurose, "Assessing the Fidelity of COTS 802.11 Snif- fers," in IEEE INFOCOM 2009, 1089–1097, 2009, doi:10.1109/INFCOM.2009.5062021.

[19] A. Abusnaina, R. Jang, A. Khormali, D. Nyang, D. Mohaisen, "DFD: Adver-sarial Learning-based Approach to Defend Against Website Fingerprinting," in IEEE INFOCOM 2020 - IEEE Conference on Computer Communications, 2459–2468, 2020, doi:10.1109/INFOCOM41043.2020.9155465.

[20] W. De la Cadena, A. Mitseva, J. Hiller, J. Pennekamp, S. Reuter, J. Filter, T. Engel, K. Wehrle, A. Panchenko, "Trafficsliver: Fighting website fingerprint- ing attacks with traffic splitting," in Proceedings of the 2020 ACM SIGSAC Conference on Computer and Communications Security, 1971–1985, 2020, doi:10.1145/3372297.3423351.

[21] F. Zhang, W. He, X. Liu, "Defending against traffic analysis in wireless net-works through traffic reshaping," in 2011 31st International Conference on Distributed Computing Systems, 593–602, IEEE, 2011, doi: 10.1109/ICDCS.2011.77.

[22] Z. Jiang, K. Zhao, R. Li, J. Zhao, J. Du, "PHYAlert: identity spoofing at-tack detection and prevention for a wireless edge network," Journal of Cloud Computing, **9**(1), 1–13, 2020, doi:10.1186/s13677-020-0154-7.

[23] Q. Xu, R. Zheng, W. Saad, Z. Han, "Device fingerprinting in wireless networks: Challenges and opportunities," IEEE Communications Surveys & Tutorials, 18(1), 94–104, 2015, doi: 10.1109/COMST.2015.2476338.

[24] I. I. A. Sulayman, R. He, M. Manka, A. Ning, A. Ouda, "LiFi/WiFi Authenti-cation and Handover Protocols: Survey, Evaluation, and Recommendation," in 2021 International Symposium on Networks, Computers and Communications (ISNCC), 1–6, IEEE, 2021, doi: 10.1109/ISNCC52172.2021.9615853.

[25] K.-C. Lan, J. Heidemann, "On the correlation of internet flow characteristics," Technical report, Citeseer, 2003.

[26] T. Chen, T. He, M. Benesty, V. Khotilovich, Y. Tang, H. Cho, K. Chen, et al., "Xgboost: extreme gradient boosting," R package version 0.4-2, 1(4), 1– 4, 2015.

[27] I. A. Alharbi, A. J. Almalki, C. C. Zou, "Hyperparameter Optimization and Comparison of Student Performance Prediction Algorithms," in 2021 Interna- tional Conference on Computational Science and Computational Intelligence (CSCI), 889–894, 2021, doi:10.1109/CSCI54926.2021.00207.

Field Oriented Control and Commutation Based on Sensorless Methods for High Speed Electrical Motors of Unmanned Multicopters

Chen Zhao[*], Weisheng Kong, Federico Percacci, Patrik Gnos

Corporate Center Motion Control, maxon motor ag, Sachseln, 6072, Switzerland

A B S T R A C T

In recent years, unmanned aerial vehicles (UAVs), especially small and light multicopters driven by electrical motors and batteries, have experienced a boom in applications. The electrical drive system is a central component of these UAVs. This paper introduces the basics of these drives and presents control methods for them using permanent magnet synchronous motors (PMSMs). Control of these drives is based on field-oriented control (FOC) optimised for high speed (for instance, 200 el. krpm). For the multicopter drives, sensorless control is preferred, i.e., no position or speed sensor on the motors is necessary. Therefore, in this paper, the rotor position is estimated by a sensorless method based on a back electromotive force (back emf) observer combined with a start-up process. The parametrisation methods of the observer and the start-up process are described as well. The observer and the integration of it in multicopter drives are the major innovative parts of this paper. These introduced methods are verified by simulation and experiments. In experiments two motors are considered. One is applied to operate at the maximal speed up to more than 200 el. krpm. The other is a special UAV drive motor and applied for experiments with propeller, under similar operating conditions as UAVs. The results prove the performance and effectiveness of the introduced methods.

1 Introduction

1.1 Multicopters using electric motors

Unmanned aerial vehicles (UAVs), especially multicopters like the one in figure 1, have experienced a surge in popularity in recent years and have found application in various fields. UAVs powered by electrical motors are easy relatively inexpensive to assemble compared to other aircraft structures.

This paper is an extension of work originally presented at the 23rd European Conference on Power Electronics and Applications (EPE21 ECCE Europe), [1]. The technical background and additional experimental results are included, as well as the analysis and discussion of the results[1].

The electric drives and their corresponding control system are one of the core components of UAVs. They are required to be power-efficient, lightweight, robust against a hostile environment, and reliable over many flight hours. Surface mounted permanent magnet synchronous motors (SMPMSMs) are the most suited for UAVs for their compactness, high efficiency, and high power and

torque density compared to other motor technologies. While compact multicopters with at least four motors are able to carry a light load, e.g. a camera, large multicopters with six or more motors can carry more equipment and are interesting for tasks such as package delivery in urban areas and the targeted application of fertilisers or pesticides on large farms. To provide the necessary thrust, the SMPMSMs for these large multicopters tend to have a high nominal current and a high number of pole pairs, for instance 20. Since multicopter propellers may be rated for top speeds of even 8000 mechanical revolutions per minute (mech. rpm), the electrical speed experienced by multicopter motors may easily surpass 100'000 electrical rpm (el. rpm).

When it comes to the control of motor current, field-oriented control (FOC) is preferred over e.g. block commutation mainly because of the more even torque generation and the higher power efficiency, especially when used with motors with a long electrical time constant. Either way, the direction of the rotor's magnetic field must be known or measured for the control of motor current. While the most convenient approach consists in measuring the rotor's angle with a position sensor, e.g. an encoder, it is possible

---

[*]Corresponding Author: Chen Zhao, Corporate Center Motion Control, maxon motor ag, Brünigstrasse 220, CH-6072 Sachseln, Switzerland, E-Mail: chen.zhao@maxongroup.com

[1]Compared to the conference paper [1], there are following extensions included in this paper: 1) technical background about power electronics and electric motors, 2) technical background about motor drive methods, 3) introduction of modulation methods, 4) the thermal behaviour of motor and motor drive, 5) experimental results of thermal behaviour, 6) additional description of the model and methods, 7) additional results and figures, 8) additional literature papers.

to infer the magnetic field's direction by careful processing of the motor's electrical quantities (voltage and current). This so-called *sensorless* form of position detection is advantageous for UAVs because it renders position sensors superfluous, thus reducing the overall weight and increasing reliability by eliminating a potential source of failure.

Figure 1: A test quadcopter (UAV)

At present, the high electrical speed and high motor current characteristic of large multicopters present a challenge for electrical drives, namely in terms of

- reliable sensorless position detection

- reliable commutation

- reliable current control.

1.2   Related work

There is much research focusing on design and build multicopters, for instance [2]. For a detailed introduction of PMSMs, [3] can be referred.

With consideration of sensorless control of PMSMs, the main approaches for sensorless position detection are two: one is based on the superposition of test signals (*signal injection*) on the voltage vector applied to motor. A number of research papers are published, [4]–[10]. For instance in [4], the Indirect Flux detection by On-line Reactance Measurement (INFORM) method is introduced. In [9], the rotor position of SMPMSMs without saliency is estimated by using periodic injection in circumference direction, interleaved with torque generating current. Whereas, the other is based on the estimation of the back electromotive force (back emf).

In this paper, less attention is paid to the signal injection methods, which are computational intensive and may lead to disturbance of motor torque. The Position estimation based on back emf is suitable and sufficient for multicopter drives: as the motors must rotate continuously at high speed during flight, the back emf is large and thus easy to estimate with satisfying accuracy.

The simplest back emf estimation method entails detecting the instants at which back emf changes sign in each motor winding. However, this method cannot be applied in FOC but only in block commutation. A Model-based method using the sliding mode back emf observer is proposed in [11]. It is still only suitable for block commutation. In [12], a load torque estimation method for sensorless control of brushless DC drives is presented, however it is also designed for 6-step commutation.

Further model-based methods compatible with FOC are the object of [9] and [13]. In particular, in [9] a back emf observer combined with signal injection is introduced. The algorithm can be improved and computation load of this method can be reduced for multicopter drives, with consideration of required operation speed. In [13], a sliding mode back emf observer is proposed for sensorless position estimation, in which the position estimation error is compensated by using an integral sliding mode observer. However, for multicopter drives, varying effects have to be considered. Beside the dynamic response and high speed performance, the computation load may also be an issue.

In addition, the performance of sensorless control using pulse width modulation (PWM) and pulse-amplitude modulation (PAM) is analysed in [14]. The focus if this paper is only losses. The control performance is not included, which is very essential for UAV applications. Furthermore, the suggested advantage of PAM is significant at a high speed range compared that of multicopter drives.

1.3   Main contribution of this paper

As aforementioned, sensorless control of PMSMs is considered in a few papers, however, the special requirements and conditions of multicopter drives are taken into account, especially the sensorless drive at high speed range using FOC. With consideration that the multicopters is one of the most interesting application areas of electric drive at present, therefore we propose and describe a control system for electrical drives for drives of multicopters. We achieve sensorless position detection with a Luenberger observer that estimates back emf. We propose a method to parametrise the observer's gains to achieve a desired dynamic response and to guarantee a maximum position estimation error at the maximum operation speed. The position estimate derived from the back emf in this way is updated at the rate of the current control task (25 kHz).

At high electrical speed, the two components of the motor current in the rotor coordinate frame are heavily coupled. While block commutation can obviate this [14], like others we add a decoupling mechanism in the current control loop [15]–[18].

After describing our proposed control system, we evaluate its performance by examining characteristics of interest of a selected multicopter drive (e.g. torque ripple) at its maximum electrical speed, both in simulation and experiment. We show that the multicopter drive with out control system can reach a speed of 200 el. krpm. To the best of our knowledge, other control systems for multicopters with these features do not exist at present.

The rest of the paper is structured as follows. The second section discusses the commutation method and explains the sensorless position detection method and the current controller designed for high speed applications. In the third section, the methods are verified by using simulations and experiments. The last section contains the conclusion.

2 Electrical drive systems

2.1 Power inverter and control

Drive systems using electric motors are very diverse. For PMSMs, the most widely applied motor drive is a voltage source inverter (VSI), [19], which is also applied in this paper. The topology of a VSI is illustrated in the Figure 2, left. The main components are the six metal–oxide–semiconductor field-effect transistors (MOSFET), T. They build three switching bridges for the three motor phases, respectively.
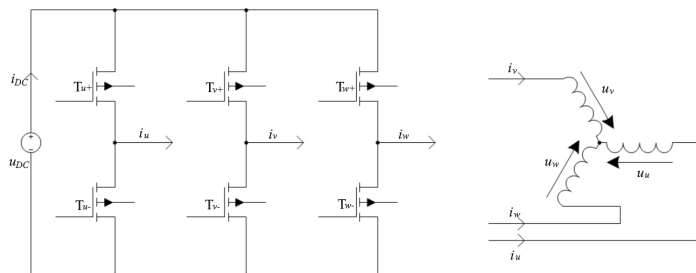

Figure 2: Structure of voltage source inverter and PMSM.

The motor winding terminals are connect to the outputs of the VSI, Figure 2, right, and can be connected to supply voltage or the ground by switching the power transistors in the left figure. In this paper, the switching pattern is determined according to space vector pulse width modulation (SVPWM) methods. Figure 3 shows simulated current in one motor phase and the corresponding PWM duty cycle as an example for generation of current using 5-segment SVPWM. The first plot illustrates the expected reference current. For an easier comparison with the actual current, the reference current is projected to the $u - v - w$ phase coordinate. According to the SVPWM method the duty cycle is calculated and the switching signals are generated, which are the third and fourth plot, respectively. Then, the generated actual current matches the reference current, shown in the second plot, except for the current ripples.
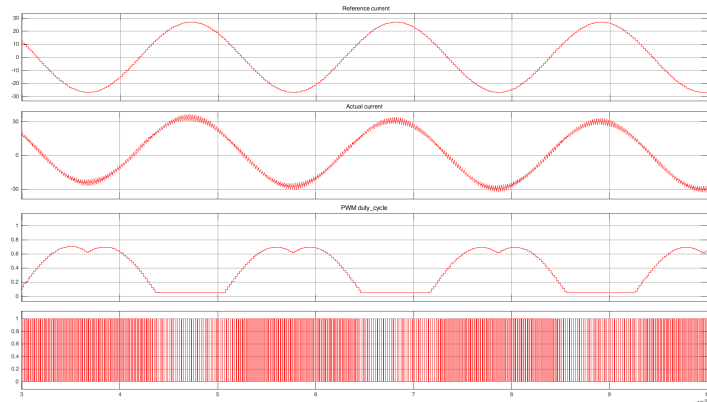
Figure 3: Example of generating current using PWM in one motor phase. The first plot, from above, is the reference current projected in $u - v - w$ phase coordinate, the second is the actual current, the third and fourth are the PWM duty cycle and switching signal, respectively. In the figure of actual current current ripple can be observed, which is caused by PWM switching process.

As mentioned in the introduction, the motor current is regulated

with FOC. The principle of FOC is to transform the total motor current flowing in the three phases into two orthogonal components, i.e., the torque generating and magnetic flux generating current by using the Clarke and Park transformations. An electric motor is a complex electrical-magnetic system. This transformations simplify this system significantly and allow the torque and magnetic flux to be controlled separately. Furthermore, the back emf observer mentioned in Section 3 is also implemented according to FOC, so that the estimated position, derived by the observer, can be applied for current control in FOC directly.

The Clarke transformation transforms motor current from phase coordinate, $u - v - w$, to stator coordinate, $\alpha - \beta$, (1). The stator coordinate is fixed with motor stator and the α axis has the same direction as the winding u.

$$\mathbf{i}_{\alpha\beta} = \begin{bmatrix} i_\alpha \\ i_\beta \end{bmatrix} = \frac{2}{3} \begin{bmatrix} 1 & -\frac{1}{2} & -\frac{1}{2} \\ 0 & \frac{\sqrt{3}}{2} & -\frac{\sqrt{3}}{2} \end{bmatrix} \begin{bmatrix} i_u \\ i_v \\ i_w \end{bmatrix} \quad (1)$$

The Park transformation transforms current from stator coordinate to rotor coordinate system, $d - q$, (2). The rotor system is fixed to the rotor magnet and rotates with the rotor.

$$i_{dq} = \begin{bmatrix} i_d \\ i_q \end{bmatrix} = \begin{bmatrix} \cos\theta & \sin\theta \\ -\sin\theta & \cos\theta \end{bmatrix} \begin{bmatrix} i_\alpha \\ i_\beta \end{bmatrix} \quad (2)$$

The aforementioned coordinate systems are shown in Figure 4. The angle, θ, between rotor and stator systems indicates also the electrical rotation angle of rotor, also known as commutation angle.
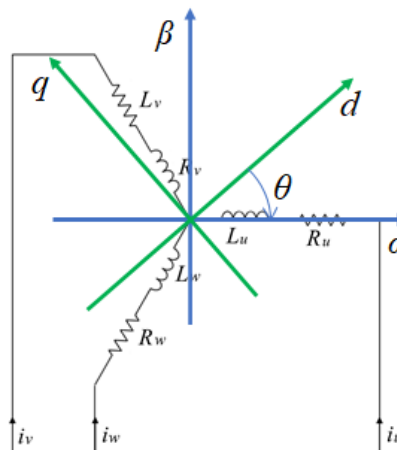
Figure 4: Coordinate systems applied in FOC, including phase, stator and rotor coordinate. θ is the angle between rotor and stator coordinate systems.

In order to control thrust, multicopter drives are operated in speed control mode. Therefore, the control system contains a PI speed controller cascaded with an PI current controller, see Figure 5. The speed feedback are derived by a speed observer or a speed filter. The configurations and gains of both controllers, observer or filter can be determined by using classical methods for electrical drives, for instance plant inversion or pole placement, [20]. As the algorithms and parametrisation methods for PI current and speed controllers are well known, they will not be introduced in this pa-

per. The next subsections describe the features that are specific to operation at high speed.
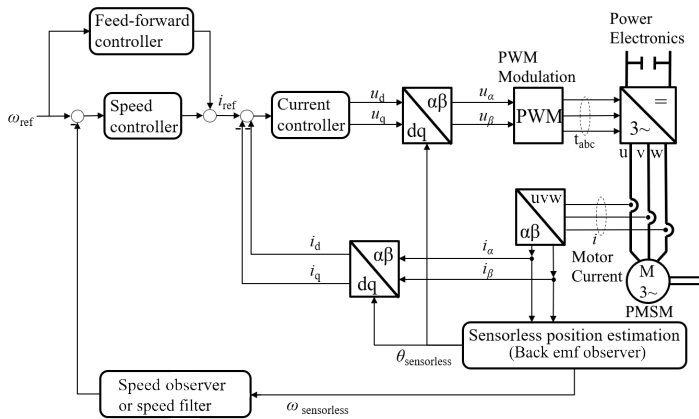
Figure 5: Control structure of multicopter drives, including speed and current control loops.
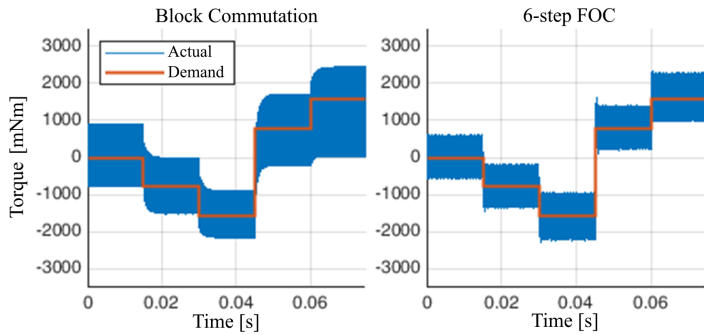
Figure 6: Simulated torque generation of block and 6-step FOC at 100 el. krpm. The FOC has faster response and smaller torque ripple compared to block commutation. The motor data are from PMSM 1 in Table 2 in the "Simulation and experimental results" section.

The output of the current controller, i.e., the demanded voltage, is converted to PWM signals via SVPWM generator. The PWM signals then drive the DC to AC power inverter, which is also included in the top-right corner of Figure 5.

2.2 Commutation method

Since multicopter drives are powered by onboard batteries, efficiency is arguably the most important optimisation criterion. In this section, block commutation and FOC are analysed and compared. If the motor speed is high enough relative to the execution frequency of current control, FOC may only generate ten or even less consecutive voltage vectors per electrical revolution, which is comparable to block commutation (six states per electrical revolution). In order to make a fair comparison between the two commutation methods, the position resolution is fixed to 6 per electrical revolution for both commutation methods in the simulation. The motor data from PMSM 1 in Table 2 in the experiment section is used for the simulation. The FOC current controller is explained in the "Current control with decoupling and delay compensation" subsection. Figure 6 and 7 show torque generation performance at two different

speeds. Figure 6 demonstrates that FOC has a faster response and lower current (torque) ripple. Besides, FOC is able to generate the demanded torque at a higher speed with the same supply voltage, see Figure 7. Therefore, FOC is chosen.
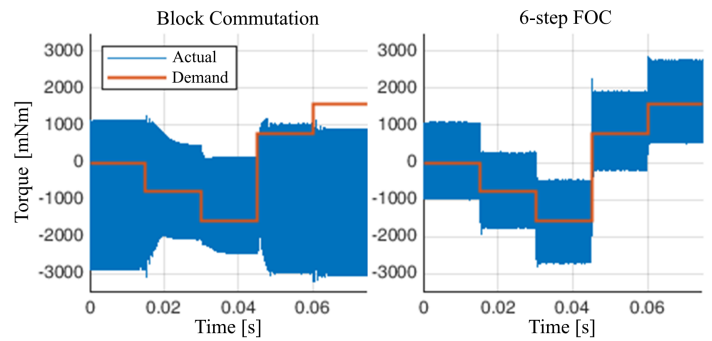
Figure 7: Simulated torque generation of block and 6-step FOC at 150 el. krpm. The FOC can generate the desired torque at 150 el. krpm, whereas block commutation fails. The motor data are from PMSM 1 in Table 2 in the "Simulation and experimental results" section. For block commutation to work at this frequency, a much higher DC supply voltage is needed.

As already mentioned, block commutation has the advantage that the rotor position can be inferred from the instant at which back emf changes sign (i.e., crosses zero) in the disconnected motor phase. However, this advantage is lost for motors with large electrical time constant operating at high speed: under these conditions, the current flowing through the body diodes in the leg of the power stage corresponding to the disconnected motor phase can shift the instant of the back emf zero-crossing.

Furthermore, for FOC, the PWM frequency and modulation methods are important parameters. In this paper, 5-level and 7-level space vector PWM (SVPWM) are considered, as shown in Figure 8. For the PWM frequency, 25 kHz and 50 kHz are considered.
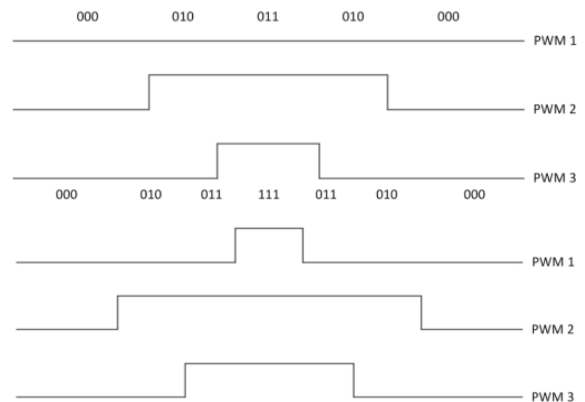
Figure 8: Example of 5-level (upper) and 7-level (lower) PWM duty cycle of a three-phase system. High and low, PWM1, PWM2 and PWM3 are according to the three phases respectively.

7-level SVPWM has lower current ripple, as shown in Figure 9. One should be aware that the difference of current ripple depends on motor characteristics, PWM frequency, and operating conditions. For motors with larger electrical time constant the difference becomes smaller.
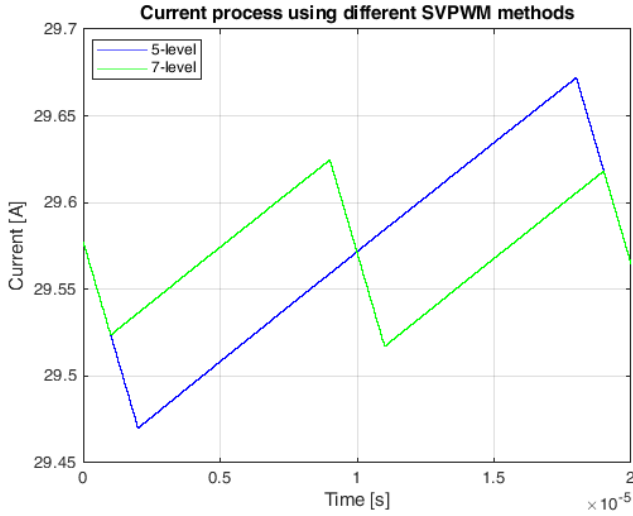
Figure 9: Simulated current process in a single PWM period using different modulation methods, current ripple of 7-level SVPWM is lower than that of 5-level.

On the other side, the switching losses on the motor controller significantly depend on the PWM frequency and modulation method. The comparison results in experiments are included in Section 4.

3 Motion control for high speed applications

3.1 Sensorless position estimation

As mentioned in the introduction, the reliability of the drive system is improved and its weight is reduced by eliminating the position sensor. There are three fundamental requirements on sensorless position detection based on back emf estimation:

1. Stability of the whole control system

2. Accuracy of back emf estimation at low speed, which is essential to use the position estimate for current control

3. Accuracy of position estimation, which affects the efficiency of torque generation.

We choose to estimate back emf with an observer. The observer requires a model of the system. For this purpose, we consider the electrical model of a SMPMSM

$$\mathbf{u}^S = \mathbf{R}^S \cdot \mathbf{i}^S + \mathbf{L}^S \frac{\mathrm{d}\mathbf{i}^S}{\mathrm{d}t} + \mathbf{e}^S \tag{3}$$

where $\mathbf{u}$ and $\mathbf{i}$ are applied voltage and motor current, which are functions of time, $\mathbf{R}$ and $\mathbf{L}$ are the motor resistance and inductance matrices, and $\mathbf{e}$ is the back emf. The superscript S indicates that the quantities are expressed in the stator coordinate system.

As with most control systems in practice, ours is implemented on a microcontroller in discrete form. The discrete implementation of the observer contains two separate steps for prediction and measurement update. The observer differs from a textbook Luenberger observer because the update step is based only on the measurement

of current and not of back emf. The prediction (4) and update (6) equations in discrete time are as follows

$$\tilde{\mathbf{i}}_k^S = \mathbf{\Phi}^S \hat{\mathbf{i}}_{k-1}^S + \mathbf{B}_d^S (\mathbf{u}_{k-1}^S - \hat{\mathbf{e}}_{k-1}^S) \tag{4}$$

$$\begin{aligned}
\hat{\mathbf{i}}_k^S &= \tilde{\mathbf{i}}_k^S + \mathbf{L}_i(\mathbf{i}_k^S - \tilde{\mathbf{i}}_k^S) \\
\hat{\mathbf{e}}_k^S &= \hat{\mathbf{e}}_{k-1}^S + \mathbf{L}_e(\mathbf{i}_k^S - \tilde{\mathbf{i}}_k^S).
\end{aligned} \tag{5}$$

where subscript k indicates the sampling instant and $\mathbf{\Phi}$ and $\mathbf{B}_d$ are the transition and input matrices of the discrete time system, respectively.

$$\mathbf{\Phi}^S = \exp\left(-\left(\mathbf{L}^S\right)^{-1}\mathbf{R}^S \Delta t\right) \tag{6}$$

$$\mathbf{B}_d^S = \left(\mathbf{I} - \mathbf{\Phi}^S\right)\left(\mathbf{R}^S\right)^{-1} \tag{7}$$

$\mathbf{L}_i = \mathrm{diag}\{l_i\}$ and $\mathbf{L}_e = \mathrm{diag}\{l_e\}$ are the observer feedback gain matrices for current and back emf, respectively. The ~ and ^ symbols indicate prediction and estimation variables, respectively. In this model, Δt is equal to the sampling time T_s.

In order to determine the values of the observer feedback gains, the electrical control loop, i.e. the linearised innermost feedback loop in Figure 5, is analysed. This loop consists of the current controller, the inverse Park transform (to the right of the "Current controller" block), the motor electrical dynamics, and the back emf observer ("Sensorless position estimation" block). This loop is stable if and only if

$$\gamma = \frac{|\mathbf{u_q}|}{|\mathbf{e}|} < \frac{1 + \phi\,(l_i - 1)}{l_e b_d}. \tag{8}$$

where ϕ and b_d are the diagonal elements of $\mathbf{\Phi}^S$ and $\mathbf{B}_d^S$ in (3). Equation (8) indicates that the operating range of the motor is constrained as a function of the motor's electrical dynamics and the observer gains. The ratio of voltage and back emf in the left hand side of (8) we call *operating point ratio*. Because the constraint also contains the observer gains, the allowed operating range can be manipulated at least to a certain extent.

The feedback gains of the observer are determined by using pole-placement with two conjugate poles. The available measurement is current and the expected output is back emf. For this reason, the transfer function in (9) from applied voltage, $\mathbf{u}$, to back emf, $\mathbf{e}$, has direct meaning in the controller and is applied. This transfer function is derived directly from the observer, according to the observer equations.

$$G(z) = \frac{e(z)}{u(z)} = \frac{l_e z}{z^2 + (l_e - 1 - \phi^S(1 - l_i))z + \phi^S(1 - l_i)} \tag{9}$$

The back emf observer's gains are calculated such that the phase lag of the transfer function $G(z)$ is below an predefined threshold at a certain frequency. This frequency corresponds to the maximum operating speed of the drive system expressed in Hertz. Because the phase lag of $G(z)$ corresponds to the error in the estimation of the back emf angle, and thus rotor position, this criterion guarantees that torque generation efficiency lies above a desired threshold in the whole operating range.

The calculation of the gains entails placing the conjugate poles' frequency a factor ten faster than the maximum intended operating

electrical speed. The corresponding expression for the observer's gains is

$$l_e = 1 - 2e^{-\xi\omega T_s}\cos\left(\omega T_s\sqrt{1-\xi^2}\right) + e^{-2\xi\omega T_s} \qquad (10)$$

$$l_i = 1 - \frac{1}{a}\left(e^{-2\xi\omega T_s} + b\gamma l_e\right). \qquad (11)$$

where ξ is the conjugate poles' damping coefficient, ω their frequency in rad/s, and T_s the sampling period, which is equal to $40\mu s$ in the experimental system. To sum up, this method requires two inputs to calculate the observer gains

1. Maximum intended operating point ratio for the present gain set

2. Maximum intended operating speed for the present gain set.

With this parametrisation method, the position obtained from the back emf estimate is reliable enough for use in current control from a speed of about 300 to 500 rpm with most motors.

3.2 Operation process

The motor drive operates under two different operating modes, the start-up mode and normal back emf mode, as long as there is not any error in the drive system. The switching between the modes is illustrated in the algorithm below.

Algorithm 1: Operating process and modes

Result: Operating process and modes
Initialisation;
while *system is enabled and reference speed is suitable* **do**
 if $|\mathbf{e_k}| > |\mathbf{e_k}|_{thr}$ **then**
  Operating in back emf mode;
 else
  Operating in start-up mode;
 end
end

We use the magnitude of back emf, $|\mathbf{e_k}|$, as a measure of the reliability of the back emf estimate for the purpose of current control. If it exceeds a predefined threshold, $|\mathbf{e_k}|_{thr}$, the position obtained from the back emf estimate is used for control: we call this operating mode "back emf mode". Compared to the speed range of propellers mentioned in the introduction (2000-8000 rpm), the speed corresponding to this back emf magnitude is low.

Below this speed, the motor operates in what we call the "start-up mode": starting at standstill, a constant-magnitude current vector is applied whose angle rotates with linearly increasing speed, i.e., constant acceleration. This is an open loop control mode, since the actual position and speed are not measured. For propeller drives, the open loop start-up mode and the transition to closed loop back emf mode works reliably, since the load is known and light. In this way, the motor is accelerated until the back emf magnitude is sufficient for closed loop control.

In addition, one must be aware that the position estimated by the back emf observer does not include the polarity of the rotor magnetic field and the rotation direction. To use the position estimate

from the back emf observer for commutation, the rotation direction must be known. This is determined by taking the cross-product of the last two consecutive position estimates from the back emf observer. The scalar product of the motor speed with the unit vector z perpendicular to the stator coordinate (α-β) plane yields s_k, which corresponds to the magnitude of rotational speed.

$$s_k = (\mathbf{e}_{k-1} \times \mathbf{e}_k) \cdot \mathbf{z}. \qquad (12)$$

In practice, since s_k is very noisy, it is low-pass filtered before evaluation of its sign.

3.3 Current control with decoupling and delay compensation

As mentioned in the introduction, cross-coupling between the current components in the rotor coordinate frame is proportional to the product of the motor's electrical time constant and of the motor's speed. If this cross-coupling is not considered when tuning the current controller, it deteriorates current control performance perceptibly. What's more, the discrete implementation of the current control system inevitably gives rise to sampling delay. To counteract the effect of cross-coupling and sampling delay in the current control loop, we apply d-q decoupling and delay compensation.

The derivation begins from the motor electrical model. Transforming the electrical model of PMSM in (3) to the rotor coordinate frame yields (13). The aforementioned cross-coupling between the d and q components, $\omega_e L$, cannot be neglected anymore

$$\mathbf{u}^R = \begin{bmatrix} R & -\omega_e \cdot L \\ \omega_e \cdot L & R \end{bmatrix} \mathbf{i}^R + \begin{bmatrix} L & 0 \\ 0 & L \end{bmatrix} \frac{d\mathbf{i}^R}{dt} + \mathbf{e}^R, \qquad (13)$$

where superscript R indicates the rotor coordinate frame and $\mathbf{e}$ is the back emf, whose magnitude is equal to the product of magnetic linkage and electrical speed, $\Psi\omega_e$.

In independent d-q current control, the cross coupling terms are neglected and the current controller is as follows

$$\begin{aligned} \mathbf{u}^R_{c,k+1} &= k_P\Delta\mathbf{i}^R_k + \mathbf{I}^R_k \\ \mathbf{I}^R_{k+1} &= \mathbf{u}^R_{c,k+1} - (k_P - k_I)\Delta\mathbf{i}^R_{k+1}, \end{aligned} \qquad (14)$$

where $\mathbf{u}_c$ is the output demand voltage, $\Delta\mathbf{i}$ is the current control error, and $\mathbf{I}$ is the integral term in PI current controller.

When $|\omega_e L|$ is comparable to or larger than R, independent control of the current components of $\mathbf{i}^R$, i.e., i_d and i_q, undermines transient performance and may even lead to instability. It is true that a higher control bandwidth can help. However, in practice the bandwidth is always limited by sampling frequency, which is determined by the computational power of the selected MCU and characteristics of the power electronics components.

We adopt the method in [17] to improve the performance of current control loop without having to increase the sampling frequency. Equation (15) describes the decoupling PI current control in discrete time.

$$\begin{aligned} \mathbf{u}^R_{c,k+1} &= k_P\begin{bmatrix} \cos(T_s\omega_e) & -\sin(T_s\omega_e) \\ \sin(T_s\omega_e) & \cos(T_s\omega_e) \end{bmatrix}\Delta\mathbf{i}^R_k + \mathbf{I}^R_k \\ \mathbf{I}^R_{k+1} &= \mathbf{u}^R_{c,k+1} - (k_P - k_I)\Delta\mathbf{i}^R_{k+1}. \end{aligned} \qquad (15)$$

In this current control method, the tuning of current controller should guarantee (16), to ensure the equivalency of discrete time and continuous time controller,

$$\frac{k_I}{k_P} = 1 - e^{-T_s \frac{\hat{R}}{\hat{L}}} \tag{16}$$

where $\hat{R}$ and $\hat{L}$ are the estimated values of phase resistance and inductance, respectively. They can be identified or obtained from the motor's datasheet.

The sampling delay is another factor which affects the high-speed performance. It results in a lower torque than desired causing a worse torque generation efficiency. To address this issue, the demand voltage $\mathbf{u}_c$ is rotated forward by $T_s \omega_e$ yielding $\mathbf{u}_c^*$, which is the final output of current controller

$$\mathbf{u}_{c,k+1}^* = \begin{bmatrix} \cos(T_s \omega_e) & -\sin(T_s \omega_e) \\ \sin(T_s \omega_e) & \cos(T_s \omega_e) \end{bmatrix} \mathbf{u}_{c,k+1}. \tag{17}$$

4 Simulation and experimental results

4.1 Simulation and experimental system

The introduced control methods are implemented in an Electronic Speed Controller (ESC), the maxon UAV-ESC 52/30, see Figure 10. The experiments are conducted using this ESC and two test motors, PMSM 1 (Figure 11) is a Ø87 mm outrunner drone motor by maxon designed for multicopters, whereas PMSM 2 (Figure 12) is a general-purpose inrunner motor, also by maxon, which can reach a high electrical speed (210 el. krpm). The MCU of the UAV-ESC 52/30 is an ARM Cortex-M microcontroller from STMicroelectronics. The modelling and simulations are according to the same hardware systems under the Matlab/Simulink environment. Specifications of the controller and test motors are summed up in Table 1 and Table 2, respectively.

Figure 11: The test motor PMSM 1, UAV motor. On the back side, left, there are three thick motor power cables and four thin cables for two motor temperature sensors, which are applied for measurement of thermal behaviour later.

Figure 12: The test motor PMSM 2.
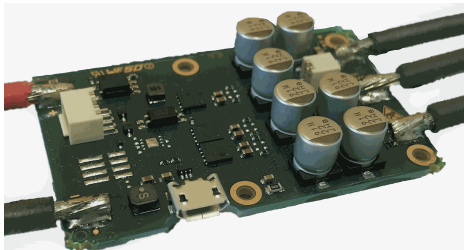
Figure 10: The UAV-ESC 52/30 without housing.
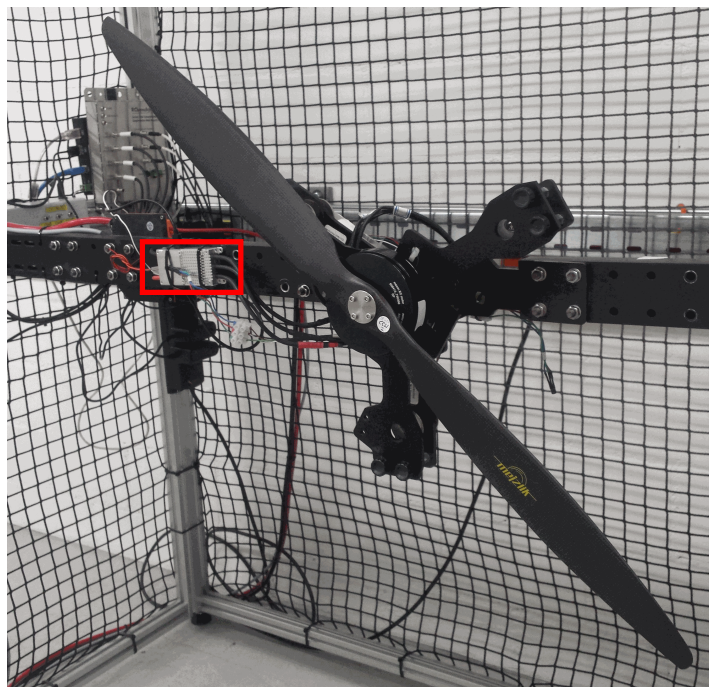
Figure 13: Experimental setup, including the test motor PMSM 1 with propeller and the controller with aluminium housing, indicated by the red rectangle.
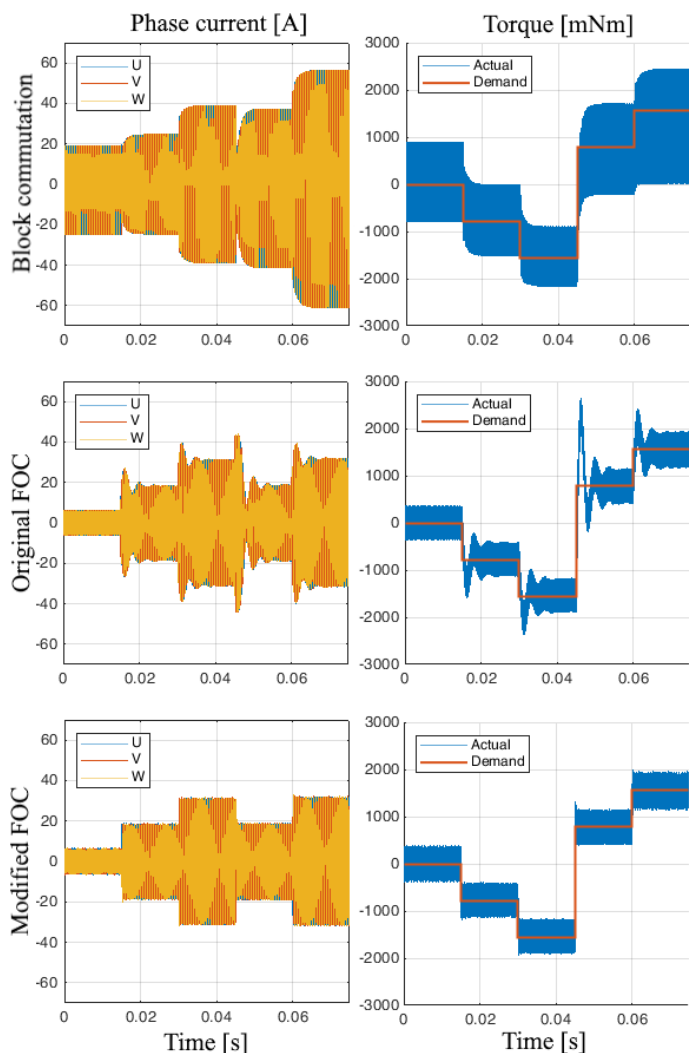
Figure 14: Simulation of motor current and torque during current step response at speed 100 el. krpm, using PMSM 1. The modified FOC has better transient performance and lower current/torque ripple compared to both block commutation and the original FOC.

Table 2: Maxon motor specification

Test motor	PMSM 1	PMSM 2
Diameter	Ø87 mm	Ø40 mm
Length	20 mm	40 mm
Max. continuous operating current	30 A	5.9 A
Max. operating current	90 A	15 A
Motor pole pair number	21	7
Motor maximum mechanical speed	6500 rpm	30000 rpm
Motor resistance (phase to phase)	0.0891 Ω	0.136 Ω
Motor inductance (phase to phase)	0.05 mH	0.0639 mH
Electrical time constant	5.61×10^{-4} s	4.70×10^{-4} s
Structure	Outer runner	Inner runner
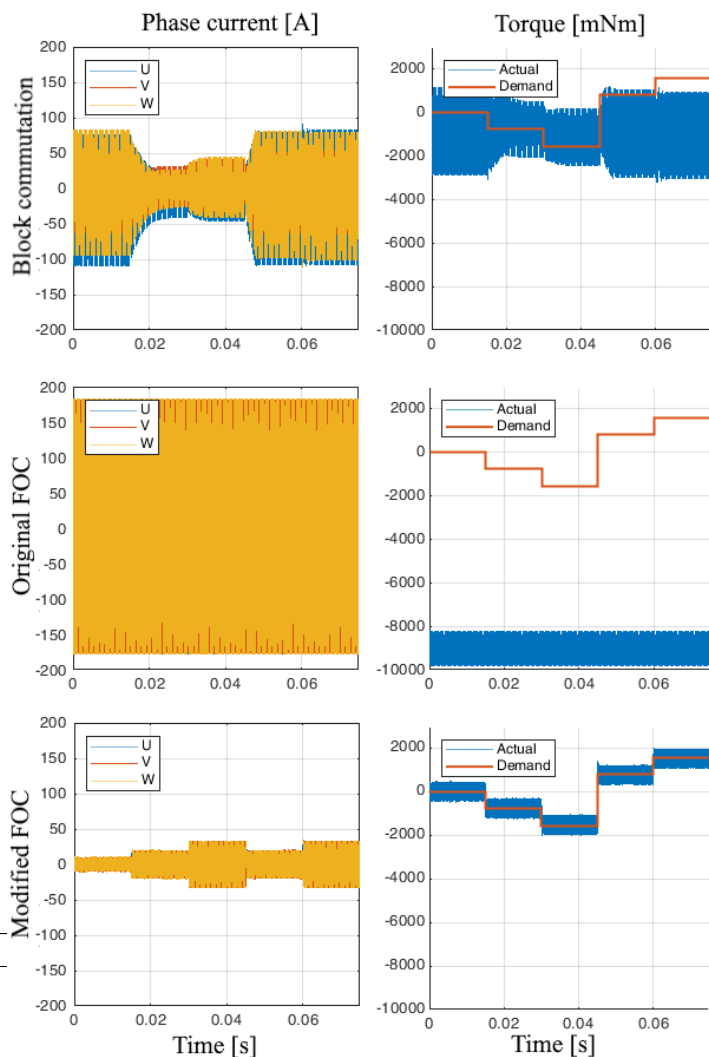
Figure 15: Simulation of motor current and torque during current step response at speed 150 el. krpm, using PMSM 1. The modified FOC performs well, whereas the block commutation cannot output the desired torque, and the original FOC becomes unstable.

Table 1: Controller specification

Type of controller	maxon UAV-ESC 52/30
Mechanical dimension:	
length	58 mm
width	36 mm
thickness	11.6 mm
Electric characteristics:	
PWM frequency	25 kHz
Current control sampling frequency	25 kHz
Position estimation frequency	25 kHz
Speed control sampling frequency	2.5 kHz
maximum continuous operating current	30 A
maximum output current	90 A
Supply voltage	12-52 V DC

The experiments are conducted with different loads. If the test motor PMSM 2 is used, the load is created by a coupled motor generating an opposing torque. On the other hand, the experiments with the test motor PMSM 1 are conducted with a propeller on the

test setup shown in Figure 13. This paper concentrates on motor control.
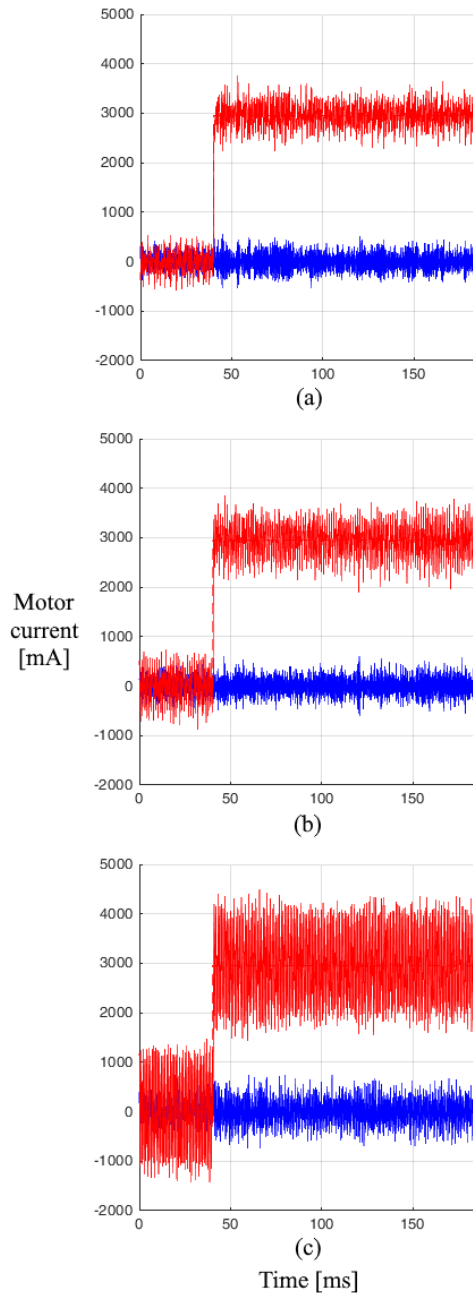
Figure 16: Motor current in experiments of current step response under current control using PMSM 2 at 40, 175, and 210 el. krpm in sub-figures (a), (b) and (c), respectively. The blue curve indicates the d-current and the red curve indicates the q-current. The current controller performs well, with increasing current ripple with operating speed.

4.2 Simulation results of control behaviour

The performance of current/torque control and commutation are simulated for different current step responses. In Figure 14, simulations show that at 100 el. krpm, FOC has a fast response and generally smaller torque/current ripple compared to block commutation. Current control with decoupling and delay compensation

("modified FOC" for short) has an even slightly smaller current and torque ripple compared to the independent d-q current control ("original FOC" for short). In particular, the modified FOC has a significantly better transient performance compared to the original FOC, with consideration of overshoot and settling time.

Figure 15 shows that at 150 el. krpm the original FOC becomes unstable. For block commutation, the DC supply voltage is not enough to correctly apply the desired torque. Instead, the modified FOC still performs well.

4.3 Experimental results of control behaviour

In experiments, different operating points and operating modes are included. Figure 16 shows current in the d-q coordinate frame. There are desired q-current steps at different constant motor speeds (140, 175, and 210 el. krpm), using the modified FOC and PMSM 2. The desired d-current is always zero. At the maximum tested speed, 210 el. krpm, there are 7.5 commutations per electrical revolution. The modified FOC is stable and sufficiently dynamic at all tested speeds, although current ripple increases with operating speed.

In Figure 17, the start-up process using PMSM 1 with propeller is illustrated. The drive starts from standstill in start-up mode. The magnitude of back emf is evaluated in each current period. As soon as the magnitude of back emf exceeds a predefined threshold, 0.35 V in this experiment, the operating mode switches to the back emf operating mode (at about 0.26 seconds in Figure 17). This back emf threshold corresponds to a mechanical speed of about 300 rpm. From then on, the position estimate obtained from the back emf estimate is considered reliable enough for use in closed loop control.
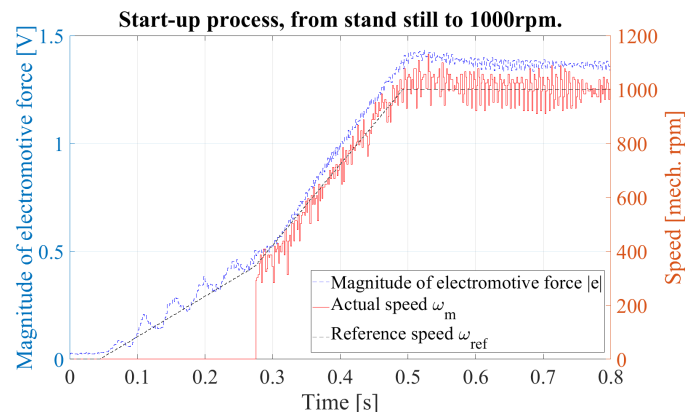
Figure 17: Start-up process from stand still to 1000 rpm, using PMSM 1 with propeller. The black dashed curve and red curve indicate the desired and measured speed, respectively. The speed in the plot is measured based on the back emf position estimation, which is available only after the switch into the back emf operating mode. The blue curve illustrates the magnitude of back emf. In this experiment, the threshold is 0.35 volts.

Further experiments of speed control are conducted. Figure 18 illustrates acceleration under speed control from 600 to 4000 rpm, using the PMSM 1 with propeller. The desired speed is implemented according to a profile acceleration of 5500 rpm/s. The drive operates in back emf mode in this speed range. The speed control and position estimation are reliable.
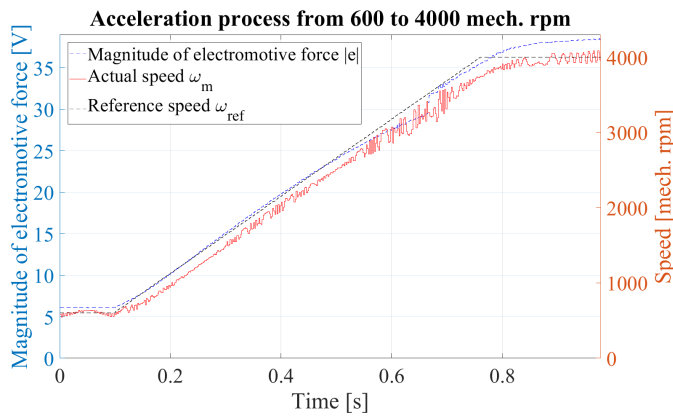
Figure 18: Acceleration using PMSM 1 with propeller, from 600 to 4000 rpm. The black dashed and red curves indicate the desired and measured speed, respectively.

Figure 19 illustrates speed control using fast acceleration from with stand still. The process of motor current is also included. The speed overshoot in this experiment is created with propose in order to illustrate a strong acceleration current, which exceeds the maximal continuous operating current for short period.
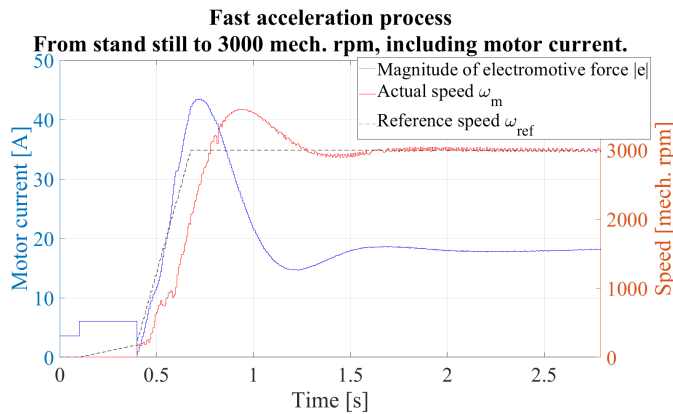
Figure 19: Acceleration using PMSM 1 with propeller, from stand still to 3000 rpm. The black dashed and red curves indicate the desired and measured speed, respectively. The blue curve indicate the motor current.

In the next experiment, true load condition of multicopters is tested. Figure 20 shows the speed control with a constant reference speed, on PMSM 1 with propeller. For propeller drives, the propeller's thrust and drag torque are both monotonic functions with respect to propeller speed. Therefore, at least under laboratory settings, the drive's torque (current) will be a monotonic function of speed. In this experiment, the drive is tested at its maximum continuous operating current, i.e. 30 amperes under similar condition as that of true UAV applications.

To achieve this high fidelity in ground experiment, the motor is under speed control. The load torque is continuously disturbed by an external mechanism on purpose, oscillating between ±10% of the maximum continuous torque. This leads to an effect that the controlled speed oscillates about ±2.5%. The speed controller is not optimised for disturbance rejection. The speed control reference is about 3390 rpm, i.e., about 71.5 el. krpm.
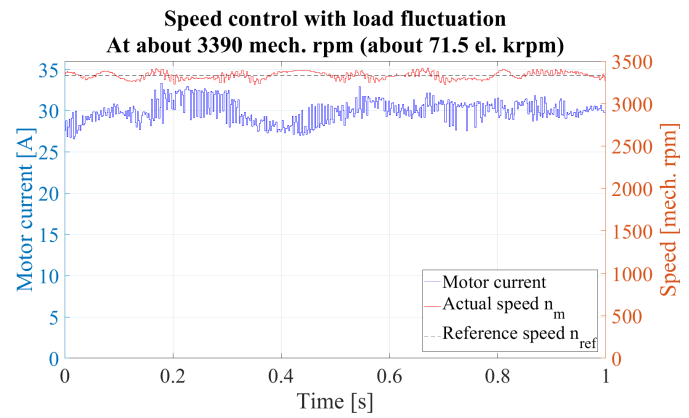
Figure 20: Speed control with maximum output power using PMSM 1. The load torque is continuously disturbed by an external mechanism, between ±10% of the maximum continuous torque. The controlled speed oscillates about ±2.5%. The black dashed and red curves are the desired and measured speed, respectively. The blue curve indicates the motor current.

4.4 Thermal behaviour

The thermal behaviour of the drive system is also experimentally investigated. In this experiment, two motors are coupled, one operates as drive (PMSM 1 in Table 2) and the other as load. The temperature of motor and power stage of motor controller is measured by using temperature sensors. A PT100 temperature sensor attached on one MOSFET in the power stage of the UAV-ESC 52/30 as shown in Figure 21. A NTC temperature sensor in the motor, shown in Figure 11, measures the temperature of the motor's windings.
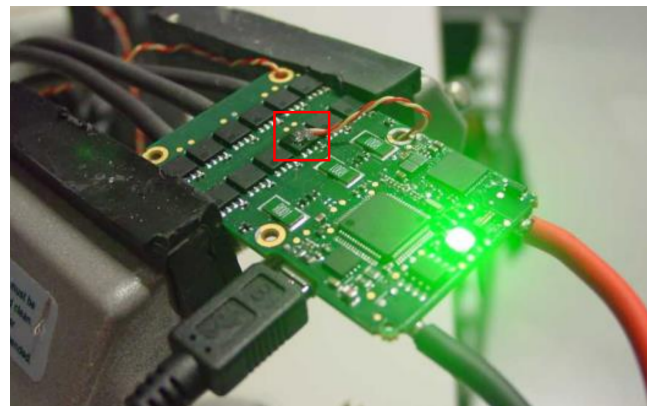
Figure 21: Installation of PT100 temperature sensor on a MOSFET of power stage, the red rectangle. There are totally 12 MOSFETs used in one UAV-ESC 52/30 controller. The red-yellow cables connect the PT100.

The results are summed up in Table 3 and 4, for motor and power stage, respectively, with consideration of using different modulation methods and PWM frequencies. The thermal losses are indicated by using relative temperature. The temperature using 7-level SVPWM with PWM frequency of 25 kHz is considered as reference temperature. The temperature difference is with respect to this reference temperature. It can be recognised that the applied 25 kHz, 7-level SVPWM is optimal for the combination of motor and power stage. According to Table 3, higher PWM frequency leads to lower motor temperature, and the temperature of 7-level SVPWM is lower than

that of 5-level SVPWM using the same PWM frequency. The reason is the smaller current ripple.

Table 3: Thermal losses on motor, indicated by relative temperature difference on motor. The motor temperature using 7-level SVPWM with PWM frequency of 25kHZ is considered as reference.

SVPWM	f_{PWM}	
method	25 kHz	50 kHz
5-level	$3.7°C$	$0.3°C$
7-level	0_{ref}	$-0.8°C$

For motor controller, the relative temperature of power electronics circuit is considered in Table 4. Analogously, the temperature of power stage using 25 kHz 7-level SVPWM is referred. Higher PWM frequency leads to higher power stage temperature, and 5-level SVPWM has lower temperature compared to 7-level SVPWM, due to less switching losses in the MOSFETs.

Table 4: Thermal losses on power stage, indicated by temperature difference of power stage. The power stage temperature using 7-level SVPWM with PWM frequency of 25 kHz is considered as reference.

SVPWM	f_{PWM}	
method	25 kHz	50 kHz
5-level	$-2.8°C$	$6.2°C$
7-level	0_{ref}	$23.2°C$

Comparing both tables, we can sum up:

1. For the tested motor, increasing PWM frequency leads to significantly more losses on power electronics, whereas the reduction of motor losses is minor, because the multicopter motor has relatively large electrical time constant. Therefore, the PWM frequency 25 kHz if preferred.

2. At 25 kHz the 5-level PWM has slightly less losses in the power stage and slightly more losses in the motor compared to 7-level PWM. Because of the better accuracy of the output voltage using 7-level compared to 5-level SVPWM, the former is preferred.

That means the configuration of 7-level SVPWM at 25 kHz, as mentioned in Table 1, is reasonable for the multicopter drive controller.

5   Conclusion

As one of the most rapidly developed application areas of electric motors, UAVs, especially multicopters, using electric motors have gotten a lot of attention. It is still a challenge to fulfil the requirements for professional multicopters, for instance for industry, agriculture and security applications. This paper focuses on these desires. Accurate sensorless control and commutation methods are developed in order to improve efficiency and extend the operation speed range.

In this paper, at first, a motor controller for multicopter drives is introduced. The technical background of electric drive systems for PMSM is introduced briefly, with consideration of power inverter, general control structure, commutation methods, including block commutation and FOC, and different modulation methods of SVPWM. The special requirements and operation conditions of multicopter drives are considered. Then, as the main innovative part of this paper, a control system for electrical drives for multicopters is introduced. The control system relies on sensorless position detection provided by a back emf observer, on a decoupling mechanism of the motor current components in the rotor coordinate frame, and on the compensation of the effect of sampling delay in the current control loop. The parametrisation method of the back emf observer is also included in order to minimise the offset of estimated position, especially at high speed. The proposed methods have taken requirements and application situations of multicopter drives into consideration. The control system is implemented in a compact motor controller. We show in simulation and experiment that the control system can drive two motors at high speed, up to 200 el. krpm. In experiments, a compact motor drive platform, maxon UAV-ESC 52/30, is used. High fidelity validation with propeller and load with disturbance and oscillation are also included in experiments. Furthermore, the thermal behaviour of the multicopter drives is analysed. Measurement of the temperature of both motors and power electronics validate the choice of PWM frequency and space vector modulation method.

Besides multicopters, these methods can also be applied in other systems with similar requirements.

References

[1] C. Zhao, W. Kong, F. Percacci, P. Gnos, "Sensorless FOC Drive Control Methods for High Speed Motors of Unmanned Multicopters," in Proc. 23rd Conference on Power Electronics and Applications (EPE'21 ECCE), 2021, doi:10.23919/EPE21ECCEEurope50061.2021.9570534.

[2] N. Michel, P. Wei, Z. Kong, A. K. Sinha, X. Lin, "Modeling and validation of electric multirotor unmanned aerial vehicle system energy dynamics," eTransportation, **12**, 100173, 2022, doi:10.1016/j.etran.2022.100173.

[3] D. Mohanraj, R. Aruldavid, R. Verma, K. Sathiyasekar, A. B. Barnawi, B. Chokkalingam, L. Mihet-Popa, "A Review of BLDC Motor: State of Art, Advanced Control Techniques, and Applications," IEEE Access, **10**, 54833–54869, 2022, doi:10.1109/ACCESS.2022.3175011.

[4] M. Schroedl, "Sensorless control of AC machines at low speed and standstill based on the 'INFORM' method," in Proc. Industry Applications Conference, 270–277, 1996, doi:10.1109/IAS.1996.557028.

[5] A. Consoli, G. Scarcella, A. Testa, "Industry application of zero-speed sensorless control techniques for PM synchronous motors," IEEE Transactions on Industry Applications, **37**(2), 513–521, 2001, doi:10.1109/28.913716.

[6] N. Bianchi, E. Fornasiero, S. Bolognani, "Effect of Stator and Rotor Saturation on Sensorless Rotor Position Detection," IEEE Transactions on Industry Applications, **49**(3), 1333–1342, 2013, doi:10.1109/TIA.2013.2253437.

[7] M. Laumann, C. Weiner, R. Kennel, "Arbitrary injection based sensorless control with a defined high frequency current ripple and reduced current and sound level harmonics," in Proc. IEEE International Symposium on Sensorless Control for Electrical Drives (SLED), 103–108, 2017, doi: 10.1109/SLED.2017.8078438.

[8] T. Slininger, M. Petit, H. Flieh, S. Chien, L. Ku, R. D. Lorenz, "Full Order Discrete-Time Modeling for Accurate and Speed-Independent Pulsating Voltage Injection Self-Sensing," in Proc. IEEE 10th International Symposium on Sensorless Control for Electrical Drives (SLED), 1–6, 2019, doi: 10.1109/SLED.2019.8896346.

[9] C. Zhao, M. Tanaskovic, F. Percacci, S. Mariéthoz, P. Gnos, "Sensorless position estimation for slotless surface mounted permanent magnet synchronous motors in full speed range," IEEE Transactions on Power Electronics, **34**(12), 11566–11579, 2019, doi:10.1109/TPEL.2019.2908408.

[10] K. Schuhmacher, S. Kleen, M. Nienhaus, "Comparison of Anisotropy Signals for Sensorless Control of Star-Connected PMSMs," in Proc. IEEE 10th International Symposium on Sensorless Control for Electrical Drives (SLED), 1–6, 2019, doi:10.1109/SLED.2019.8896351.

[11] H. Fakham, M. Djemai, K. Busawon, "Design and practical implementation of a back-EMF sliding-mode observer for a brushless DC motor," IET Electric Power Applications, **2**, 353–361, 2008, doi:10.1049/iet-epa:20070242.

[12] A. Darba, P. D'haese, F. D. Belie, J.Melkebeek, "Rotor speed, position and load torque estimation using back-EMF sampling for self-sensing brushless DC machine drives," in Proc. IEEE 5th International Symposium on Sensorless Control Elect. Drives, 1–7, 2014, doi:10.1109/SLED.2014.6844968.

[13] Y. Shao, B. Wang, Y. Yu, Q. Dong, M. Tian, D. Xu, "An Integral Sliding Mode Back-EMF Observer for Position-Sensorless Permanent Magnet Synchronous Motor Drives," in Proc. 22nd International Conference on Electrical Machines and Systems (ICEMS), 1–5, 2019, doi:10.1109/ICEMS.2019.8922158.

[14] L. Schwager, A. Tüysüz, C. Zwyssig, J. W. Kolar, "Modeling and Comparison of Machine and Converter Losses for PWM and PAM in High-Speed Drives," IEEE Transactions on Industry Applications, **50**(2), 995–1006, 2014, doi:10.1109/TIA.2013.2272711.

[15] F. Briz, M. W. Degner, R. D. Lorenz, "Analysis and design of current regulators using complex vectors," IEEE Transactions on Industry Applications, **36**(3), 817–825, 2000, doi:10.1109/28.845057.

[16] H. Kim, M. W. Degner, J. M. Guerrero, F. Briz, R. D. Lorenz, "Discrete-time current regulator design for AC machine drives," IEEE Transactions on Industry Applications, **46**(4), 1425–1435, 2010, doi:10.1109/TIA.2010.2049628.

[17] B. Bon-Ho, S.-K. Sul, "A compensation method for time delay of full-digital synchronous frame current regulator of PWM AC drives," IEEE Transactions on Industry Applications, **39**(3), 802–810, 2003, doi:10.1109/TIA.2003.810660.

[18] J.-S. Yim, S.-K. Sul, B.-H. Bae, N. R. Patel, S. Hiti, "Modified current control schemes for high-performance permanent-magnet AC drives with low sampling to operating frequency ratio," IEEE Transactions on Industry Applications, **45**(2), 763–771, 2009, doi:10.1109/TIA.2009.2013600.

[19] D. Schröder, Elektrische Antriebe –RegelungvonAntriebssystemen, Springer-Verlag, 2009.

[20] D. Schröder, Leistungselektronische Schaltungen, Springer-Verlag, 2008.

ASTES

Bangla Speech Emotion Detection using Machine Learning Ensemble Methods

Roy D Gregori Ayon, Md. Sanaullah Rabbi, Umme Habiba, Maoyejatun Hasana[*]

Department of Computer Science and Engineering, Asian University of Bangladesh, Dhaka, 1341, Bangladesh

A R T I C L E I N F O	A B S T R A C T
	Emotion is the most important component of being human, and very essential for everyday activities, such as the interaction between people, decision making, and learning. In order to adapt to the COVID-19 pandemic situation, most of the academic institutions relied on online video conferencing platforms to continue educational activities. Due to low bandwidth in many developing countries, educational activities are being mostly carried out through audio interaction. Recognizing an emotion from audio interaction is important when video interaction is limited or unavailable. The literature has documented several studies on detection of emotion in Bangla text and audio speech data. In this paper, ensemble machine learning methods are used to improve the performance of emotion detection from speech data extracted from audio data. The ensemble learning system consists of several base classifiers, each of which is trained with both spontaneous emotional speech and acted emotional speech data. Several trials with different ensemble learning methods are compared to show how these methods can yield an improvement over traditional machine learning method. The experimental results show the accuracy of ensemble learning methods; 84.37% accuracy was achieved using the ensemble learning with bootstrap aggregation and voting method.

1. Introduction

Emotions play an important role in understanding human behaviors, thoughts, and actions. There is a plethora of applications such as human-to-human communication [1], human computer interaction [2], affective computing [3], remote patient monitoring system [4], etc. where emotion detection is a vital part for decision making, problem solving or understanding the mental state of a subject. Human emotions can be divided into primary and compound emotions. Primary emotions consist of eight types of emotions such as anger, fear, sadness, disgust, surprise, anticipation, acceptance, and joy. Compound emotions can be derived by conjugating two or more primary emotions. On the other hand, emotions may vary not only from person to person but also in different contexts, communities, cultures, and languages. This work detects emotions from Bangla speech data extracted from audio.

Working with Bangla speech data to detect emotions is quite difficult and different in terms of accent, pitch, rhythm,

intonation, pronunciation, and voice modulation. Selecting the right set of features is necessary to correctly classify emotions from Bangla speech data. There are several feature extractions approaches such as perceptual linear prediction (PLP), linear prediction coding (LPC) and Mel-frequency Cepstrum Coefficients (MFCC), which have been used for speech recognition from speech data. In this study, MFCC is used to extract features from Bangla audio speech data collected from Bangla speaking participants.

Literature has documented numerous traditional machine learning approaches to classify an emotion from different types of data such as text, audio, video, image, brainwaves, etc. There are few notable works that detect emotions from Bangla speech data [5]-[9]. In [5], the authors have investigated the optimum number of MFCCs to recognize an emotion from speech data and suggested that MFCCs should be 25. In [6], the authors have developed a Gated Recurrent Unit (GRU) based deep neural network model to classify users' comments on Facebook pages. The authors have collected 5,126 Bangla comments and classified them into six classes: hate speech, communal attack, inciteful, religious hatred, political comments, and religious

[*]Corresponding Author: Maoyejatun Hasana, Asian University of Bangladesh, Dhaka-1341, Bangladesh, mjhasana@aub.edu.bd

comments. The accuracy of GRU based model is 70.10%. In [7], the Recurrent Neural Network (RNN) is used to classify six emotions: joy, sadness, anger, surprise, fear, and disgust from Bangla speech and achieved 51.33% accuracy. In [8], Gaussian Mixture Model-Hidden Markov Model (GMM-HMM) and Deep Neural Network-Hidden Markov Model (DNN-HMM) are used to search emotions from 49 different speakers of a vocabulary of 500 unique words. The performance criterion of the models is considered Word Error Rate (WER) and achieved 3.96% WER for GMM-HMM, whereas 5.30% WER for DNN-HMM. In [9], an ensemble method of several supervised classifiers has been used to classify emotions from speech data and achieved 70% accuracy. We can see that the existing works have not achieved significant accuracy in detecting, and/or recognizing emotions from audio data. This work uses ensemble machine learning methods to detect four types of emotion such as happy, sad, angry, and neutral. Different trials of ensemble machine learning methods have been conducted to achieve better accuracy. The specific contributions of this work are as follows:

- Bangla speech data collection with a careful avoidance in data biases.
- Implementation of a noise reduction module which has been used during pre-processing.
- Apply a different set of ensemble machine learning methods to achieve better accuracy in emotion detection.

The rest of this paper is organized as follows. Related research is given in the next section. Dataset information is given in section 3. After that, the detail of the proposed method is described in section 4. Following the methodology, results and analysis are drawn from the experiments. Then a conclusion is drawn.

2. Related Work

From the last few decades, enormous research works have been accomplished in the field of emotion detection, recognition, and/or classification. Emotional intelligence is widely used to develop an emotionally aware healthcare monitoring system or a safe driving system or during computer games. This section will focus on reviewing different studies on emotion detection as well as studies other than the English language.

2.1. Study of Speech Emotion Detection

In [10], the authors developed a machine learning model for automatic emotion detection from speech. The model is used to monitor public emotions. The authors chose a manually annotated dataset and represented it as text using a vectorization method. Deep learning methods, convolutional, recurrent neural networks, and perception are used to detect emotions in textual data. The accuracy of the obtained classification model is quite low, which is 77% for random forest, 74% for regression, and 73.5% for naive Bayesian classifier.

In [11], the authors presented an ANN approach to predict emotion in the field of Music Emotion Recognition. 167 voices were analyzed, and 76 features were extracted from International Affective Digital Sounds Dataset (IADS). This audio dataset was segmented into three parts for the purpose of training (70%), validation (15%) and testing (15%). In the prediction stage, the

ANN model accounted for 64.4% in arousal and 65.4% in valence. The result showed that the shallow neural network performs better than the regression model.

In [12], the authors presented a method for detecting emotion using speech using IoT based deep learning. The authors implemented a real time system based on IoT, and then classified emotions. The authors proposed an integrated deep learning model named Speech Emotion Detection (SED) using 2D convolutional neural network. The accuracy rate achieved by SED is approximately 95%.

In [13], the authors presented a new set of acoustic features for automatic emotion recognition from audio. The author proposed a feature based perceptual quality metric which is based on the masked perceptual loudness. The features computed emotion based on emotional difference such as "happy/excited", "angry/anxious", "sad/bored", and "relaxed/serene" in the reference set of data. The authors used the proposed set referred as a perceptual feature set that consists of a 9-dimensional feature vector with 7 low level and 2 statistical descriptors. GMM and SVM classifiers are used for computing emotions. A decision rule to be interpreted as an S-MV rule was proposed by the authors and it showed an improved recognition performance specially for valence which was valid in both acted and natural emotions.

In [14], the authors explained architecture for modeling conversation through language models encoding, and classification stages. The authors used transfer learning through the universal language modeling that is composed of Bi-LSTM units. The authors also list the hyperparameters which are used for building and training these models. The F1-score of this model is 0.7582.

The EmoDet2 system is presented in [15] to detect emotion using a deep learning approach. EmoDet2 takes English textual dialogue as an input, and from text it detects four types of emotion such as happy, sad, angry, and others. The authors combined neural network architecture and BiLSTM neural network to obtain substantial improvement over the baseline model. The performance of EmoDet2 is quite satisfactory, with an F1-score of 0.78.

In [16], the authors developed a system to detect emotion from the Roman Urdu text. The authors developed a comprehensive corpus of 18k sentences that converged from distinct domains, and annotated it with six different classes. The authors also applied different baseline algorithms like KNN, Decision tree, SVM, Random Forest on their corpus. The authors gained an accuracy rate of 69.4% and an F-measure of 0.69.

A method to recognize emotion collected from social media like Twitter is described in [17]. The authors classify English text into six different emotions which are happiness, sadness, fear, anger, surprise, and disgust. The authors used natural language processing and machine learning classification

algorithms. The authors also managed to create a large bag of emotional words along with their emotion-intensities. The authors achieved an accuracy of 91.7% for SMO and 85.4% for J48.

In [18], the authors presented a model to detect multiclass emotion detection from Bangla text. The authors used a Multinomial Naïve Bayes (MNB) classifier with various features. The model can classify three emotions: happy, sad, and angry from text with an accuracy of 78.6%.

In [19], the authors explained a machine learning method to recognize four major types of human emotions which are anger, sadness, joy, and pleasure. The authors incorporated electrocardiogram (ECG) signals to recognize emotions. The authors combined four ECG signal-based techniques which are heart rate variability, empirical mode for decomposition within beat analysis, and frequency spectrum analysis. The frequency spectrum analysis used in this work is proposed in this work. By comparing it with the best biosensor-based model, this ensemble model attained an accuracy rate of 10.77%.

In [20], the authors presented a framework of Long Short-Term Memory (LSTM) and 2D Convolutional Neural Network (CNN) to detect emotion from physiological signals acquired using wearable, low-cost sensors. In [21], the authors used two ensemble classification schemes: stacked generalization and unweighted voting for spoken emotion recognition. Stacked generalization is an approach to combining predictions from multiple classifiers. In an unweighted voting method, the class predictions of the base-level classifiers are abridged and the class which gets majority votes is selected as the final class. Numerous deep learning architectures have been used in [22] for emotion detection from both speech and text data.

Most of these works have been conducted to recognize emotions in English language, which could not be useful for detecting emotions in languages other than English.

2.2. Study of speech emotion detection in languages other than English

Beyond the English language-based speech emotion detection studies, researchers have worked on many other languages such as Persian [23], Urdu [24], Arabic [25], Hindi [26], etc. Since each language has different kind of expressions to show emotional states, generalizing emotions for all languages would be a difficult task. Hence, speech emotion detection systems are generally developed language-dependently. As native speakers of Bangla language, we choose to work on emotion detection from spoken Bangla using our own dataset.

3. Dataset

To detect different emotions from speech audio data, we needed to develop an emotion speech dataset. In this work, we have collected data from 20 participants, of which 12 are males, and 8 are females. All participants are native speakers of Bangla language. Table 1 and Table 2 show the detailed information of participants' age, gender, and occupation. We have collected data from different age groups ranging from 18 to 32 years, and with different occupations such as job holder, student, businessman,

and self-employed. We have collected 452 samples and the duration of each sample is from 3 to 5 seconds. We have labeled these samples in four emotional categories based on the type of speech data. The emotion categories are angry, happy, sad, and neutral. We have recorded the speech audio data on smartphones. Since the participants had different models of smartphone, we had to convert the recorded data into one common audio format. In this work, we have converted the data into wav format. The volume of our dataset is not large compared to other datasets such as RAVDESS multimodal database [27]. However, we could achieve a good accuracy with fewer samples of data that is discussed in the result section.

Table 1: Age and gender of the participants

Gender	Age			Total
	18-22	23-27	28-32	
Male	04	05	03	12
Female	03	04	01	08

Table 2: Occupation of the participants

Gender	Occupation			
	Job Holder	Student	Business	Self-Employed
Male	02	06	01	03
Female	01	05	00	02

4. Methodology

Voice is the prominent medium to communicate. Our objective is to detect the emotion from audio data using several machine learning models including traditional, and ensemble models. We have gone through a number of pre-processing steps before training our dataset. The pre-processing is done to remove any unwanted noises from the audio data. We will discuss each phase of pre-preprocessing in the next subsection.
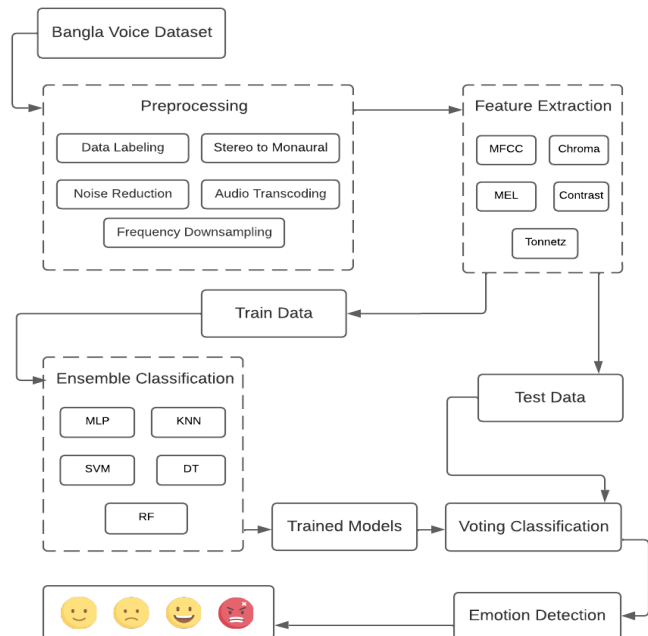

Figure 1: Architecture of the proposed methodology

A block diagram of emotion detection methodology is shown in Figure 1 where the pre-processed data go through the feature extraction phase. Here, we extract several voice features such as MFCC, MEL, contrast, tonnetz, etc. After the feature extraction phase, the audio data are sent to ensemble machine learning models for training. After training the models, our next step is to detect different types of emotions from test data.

4.1. Pre-processing

Pre-Processing is a technique that transforms raw data into understandable format. It is not suitable for feature extraction modules with raw data directly because the data are collected from different platforms and environments. Our dataset was collected in various formats such as MP3, MP4 AAC, M4A, WMA, FLAC, OGG, etc. Also the dataset was not properly labeled, and was contaminated with a lot of extra unwanted noises. In order to simplify the further steps, we processed the dataset and cleaned them as follows:

- Data Labeling: Our dataset is formatted based on RAVDESS multimodal database [27] of emotional speeches and songs. Each of the 452 samples has been labeled based on the speech emotion data. The filename consists of a 7-part numerical identifier (e.g., 03-01-05-01-02-01-12.wav). These identifiers define stimulus characteristics of the speech data. Third identifier of the filename is defined as Emotion (e.g., 01 = neutral, 03 = happy, 04 = sad, 05 = angry). For example in the filename: 03-01-05-01-02-01-12.wav, the 3rd identifier is 05, and is referred to emotion angry. The other identifiers are not necessary for this study.

- Audio Transcoding: We have used the *librosa* module to convert the audio data. This module returns WAV audio format from raw data such as MP3, MP4 AAC, M4A, WMA, FLAC, OGG etc. Audio transcoding is done to convert different audio formats to one common audio format.

- Noise Reduction: Noise reduction is the process of removing noise from a signal. Noise reduction techniques exist for audio and images. In this work, a python module *pydub* is used for audio segmentation to remove extra noise from audio data.

- Stereo to Monaural: Monaural or monophonic sound (mono) reproduction is sound intended to be heard as if it is emanating from one position. Mono channel is used when there is only one source of audio, and the stereo channel is used when there are multiple sources of audio. Since we are only taking speech data without contamination of any music or instruments, we have converted stereo to mono channel to reduce the usage of bandwidth and storage space. We have used *FFmpeg* multimedia framework for converting our audio data from stereo to mono.

- Frequency Downsampling: We downsampled the audio data to adjust frequency to 16kHz using *FFmpeg* multimedia framework.

4.2. Feature extraction

Choosing a suitable set of features is an important step in detecting emotions from speech data. Speech features can be divided into spectral, excitation, acoustic features [25]. We have selected several features such as MFCC, Chroma feature, LFCC, LPC, RC, Contrast, Tonnetz, etc. We use a minimal set of features to reduce the complexity in emotion detection. Since there is no general agreement on the right number of features for detecting emotions from speech data, we have chosen features that are effective and computationally efficient.

4.3. Train model

After the feature extraction phase, the extracted features are used to train machine learning models. In this stage, different machine learning models are trained using the dataset. For this, the dataset is split into 85% for training and 15% for testing. Since the volume of our dataset is small, we have split the dataset based on empirical findings. After training a model, the dataset is gone through the testing phase to evaluate model's accuracy.

4.4. Detection of emotion

Machine learning classifiers have been used in predicting, recognizing, and detecting the desired target of a given dataset. In this work, we have trained and tested traditional and ensemble machine learning models to detect emotions from Bangla speech audio data.

4.4.1. Traditional Machine Learning Models

Five traditional machine learning models are used in this work. They are Multi-Layer Perceptron (MLP), K-Nearest Neighbors (KNN), Decision tree (DT), Random Forest (RF), and Support vector machines (SVM). These machine learning approaches are used in detecting different emotional states such as happy, sad, angry, and neutral from the extracted speech data.

4.4.2. Ensemble Machine Learning Model

Ensemble machine learning model is a combination of different sets of models. It provides a final output by combining several outputs of different ML models. Hence, ensemble machine learning model gives more accurate performance. The final decision can be taken by the ensemble model by using different methods such as hard voting, bootstrap aggregations, boosting, etc. It provides more accurate results by relying on a decision tree rather than one model as shown in Figure 2.
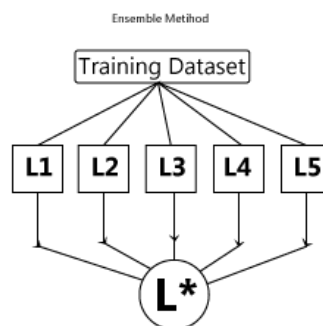

Figure 2: An example ensemble method

In Figure 2, there are 5 weak learners that are L_1, L_2, L_3, L_4 and L_5. They are going through training models to become a vigorous learner as L*.

In this work, we used a bagging ensemble model. Bagging (Bootstrap Aggregation) is generally used to reduce the contradiction. In bootstrap aggregation, multiple similar algorithms are trained separately, and then merge them all to determine the model's average. We used five different types of algorithms for the bootstrap aggregation method. In Figure 3 shows ensemble method with bootstrap aggregation.
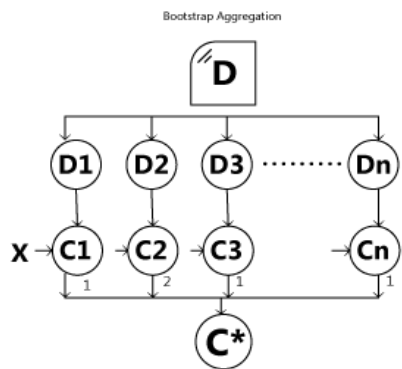

Figure 3: An example of Bootstrap Aggregation

In Figure 3, we have provided an original dataset. The bootstrap aggregation process generates multiple subsets which are D_1, D_2, D_3, … D_n from the given dataset. On each subset, a machine learning algorithm is fitted. The fitting algorithm is then trained using multiple subsets to produce various models which are C_1, C_2, C_3, … C_n. The produced models are called weak learners or base models. Now, we have our multiple base models which are trained in parallel at this stage. In the last stage, the multiple predictions made by the base models are combined to produce a single final model which is C*. The final model C* will have low variance and a high accuracy score.

5. Result and Discussion

In order to evaluate the performance of our work, we have considered precision, recall, and F1-score for each emotion class and then we have calculated the average accuracy. We have experimented with different ML models to find out which model performs better in terms of detecting emotions with higher accuracy.

We have tested multiple machine learning models for our work. Since these machine learning models failed to give our desired result, we go with ensemble methods with bootstrap aggregation that not only give the better accuracy but also improve the stability of machine learning models, prevent model overfitting, and reduce variance.

Table 3 gives the precision, recall and the weighted-average F1-scores for the multiclass classification using ensemble model with SVM, MLP, KNN, DT and RF classifiers for training dataset. In Table 3, DT with ensemble model performs better than other classifiers with an average accuracy of 99% approximately.

Table 4 shows the precision, recall and the weighted-average F1-scores for test dataset. The RF model gives slightly better accuracy than other models, which is 78%. Here, we also see that, DT has the accuracy score of 77%, while KNN has 74%,

and MLP has 71% accuracy. On the other hand, precision, recall, f1-score and accuracy percentage are quite low for the SVM classifier compared to other classifiers. SVM gives only 65% accuracy.

Table 3: Comparison of different ensemble ML models for training dataset

ML Model	Emotion	Precision	Recall	F1-score	Average accuracy
Decision Tree	angry	1.00	0.98	0.99	0.99
	happy	0.94	0.98	0.96	
	neutral	0.99	0.97	0.98	
	sad	0.98	1.00	0.99	
Random Forest	angry	1.00	0.98	0.99	0.96
	happy	0.89	0.97	0.93	
	neutral	0.92	0.96	0.94	
	sad	0.97	0.99	0.98	
KNN	angry	1.00	0.98	0.99	0.98
	happy	0.94	0.98	0.96	
	neutral	0.99	0.97	0.98	
	sad	0.98	1.00	0.99	
MLP	angry	0.96	0.98	0.97	0.93
	happy	0.90	0.95	0.93	
	neutral	0.91	0.93	0.92	
	sad	0.95	0.86	0.90	
SVM	angry	0.98	1.00	0.99	0.97
	happy	0.93	0.97	0.95	
	neutral	0.97	0.99	0.98	
	sad	0.95	0.97	0.96	

Table 4: Comparison of ensemble ML models for test dataset

ML Model	Emotion	Precision	Recall	F1-score	Average accuracy
Decision Tree	angry	0.85	0.73	0.79	0.77
	happy	0.79	0.75	0.77	
	neutral	0.71	0.79	0.75	
	sad	0.75	0.81	0.78	
Random Forest	angry	0.64	0.94	0.79	0.78
	happy	0.95	0.57	0.76	
	neutral	0.69	0.71	0.70	
	sad	0.79	0.94	0.87	
KNN	angry	0.76	0.80	0.78	0.74
	happy	0.83	0.57	0.70	
	neutral	0.68	0.78	0.73	
	sad	0.67	0.81	0.74	
MLP	angry	0.63	0.73	0.68	0.71
	happy	0.79	0.71	0.75	
	neutral	0.77	0.69	0.73	
	sad	0.65	0.77	0.71	
SVM	angry	0.55	0.69	0.62	0.65
	happy	0.61	0.71	0.66	
	neutral	0.65	0.57	0.61	
	sad	0.76	0.69	0.71	

As we progressed, we see that we are not getting our desired result. So, we have applied an ensemble voting classifier for better accuracy. The intuition behind using hard voting is that to label the emotion that has been chosen most frequently by the classification models.

Hard voting is the simplest case of majority voting. Here, we label a class ŷ via majority (plurality) voting of each classifier C_j:

$$\hat{y} = mode\{C1(x), C2(x), \ldots, Cm(x)\}$$

Here C represents the models. We combine our five models in the voting classifier to get better performance in detecting emotions.

Table 5: Accuracy of ensemble methods with voting

Ensemble Method	Emotion	Precision	Recall	F1-score	Average accuracy
Voting classifier	angry	0.76	0.82	0.79	**0.84**
	happy	0.83	0.89	0.86	
	neutral	0.82	0.86	0.84	
	sad	0.83	0.91	0.87	

In Table 5, we have calculated the F1-score of four types of emotions: a79.5% for angry, 86.25% for happy, 84.75% for neutral and 87% for sad emotions. The average accuracy is 84.37% using the voting classifier. So, we can say that if we test any sample of Bangla speech data, we can get the success rate of emotion detection of 84.37%. During evaluation of ensemble model in our work, we have found that the size of the dataset, the number of features, and the classifiers affect the detection of emotions to some extent.

In Figure 4 and Figure 5, we have showed the ensemble bootstrap aggregation model accuracy for training and test dataset respectively. In our emotion recognition journey, we try to find out which classifier detects emotion accurately, so we have compared the ensemble classifiers and traditional classifiers. In Figure 5, we clearly see that our ensemble classifier gives better performance compared to traditional classifiers.
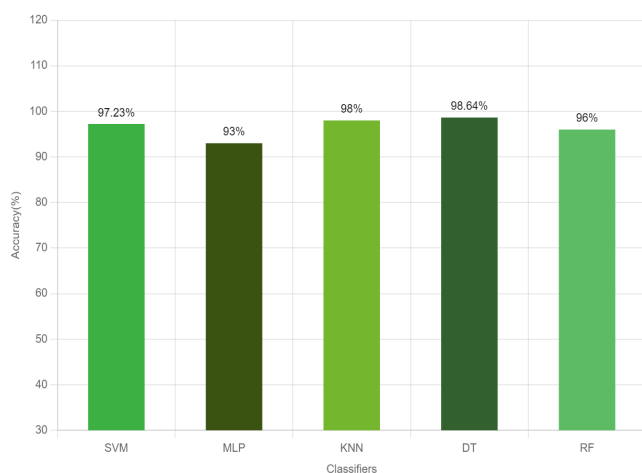
Figure 4: Ensemble bootstrap aggregation training model accuracy

In Figure 6, we have shown the emotion detection success rate using ensemble model with voting. From our observation, we can say that by using ensemble voting method, we can get better accuracy in compared to traditional methods, which is 84.37%.
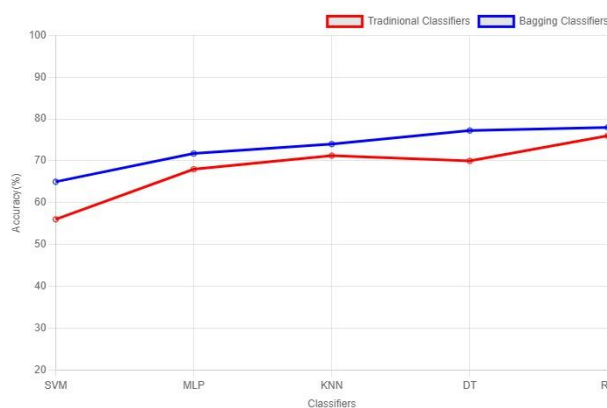
Figure 5: Comparison between begging classifier and traditional classifier
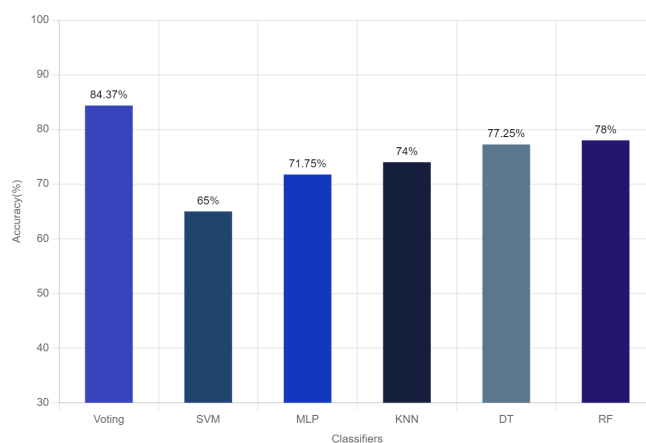
Figure 6: Accuracy of ensemble method with voting

6. Conclusion

In this work, we have explored emotion detection in Bangla language. We have presented an ensemble machine learning model with voting to detect emotion from speech data. The ensemble learning model with voting outperformed traditional machine learning models with better accuracy. However, our dataset has fewer samples of speech data. The amount is not sufficient to achieve a better result. Therefore, in future, more data samples would be considered for detecting broad ranges of emotions from Bangla speech data.

References

[1] S. C. Hauser, S. McIntyre, A. Israr, H. Olausson, G. J. Gerling, "Uncovering human-to-human physical interactions that underlie emotional and affective touch communication," in 2019 IEEE World Haptics Conference, 407–412, 2019, doi: 10.1109/WHC.2019.8816169.

[2] A. Al-Nafjan, K. Alharthi, H. Kurdi, "Lightweight building of an electroencephalogram-based emotion detection system," Brain Sciences, **10**(11), 781, 2020, doi:10.3390/brainsci10110781.

[3] S. Pal, S. Mukhopadhyay, and N. Suryadevara, "Development and progress in sensors and technologies for human emotion recognition," Sensors, **21**(16), 2021, doi:10.3390/s21165554

[4] C. Athavipach, S. Pan-Ngum, and P. Israsena, "A wearable in-ear EEG device for emotion monitoring," Sensors, **19**(18), 4014, 2019, doi:10.3390/s19184014.

[5] M.R. Hasan, M.M Hasan, M.Z. Hossain, "How many Mel-frequency cepstral coefficients to be utilized in speech recognition?," The Journal of Engineering, 12, 817-827, 2021, doi:10.1049/tje2.12082.

[6] A.M. Ishmam, S. Sharmin, "Hateful Speech Detection in Public Facebook Pages for the Bengali Language," in 18th IEEE international conference on machine learning and applications (ICMLA), 555-560, 2019, doi:10.1109/ICMLA.2019.00104.

[7] H.M. Hasan, M.A. Islam, "Emotion recognition from bengali speech using rnn modulation-based categorization," In 2020 third international conference on smart systems and inventive technology (ICSSIT), 1131-1136, 2020, doi:10.1109/ICSSIT48917.2020.9214196.

[8] J.R. Saurav, S. Amin, S. Kibria, M.S. Rahman, "Bangla speech recognition for voice search," in 2018 international conference on Bangla speech and language processing (ICBSLP), 1-4, 2018, doi:10.1109/ICBSLP.2018.8554944.

[9] N.T Ira, M.O. Rahman, "An efficient speech emotion recognition using ensemble method of supervised classifiers," in 2020 Emerging Technology in Computing, Communication and Electronics (ETCCE), IEEE, 1-5, 2020, doi:10.1109/ETCCE51779.2020.9350913.

[10] N. Kholodna, V. Vysotska, S. Albota, "A Machine Learning Model for Automatic Emotion Detection from Speech," in CEUR Workshop Proceedings, 2917, 699-713, 2021.

[11] S. Cunningham, H. Ridley, J. Weinel, R. Picking, "Supervised machine learning for audio emotion recognition," Personal and Ubiquitous Computing, **25**(4), 637-650, 2021, doi: 10.1007/s00779-020-01389-0.

[12] Z. Tariq, S.K. Shah, Y. Lee, "Speech emotion detection using iot based deep learning for health care," in 2019 IEEE International Conference on Big Data, 4191-4196, 2019, doi: 10.1109/BigData47090.2019.9005638.

[13] M.C. Sezgin, B. Gunsel, G.K. Kurt, "Perceptual audio features for emotion detection," EURASIP Journal on Audio, Speech, and Music Processing, **2012**(1), 1-21, 2012, doi:10.1186/1687-4722-2012-16.

[14] W. Ragheb, J. Azé, S. Bringay, M. Servajean, "Attention-based modeling for emotion detection and classification in textual conversations," arXiv preprint arXiv:1906.07020, 2019, doi:10.48550/arXiv.1906.07020.

[15] H. Al-Omari, M.A. Abdullah, S. Shaikh, "Emodet2: Emotion detection in english textual dialogue using bert and bilstm models," in 2020 11th International Conference on Information and Communication Systems (ICICS), 226-232, 2020, doi: 10.1109/ICICS49469.2020.239539.

[16] A. Majeed, H. Mujtaba, M.O Beg, "Emotion detection in roman urdu text using machine learning," in Proceedings of the 35th IEEE/ACM International Conference on Automated Software Engineering Workshops, 125-130, 2020, doi: 10.1145/3417113.3423375.

[17] B. Gaind, V. Syal, S. Padgalwar, "Emotion detection and analysis on social media," arXiv preprint arXiv:1901.08458, 2019, doi:10.48550/arXiv.1901.08458.

[18] S. Azmin, K. Dhar, "Emotion detection from Bangla text corpus using Naïve Bayes classifier," in 2019 4th International Conference on Electrical Information and Communication Technology (EICT), 1-5, 2019, doi: 10.1109/EICT48899.2019.9068797.

[19] T. Dissanayake, Y. Rajapaksha, R. Ragel, I. Nawinne, "An ensemble learning approach for electrocardiogram sensor based human emotion recognition," Sensors, **19**(20), 4495, 2019, doi:10.3390/s19204495.

[20] M. N. Dar, M.U. Akram, S.G. Khawaja A.N. Pujari, "CNN and LSTM-Based Emotion Charting Using Physiological Signals," Sensors, **20**(16), 4551, 2020, doi:10.3390/s20164551.

[21] D. Morrison, R Wang, L.C. De Silva, "Ensemble methods for spoken emotion recognition in call-centres," Speech communication, **49**(2), 98-112, 2007, doi:10.1016/j.specom.2006.11.004.

[22] M. de Velasco, R. Justo, J. Antón, M. Carrilero, M.I. Torres, "Emotion Detection from Speech and Text," in IberSPEECH, 68-71, 2018, doi:10.21437/IberSPEECH.2018.

[23] O.M. Nezami, P.J. Lou, M. Karami, "ShEMO: a large-scale validated database for Persian speech emotion detection," Language Resources and Evaluation, **53**(1), 1-16, 2019, doi:10.1007/s10579-018-9427-x.

[24] A. Asghar, S. Sohaib, S. Iftikhar, M. Shafi, K. Fatima, "An Urdu speech corpus for emotion recognition," PeerJ Computer Science, 8, p.e954, 2022, doi:10.7717/peerj-cs.954.

[25] S. Klaylat, Z. Osman, L. Hamandi, R. Zantout, "Emotion recognition in Arabic speech," Analog Integrated Circuits and Signal Processing, **96**(2), 337-351, 2018, doi:10.1007/s10470-018-1142-4.

[26] A. Agrawal, A. Jain, "Speech emotion recognition of Hindi speech using statistical and machine learning techniques," Journal of Interdisciplinary Mathematics, **23**(1), 311-319, 2020, doi:10.1080/09720502.2020.1721926.

[27] S.R. Livingstone, F.A. Russo, "The Ryerson Audio-Visual Database of Emotional Speech and Song (RAVDESS): A dynamic, multimodal set of facial and vocal expressions in North American English," PloS one,**13**(5), p.e0196391, 2018, doi:10.1371/journal.pone.0196391.

The Security of Information Systems and Image Processing Supported by the Quantum Computer: A review

Tarek Nouioua[*,1,2], Ahmed Hafid Belbachir[2]

[1]*Department of Mathematics and Computer Sciences, Faculty of Exact sciences and sciences of Nature and life, University of Tebessa, Tebessa, 12000 , Algeria*

[2]*Laboratory of Analysis and Application of Radiation (LAAR), Engineering Physics Department, Faculty of Physics, University of Sciences and Technology of Oran Mohamed Boudiaf, Algeria, Oran, 31000, Algeria*

ARTICLE INFO

ABSTRACT

The knowledge and understanding of the technology of quantum computers and their superiority over classical computers are still insufficient or uncertain for many communities of researchers, manufacturers, investors and the general public. For this reason, we try in this article to present and explain some of the basic concepts of quantum computers. We explain how the quantum phenomena may be employed to conceive a quantum computer by defining the qubit that will represent the data entity corresponding to the bit in the classical computer and how this computer can effectively be powerful. We address the issue of strengthening the information system security through a simulation of a spy hunter and the importance of image processing security using the quantum computer, which will minimize the data processing time regardless of the amount of data to be processed. The security of the images will lead us to introduce the new prospects of using multilevel systems instead of binary systems, which will exponentially increase the gain in the size of the memory used.

1 Introduction

This paper is an extension of a work initially presented at the International Conference on Recent Advances in Mathematics and Informatics (ICRAMI) [1]. The main objective is to contribute to attracting attention to the importance of the quantum computer in the future for those who now use classical computers in all their different fields or who work in the development of technology and the computer industry and anyone related to this advanced technology.

To be convincing, an example of a spy hunter simulation will be presented and discussed. The relevance of using quantum computers in image processing security will also be presented and discussed. The impact of using multilevel or ternary quantum systems compared to binary quantum systems will be presented to argue their advantage in minimizing the memory size in image processing.

The technological evolution of the processors has considerably improved their efficiency, namely the calculation time and the energy consumption. However, the processor's physical core is changing as well as the nature of the data which will be represented by the qubit instead of the bit, by studying quantum physics.

Studying quantum physics and aiming to make it representative of the information will help us conceive the quantum computer and use it efficiently. Following that idea, several laboratories invest budgets in research to have the first quantum computer and benefit from quantum physics.

Quantum physics history goes back to the 1940s and plays a central role in manufacturing computers' electronic components. In 1982 [2], the author was the first to propose the concept of the quantum computer, and in 1986 by another paper [3], he confirmed his thought. However, quantum computing got its big break in the 1990s. The most important being that idea [4, 5], where the author used a quantum algorithm for the factorization of prime numbers of size n in a time $O((n)^3)$ and space $O((\log n))$.

Another idea of a quantum algorithm in 1992 was developed [6], which did not have significant importance. But in 1996, another one [7], developed a quantum algorithm which consists in searching one or more elements out of N elements within a time proportional to $\sqrt{N}$, with a storage space which is proportional to $logN$.

*Corresponding Author: Tarek Nouioua, Department of Mathematics and Computer Sciences, Faculty of Exact sciences and sciences of Nature and life, University of Tebessa, Algeria, tarek.nouioua@univ-tebessa.dz

Security requirements are essential for a secure transaction on a transmission canal using an asymmetric encryption algorithm. Information systems exchange data over the transmission canal using the RSA (Rivest-Shamir-Adleman) algorithm; since the encryption key is different from the decryption key, it is difficult to break the RSA keys.

So far, no one has been able to break RSA keys. Once we are in the era of quantum computers, it will be possible to factorize large numbers in a fast time and, consequently, RSA keys may be broken and the security of the information systems would be at risk. Therefore it will be necessary to think of a post-quantum cryptography [8].

Quantum Image Processing (QIP) using Quantum image-based data security techniques are more efficient and provide higher security than conventional image processing. The processing speed and the amount of data processed in image processing are the most advantages guaranteed by QIP. The strength of this approach is subject to quantum physics rules which we do not have in classical image processing.

The rest of this paper is organized as follows. In 2, Literature review is presented. In 3, Basics of quantum computer are presented. In 4, Computation using Quantum computer will be described. In 5, The quantum computer and data security are presented. And finally, in 6 The conclusion.

2 Literature review

It is noteworthy that after a rising technological revolution, it has been quite a while since a scientific work on information processing using quantum physics was published [2, 3, 9].

In [10], the authors presented in their survey on quantum computing the basic components that are required to build a real quantum computer. They also have pointed out the basics of each capability to be translated from a classical environment to a quantum environment and vice versa.

In [11], the authors proposed initial ideas and several schemes for quantum computing architectures that satisfy the physical constraints; the architectures restrict the way to map the logical qubits used to describe the algorithm to the physical qubits to realize the corresponding functionality.

In a paper [12], the authors presented the difference between classical and quantum cryptography and have pointed out the implications of quantum computing in current cryptography and introduced the basic post-quantum algorithm and said that it deals with different quantum keys distribution methods and mathematically based solutions.

In [13], the authors discussed the connection between the strong testing, which they referred to as the purity testing and the quantum ciphertext authentication (QCA), and have reported that it may offer higher security.

In [14], the authors reported on the relevance of using quantum computing in the biological sciences and how the problems posed by quantum algorithms in this area could provide increased computational efficiency, which was much lacking.

In [15], the authors mentioned that the major challenges faced in designing a quantum computer are related to the errors generated by the quantum computer during computation, which decreases its efficiency. To minimize these errors, they suggested the deployment of quantum error-correcting code, and to achieve fault-tolerance, it will be important to make advancement in engineering.

In their work [16], the authors compared different methods of image storage, image representations and image retrievals in a quantum system. They have also presented and discussed the advancement in quantum image processing.

Another review article[17], the authors reported an outline of the QIMP as well as a diagnostic analysis of the enhancement of existing models of quantum image representations, the design of quantum algorithms to solve sophisticated operations, and the further development of physical hardware and software architecture to both capture and manipulate quantum images.

In a recent paper [18], the authors highlighted that a prominent example is secure communication and presented the cryptographic requirement of transmitting confidential messages from one location to another.

In [19], the authors presented in their work the possibilities that quantum mechanics can add to strengthen the cypher code to be unbreakable.

In [20], the authors discussed details in their work towards applying quantum computation to image processing which can be improved through the application of Quantum Computing.

In a recent work [21], the authors presented in their paper the role of quantum mechanics on image and data processing, they presented three quantum algorithms for comparing the similarity between two quantum images and declared that their proposed algorithms achieve exponential acceleration than the existing quantum and classical methods in all three cases.

Table 1 represents a summary of the different works of the selected articles in literature in relation to our present paper.

3 Basics of a quantum computer

The item *bit* is the basic element for data representation in conventional computer science, which can only have one value among two values 0 or 1. In quantum physics, a third situation is possible, the *qubit* (quantum bit), which represents the new item for the basic element of data representation, can be in a superposition of two states $|0\rangle$ and $|1\rangle$ that can be represented by (1):

$$|\psi\rangle = \alpha|0\rangle + \beta|1\rangle \tag{1}$$

where α, $\beta \in \mathbb{C}$ with $|\alpha|^2 + |\beta|^2 = 1$ and $|\psi\rangle$ is a unit vector in a complex vector space of dimension 2, whose basis vectors are denoted as in (2):

$$|0\rangle = \begin{pmatrix} 1 \\ 0 \end{pmatrix} \quad and \quad |1\rangle = \begin{pmatrix} 0 \\ 1 \end{pmatrix} \tag{2}$$

A geometric representation in a three-dimensional sphere called Bloch Sphere [22] (see Figure 1), is used to describe many operations of a single *qubit*, for multiple qubits, there is no generalization known of the Bloch sphere. In such a situation, in the whole sphere, we can have an infinity of information represented by an infinity of states.

Table 1: A Review Summary

Related work \ Focused study	Quantum computer architecture	Quantum cryptography	Quantum Image processing	Other Quantum interests
Paper [10]	✓			
Paper [11]	✓			
Paper[12]		✓		
Paper [13]		✓		
Paper [14]				✓
Paper [15]	✓			
Paper [16]			✓	
Paper [17]		✓		
Paper [18]		✓		
Paper[19]		✓		
Paper [20]		✓		
Paper [21]		✓		
Present paper	✓	✓	✓	
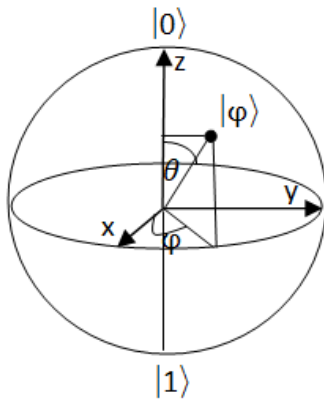
Figure 1: *Qubit* representation by Bloch Sphere

In computer science, all useful information is represented using a succession of bits of 0's and 1's in low-level codes that can be decoded using low-level to high-level transcription programs for different purposes, such as displaying, reading and writing or even other useful purposes, each bit has to be 0 or 1 but not both.

By using a superposition of two states $|0\rangle$ and $|1\rangle$, the *qubit* have the potential to represent both values 0 and 1 at the same time in a state $|\psi\rangle$ that can be noted in (3).

$$|\psi\rangle = \frac{1}{\sqrt{2}}|0\rangle + \frac{1}{\sqrt{2}}|1\rangle \tag{3}$$

In Equation (3), at the moment of measurement, the state $|\psi\rangle$ will be $|0\rangle$ with a probability equal to $(\frac{1}{\sqrt{2}})^2$ or $|1\rangle$ with a probability equal to $(\frac{1}{\sqrt{2}})^2$, and this is known in quantum physics as decoherence [23], which has to be exactly the same *bit* case of coventional computer.

To make calculations using *qubits*, we must have to leave the measurement at the end to avoid losing the state superposition due to *qubit* decoherence, which means we must maintain the *qubit* coherence as long as possible, for this reason, we should eliminate the constraints that help the *qubit* decoherence and especially minimize

the *qubit* interaction with its environment. In [24], was mentioned five requirements, one of them being to minimize the interaction of the *qubit* with its environment, otherwise, the computation will collapse and then the complete system will collapse.

If we need a numerical analysis of the possible coherence time of a *qubit*, in an experiment [25], where the authors made atoms interact with photons one by one, measured the time it takes to observe progressive decoherence, and they obtained a time of about $100\,\mu$ seconds for only ten atoms, and this was considered too small to be measured which means that when we increase the number of atoms, the time will decrease exponentially and this will affect the coherence of the *qubit*.

For a given computation time and considering the microprocessor's technological evolution; with $100\,\mu$ seconds we can perform a lot of computations, but considering the gate's latency, we will have to increase this time so that it is appropriate to a given computation.

We can have a comparison with the frequency of a conventional processor to see how many quantum processes it can manage, for that purpose, we can convert the qubit coherence time into a frequency that we can obtain a ratio $S_{C/Q}$ that we can calculate using (4); a number which represents the number of cycles that a conventional processor can handle.

$$S_{C/Q} = \frac{F_{CP}}{F_{DQub}} \tag{4}$$

where:

- F_{CP} is the coventional Processor frequency,

- F_{DQub} is the *qubit* decoherence rate,

- $S_{C/Q}$ represents the speed ratio between the conventional processor frequency and the *qubit* decoherence rate.

If we consider a conventional processor frequency of 3.2 GHz, and if we transform the *qubit* coherence time into a frequency, we will have 10 KHz. By using (4), we can calculate the ratio between the conventional processor frequency and the coherence frequency that gives us 320000 times faster, which means that the conventional processor can manage 320000 *qubit's* cadencies (see Figure 2).

Figure 2: Illustration of cadency of $S_{C/Q}$ *qubits* by a conventional processor rate time

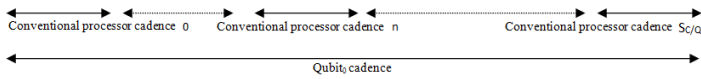To increase the number $S_{C/Q}$ it is only sufficient to increase the frequency of the conventional processor, or to reduce the decoherence rate (i.e. to extend the decoherence time), and for that purpose Chapter 10 of the book [26] discusses various approaches to extend the decoherence time effectively.

The conventional computer's technological evolution makes it possible to have the classical processor's frequency increased. But it is a difficult mission to reduce *qubit* decoherence rate because it is not easy to isolate the *qubit* from its environment.

3.1 Concepts and Physical realisation of the qubit and the quantum computer

To have a quantitative evaluation and to see the measurable size of a *qubit*, in [27],The authors succeeded in fabricating a 60 μm *qubit* in a 6 GHz resonant system. The realized *qubit* is considered giant compared with the size of an atom, which means that with this *qubit* size, we have the horizon opened to the fabrication of quantum electronic chips that are also considerably larger than the size of an atom.

A *qubit* is a fundamental unit of data representation and a basic element of the quantum computer's hardware architecture. This architecture, quite particular compared to the classical one, needs to meet certain engineering requirements to be able to engineer a quantum computer. These requirements are linked to quantum physics specificities, which cannot be found in the classical one.

One of the relevant concepts in quantum physics is energy, which forms discontinuous scales known as a quantum leap. In their experiment [28], by using Barium, the authors measured the quantum leap, which confirms that, by the quantum physics nature, an electron can occupy two energy levels at the same time; that is known as a states superposition.

For the concept of entanglement, where two electrons or two photons will be linked to each other; namely, if we act on one automatically we act on the other instantaneously, and if one chooses its state whether it is $|0\rangle$ or $|1\rangle$ the other one automatically is in the opposite state. This phenomenon was described as strange and mentioned in a scientific paper [29] known as the EPR paradox, since no velocity, until today, is higher than the velocity of the light.

In a recent experiment [30], Chinese researchers, have proven and demonstrated that even at large distances (1203 km), photons were entangled.

For example, taking two superposed electrons where we have four possibilities $|11\rangle$ $|10\rangle$ $|01\rangle$ $|00\rangle$. The most relevant case is $|10\rangle$ $|01\rangle$ called the entangled states, where the two electrons are irremediably linked to each other, when measuring one of them we necessarily interact with the other one, i.e. the entangled systems are linked each to other, and this is proved by experiments [30, 31].

4 Computation using Quantum computer

Computing with a quantum computer is quite different from computing with a classical computer. The entanglement and the superposition of the states of a *qubit* are very fragile that we can only make measurements at the end of the calculation for fear that the entanglement and the superposition of the states will collapse. To overcome this problem, we can use an ingenious solution which consists in duplicating thousands of copies of the *qubit* and making the calculation, two scenarios are to be considered; we check the calculation and it is good so we go ahead, otherwise, we stop it and start again.

When doing computations, we cannot escape from the computational errors which are so far in the range of $\frac{1}{1000}$, and by taking into account the number of *qubits* to be handled, we can expect to have one million of *qubits* to carry out an appropriate computation.

If we assume having a decoherence time four times the time observed in the experiment [25], i.e. a decoherence time of 400 μ seconds, which represents a frequency of 2.5 kHz and let's take (4) to calculate the quotient $S_{C/Q}$ for a conventional processor frequency of 3.2 GHz, we obtain 1280000 cadences. If we duplicate copies of the *qubits* and we verify at a given moment if the calculation is good or not, and let's say that everything is good and that the calculation we are doing is correct without collapsing as shown in Figure 3, in this case, the total time T is equal to the time at the end of the computation, i.e. equal to the *qubit* decoherence, but if we were in the second case (see Figure 4), where the computation is not correct and therefore we stop it and start again, in this case, the total time is *T1* and is different from *T*, it will be equal to $m \times$ Conventional Processor instruction time, where m represents the number of repetitions.
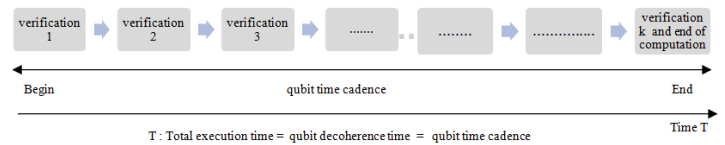
Figure 3: Time computation T: Computation verification without errors
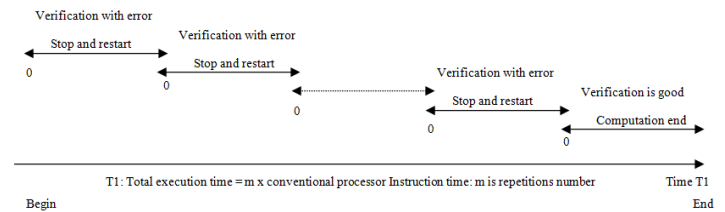
Figure 4: Time computation T1 : Computation verification error with stop and restart

We point out that even though the calculation is correct, this does not mean that there are no errors; this is due to the probabilistic measurements and the superposed states that occur each with a probability. Also, the quantum computer runs on a different clock separated from that of a conventional computer.

Quantum programming cannot replace conventional programming completely, it is estimated only for solving some complex

problems that are difficult to solve using a classical computer. In [32], a list of 50 sample problems was compiled that may be interesting to use as examples for writing quantum programs.

Quantum computer can be considered as a co-processor for the conventional computer, in which our programs are divided into two different parts; a conventional programming part for the conventional computer side, and another quantum programming part for the quantum computer as shown in Figure 5.
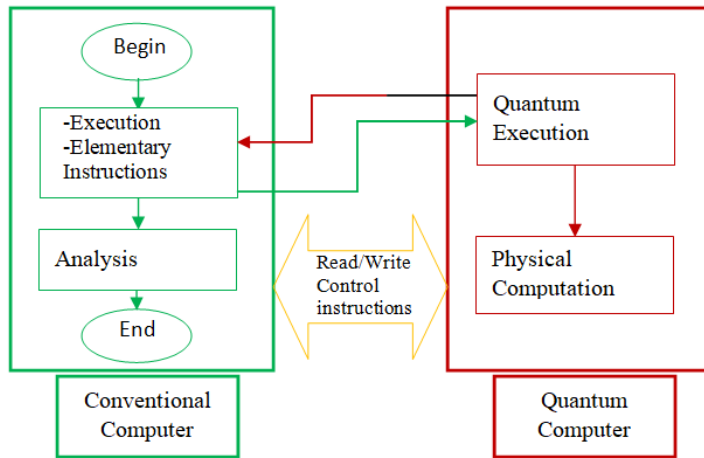
Figure 5: Illustration of two programming parts

5 The Quantum computer and data security

5.1 Internet Security and the RSA encryption method

Internet at high speed is difficult to define, as what constitutes "high speed" changes over time as technology advances and applications develop. There are advantages and weaknesses in each technology. The final selection should attend to the specific requirements of the Internet application, mainly determined by the factors that affect Internet objectives: low power, low cost, high number of devices, and medium-long range [33]. The high-speed of the Internet has affected many areas, especially those that use it as a medium for communication and data exchange.

In the era of information technology, data exchange has rapidly progressed, especially with the availability of high-speed communication such as the internet. However, data exchange is subject to hackers' attacks to hack the information, which has led us to use technical solutions to protect our information systems as well as the data exchanged on the Internet.

The RSA encryption method [34, 35], is an asymmetric algorithm used to exchange data on the Internet. This algorithm depends on two keys: a public key and a private key. No one has been able to break these keys, but once we have the quantum computer, these keys may be compromised, and the information system will then be at risk.

To address this risk, we develop quantum cryptography methods to secure the information system and the data exchange algorithm.

The technology used to design a qubit plays a huge role in the accuracy of computations performed with a quantum computer, but

the question arises seriously: is quantum computing accurate? In order to provide an answer, we need to look at one of the latest works done. In [36], the authors mentioned that quantum operations are accurately characterized using gate set tomography (GST), resulting in average single-qubit gate fidelities of up to 99.95%, average two-qubit gate fidelities of 99.37%, and two-qubit preparation/measurement fidelities of 98.95%. They precised that these three metrics are approaching the performance demanded in fault-tolerant quantum processors. which means that by the time the first generation of quantum computer appears, we will be able to achieve 100% accuracy.

To take advantage of quantum physics, we can benefit from the concepts of entanglement and superposition of qubit states, and since the measurement can only be performed at the end of the computation to avoid the system collapse. We have simulated an *8-qubits* (i.e. a *quByte*) code, Based on the original sample code example [37], to illustrate how can we do to perform a secure data exchange.

The spy hunter continuously checks and tunes the transmission channel to get accurate information by hacking the data. They use sophisticated tools and devices to get powerful that give them techniques to decrypt any data. With the quantum computer, spies can easily intercept and decipher data, and it is of great interest to understand quantum physics to know how to manage a secure transmission medium.

By capturing the data, they behave as if they had not caught it and send it back to the receiver (Bob). When Bob receives the data, and before reading, Alice informs him that she had applied a quantum gate (and maybe a combination of quantum gates) to the data, and then Bob applies the inverse of the quantum gate to the received data and compares it with Alice's data. If their data are identical, Bob and Alice conclude that the data has not been hacked, otherwise, they understand that it has been hacked.

In the case of applying quantum gates, and even if the hackers intercept the data, they will not be able to read it because they will never be able to guess the combination of quantum gates applied to the data before sending it.

Figure 6 represents the result of the simulation using QCEngine, and Figure 7 represents the result of the simulation using Qiskit.

For illustration presented on Algorithm 1, Alice wants to send some data to Bob (as example here data are an arbitrary information coded on 8 Qubits).

It is necessary to secure our information systems by thinking about post-quantum-cryptography solutions; i.e. working a lot in the technological field of quantum cryptography to prevent the RSA key from being broken because 1024-bit or even 2048-bit keys will be broken using quantum computers.

One day we will be in an era where the use of the quantum computer will be available to everyone, and then the spies of the computer will have the possibility to factorize long numbers, thereafter, they will be able to break the RSA algorithm keys. However, we have seen from the presented example that it will be guaranteed to ensure the security of our information systems and the strength of the RSA keys, while based on the characteristics of quantum physics.

The field of quantum programming is expanding, and we look forward to the first real and commercialized quantum computer
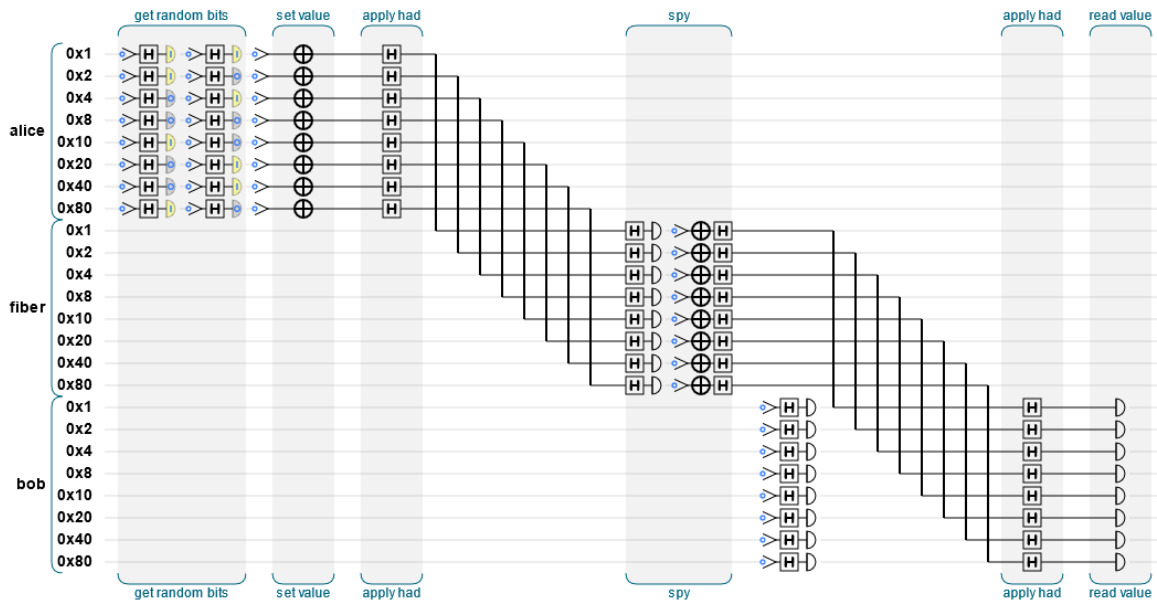
Figure 6: Illustration of spy hunter quantum program simulation using QCEngine
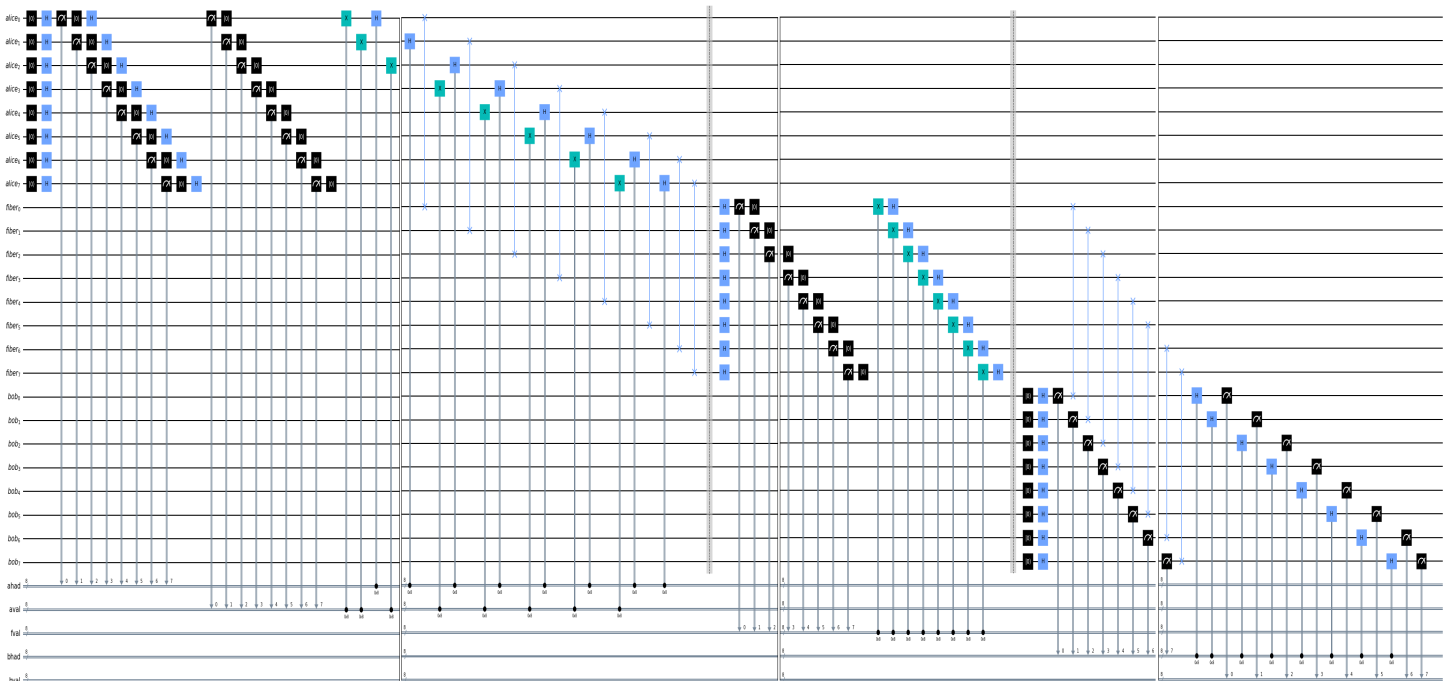
Figure 7: Illustration of spy hunter quantum program simulation using Qiskit

Algorithm 1: Spy Hunter

```
#Use Alice's QPU to prepare Alice's qubit
qc.measure(alice, alice_had);
qc.measure(alice, alice_val);
if (apply a HAD) then
    qc.h(alice)=alice_had
    else
    │   qc.x(alice)=alice_val
    end
end
# Send the qubit!
qc.swap(alice, fiber)
# Activate the spy
spy_is_present = True
if (spy_is_present) then
│   qc.barrier()
end
spy_had = True
if (spy_had) then
│   qc.h(fiber)
end
qc.measure(fiber, fiber_val); qc.reset(fiber);
if (fiber_val) then
│   qc.x(fiber)
end
if (spy_had) then
│   qc.h(fiber)
end
qc.barrier()
# Use Bob's QPU to prepare data...
# Receive the qubit!
qc.swap(fiber, bob)
if (bob_had) then
│   qc.h(bob)
end
qc.measure(bob, bob_val)
# If the setting matches and the value
#does not, there's a spy!
counts = result.get_counts(qc);
print('counts:',counts)
caught = False
for key,val in counts.items() do
│   alice_had,alice_val,f,bob_had,bob_val =(int(x)
end
for (x in key.split(' ')) do
│   if (alice_had == bob_had) then
│   │   if (alice_val != bob_val) then
│   │   │   print('Caught a spy!') caught = True
│   │   │   else
│   │   │   │   not caught: print('No spies detected.')
│   │   │   end
│   │   end
│   end
end
```

to apply everything we know as quantum algorithms, but we may   state that this is only for certain applications that need fast solu-

tions, and anything we use in a conventional computer, for example, Word or all our existing applications cannot be replaced by quantum programs.

5.2 Quantum Image Security

In cryptography, encryption is the process of hiding information to make it unreadable without special knowledge. In steganography or in watermarking, the technique used to hide information seems to be more secure because it is not easily detected by hackers. However, its major problem is a large amount of information that can be hidden inside an image without distortion of its visual imperceptibility.

In 2012, the authors of [38] have proposed the first quantum image security protocol, by a scheme of watermarking and authentication of quantum images (WaQI), and was based on restricted geometric transformations on the images.

In 2013 [39], a novel watermarking scheme based on Quantum Wavelet Transform (QWT) was proposed , and in 2014 [40],another watermarking scheme based on Hadamard transform was proposed .

In [41], the authors have proposed an improvement of the watermarking protocol proposed in [39].

In the field of quantum image encryption, methods are classified into spatial domain-based strategies or frequency domain-based strategies, on which quantum image encryption algorithms focus [42].

5.3 Multilevel Quantum Systems

In many works in literature, various models of quantum image representation have been proposed, and many of the proposed models are based on a binary quantum system.

Instead of a binary quantum system, a ternary quantum system is a new tendency to represent and process the quantum image.

A ternary quantum system is a 3-level quantum system having three mutually orthogonal states $|0\rangle$, $|1\rangle$ and $|2\rangle$ that form a basis in the Hilbert space $\mathcal{H}^3$ called qutrit.

As in a quantum binary system for a qubit, the superposition state of a qutrit can be formulated as:

$$|\psi\rangle = \alpha|0\rangle + \beta|1\rangle + \gamma|2\rangle \tag{5}$$

with $|\alpha|^2 + |\beta|^2 + |\gamma|^2 = 1$

In [43], the authors have proposed an RGB color image represented and stored on a ternary (3-levels) quantum system. They postulate that "*i*mages on quantum computers can be represented in the form of a normalized state which captures information about colors ($|c\rangle$) and their corresponding positions ($|p\rangle$) in the images". The image can be represented as:

$$|I\rangle = |c\rangle \otimes |p\rangle \tag{6}$$

$$|I\rangle = \frac{1}{2^n} \sum_{i=0}^{2^n-1} (cos\theta_i|0\rangle + sin\theta_i|1\rangle) \otimes |p\rangle \tag{7}$$

where, $\theta_i \in [0, \pi]$, i= 0, 1, 2,. . . , 2^{2n} - 1 and $\theta = \theta_0, \theta_1, . . . , \theta_{2^{2n}-1}$ is the vector of angles encoding colors.

In the case of the qutrits-based quantum system, According to Klimov qutrit phase model [44] can be represented as:

$$|I\rangle = \frac{1}{3^n} \left(\sum_{i=0}^{3^{2n}-1} sin(\frac{\xi}{2})cos(\frac{\theta}{2})|0\rangle + \right.$$
$$exp^{i\phi_{01}} sin(\frac{\xi}{2})cos(\frac{\theta}{2})|1\rangle +$$
$$\left. exp^{i\phi_{02}} cos(\frac{\xi}{2})|2\rangle \right) \otimes |p\rangle \tag{8}$$

where, θ and ξ represent the magnitudes of the components of $|\phi\rangle$, and ϕ_{01} is interpreted as the phase of $|0\rangle$ relative to $|1\rangle$ and analogously for ϕ_{02}.

The multilevel quantum system was implemented and designed in various works for different image processing purposes. In their work [45], the authors designed a circuit-level implementation of the quantum multilevel threshold-based color image segmentation technique.

Using multilevel quantum system have more advantages compared to binary quantum system in the most cases that can be stated for example:

> With the same amount of physical resources, the use of higher-dimensional quantum states increases exponentially the available Hilbert space.

> An n-qutrit quantum system can be represented by a superposition of 3^n basis states, thus a quantum register of size n can hold 3^n values simultaneously, in the other side an n-qubits register can only hold 2^n values.

> More efficient ternary logical gates implementation are used in multilevel quantum system.

> For representing, storing and processing the color images, ternary quantum system is more beneficial than binary quantum system.

6 Conclusion

In this paper, we describe how we can profit from the quantum computer to strengthen the security of our data on the Internet using quantum physics, based on the principles of quantum physics that we do not have in classical computers.

The unequalled power of the quantum computer led us to think of using it to represent and process big-size images. We have presented the new tendency of using ternary quantum systems compared to binary ones.

In future work, we will use the idea of sending a scrambled image with a ternary quantum system, which will guarantee us better security and an exponential gain in processing time and memory.

Conflict of Interest The authors declare no conflict of interest.

References

[1] T. Nouioua, A. H. Belbachir, "The Quantum Computer and the Security of Information Systems," in 2021 International Conference on Recent Advances in Mathematics and Informatics (ICRAMI), 1–9, 2021, doi:10.1109/ICRAMI52622.2021.9585929.

[2] R. P. Feynman, "Simulating physics with computers," Int. J. Theor. Phys., **21**, 467–488, 1982.

[3] R. P. Feynman, "Quantum mechanical computers," Foundations of Physics, **16**, 507–531, 1986.

[4] P. W. Shor, "Algorithms for Quantum Computation: Discrete Logarithms and Factoring," in in Proceedings of the 35th Annual Symposium on the Foundations of Computer Science, 124–133, 2021.

[5] P. W. Shor, "Polynomial-time algorithms for prime factorization anddiscrete logarithms on a quantum computer," SIAM review, **41**, 303–332, 2020.

[6] D. Deutsch, R. Jozsa, "Rapid solution of problems by quantum computation," SIAM review, **439**, 553–558, 2020.

[7] L. K. Grover, "A fast quantum mechanical algorithm for database search," in In Proceedings of the twenty-eighth annual ACM symposium on Theory of computing, 212–219, 1996.

[8] J. A. Buchmann, D. Butin, F. Göpfert, A. Petzoldt, "Post-Quantum Cryptography: State of the Art," Lecture Notes in Computer Science, **9100**, 2016, doi:10.13140/RG.2.2.29502.18243.

[9] M. A. Nielsen, I. L. Chuang, Quantum Computation and Quantum Information, Cambridge University Press, 2011.

[10] S. M. Pranav, M. Ritwik, "A Comprehensive but not Complicated Survey on Quantum Computing," in In Proceedings of the twenty-eighth annual ACM symposium on Theory of computing, 144–152, 2014, doi:10.1016/j.ieri.2014.09.069.

[11] D. Arighna, D. Gerhard W, W. Robert, "Towards exploring the potential of alternative quantum computing architectures," in Proceedings of the 23rd Conference on Design, Automation and Test in EuropeMarch, 682–685, 2020.

[12] M. Vasileios, V. Kamer, M. D. Zych, A. Jøsang, "The Impact of Quantum Computing on Present Cryptography," International Journal of Advanced Computer Science and Applications, **9**, 2018.

[13] Y. Dulek, F. Speelman, "Quantum Ciphertext Authentication and Key Recycling with the Trap Code," Leibniz International Proceedings in Informatics, 1–17, 2020.

[14] P. S. Emani, J. Warrell, A. Anticevic, "Quantum computing at the frontiers of biological sciences," Nat Methods, **18**, 701–709, 2021, doi:10.1038/s41592-020-01004-3.

[15] D. C. Doimari, "computing versus classical computing in the field of Biological Sciences," E-ZINE OF BIOLOGICAL SCIENCES, 2020, doi:10.1038/s41592-020-01004-3.

[16] S. Chakraborty, S. B. Mandal, S. H. Shaikh, "Quantum image processing: challenges and future research issues," International Journal of Information Technology, 1–15, 2018.

[17] F. Yan, S. E. Venegas-Andraca, K. Hirota, "Toward implementing efficient image processing algorithms on quantum computers," Soft Computing, 1–13, 2022.

[18] P. Christopher, R. Renato, "Renato,Security in quantum cryptography," Rev. Mod. Phys, 2022, doi:10.1103/RevModPhys.94.025008.

[19] Bennett, H. Charles, G. Brassard, A. K. Ekert, "Quantum Cryptography," Scientific American 267, **4**, 50–57, 1992.

[20] G. Beach, C. Lomont, C. Cohen, "Quantum image processing (QuIP)," in 32nd Applied Imagery Pattern Recognition Workshop, Procedongs, 39–44, 2003, doi:10.1109/AIPR.2003.1284246.

[21] Y. Liu, Z. Qi, Q. Li, "Comparison of the similarity between two quantum images," Sci Rep 12, 50–57, 2022, doi:10.1038/s41598-022-11863-9.

[22] M. A. Nielsen, I. L. Chuang, Quantum Computation and Quantum Information, Cambridge University Press, 2010.

[23] C. Kiefer, E. Joos, "Quantum Future From Volta and Como to the Present and Beyond," Lecture Notes in Physics, 1999, doi:10.1007/BFb0105342.

[24] D. P. DiVincenzo, "The Physical Implementation of Quantum Computation," Fortschr. Phys., **48**, 771–783, 2000, doi:10.1002/1521-3978(200009)48:9/11⟨771::AID-PROP771⟩3.0.CO;2-E.

[25] M. Brune, . Hagley, J. Dreyer, X. Maître, A. Maali, C. Wunderlich, J. M. Raimond, S. Haroche, "Observing the Progressive Decoherence of the "Meter" in a Quantum Measurement," Phys. Rev. Lett, **77**, 301, 1996.

[26] N. Mikio, O. Tetsuo, Quantum Computing - From Linear Algebra to Physical Realizations, CRC Press, 2010.

[27] A. D. O'Connell, M. Hofheinz, M. Ansmann, B. Radoslaw, M. Lenander, L. Erik, M. Neeley, D. Sank, H. Wang, W. Martin, J. Wenner, M. John, A. Cleland, "A. Quantum ground state and single-phonon control of a mechanical resonator," Nature, **464**, 697–703, 2010, doi:10.1038/nature08967.

[28] T. Sauter, W. Neuhauser, R. Blatt, P. E. Toschekt, "Observation Of Quantum Jumps," PHYSICAL REVIEW LETTERS, **57**, 697–703, 1986.

[29] A. Einstein, B. Podolsky, N. Rosen, "Can Quantum-Mechanical Description of Physical Reality Be Considered Complete? ," PHYSICAL REVIEW, **47**, 1935.

[30] J. Yin, Y. Cao, Y.-H. Li, S.-K. Liao, L. Zhang, J.-G. Ren, W.-Q. Cai, W.-Y. Liu, B. Li, H. Dai, G.-B. Li, Q.-M. Lu, Y.-H. Gong, Y. Xu, S.-L. Li, F.-Z. Li, Y.-Y. Yin, Z.-Q. Jiang, M. Li, J.-J. Jia, G. Ren, D. He, Y.-L. Zhou, X.-X. Zhang, N. Wang, X. Chang, Z.-C. Zhu, N.-L. Liu, Y.-A. Chen, C.-Y. Lu, R. Shu, C.-Z. Peng, J.-Y. Wang, J.-W. Pan, "Satellite-Based Entanglement Distribution Over 1200 kilometers ," Science, **356**, 1140–1144, 2017, doi:10.48550/arXiv.1707.01339.

[31] A. Aspect, J. Dalibard, G. Roger, "Experimenta lTest of Bell's Inequalities Using Time-Varying Analyzers ," Physical Review Letters, **49**, 1982.

[32] "quantum algorithm zoo," 2020.

[33] G. D. Campo, I. Gomez, G. Canada, L. Piovano, A. Santamaria, "Guidelines and criteria for selecting the optimal low-power wide-area network technology ," LPWAN Technologies for IoT and M2M Applications, 281–305, 2020, doi:10.1016/b978-0-12-818880-4.00.

[34] N. Shireen, F. Mohammed, "RSA Public Key Cryptography Algorithm. A Review ," International Journal of Scientific and Technological Research, **6**, 187–191, 2017.

[35] X. Zhou, X. Tang, "Research and implementation of RSA algorithm for encryption and decryption," 2011, doi:10.1109/IFOST.2011.6021216.

[36] M. T. Madzik, S. Asaad, A. Youssry, B. Joecker, K. M. Rudinger, E. Nielsen, K. C. Young, T. J. Proctor, A. D. Baczewski, A. Laucht, V. Schmitt, F. E. Hudson, K. M. Itoh, A. M. Jakob, B. C. Johnson, D. N. Jamieson, A. S. Dzurak, C. Ferrie, R. Blume-Kohout, A. Morello, "Precision tomography of a three-qubit donor quantum processor in silicon ," Nature, **601**, 348, 2022, doi:10.1038/s41586-021-04292-7.

[37] E. R. Johnston, N. Harrigan, M. Gimeno-Segovia, Programming Quantum Computers: Essential Algorithms and Code Samples, O'Reilly Media, 2019.

[38] A. Iliyasu, P. Le, F. Dong, K. Hirota, "Watermarking and authentication of quantum images based on restricted geometric transformations," Inf. Sci., **186**, 126–149, 2012.

[39] X. Song, S. Wang, S. Liu, A. A. El-latif, X. Niu, "A dynamic watermarking scheme for quantum images using quantum wavelet transform," Quantum Information Processing, **12**, 3689–3706, 2013.

[40] X. Song, S. Wang, A. A. El-latif, X. Niu, "Dynamic watermarking scheme for quantum images based on Hadamard transform," Multimedia Systems, **20**, 379–388, 2014.

[41] Y. Yang, P. Xu, J. Tian, H. Zhang, "Analysis and improvement of the dynamic watermarking scheme for quantum images using quantum wavelet transform," Quantum Information Processing, **13**, 1931–1936, 2014.

[42] F. Yan, A. M. Iliyasu, P. Q. Le, "Quantum image processing: A review of advances in its security technologies," International Journal of Quantum Information, **15**, 1730001, 2017.

[43] S. Chakraborty, S. B. Mandal, , S. H. Shaikh, L. Dey, "Ternary quantum circuit for color image representation," In Advanced Computing and Systems for Security, 95–108, 2017.

[44] A. B. Klimov, L. L. Sánchez-Soto, H. de Guise, G. Bjork, "Quantum phases of a qutrit," Journal of Physics A, **37**, 4097–4106, 2000.

[45] S. Chakraborty, S. B. Mandal, S. H. Shaikh, "Design and implementation of a multivalued quantum circuit for threshold based color image segmentation," Intell. Decis. Technol., **12**, 251–264, 2018.

A Cloud Telemedicine Platform Based on Workflow Management System: A Review of an Italian Case Study

Gianvito Mitrano*,[1], Antonio Caforio[2], Tobia Calogiuri[1], Chiara Colucci[3], Luca Mainetti[1], Roberto Paiano[1], Claudio Pascarelli[1]

[1]*University of Salento, Department of Engineering for Innovation, Via per Monteroni, Lecce, 73100, Italy*

[2]*A-thon s.r.l., Via dei Tufi 4, Monteroni di Lecce (Le), 73047, Italy*

[3]*National Interuniversity Consortium for Informatics, Via Ariosto 25, Roma, 00185, Italy*

ARTICLE INFO

ABSTRACT

The paper aims to describe a new technological and organizational approach in order to manage teleconsultation and telemonitoring processes involving a Physician, who remotely interacts with one or more Specialists, in order to evaluate and discuss the specific clinical conditions of a patient, based primarily on the sharing of digital clinical data, reports and diagnostic images. In the HINT project (Healthcare INtegration in Telemedicine), a teleconsultation and telemonitoring cloud platform has been developed using a Hub and Spoke architecture, based on a Business Process Management System (BPMS). The specialized clinical centres (Hubs) operate in connection with the territorial hospital centres (Spokes), which receive specific diagnostic consultations and telemonitoring data from the appropriate Specialist, supported by advanced AI systems. The developed platform overcomes the concepts of a traditional and fragmented teleconsultation and consequently the static organization of Hubs and Spokes, evolving towards an integrated clinical workflow management. The project platform adopts international healthcare standards, such as HL7 FHIR, IHE (XDS and XDW) and DICOM for the acquisition and management of healthcare data and diagnostic images. A Workflow Management System implemented in the platform allows to manage multiple and contemporaneous processes through a single platform, correctly associating the tasks to the Physicians responsible for their execution, monitoring the status of the health activities and managing possible clinical issues.

1. Introduction

This paper is an extension of work originally presented in the *10th International Conference on Information Systems and Technologies (ICIST 2020)* entitled *"HINT project: a BPM teleconsultation and telemonitoring platform"* [1]. It is focused on the implementation of a telemedicine (teleconsultation and telemonitoring) platform, based on diagnostic imagines, which supports the *Hub and Spoke* clinical model.

In particular, optimized teleconsultation processes, supported by proper technological infrastructures, allow: i) to share data and diagnostic images between several professionals; ii) to have the

first or second opinion evaluations in a very short time; iii) to prevent the patient from moving between Physicians for consultations; iv) to provide precise evaluations and diagnoses to the patient by reducing waiting times. Moreover, telemonitoring allows to control the specific vital parameters of each patient and to manage alerts if necessary [2], [3].

Over the years, many definitions of telemedicine have been given, based on the use of IT (Information and Telecommunication Systems) for remote clinical data exchange between the medical team (Physician, Nurses, Specialist) and patients, in order to provide the remote healthcare treatment. Some of these definitions are given below.

The American Telemedicine Association gives a definition of telemedicine as "The use of medical information exchanged from

*Corresponding Author: Gianvito Mitrano, University of Salento, Department of Engineering for Innovation, Via per Monteroni, 73100, Lecce, Italy - gianvito.mitrano@unisalento.it

one site to another via electronic communications to improve a patient's clinical health status" [4].

The World Health Organization (WHO) defines telemedicine as follows: "The delivery of healthcare services, where distance is a critical factor, by all healthcare professionals using information and communication technologies for the exchange of valid information for diagnosis, treatment and prevention of diseases and injuries, research and evaluation, and for the continuing education of healthcare providers, all in the interests of advancing the health of individuals and their communities" [5].

The outcomes of telemedicine services can be: i) accessibility to healthcare in remote areas, allowing consistent and reliable communication; ii) fast, affordable, and reachable care; iii) h24 diagnosis (also known as night-hawking); iv) efficiency in care delivery like telestroke scenario; v) cost and time optimization and saving; vi) better collaboration between Specialists [6].

Telemedicine can also reduce the risk of hospitalization, thanks to its ability to decrease in-clinic visits, promoting remote services for patients [7]. Another important outcome can be a more effective patient engagement and evolvement, which could help users to be informed overtime about their care plan and become more aware of their health. Telemedicine can also represent an effective way to treat depression and other mental health conditions, helping patients with mental disorders unwilling to seek any treatment in normal circumstances, and making use of video or remote controls.

Telemedicine services can be divided into synchronous and asynchronous services. In the former case, the service establishes an interaction and connection in real time (through audio or video-conferencing technologies) between the parties requiring their presence at the same time; in the latter case, clinical and medical data are temporarily stored and later transmitted to the Physician or medical Specialist for an offline assessment. Synchronous telehealth models can help to provide timely care, especially for emergency care or urgent situations. On the other hand, asynchronous models are ideal for evidence-based and not emergency care [8].

In healthcare, especially in telemedicine, some fundamental aspects concern the quality of data, clinical documents, diagnostic images and the modality to exchange. Physicians and healthcare professionals need to access and share all the patient's information and clinical data, also deriving from telemonitoring activities, and it is, therefore, necessary the interconnection between different Information Systems and the consequent interoperability based on clear and possibly open rules and standards [9], [10].

Interconnected and interoperable systems are defined as integrated if, thanks to the use of standard languages, protocols and formats, they allow to define the methods of transmission and reception of data, as well as their representation (syntax) and their semantics [11].

In the healthcare sector, there are several models and open standards for the information and clinical data management and exchange, among which, for the best of authors' knowledge, the most widely used are IHE (Integrating the Healthcare Enterprise), DICOM (Digital Imaging and Communications in Medicine) and HL7 (Health Level Seven) for the diagnostic images sharing [12].

These standards are used in order to have an effective interoperability between the Health Information Systems (HIS)such as hospital RIS (Radiology Information System), PACS (Picture Archiving and Communication System) and booking centers (e.g., the Italian CUP) [13].

Alongside the standards and new healthcare information technologies mentioned above, it is important to define and optimize clinical processes through the use of management approaches such as the BPM (Business Process Management), which allows to model, define, organize, execute and monitor the clinical activities of interest.

In this paper, after an initial overview of the motivation behind this work, section two provides a narrative literature review about telemonitoring and teleconsultation applications. The third section describes the HINT project, that has developed a cloud platform based on a *Hub and Spoke* architecture where telemedicine processes are managed by a BPM workflow system. The fourth section illustrates these processes modelled through the BPMN notation, with a detailed analysis of the following scenarios: Neuro-Radiological Teleconsultation, Dermatological Teleconsultation and Obstructive Sleep Apnoea Syndrome Telemonitoring. Finally, discussion and conclusions close the paper.

1.1 Motivation

Different telemedicine projects propose generic solutions with static Hub and Spoke architecture [14], [15], in which the teleconsultation and the exchange of clinical data and information take place through traditional clinical assessment, in absence of a single management platform and digitalized telemedicine pathways for the real time sharing of reports, diagnostic images and documents. To overcome a typical static organization, the HINT project envisages the use of a workflow engine for the complete routing and management of the consultation request and parameter monitoring to the appropriate and available Hub.

Moreover, the Hub Specialist can be helped in his/her clinic evaluation by Decision Support Systems (DSSs) based on Deep Learning, which can analyse and classify dermatological images and to manage out-of-threshold values with alerts. Specifically, the project proposal is an advanced teleconsultation and telemonitoring system, in which Physicians can: i) receive technological support through DSSs; ii) are aware of the consulting request status in every moment and iii) provide detailed clinical information to make assessments and final diagnoses. The HINT *Hub and Spoke* system allows the identification of the most appropriate available Specialist for the dermatological case to be treated, who responds on a single, integrated platform with his/her second opinion evaluations. It is particularly valuable in all the cases requiring high healthcare specializations, especially in remote areas where they are not immediately available.

Furthermore, the HINT platform wants to guarantee timely and constant monitoring of specific vital parameters in the treatment of sleep apnoea through UWB devices. It is supported by the implementation of a Workflow Management System for healthcare process digitalization through the application of the IHE standard (XDW) for the definition and traceability of all the steps, actors and documents produced in the clinical care processes.

2. Literature review

In this section, a literature study is carried out to analyse the different telemedicine services implemented in the HINT system,

which are teleradiology, teleconsultation and telemonitoring. A review on information systems and standards is also provided.

Teleradiology is implemented in different countries in order to face the following issues [1], [16]:

1. out-of-hour coverage by means of intramural services (at-home control);
2. out-of-hour coverage by means of extramural services;
3. rural or regional hospital coverage;
4. Specialist's second opinion.

In [16], the authors summarize some of the key aspects in image acquisition, transmission, and interpretation, with a discussion of the clinical practice of teleradiology.

A survey [17] states that 44% of the European radiologists use at-home control instead of call referral. In many cases this procedure is not based on a structured *Hub and Spoke* architecture, but only on the diagnostic image transmission to the Radiologist who sends the referral to the Physician by email or phone (79% of the cases).

It is also important to mention the Kaiser Permanente hospital [18] where, during the out-of-hours, there are only 2 radiologists sending medical reports for 11 different image acquisition sites, instead of having a specific Radiologist, called when needed, in each hospital.

In the U.S., it is estimated that over than 50% of the hospitals use out-of-hours reporting or night-hawking [19]. It is possible to gain an advantage from the different time zones by using extramural services. For example, in [20] radiologists from Sydney are called by a Swedish hospital for emergency; while in [21] an American hospital requests a consultation to radiologists located in India. Moreover, in [22] the authors report that radiology delays are shorter when teleradiology is used [1].

In [23], the authors delineate the main reasons for the medical imaging demand growing in Europe and U.S., explaining why teleradiology is critical to support this development in Europe. In particular, the paper presents three different teleradiology case studies regarding successful data sharing and innovative workflow models through single imaging implementations.

Furthermore, radiology is becoming increasingly specialised in recent years. The studies [24], [25] illustrate the improvement associated with producing a subspecialist report compared to a general one. In this context, teleradiology can be used to gain access to radiologists who are well trained in a particular field. Regarding this aspect, [26] underlines that teleradiology is an important component in radiology field for many aspects, one of which is the possibility to facilitate seeking a second opinion from an expert, improving in this way the efficiency and effectiveness of healthcare system. In particular, the paper presents a model based on second opinion teleradiology consultation service, which involves an Israel health insurance company and a premier medical center in San Francisco, showing in detail the operational procedure of this second opinion service [26].

In [27], the authors state that fast wireless network and mobile technologies allow to evaluate diagnostic images with a comparable accuracy to PACS workstations. In [28], the authors design and develop an economic web based platform for the diagnostic images referral by means of IT technologies. For more details about this approach, [29] gives a complete historical overview of the applications in the teleradiology sector [1].

Moreover, the tele-imaging application represents a significant chance for the future and it is a central practice for telemedicine. In particular, it includes the transmission of medical digital images and has an important role in all fields of telemedicine, such as expertise, consultation, teaching and research activities [30].

Another field of tele-imaging concerns teleconsultation, whose overall goal is to overlook geographical and functional distance between two or more geographically separated healthcare providers, using information and communication technology [31]. Surgery and general medicine are among the most common topics in adult teleconsultations. In particular, surgery teleconsultations are generally performed by sending radiology images (teleradiology), clinical pictures or videos, in order to reduce unnecessary patient transfers or travels with related costs, and also to support prompt decision making with high diagnostic accuracy, improving the future of the healthcare delivery [31].

In this context, teleconsultation is increasingly becoming an integral part of the hospital procedures. A European survey [14] estimates that 65% of all radiologists currently use teleradiology for the images sharing within the organisation and for on-call readings from home [32].

Moreover, some hospitals, especially in the United States, use teleconsultation to manage out-of-hour reporting by adopting a complete *Hub and Spoke* architecture. The architecture involves configurations which are centers of excellence opened 24 hours a day, providing highly complex diagnostic-therapeutic services (Hubs), and other configurations which aim to create a territorial network of services for the management of patients once overcome a certain clinical severity threshold (Spoke) [1], [33].

Additionally, teleconsultation is also applied in emergency or urgent situations, for example during pre-hospital critical care situations [34] or for emergency orthopaedic patients by mobile phone messages [35] or even for ophthalmic emergency consultation, through the use of a smartphone App or PC and a webcam [36].

There are also many studies about telemonitoring application; in particular, an analysis presented in [37] and conducted on 65 studies in the field of telemonitoring for cardiovascular, pulmonary, hypertension and diabetes diseases, describes the maturity and reliability of remote monitoring technologies [1]. Telemonitoring has also demonstrated the ability to identify changes in the condition of chronic patients at an early stage of their disease, obtaining fast intervention and avoiding complications [31]. An example is reported in [38], which refers to diabetic patients affected by a reduction in haemoglobin A1c and a significant blood glucose increase. For patients affected by hypertension, [39] reports how to respond through telemonitoring to a systolic and diastolic blood pressure reduction. In [40], [41], the authors report a high level of satisfaction of telemonitoring processes and [42], [43] emphasize the positive contribution given by telemonitoring to the decrease of hospital admissions for heart and pulmonary diseases.

Through telemonitoring it is also possible to analyse the Continuous Positive Airway Pressure (CPAP) in patients with Obstructive Sleep Apnoea (OSA) [44]. In particular, a study [45] based on [46], [47], shows that CPAP compliance is significantly higher in the Telemonitor (TM) care group compared with the usual care group, thanks to current technological advances and to the use of innovative medical devices which allow patients to control some vital parameters at home.

Telemonitoring is also applicable in the cardiology sector, for example through the development of a phone-based and rule-based expert system for heart failure telemonitoring, designed to provide remote clinical support for patients with cardiological problems [48], [49]. Another important field of application of telemonitoring concerns the control of elderly people [1], [50].

A complete review of telemedicine, is proposed into [51], which contains detailed information about: telecardiology, telestroke, teleradiology, teleoncology, teledermatology, telepathology and telemonitoring.

2.1. Health information systems and standards

An Information System (IS) can be defined as a technical and organizational system designed to collect, process, store, and exchange information and data [52].

In healthcare organizations (i.e. hospitals, radiology departments), IS manages all clinical data, diagnostic images, and reports. HIS (Hospital Information System), RIS (Radiology Information System), PACS (Picture Archiving and Communication System) are some of the most important clinical Information Systems applied in healthcare organizations [53], [54]:

- HIS: system based on IT used in healthcare to manage the administrative and clinical flows of a hospital;
- RIS: system used to manage the radiology data flow, with the purpose to collect, manage and display data and information produced in the Radiology Department;
- PACS: system used for archiving images acquired from modalities applications, managing worklists, and accessing images from reporting stations (workstations) [55].

The RIS is a HIS subsystem, while the PACS, an independent system integrated with the others, deals with the diagnostic images management.

The integration among the different systems and, in particular, between the RIS and the PACS within Radiology Department should lead to: i) use a single medical registry; ii) have a simultaneous display of images and reports; iii) facilitate the automatic distribution of images through departments [56].

Generally, every healthcare organization has a PACS which manages the various modes of digital image acquisition. A structured PACS comprises an image acquisition system and a secure network connecting radiology workstations (on-site or off-site) with a centralized archive [1]. The DICOM standard is used in order to simplify the interoperability of different devices in acquisition, transmission and saving of images.

Digital Imaging and Communications in Medicine (DICOM) was developed by the American College of Radiology and the National Electrical Manufacturers' Association [57], in order to use fully digital images with high resolution instead of physical X-ray films [58].

DICOM is an international standard for all clinical images and relevant metadata and concerns the handling, storing, printing and transmitting phases [59], [60]. This standard allows to manage different types of medical images with other data such as: patient name, reference number, study number, dates and reports [61].

The DICOM standard is widely adopted in radiology, cardiology and radiotherapy imaging, and it is progressively expanding in other medicinal areas, like ophthalmology and dentistry [62].

Health Level Seven (HL7) is another important standard which allows the standardisation of the exchange of electronic health information. It is focused on data communication and not on data storage and presents the following versions: HL7 v2, HL7 v3 and the most recent FHIR (Fast Healthcare Interoperability Resources) which uses real-time RESTful interfaces [1]. In particular, HL7 v2 is chosen from local hospital for the exchange of healthcare information, including electronic medical record information [63]. HL7 v3 is designed to be the successor to v2 and overcomes the v2's shortcomings. Finally, FHIR combines the features of HL7 v2 and v3 with the modern web technologies such as the REST architecture, in order to facilitate its implementation [63], [64]. In particular, differently from v2, FHIR is not based on the exchange of messages when certain events occur but on the availability of data and information exposed through a server, defining in this way the Resources (patient, encounter, condition, observation, procedures, care plan, goal and appointment), which are organized into modules, each representing a different functional area.

Modules are structured in 3 groups and 5 levels: infrastructure (levels 1 and 2), content (levels 3 and 4) and reasoning (level 5) [65].

In order to support the adoption of international standards such as DICOM or HL7, a consortium of professionals and industries named Integrating the Healthcare Enterprise (IHE) has been defined. IHE preserves a list of domains such as cardiology, radiology, pharmacy, IT system and patient care. In this context, it is important to mention the Cross Enterprise Basic eReferral Workflow Definition Profile (XBER-WD), which defines and standardises the workflow related to an eReferral Document, the actors involved and the digital documents related with the process [66]. XBER-WD is a standard based on a document type called Cross-Enterprise Document Workflow (XDW), in which the tasks completed in the workflow, the inputs and the outputs are stored [1].

The XDW standard supports participants in a complex environment to track and manage tasks related to clinical workflows, providing a common interoperability infrastructure to support them. All the documents can be exchanged between organisations through Cross-Enterprise Document Sharing (XDS) repositories, which facilitate the registration, sharing and storage across health enterprises of the patient electronic health records, in order to associate documents containing medical data to a specific workflow [67], [68].

3. HINT project

The HINT (Healthcare INtegration in Telemedicine)[1] project aims to implement a clinical support network both in cases requiring high specialization and to cover areas without specific expertise. The project develops a platform for the management of cases requiring access to diagnostic images, with the possibility of

---

applying specific medical expertise even when no one is physically present where the images are produced. Specifically, the project envisages the realization of technological solutions aimed at optimizing the communication between the multi-disciplinary teams involved in a clinical case. Research activities also focus on defining tools which improve clinical data collection and healthcare information management, as well as on the clinical workflow efficiency, supporting the Physician in the decision-making process. HINT aims to realise a multi-target approach by integrating Physician support with the suggestion of diagnostic pathways, relying on a computational architecture capable of managing large data sets and algorithms for process mining and deep learning [1].

The research topics addressed by the project concern innovation in the area of:

- Cloud architectures in the clinical health field;
- Clinical Decision Support Systems and Computer Aided Diagnosis systems;
- Deep Learning models and algorithms;
- Integration and management standards for clinical processes;
- Secure data storage.

3.1 The BPM approach and lifecycle applied to the project

Looking at the approaches used in recent years, it is possible to note that there have been health and telemedicine projects which have used Workflow Management Systems based on the Business Process Management (BPM) approach and on the Business Process Model and Notation (BPMN) [69]. The BPM and BPMN tools allow to optimize clinical processes, tracking the key health parameters of an individual patient, organizing and monitoring all the healthcare activities, in order to support health organizations [70], [71].

The business processes are intended as "logically related tasks performed to achieve a defined business outcome" [72]. The BPM approach embodies methods and technologies which enable organizations to analyse, manage and optimize business processes [1], [73].

In [74], the authors analyse three BPM lifecycle proposals: the BPM lifecycle defined by Van der Aalst, the BPM lifecycle proposed by Netjes, and the BPM lifecycle proposed by Weske.

The first author proposes the BPM lifecycle with four steps: i) process design; ii) system configuration; iii) process enactment; iv) diagnosis phase, concerning processes' monitoring and analysis [75].

The second approach includes five steps: i) design; ii) configuration; iii) execution; iv) control; v) diagnosis, which provides information in order to identify opportunities for improvement, workflow bottlenecks and any other critical points [76].

The last approach presents a cycle consisting of the following four steps: i) design and analysis; ii) configuration; iii) enactment; iv) evaluation of the business processes' performance [77].

Taking the cue from the models proposed, the lifecycle of the health processes managed in the project (starting from modelling to optimization) are described and shown in the following revised phases and in Figure 1 [1], [78]:

1. Process analysis and modelling;

2. Process implementation;
3. Process execution;
4. Process monitoring.
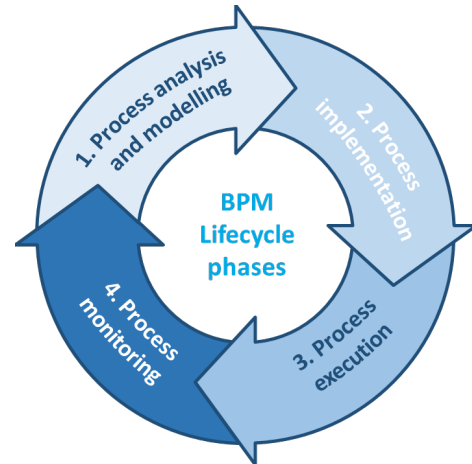
Figure 1: BPM lifecycle phases in HINT project

In the analysis phase, a business problem is highlighted and studied, in order to identify and analyse the related processes. The outcome of the process analysis is a new or updated process model which makes available a complete overview of the organization processes. In the modelling step, the current state of processes and the related activities are designed and modelled using tools and notations as BPMN, DMN (Decision Model and Notation), CMMN (Case Management Model and Notation) [1].

Then, in the implementation phase, the changes required to shift from the As-Is process to the To-Be process are defined and performed [63]. In particular, this phase involves two different aspects: the organizational change management and the process automation. Once the process has been mapped and illustrated, during the execution phase, it is run and tested, allowing its adaptation to the users' needs. Then, a series of logs and measurements are collected and used in the monitoring phase, in order to analyse the process performance through specific Key Performance Indicators (KPI) and targets [1]. The notations mentioned above can be used for the process modelling: BPMN, CMMN and DMN, which can support the clinical process management.

In particular, an application example can be seen in [79], which recreates a guideline for stable ischemic heart disease, and considers the advantages and limitations of representing clinical pathways with these three notations. Moreover, [80] presents a clinical pathway for living donor liver transplantation using a combined approach which involves the event processing (BPMN) and the case management (CMMN) [81]. Another applicative case is presented in [82], which reports a study in healthcare sector, using DMN and BPMN approaches in an integrated manner, analysing a pediatric surgery process in a mid-size hospital. Finally, [83] combines the BPMN and DMN notations for modelling care pathways in a standardised manner.

As previously analysed, the BPM proved its usefulness to improve the design and therefore the telemedicine processes' implementation. Indeed, there are some cases of the BPM application in the field of telemedicine projects, regarding, for example, de-hospitalization services with focus on e-Health

solutions [84], or related to chronic pathologies such as Chronic Obstructive Pulmonary Disease (COPD) with a patient-centered approach based on telemedicine devices [85]. There is also a study concerning the use of the BPM methodology in healthcare with reference to the end-user interaction with EHR interface [86], as well as a study involving patients with hypertension whose healthcare processes are modelled using the BPM paradigm in order to identify weaknesses and mitigate them, for a better patient empowerment [87]. These studies underline that BPM applied to telemedicine is an efficient approach which can improve the management of the all-internal processes, the work of healthcare operators, with a positive impact on the quality of care and life of the patients.

In fact, in recent years, different clinical organisations have applied a BPM-based technology approach in order to improve the process management in healthcare sector.

In this way the quality and efficiency of processes can be increased, ensuring a better and continuous relationship with the patient. The use of BPM can also support medical practices by monitoring care processes, managing and analysing the clinical workflow and specific activities. A structured knowledge of the business context could be useful for the analyst in these activities [88], [89].

Table 1 summarizes and describes the BPM lifecycle phases in telemedicine processes, outlines the possible actors involved (Physicians, Specialists, Developers, Analysts) and identifies the clinical profiles, the standards (i.e. HL7, IHE, DICOM) and notations for process modelling and rule management [1].

3.2 HINT architecture

The HINT project intends to develop a cloud platform with *Hub and Spoke* architecture for telemedicine based on imaging, which, by using international standards (DICOM, HL7, IHE), allows the integration of processes, health data and diagnostic images [1].

The cloud platform developed includes components which support Physicians and healthcare workers in the clinical cases management, enabling them to authenticate and authorise users, to manage roles, to search and consult the patient list, to manage examinations, to consult documents in the patient medical record, to open a clinical case, to record data in the required formats and to initiate and manage predefined diagnosis and treatment paths through the Workflow Manager functions whose interrelations will be highlighted later.

The core components developed, and described below, are: Portal, *Hub and Spoke* applications to manage Telemedicine services, DSS (Decision Support System), Workflow Management System, ESB (Enterprise Service Bus), VA (Virtual Archive) (Figure 2).

These components ensure [1]:

- user access to the different applications;
- the availability of basic record management services;
- access to integration services, allowing messages to be converted into the standard formats used in the health field;
- access to the necessary terminology management services;
- standard access to document archiving services.

Table 1 – BPM lifecycle phases, with related actors and clinical standards applied in the HINT project

| BMP Lifecycle	Description	Actors	Standards
1. Business process analysis and modelling	The phase involves the identification and study of the relevant business processes and the As-Is process definition	Business/Process Analyst Clinical domain experts (General Practitioner, Specialist, Healthcare Manager)	BPMN CMMN DMN
2. Business process implementation	The phase involves changes preparation needed to move from the As-Is process to the To-Be process in terms of process automation and management	Software Developer Process Developer	CDA HL7 DICOM XBER-WD (IHE) XDS (IHE) DSUB (IHE)
3. Business process execution	The phase involves To-Be process running and testing, with measurements and logs collection needed in the monitoring phase	Physician and Specialist Users RIS/PACS systems DSS UWB devices	DICOM XDW (IHE) FHIR
4. Business process monitoring	The phase involves the collection of relevant data in order to define the process performance in relation to its KPIs	Clinical Data Analyst Clinical Risk Manager	XDW (IHE) AUDIT LOG
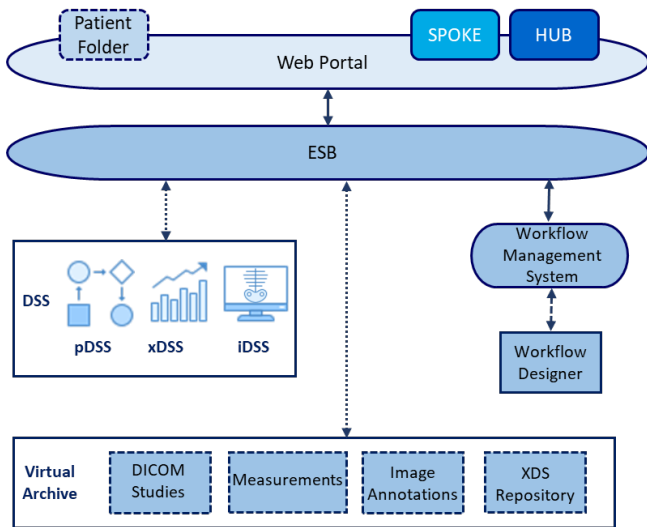
Figure 2 – HINT project architecture components

Portal

The HINT Portal provides the general services of the platform. It consists of a web interface hosting all the user applications (Web Container), such as the Patient Folder, the agenda management, the visit management, etc. and allows access to the specific applications for *Hub and Spoke* telemedicine processes described in the scenarios.

The Portal allows basic consultation to the patient medical record, in which it is possible to examine the patient's documents, the active pathways and the visit management through acceptance and discharge procedures.

The Portal offers a layer of back-end services to the other applications of the platform and has a local archiving component. This layer mainly offers:

- Single Sign-On services (SSO);
- services for the univocal patient data management (Master Patient Index) and for the patients' identification;
- EHR services.

Spoke

The Spoke represents a set of platform applications which enable the implementation of specific functionalities of a particular clinical-health task. Basically, a Spoke application identifies, for a requesting structure, the hardware and software equipment used to digitally record and archive the patient's physiological data, documents and clinical studies, i.e. to make use of that set of information to perform the task and obtain a diagnosis. For HINT, Spoke functionality also includes the generation of requests for examinations and consultations (Neuro-Radiological and Dermatological teleconsultation).

The Spoke hardware and software equipment can be represented by a specific software application and by the following devices: medical devices (including UWB devices - Ultra Wide Band), diagnostic apparatus, RIS/PACS system.

Hub

The Hub represents a set of applications of the platform which allows to receive the notification and proceed to the completion of a particular clinical-health task. Basically, a Hub application identifies, for the supplying structure, the system used to consult data, documents and images and to record the diagnosis in a medical report. The Hub may be the display component of a teleconsultation, telemonitoring or teleassistance system, or even a RIS/PACS system.

ESB

The integration services of the HINT platform enable communication between the different components by sorting and transforming messages into formats supported by the final components.

The Enterprise Service Bus (ESB) component implements services dealing with the exchange of information between the front-end of the Portal together with the user applications (including *Hub and Spoke*) and the back-end components of the platform.

These services implement, when required, the transformation of the messages sent by the clients in JSON (XML format) for data and documents, and in JPEG format, for images, into the health standard formats (HL7, CDA, DICOM).

DSS

The Decision Support System (DSS) component allows the following activities: feature extraction; image classification and diagnostic support by means of a neural network (iDSS); diagnostic logs analysis for the identification of the diagnostic process patterns (pDSS); control of physiological data and alerts reporting (xDSS) [1].

Workflow Management System

The Workflow Management System is responsible for managing the execution of clinical processes modelled in BPMN, which comply with the specifications of the workflow definition profile standard defined by XBER-WD and for the storage of workflow documents in the XDS.

The Workflow Management System consists of these sub-systems:

- Workflow Engine and related services;
- Workflow Document Management and storage system.

The Workflow Engine manages the execution of processes and controls activities involving actors and applications. It receives communications which allow tasks to be updated through services compliant with the FHIR standard. Moreover, it manages the assignment of tasks, the progress of processes and the notifications to external components.

Virtual Archive

The Virtual Archive implements repository services for archiving clinical-health data, documents and images. The VA defines a unique interface layer for the portal and identifies the applications which need to archive data and documents generated during the execution of the processes supported by the platform.

4. HINT telemedicine processes

4.1 Neuro-Radiological Teleconsultation

This process describes the remote consulting activity between Physicians (Requesting Physicians and Clinical Specialists) who, being in two different places, can communicate with each other via ICT systems. In the specific case, the specialized organization (Hub), where the Clinical Specialist provides health services, gives, when required, medical consultations to the local organization (Spoke), which has available clinicians providing only some basic health services.

The principal activity regards the evaluation of the patient's condition for first or second opinion by a Clinical Specialist, based on shared diagnostic images and clinical reports.
The entire process can be divided into the following phases [1]:

- Creation of a Referral Request;
- Consultation Scheduling;
- Clinical data control and evaluation by the Clinical Specialist (creation of report).

The HINT portal can manage the initial step concerning the admission of the patient to the clinical organization, the acquisition of the exam reports (MRI, PET, CT, diagnostic tests) carried out and the subsequent neurological evaluation during the first control visit. If the Requesting Physician of the Spoke Organization needs to perform a neuroradiology consultation by contacting the Hub Clinical Specialist, he/she can use the HINT system based on a workflow engine to create a *Teleconsultation Referral Request*. The Requesting Physician enters all the data regarding the teleconsulting request in the first free Hub.

The data to be entered in order to define the Request are: the patient's personal data, request type (e.g., first neuro-radiological control, diagnostic valuation for second opinion), clinical history (e.g. trauma, potential stroke, dementia), urgency level, the list of past clinical exams (reports and digital images).

The *Scheduling* task creates a list of Hub structures (and related Clinical Specialists) which can take charge of the teleconsultation execution. The Requesting Physician can then select one of them from the list. A decision table based on specific rules (for example Physician specialization, his/her time-sheet and available days and times, intervention mode type) will create the list of potential Hub organizations which can take responsibility for the clinical services. The request is repeated until the referral has been assigned and executed by the available Hub.

When the Hub organization takes charge of the teleconsultation request, the Clinical Specialist performs the consultation and sends the file reference containing the diagnosis and the related report. If the Hub does not take charge of the request within a predefined time interval based on the case urgency, it is sent to another organization. The Clinical Specialist can acquire and display all the patient's data and information regarding his/her clinical case.

After a thorough study of the specific case, the Clinical Specialist provides his/her consultation by first or second opinion. The Spoke application which has started the process receives a notification of final diagnosis, so the related Requesting Physician can analyse the consultation report provided by the colleague [1]. The BPMN model of the teleconsultation process, realised with the open-source Signavio software, is represented in Figure 3 and Figure 4, the latter represents the related sub-process.

4.2 Dermatological Teleconsultation

The periodic check of the moles is fundamental for prevention and early detection of the presence of any skin cancers or melanomas, and it can improve significantly the chances of cure. In fact, early diagnosis is an important factor to treat this type of skin pathologies in time.

Another teleconsultation process analysed and implemented in the project, regards specifically the melanoma pathologies, which is similar to the one described for the neuro-Radiological teleconsultation. In fact, the process steps are based on these phases: Dermatological image acquisition, Request for teleconsultation referral and its Scheduling, in order to find a specific Dermatology Clinical Specialist and the clinical evaluation through artificial neural network with the final report.
In this process, the platform must acquire the patient's data in order to perform analyses through a neural network and to provide predictions referring to the type of skin lesions and related statistics.

Unlike the previous scenario, a DSS is used by the Dermatology Clinical Specialist to support the evaluation of the clinical situation. It is focused on the analysis of images assimilated in previous diagnostic cases of melanoma. The imaging DSS (iDSS) is based on specific images fingerprint extraction (features) and it permits a diagnostic image classification through the neural network [1].

The application can acquire all biometrics data (phenotype, ethnicity), personal data (region and province of residence, age, sex) and dermoscopic images (png, jpeg, jpg or DICOM) of a patient. In this way, it is possible to carry out analyses based on these data through a neural network, to return the predictions referred to the typology of the cutaneous lesions and to characterize any melanomas.

In this clinical scenario, the Spoke Requesting Physician visits the patient and enters in the platform all his/her personal data and past clinical information (exams reports, dermatological images). The Requesting Physician may indicate the diagnosis regarding the specific case, if the clinical situation is clear after the first visit.
If necessary, the Requesting Physician can send a teleconsultation request to the Dermatology Clinical Specialist of a Hub for a first opinion (when the initial diagnosis has not been made and the case is sent to the Dermatology Clinical Specialist immediately) or for a second opinion after the diagnosis. The Dermatology Clinical Specialist who takes over the case can be supported in his/her analyses by a neural network which can:

- request the prediction of specific skin pathology evaluation returned as the most likely disease class;
- check the 5 similar cases retrieved from the dataset and compared with the image linked to the patient.

In this way, the Requesting Physician is supported in detecting the presence of possible melanomas. Thanks to the neural network (DSS), the Dermatology Clinical Specialist has the opportunity to compare the new dermoscopic images acquired regarding the suspected lesions or moles of a patient with those present in the system dataset. A comparison is then made to identify any similarities and consequently to provide the Requesting Physician
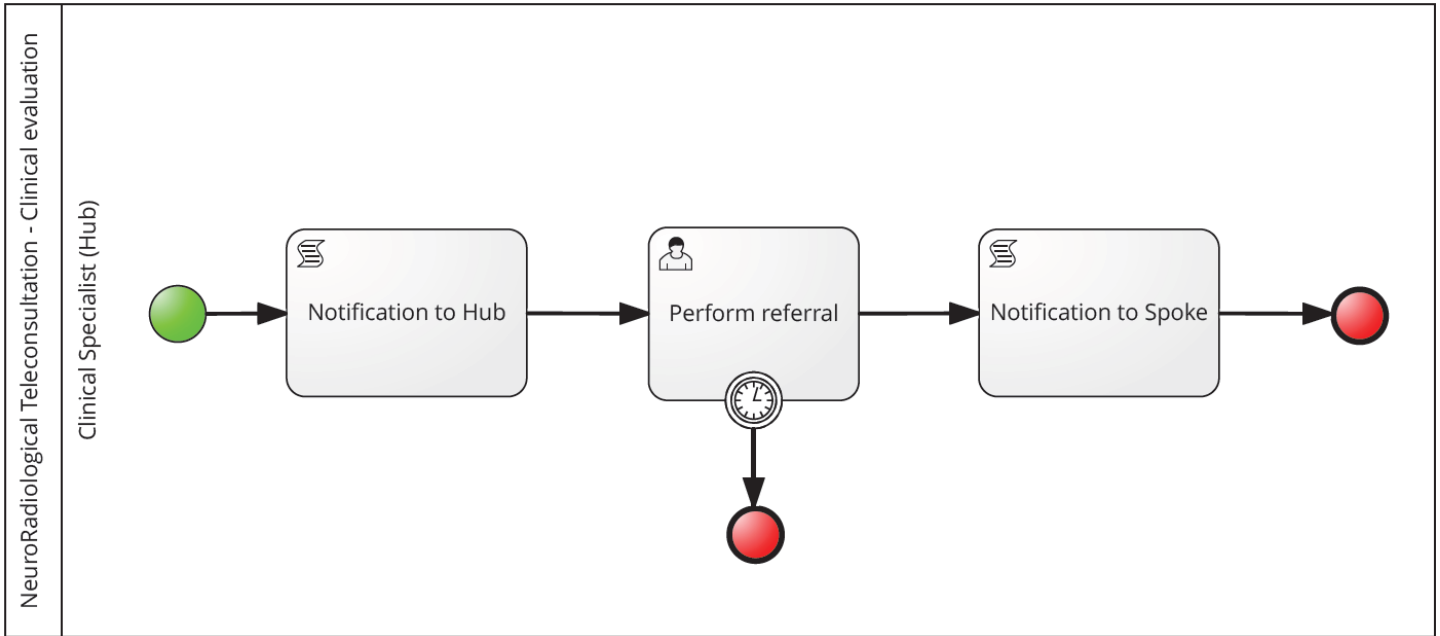
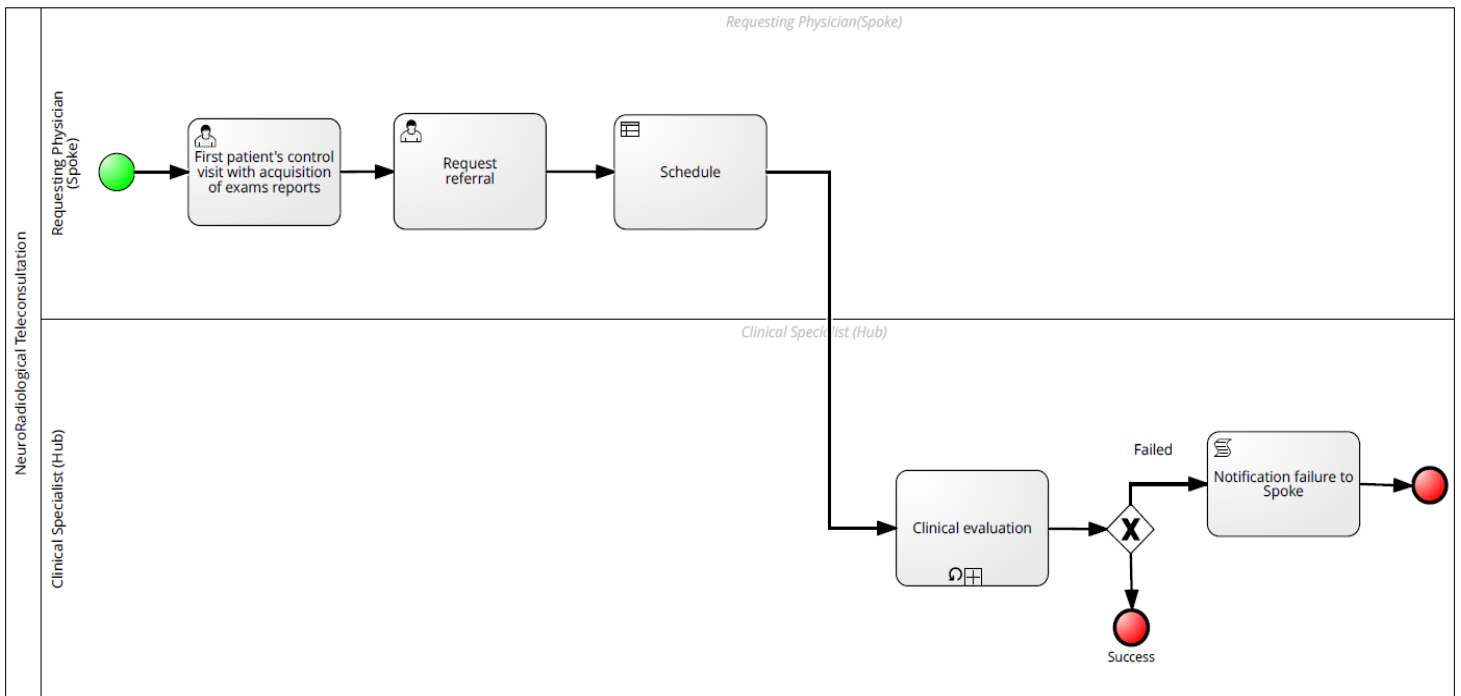Figure 3 – NeuroRadiological Teleconsultation

Figure 4: NeuroRadiological Teleconsultation Subprocess: Clinical evaluation
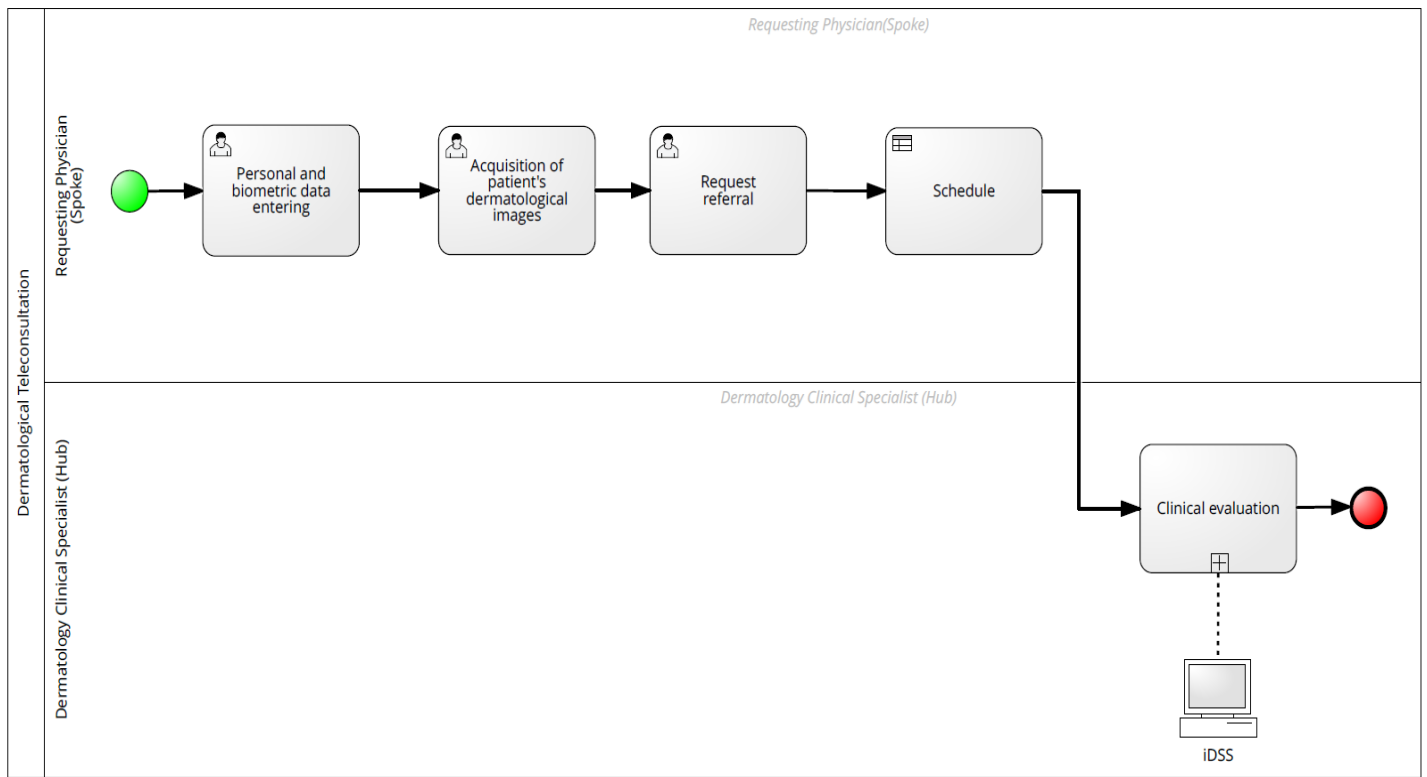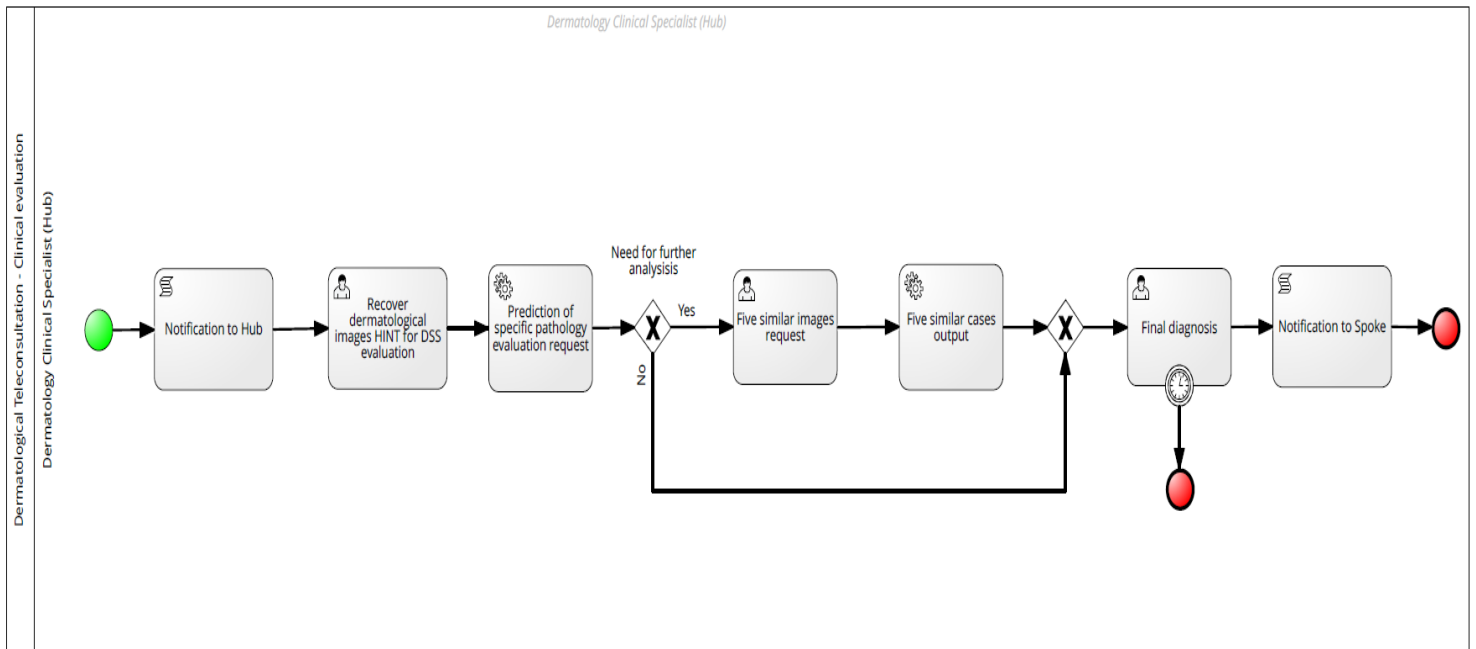
Figure 5: Dermatological Teleconsultation

Figure 6: Dermatological Teleconsultation Subprocess: Clinical evaluation
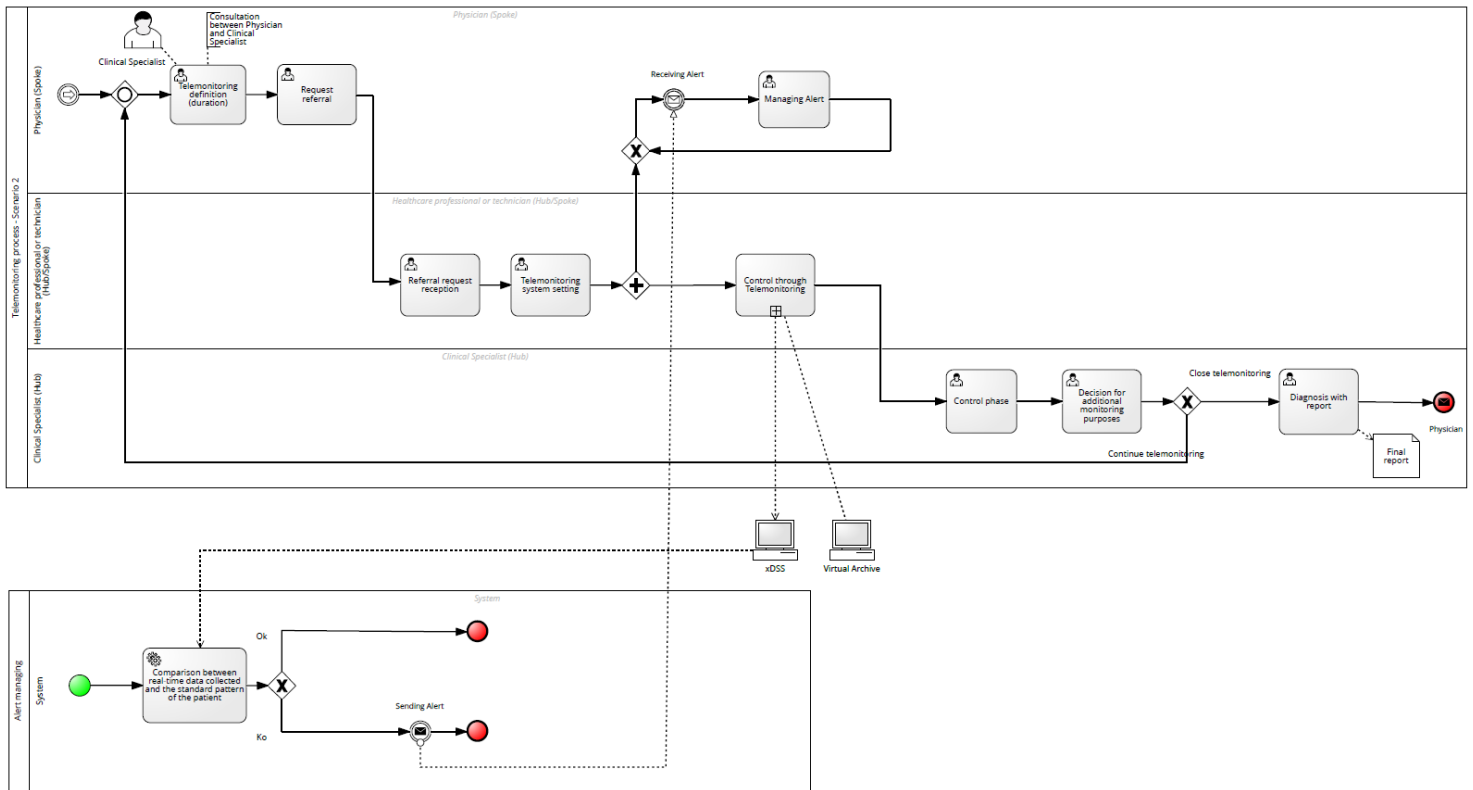
Figure 7: Telemonitoring process - Scenario 1
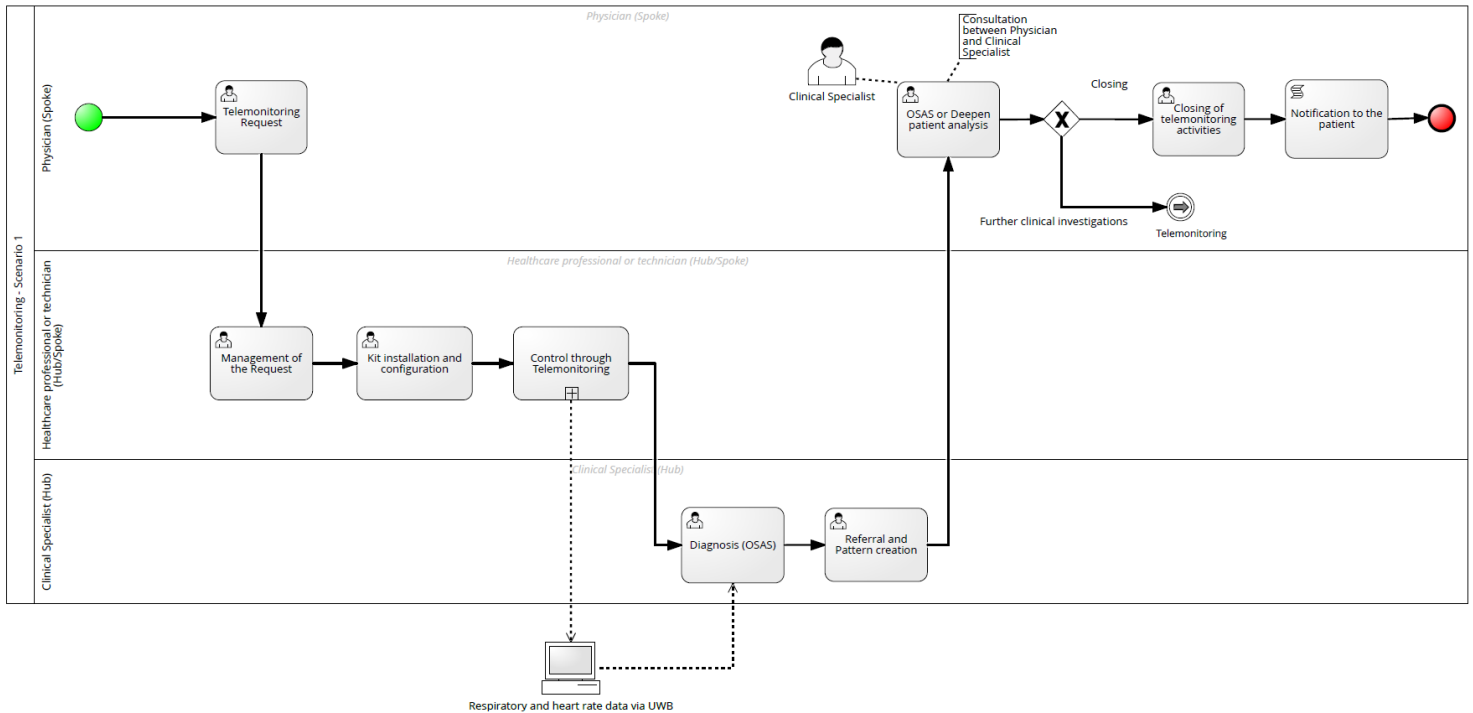
Figure 8 – Telemonitoring process - Scenario 2
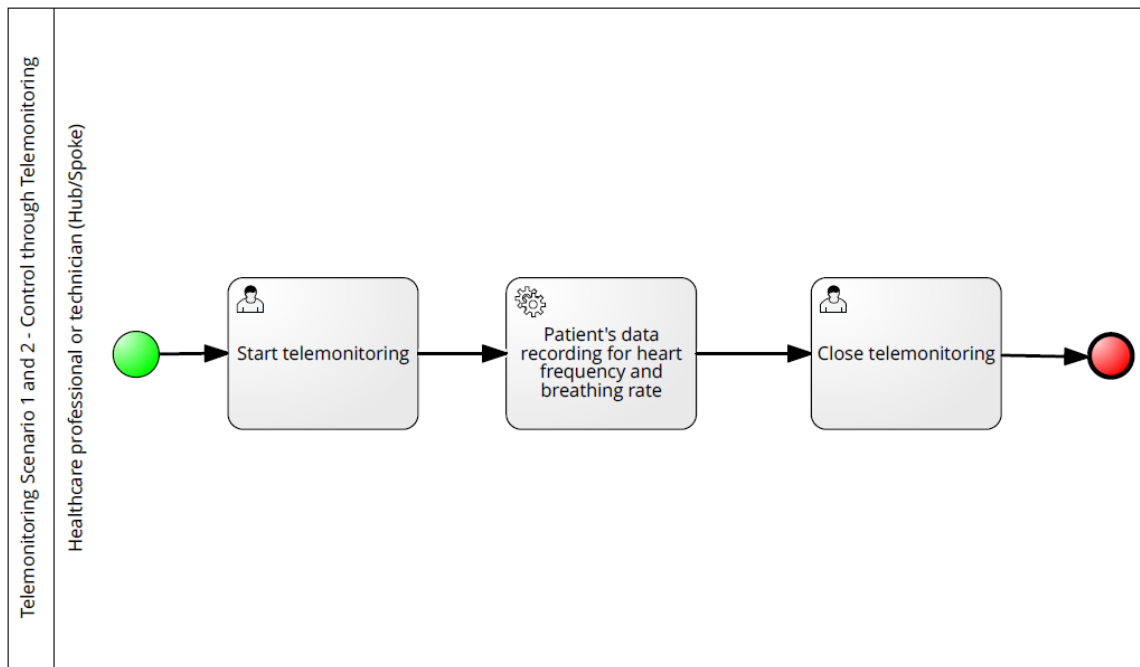
Figure 9 – Telemonitoring process Subprocess: Control through telemonitoring

with specific classes and coefficients of cosine similarity (fingerprints comparison).

The steps of the Dermatology Clinical Specialist for the evaluation of a clinical case via neural network and 5 similar cases are:

- the Dermatology Clinical Specialist selects the clinical case for which he/she wants to obtain a prediction regarding the acquisitions of data and images he/she has made;
- the neural network returns the predicted class with the probabilities of all other similar classes;
- the Dermatology Clinical Specialist can also request the 5 most similar acquisitions;
- the neural network returns the 5 images acquisition having the greatest correspondence with the patient's image, in order to be evaluated on the basis of a coefficient of similarity.

The Requesting Physician may use the results provided by the system to write the Dermatology Clinical Specialist diagnosis regarding the selected clinical case. In addition, statistics can be extracted by analysing biometric and personal data using DSS techniques. Also in this scenario, the Spoke organization which has initiated the process, receives a notification of completed diagnosis made by the Hub organization. The BPMN model of the dermatological teleconsultation process is represented with the open-source Signavio software in Figure 5 and Figure 6, the latter represents the related sub-process.

4.3. Telemonitoring – OSAS Syndrome Diagnosis

This process analyses the telemonitoring of the patient's heart and respiratory rate during sleep time to diagnose the Obstructive Sleep Apnoea Syndrome (OSAS). The system uses a non-invasive Ultra-Wide Band (UWB) technology, thanks to which it is possible to acquire data related to the patient's heart and breathing rate during sleep time in a non-invasive way.

The Physician of a health organization (public or private hospital) forwards the request for sleep monitoring in order to analyse the clinical situation of the patient, while a specific health operator of the Hub/Spoke assigned to the service, responds to this request. The service can also be provided at patient's home by activating a monitoring system based on digital devices. This home system is able to acquire, in contactless mode, clinical data from the patient during sleep. In addition, there is a tablet acting as a gateway, which receives the recorded data from the UWB device and retransmits them to the system [1].

The processes for this telemonitoring case are basically two and both involve the Physicians, the Clinical Specialists, the healthcare operators and the patients as follows:

1. the diagnosis formulation based on sleep data collected in a predefined period;
2. the subsequent real-time sleep telemonitoring finalized to continue the evaluation of the clinical case over time.

Formulation of diagnosis by telemonitoring

The steps of the first process leading to the formulation of the diagnosis by telemonitoring and to the subsequent report definition are specified below:

- Creation of pre-diagnosis sleep telemonitoring request;
- Receiving pre-diagnosis telemonitoring request;
- Configuration and installation of sleep telemonitoring kit;
- Start and end of data collection;
- Sleep monitoring data recovery for the patient;
- Diagnosis and report formulation.

After the request has been sent, the system assigns the task to the most suitable Hub/Spoke operator, who can manage the activity and supervise the process until its conclusion, with the production of the final report by the Hub Clinical Specialist.

The Physician who started the telemonitoring request, can recover the patient's monitoring data in order to evaluate his/her clinical condition. In the first phase regarding the *Pre-diagnosis*, the initial clinical information about the patient's condition and the data collected from the monitoring for a given time interval (time series of hearth and breath rate) are recorded in the local database and indicated as reference model to the patient.

After this monitoring phase, the Clinical Specialist can examine the patient's pattern to diagnose the eventual Obstructive Sleep Apnoea Syndrome and produce the associated report which will be saved in the system. Once the diagnosis has been defined, the Physician, consulting with the Clinical Specialist, can decide to perform a successive telemonitoring phase to record the patient's sleep apnoea episodes for an extended period. If further telemonitoring activity is not necessary, the Physician communicates the final diagnosis to the patient (Figure 7 and Figure 9, the latter represents the related sub-process) [1].

Telemonitoring and real-time evaluation

If the patient is afflicted with OSAS or the Physician needs to further investigate the patient's clinical situation, he/she can decide to set up a telemonitoring process, in order to control the evolution of the medical case in a medium or long period.

In this second scenario (Figure 8 and Figure 9, the latter represents the related sub-process), the activities regarding the telemonitoring and real-time evaluation are defined. They are aimed at detecting any critical situation on the basis of clinical data acquired which show a deviation from normal values (reference pattern) and, consequently, provide indications for a timely intervention and a possible change of care plan.

The steps of this second process are:

- Telemonitoring plan definition;
- Creation of sleep telemonitoring request;
- Receiving of telemonitoring request;
- Telemonitoring kit configuration;
- Start of telemonitoring activities and data collection;
- Data processing from xDSS;
- Management of possible alert sent to the system and their visualization by the Physician;
- Control phase for a possible extension of telemonitoring service at the end of the predefined period;
- Final clinical evaluation by the Specialist.

In this situation, there is an initial phase of telemonitoring programme definition, followed by its subsequent referral to the Hub/Spoke operator, who then configures the telemonitoring kit.

After the telemonitoring process has been defined and started, the real time data collected from the patient's UWB device, with the standard model data collected during the pre-diagnosis monitoring, are given as input to the platform's xDSS. The xDSS allows the analysis of patient data from the activated monitoring and, in case of significant deviations between the data collected in the pre-diagnosis and the data acquired through real-time telemonitoring, an alert message is sent by the system to the deputy Physicians. In this way, the system processes the real-time data and compares them with the patient's standard pattern, promptly notifying the presence of its deviation, such as an ongoing night apnoea episode [1]. The potential alert generated by the platform can, then, be viewed and managed by the Physician. At the end of the process, the Specialist makes an assessment of the OSAS data from the telemonitoring and makes it available and viewable to the requesting Physician.

5. Discussion and Conclusions

The use of telemedicine systems, supported by an efficient territorial health service, can reduce the number of admissions and inappropriate hospitalization, making home monitoring and treatments more effective [90]. This approach can allow a better interaction with Specialists and an accurate control of patients' clinical situation through the use of medical IoT devices.

The HINT project fits perfectly this context, as it has provided a comprehensive and optimized framework based on a flexible and workflow-focused teleconsultation and telemonitoring platform.

The new *Hub and Spoke* architecture proposed in this project allow Physicians (Hub) to find Specialists (Spoke) for a consultation even in remote areas, where medical specialists are not physically present, thanks to innovative teleradiology, teleconsultation and telemonitoring solutions.

An important innovation in the HINT project concerned the introduction of a Decision Support System for dermatological teleconsultation within a cloud telemedicine platform, which allows the classification of dermoscopic images of skin lesions, thanks to Artificial Intelligence and Deep Learning techniques.

Another important innovation, in the field of Obstructive Sleep Apnoea Syndrome, concerned the introduction of advanced monitoring devices.

Moreover, a workflow management component within the HINT platform, based on BPM, allowed the automated management of the clinical processes' activities and related data sharing. The steps of the BPM lifecycle were implemented specifying, for each phase, the healthcare standards used and the actors involved, in order to re-engineer the clinical processes analysed (see Table 1).

The technological and organisational innovations led to the definition of a prototype, whose components and functionalities have been tested but not in a real clinical setting. However, the HINT technological applications have been successfully used in the Italian LHA (Local Health Authority) by some partners after the project conclusion.

Many potential advantages deriving from HINT telemedicine solutions, involve different end-users. In particular, Physicians can be supported in finding the most suitable patient's diagnostic process, through telemonitoring and telehealth appointments.

Furthermore, in emergency situations, telemedicine can represent a guidance for Specialist Consultants (SPs) and for hospital admission, since, thanks to telemonitoring systems combined with possible teleconsultations with other Physicians, it is possible to know the patient's clinical situation before he/she arrives at the hospital. For private or public healthcare organisations, telemedicine systems can give the possibility to ensure an effective coverage of the largest number of clinical cases as well as a service homogeneity offered on the territory, thanks to

the support of integrated platforms enabling advanced care systems. The support in the diagnosis phase through IT systems based on telemedicine services can help the Specialist Physicians, who can work also remotely in a more efficient and effective way [1].

The advantages for patients can concern the availability of more specialist services within the hospital or territory healthcare processes. They can also benefit from the empowerment process ensured by telemedicine services, thanks to which they can be more involved in their diagnosis processes and in healthcare treatments.

Finally, using telemedicine systems, patients can reduce time and costs needed to get efficient medical care.

Conflict of Interest

The authors declare no conflict of interest.

Acknowledgements

References

[1] A. Caforio, T. Calogiuri, M. Lazoi, G. Mitrano, R. Paiano, "HINT project: a BPM teleconsultation and telemonitoring platform", in Proceedings of the 10th International Conference on Information Systems and Technologies, Lecce Italy, 1–8, 2020. doi: 10.1145/3447568.3448542.

[2] A.V. Gaddi, F. Cascini, E. Chiarolla, B. Delfrate, S. Forti, M. Marchetti, "Telemonitoraggio e telecontrollo per i cittadini con malattie cardiologiche, respiratorie e diabete", MONITOR, 47, 21–26, 2022.

[3] J. Wiegel, B. Seppen, M. van der Leeden, M. van der Esch, R. de Vries, W. Bos, "Adherence to Telemonitoring by Electronic Patient-Reported Outcome Measures in Patients with Chronic Diseases: A Systematic Review", IJERPH, 18(19), 2021, doi: 10.3390/ijerph181910161.

[4] D. Voran, "Telemedicine and beyond", Mo Med, 112(2), 129–135, 2015.

[5] I. Khemapech, W. Sansrimahachai, M. Toahchoodee, "Telemedicine – Meaning, Challenges and Opportunities", Siriraj Med Bull, 71(3), 246–252, 2019, doi: 10.33192/Smj.2019.38.

[6] J. Adler, C. Yu, M. Datta, "The changing face of radiology: from local practice to global network", Medical Journal of Australia, 190(1), 20–23, 2009, doi: 10.5694/j.1326-5377.2009.tb02256.x

[7] C.L. Snoswell, M.L. Taylor, T.A. Comans, A. C. Smith, L.C. Gray, L.J. Caffery, "Determining if Telehealth Can Reduce Health System Costs: Scoping Review", J Med Internet Res, 22(10), 17298, 2020, doi: 10.2196/17298.

[8] E.B. Allely, "Synchronous and asynchronous telemedicine", J Med Syst, 19(3), 207–212, 1995, doi: 10.1007/BF02257174.

[9] M. Batool, A. Jalal, K. Kim, "Telemonitoring of Daily Activity Using Accelerometer and Gyroscope in Smart Home Environments", J. Electr. Eng. Technol., 15(6), 2801–2809, 2020, doi: 10.1007/s42835-020-00554-y.

[10] D. Dias, J. Paulo Silva Cunha, "Wearable Health Devices—Vital Sign Monitoring, Systems and Technologies", Sensors, 18(8), 2414, 2018, doi: 10.3390/s18082414.

[11] A. Rosotti, Informatica medica. Sistemi informativi sanitari e reti di telemedicina. McGraw-Hill Education, 2021.

[12] ACR Data Science Institute, "ACR DSI and Standards Bodies Active in Artificial Intelligence Space", ACR DATA SCIENCE INSTITUTE, American College of Radiology.

[13] A.K. Gupta, A. Garg, M.S. Sandhu, "Diagnostic radiology: advances in imaging technology, Third edition", Medical Publishers, 2019.

[14] R. Nuzzi, P. Marolo, A. Nuzzi, "The Hub-and-Spoke Management of Glaucoma", Front. Neurosci, 14, 180, 2020, doi: 10.3389/fnins.2020.00180.

[15] T. Chong et al., "The California Telepathology Service: UCLA's Experience in Deploying a Regional Digital Pathology Subspecialty Consultation Network", Journal of Pathology Informatics, 10(1), 31, 2019, doi: 10.4103/jpi.jpi_22_19.

[16] G. Boland, J.T. Schlakman, J.H. Thrall, "Teleradiology", in PACS, K. J. Dreyer, J.H. Thrall, D.S. Hirschorn, e A. Mehta, A c. di New York: Springer-Verlag, 523–560, 2006, doi: 10.1007/0-387-31070-3_26.

[17] E.R. Ranschaert, F.H.B. Binkhuysen, "European Teleradiology now and in the future: results of an online survey", Insights Imaging, 4(1), 93–102, 2013, doi: 10.1007/s13244-012-0210-z.

[18] B. Horn, D. Chang, J. Bendelstein, J.C. Hiatt, "Implementation of a Teleradiology System to Improve After-Hours Radiology Services in Kaiser Permanente Southern California", TPJ, 10(1), 47–50, 2006, doi: 10.7812/TPP/05-119.

[19] R.S. Lewis, J.H. Sunshine, M. Bhargavan, "Radiology Practices' Use of External Off-Hours Teleradiology Services in 2007 and Changes Since 2003", American Journal of Roentgenology, 193(5), 1333–1339, 2009, doi: 10.2214/AJR.09.2984.

[20] H. Eklöf, E. Radecka, P. Liss, "Teleradiology uppsala–sydney for nighttime emergencies: preliminary experience", Acta Radiol, 48(8), 851–853, 2007, doi: 10.1080/02841850701422120.

[21] A. Kalyanpur, J. Weinberg, V. Neklesa, J.A. Brink, H.P. Forman, "Emergency radiology coverage: technical and clinical feasibility of an international teleradiology model", Emergency Radiology, 10(3), 115–118, 2003, doi: 10.1007/s10140-003-0284-5.

[22] A. Martinon et al., "Teleradiology saves times in cases of vital emergencies: A comparative study with on-call radiology in two urban medium-sized French hospitals", European Research in Telemedicine / La Recherche Européenne en Télémédecine, 3(4), 151–160, 2014, doi: 10.1016/j.eurtel.2014.10.001.

[23] T.C.M. Pechet, G. Girard, B. Walsh, "The value teleradiology represents for Europe: A study of lessons learned in the U.S.", European Journal of Radiology, 73(1), 36–39, 2010, doi: 10.1016/j.ejrad.2009.10.019.

[24] C. Eakins et al., "Second Opinion Interpretations by Specialty Radiologists at a Pediatric Hospital: Rate of Disagreement and Clinical Implications", American Journal of Roentgenology, 199(4), 916–920, 2012, doi: 10.2214/AJR.11.7662.

[25] E. Zan, D.M. Yousem, M. Carone, J.S. Lewin, "Second-Opinion Consultations in Neuroradiology", Radiology, 255(1), 135–141, 2010, doi: 10.1148/radiol.09090831.

[26] H.K. Huang, "Teleradiology technologies and some service models", Computerized Medical Imaging and Graphics, 20(2), 59–68, 1996, doi: 10.1016/0895-6111(96)00032-8.

[27] G.A. Naqvi, M. Daly, A. Dawood, A. Kurkuri, S. Kutty, "Smart consultation for musculoskeletal trauma: Accuracy of using smart phones for fracture diagnosis", The Surgeon, 12(1), 32–34, 2014, doi: 10.1016/j.surge.2013.09.001.

[28] F.J. Kammerer, M. Hammon, P.M. Schlechtweg, M. Uder, S.A. Schwab, "A web based cross-platform application for teleconsultation in radiology", J Telemed Telecare, 21(6), 355–363, 2015, doi: 10.1177/1357633X15575237.

[29] J.H. Thrall, "Teleradiology Part I. History and Clinical Applications", Radiology, 243(3), 613–617, 2007, doi: 10.1148/radiol.2433070350.

[30] A. Bonnin, "Medical tele-imaging: a good chance for the future", Bull Acad Natl Med, 183(6), 1123–1134, 1999.

[31] K. Deldar, K. Bahaadinbeigy, "Teleconsultation and Clinical Decision Making: a Systematic Review", Acta Inform Med, 24(4), 286, 2016, doi: 10.5455/aim.2016.24.286-292.

[32] S. Conway, "Teleradiology and telemedicine: They are not equal", Managing Quality, Safety, and Cost in Radiology, and Learning to Wear it Well, 28–29, 2016.

[33] Sanitanova, "Concept Hub & Spoke", Monitor dolore - Sanitanova..

[34] M. Skorning et al., "Teleconsultation in pre-hospital emergency medical services: Real-time telemedical support in a prospective controlled simulation study", Resuscitation, 83(5), 626–632, 2012, doi: 10.1016/j.resuscitation.2011.10.029.

[35] C. Chandhanayingyong, B. Tangtrakulwanich, T. Kiriratnikom, "Teleconsultation for emergency orthopaedic patients using the multimedia messaging service via mobile phones", J Telemed Telecare, 13(4), 193–196, 2007, doi: 10.1258/135763307780908049.

[36] H. Bourdon et al., "Teleconsultation in primary ophthalmic emergencies during the COVID-19 lockdown in Paris: Experience with 500 patients in March and April 2020", Journal Français d'Ophtalmologie, 43(7), 577–585, 2020, doi: 10.1016/j.jfo.2020.05.005.

[37] G. Pare, M. Jaana, C. Sicotte, "Systematic Review of Home Telemonitoring for Chronic Diseases: The Evidence Base", Journal of the American Medical Informatics Association, **14**(3), 269–277, 2007, doi: 10.1197/jamia.M2270.

[38] S. Crossen, N. Glaser, H. Sauers-Ford, S. Chen, V. Tran, J. Marcin, "Home-based video visits for pediatric patients with poorly controlled type 1 diabetes", J Telemed Telecare, **26**(6), 349–355, 2020, doi: 10.1177/1357633X19828173.

[39] K.L. Margolis et al., "Effect of Home Blood Pressure Telemonitoring and Pharmacist Management on Blood Pressure Control: A Cluster Randomized Clinical Trial", JAMA, **310**(1), 46, 2013, doi: 10.1001/jama.2013.6549.

[40] R. Bellazzi et al., "A telemedicine support for diabetes management: the T-IDDM project", Computer Methods and Programs in Biomedicine, **69**(2), 147–161, 2002, doi: 10.1016/S0169-2607(02)00038-X.

[41] B. Morlion, C. Knoop, M. Paiva, M. Estenne, "Internet-based Home Monitoring of Pulmonary Function after Lung Transplantation", Am J Respir Crit Care Med, **165**(5), 694–697, 2002, doi: 10.1164/ajrccm.165.5.2107059

[42] C. Maiolo, E.I. Mohamed, C.M. Fiorani, A. de Lorenzo, "Home telemonitoring for patients with severe respiratory illness: the Italian experience", J Telemed Telecare, **9**(2), 67–71, 2003, doi: 10.1258/135763303321327902.

[43] N.B. Shah, E. Der, C. Ruggerio, P.A. Heidenreich, B.M. Massie, "Prevention of hospitalizations for heart failure with an interactive home monitoring program", American Heart Journal, **135**(3), 373–378, 1998, doi: 10.1016/S0002-8703(98)70310-2.

[44] G. Labarca et al., "Efficacy of continuous positive airway pressure (CPAP) in patients with obstructive sleep apnea (OSA) and resistant hypertension (RH): Systematic review and meta-analysis", Sleep Medicine Reviews, **58**, 101446, 2021, doi: 10.1016/j.smrv.2021.101446.

[45] C. Chen, J. Wang, L. Pang, Y. Wang, G. Ma, W. Liao, "Telemonitor care helps CPAP compliance in patients with obstructive sleep apnea: a systemic review and meta-analysis of randomized controlled trials", Therapeutic Advances in Chronic Disease, **11**, 2020, doi: 10.1177/2040622320901625.

[46] C. Turino et al., "Management of continuous positive airway pressure treatment compliance using telemonitoring in obstructive sleep apnoea", Eur Respir J, **49**(2), 1601128, 2017, doi: 10.1183/13993003.01128-2016.

[47] N. Fox et al., "The Impact of a Telemedicine Monitoring System on Positive Airway Pressure Adherence in Patients with Obstructive Sleep Apnea: A Randomized Controlled Trial", Sleep, **35**(4), 477–481, 2012, doi: 10.5665/sleep.1728.

[48] E. Seto, K.J. Leonard, J.A. Cafazzo, J. Barnsley, C. Masino, H.J. Ross, "Developing healthcare rule-based expert systems: Case study of a heart failure telemonitoring system", International Journal of Medical Informatics, **81**(8), 556–565, 2012, doi: 10.1016/j.ijmedinf.2012.03.001.

[49] S. Wali et al., "Expanding Telemonitoring in a Virtual World: A Case Study of the Expansion of a Heart Failure Telemonitoring Program During the COVID-19 Pandemic", J Med Internet Res, **23**(1), 2021, doi: 10.2196/26165.

[50] World Health Organization, WHO global report on falls prevention in older age. Geneva, Switzerland: World Health Organization, 2008.

[51] H. Eren e J.G. Webster, Telemedicine and electronic medicine. Boca Raton: CRC Press, Taylor & Francis Group, 2016.

[52] S.K. Boell, D. Cecez-Kecmanovic, "What is an Information System?", in 2015 48th Hawaii International Conference on System Sciences, HI, USA, 4959–4968, 2015. doi: 10.1109/HICSS.2015.587.

[53] A.R. Bakker, "HIS, RIS, and PACS", Computerized Medical Imaging and Graphics, **15**(3), 157–160, 1991, doi: 10.1016/0895-6111(91)90004-F.

[54] T. Nakamura, H. Hitsuishi, T. Harada, "Cooperation between the Hospital Information System and the File Maker Pro", in 2007 IEEE/ICME International Conference on Complex Medical Engineering, Beijing, China, 291–294, 2007. doi: 10.1109/ICCME.2007.4381741.

[55] B. Mansoori, K.K. Erhard, J.L. Sunshine, "Picture Archiving and Communication System (PACS) Implementation, Integration & Benefits in an Integrated Health System", Academic Radiology, **19**(2), 229–235, 2012, doi: 10.1016/j.acra.2011.11.009.

[56] S. Boochever, "HIS/RIS/PACS integration: getting to the gold standard", Radiology management, **26**(3), 16–24, 2004.

[57] M. Gupta, N. Singh, K. Shrivastava, P. Mishra, "Significance of digital imaging and communication in medicine in digital imaging", Digit Med, **1**(2), 63, 2015, doi: 10.4103/2226-8561.174769.

[58] M. Hosseini, B.E. Dixon, "Syntactic Interoperability and the Role of Standards", in Health Information Exchange, Elsevier, 123–136, 2016, doi: 10.1016/B978-0-12-803135-3.00008-6.

[59] I.D. McLean, J. Martensen, "Specialized Imaging", in Clinical Imaging, Elsevier, 44–78, 2014, doi: 10.1016/B978-0-323-08495-6.00002-6.

[60] M. Licurse, W. Boonn, Computers in radiology, 26, 2016.

[61] R. Bibb, D. Eggbeer, A. Paterson, Medical modelling: the application of advanced design and rapid prototyping techniques in medicine, Second edition. Amsterdam Boston Cambridge Heidelberg: Elsevier/ Woodhead Publishing, 2015.

[62] M.M. Cruz-Cunha, I.M. Miranda, P. Goncalves, Handbook of research on ICTSs and management systems for improving efficiency in healthcare and social care. Hershey PA: Medical Information Science Reference, 2013.

[63] D. Bender, K. Sartipi, "HL7 FHIR: An Agile and RESTful approach to healthcare information exchange", in Proceedings of the 26th IEEE International Symposium on Computer-Based Medical Systems, Porto, Portugal, 326–331, 2013, doi: 10.1109/CBMS.2013.6627810.

[64] R. Noumeir, "Active Learning of the HL7 Medical Standard", J Digit Imaging, **32**(3), 354–361, 2019, doi: 10.1007/s10278-018-0134-3.

[65] M. Mangia, "Alla scoperta di FHIR", Salute digitale, 2022.

[66] Integrating the Healthcare Enterprise, IHE Patient Care Coordination (PCC) Technical Framework, 1, 2016.

[67] Integrating the Healthcare Enterprise, IT Infrastructure (ITI) Technical Framework, 1, 2022.

[68] A. Sakellarios, "A cloud-based platform for the non-invasive management of coronary artery disease", Enterprise Information Systems, **14**(8), 1102–1123, 2020, doi: 10.1080/17517575.2020.1746975.

[69] P. Szmodics, "Evaluating the organizational knowledge based on business process management", PhD, Corvinus University of Budapest, Budapest, 2018. doi: 10.14267/phd.2018020.

[70] A. Capodieci, G. Del Fiore, L. Mainetti, "Adopting Collaborative Business Processes To Prevent The Loss Of Information In Public Administration Organisations", 2014, doi: 10.5281/ZENODO.1092317.

[71] U. Barchetti, A. Capodieci, A. L. Guido, L. Mainetti, "Information Systems for Knowledge Workers: The Kpeople Enterprise 2.0 Tool", in Web Information Systems Engineering - WISE 2012, X. S. Wang, I. Cruz, A. Delis, e G. Huang, A c. di Berlin, Heidelberg: Springer Berlin Heidelberg, 7651, 804–807, 2012, doi: 10.1007/978-3-642-35063-4_71.

[72] T. Davenport, J. Short, The new Industrial Engineering: Information Technology and Business Process Redesign. 2015.

[73] P. Harmon, Business process change: a guide for business managers and BPM and six sigma professionals, 2nd ed. Amsterdam ; Boston: Elsevier/Morgan Kaufmann Publishers, 2007.

[74] R. Macedo de Morais, S. Kazan, S. Inês Dallavalle de Pádua, A. Lucirton Costa, "An analysis of BPM lifecycles: from a literature review to a framework proposal", Business Process Management Journal, **20**(3), 412–432, 2014, doi: 10.1108/BPMJ-03-2013-0035.

[75] W.M.P. van der Aalst, "Business Process Management Demystified: A Tutorial on Models, Systems and Standards for Workflow Management", in Lectures on Concurrency and Petri Nets, 3098, Springer Berlin Heidelberg, 1–65, 2004, doi: 10.1007/978-3-540-27755-2_1.

[76] M. Netjes, H.A. Reijers, W.M.P. Van der Aalst, "Supporting the BPM life-cycle with FileNet", EMMSAD, 135–146, 2006.

[77] M. Weske, Business process management: concepts, languages, architectures, 2nd ed. Berlin, Springer, 2012.

[78] M. Dumas, M. La Rosa, J. Mendling, H.A. Reijers, Fundamentals of business process management. Berlin: Springer, 2015.

[79] J. Chae, B.H. Park, M. Jones, M. Ward, J. Nebeker, "Converting Clinical Pathways to BPM+ Standards: A Case Study in Stable Ischemic Heart Disease", in 2020 IEEE 33rd International Symposium on Computer-Based Medical Systems (CBMS), Rochester, MN, USA, 453–456, 2020, doi: 10.1109/CBMS49503.2020.00092.

[80] N. Herzberg, K. Kirchner, M. Weske, "Modeling and Monitoring Variability in Hospital Treatments: A Scenario Using CMMN", in Business Process Management Workshops, F. Fournier e J. Mendling, A c. di Cham: Springer International Publishing, 202, 3–15, 2015, doi: 10.1007/978-3-319-15895-2_1.

[81] C. Combi, B. Oliboni, A. Zardini, F. Zerbato, "A Methodological Framework for the Integrated Design of Decision-Intensive Care Pathways—an Application to the Management of COPD Patients", J Healthc Inform Res, **1**(2), 157–217, 2017, doi: 10.1007/s41666-017-0007-4.

[82] A. Bianchi, M. Mortari, C. Pintavalle, G. Pozzi, "Putting BPMN and DMN to Work: a Pediatric Surgery Case Study", in 2021 IEEE International Conference on Digital Health (ICDH), Chicago, IL, USA, 154–159, 2021, doi: 10.1109/ICDH52753.2021.00028.

[83] I. Essefi, H.B. Rahmouni, M.F. Ladeb, "Integrated privacy decision in BPMN clinical care pathways models using DMN", Procedia Computer Science, **196**, 509–516, 2022, doi: 10.1016/j.procs.2021.12.043.

[84] E. Sulis et al., "Monitoring patients with fragilities in the context of de-hospitalization services: An Ambient Assisted Living Healthcare Framework for e-Health applications", in 2019 IEEE 23rd International

Symposium on Consumer Technologies (ISCT), Ancona, Italy, 216–219, 2019, doi: 10.1109/ISCE.2019.8900989.

[85] M. Szelągowski, J. Berniak-Woźny, C. Lipiński, "BPM Support for Patient-Centred Clinical Pathways in Chronic Diseases", Sensors, **21**(21), 7383, 2021, doi: 10.3390/s21217383.

[86] J. Gomes, F. Portela, M.F. Santos, "Introduction to BPM approach in Healthcare and Case Study of End User Interaction with EHR Interface", Procedia Computer Science, 141, 519–524, 2018, doi: 10.1016/j.procs.2018.10.132.

[87] D. Ruiz-Fernández, D. Marcos-Jorquera, V. Gilart-Iglesias, V. Vives-Boix, J. Ramírez-Navarro, "Empowerment of Patients with Hypertension through BPM, IoT and Remote Sensing", Sensors, **17**(10), 2273, 2017, doi: 10.3390/s17102273.

[88] A. Caione, A.L. Guido, A. Martella, R. Paiano, A. Pandurino, "Knowledge base support for dynamic information system management", Inf Syst E-Bus Manage, **14**(3), 533–576, 2016, doi: 10.1007/s10257-015-0294-3.

[89] R. Paiano, A. Caione, "A Knowledge Base Guided Approach for Process Modeling in Complex Business Domain", in Proceedings of the 11th International Joint Conference on Software Technologies, Lisbon, Portugal, 169–176, 2016, doi: 10.5220/0005974801690176.

[90] N.D. Brunetti, S. Scalvini, G. Molinari, "Innovations in telemedicine for cardiovascular care", Expert Review of Cardiovascular Therapy, **14**(3), 267–280, 2016, doi: 10.1586/14779072.2016.1140572.

Redesign and Improvement in the Management of the Raw Material Inventory Control Process with Oracle APEX

Jhoys Alinson Delgado Delgado, José Sulla-Torres[*]

Universidad Católica de Santa María, Escuela de Ingeniería de Sistemas, Arequipa, 04000, Perú

A R T I C L E I N F O	A B S T R A C T
	Having reasonable inventory control is a priority for any company because a lack of inventory could incur economic losses. Not having the necessary stock for the timely production of your orders could generate dissatisfaction in your customers and possibly cause them to lose them. Likewise, reasonable inventory control allows quick decision-making for the company's benefit. The study's objective was to improve the management of the request process, and quality control of the raw material of a textile supplier exporter of Peruvian alpaca yarn and an exporter of the textile company focused on transforming alpaca fiber and other natural fibers into high-value-added products. It was redesigned under the Process Management approach, developing and implementing software to control raw materials and requests following the Scrum framework and using the Oracle Apex tool. The results obtained with the new system were very positive, increasing workers' productivity, eliminating manual tasks and calculations, avoiding confusion in the allocation of material to scheduled orders, and the response time of the delivery date of orders and, therefore, customer satisfaction. Concluding that, it was possible to lower from an initial 30% to 0.08% of the requests answered in a period greater than 48 hours with the application of the developed system that allows rapid decision-making.

1. Introduction

The quality control of the raw material is one of the most critical issues in the manufacturing process of products with the advancement of technology [1]. To meet the high technical requirements, effective quality control at the initial stage of raw material can significantly reduce the quality risk during the manufacturing process [2].

This problem is not unrelated to the textile industry [3]; one of the most important companies in the textile industry, a supplier of Peruvian alpaca yarn and internationally recognized for its fine quality products, in one of its critical processes for handling orders: the control and request of raw material, this process is obsolete and takes a long time (hours/worker) to be able to carry it out correctly, for this reason, said control is reviewed once a week, and on certain occasions depending on the urgency, it is it can review up to three times maximum, also generating a delay in the other activities of the worker, which is critical for the company since it strictly depends on the availability of raw material to be able to produce and deliver its orders on time.

On the other hand, inventory management represents a key factor within any organization. A company's poor inventory management practices influence its productivity, leading to raw material shortages, production delays, rework, and material loss [4].

For this reason, the research seeks to satisfy the need of a textile company to improve its control process and raw material request to achieve better productivity [5] in its workers, keeping the information updated and available for decision-making and high command decisions. The contribution and novelty of the work is to analyze and redesign the process under the Process Management approach, to develop and implement software that adapts to the new process flow, following the agile Scrum framework and using the Oracle APEX tool.

The new flow of the process will seek to: improve the response time to requests for the delivery date of new orders to avoid loss of sales due to a slow response to requests or avoid delays in the delivery of orders, also contributing to an improvement in the level of customer satisfaction. Likewise, it will seek to avoid errors in allocating material for scheduled orders, increase the productivity

[*]Corresponding Author: José Sulla-Torres,   jsullato@ucsm.edu.pe

of the users involved in the process, and speed up decision-making when dealing with orders.

2. Related Work

Inventory control in an industrial company has become a critical process since inventories represent a considerable investment on the company's part. Their absence generates delays in order delivery dates, loss of sales or customers, and economic losses.

According to [6], reasonable inventory control allows one to have a broad knowledge of the rotation of the products and, based on that, to be able to make purchasing decisions; where they indicate that the benefits of an Inventory Control System are a better cash flow in the company, improvement of the quality indicator of customer service, customer loyalty, recognizing products with little demand, higher inventory turnover, theft detection and optimized space in warehouses.

Comprehensive inventory management is critical to efficiently operating any facility that uses and stores products. Since today's technologies are essential to support all processes within a company, In [7], the author indicates the benefits of having inventory management software. Most of the inventory management software available in the market focuses on regulation or acquisition and usually comes with monthly or upfront fees.

To use technologies as a support tool, it is first necessary to have a well-defined process that will be automated; for this, there is Process Management. Today is critical for any organization since processes are the heart of it; automating, optimizing, or redesigning these processes saves time and money, representing a notable competitive advantage over any other organization.

In [8], the author mention that Purpose Comprehensive management systems, such as ISO 9001 or ISO 14001, are designed to help organizations improve processes, ensure customer satisfaction, efficient information flow, efficient use of resources, and many other thriving management areas. These systems can also have unintended direct and indirect effects on organizations.

Once the process is well defined, it is proceeded to automate with software that suits the needs of the same and the users; given the complexity of the type of business of the company in question and the size of it would be much more efficient and effective if the software is custom developed. Today there are different methodologies for implementing this, which support us when performing this task. Like any organization, the most sought-after is a straightforward methodology to understand and, above all, very efficient, such as the well-known Agile Methodologies. In [9], the author indicates that since the agile manifesto was created in 2001, the research community has paid much attention to agile software development.

Specifically, they delineate the conceptual framework underlying agile scholarship by analyzing authors who have made notable contributions to the field. Agile methodologies are born from the need to respond rapidly to change to increase customer satisfaction by delivering operational functionality and continuous feedback to the customer during the project.

Nowadays, using these methodologies is essential since they help reduce the project's completion time because everything would already be very well organized, and the tasks would already be ordered by priority. These methodologies help to have an exact idea of what is being done at any point in its development and, in turn, encourage constant communication between the project members so that the result is successful.

In [10], the author state that to optimize and improve processes, in most cases, information systems have been developed using traditional methodologies that have fulfilled their function over time but that, however, have a lower probability of success. Not meeting all the needs of the client because the requirements may have changed, and these changes cannot be alerted or validated at the end of the project. The same authors refer to the fact that agile methodologies show promising results in projects that present constant changes in the definition of their requirements due to the different business environments; the agile team works much better from the moment they understand that a product that gives value to the client, and therefore they will have to consider that after each review with the client and after the development of each deliverable, changes could be requested. They also mention that agile teams are self-organized and multidisciplinary since they can develop their skills, knowledge, and experience, which means the same level of responsibilities for the entire team; It should also be noted that constant communication allows the team to make timely decisions.

Likewise, in the study [11], work points out that software development depends significantly on team performance, as does any process involved. According to [12] point out that within the Peruvian economy, there are critical business sectors, such as mining, mainly because their products are in great demand as essential components used by other industries, such as construction, mining, and textiles, which includes evaluating productivity in terms of growth rates and levels. They use Lean Manufacturing tools to measure these indicators and propose improvements or solutions to generate added value for the company.

In addition, the work of [13] indicates that in Peru, many small and medium-sized companies (SMEs) do not have a system focused on Human Resources because companies do not have the necessary technology to implement it, they do not know it, or the prices are pretty high. That is why they designed a payroll control and monitoring system based on the Agile Scrum Methodology, taking as an example the textile company Chalicen S.A.C, which is within the range of small companies.

On the other hand, Oracle Apex has become an exciting tool for developing effective and efficient applications. In [14], the author presented a technology solution integrating Oracle Apex and Python development software, where open-source libraries powered by Python provide an approach to Big Data analysis. On the other hand, the powerful database management offered by Oracle, powered by Apex application creation software, requires the cooperative use of such intellectual processing tools. Similar work on inventory management software developed with Apex was presented in [15].

Given the references, we will seek to redesign the current raw material control and request process based on process management

and, in turn, develop and implement software based on the Scrum framework. This software should cover the company's needs to improve the time hours/worker, keeping the information in real-time and available for any decision-making of the high command. It should be noted that it will be developed under the Oracle Apex tool.

3. Material And Method

The analysis of the process will be carried out with the following activities.

3.1. Description of the Company

The textile company under study is classified as a macro-company. It is one of the most important companies within the exporting suppliers of Peruvian alpaca yarn, internationally recognized for its fine quality products. It is worth mentioning that it is also one of the pioneer companies worldwide in offering 100% certified organic alpaca.

According to its vision and mission, this company aims to transform alpaca fiber and other natural fibers into products with high added value, satisfying the world's needs, promoting its use globally, and caring for the community and the environment. It aims to be the world leader in providing warmth and shelter with the best alpaca and natural fiber products. It offers unique experiences to our customers and community sustainably and innovatively through a committed and empowered team.

In Figure 1, its traceability circle is shown; it begins with the raising of alpacas on its farm, then it goes through a fiber treatment, and finally, it goes through the spinning of these. They have industrial processes of washing, carding, combing, spinning, dyeing, and weaving, ending in the dispatch of the product.
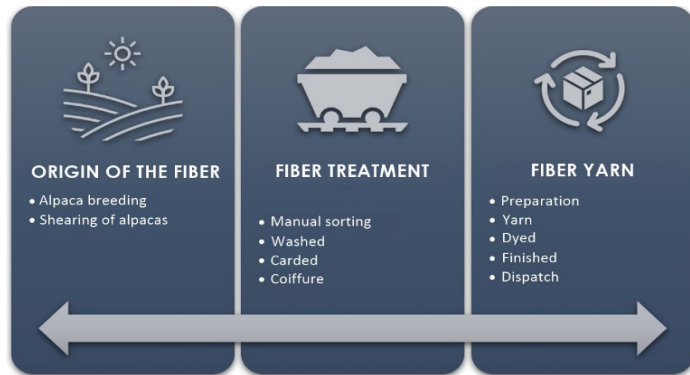
Figure 1: Traceability of the textile company

Figure 2 shows the dynamics of the company: the alpacas raised on the farm go through a shearing process to extract their wool, which goes through a treatment process, thus becoming Alpaca fiber Tops; mention that the company not only uses fibers extracted from the farm but also works with other fibers such as sheep, silk, cotton, nylon, linen, among others, which are acquired from other national or international suppliers, these fibers are mixed between yes, according to the percentages requested by the client through the spinning processes, obtaining three yarn presentations: yarn for machine weaving in cones and skeins and yarn for hand weaving in balls and skeins, they also offer accessories and garments made of fabric knit and flat knit.

Figure 2: Dynamics of the textile company.

3.2. Process Discovery

Within the three disciplines of value: product leadership, operational excellence, and intimacy with the client, the value proposition of the company in question are based on the discipline "Product Leadership," which is this: supply the best product menu diversified in terms of quality, fineness, and color of alpaca fiber to the world, through systems, efficient processes and committed personnel that is capable of providing the best service; according to this, Figure 3 shows the process map, since the problem occurs in the current process of Control and Request for Raw Material, the areas involved have been highlighted: Programming and Control, Industrial Development, Warehouse, Inputs and Parts, and Logistics.

Figure 3: Process map of the textile company.

The process map of the textile company under study is presented, highlighting the processes involved in the investigation in red color.

- *Initial process model*: With the Bizagi tool's help, the initial raw material control process diagram is presented, referring to scheduled and pending orders or to be scheduled. Figure 4 shows the graph of the initial process of raw material control. Figure 5 shows the initial process of requesting raw materials for alpaca and national sheep.

In the general process of raw material control, where the following waste is observed:

- *Overprocessing*: By breaking down all the orders again each time the information is required, the correct thing would be to store a history of previously made breakdowns.
- *Defects*: As the order breakdown process is not well defined, the end of the data generation presents errors or shortcomings that must be corrected or added manually by the user.
- *Waiting*: It is evident that there is a very high waiting time since it is impossible to make any decision without the data generated from the said process.
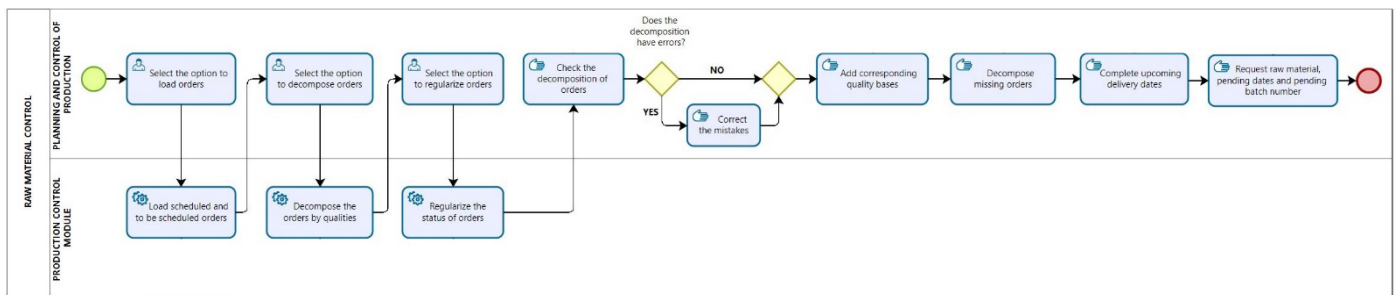
Figure 4: Diagram of the initial raw material control process.
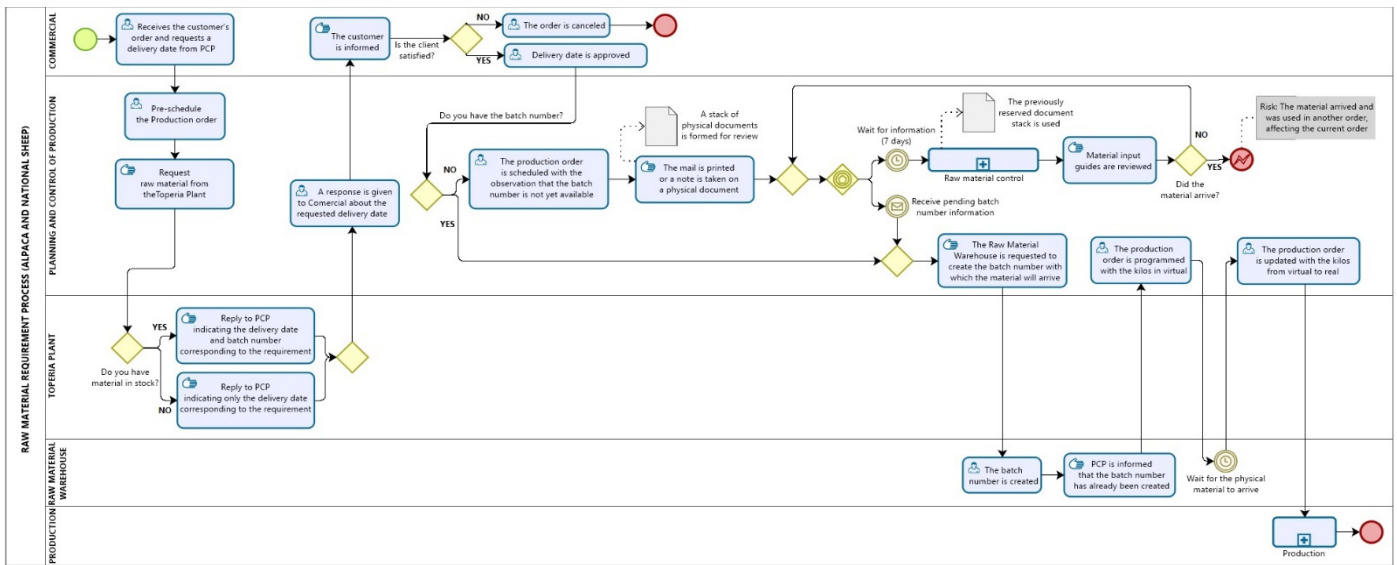
Figure 5: Diagram of the initial process for requesting raw material for alpaca and national sheep.
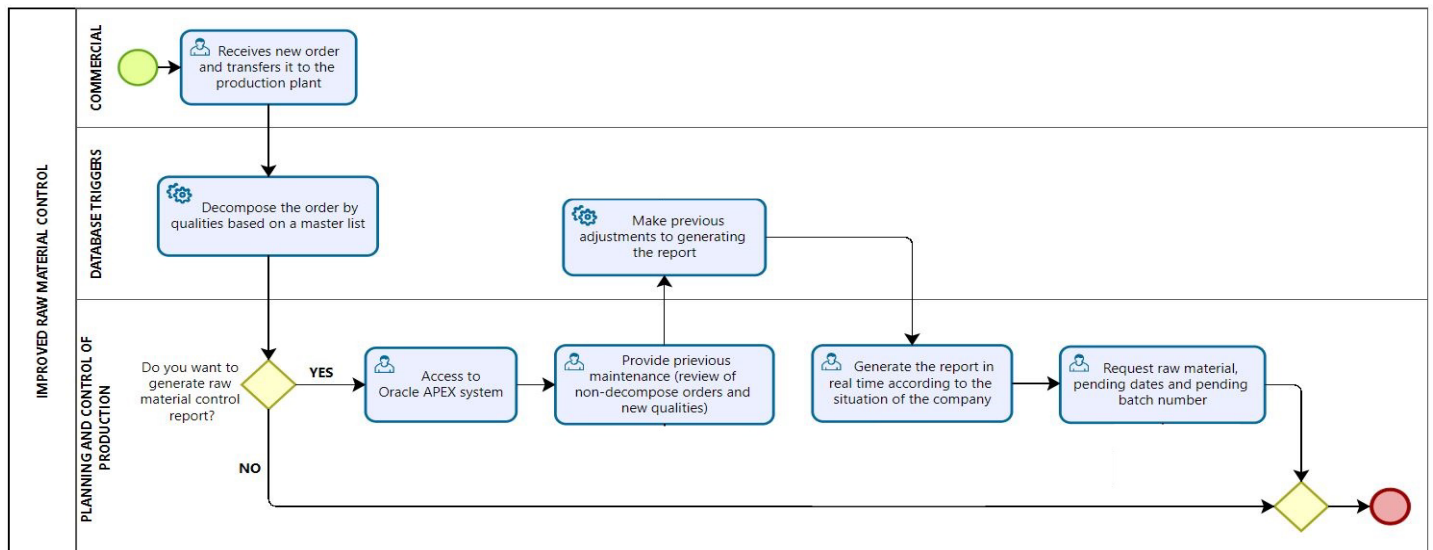
Figure 6: Diagram of the improved raw material control process.

Then there is the process of requesting raw material for alpaca and national sheep, where the following waste is observed:

- *Overprocessing*: By constantly modifying the production order, generating a stack of physical documents to control

the delivery of the material, and requesting the creation of the batch number.

- *Defects*: By having an inefficient process, there is confusion with the material's assignment to the scheduled orders, causing their delay.

- *Waits*: The most significant delay occurs when waiting for the confirmation of the batch number to finish programming the production order.

In both raw material request processes, it is evident that there is a more common waste, and that is the waste of human talent, by outsourcing activities.

3.3. Process Redesign

An improved raw material control process is carried out regarding scheduled and pending orders or orders to be scheduled. Figure 6 shows the diagram of the improved raw material control process. Figure 7 shows the enhanced process for requesting raw materials for alpaca fiber and national sheep.

The new raw material control process begins when a new order is entered in the Commercial area and is transferred to the Programming and Production Control area in the request of a delivery date, automatically entering decomposition by the system with the help of a defined Master of Qualities and bases, in this way when the user requires it, he will already have the stored information of the decomposition of all the orders.

Before generating the report, a prior review should be given to see if any order was partially decomposed or if one was not since a new quality may have been created in some order, which has not yet been considered in the Master of Qualities and bases. The user must add the unique quality to the master; once added, the system will automatically decompose all the pending orders that contain this new quality.

Once the report is generated, there should be complete information on all breakdowns and the stock of raw materials: stock in a warehouse, stock in production, supply in request, and missing stock; with this information, the user will be able to make decisions quickly.

3.4. System Development with Scrum and Oracle Apex

The agile Scrum methodology [16] will be used to construct the software. The Scrum guide was recently updated by its authors Ken Schwaber and Jeff Sutherland in November 2020, making it intelligible since they decided to reduce the prescriptive language and point to a general language applicable to different areas and not only to technology areas; It is also highlighted that the guide shows how essential it must be to implement it; however, it is possible to complement it with other processes, techniques, and methods [17].

Given the need of the company in question and the characteristics of the process analyzed, it is decided to take the strategy of division by process flow, thus leaving a division of five Sprints ordered by priority based on the collected user stories.

Within the five sprints, the following non-functional requirements will be taken into consideration: a) System accessibility, b) System portability, c) Friendly user interface, d) Reliable information, e) System scalability, f) System flexibility, and g) Can be integrated into the current system.
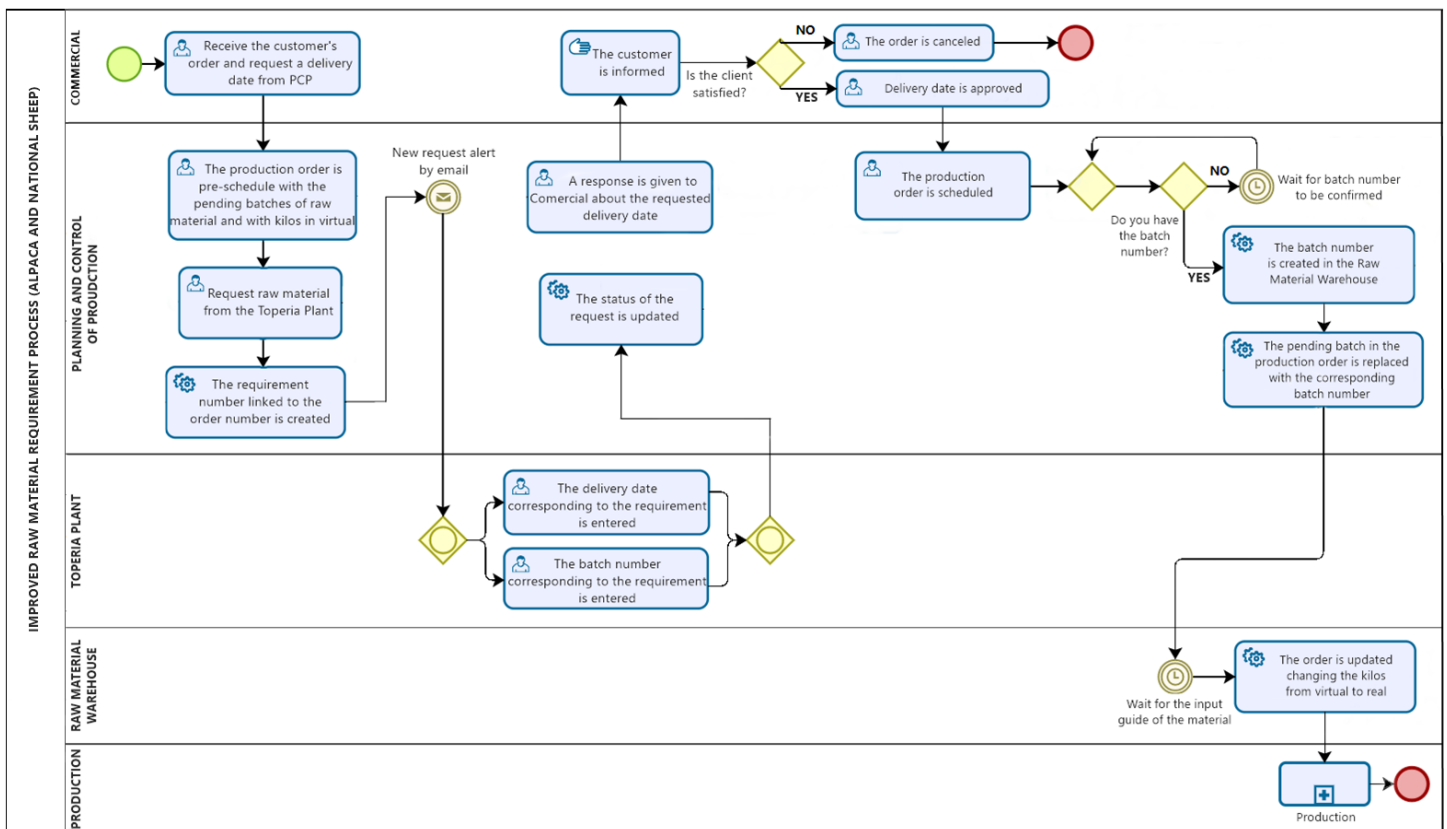
Figure 7: Diagram of the improved process for requesting raw material for alpaca and national sheep.

- Data Model: Figure 8 shows the data model of the base tables for the Master of Qualities, where the names of the fields are observed together with the type of data, data length, and the relationships between the tables.
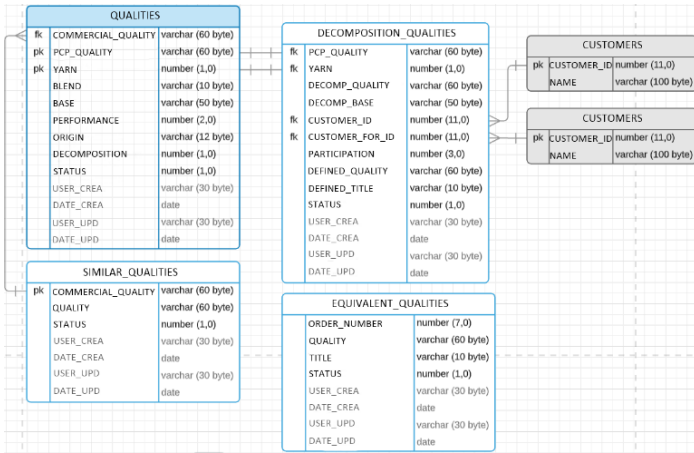
Figure 8: The master relational model of qualities.

- *Oracle APEX*: Oracle APEX, being a low-code graphical tool, as mentioned by Baggia1, Leskovar, and Rodič [18], allows us to prototype while it is being developed, representing significant time savings in the development of the project. These pre-prototyped interfaces can be adjusted or modified in a matter of minutes, which fits with the Scrum framework regarding the adoption of changes by the customer.

Before starting with the development documentation, it should be clarified that the project was led and developed by the same person due to the mechanics of the Systems and IT area in the textile company.

When entering the interface of the master of qualities shown in Figure 9, three columns will be observed: the first shows the header

of the master, the second that shows the detail of the decomposition of qualities, and the third where the similar attributes will be registered; All the related information will be displayed from the header, selecting the magnifying glass icon, the rate will be painted green when it has similar qualities registered.

Figure 10 shows the deliverable of the data model of the table that will store the history of the decompositions of the orders transferred to the plant; from this history, it is that the summary report of the raw material can be generated for correct control.

- *Iterative algorithm:* As part of the second deliverable, the quality decomposition procedure is presented; this will start when there is a transfer of an order from the commercial area to the plant; the order will automatically enter decomposition and will generate the information that will be stored in the decomposition history table. Figure 11 defines the algorithm that was developed to decompose the orders.

To better understand the decomposition of qualities, a practical case of the decomposition of an order is shown in Figure 12. The order is entered with three mandatory data: the rate, the mixture, and the number of kilos requested. In this case, the order is entered with mixed quality, and the mixed data corresponds to the percentage of participation of each pure quality identified in the mixed quality. The first step would be to break down the mixed quality into its pure qualities according to the order of the chain with the highest number of characters, with the pure quality W24.5 being found first, then AC-F, and finally FS. For each pure grade, its blend % is assigned according to the blend data received in the order; then, the grade is searched for in the graded master, assigning its yield % and identifying if the grade has decomposition. If the quality has decomposition, a % of participation must also be given for each component. Finally, the calculation is made according to the established formula, thus obtaining all the details of the order.

Figure 9: Oracle APEX interface of the quality master.
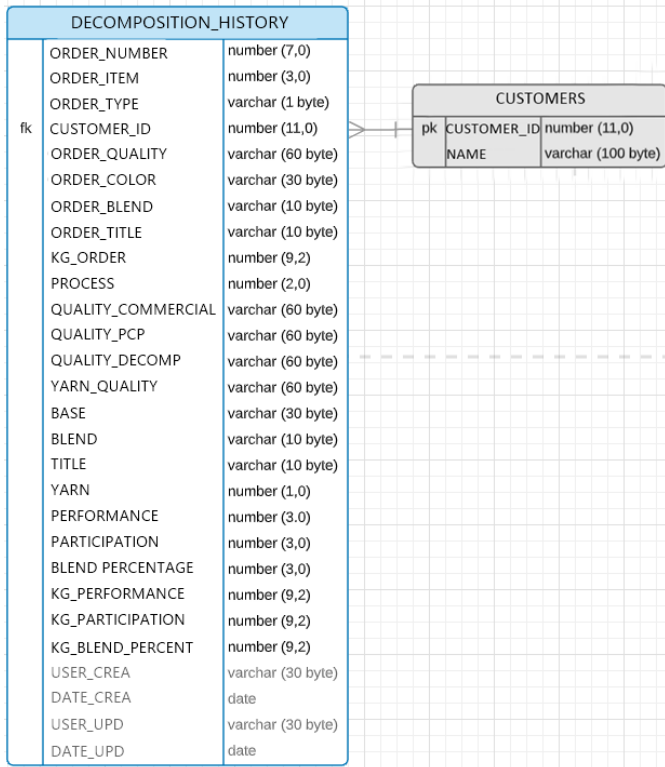
Figure10: Entity relationship history model of quality decomposition.

The logistics raw material requirements interface shown in Figure 13 is like the Topería requirements interface because it also has editable fields and an option to send the requirement. Still, it is handled in a different way distinct.

This interface can send several requests in a single order to Logistics and cancel the request in a cascade. The fields title, weight, kilos required, reference batch type, and good service code must be filled in before sending the request. In the same way as the interface to Topería, there is the option to download the information to excel, create a manual submission, and display the date and kilos of the material entered.

Figure 14 shows the interface of the raw material referring to the Top type qualities. Links have been added in the QUALITY and ORDER fields to access detailed information. Similarly, in the upper right part of the interface, a couple of buttons were added to access the information on the stock in production and the lots with virtual kilos. Below these information buttons are links to report downloads. in PDF formats. A region is highlighted in red; this indicator will alert the user that these orders are not covered by the existing stock or any raw material requirement. You can break down an order again if the user requires it

4. Results

4.1. Analysis of the Average Time of the General Process

The average time it would take to execute the general Raw Material Control process was analyzed as part of the system evaluation. Figure 15 shows that the previous process took approximately 3 hours and 15 minutes, plus 2 hours for a coordination meeting between the different areas of interest. Whereas, with the new approach, it takes 10 minutes to control raw material correctly.
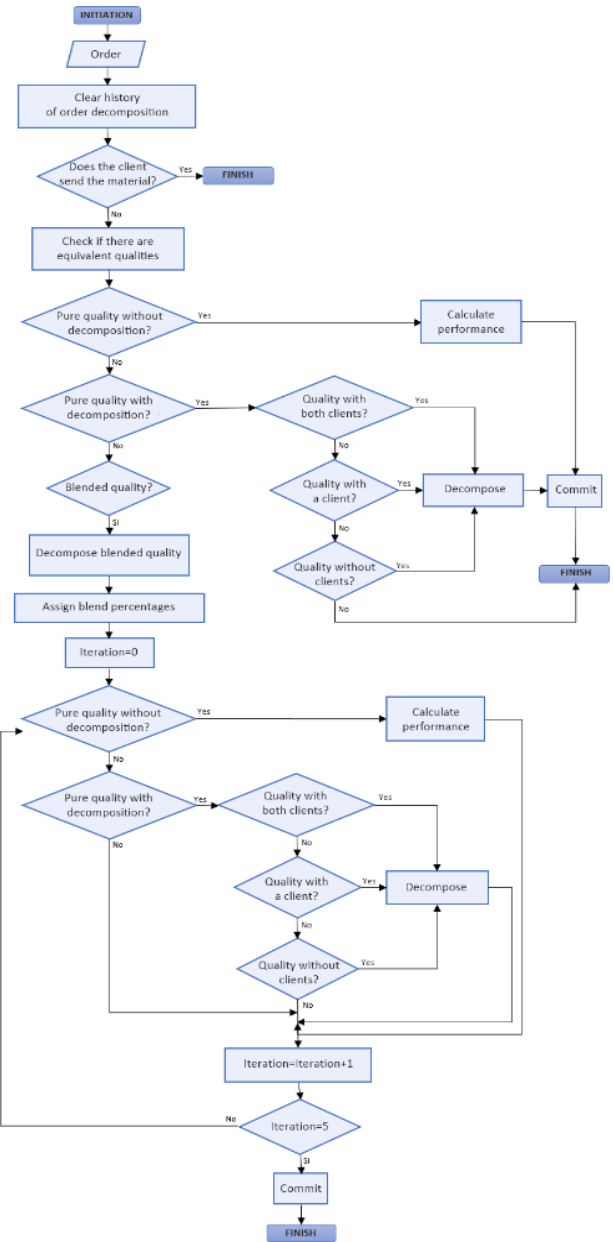
Figure 11: Flowchart of the iterative algorithm of the quality decomposition.
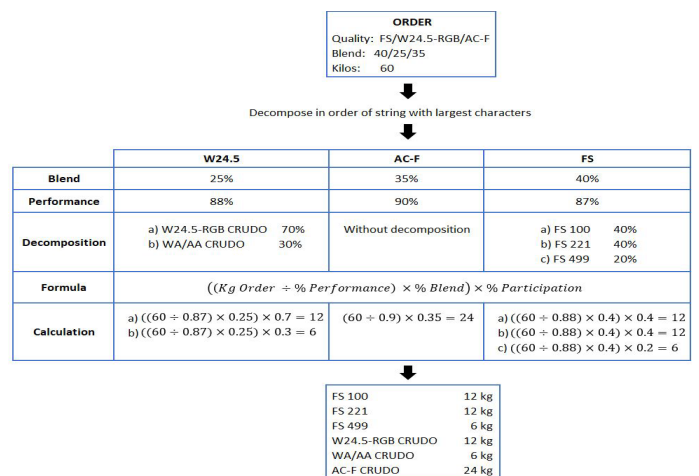
Figure 12: A case study of the decomposition of an order.
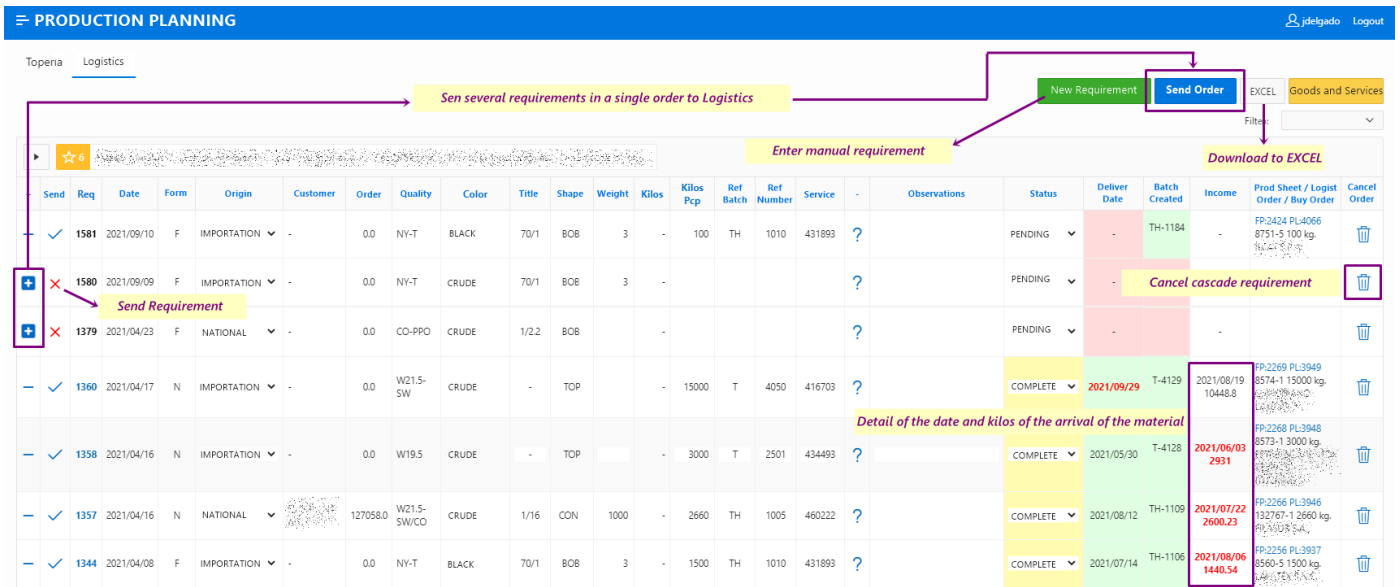
Figure 13: Time analysis of the Raw Material Control process.
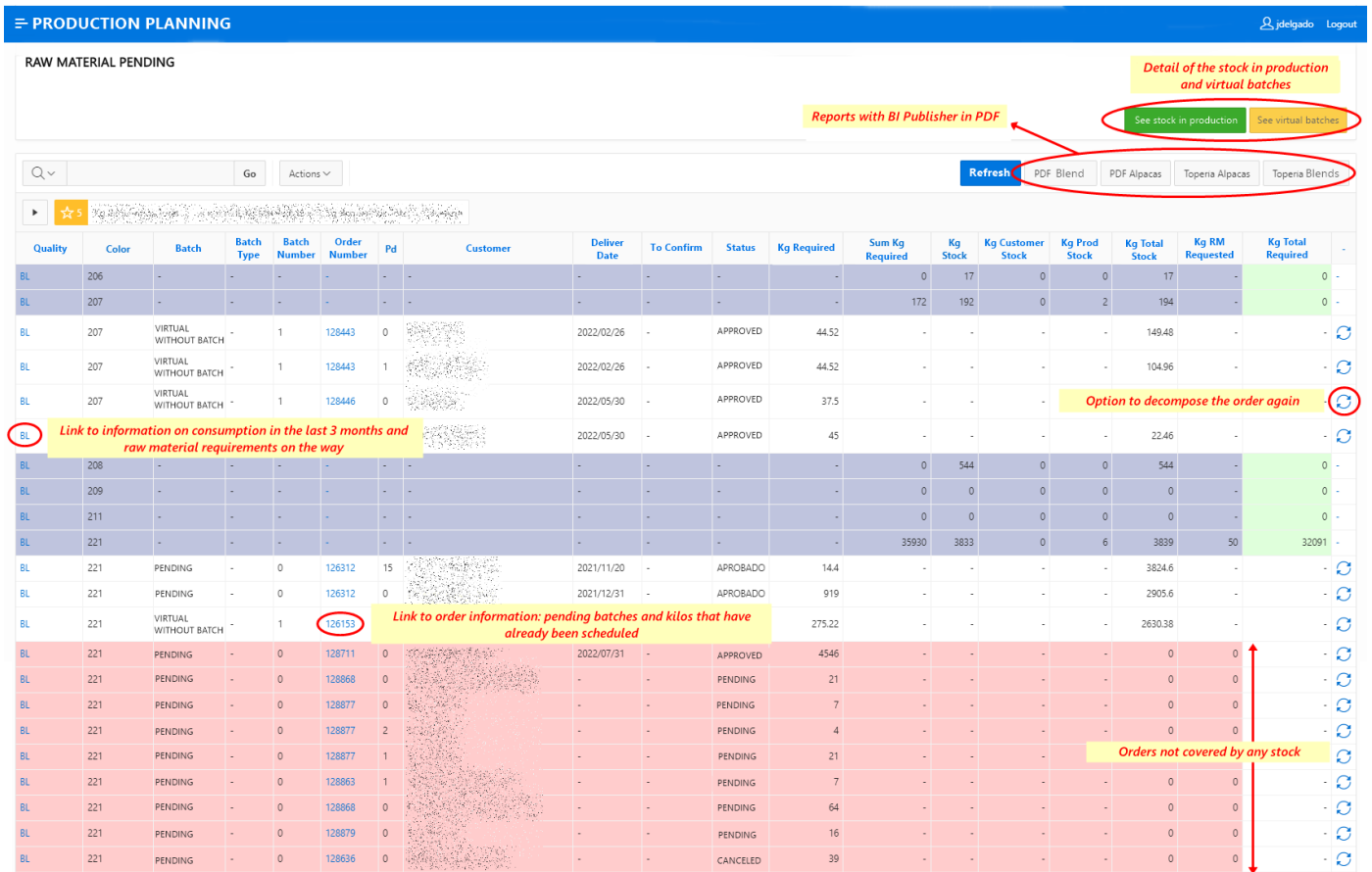
Figure 14: Time analysis of the Raw Material Control process.

4.2. Analysis of Response Time to Delivery Date Requests

In analyzing the process problems, the indicator of response time to delivery date requests was implemented, which classifies why the response exceeds 48 hours. In 2020, it was found that approximately 31% of the proposals that exceeded the 48-hour response time were due to a pending raw material request.

Figure 16 shows the analysis of the response time so far in the year 2021; the level of response exceeding 48 hours per raw material request seems to have decreased.
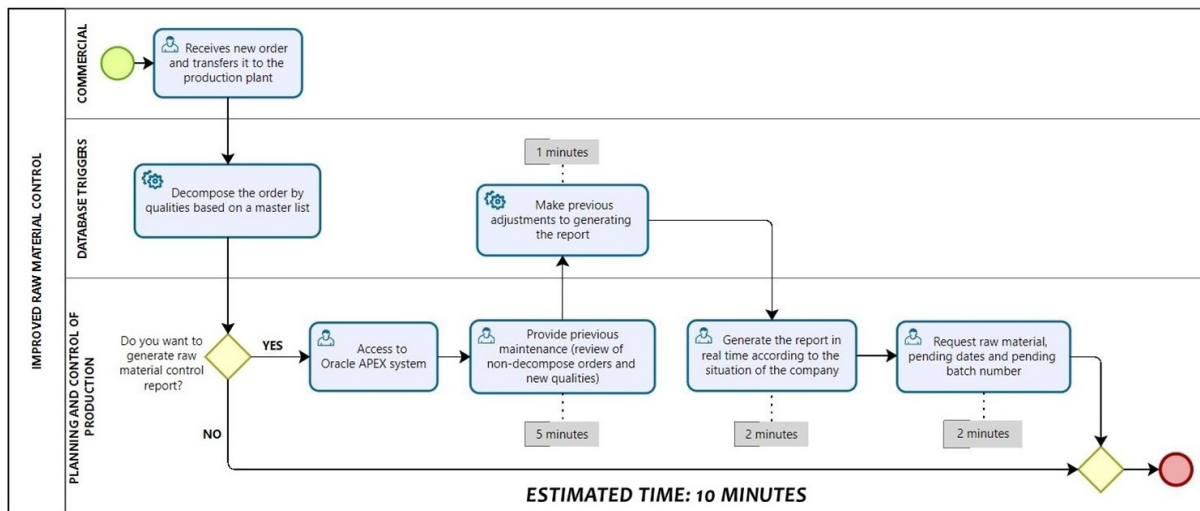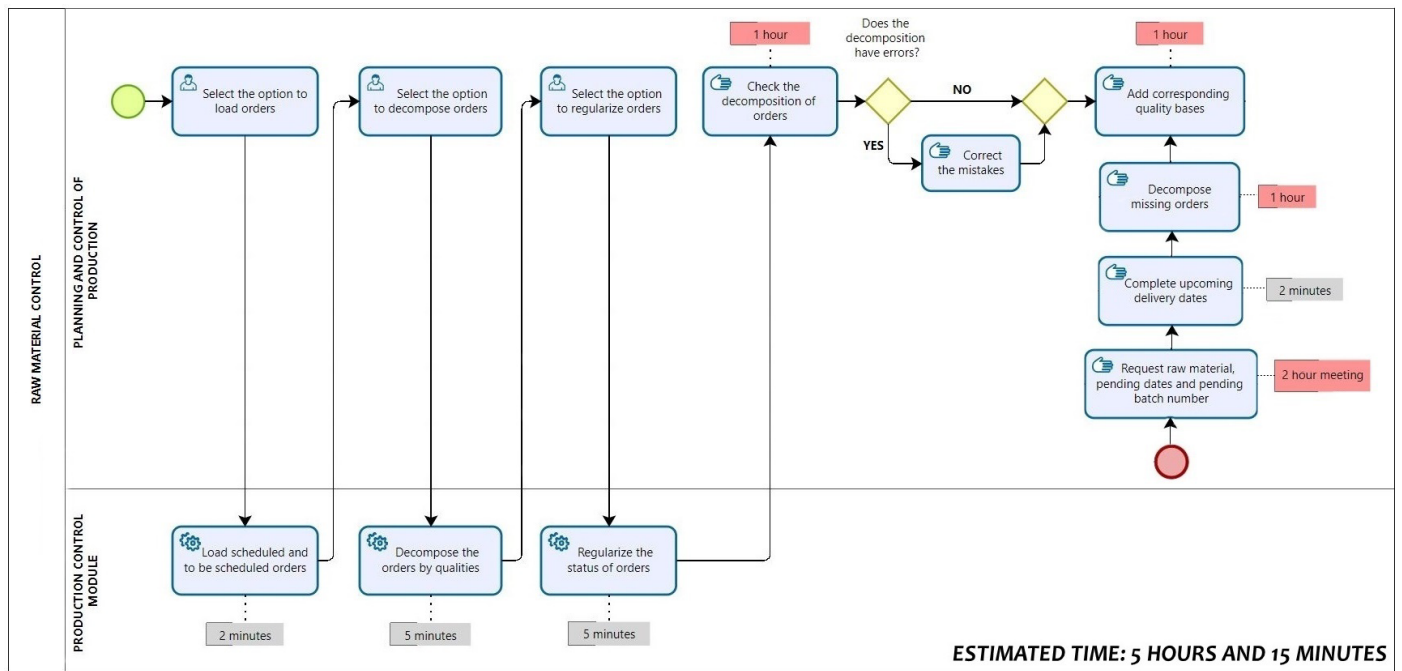
Figure 15: Time analysis of the Raw Material Control process.
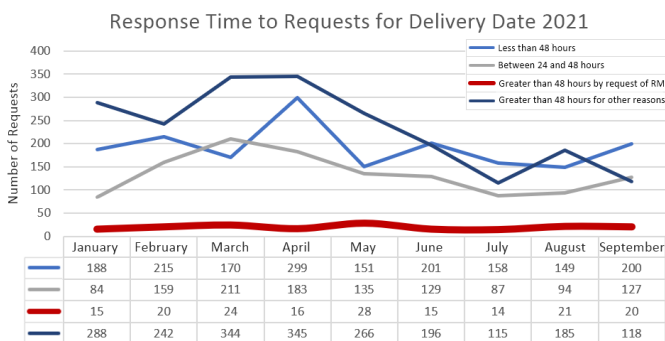
Figure 16: Response time to delivery date requests.

In Figure 17, we compare the values for 2020 against those obtained for 2021 concerning the response time for raw material requests exceeding 48 hours. It is confirmed that the percentage was considerably reduced from 30% to 0.08% of requests

answered over 48 hours. With this, we can say that the objective of improving the response time for delivery date requests has been met.

Figure 17: Comparison of response time per raw material request 2020-2021.

5. Discussion

Our results show that with the developed system, we obtained a considerable reduction in the execution time of the process; likewise, we were able to reduce from an initial 30% to 0.08% of

the requests answered in a period longer than 48 hours, in addition to eliminating different tasks and manual calculations such as the calculation of yields, manual control of the number of lots in the warehouse, decomposition of yarn qualities, among others. It was also possible to avoid confusion in assigning material to programmed orders. Likewise, the control and the raw material process were successfully optimized by redesigning its flow, developing a system in Oracle APEX, and implementing it through the SCRUM methodology.

These results coincide with those of [4]. They demonstrate that implementing the management model in the textile company in their study can increase effective operational productivity from 82.61% in the current system to 130.43% in the proposed approach. Similarly, a reduction in the rate of defective products from 20.83% to 6.25% is identified. Finally, 100% compliance with scheduled deliveries was achieved; in other words, the order was delivered within the agreed time. Likewise, it coincides with the importance of analyzing the inventory life cycle in textile equipment and its evaluation using the software as input data, among others, the raw material [19].

Through the analysis of the operation of the raw material control and request process of the textile company, the main flows were identified, as well as their critical points: Raw material control, raw material request (alpaca and domestic sheep), and raw material request (imported sheep and yarn).

Under the Process Management approach, it was possible to redesign the raw material control and request process, eliminating the identified wastes of over processes, defects, and waiting times in the process flows.

Using the Scrum methodology, we were able to meet the needs of the users and the textile company: (i) improve the response time to delivery date requests, (ii) avoid the loss of sales due to a slow response to requests, (iii) avoid errors in the allocation of material in scheduled orders, (iv) avoid delays in the delivery of orders, (v) improve the level of customer satisfaction, (vi) increase the productivity of the users involved and finally (vii) facilitate rapid decision making.

The software necessary for the new flow of the raw material control and request process was developed and implemented, proving that the tool used (Oracle APEX) allows the development of basic applications, as well as much more advanced applications, which makes its use possible in small, medium, and large companies. This coincides with the work of [20], where Oracle Apex facilitates the creation of secure and scalable applications with outstanding features. Likewise, comparing it with other works that showed the benefits of using Oracle Apex as in [21] where the use of the APEX Oracle platform for the development of their application and analysis of the data set gave them a data accuracy of 78% compared to any other existing technique, which is similar to the results achieved in the present study. Other studies highlight the benefits of using Oracle APEX as [22] and [23].

6. Conclusions

The study has covered the process of controlling and requesting raw materials from a textile company in Arequipa-Peru.

After the implementation of the proposed system, the main result was a considerable reduction in the execution time of the process; likewise, it was possible to lower from an initial 30% to 0.08% the requests answered in a period greater than 48 hours, In

addition, different tasks and manual calculations were eliminated, such as the calculation of yields, manual control of the number of batches in the warehouse, decomposition of yarn qualities, among others. Confusion in assigning material to scheduled orders was also avoided.

It can be concluded that the implementation of the new raw material control and request process flow was successful and facilitated the work of the users involved; likewise, the new flow improves the response time to delivery date requests.

For future work, it is recommended to carry out a continuous improvement cycle in all the company's processes, under the Process Management approach, in order to ensure the quality of its systems and obtain growth opportunities. Likewise, applying the same raw material request procedure in the Research and Development area is proposed since it would be the only link not considered in the analyzed flow. From this area, raw material requests are made with a few kilos because they are used for testing new fabrics; however, it is essential to account for these raw material revenues.

Conflict of Interest

The authors declare no conflict of interest.

References

[1] V.S. Guan, J. Shui, K. Chang, "The quality control application for abnormal raw material early detection," in IEEE International Conference on Industrial Engineering and Engineering Management, 2014, doi:10.1109/IEEM.2013.6962597.

[2] X. Shui, A. Shangguan, Y. Yu, H. Gao, "Advanced quality control at raw material kickoff stage," in IEEE International Conference on Industrial Engineering and Engineering Management, 2016, doi:10.1109/IEEM.2015.7385788.

[3] A.R. Guevara-Yarasca, G.F. Falla-Marcelo, J.C. Quiroz-Flores, J.C. Alvarez-Merino, "Supply Model for Dependent Demand in the Peruvian Textile Industry: A Case Study," in IEEE International Conference on Industrial Engineering and Engineering Management, 2019, doi:10.1109/IEEM44572.2019.8978862.

[4] K. Argumedo-Gonzales, A. Pumahuare-Ayala, E. Aparicio-Lora, E. Altamirano-Flores, C. Nunura-Nunura, "Proposal to Improve the Inventory Management Model in a Textil SME based on the Plan for Every Part," in Proceedings of the LACCEI international Multi-conference for Engineering, Education and Technology, 2021, doi:10.18687/LACCEI2021.1.1.498.

[5] A. Kumbara, A. Hariadi DP, "Expanded the Production Effectiveness Through Production Planning, Raw Material Control, Schedule Control And Production Control AT PT. LPA," Dinasti International Journal of Education Management And Social Science, **2**(5), 2021, doi:10.31933/dijemss.v2i5.945.

[6] C.A. Quinde Espinoza, T.K. Ramos Alvarado, "Valuación y Control Del Inventario y Su Efecto En La Rentabilidad," Revista Observatorio de La Economía Latinoamericana, **0**(0), 2018.

[7] M.K. Payne, A.W. Nelson, W.R. Humphrey, C.M. Straut, "The Chemical Management System (CMS): A Useful Tool for Inventory Management," Journal of Chemical Education, **97**(7), 2020, doi:10.1021/acs.jchemed.9b00905.

[8] D. Zimon, P. Madzík, S. Dellana, R. Sroufe, M. Ikram, K. Lysenko-Ryba, "Environmental effects of ISO 9001 and ISO 14001 management system implementation in SSCM," TQM Journal, **34**(3), 2022, doi:10.1108/TQM-01-2021-0025.

[9] T. Dingsøyr, S. Nerur, V. Balijepally, N.B. Moe, A decade of agile methodologies: Towards explaining agile software development, Journal of Systems and Software, **85**(6), 2012, doi:10.1016/j.jss.2012.02.033.

[10] L.M. I., V.A. M., "Hybrid method for agile software develop mobile devices [Método ágil híbrido para desarrollar software en dispositivos móviles]," Ingeniare, **23**(3), 2015.

[11] N.B. Moe, T. Dingsøyr, T. Dybå, "A teamwork model for understanding an agile team: A case study of a Scrum project," Information and Software Technology, **52**(5), 2010, doi:10.1016/j.infsof.2009.11.004.

[12] J. Cruz-Rojas, R. Rojas-Villa, F. Maradiegue, C. Raymundo, Lean Production Management Model Using an Agile Approach Applied to Increase Productivity in Small and Medium-Sized Chemical, Education Excellence And Innovation Management: A 2025 Vision To Sustain Economic Development During Global Challenges, 6354–6363, 2022.

[13] A. Delgado, "Web System Design for Human Resources Management in an SME in the Textile Sector," International Journal of Emerging Trends in Engineering Research, **8**(4), 2020, doi:10.30534/ijeter/2020/87842020.

[14] V.N. Timokhin, N. V Timokhin, A.N. Medvedev, "Big data analysis with Python and Oracle APEX integration," in AIP Conference Proceedings, 110029, 2022.

[15] J.D. Patiño Parra, A.K. Acosta Quintero, J.A. Ramirez Morales, "Software para la gestión de inventarios desarrollado con apex (Oracle Application Express)," M. BV Álvarez. Modelos Económicos Matemáticos II. La Habana: Editorial Félix Varela., 2006, Pp.15., 2019.

[16] K. Schwaber, SCRUM Development Process, 117–134, 1997, doi:10.1007/978-1-4471-0947-1_11.

[17] K. Schwaber, J. Sutherland, The scrum guide the definitive guide to scrum: The rules of the game, 2020.

[18] A. Baggia, R. Leskovar, B. Rodič, "Low code programming with oracle APEX offers new opportunities in higher education.," ITEMA, 2019, doi:10.31410/ITEMA.S.P.2019.91.

[19] R.M. Aileni, R.I. Radulescu, L. Chiriac, L. Surdu, "Life cycle assessment of the electroconductive textiles functionalized by advanced technologies (plasma) and metallic micro/nanoparticles deposition," Industria Textila, **70**(3), 2019, doi:10.35530/IT.070.03.1476.

[20] K. Talesra, N. G. S., "Low-Code Platform for Application Development," International Journal of Applied Engineering Research, **16**(5), 2021, doi:10.37622/ijaer/16.5.2021.346-351.

[21] V. Pathania, S.Z.D. Babu, S. Ahamad, P. Thilakavathy, A. Gupta, M.B. Alazzam, D. Pandey, A Databasde Application of Monitoring COVID-19 in India, Springer: 267–274, 2023. DOI: 10.1007/978-981-19-0151-5_23

[22] S. Farshidi, S. Jansen, S. Fortuin, "Model-driven development platform selection: four industry case studies," Software and Systems Modeling, **20**(5), 2021, doi:10.1007/s10270-020-00855-w.

[23] E. Bašić, Organizacija vjenčanja-poslovna aplikacija nad relacijskom bazom podataka (Oracle APEX), University of Rijeka. Department of Informatics, 2021.

Developing CubeSat and AI Framework for Crowd Management Case of Short-Term Large-Scale Events

Faris Abdullah Almalki[*], Asrar Mohammed Mutawi, Ibtihal Abduljalil Turkistani, Lujain Khalaf Alqurashi, Maha Talat Fattah, Malak Tammam Almogher, Reem Shaman Aldaher, Ruzan Ahmed Wali, Wafa Muidh Almalki, Yusra Muhamed Almubayed

Taif University, Department of Computer Engineering, College of Computers and Information Technology, Taif City, 21944, Saudi Arabia

A B S T R A C T

Many consequences can be resulted in mismanagement of crowd, which might get people injured or even lose their lives. Thus, crowd management helps in controlling overcrowded areas during events, and allowing authorities to monitor, manage and reduce incidents. Space science and technology have made huge leap in crowd management, let alone when this technology integrated with Artificial intelligent. Hence, space-based systems like CubeSats are seen as the best approach to help monitoring and providing various reasons. For instance, wide coverage footprint, collect specific area data simultaneously, assist in aerial photography, as well as providing wide range of wireless communications services that can integrate appropriately with AI and wearable devices. This work aims to design a CubeSat vehicle to manage crowds during short-term, large-scale events. The proposed system is, also, coupled with AI framework along with the camera and wearable devices to monitor the crowds' performance continuously by relying on two aspects: Firstly, aerial imaging (e.g., photos and videos). Secondly, using wearable devices that can be worn to monitor vital signs of crowds. Moreover, the proposed system can independently relieve congestion, as well as notify the ground controller of all problems to take further actions. The obtained results confirm that the proposed innovative solution is for crowd management with accuracy reached 95%, and MSE equal to 0.049.

1. Introduction

CubeSats are small cubic shape satellites designed in 1999 orbits around the earth in the (LEO) layer with is the low earth at +400 km height form the sea surface. These aerial nano vehicles can do missions despite their differences in size and structures (e.g., 1U, 2U, up to 6U), where mass ranges from 1k to 6kg. A CubeSat has two types of components Payload (which are the physical components of the CubeSat) and Platform (which are several systems to fulfil the mission). Unquestionably that CubeSat is less expensive than large satellites in terms of manufacture and launch, besides its close distance to the ground that gives advantages of rapid data transmission. Noticeably, these nano satellites are more accessible to various companies or even individuals since its affordable cost and short time to development and implementation [1-3].

Figure 1: CubeSat wide range of applications.

*Corresponding Author: Faris Abdullah Almalki, m.faris@tu.edu.sa

The Fourth Industrial Revolution conceptualizes fast change to technology, industries, and societal patterns and processes in the 21st century. Where it changes the way businesses operate in daily tasks with information technologies, allows improving operations, decreasing costs, improving the quality of life and processes. Including Artificial Intelligence (AI), Internet of Things (IoT), Internet of Medical Things (IoMT), and wearable devices. These technologies can integrate with CubeSat and deliver wide range of smart applications. Figure 1 demonstrates Cubesat wide range of applications that around topics like telecommunications, science space, and earth observations [4-6].

Temporary event or short-term large-scale events (e.g., sports, social, cultural) require an extra measure of planning, coordination, and management; thus, they can heavily benefit from CubeSat and its wide range applications such as commercial applications (e.g., telecommunications, remote sensing, high-resolution aerial imagery, ship tracking and monitoring). Additionally, such small satellites help in more domains like [7-9]:

- Technology demonstration in strict environment of space to test new instruments or materials.
- Academia and educational projects to get a unique hands-on experience in emerging space undertakings from design to launch and operations
- Crowd management via integration between an aerial imaging capability with AI that help to describe crowd movements, issue early warning, and then take actions. Where authorities and countries need to manage the crowds' events especially those large-scale short-term events, where the safety and security of people must be ensured.

Many authors have stressed the that the research on CubeSats for communications is still in its early phase. IoT, Internet of Space Things (IoST), low-power long-range networks, Iridium communications, earth-remote sensing, and machine learning are opened research areas for CubeSats. The following section 2 presents related study review work in support to the design; then concludes by highlighting research gaps and our own research motivations. Section 3 describes the proposed model design from communication and serious gaming perspectives. Then, evaluation of the proposed framework and discussing results is presented in section 4. Section 5 concludes.

2. Related Study

This section presents a representative illustration of the related research works in the literature, where a set of criteria have been used to meet this research's scope. The criteria of this related study include different aerial platform type, aerial imaging and crowed management using AI techniques at low-altitude missions. This section concludes by highlighting research gaps and draw our own research motivations.

Researchers in [10] have proposed a framework via Unmanned aerial vehicle (UAV) for Crowd Control and Health Management System (CCHMS). The CCHMS system consists of two subsystems. The first is a Disaster Control and Management System (DCMS), which aimed at reducing the risk of stampedes and other disasters; while the second is a Healthcare Management System (HMS) to ensure safety and wellbeing of people in crowded zones. Their system is used various kinds of wireless and mobile tools including: Fog Computing, Smart Phones, Smart Digital Street, IP-Cameras, Radio Frequency Identification (RFID), Voice Alarm, Light Alarm, and Global Positioning System (GPS). The Proposed Algorithm for Stampede Detection (ASD) depends on integration among the number of objects, edge detection, and Hough transformation to ensure higher reliability when sending notifications to human observer in order to take suitable decisions and actions promptly. We noticed that the accuracy of headcount by ASD was more than 94% in most of ASD applied to a virtual image.

Authors in [11] followed a predictive approach to crowd analysis via ground camera, where they tend used geometric methods such as ORCA system to struggle in medium density scenarios where agile manoeuvres are important and it is provide to estimate the accuracy of the simulation for a particular crowd situation. This technique is based on scanning the area and then identifying the crowd and its density, finally tracking it.

A crowd counter technique is introduced in [12] that counts the crowds' heads using a Canon crowd counting technology. Obtained results show that using this a high-quality network camera in conjunction with AI framework offered a notable advantage of minimal distortion and a high-resolution result. Attention-Based Real-time CrowdNet (ARCN) decoding model is presented in [13], which is a computationally efficient density estimation-based crowd counting model that perform crowd-counting from UAV images in real-time with high accuracy. The key idea of this model is to add a "Convolution Block Attention Module" (CBAM) blocks between the bottleneck layers of the MobileCount architecture to focus on crowds and ignore background information of the obtained images. The proposed ARCN model achieved low error rates as it was a Mean Absolute Error (MAE) of 19.9 and Mean Squared Error (MSE) of 27.7.

Researchers in [14] presented a study for crowd monitoring system using UAV that equipped with sensors, and communication infrastructure to transmit sensory data to a control station. This can be done by estimating and geo-referencing of the crowd density levels using image processing tools. The process starts with people detection using image segmentation and geo-referencing for mapping the crowd levels. Then, the density of the crowds can be estimated through converting segmented images into binary images. Where these imaged appear as white region, while other images feature appear in black colour to calculate image properties (e.g., area). The proposed work showed that the image segmentation used can detect and distinguish people and estimate crowd-level density with good results. However, the position and direction of camera movement on the UAV should be optimized.

Authors in [15] use a real-time crowd monitoring and management system to classify social distance using YOLO V4 object detection technology. The detected people are tracked by surrounding boxes using Deepsort, overlapping sites become symbolize high density. The whole system is about social distance detection, network design, deep sorting-based tracking, and distance classification algorithm. Results seem reasonable only for short range distances using cameras installed via ground camera.

Researchers in [16] propose a method to manage the crowd by keeping track of the count of the people. They have developed a

system using a Raspberry Pi 3 board that consists of an armv8 CPU to detect human heads as dots and provide a count of humans in the region using OpenCV-Python. Human tracking is achieved by indicating the direction of movement of a person. The obtained results showed an average level of accuracy where not every head in the frame was detected.

Researchers in [17] proposed an approach for crowd counting method called SCNet via drone images. The method based on cascaded deep convolutional neural networks (CNN). It works by extracting high-level features to generate density maps that represent an estimation of the crowd count with respect to the scale variations in the images. A dataset named ViseDrone2020 used for training and testing of the proposed method. The evaluation process was done by comparing the proposed method with ten state-of-the-art methods, in addition to testing the proposed method on different datasets and noisy images. The experiments shows that the proposed model (SCNet) was more efficient for crowd counting and the quality of the density map. Besides the quantity of the crowd count estimation was comparatively better than other existing methods without the presence of noise.

In [18], low-altitude aerial images collected by a UAV that integrated with an AI model was presented to count crowds in a specific situation. The basic idea of their approach was to deploy an end-to-end CNN model to generate a density estimation map on edge of AI devices. They evaluated a range of neural network architectures to find ones appropriate for on-board image processing using edge computing devices. Through these experiences, it has been concluded that using a Xavier NX platform shows a sufficient computational power with good accuracy. Also, noticed that the accuracy of the input image greatly affects the prediction quality and should be considered an important factor before moving on to a more complex neural network model to improve accuracy.

Authors in [19] proposed an approach for tackling crowd management via satellite. Many modules have been proposed for crowd management, some were visual sensing methods such as satellite images, video sequences or infrared thermography; while others were non-visual sensing methods such as smart bracelets or hotspot Wi-Fi in smartphones. The proposed collaboration was between satellite images, thermography, and wearable devices. Results of the proposed system showed high accuracy for proper crowd management. Yet, crowd density should be calculated in a real-time to make decisions.

Authors in [1] proposed a novel lightweight and fast convolutional neural network (FCN) to learn a regression model for crowd counting via images captured from drones. A learning system was initially based on a multi-input model trained on two different views of the same input. First, real-world images; Second, corresponding synthetically created "crowd heatmaps", which was used to help the FCN focusing on the most important parts of the images. The derived model achieved promising results on the tested images. Researchers in [20] developed an automatic people counting system using digital image processing technique that integrate with a drone called "Otsu's method". The captured images were firstly compared between RGB and HSV colour model. Then, the HSV colour model has been chosen for the thresholding process due to its high accuracy. Results of the

proposed system has achieved a good image processing with total accuracy of 91%.

Authors in [21] present a multi-UAV for crowd monitoring system to monitor group of moving walking individuals using an auction paradigm that distribute targets among UAVs and genetic algorithms. The monitoring aims to track and record the position of targets, where all targets should be visited during a surveillance period and reducing time between the visits made to each target. The system can be used for law enforcement applications, helping authorities monitor crowds to identify and track suspicious individuals. System results show a good performance under various situations.

A decision-making process on board a UAV was proposed in [22] to enhance search and rescue operations during natural or man-made catastrophes via multi-agent architecture. It was used to deploy multi-agent systems aimed at retrieving and analysing information by using mobile robots, which are usually UAVs, and for providing support to the decision-making process in environments affected by natural disasters. The architecture has been structured into layers provides communication and cooperation mechanisms among agents and envisages defining a set of agents with different roles. This work shows a good example when using space-based system for aerial imaging that serve different purposes.

Researchers in [23] used a Digital Elevation Model (DEM) to detect individuals in crowded areas from very high-resolution satellite images using street classification approach. The proposed approach aims to eliminate high objects on streets using shadow information, and using DEM of the region, which is automatically generated using stereo satellite images to eliminate buildings. After applying feature selection using selected local features as observations, a probability density function (pdf) was generated. Obtained pdf helps detecting crowded regions and some of the individual people automatically. Results indicate the possible usage of the proposed approach in real-life for mass events to provide a rough estimation of the location and size of crowds from satellite data. Table 1 shows a comparison of the related research windup.

Table 1: Related study wind-up.

Ref.	Platform	Intelligent Framework	Contribution	Issues
[1]	UAV	FCN	Lightweight and fast convolutional method to create heat maps of crowds to enrich the semantic contents	Images should be enhanced, while maintaining computing power & real-time response
[10]	UAV	CCHMS	Higher reliability and accuracy of headcount	Short distance, and limited crowds
[11]	Ground Cameras	ML	Crowds are represented as dots for better crowd management	It is not clear if the crowd is passing through a confined space
[12]	UAV	AI	A counter on several cameras that count crowds & represent them as dots	Coordination and well-mounted cameras are needed for better coverage
[13]	UAV	CNN	Good level of accuracy	Complexity and Giga flops increase

[14]	UAV	Image processing tools	The control station processes the sensory data and if any urgent situations noticed, alert the field staff	Similarity in colours of the surrounding setting lead to less crowds management
[15]	Ground Cameras	DL & Tracking Techniques	Prevention of Covid-19 in public places	Due to short monitoring distance complexity increases and more cameras is required
[16]	A camera on walls	OpenCV-Python	Average level of accuracy	The camera cannot track in large or crowded places
[17]	UAV	CNN and VGG-16	Density map quality and crowd count estimation are comparatively better than other existing methods without the presence of noise	Increase UAV altitude, and weather conditions would affect accuracy and increase noise
[18]	UAV	CNN	Good level of prediction accuracy	UAV altitude affect the quality of the prediction, it should be optimized
[19]	Satellite	Image processing tools	Combination between two or more different image processing tools creates accurate results.	- High complexity, so optimization is needed - High altitudes reduces resolution
[20]	UAV	Otsu's	Successful estimation of crowds and good image processing with total accuracy	Difficulty to remove the unwanted objects from images less than 2500 pixels
[21]	UAV	GAs	Good level of monitoring the position of individual targets	Complexity and delay for processing
[22]	UAV	Multi-agent	Good performance for fusing info to assess the level of risk	Natural disasters could affect the UAV performance due to low altitude
[23]	Satellite	DEM	Detect crowds automatically and remotely with very high-resolution	DEM images lead to the inability to determine the crowds properly

Based on the wind-up related studies on Table 1, the research gaps have been identified, so we draw our own research motivations and proposed model. To our best knowledge and based on the related study, no work has been done to have a fully CubeSat that integrate with integrate properly with AI and wearable devices for crowd management in short-term large-scale events and help in making smart decisions. Therefore, our proposed novel contribution is motivated to cover this gap, and to achieve such an aim the following objectives need to be pursued:

O1. Designing CubeSat platform with its software and hardware capabilities for crowed management.

O2. Developing an AI framework to integrate with CubeSat and wearable devises to monitor crowds and their health status.

O3. Manufacturing and implementing intelligent CubeSat.

3. Proposed System Model

The consequences of poor crowd management are catastrophic, where people can be injured or lose their lives. Therefore, crowd management aims to provide a healthy environment that adheres to the highest standards of prevention and safety. It is rational to consider advanced technologies to design a system that can fulfil the crowd management. This paper is aimed to manage crowds and monitor their health status in temporary events using integrated AI framework, and wearable devices that worn by terrestrial crowds. This has been done by coupling a fully autonomous CubeSat that paired with Histogram of Oriented Gradients (HOG) and OpenCV techniques that work harmoniously together to enhance crowed management. Using wearable devices that can be worn to monitor vital signs of crowds. Moreover, the proposed system can independently relieve congestion, as well as notify the ground controller of all problems to take further actions. This section is mainly focusing on two parts, which are: conceptual model, followed by mathematical calculation of the proposed system.

3.1. Conceptual Model

The proposed system has a CubeSat with its payloads to manage crowds of temporary events using integrated AI framework, and wearable devices that worn by terrestrial crowds. The integrated system can be visualized as per Figure 2, which consists of the space segment and ground segment. The former has a CubeSat platform with its payloads including an ultraHD camera paired with the proposed AI framework, a GPS sensor, a transceiver module, which is responsible for wireless communication between the CubeSat and ground segment before transmitting the gathered data to the cloud for further storage and analysis. The latter segment includes a Ground Control Centre (GCC), which acts as a focal point between two segments and host gateways to external networks. This segment deals with the wearable device that worn by terrestrial crowds to monitor vital signs, which in turn help detecting health status of them and then give solutions and/or take actions when needed.

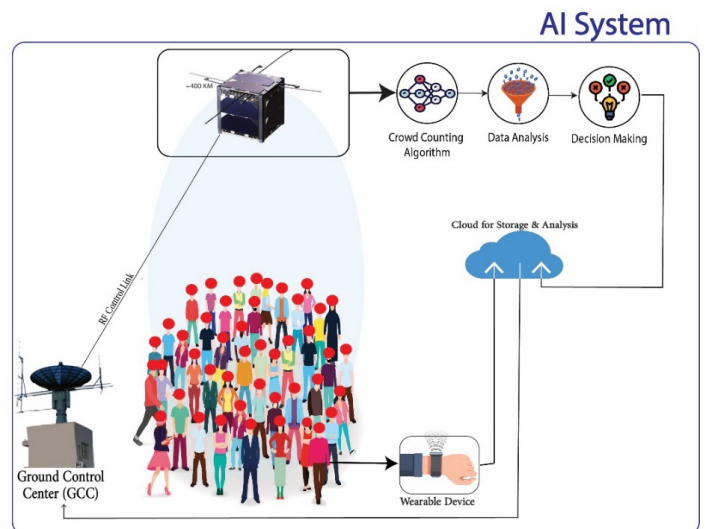Figure 2: Proposed Work System.

The CubeSat is responsible for collecting multimedia data and then transmitting them to the cloud for proposing and storage. The CubeSat along with its integrated AI system will take a picture of the crowds and treat them as dots. Additionally, the proposed system includes a crowd counter algorithm to calculate the crowded area. Then, analyses of these data to make appropriate

decision, which can be predefined actions, which makes crowd management much easier as there is no need for human intervention in some situations. For instance, guide the crowds towards empty paths, open and /or close the doors. Through wearable devices that allow us more accurate results not only by monitoring health status of the crowds, but also in counting them via Wi-Fi sensors that can be distributed in the target area. It is worth to mention that the cloud should deal with two inputs: input from the CubeSat, which provides aerial imaging and numbers; input from the wearable devices. The data can be visualized and analysed in the database associated with the user interface.
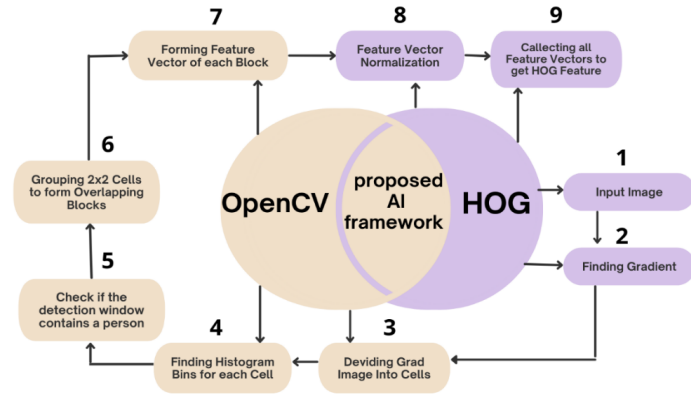

Figure 3. The Proposed System Algorithm.

The proposed AI framework consist of two brains as per Figure 3; First, the HOG, which is responsible for the Accumulated method to count the crowds and deal with them as dots. It directly extracts feature from the scene and uses a regression model to map the relationship between the extracted features and the people count does not need to precisely detect each individual or track every motion pattern. Which is more flexible and scalable. The HOG prosses starts by dividing an aerial image into cells and localize features are extract from each cell region. Second: Using the OpenCV library, the SVM classification is applied to decide if the detection window contains a person using the block histograms. Every cell needs to train a regression function mapping localized features to local count and the global count is obtained by accumulating all the local counts processing speed is proved to be fast enough for real-time application.

The workflow of the proposed system focuses on the collaboration between multimedia that obtained from the CubeSat and wearable devices to manage the crowd. Where the CubeSat can cover a large footprint area as well as participate in making decisions to manage the crowd; While the wearable devices integrate with CubeSat and help identifying people as points and keep them connected to the Internet and transmit their health status, besides help in monitoring the crowds. The proposed system workflow as the following steps:

- CubeSat start operation by monitoring a targeted area,
- CubeSat counts the crowds and consider them as dots using HOG framework,
- Wearable devices start operation by monitoring the crowds' health status,
- The proposed AI framework analyses multimedia to understand crowd conditions and detect health status,

- When actions needed, solutions would be either predefined actions, or admin actions,
- Notifications should be sent regularly to the GCC.

3.2. Mathematical calculation

This subsection gives a mathematical outline of both the link budget predictions, as well as the proposed AI framework [24-29]. Regarding the link budget predictions this would include Free Space Path Loss (FSPL), Receiver Signal Strength (RSS), Signal to Interference and Noise Ratio (SINR), and Throughput. Used FSPL assumes a transmit antenna and a receive antenna to be located in an otherwise empty environment. Neither absorbing obstacles nor reflecting surfaces are considered. In particular, the influence of the earth surface is assumed to be entirely absent. RSS it is a measurement of the discrepancy between the data and an estimation model and when the receiver moves away from the transmitter RSS helps to estimate the coverage range when the signal weakens. SINR is a measure of Signal Quantity and Interference and Noise Quantity RSS is effective through distance, when distance increase RSS decrease. Throughput is the amount of data received by the user in a unit of time. Therefore, equations of the link budget predictions can be seen as per equations (1) to (4):

$$FSPL = 20log((\frac{4\pi d}{\lambda})) \tag{1}$$

$$RSS = (P_t + h_t + h_r - FSPL - L) \tag{2}$$

$$SNR = \frac{RSS}{N+l} \tag{3}$$

$$Throughput = (B * log(1 + SNR)) \tag{4}$$

where d denotes the distance beween the receiver and transmitter, λ represent Wavelength, Pt denotes the Power of the transmitter, ht denotes transmitter antenna's height , hr denotes receiver antenna's height and L denotes system losses, N denotes noise, I denotes interference power, B denotes channel bandwidth.

The mathematical representation of the proposed AI framework that include HOG and OpenCV techniques can be seen as per equations (5) to (25):

$$G_x(x,y) = I(x + 1, y) - I(x - 1, y) \tag{5}$$

$$G_y(x,y) = I(x, y + 1) - I(x, y - 1) \tag{6}$$

$$Magnitude(\mu) = \sqrt{Gx^2 + Gy^2} \tag{7}$$

$$Angle(\theta) = |tan^{-1}\frac{G_y}{G_x}| \tag{8}$$

where G_x and G_y are the coordinate of the pixel in the image, will be count the pixel at X with a difference of -1 and +1 on the X-axis and the same for Y (Y-axis). μ and θ to find the size and angle of each pixel in the input image.

$$No. of\ bins = 9(0^o\ to\ 180^o) \tag{9}$$

$$Step\ size(\Delta\theta) = \frac{180^o}{No.of\ bins} \tag{10}$$

$$[\Delta\theta * j, \Delta\theta * (j + 1)] \tag{11}$$

$$C_j = \Delta\theta(j + 0.5) \tag{12}$$

Each part is divided into cells (there is no specific number to choose cell, the larger the image, the more cells), and each cell contains dots, and each dot is a bin, so will be use equation 9 (No. Of bins) and 10 ($\Delta\Theta$) to find number of bins, equation 11 is to find bin boundaries, finally C_j (equation 12) is to find centre of the bin, then will be collect all the cells, the block, the features and convert them to vector.

$$Vj = \mu * [\frac{\theta}{\Delta\theta} - \frac{1}{2}] \quad (13)$$

$$V_{j+1} = \mu * [\frac{\theta - cj}{\Delta\theta}] \quad (14)$$

$$L * H * f_{bi} \quad (15)$$

where V_j (equation 13) and V_{j+1} (equation 14) are vectors values to find the histogram bins for each cell, L is length , H is high (width) and f_{bi} is feature block so equation 15 is to calculate how much a 2x2 square takes for the length and width.

$$fbi \leftarrow \frac{fbi}{\sqrt{\|fbi\|^2 + \in}} \quad (16)$$

$$fbi = [b1/k, b2/k, b3/k, ... b36/k] \quad (17)$$

$$k = \sqrt{b1^2 + b2^2 + b3^2 + ... + b36^2} \quad (18)$$

$$fbi = [b1, b2, b3, ... b36] \quad (19)$$

where values of f_{bi} for each block to normalize it, equation 16 and 17 same as equation 18 but using the k coefficient and its equation, collecting all feature vectors to get the HOG feature as per equation 19. Equation 20 to 25 are related to the OpenCV technique. First step is to manipulate the source image duo to code ability. In equations (20) & (21) dilates the source image using structuring element that determines the shape of a pixel neighbourhood over which the maximum limit is:

$$dst(x,y) = max_{(x',y'):element(x',y')\neq 0} src(x + x', y + y') \quad (20)$$

$$dst(x,y) = min_{(x',y'):element(x',y')\neq 0} src(x + x', y + y') \quad (21)$$

where src is the input image; the number of channels can be arbitrary, dst is output image of the same size and type as src.

Then, by using equation (22) the horizontal and vertical lines are detected over the image and the lines intersection point. The histogram of src is calculated. Considering that the sum of histogram bins is 255.

$$H_i' = \sum_{0 \leq j < i} H(j) \quad (22)$$

Now equation (23) is used to find the bins value and vectors of image blocks for corner detection. For every pixel p, the function considers a blockSize × blockSize neighborhood S(p). It calculates the covariation matrix of derivatives over the neighborhood as:

$$M = \begin{bmatrix} \sum_{S(p)}(dI/dx)^2 & \sum_{S(p)}dI/dxdI/dy \\ \sum_{S(p)}dI/dxdI/dy & \sum_{S(p)}(dI/dy)^2 \end{bmatrix} \quad (23)$$

After that, it finds vectors and values of M and stores them in the destination image as (λ1, λ2, x1, y1, x2, y2). Where λ1, λ2 are the non-sorted values of M, x1, y1 are the vectors corresponding to λ1, x2, y2 are the vectors corresponding to λ2. Then, for each pixel (x,y) a 2×2 gradient covariance

matrix M(x,y) over a blockSize×blockSize neighbourhood is calculated as the local maxima. Then, the horizontal and vertical lines are used to detect people which is compute as following is equation (24):

$$dst(x,y) = detM^{(x,y)} - k \cdot (trM^{(x,y)})^2 \quad (24)$$

where XblockSize is neighborhood size, k size is the aperture parameter for the Sobel operator, and BorderType is pixel extrapolation method.

Equation (25) calculates the complex spatial derivative-based function of the source image. If the source image size was 224x244 pixels so it will be return to 224x224 pixels after being manipulated to detected people.

$$dst = (D_x src)^2 \cdot D_{yy} src + (D_y src)^2 \cdot D_{xx} src - 2D_x src \cdot D_y src \cdot D_{xy} src \quad (25)$$

where D_x, D_y are the source image derivatives, D_{xx}, D_{yy} are the delivered image derivatives, and D_{xy} is the mixed derivative of them.

4. Simulation and Experimental Setup

This section aims to present the main components of simulating the proposed system. Then, outlining the hardware specifications of the experiment setup and the testbed structure. Figure 4 shows the CubeSat network communication architecture using Satellite Communications Simulation Toolbox in MATLAB. It is very useful tool to simulate, analyse, and visualize the motion and dynamics of CubeSat. This simulation toolbox provides standards-based tools and enormous parameters and network configurations for designing, simulating, and verifying satellite communications systems and links. This simulation step is vital to get early link budget predictions of the proposed CubeSat from perspectives of communication, size, and animation properties, before start manufacturing the CubeSat structure using 3D printers.
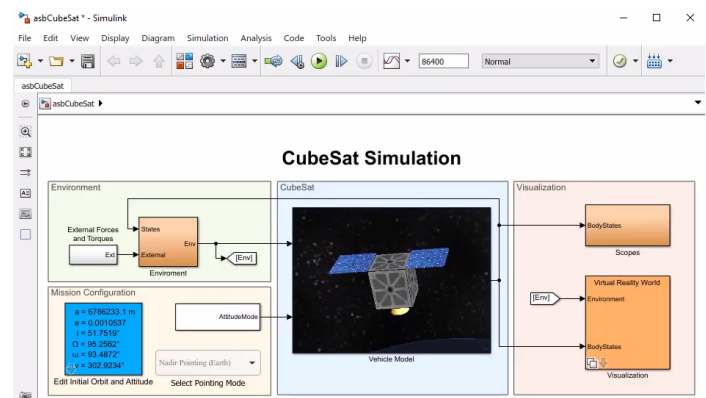
Figure 4: CubeSat network communication architecture.

Figure 5 shows the final CubeSat installation with all its hardware elements. We can see that the CubeSat contains kit of Cubesat: Structure, Raspberry Pi 4B, lens Camera Module, GPS Module, Wi-Fi Module (Transceiver), Power system includes power management, Solar Panel Cells and Battery; a HD camera is used for aerial imaging, GPS sensor for coordinating location of the CubeSat, a 5GHz module transceiver module to connect the

drone with the GCC, a power system receives power from two sources that have been connected to a power management: Source 1: Solar Panel Cells that covers the CubeSat structure; Source 2 Battery as pack up if solar power somehow gets too low. All these hardware components are connected to the Raspberry Pi 4B microcontroller, which is fitted onboard the CubeSat.
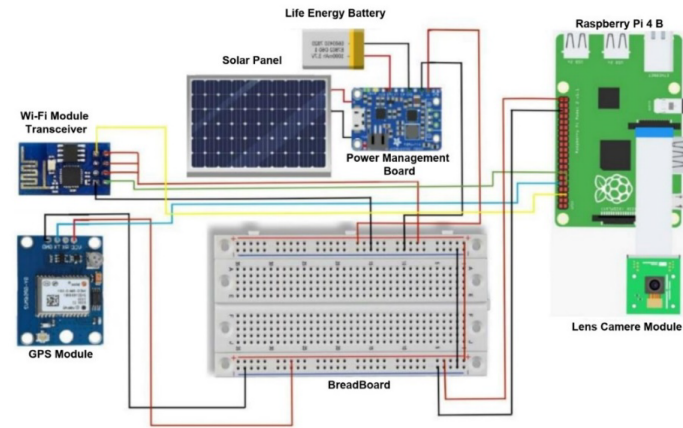
Figure 5: CubeSat Connection Diagram.

(a) (b)

(c) (d)
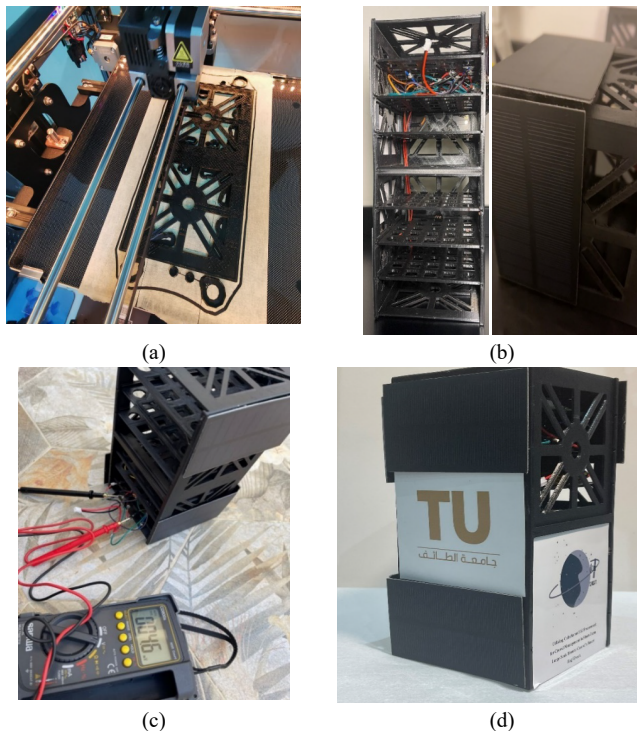
Figure 6: CubeSat structure, components, calibration, and final CubeSat platform.

Figure 6 (a) shows the CubeSat structure that is fabricated using a 3D printer, (b) represents the CubeSat structure when installing solar panels and other hardware components, (c) demonstrates the CubeSat platform under calibration and functional testing, (d) displays the final CubeSat platform. For the sake unification with global stranders, the CubeSat has been designed to meet the size and the weight capability of the 2U CubeSat, which is 10 cm × 10 cm × 22.70 cm; yet scalability is possible to be structure size of 3U, 6U, or 12U. The experiment was taken place in Taif city, Saudi Arabia, under supervision from Computer Engineering department at Taif university on the 9th of

May 2022 at 15m altitudes. The experiment's longitude and latitude are 40.4867323, and 21.3320348, respectively. A mission planner VNC software has been used when floating the CubeSat.
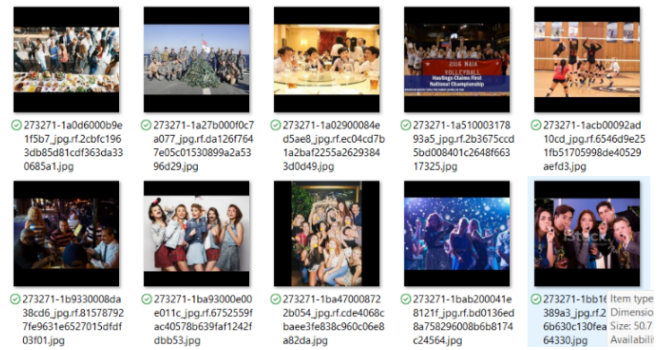
(a) Human dataset.
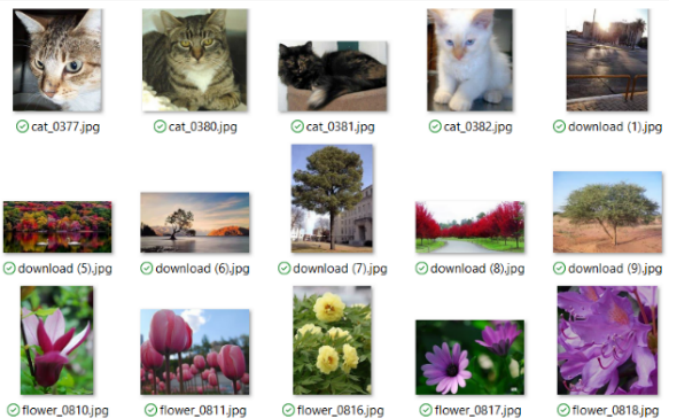
(b) Non-human dataset.

Figure 7: Samples of the dataset.

1700 images used as dataset, where 70% for training, 15% for testing, and 15% for validation. Figure 7 shows a sample of the dataset that includes (a) human dataset, (b) non-human dataset. The dataset is sourced from [30-34]. The sample of these two types has been chosen to make the model able to differentiate better between people in crowds and other elements. Another consideration has been taken is that dataset contains different crowds in different places and locations to train the model more precisely.

5. Implementation and Discussion

After defining the main parts of the proposed CubeSat design system along with the main structure of the testbed, this section highlights simulation predictions and practical measurements, respectively.

5.1. Simulation Predictions

The role of this subsection is to summarize and analyse simulation results of the proposed system in a way that will yield maximum insight and help with decision-making when implementing the model practically. So, a simulation work of the proposed CubeSat system has been discussed from two angles:

a) Communication
b) AI accuracy

5.1.1. Communication Predictions

The simulation has considered 5G multiple-input and multiple-output (MIMO) antenna to enhance diversity performance of the channel capacity, and therefore boost the reliability of wireless communication via the CubeSat. Such a consideration would not only contribute effectively to a last-mile connectivity, but also helps in reducing power consumption. Simulations have been done using Satellite Communications Simulation Toolbox in MATLAB. This subsection provides a description and interpretation of the simulation predictions based on the 2U CubeSat structure.

Figure 8 illustrates the predicted results of the PL, RSS, SINR, and T via the PL propagation model at CubeSat's altitude of 400km, where neither absorbing obstacles nor reflecting surfaces are considered. The PL predicted result, where this parameter is seen as a crucial factor to monitor channel model performance and footprint range. The obtained PL are below the maximum permissible, which is 157dB. Clearly, PL increases with distance.

The RSS predicted result is mathematically depends on PL, so both predicted results appear comparable characteristics. Obtaining RSS help in approximating the coverage range, so wireless signals get weaker as the receiver moves away from the transmitter (the CubeSat in our case). The produced RSS were within the acceptable range and below the threshold, which is 140dBm. Boosting the RSS requires tunning of different parameters like transmission power to be increased. Yet, this might reduce flight time, so compromise should be applied. The SNR predicted result demonstrates a vital parameter that seen as a wireless link quality indicator. The SNR value is ranging between upper and lower bounds, where above values are viewed as wasted transmitter power, while lower ones are considered undesirable [35-38].

The predicted result of T considers as a vibrant parameter for livestreaming and/or HD multimedia transmission. Predicted result achieved high level of T that ranges around 70Mb/s at altitude of 400km, where there is a negative correlation with distance increase. Another observation is that using 5G MIMO antenna with its diversity capacities has helped in enhancing the throughput predictions.
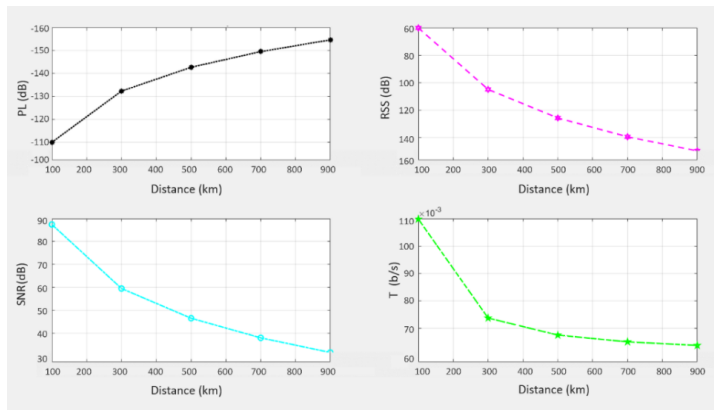
Figure 8: Link budget parameters of simulating the CubeSat.

Overall, the simulated propagation models and their generated predicted results of the full range of link budget parameters has been carried out at to monitor system performance, network planning and coverage to achieve perfect reception of the FSPL propagation model. Since this model is heavily depends on a Line of Sight (LoS) connectivity when calculating the link budgets, thus, it experiences less effect of shadowing and reflections, which in turn leads to wider coverage footprint. Unsurprisingly, reasonable results of link budget parameters would help in bridging wireless communication links between the CubeSat and GCC, ground users, as well as wireless to the cloud for storage and analysis in an efficient and timely manner [39-43].

5.1.2. AI Accuracy Predictions

The proposed AI framework trained with dataset contains 2000 different images that been sourced from [44-46]. The dataset was divided as dataset 70% training, 15% testing, 15% validation. The simulation conducted using Python in visual studio code software. Mean Sequard Error (MSE), Confusion matrix for classification, and overall accuracy are the main performance indicators that used to evaluate the proposed AI model. The proposed AI framework trained into two stages:

First stage of training aims to focus on making the model differentiate between images that contain people or not using the HOG algorithm. Where after training, the accuracy reached 95% as Figure 9 shows.

Second stage of training aims to focus on crowd management, where it divides any crowd into three situations with a different colour represent each one: Normal, Medium, and Dangerous, as Table 2 shows. The number of people is adjustable and considered here for simplicity. Thus, an interface that developed by Anaconda3 specifically QT Designer tool software to show the result of via a detected image, so the interface shows the situation and them a suitable decision can be made.
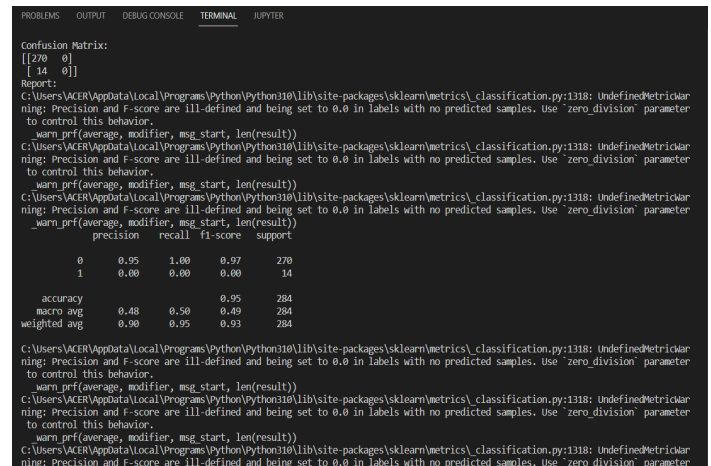
Figure 9: MSE accuracy of the trained AI model.
Table 2: Three situations of crowd management.

Situation	Means	Action
Normal Situation	People < 15	Watch only – no action is needed
Medium Situation	People 15-35	Warning: a crowd began to form
Dangerous Situation	People > 35	Alarm: take actions

5.2. Practical Measurement and Implementation

This subsection presents the experimental results when implementing the proposed system. Where results are presented from two perspectives: Communication; then AI Accuracy, respectively. The launch of our CubeSat cannot be attained using a rocket since this need long logistics with national authorities. So instead, a trial launch of our CubeSat has been done with a tethered balloon that inflated with helium gas and anchored to the ground with a polyethylene rope. This simulates the aerial space environment with more control of the CubeSat platform. Before the launch, the weather forecast has been checked to ensure stability of both the CubeSat and the tethered balloon; hence, better connectivity and high multimedia resolution.

Figure 10 illustrators the implementation of the proposed CubeSat with it all payload components at 15m altitude. To check crowd management performance, some people have been gathered to check different crowding scenarios. Two communication software were utilized in this implementation: Acrylic, and Netspot. The first software uses 5G Wi-Fi Module, which is a complete set of Wi-Fi to diagnose the Wi-Fi performance including Wi-Fi coverage, security analysis and networks. The second software is used to collect all the details about the surrounding Wi-Fi networks and presents the wireless data as an interactive table. This allows to troubleshoot and improve your network coverage, capacity, performance, access point configurations, signal level, interference, noise, and many others.

Results from communication perspective are shown in Figures 11 and 12, where they present communication performance indicators of the proposed CubeSat to 5G Wi-Fi ground station at 15m altitude. Figure 11 shows the RSS and signal coverage levels using the Acrylic tool. The obtained RSS shows a reasonable average -75 dBm, where wireless signals get weaker as the receiver moves away from the CubeSat. It is worth to mention that RSS depends on PL, so both results appear comparable characteristics. Obtaining RSS help in approximating the coverage range, and strength. Figure 12 shows SNR is seen as a wireless link quality indicator. The obtained SNR result floats around 56 dB, which is a desirable value and viewed as acceptable level of power consumption.

Figure 10: implementation of the proposed CubeSat with it all payload components.
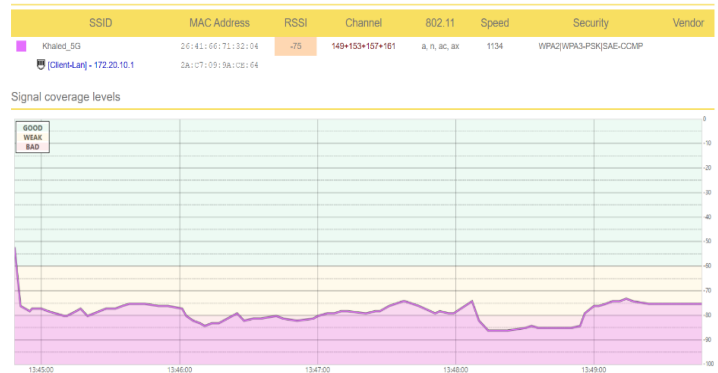
Figure 11: RSS and signal coverage levels of the proposed system using Acrylic tool.
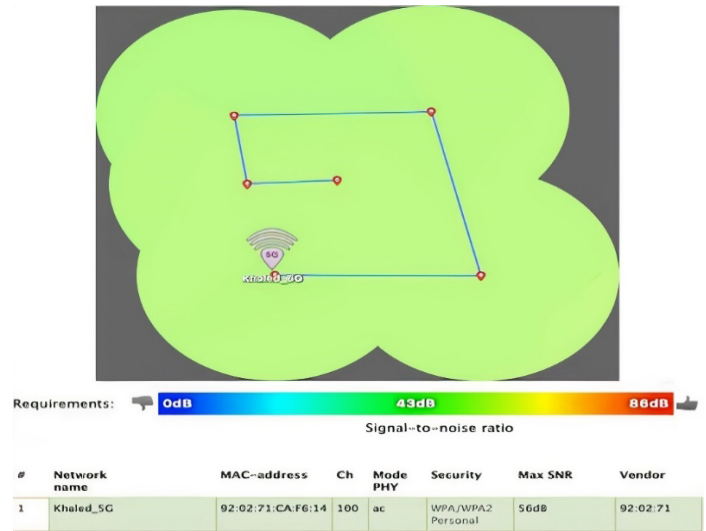
Figure 12: Signal & Noise of the proposed system using NetSopt tool.

Results from the AI framework performance perspective are presented in Figure 13 where it shows three crowd situations with a different colour represent each one. These three different situations have been evaluated from an altitude of 15m above the ground where the CubeSat locates. The first situation is being represented in green, which is normal status, so watch only – no action is needed. The second situation is yellow, which means a briefed action is needed. The third situation is red, which means dangerous, and actions must be taken. Where actions can be done by admin, and/or can be pre-defined ones, so the platform (CubeSat in our scenario) can act without the admin intervention (e.g., automatic opening or closing doors, directing people to alternative routes).

To note, the proposed AI framework includes the HOG technology, which enables tracking and detecting the places of people as dots to monitor the crowds. This has been completed with an efficient timeframe that does not exceed 4 seconds. Overall, all these three different situations have performed well based on the thresholds that have been assigned for each one. Another observed point is that the proposed AI framework deal with crowds as dots, which means it can count the number heads and send emergency alerts if needs be.
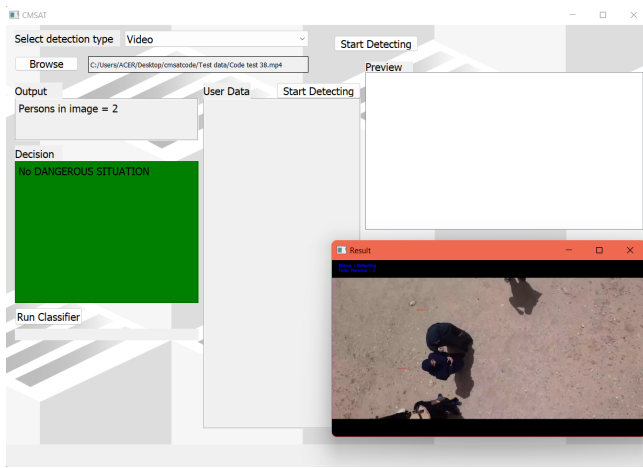
(a) Normal situation
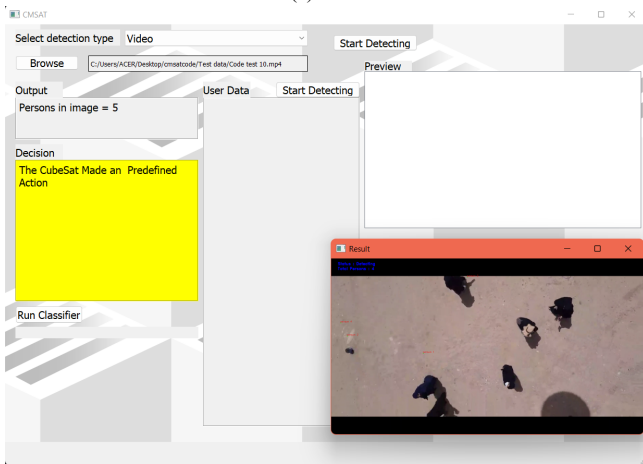
(b) Medium Situation
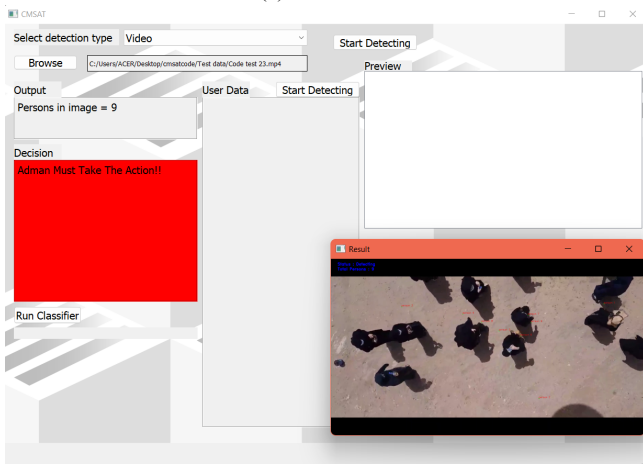
(c) Dangerous Situation

Figure 13: Three situations of crowd management using the proposed AI framework

Figure 14 shows that the crowds' health status has direct link to crowd management. Hence, when crowds' health status is good, that means no sequences happen that may affect the crowd management, as Figure 14 shows. On the other hand, in case of a health status of an individual inside the crowd is above the threshold (e.g., high temperature) the CubeSat take actions to manage the crowd correctly, which in turn can save lives. An example of this case, when the CubeSat locates the effected individual inside the crowd, send a notification to paramedics to provide the proper healthcare, besides if the CubeSat get linked to electronic doors to implement the decision to open and close the doors so that the congestion does not reach the stage of danger.

For sake of validation, a comparison graphic is shown in Figure 15 between the proposed system in relation to existing ones. Where it compares between to the MSE against signal to noise ratio (SNR). The average evaluation of the MSE at 1×10^{-5} MSE shows that the proposed system is better than the other ones, where SNR is 12dB; While FCN and CNN recorded 21dB and 13.5dB, respectively. Clearly, the obtained value of the proposed system indicates 5% to 40% of an enhancement degree.
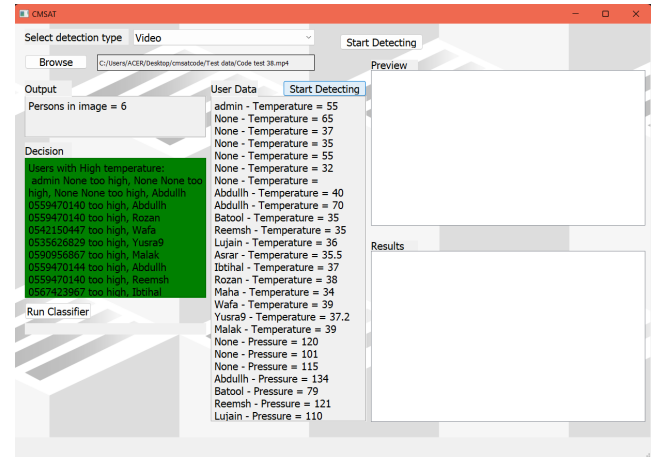
Figure 14: Crowds' health status.
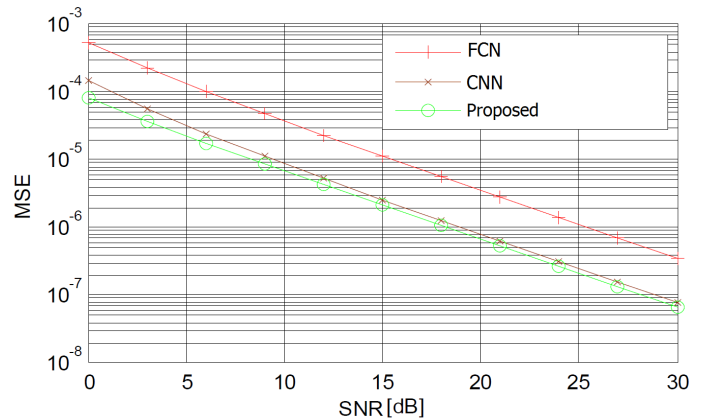
Figure 15: Crowds' health status.

6. Conclusion and Future Work

To produce and organize a successful massive event, it requires set of procedures and planning to allow the crowds move in harmony and order. Therefore, developing an advanced system plays an important role in analysing the movement features of the crowds in crowded events and alerting about an ensuing stampede. To have such a system could reduce human intervention, help in ensuring security and safety of individuals and manage crowded areas by taking the necessary decisions in an efficient and intelligent manners effort. This paper aims to develop to create a CubeSat vehicle that contains an integrated with AI framework to manage crowds a short-term, large-scale events.

Both software and hardware capabilities have been considered in this work to monitor and evaluate various performance indicators of the proposed system. Preliminary results are shown the effectiveness of the proposed CubeSat with AI framework. Work has been done to train and test the algorithm and to ensure the highest accuracy rate and the lowest error rate. Developing an intelligent aerial inspection for crowd management can extended in the future to include multilayer aerial system (e.g., drone, balloon) for more heterogenous capability. Additionally, full deployment of these space-based vehicles and send them to space for real-life trail.

Conflict of Interest

The authors declare no conflict of interest.

Acknowledgment

References

[1] G. Castellano, C. Castiello, M. Cianciotta, C. Mencar, G. Vessio, Multi-view Convolutional Network for Crowd Counting in Drone-Captured Images, 588–603, 2020, doi:10.1007/978-3-030-66823-5_35.

[2] I.U. Zaman, A. Eltawil, O. Boyraz, "Wireless Communication Technologies in Omnidirectional CubeSat Crosslink: Feasibility Study and Performance Analysis," IEEE Journal on Miniaturization for Air and Space Systems, **2**(3), 157–166, 2021, doi:10.1109/jmass.2021.3079102.

[3] F. A. Almalki, "Comparative and QoS Performance Analysis of Terrestrial-aerial Platforms-satellites Systems for Temporary Events," International Journal of Computer Networks & Communications, **11**(6), 111–133, 2019, doi:10.5121/ijcnc.2019.11607.

[4] S.A. Alhusayni, S.K. Alsuwat, S.H. Altalhi, F.A. Almalki, H.S. Alzahrani, "Experimental Study of a Tethered Balloon Using 5G Antenna to Enhance Internet Connectivity BT - Intelligent Computing," in: Arai, K., ed., Springer International Publishing, Cham: 649–663, 2021.

[5] F.A. Almalki, B.O. Soufiene, "Modifying Hata-Davidson Propagation Model for Remote Sensing in Complex Environments Using a Multifactional Drone," Sensors, **22**(5), 1786, 2022, doi:10.3390/s22051786.

[6] C. Essid, C. Abdelhamid, F.A. Almalki, O. Ali, H. Sakli, "New MIMO Antenna with Filtration for the Future Multiuser Systems in Satellite Communications," Wireless Communications and Mobile Computing, 2022, 1–12, 2022, doi:10.1155/2022/1040333.

[7] F.A. Almalki, A.A. Albraikan, B.O. Soufiene, O. Ali, "Utilizing Artificial Intelligence and Lotus Effect in an Emerging Intelligent Drone for Persevering Solar Panel Efficiency," Wireless Communications and Mobile Computing, 2022, 1–12, 2022, doi:10.1155/2022/7741535.

[8] F.A. Almalki, S.H. Alsamhi, M.C. Angelides, Internet of X-Enabled Intelligent Unmanned Aerial Vehicles Security for Hyper-connected Societies, Springer Nature Singapore, Singapore: 75–100, 2022, doi:10.1007/978-981-19-1960-2_5.

[9] F.A. Almalki, M. Aljohani, M. Algethami, B.O. Soufiene, "Incorporating Drone and AI to Empower Smart Journalism via Optimizing a Propagation Model," Sustainability, **14**(7), 3758, 2022, doi:10.3390/su14073758.

[10] M. Yamin, A.M. Basahel, A.A. Abi Sen, "Managing Crowds with Wireless and Mobile Technologies," Wireless Communications and Mobile Computing, 2018, 1–15, 2018, doi:10.1155/2018/7361597.

[11] I. Karamouzas, N. Sohre, R. Hu, S.J. Guy, "Crowd space," ACM Transactions on Graphics, **37**(6), 1–14, 2018, doi:10.1145/3272127.3275079.

[12] D. Cazzato, C. Cimarelli, J. L. Sanchez-Lopez, H. Voos, and M. Leo, "A Survey of Computer Vision Methods for 2D Object Detection from

Unmanned Aerial Vehicles," Journal of Imaging, **6**(8), 78, Aug. 2020, doi: 10.3390/jimaging6080078.

[13] S. Nag, Y. Khandelwal, S. Mittal, C.K. Mohan, A.K. Qin, "ARCN: A Real-time Attention-based Network for Crowd Counting from Drone Images," in 2021 IEEE 18th India Council International Conference (INDICON), IEEE: 1–6, 2021, doi:10.1109/INDICON52576.2021.9691659.

[14] A. Al-Sheary and A. Almagbile, "Crowd Monitoring System Using Unmanned Aerial Vehicle (UAV)," Journal of Civil Engineering and Architecture, **11**(11), Nov. 2017, doi: 10.17265/1934-7359/2017.11.004.

[15] S. Yadav, P. Gulia, N.S. Gill, J.M. Chatterjee, "A Real-Time Crowd Monitoring and Management System for Social Distance Classification and Healthcare Using Deep Learning," Journal of Healthcare Engineering, 2022, 1–11, 2022, doi:10.1155/2022/2130172.

[16] S.S.A. Abbas, P.O. Jayaprakash, M. Anitha, X.V. Jaini, "Crowd detection and management using cascade classifier on ARMv8 and OpenCV-Python," in 2017 International Conference on Innovations in Information, Embedded and Communication Systems (ICIIECS), IEEE: 1–6, 2017, doi:10.1109/ICIIECS.2017.8275988.

[17] O. Elharrouss, N. Almaadeed, K. Abualsaud, A. Al-Ali, A. Mohamed, T. Khattab, S. Al-Maadeed, "Drone-SCNet: Scaled Cascade Network for Crowd Counting on Drone Images," IEEE Transactions on Aerospace and Electronic Systems, **57**(6), 3988–4001, 2021, doi:10.1109/TAES.2021.3087821.

[18] B. Ptak, D. Pieczyński, M. Piechocki, M. Kraft, "On-Board Crowd Counting and Density Estimation Using Low Altitude Unmanned Aerial Vehicles—Looking beyond Beating the Benchmark," Remote Sensing, 14(10), 2288, 2022, doi:10.3390/rs14102288.

[19] A.M. Al-Shaery, S.S. Alshehri, N.S. Farooqi, M.O. Khozium, "In-Depth Survey to Detect, Monitor and Manage Crowd," IEEE Access, 8, 209008–209019, 2020, doi:10.1109/ACCESS.2020.3038334.

[20] M.S. Saidon, W.A. Mustafa, V.R. Rajasalavam, W. Khairunizam, "Automatic People Counting System Using Aerial Image Captured by Drone for Event Management BT - Intelligent Manufacturing and Mechatronics," in: Bahari, M. S., Harun, A., Zainal Abidin, Z., Hamidon, R., and Zakaria, S., eds., Springer Singapore, Singapore: 51–65, 2021, doi: 10.1007/978-981-16-0866-7_4

[21] R.S. de Moraes, E.P. de Freitas, "Multi-UAV Based Crowd Monitoring System," IEEE Transactions on Aerospace and Electronic Systems, 56(2), 1332–1345, 2020, doi:10.1109/TAES.2019.2952420.

[22] D. Vallejo, J.J. Castro-Schez, C. Glez-Morcillo, J. Albusac, "Multi-agent architecture for information retrieval and intelligent monitoring by UAVs in known environments affected by catastrophes," Engineering Applications of Artificial Intelligence, **87**, 103243, 2020, doi:10.1016/j.engappai.2019.103243.

[23] B. Sirmacek, P. Reinartz, "AUTOMATIC CROWD ANALYSIS FROM VERY HIGH RESOLUTION SATELLITE IMAGES," The International Archives of the Photogrammetry, Remote Sensing and Spatial Information Sciences, XXXVIII-3/, 221–226, 2013, doi:10.5194/isprsarchives-XXXVIII-3-W22-221-2011.

[24] F.A. Almalki, A.A. Alotaibi, M.C. Angelides, "Coupling multifunction drones with AI in the fight against the coronavirus pandemic," Computing, 104(5), 1033–1059, 2022, doi:10.1007/s00607-021-01022-9.

[25] N.-D. Nguyen, D.-H. Bui, X.-T. Tran, "A Novel Hardware Architecture for Human Detection using HOG-SVM Co-Optimization," in 2019 IEEE Asia Pacific Conference on Circuits and Systems (APCCAS), IEEE: 33–36, 2019, doi:10.1109/APCCAS47518.2019.8953123.

[26] F.A. Almalki, M.C. Angelides, "Autonomous flying IoT: A synergy of machine learning, digital elevation, and 3D structure change detection," Computer Communications, **190**, 154–165, 2022, doi:10.1016/j.comcom.2022.03.022.

[27] OpenCV Open Source Computer Vision 4.6.0-dev, docs.opencv.org. [Online]. Available: https://docs.opencv.org/4.x/d7/dbd/group__imgproc.html

[28] K.S. Alqarni, F.A. Almalki, B.O. Soufiene, O. Ali, F. Albalwy, "Authenticated Wireless Links between a Drone and Sensors Using a Blockchain: Case of Smart Farming," Wireless Communications and Mobile Computing, 2022, 1–13, 2022, doi:10.1155/2022/4389729.

[29] F.A. Almalki, M.C. Angelides, "An enhanced design of a 5G MIMO antenna for fixed wireless aerial access," Cluster Computing, 25(3), 1591–1606,

2022, doi:10.1007/s10586-021-03318-z.

[30] Segmented nature, Kaggle.com, 2021 to 2022. [Online]. Available: kaggle datasets download -d lprdosmil/segmented-nature.

[31] Cat and Dog, Kaggle.com, 2018. [Online]. Available: kaggle datasets download -d tongpython/cat-and-dog.

[32] Animal Faces, Kaggle.com, 2020. [Online]. Available: kaggle datasets download -d andrewmvd/animal-faces.

[33] Crowd Counting, Kaggle.com, 2018. [Online]. Available: kaggle datasets download -d fmena14/crowd-counting.

[34] Human Crowd Dataset, Kaggle.com, 2021 to 2022. [Online]. Available: kaggle datasets download -d hilongnguyn/human-crowd-dataset.

[35] S.N. Chaudhri, N.S. Rajput, S.H. Alsamhi, A. V Shvetsov, F.A. Almalki, "Zero-Padding and Spatial Augmentation-Based Gas Sensor Node Optimization Approach in Resource-Constrained 6G-IoT Paradigm," Sensors, **22**(8), 3039, 2022, doi:10.3390/s22083039.

[36] S.H. Alsamhi, F.A. Almalki, H. AL-Dois, A. V Shvetsov, M.S. Ansari, A. Hawbani, S.K. Gupta, B. Lee, "Multi-Drone Edge Intelligence and SAR Smart Wearable Devices for Emergency Communication," Wireless Communications and Mobile Computing, 2021, 1–12, 2021, doi:10.1155/2021/6710074.

[37] F.A. Almalki, S.H. Alsamhi, R. Sahal, J. Hassan, A. Hawbani, N.S. Rajput, A. Saif, J. Morgan, J. Breslin, "Green IoT for Eco-Friendly and Sustainable Smart Cities: Future Directions and Opportunities," Mobile Networks and Applications, 2021, doi:10.1007/s11036-021-01790-w.

[38] S.H. Alsamhi, F.A. Almalki, O. Ma, M.S. Ansari, M.C. Angelides, "Correction to: Performance optimization of tethered balloon technology for public safety and emergency communications," Telecommunication Systems, 72(1), 155–155, 2019, doi:10.1007/s11235-019-00589-1.

[39] F.A. Almalki, "Utilizing Drone for Food Quality and Safety Detection using Wireless Sensors," in 2020 IEEE 3rd International Conference on Information Communication and Signal Processing (ICICSP), IEEE: 405–412, 2020, doi:10.1109/ICICSP50920.2020.9232046.

[40] S.H. Alsamhi, M.S. Ansari, O. Ma, F. Almalki, S.K. Gupta, "Tethered Balloon Technology in Design Solutions for Rescue and Relief Team Emergency Communication Services," Disaster Medicine and Public Health Preparedness, 13(02), 203–210, 2019, doi:10.1017/dmp.2018.19.

[41] F.A. Almalki, M.C. Angelides, "A machine learning approach to evolving an optimal propagation model for last mile connectivity using low altitude platforms," Computer Communications, 142–143, 9–33, 2019, doi:https://doi.org/10.1016/j.comcom.2019.04.001.

[42] S.H. Alsamhi, O. Ma, M.S. Ansari, F.A. Almalki, "Survey on Collaborative Smart Drones and Internet of Things for Improving Smartness of Smart Cities," IEEE Access, **7**, 128125–128152, 2019, doi:10.1109/ACCESS.2019.2934998.

[43] F.A. Almalki, M.C. Angelides, "Propagation modelling and performance assessment of aerial platforms deployed during emergencies," in 2017 12th International Conference for Internet Technology and Secured Transactions (ICITST), IEEE: 238–243, 2017, doi:10.23919/ICITST.2017.8356391.

[44] ShanghaiTech With People Density Map, Kaggle.com, 2019. [Online]. Available: kaggle datasets download -d tthien/shanghaitech-with-people-density-map.

[45] F.A. Almalki, S. Ben Othman, "Predicting Joint Effects on CubeSats to Enhance Internet of Things in GCC Region Using Artificial Neural Network," Mobile Information Systems, 2021, 1–16, 2021, doi:10.1155/2021/1827155.

[46] S.H. Alsamhi, F.A. Almalki, F. Afghah, A. Hawbani, A. V Shvetsov, B. Lee, H. Song, "Drones' Edge Intelligence Over Smart Environments in B5G: Blockchain and Federated Learning Synergy," IEEE Transactions on Green Communications and Networking, **6**(1), 295–312, 2022, doi:10.1109/TGCN.2021.3132561.

Extended Buffer-referred Prefetching to Leverage Prefetch Coverage

Jinhyun So[*], Mi Lu

Texas A & M University, Department of Electrical & Computer Engineering, College Station, TX 77843, US

A R T I C L E   I N F O

A B S T R A C T

This paper is an extension of the work originally presented in the 26th International Conference on Automation and Computing. This study regarding hardware prefetching aims at concealing cache misses, leading to maximizing the performance of modern processors. This paper leverages prefetch coverage improvement as a way to achieve the goal. Original work proposes two different storage buffers to enhance prefetch coverage; block offset buffer and block address buffer. The block offset buffer updates its contents with the offsets of a cache block accessed, while the block address buffer contains the address of a cache block prefetch-issued. The offset buffer is utilized to speculate a local optimum offset per page. The offset buffer is proposed to adopt multiple lengths of delta history in observing offset patterns from completely trained table. This paper advances to employ incompletely trained table as well, while in other prefetching methods including original work, only completely trained candidates are utilized. Furthermore, we construct the table on the fly. Rather than using only completely built tables, we offer utilizing and updating table concurrently. This paper also proposes a refined metric from existing prefetch accuracy metric, to measure net contribution of a prefetcher. Compared to the original work, we have 2.5% and 3.8% IPC speedup increment with single- and 4-core configuration, respectively, in SPEC CPU 2006. In SPEC CPU 2017, our work achieves 4.5% and 5.5% IPC speedup improvement with single- and 4-core configuration, respectively, over the original work. Our work outperforms the 2nd best prefetcher, PPF, by 2.9% and 2.7% IPC speedup with single- and 4-core configuration, respectively, in SPEC CPU 2006. In SPEC CPU 2017, our work surpasses both Berti by 1% and SPP by 2.1% IPC speedup with 4-core configuration in SPEC CPU 2017.

1   Introduction

IN [1], the author necessitates the implementation of memory hierarchy, which attempts to greatly shorten the average memory access time due to huge performance gap between the processor execution speed and memory latency. The execution speed of the processor has significantly increased while memory has pursued higher densities that causes increased memory latency. The enormous gap has been increasing due to the different objectives in developing the processor and memory. Hierarchy of cache memory has been introduced to reduce the performance gap by improving average memory access time, depending on two kinds of memory reference locality; temporal and spatial locality. However, the cache memory is still limited in reducing the gap with a trade-off between its capacity and the speed of cache hierarchy levels. That is, the cache levels closer to the cores are smaller size but have shorter latency. On the contrary, the cache levels farther apart from cores are of larger size but have longer latency. So, prefetching

has been proposed as an effective technique that can bridge the performance gap by proactively fetching data ahead of processor's request into the cache closer to the cores. This paper proposes an effective technique in terms of prefetch coverage.

Prefetching is a mechanism that comprehends the memory access pattern of the program, and speculatively predicts and issues memory addresses ahead of the program's access to them. Hardware prefetching is to employ a standalone hardware that is dedicated to the prefetching. That is, hardware prefetcher predicts the future access to a memory data based on the observed access pattern of memory addresses in the past. Then, the prefetcher requests the data from low level of the memory hierarchy and stores it into a higher level cache close to the processor. Thus, by prefetching data, the prefetcher helps prevent cache misses due to the future access to the data, hiding long latency of low level cache access.

The objective of hardware prefetching is to proactively continue to fetch useful cache blocks from low level cache throughout run time based on memory access patterns. Usually, the algorithm

---

of a hardware prefetcher observes the past memory access patterns, predicts a future memory data access, and issues the address of the data. The patterns of a past memory access can be found based on the presumption of the existence of spatial and temporal locality of memory accesses.

In this paper, we propose an extended work of one of state-of-art prefetcher [2] with effective techniques maximizing prefetch coverage[1] at a moderate cost of prefetch accuracy. The contributions of this paper are categorized into the following three parts.

1.1 Efficient use of hardware storage

Following two buffers are employed for prefetching; one is block offset buffer and the other one is block address buffer to store the offset of a block and the address of prefetched block, respectively, in a FIFO manner. The offset buffer provides a reduction of hardware overhead by generating virtual tables[2] for prefetching instead of real table. The offsets of cache blocks are stored in the tables virtually generated whenever they are needed; storing the original offsets and generating the virtual tables can save hardware overhead by 45%[3] in terms of total hardware overhead.

1.2 Maximizing prefetch coverage

We propose following techniques for maximizing prefetch coverage from the two buffers as an offset prefetching: We use the history of a delta in multiple lengths to find diverse access patterns through access history. We mine access patterns from completely trained (virtual) table. Besides, they are also mined from incompletely trained (virtual) table.[4] Access patterns from the incompletely trained table are utilized until the table's training is completed. After the training is finished, access patterns from the completely trained table are used. Moreover, we also utilize an on-the-fly table that is on-going in building its entries. Taking advantage of the access patterns in the table under construction, prefetching can start as soon as possible even though there are few access patterns when new page is accessed for the first time. Moreover, to expand the opportunity in exploiting access patterns, we advance to make a use of entries of other table built for different pages. Especially, by referencing access patterns from the preceding pages, currently accessed page can have more diversified access patterns.

1.3 Better accuracy metric

We propose a modified metric in measuring prefetch accuracy by excluding the undetermined prefetches in existing metric. We name the metric as "accuracy ratio", which is the ratio of number of useful prefetches to the sum of number of useful prefetches and number of useless prefetches. The denominator of the existing metric is total number of prefetches which contains the undetermined prefetches in it. So, we construct denominator only with a deter-

mined portion, useful prefetches and useless prefetches, in order to well reflect prefetch accuracy.

2 Background

One of the early proposed hardware prefetching techniques is the simplest sequential prefetching, next line prefetching [3]. The next line prefetching is to prefetch a cache line that follows immediately the miss of the cache line. More advanced prefetching methods employ a prediction table by means of detecting memory access patterns. The table is used to record memory access history and identify its pattern. Also, a prefetching method is proposed for constant stride access pattern that refers to a sequence of memory accesses in which the distance of consecutive accesses is constant [4, 5]. The constant stride pattern also appears in pointer-based data structures [6].

In [7, 8], the author is proposed to find the most likely next address for currently accessed addresses by representing probabilistic correlation between accessed addresses with Markov model. This method needs not only a large storage to store the addresses into a table but it also requires high computational cost to calculate the correlation. Furthermore, Markov prefetching has stale data problem in the table.

Global history buffer (GHB) [9] as a FIFO manner is proposed to reduce a storage overhead as well as to solve a stale data problem. GHB holds recent miss addresses in the FIFO buffer and chains the same miss addresses in the buffer. Following the chain, deltas[5] are computed and adjacent deltas form a pair used as a prefetch key.[6]

Recent prefetching methods adopt a learning system since these mechanisms are possible to give a feedback of varying accuracy and coverage, depending on workloads [10]–[12]. In [12], the author dynamically adjusts prefetching aggressiveness in both positive and negative ways through a feedback system, to achieve better performance and bandwidth-efficiency.

Signature Path Prefetcher (SPP) [13] uses confidence value to adjust the length of a signature path to strike a balance between accuracy and coverage. SPP speculatively predicts memory access patterns, based on a 12-bit signature that represents a sequence of memory access. The 12-bit signature is calculated in the fashion of combining consecutive strides between adjacent accessed cache lines. The signature and a subsequent stride form a pair, used as a prefetching key and a prefetch prediction, respectively.

Perceptron-based Prefetch Filtering (PPF) [14] proposes an additional filter layer enhancing SPP as a way to increase prefetch coverage. PPF is a filter that uses a hased perceptron model to evaluate the usefulness of each prefetch generated by SPP, in order to reach better coverage. The perceptron model uses several features such as physical address, cache line, and page address, etc. to train PPF layer.

Recently, many offset prefetching descendants [11, 15, 16, 19]

---

[1] Prefetch coverage means the number of memory access patterns that are detected by prefetches. The coverage will be discussed in Sec. 2

[2] Virtual table refers an actually generated table for prefetching but it merely needs temporary hardware storage instead of permanent one

[3] Hardware overhead will be discussed in Sec. 4

[4] Incompletely trained table indicates a table of which the training period is in progress.

[5] Delta is a value of address difference between two adjacent addresses

[6] Each prefetch key has a corresponding prefetch prediction. Different prefetch keys may make different predictions.

have been proposed after Sandbox prefetching (SP)[20] was proposed. SP attempts to find a block offset that gives high performance. The offset is chosen from a set, named sandbox, of pre-selected offset candidates, based on calculated accuracy score of each offset candidate during run-time. Best-offset prefetching (BOP) [11] adds timeliness consideration to SP in order to pursue timely prefetching. BOP tests pre-selected offsets with arrived prefetch-requested block to figure out which offsets fit better in terms of latency of the arrival of prefetched block; BOP checks if the base address of previously prefetched block are equal to currently accessed block's address minus offset. If the equality is satisfied, the score for offset will increase. Otherwise, the score will decrease.

In [15], the author attempts better timely prefetching by calculating best offset page-by-page as compared to BOP's global best offset. The offset is calculated by recording access timing of each cache line in terms of the number of cycles. The measured cycles are referred to decide the proper latency of two arbitrary accessed cache lines in the same page. If there are cache lines accessed within the chosen latency, Berti uses burst mode for them.

Instruction Pointer Classifier based Prefetching (IPCP) [17] proposes two cache level, L1 and L2, prefetching at the same time with multiple instruction pointers to speculate different access patterns and cover a wide spectrum of access patterns. IPCP classifies instruction pointers into constant stride, complex stride, and stream. IPCP suggests different prefetching methods based on the type of instruction pointer.

In [18], the author introduces a reinforcement learning algorithm of prefetching to evaluate prefetch quality, pursuing system-aware prefetching. Observing the current memory bandwidth usage, Pythia intends to obtain highly accurate, timely prefetching by correlating program context information such as cache line address, program counter value, etc. to prefetch decision.

2.1 Useful and Useless prefetch

Usefulness of a prefetch is determined by whether a prefetched block is accessed by a program or not. In implementation, a prefetch bit of a block is employed to evaluate the usefulness of the prefetch. The prefetch bit is set when a prefetched block is inserted into cache memory. Then, it is unset when the block is accessed by the program. If the prefetch bit of a prefetched block is unset within the time that the block is evicted, corresponding prefetch will be regarded as a useful prefetch. In other words, the useful prefetch fetches a block that is accessed in the near future so the access occurs before the block is evicted. With the access, the useful prefetch results in eliminating a cache miss. On the contrary, if the prefetch bit remains set, corresponding prefetch will be considered as a useless prefetch. That is, useless prefetch fetches a block that is evicted with no access to it. So, the prefetch wastes cache space and memory bandwidth.

2.2 Temporal and Spatial Locality

Locality is that a program exhibits a tendency to reference the same data accessed recently or a data located closely to the recently accessed data. The principle of temporal locality is that recently ac-

cessed memory addresses by a program are likely to be accessed again in the near future.[21] The principle of spatial locality is that other nearby memory addresses have a likelihood of being referenced if a memory address is referenced. For example, sequential prefetching takes advantage of spatial locality; the simplest sequential prefetching scheme is to prefetch next cache block, one block lookahead of current access block[3].

2.3 Physical page contiguity

An address translation is an essential mechanism that maps a virtual address into a physical address to support virtual memory for modern processors. The translation is page-based operation so each virtual page corresponds to a physical page. The transfer between the two different address space can be a challenge to a hardware prefetcher since the translation can separate two contiguous virtual addresses into two distant addresses in physical address space. Hardware prefetcher has no knowledge of the translation since it is located at the side of a cache [4, 11, 22, 23]. So, prefetching should stop if prefetched data crosses over a page boundary of reference address.

Sequence: A, A+1, A+3, A+4, A+6, A+7, A+9, A+10, A+12, A+13, A+15, A+16, A+18, ...
   Delta: +1 +2 +1 +2 +1 +2 +1 +2 +1 +2 +1 +2
(a) Original sequence and delta pattern

Sequence: A, A+1, A+3, A+4, (A+6), A+7, A+9, (A+10), A+12, A+13, (A+15), A+16, A+18, ...
   Delta: +1 +2 +1 +3 +2 +3 +1 +3 +2
(b) Changed sequence and delta pattern
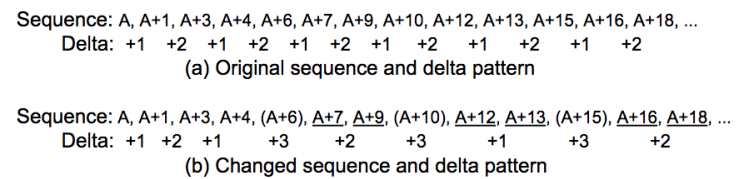
Delta Pattern Table	
Delta(prefetch key)	Delta Prediction
1	2
2	1

Figure 1: Effect of Prefetching on Miss Address Stream

2.4 Miss addresses and Prefetch hit

Miss addresses have been used for prefetching as a reference of memory access history. The miss addresses can be affected by prefetching; some of cache misses can be removed by useful prefetches. That is, correct prefetching based on miss addresses in the past changes the subsequent miss addresses, resulting in incorrect prefetching unless the prefetching reflects the change in the miss addresses.

Figure 1 is an example that shows the change in a miss address stream by prefetching. We ignore access latency for simplicity. We start with how to construct the Delta Pattern Table from the stream, and then explain about how a prediction from the table changes the miss address stream.

The original sequence shown in Figure 1a starts with a base address of A and shows a Delta pattern of 1 and 2, alternatively. The Delta Pattern Table shown in Figure 1c is constructed based on the Deltas observed in the sequence shown in Figure 1a. It is indexed by Delta (prefetch key) 1 and 2 accordingly. For each Delta, the Delta Prediction is entered. For example, from A to A+1, the table stores Delta 1. The next address is from A+1 to A+3 between

which the Delta is 2, so the table stores in entry Delta Prediction 2. In the sequence, Delta 1 is followed by Delta 2. For the table lookup, the entry of Delta with value 1 will find in the corresponding entry, Delta Prediction, a value 2. For example, address A+6 can be predicted from address A+4 by the Delta Pattern Table since the Delta of 1 observed from A+3 to A+4 is matched with the Delta (prefetch key) in the first entry in the table. So, its corresponding Delta Prediction is 2 so the table predicts address A+6 by adding 2 to address A+4. Then, the address A+6 is changed to be a hit address (the parenthesis with A+6 shown in Figure 1b indicates a hit address); the A+6 is no longer used as a reference. Therefore, the Delta, +2 (circled in Figure 1a), is not observed in Figure 1b. Due to the missing Delta, next incoming address A+7 cannot be predicted by the table. Furthermore, next incoming address A+9 cannot be predicted since the observed delta between A+4 and A+7 is 3 that does not match with any Delta (prefetch key) in the table. Likewise, correct prediction of address A+10 disturbs next two incoming addresses, A+12 and A+13, to be predicted by the Delta Pattern Table. In Figure 1b, underlined addresses indicates such addresses.

Reconstruction of the pattern table could be proposed as a solution to above issue due to the changed miss address stream. However, the update of the table cannot be effective in reflecting the miss address patterns since the original sequence of the memory access does not hold the new delta value, 3, in this example sequence. Therefore, it is important to keep prefetch hit addresses to identify patterns from miss address stream. Also, it is necessary to record which address has been prefetched by a prefetcher.
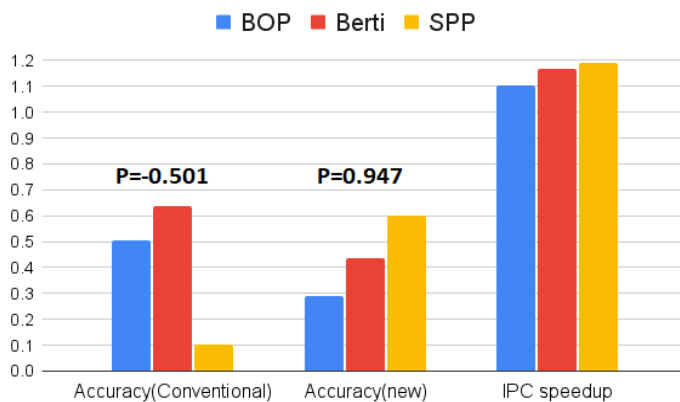
Figure 2: Pearson's Coefficient

2.5 *Evaluation Methodology*

There are two metrics to evaluate the performance of prefetching; prefetch accuracy and prefetch coverage. Prefetch accuracy measures a prefetcher in that how accurately the prefetcher predicts which memory addresses will be accessed in the future; on the other hand, prefetch coverage measures a prefetcher in that how diverse access patterns the prefetcher is capable of detecting against variations of the access patterns.

The accuracy and coverage has a relationship of inherent trade-off between them. For example, next line prefetcher can make a

prediction for simple access pattern having a stride of 1 with a high accuracy but has a limited scope in coverage, meaning that the prefetcher cannot generate diverse predictions other than the stride of 1. On the other hand, if a prefetcher wants to achieve a wide scope in coverage, it should sacrifice its accuracy as a cost. This is, for a wide scope in coverage, a prefetcher should consider a wide change in simple to complex access patterns. So, regarding the broad variation on all the patterns would be more likely to lead a prefetcher to an inaccurate prediction. The imprecise prediction results in useless cache blocks to be fetched so that cache space can be wasted as well as cache pollution and memory bandwidth consumption can increase. Consequently, the inaccuracy of a prefetcher degrades the system performance.

We propose a refined metric for prefetch accuracy in order to make the accuracy metric more relevant to IPC speedup performance. Existing accuracy metric is the ratio of the number of useful prefetches to the total number of issued prefetches[12]. The numerator, the number of useful prefetches, in the metric is directly proportional to the IPC speedup performance since useful prefetches hides cache miss latency. However, the denominator, total number of issued prefetches, shows low correlation to IPC speedup performance. The total number of issued prefetches counts all the prefetches that are issued during only the "current" IPC speedup measure period. Actually, the IPC speedup measured in the current measure period can be affected by the prefetches issued in the "past"(before current) measure period. During the current measure period, the hit(or miss) of the prefetch issued in the past period increases(or decreases) IPC speedup. In other words, the total number of issued prefetches does not count the prefetches that were issued in the past period which, however, impacts the currently measured IPC speedup

Another reason of the low correlation between the total number of issued prefetches and IPC speedup is that the total number of issued prefetches contains the number of prefetches that turn out to be neither useful nor useless by the end of current IPC speedup measure period. They can be determined as either hit or miss "after" the current measure period. Thereby, in the current measure period, we do not have enough information about how those prefetches affects IPC speedup. However, in the conventional metric, such prefetches constitutes a portion of the total number of issued prefetches which is inversely proportional to the IPC speedup.

The low correlation between existing prefetch accuracy metric and IPC speedup is shown in Figure 2 with Pearson's correlation coefficient of -0.501. The value close to 0 means a low correlation while the value close to +1 or -1 indicates a linear correlation. One can see that in Figure 2 the prefetcher SPP has the lowest accuracy in the conventional metric but the IPC speedup of this prefetcher shows the highest IPC speedup, compared to other two prefetchers, BOP and Berti. We run the three prefetchers, BOP, Berti, and SPP, since they show almost the same value in the other metric, called prefetch coverage, in SPEC CPU 2006 benchmark to exclude the effect of prefetch coverage on the IPC speedup. We propose the modified metric, named prefetch accuracy ratio in this paper, as shown in Equation 1.

Prefetch Accuracy Ratio

$$= \frac{\text{Number of Useful Prefetches}}{\text{Number of Useful Prefetches} + \text{Number of Useless Prefetches}} \quad (1)$$

Figure 3: Overall BRP Structure[2]

Equation 1 evaluates the accuracy of a prefetcher based on the prefetches evaluated as useful and useless during "current" measure period only. The equation directly compares the useful prefetches and useless prefetches that are detected during the "current" measure time. Therefore, the metric, prefetch accuracy ratio, can show how much the useful prefetches contribute to the performance improvement over a performance degradation from useless prefetches. For example, a prefetch accuracy ratio of 1 means that a prefetcher gives only a positive effect to the system performance by generating only useful prefetches with no useless prefetches. As shown in Figure 2, Pearson's coefficient value of 0.947 shows a high correlation between the prefetch accuracy ratio and IPC speedup, so SPP represents the highest accuracy ratio, leading to the highest IPC speedup.

Another metric, prefetch coverage, is defined as the number of useful prefetches over the number of cache misses with no prefetching; prefetch coverage is proportional to the number of useful prefetches as shown in Equation 2:

$$\text{Prefetch coverage} = \frac{\text{Number of Useful Prefetches}}{\text{Total Number of Cache Misses}} \quad (2)$$

From Equation 1 and 2, we can conclude that the number of useful prefetch can be a key factor to achieve both high accuracy and wide coverage at the same time. The number of useful prefetches would not be proportional to the prefetch accuracy since increase in the number of useful prefetches involves increase in the number of useless prefetches in general. On the other hand, the number of useful prefetches is proportional to prefetch coverage since the change in the number of useful prefetches does not affect total number of cache misses.

Based on aforementioned metrics, we evaluate existing prefetchers and our proposed prefetcher in terms of IPC[7] speedup in section 3 and 4.

3 Design

Figure 3 illustrates the overall structure of our prefetcher, BRP. Both L2 cache miss and prefetch hit addresses trains our prefetcher. BRP sends a request to fill a prefetch into either L2 cache or last-level cache (LLC); LLC is requested to be filled by the prefetch when miss status holding register (MSHR)[8] has no opening because it is full of its items.
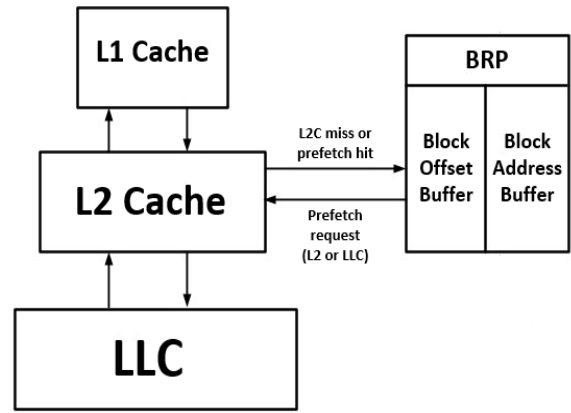
The BRP module consists of two buffers as a storage; block offset buffer and block address buffer. The block offset buffer stores an offset of each block page-by-page. On the other hand, the block address buffer stores the address of blocks that are prefetched. The two buffers updates their data, according to FIFO manner; the oldest one is evicted first and the latest one is stored as a last item in the buffer, as avoiding stale data problem. In this section, we discuss how the two buffers are employed in reaching moderate accuracy ratio while maximizing prefetch coverage. Another feature of our BRP is that it does not request a prefetch in the case that it traverses a boundary of the page to which referred data belongs as discussed in Section 2.3.
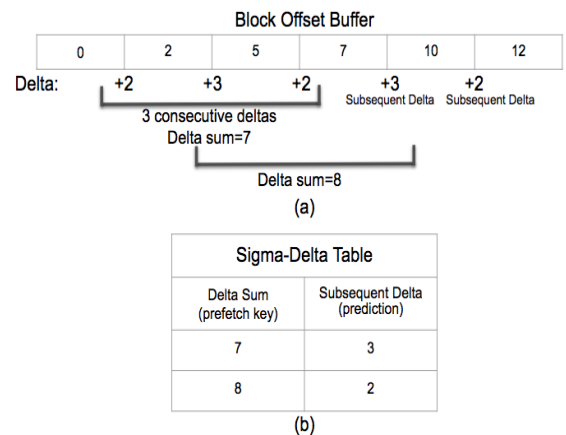
Figure 4: Example of Sigma-Delta Table generation (b) from block offset buffer (a) with delta history length of 3.

3.1 Offset Buffer

Offset buffer stores a block offset of pages that have been accessed recently. Based on the tag attached to the buffer, block offsets can be stored to a offset buffer with the same tag. That is, One of the offset buffers, of which the tag is the same as it of the page of the block accessed, collects the latest offset of the block. If a new page

---

[7]All IPCs, instruction per cycle, are computed as arithmetic average of the IPC across the benchmarks

[8]MSHR holds pending load/store accesses that refer to the missing cache

is accessed for the first time, a new tag is generated based on a base address of the page, and a new offset buffer attached to the new tag is also built, loading the offset on it. The storage capacity of the buffer is set by users. If all the buffer is fully occupied by its offsets, the buffer evicts its oldest one and stores the latest offset as a last item in it.

The purpose of collecting block offsets is to observe the pattern of deltas among offsets; the delta is the arithmetic difference between the values of two block offsets that are successively accessed in the same page. [2] suggests a table, named Sigma-Delta Table, to identify the delta pattern from delta sequence as shown in Figure 4. Delta Sum, the sum of number of consecutive deltas, is used as an index; corresponding to it is the subsequent delta, the delta coming next.

Figure 4 represents an example of how a Sigma-Delta Table is generated from an offset buffer containing block offsets of 0, 2, 5, 7, 10 and 12. The example shows a case that three consecutive deltas are added up. The generated delta sequence is 2, 3, and 2 from the offset sequence of 0, 2, 5, and 7 as shown in Figure 4a, of which the sum is 7. The next Delta is 3 (to move from offset 7 to 10). So, the sum of 7 and the subsequent delta of 3 constructs a pair as an entry of the table shown in Figure 4b. In the table, in the case that Delta Sum 7 is given, from the same row and next column under Subsequent Delta, a value of 3 is read out.

In implementation, the number of consecutive deltas is set by users with regard to hardware overhead. In fact, the Sigma-Delta Table is built as a virtual table that does not require a permanent hardware overhead. That is, all the entries in the table is derived from offsets in the buffer only when they are referenced for prefetching. Hardware overhead of the table will be discussed in Sec. 4.

Sigma-Delta Tables are built; That is, each table belongs to different delta history length. Different number of consecutive deltas are used to construct the Sigma-Delta Table. All the generated sigma-delta pattern tables are subject to being used for prefetching.

The higher prefetch coverage is achieved by the proposed method as shown in Figure 5b, compared to the method of using single delta history length shown in Figure 5a. IPC speedup shown in Figure 5a gets decreased by the coverage reduction as a single delta history length increases. Compared to the decrease, in Figure 5b, IPC speedup is sustained as more multiple lengths of delta history gets involved. This is because the multiple delta history lengths cause an increase in prefetch coverage that cancels out the IPC speedup decrement caused by accuracy ratio reduction.

Briefly, multiple delta history lengths improves prefetch coverage by generating more useful prefetches, resulting in IPC speedup improvement. Several methods will be discussed to reach further increase in prefetch coverage in the section onward.

(a) Complete trained table only (b) (Complete+Incomplete) trained table
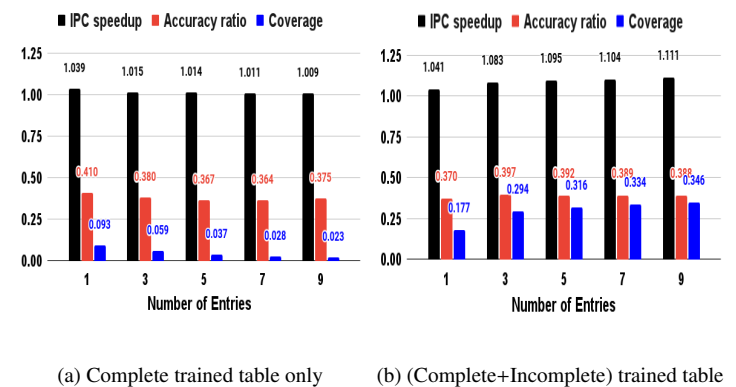
Figure 6: Completely and Incompletely Trained Table (a) complete only (b) complete+incomplete

(a) Single Delta History Length (b) Multiple Delta History Length

Figure 5: Comparison of delta history length (a) single (b) multiple

3.1.1 Multiple delta history length

As aforementioned, the Sigma-Delta Table is built by pairs of delta sum and subsequent delta which is calculated by deltas. The number of deltas used is equal to the delta history length. [2] suggests a method of using multiple delta history lengths rather than a single delta history length. So, the multiple Sigma-Delta Tables are built according to multiple delta history lengths. For example, if the maximum length of the delta history is set to be 4, four of the

3.1.2 Complete/Incomplete training

After a Sigma-Delta Table fills all of its entries, training session is started to evaluate the validity of the patterns that the table stores. Surely, we use a Sigma-Delta Table of which the training session is completely finished with its validity for prefetching. In addition, we propose to utilize the Sigma-Delta Table for prefetching while its training session is in progress in order to avoid no prefetch issued during the training session. Adopting the table with on-going training helps increase the scope of prefetch coverage. Figure 6b reflects the effect of the incompletely trained table additionally used, as compared to Figure 6a. Figure 6b exhibits a coverage increase by 2 to 15 times, compared to the coverage shown in Figure 6a, a result from using the completely trained table only. The increased coverage is due to the increase in the number of useful prefetches that a table under its training generates.

Furthermore, in Figure 6a, coverage decreases as the number of entries increases since the increase in the number of entries in the table requires longer training session. As a result, no prefetching duration increases, resulting in decrease in useful prefetches. However, Figure 6b shows the effectiveness of our proposed method

especially when more entries are employed. This is because the increased duration of training session for the case of more entries makes incompletely trained tables having longer time to generate more useful prefetches.

According to our design intention, the IPC speedup increases by 1 to 11% due to the increased coverage; IPC speedup is 1.04 to 1.11 in Figure 6b versus 1.03 to 1.01 in Figure 6a. The proposed method is more effective in the case of greater number of entries in a Sigma-Delta Table. One interesting observation in Figure 6b is that the additional use of the table continuing its training provides slight increase in accuracy ratio, as compared to Figure 6a, except the case of single entry of Sigma-Delta Table; 3 to 7% increase across 3 to 9 entries and 10% decrease in single entry. Another interesting observation from Figure 6b is that the case of 3 entries exhibits better results in both accuracy ratio and coverage than the results of single entry.

Training mechanism adopted in this work is to check the validity of collected delta patterns stored in the Sigma-Delta Table. The training is to compare values of entries in the Sigma-Delta Table with subsequently accessed block offsets that update a block offset buffer; to check if the pair of delta sum and delta prediction in the entry is equal to a pair of them calculated from the updated offsets in the offset buffer. If the equality happens, the table will get a hit, so called table hit. Otherwise, the table will get a table miss.

In implementation, we employ a flag to denote whether each Sigma-Delta Table obtains a table hit or not. On the other hand, a table miss score is counted with 2-bit saturating counter. If a table reaches a maximum table miss score, 3 with the 2-bit counter, all the entries in the table will be removed and new entries will, then, be generated by more recent offsets stored in the offset buffer. After training is finished, the table attaining a table hit and having lowest table miss score is used as top priority for prefetching.
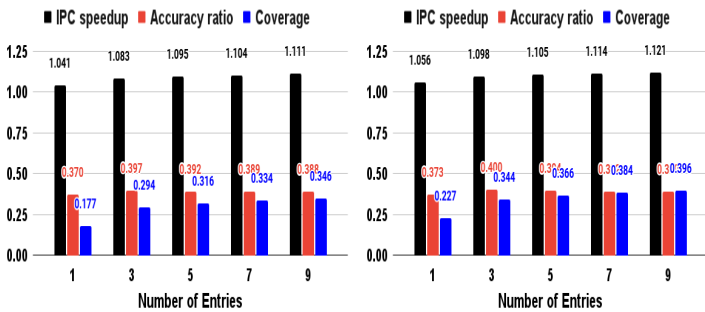
(a) Sigma-Delta Table with no on-the-fly   (b) Sigma-Delta Table with on-the-fly

Figure 7: Sigma-Delta Table usage (a) no on-the-fly (b) on-the-fly

3.1.3 On-the-fly table

We propose to use the Sigma-Delta Table on the fly to avoid no prefetching issued until the table is full of its entries. That is, we employ the table even under construction to generate a candidate of a prefetch to reach further increase in coverage. The on-the-fly table is effective in increasing coverage since it can generate a

prefetch while the table either accumulates its entries or replaces its existing entries with new entries due to reaching a maximum table miss score. Also, the table can generate prefetches sooner based on the few patterns that belong to the new page accessed for the first time. According to our design intention, the IPC speedup increases by 1.3% due to the increased coverage; IPC speedup is 1.055 to 1.126 in Figure 7b versus 1.04 to 1.11 in Figure 7a.

3.1.4 Referring to other pages

Multiple Sigma-Delta Tables are generated to figure out the offset patterns for individual page. In [2], the author proposes referring to those tables so other near pages can reference the offset patterns to issue their prefetches. In other words, each page refers to the offset pattern, the pairs of Delta Sum and a Delta, in the table that has been accessed little earlier. So, the patterns detected from both currently accessed page and earlier accessed pages are utilized for current prefetch issue. Especially, this referring method should be effective in generating diverse prefetches when the page does not have enough identified patterns due to first time access to the page, early stage of building the Sigma-Delta Table, etc.
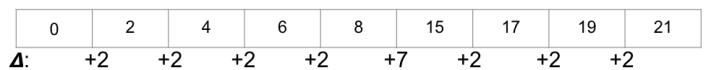
Figure 8: *libq*: Example of Spike Pattern
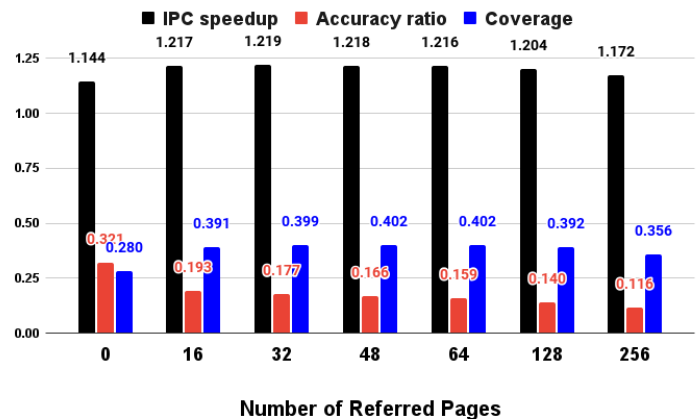
Figure 9: Number of Referred Pages Sensitivity

Furthermore, the referring mechanism gives a chance to mine performance improvement from irregular pattern. For example, spike pattern, the delta sequence with the single delta of +7, shown in Figure 8 from *leslie* benchmark is hard to be predicted due to its minority in patterns. Also, the delta spike can appear irregularly and its magnitude can be variable. Based on locality property among near pages, it is possible that preceding pages go through both the same timing and magnitude of spike pattern. So, we leverage access patterns of the preceding page in generating prefetches for subsequently accessed pages.

Obviously, there should be a cost of an initial miss in capturing the irregular pattern when the pattern shows up for the first time. With the sacrifice of the initial miss, the the pattern can be identified and referred by other near pages that may go through the same access pattern. This method is very effective to performance improvement for some benchmarks such as *calculix*, *lbm*, *leslie*, *libq*, *soplex*, etc. through simulation. In those benchmarks, some of the pages that are accessed sequentially tends to have the same offset patterns.

Compared to other prefetchers, BOP[11] is not successful in identifying the delta spike pattern since the prefetcher focuses only on globally optimal offset, using only delta value of +2 as a majority. GHB[9] could succeed in predicting the pattern as it captures two consecutive deltas as a pair, preserving the sequence of individual delta. By maintaining the delta sequence, GHB constructs pairs of two adjacent deltas such as (+2,+2), (+2,+7), and (+7,+2) that are used as a prefetch key. So, the pair, (+2,+2), is used to predict the spike delta, +7. However, in the case that the magnitude of next delta spike varies, GHB is hard to predict correct spike delta. Furthermore, GHB needs hardware storage in order to store the pairs of two deltas.

The performance improvement from referring to other pages is shown in Figure 9 with different number of referred pages. There is a 39% increase in prefetch coverage between no page referred and 16 pages referred. On the other hand, there is a 40% decrease in accuracy ratio between them. As a result, IPC speedup increases by 6%. On the other hand, coverage, accuracy ratio, and IPC speedup are almost the same among 16 to 128 referred pages. Also, referring to 256 pages degrades IPC speedup by 3.9% due to the decrease in prefetch coverage by 9.3%. Performance degradation occurs in the case that we refer many pages, which contains pages accessed in the distant past. With the observation, 32 pages are set to be referred.

pattern of the miss addresses. The paper offers a block address buffer to store the history of recent prefetch addresses. The record is used for multi-degree prefetching that indicates issuing multiple prefetchings per prefetch prediction. Additionally, the history helps filter out duplicate prefetches that are issued in the past.

As shown in Figure 10, there is an IPC speedup increase of 3.7% between no prefetch buffer and 12 prefetch buffers, because prefetch coverage increases by 76% while accuracy ratio decreases by 14%. On the other hand, compared to 12 buffers, 32 buffers shows 0.27% increase in IPC speedup. Also, there is no significant IPC speedup improvement with more than 32 buffers. The result represents that an optimal number of buffers is 32 since more than 32 buffers requires more hardware overhead with little return.

4 Performance Evaluation

We evaluate the performance of the prefetcher, BRP, with added techniques mentioned in the previous section. We compare it with other prefetchers' performance in terms of IPC speedup, accuracy ratio, and coverage, in this section.

4.1 Simulation Methodology

To evaluate BRP and other prefetchers, a subset of both the SPEC CPU 2006 benchmark[24] and 2017 benchmark[25] is used since the SPEC CPU 2006 benchmark is known as memory-intensive characteristics and SPEC CPU 2017 is developed recently. We use individual thread for a single core simulation and 4-thread mixes randomly selected from the benchmark for 4-core simulation. Simpoints [26], of which the interval is 10M instructions, are used to measure the IPC speedup. We simulate 200M instructions as a warmup and then measure the performance with the following 200M instructions. ChampSim simulator[27] is used for the evaluation. The framework of the Champsim simulator is the 3rd Data Prefetch Championship.

Table 1: Processor Configuration

Core Parameters	1-4 Cores, OoO, 4GHz, 256 entry ROB, 4-wide
Branch Predictor	16K entry bimodal, 20 cycle misprediction penalty
Private L1 Dcache	32KB, 8-way, 8 MSHRs, LRU, 4 cycles
Private L2 Cache	256KB 8-way, 16 MSHRs, LRU 8 cycles, Non-inclusive
Shared L3 (LLC)	2MB/core, 16-way, LRU 12 cycles, Non-inclusive
Main Memory	4GB, 1-2 64 bits channels, 8 ranks/channel, 8 bank/rank, 1600MT/s

Figure 10: Block Address Buffer Sensitivity

Table 1 summarizes the simulation configuration for the testing systems. The CPU is clocking at 4 GHz clock rates per core with an out-of-order scheduler. Each CPU core has its private cache; L1 and L2 cache. All the four cores shares a single L3 cache. The L1 cache is divided into instruction and data cache, of which size is 32 KB. L2 cache size is 256KB. The block size and page size of the cache is 64B and 4KB, respectively. In the single core simulation, single DRAM channel is adapted. In the 4-core simulation, two

3.2 Block Address Buffer

As discussed in Section 2.4, [2] proposes recording memory addresses that have been prefetch requested, including prefetch hit addresses. So, the access pattern can be preserved as the original

DRAM channels are adapted. Also, L1 and L2 cache contain 8 and 16 prefetch queues, respectively.

L1 and L2 cache have 8 and 16 miss MSHRs, respectively. The prefetch queue temporarily holds the block address which is requested for prefetching until it is issued. The MSHR and prefetch queue helps CPU continue to execute following instructions of a program since they store pending cache misses and prefetches. Only L2 cache access initiates the prefetcher and no prefetcher exists in other cache levels. All the prefetched data are stored into either L2 cache or L3 cache.

The performance of this work is compared with the origin work, BRP, as well as prefetchers such as SPP, PPF, BOP, and Berti, which are discussed in section 2. Those prefetchers are compared in terms of following three metrics; IPC speedup, prefetch accuracy ratio, and prefetch coverage. We use the original code of these prefetchers submitted to DPC-2 and DPC-3. We follows BRP's configuration which is set as follows: 1) Delta history length up to 3; length of 1, 2, and 3. 2) Maximum entries of 3 in sigma-delta table. 3) Block offset buffers for 512 pages. 4) Referring 32 pages. 5) 25 block address buffers.

4.2 Single Core Performance

Figure 11 shows the average IPC speedup of all the prefetchers with both SPEC 2006 and 2017 benchmark. The IPC speedup is a normalized IPC value to the IPC value of no prefetching baseline. Our work outperforms all the other prefetchers with the best average IPC speedup of 1.257 and 1.143 on SPEC CPU 2006 and 2017 benchmark, respectively, due to the widest prefetch coverage. As shown in Figure 11a, in SPEC CPU 2006 benchmark, our work exhibits 58.2%, 50.3%, 36.3%, 15.4%, and 3.5% improvement in coverage over BOP, SPP, Berti, PPF, and BRP, respectively, as our work shows the lowest accuracy ratio according to the design intention. So, our work achieves 25.7% IPC speedup improvement, which is 15.3%, 8.9%, 6.7%, 2.9%, and 2.5% more than the BOP, Berti, SPP, PPF, and BPR, respectively. Also, in SPEC CPU 2017 benchmark, as shown in Figure 11b, our work exhibits 50.5%, 47.9%, 35.6%, 16%, and 6.5% improvement in coverage over BOP, SPP, Berti, PPF, and BRP, respectively. So, our work achieves 14.3% IPC speedup improvement, which is 7.7%, 6.4%, 3.2%, 2.7%, and 4.5% more than the BOP, Berti, SPP, PPF, and BPR, respectively.

(a) SPEC 2006: IPC speedup by individual benchmark
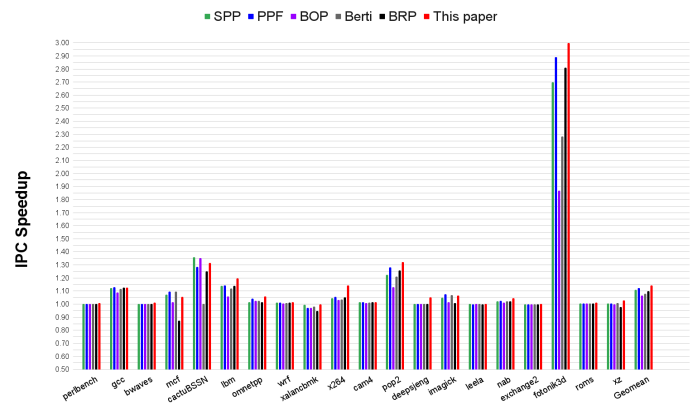
(b) SPEC 2017: IPC speedup by individual benchmark

Figure 12: IPC speedup by Benchmark

(a) SPEC 2006: The impact of prefetch accuracy ratio and coverage on IPC speedup

(b) SPEC 2017: The impact of prefetch accuracy ratio and coverage on IPC speedup

Figure 11: Single-core IPC speedup

Figure 12 represents IPC speedup by individual benchmark. In SPEC CPU 2006(Fig. 12a), our work shows significant IPC improvement from benchmarks such as *GemsFDTD*, *leslie*, *libq*, *so-*

plex, *sphinx*, *xalancbmk*, and *zeus*, as compared to no prefetching baseline. This is because our work achieves high coverage from them by generating large number of useful prefetches as shown in Figure 13a. Especially, our work achieves the best IPC speedup in 10 applications such as *calculix*, *gromacs*, *leslie*, *soplex*, etc., compared to other prefetchers. As compared to the original work, BRP, our work shows better IPC speedup across nearly all the benchmarks. For example, our work exhibits 5%, 8%, and 7% IPC speedup improvement in *leslie*, *sphinx*, and *xalancbmk*, respectively.

In SPEC CPU 2017(Fig. 12b), our work shows outstanding IPC improvement from applications such as *cactuBSSN*, *pop2*, and *fotonik3d*, as compared to no prefetching baseline. This is because our work achieves high coverage from them by generating large number of useful prefetches as shown in Figure 14a. Especially, our work achieves the highest IPC speedup in 16 out of 20 benchmarks. As compared to BRP, our work also shows better IPC speedup across nearly all the benchmarks; especially, our work exhibits 20%, 8%, and 6% IPC speedup increase in *mcf*, *x264*, and *fotonik3d*, respectively.

zeus so that we have the highest IPC speedup. For those applications, high coverage is a key to predict their patterns, which would be diverse and irregular. On the other hand, in those applications such as *gcc* and *mcf*, our work generates the largest number of useful prefetches, which brings the highest coverage on them, but our work does not reach the highest IPC speedup. This is because that the comparable accuracy ratio would be also required to achieve better IPC speedup.
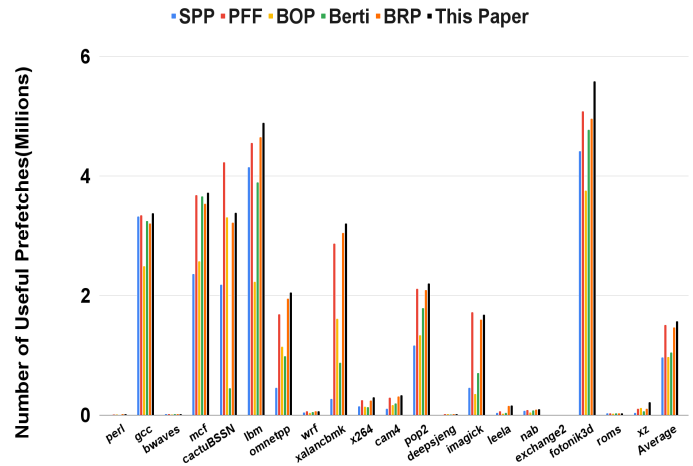
(a) SPEC CPU 2017: The number of useful prefetches by Individual Benchmark

(a) SPEC CPU 2006: The number of useful prefetches by Individual Benchmark
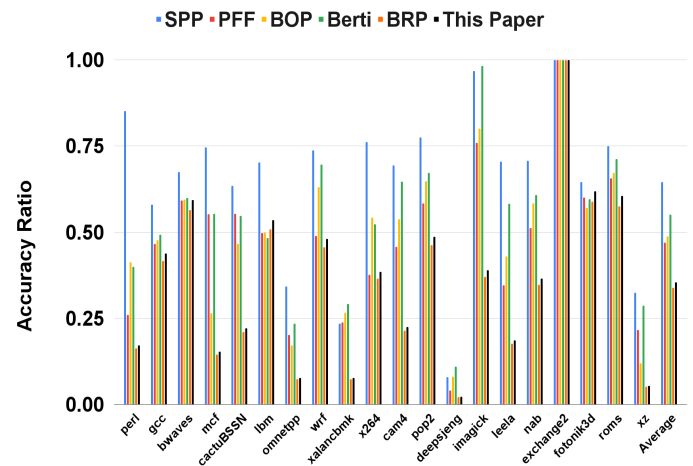
(b) SPEC CPU 2017: Accuracy Ratio by Individual Benchmark

Figure 14: Coverage and Accuracy Ratio with SPEC CPU 2017

(b) SPEC CPU 2006: Accuracy Ratio by Individual Benchmark

Figure 13: Coverage and Accuracy Ratio with SPEC CPU 2006

As shown in SPEC CPU 2006(Fig. 13a), our work generates the largest amount of useful prefetches in the applications such as *bzip2*, *calculix*, *gromacs*, *lbm*, *leslie*, *sphinx*, *xalancbmk*, and

As shown in SPEC CPU 2017(Fig. 14a), our work generates the largest amount of useful prefetches in the applications such as *lbm*, *omnetpp*, *xalancbmk*, *x264*, *pop2*, *deepsjeng*, *nab*, *fotonik3d*, and *xz* so that we have the highest IPC speedup on them, accordingly. For those applications, high coverage is a key factor to achieve the high IPC speedup because they would have diverse and irregular patterns. On the contrary, in those benchmarks such as *mcf* and *camp4*, our work does not achieve the highest IPC speedup even though the highest coverage is reached with the largest number of useful prefetches. This is because the enough accuracy ratio would be also involved.

Table 2: SPEC CPU 2006: Multi Programmed Workloads

mix0	GemsFDTD, astar, bzip2, cactusADM
mix1	calculix, gcc, gromacs, h264ref
mix2	lbm, leslie3d, mcf, soplex
mix3	sphinx, tonto, xalancbmk, zeus

Table 3: SPEC CPU 2017: Multi Programmed Workloads

mix0	perlbench, gcc, bwaves, mcf
mix1	cactuBSSN, lbm, omnetpp, wrf
mix2	xalancbmk, x264, cam4, pop2
mix3	exchange2, fontonik3d, roms, xz

(a) SPEC CPU 2006

(b) SPEC CPU 2017
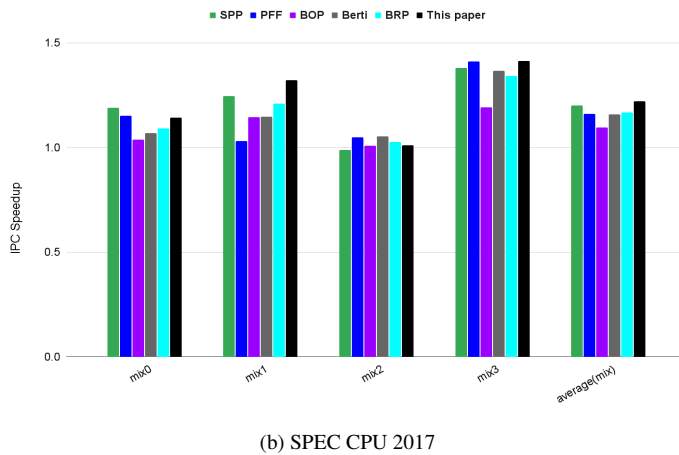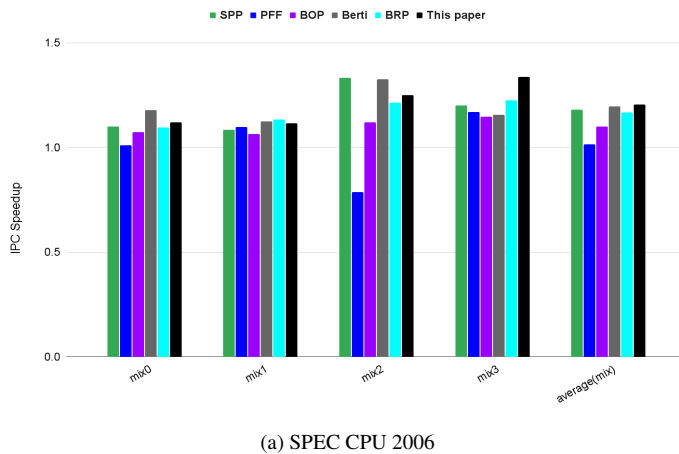
Figure 15: 4-core IPC speedup

4.3 Multi-Core Performance

We generate 4 multi-programmed mixes, each consists of 4 traces as shown in the two tables; table 2 and table 3. Each trace in the mix is assigned to a different core for the multi-core simulation.

In SPEC CPU 2006(Fig. 15a), our work accomplishes 20.6% geometric mean IPC speedup increment across 4 mix workloads, compared to no prefetching baseline. Especially, our work exhibits 33.8% IPC speedup improvement in mix3 over the baseline, since

our work is effective to appllications such as *sphinx*, *xalancbmk* and *zeus* in 4-core configuration as well. The performance improvement of our work is the best among all the prefetchers. our work surpasses the second highest one, Berti, by a 1.0% IPC speedup. Compared to single core test, in multi-core test, the IPC speedup improvement of our work over Berti reduces by 7.9% since the our work issues more prefetches than berti, throttling LLC and DRAM bandwidth.

In SPEC CPU 2017(Fig. 15b), our work accomplishes 22% geometric mean IPC speedup increase over no prefetching baseline across 4 mix workloads, which is the best performance improvement among all the prefetchers. Especially, our work shows 41.2% IPC speedup improvement in mix3 over the baseline, since our work is effective to appllications such as *fontonik3d* and *xxz* in 4-core configuration as well. Our work outperforms the second highest one, SPP, by a 2.1% IPC speedup. Compared to single core test, in multi-core test, the IPC speedup improvement of our work over SPP reduces by 1.2% since the aggressive prefetching of our work throttles LLC and DRAM bandwidth more in the multi-core configuration by generating both high number of useful and useless prefetches.

(a) SPEC CPU 2006

(b) SPEC CPU 2017
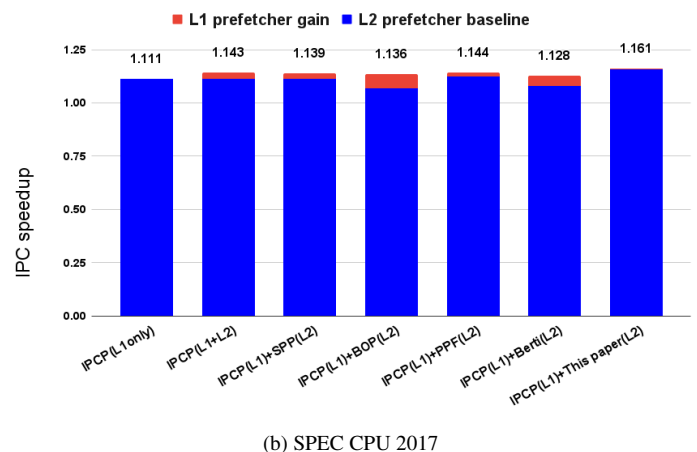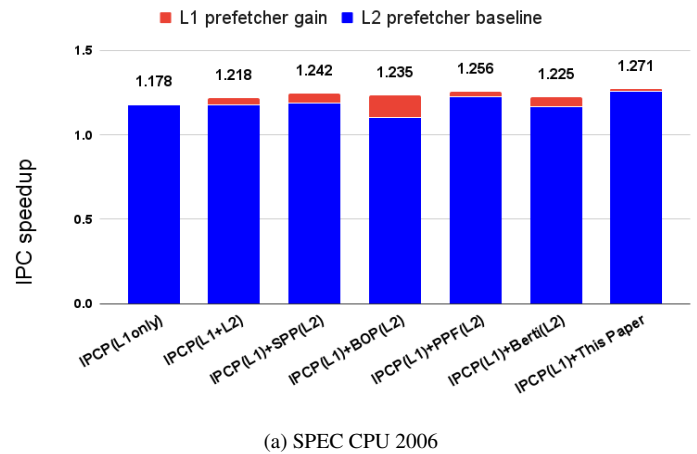
Figure 16: Single-Core: L1$ and L2$ prefetching IPC speedup

4.4 Multi-level prefetching performance

We added an L1 cache prefetcher to the test configuration to compare the performance of the prefetchers with IPCP which proposes multi-level prefetching, by an L1 prefetcher and an L2 prefetcher at the same time. We combine the IPCP L1 prefetcher with other proposed prefetchers acting as L2 prefetchers to conduct the test.

The L1 prefetcher of IPCP provides 17.8% and 11.1% IPC speedup in SPEC CPU 2006 and 2017, respectively, as compared to no prefetching. As shown in Figure 16a, our work shows the highest IPC speedup with an additional of 0.093% IPC speedup made by the L1 prefetcher in SPEC CPU 2006 benchmark; Our work outperforms the second highest, PPF, by 1.2% IPC speedup. In this test, BOP receives the maximum benefit of 0.131% IPC speedup, an increase from 1.104% to 1.235%, due to the IPCP L1 prefetcher. As shown in Figure 16b, in conjunction with the IPCP L1 prefetcher, our work also achieves the highest IPC speedup, surpassing the second highest, IPCP(L1+L2), by 0.018% in the IPC speedup. Please note, the L1 prefetcher gain here is only 0.004%, of the lowest amount.
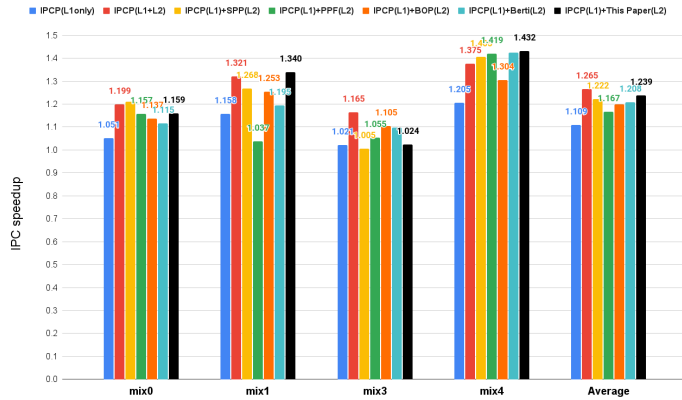
Figure 17: Multi-Core: L1$ and L2$ prefetching IPC speedup

In 4-core simulation, the two level IPCP prefetcher reached the hightest IPC speedup in SPEC CPU 2017, with 1.265 in average. As indicated in Figure 17, our work achieved the second highest performance in average, with an IPC speedup of 1.239, surpassed by the IPCP(L1+L2) only by 0.026%.

Table 4: Prefetcher Storage Overheads

Buffer-referred Prefetching(BRP)	5.512KB
Signature Path Prefetching(SPP)	5.507KB
Perceptron-Based Prefetch Filtering(PPF)	39.34KB
Best-Offset Prefetching(BOP)	1.85KB
Best-Request-Time Prefetcher(Berti)	22.1KB

4.5 Storage Overhead And Performance Contribution

The total hardware storage of our work is equal to the hardware overhead of the original work, BRP, of which the overhead is 5.512KB, with each individual component shown in Table 5. Our work does not increase the hardware overhead from the original

work. There is no extra hardware overhead required with the introduced mechanism of employing incompletely trained Sigma-Delta Tables for generating prefetch candidates. Furthermore, we utilize the original Sigma-Delta Table under construction so no additional hardware is needed. The component with the largest overhead is block offset buffer (3.32KB). The buffer stores multiple 6-bit offsets per page. Berti holds heavy hardware overhead of 22.1KB, because it pursues an increase in both prefetch coverage and accuracy at the same time. Especially, the heavy overhead of Berti is caused by adapting diverse features such as instruction pointer, recorded page table, etc. in order to ensure prefetch accuracy. As shown in Table 5, BOP has the lowest overhead since its storage contains a few cache lines that has been requested recently. However, BOP derives low performance since the storage is employed to find out global best offset value as a simple manner.

Table 5: BRP Storage Overhead

Structure	Quantity	Component	Storage
Block Offset buffer	512	Offsets(6bit), Tag(16bit), lru(9bit), burst mode(2bit), aggressiveness(2bit),	33280 bits
Sigma-delta table accessories	1536	history length(2bit), valid(1bit), miss count(2bit), hit flag(1bit)	9216 bits
Block Address buffer	25	address(64bit)	1600 bits
Total = 33280 + 9216 + 1600 = 44096 bits = 5.512KB			

With the virtual Sigma-Delta Tables, nearly 45% of hardware storage is saved against using real Sigma-Delta Tables in total storage overhead. Hardware storage is allocated for storing block offsets in the buffers but then the table is virtually generated only when they are used, instead of giving permanent hardware storage for the real tables. The block offset buffers only except its accessories occupy 2.304KB; 512 buffers exist(each for a single page), each buffer has 6 block offsets, and each offset is 6-bit long. On the other hand, when the real Sigma-Delta Table is adapted with assigned constant storage, the total hardware overhead occupies 6.912KB; 3 tables exists per page (total 512 pages), there are 3 entries per table and each entry is of 12 bits (6 bits for delta sum and the other 6 bits for delta prediction). About 67% storage is reduced in terms of constructing pattern tables for prefetching, and about 45% hardware overhead decreases in terms of total hardware overhead.

5 Conclusion

In this paper, we have shown an extended work of Buffer-referred Prefetching, achieving high performance gain with low hardware overhead. First of all, it provides techniques that increase the prefetch coverage with no additional hardware overhead, compared to the original work. With such techniques, our work helps bring

out lots of useful prefetches from Sigma-Delta Tables under construction even though the table is not complete in its training. The technique is effective to the cases that few access patterns generated due to new page access, pattern transfer within the same page, and irregular patterns. This paper also offers a refined metric, called accuracy ratio, for measuring prefetch accuracy in order to directly take into account both performance improvement and degradation from a prefetcher. Future work would be to add a perceptive filter as a replacement of the block address buffer to achieve better prefetch filtering or well-tuned aggressive prefetching. Our work accomplishes 25.7% and 20.6% IPC speedup improvement over no prefetching baseline with single- and 4-core configuration, respectively, in SPEC CPU 2006 benchmark. In SPEC CPU 2017 benchmark, our work reaches 14.3% and 22.1% IPC speedup increase over no prefetching baseline with single- and 4-core configuration, respectively. Compared to the original work, we have 2.5% and 3.8% IPC speedup increment with single- and 4-core configuration, respectively, in SPEC CPU 2006. In SPEC CPU 2017, our work achieves 4.5% and 5.5% IPC speedup improvement with single- and 4-core configuration, respectively, over the original work. Our work outperforms the 2nd best prefetcher, PPF, by 2.9% and 2.7% IPC speedup with single- and 4-core configuration, respectively, in SPEC CPU 2006. In SPEC CPU 2017, our work surpasses both Berti by 1% and SPP by 2.1% IPC speedup with 4-core configuration in SPEC CPU 2017.

References

[1] W. A. Wulf and S. A. McKee. Hitting the memory wall: implications of the obvious. SIGARCH Comput. Archit. News, **23**(1),20–24, 1995.

[2] J. So and M. Lu, Buffer-referred Data Prefetching: An Effective Approach to Coverage-Driven Prefetching, 2021 26th International Conference on Automation and Computing (ICAC), 2021, 1-6, doi: 10.23919/ICAC50006.2021.9594139.

[3] A. J. Smith. Sequential program prefetching in memory hierarchies. In IEEE Transactions on Computers, **11**, 7–21, 1978.

[4] J. W. C. Fu, J. H. Patel,and B. L. Janssens. Stride directed prefetching in scalar processors. In Wen-mei W. Hwu, editor, Proceedings of the 25th Annual International Symposium on Microarchitecture, Portland, Oregon, USA, November 1992, pages 102–110. ACM / IEEE Computer Society, 1992.

[5] J.Baer and T. Chen. An effective on-chip preloading scheme to reduce data access penalty. In Joanne L. Martin, editor, Proceedings Supercomputing '91, Albuquerque, NM, USA, November 18-22, 1991, pages 176–186. ACM, 1991.

[6] F. Dahlgren and Per Stenstroom. Effectiveness of hardware-based stride and sequential prefetching in shared-memory multiprocessors. In Proceedings of the 1st IEEE Symposium on High-Performance Computer Architecture (HPCA 1995), Raleigh, North Carolina, USA, January 22-25, 1995, 68–77. IEEE Computer Society, 1995.

[7] D. Joseph and D. Grunwald. Prefetching using markov predictors. In Proceedings of the 24th Annual International Symposium on Computer Architecture, ISCA '97, pages 252–263, New York, NY, USA, 1997. ACM.

[8] P. Pathak, M. Sarwar, and S. Sohoni. Memory prefetching using adaptive stream detection. In Proceeding of 2nd Annual Conference on Theoretical and Applied Computer Science 5 November 2010.

[9] K. J. Nesbit and J. E. Smith.Data cache prefetching using a global history buffer. In In Proceedings of the International Symposium on High-Performance Computer Architecture, 2004.

[10] I. Hur and C.Lin. Memory prefetching using adaptive stream detection. In 39th Annual IEEE/ACM International Symposium on Microarchitecture (MICRO-39 2006), 9-13 December 2006, Orlando, Florida, USA, 397–408. IEEE Computer Society, 2006.

[11] P. Michaud. Best-offset hardware prefetching. In 2016 IEEE International Symposium on High Performance Computer Architecture (HPCA), pages 469–480, 2016.

[12] S. Srinath, O. Mutlu, H. Kim, and Y. N. Patt. Feedback directed prefetching: Improving the performance and bandwidth-efficiency of hardware prefetchers. In 13st International Conference on High-Performance Computer Architecture (HPCA-13 2007), 10-14 February 2007, Phoenix, Arizona, USA, pages 63–74. IEEE Computer Society, 2007.

[13] J. Kim, S. H. Pugsley, P. Gratz, A. L. N. Reddy, C. Wilkerson, and Z. Chishti. Path confidence based lookahead prefetching. In The 49th Annual IEEE/ACM International Symposium on Microarchitecture, 1-6, 2016.

[14] E. Bhatia, G. Chacon, S. H. Pugsley, E. Teran, P. Gratz, and D. A. Jimenez. Perceptron-based prefetch filtering. In in Proceedings of the 46th International Symposium on Computer Architecture, 2019.

[15] A. Ros. Berti: A per-page best-request-time delta prefetcher. In 3rd Data Prefetching Championship, 2019.

[16] M. Shakerinava, M. Bakhshalipour, P. Lotfi-Kamran,and H. Sarbazi-Azad. Multi-lookahead offset prefetching. The Third Data Prefetching Championship, 2019.

[17] S. Pakalapati and B. Panda, Bouquet of instruction pointers: Instruction pointer classifier-based spatial hardware prefetching, 2020 ACM/IEEE 47th Annual International Symposium on Computer Architecture (ISCA), 118–131, 2020

[18] R. Bera, K. Kanellopoulos, A. Nori, T. Shahroodi, S. Subramoney, and O. Mutlu, Pythia: A customizable hardware prefetching framework using online reinforcement learning, 54th Annual IEEE/ACM International Symposium on Microarchitecture, 1121–1137, 2021

[19] D.Yadav and C. Paikara. Arsenal of hardware prefetchers. Computing Research Repository, abs/1911.10349, 2019.

[20] S. H. Pugsley, Z. Chishti, C. Wilkerson, P. F. Chuang, R. L. Scott, A. Jaleel, S.-L. Lu, K. Chow, and R. Balasubramonian. Sandbox prefetching: safe runtime evaluation of aggressive prefetchers. In 2014 IEEE International Symposium on High Performance Computer Architecture (HPCA), 2014.

[21] S. Mittal. A survey of recent prefetching techniques for processor caches. ACM Comput. Surv., 49(2):35:1–35:35, 2016.

[22] S. Somogyi, T. F. Wenisch, M. Ferdman, and B. Falsafi. Spatial memory streaming. J. Instr. Level Parallelism, 13, 2011.

[23] M. Shevgoor, S. Koladiya, R. Balasubramonian, C. Wilkerson, S. H. Pugsley, and Z. Chishti. Efficiently prefetching complex address patterns. In Milos Prvulovic, editor, Proceedings of the 48th International Symposium on Microarchitecture, MICRO 2015, Waikiki, HI, USA, December 5-9, 2015, pages 141–152. ACM, 2015.

[24] SPEC CPU 2006.https://www.spec.org/cpu2006.

[25] SPEC CPU 2017.https://www.spec.org/cpu2017.

[26] T. Sherwood, E. Perelman, G. Hamerly, and B. Calder. Automatically characterizing large scale program behavior. In Kourosh Gharachorloo and David A. Wood, editors, Proceedings of the 10th International Conference on Architectural Support for Programming Languages and Operating Systems (ASPLOS-X), San Jose, California, USA, October 5-9, 2002, pages 45–57, 2002.

[27] DPC-3.The champsim simulator. https://github.com/ChampSim/ChampSim.

ASTES

Prototype to Mitigate the Risks, Vulnerabilities and Threats of Information to Ensure Data Integrity

Segundo Moisés Toapanta Toapanta[1,*], Rodrigo Humberto Del Pozo Durango[2], Luis Enrique Mafla Gallegos[3], Eriannys Zharayth Gómez Díaz[4], Yngrid Josefina Melo Quintana[4], Joan Noheli Miranda Jimenez[5], Ma. Roció Maciel Arellano[6], José Antonio Orizaga Trejo[6]

[1]*Universidad Católica de Santiago de Guayaquil (UCSG), Guayaquil 090615, Ecuador*

[2]*Uniuersidad Estatal de Bolívar (UEB), Guaranda, Km. 3 1/2 vía San Simón, Ecuador*

[3]*Faculty of Systems Engineering, Escuela Politécnica Nacional (EPN), Quito, 17-01-2759, Ecuador*

[4]*Research Department, Instituto Tecnológico Superior Rumiñahui, Sangolquí, 171103, Ecuador*

[5]*Department of Investigation, Gestión de Tecnologías para el Mundo (GTM), Quito, N35-100, Ecuador*

[6]*Department of Information Systems (CUCEA), Universidad de Guadalajara (UDG), Guadalajara, 45100, México*

A B S T R A C T

The constant evolution of Information and Communication Technologies, Internet, access to different free software, among others; they generate problems in the management of information security in companies; to mitigate risks, vulnerabilities, and information threats, an alternative was presented considering that information security systems are the basis for decision-making at the government, strategic, tactical, and operational levels. The objective is to design a security prototype applied to business management to mitigate risks, vulnerabilities and threats to information. The deductive method and exploratory research were used for the analysis of the information. Turned out prototypes that allow mitigating risks, vulnerabilities and threats in information management for data control and integrity. It was concluded that the security prototype proposed for a commercial information system; it is security system suitable for public and private companies. In the simulation carried out, it was determined that if the number of risks and threats is high, there will be a greater probability that a problem will arise in the security of the system.

1. Introduction

Information security problems are persistent in most public and private institutions according to what the author's state in this document. To mitigate vulnerabilities, threats and information risks, they define a basic methodology based on Coras, Ebios, Magerit, Cramm, Octave, which have relevant advantages. This document is taken as a reference to continue with the investigation with the objective of presenting additional alternatives [1]. With the constant advances in technology and internet access, it has become easier to access information that is not protected, causing more frequent information security problems, putting at risk the proper management of

information, which is one of the main assets of commercial companies [2]. Guaranteeing the correct functioning of the data and the transmission of information from one user to another. The misuse, modification or unauthorized access to information, whether commercial or of any other kind, can affect the privacy or well-being of an organization, person and society. Security models based on rules and policies should be used [3]. The vulnerability is a weakness in the operating system that allows to violate the confidentiality, integrity, availability, access control in systems [4]. The existence of vulnerabilities gives way to threats, which can be external or internal. The threat assessment process is the biggest problem in information security, because the source of vulnerability and threat in an information system can be hidden until the attack begins,

which generates insufficient security controls that generate a high level of risk to the organization [5]. To minimize the availability of threats and vulnerabilities in organizations, the risk assessment process is defined, which must be carried out by an expert[6]. By information asset, we mean any good or service used so that institutions or organizations can operate and meet the objectives established in their mission and business vision[7]. Adequate information security requires that organizations determine the risks to which they are exposed, since companies that are dedicated to commercial or economic management frequently report losses due to failures and attacks on their servers. Due to the problems that arise, controls are established for the configuration of processes, hardware equipment, applications and operating systems[8]. Currently, security prototypes must be implemented that determine, analyze, evaluate and classify risks, to implement control mechanisms and prevention measures that will be implemented in the short and long term[9]. Avoiding attacks like DDoS (DDoS attacks take advantage of network capacity limits, allowing them to send multiple requests either in the form of emails with malicious files or links to web pages); Black Hat, Gray Hat, etc. taking into account four main strategies of risk treatment such as: risk avoidance, acceptance, transfer and treatment[10].

Why is it necessary to generate a security prototype to mitigate risks, vulnerabilities and threats for the control and integrity of data in business management?

To mitigate risks in information systems, to avoid large financial losses and reputational damage from misuse of technology by users of an organization.

The objective is to design a security prototype applied to business management to mitigate risks, vulnerabilities and threats to information.The deductive method is applied, exploratory research for the analysis of information related to the research topic.Turned out prototypes that allow mitigating risks, vulnerabilities and threats in information management for data control and integrity.

It is concluded that the security prototype proposed for a commercial information system; it is security system suitable for public and private companies. In the simulation carried out, it was determined that if the number of risks and threats is high, there will be a greater probability that a problem will arise in the security of the system.

2. Materials and Methods

The information from the references detailed below was used to analyze the prototypes oriented to information security in different organizations; to determine which prototype is the most suitable and optimal for security. The design of a prototype takes into account the architecture of the security infrastructure validated in different layers using elements suitable for the infrastructure.

2.1. Related Jobs

Information security is important and a priority for business management; the threats put at risk the operations

of the companies the same ones that the CIA can protect[11]. They explore the structure of knowledge, development and future trends in the area of information security; in order to provide a comprehensive review of the literature on information security risks; when incidents occur and cause serious damage to information[12]. Risk assessment processes are one of the most important factors for the development of an information system[13]. They present a comprehensive methodology for IT risk management based on globally accepted standards such as ISO 31000 and ISO/IEC 27005, which define the appropriate requirements for risk management; nevertheless[14]. The authors define those cyber threats generate risks for an organization. To quantify the risks, the differences between the risks of cyber threats and other compliance vectors are analyzed. Results determine actual and potential losses from cyber threats[15]. Absolute reliance on control, monitoring and surveillance mechanisms should be considered risky. They prove to be a useful instrument to indicate the importance of successful information system measures and to reveal weaknesses[16]. A security assessment management database can be used that can store and manage all available versions and translations of the ISO / IEC 15408 and ISO / IEC 18045 series, related documents and all intermediate products in a secure and convenient way[17]. Flexible AC transmission system devices and associated data exchange cybersecurity are necessary for the control of wide-area power networks. They verify published cybergraphic which can significantly hide data sharing[18]. This article focused on the vulnerability of software and the internet and the accumulation of raw information in big data, which are serious problems in computing[19]. The authors proposed the technological capacity they have to mitigate internal threats in computer security systems, with a systematic review of mixed methods[20]. The COBIT guide identifies the level of maturity in ICT management; that allows project management to be more effective and efficient in different areas such as: Information security, software development, etc.[21]. The Chinese Wall security model regulates the binary relationship "Conflict of interest", considers the CIR to be an equivalence relationship, using the Chinese Wall policy as a security model. A security model is a design that promotes consistent and effective mechanisms for defining and implementing controls[22].

In the table 1. Contains the best-known security models. These security models are used to guarantee the confidentiality of the information, because the security models are more precise and detailed, and are used as guidelines to create and evaluate systems.

Table 1: Security Models

Model	Concept	Ref.
Clark-Wilson model	Seeks the security of data integrity, managing the modification of the access control mechanism.	[23]

	This model is based on the classification of applications establishing an order.	
Chinese Wall Model	Oriented to guarantee confidentiality by reducing conflicts of interest, implementing security policies.	[22]
	It consists of access policies implemented on the data, whether applications or databases, preventing the same person from entering two databases of different companies that are in the same business area.	
Bell-LaPadula Model	They focus on the roles of users and objects. They consider arrays to be able to provide access.	[24]
	In this model, it must be checked if the user has authorized access in the assigned security mode, based on their role or work profile.	

The authors conclude that cloud computing is an emerging technology that uses the Honey Bee. Which is similar to cloud access control mechanism [24]. The authors determined an area of cognitive cryptography that is connected with universal cryptosystems, to link cognitive computational models with classical cryptographic procedures. With the combination of cryptographic techniques and cognitive approaches define cognitive cryptography [25]. The authors conclude that security solutions are centralized in the scalability of IoT environments. The IoT ecosystem can include DLT as a layer so that more devices can benefit from its features[26]. Define that cloud computing can provide various server attributes to process information in the cloud, which makes Smart-meter a suitable device [27], OCTAVE Allegro is a guide used by banks for information system risk management. The implementation of risk management focuses on the threats and vulnerabilities of each critical asset it owns, the bank can discover the risks, threats, vulnerabilities with their respective impact on each critical asset [28].

Table 2: Types of Risks

Type	Concept	Ref.
Business Risk	It comes from the effect of uncertainty that arises from the organization's business objectives.	[28]
Investment Risk	It comes from the effect of the uncertainty of the investment objectives of the organization.	[28]
Quality Risk	It comes from the effect of uncertainty towards the quality objectives of the organization.	[28]
Operational risk	It comes from the effect of uncertainty of the operational objectives of the organization.	[28]
Technological Risk	It comes from the effect of uncertainty of the technological objectives of the organization.	[28]
Financial risk	It comes from the effect of uncertainty of the financial objectives of the organization.	[28]

In the table 2. Contains the evaluation of the concepts of the different types of risks implemented in relation to the reviewed articles.

They conclude that an artificial intelligent network is a new way of manipulating an electrical network, which combines information and communication technology; in order to provide more effective and efficient services [29]. The authors determined that large parts of an organization's critical data currently reside in databases, making them an attractive target for cyber attackers. At the same time, cyber attackers increased their skill set leading to sophisticated attacks in the recent past [30]. The authors concluded that real threats can be detected through the assessment of risk values using the expression approach based on quantitative values. Assessment of risk values on qualitative scales is easier for practical implementation [31]. They concluded that a cloud model is qualitative and uses three digital features. They determine that the use of an uncertainty transformation model reflects the theories of confounding and randomness [32]. This article focused on demonstrating the value that a formal risk assessment technique such as EBIOS can have when considering the use of the smart grid, with respect to security solutions [33]. The authors proposed the use of cyber risk insurance products to reduce losses from cyber risk, showing future financial rewards and the benefits of obtaining cyber insurance [34]. The authors propose a risk management model based on the OCTAVE-S methodology and the ISO/IEC 27005 standard. The model has a quantitative approach that calculates the residual risks based on the effectiveness of the assigned controls [35]. They propose a CMMI model that allows the identification of gaps or weaknesses to establish continuous improvement processes [36]. The authors propose that companies, in order to optimize ICT management, should consider a customized standard prototype or model to save resources; considering methodologies and standards such as: Cobit, ITIL, Coso, ISO 27001, among others [37]. They propose a MePRiSIA security prototype, designed as a risk prevention methodology; considering the human factor in all phases [38]. This article focuses on comparing different methods for measuring and evaluating security risks, highlighting the importance of risk management assessment standards and methods [39]. The authors mention that when administrative processes are affected by cyberattacks, the management of public organizations has serious problems in decision-making [40]. The authors proposed several types of methods that allow to optimize processes and flow

in information security; considering as a starting point the definition of vulnerabilities and risk analysis [41]. The authors analyze the practical architecture of vulnerability information exchange for security risk analysis in the automotive sector [42]. The authors propose a model to determine the threats and to be able to calculate the probability of the attacks and the costs of the attacker. They determine that the logs delivered by the IoTRiskAnalyzer program help IoT specialists to define proper system configurations [43]. The authors proposed an ISRM process model that complements information security risk management processes. The ISRM model was adapted from Endsley's situational awareness model [44]. The authors proposed a quantitative method for risk assessment, using formal mathematical distributions with historical data to improve granularity, and make the assessment more realistic with respect to cyber-physical systems in computer systems that use cloud services in general. This methodology supports risks to associated asset-based processes running in the cloud [45]. The authors proposed a quantitative model, so that the interested parties that use the system quantify the risks they assume with the security of their assets regarding the threats, so that the organizations make adequate security decisions. It also allows defining average costs for the problems that are generated by the failure of the systems [46]. The authors propose a semantically enhanced model for security management; classifying the security threats identified by the IDS. The system allows management decisions regarding the selection of security controls to obtain a maximum return on investment in security [47]. They propose a risk assessment method to assess quantitative risk, using fuzzy rules to assess vulnerabilities and uncertainty [48]. They propose a software system with a web application format, to identify, evaluate and neutralize the risks of information and other systems from anywhere [49]. The CORAS method allows the evaluation of security risks for hierarchical processes that can be considered as the basis for the analysis in this investigation [50]. The ISO31000:2009 that allows enterprise risk management (ERM), to improve security management in companies at the corporate level [51].

2.2. Methods

The related methods are detailed below: Cyber Attacks List, Methodologies and security prototype models, Security Prototype Comparative Table, Risk Matrix and Methodology to generate results.

2.2.1. Cyber Attacks List

Computer attacks are considered as malicious attempts or acts by a group of people seeking to identify vulnerabilities with the aim of causing damage or problems to a computer system or network, they occur as a result of some vulnerability or weakness in software or hardware.

Table 3: Cyber Attacks List

Attack	Process	Ref.
Two	Disables access to a system, an application or a machine, in order to block the service for which it is intended; This attack is known as HTTP DoS.	[52]
Cyber espionage	It involves the attacker obtaining confidential information from a user without permission.	[30]
Black hat	They are based on tricking search engines to obtain sensitive information from vulnerable users for malicious purposes.	[53]
Gray hat	Use artificial links with natural patterns, to be able to access in an unnoticed way without using massive or abusive methods.	[40]
Unauthorized access	It consists of unauthorized access to an information system, to obtain access codes or passwords.	[54]

Table 3. described the different attacks that can affect the different information systems.

2.2.2. Methodologies and security prototype models

The methodologies allow a correct analysis of information security risks, which allow creating security prototypes to mitigate security problems.

2.2.3. MAGERIT

It is a public methodology that belongs to the Ministry of Public Administrations and was developed by the Superior Council of Electronic Administration, determining the threats to generate control and improve the protection of assets. Magerit, supports organizations to carry out the evaluation, audit ertification or accreditation process. The only disadvantage of this methodology is that its implementation is expensive, since the assets are converted into economic values, it uses both a qualitative and quantitative model to perform the risk assessment[45].
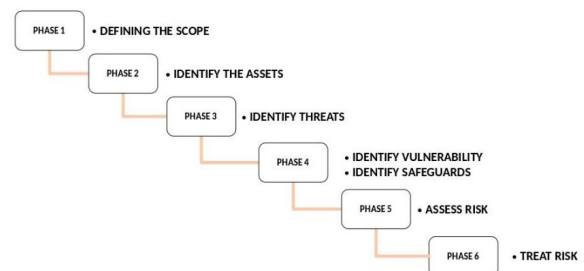
Figure 1: Phases of the Magerit process

In the Figure 1. Each phase a set of equations can be found that will allow to find the value of the estimated annual loss or residual risk. Given the MAGERIT methodology, the following equations can be proposed to find the residual risk value, taking into account the assets that the organization owns, threats and risks that may arise.

$$I = A * D(\%) \tag{1}$$
$$R = I * FA \tag{2}$$
$$RR = [R * (1 - S(\%))] * [0.1 * (1 - ES(\%))] \tag{3}$$

where:

I = Impact
A = Asset Value
D (%) = Percentage of Degradation of a Threat
R = Risk
FA = Estimated annual frequency
S (%) = Percentage of Effectiveness of Safeguards on Impact
ES (%) = Percentage of Effectiveness of Safeguards over frequency
RR = Residual Risk

2.2.4. OCTAVE

This prototype has an account of the operational risks regarding internal users. Identifies and assesses critical assets and/or threats to the organization, tracks risks, and establishes key components and technical vulnerabilities causing the risks[45].

Table 4: Advantages and Disadvantages of the OCTAVE methodology

Advantage	Disadvantages	Reference
Modification of the information system in the early stages of development.	Its administration is difficult.	[45]
It allows the developer to know the requirements of the users and / or clients.	It can only be implemented in medium and small institutions.	[45]
Initial changes during project development are less expensive.	Unforeseen changes arise that slowly down the advance of the prototype.	[45]
Includes risk analysis and management processes in organizations.	Deep technical knowledge is required for its implementation.	[45]

Table 4 shows the advantages and disadvantages of the OCTAVE methodology.

In the figure 2. Shows the operational process of the OCTAVE model, which has three phases. Phase 1 deals with the vision of the organization, in this phase the elements are specified as assets; vulnerabilities; threats and security requirements. This phase is responsible for arranging and organizing the entire plan to be executed in the risk analysis. Phase 2: Technological vision, in this phase the key

components and technical vulnerabilities of information systems are analyzed. Phase 3: planning of measures and risk reduction, this phase is responsible for classifying the risk assessment, strategies, risk weighting and the risk reduction network plan, in this phase an appropriate strategy must be sought to risk management.
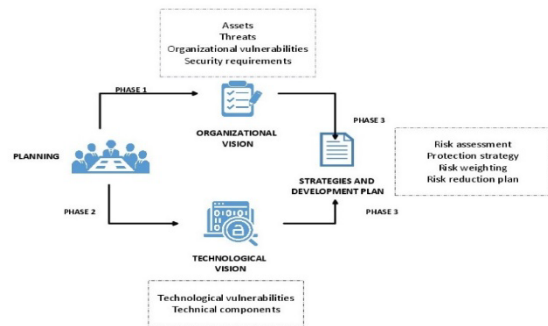
Figure 2. OCTAVE prototype process

A risk assessment is very particular to each organization and it would not be appropriate to develop assessments based on results obtained from other organizations.

2.2.5. MEHARI

It is a methodology that provides a set of tools that allow a quantitative and qualitative risk analysis to be carried out, it is designed to unite the processes of business risk analysis and future risk analysis. Its analysis is carried out based on three criteria [36]:

- Confidentiality
- Integrity
- Availability

This methodology depends on the use of a database of information and computerized techniques to carry out the evaluation of each one of the risks

2.2.6. CRAMM

It is a method of analysis and risk control that allows identifying, measuring and minimizing the attacks to which organizations are exposed. It performs a qualitative and quantitative risk analysis, known as a mixed methodology, in order to have a clear vision of the threats, based on a matrix where the rows represent the assets and the columns the risks that could affect the integrity, availability and confidentiality of the information. CRAMM is a simpler and lower cost methodology compared to the MAGERI methodology[3]. To carry out a risk analysis with the CRAMM methodology, elements such as:

- Goods
- Vulnerabilities
- Risks
- Threats
- Countermeasures
- Implementation
- Audit

2.2.7. EBIOS

Its acronym stands for Expression of Needs and Identification of Security Objects; it is a methodology created by DCSSI (Central Directorate for Information Systems Security). Its objective is to facilitate communication with the internal and external clients of an organization in order to contribute to the process of managing information systems security risks. It allows organizations to have a better knowledge of their assets, identifying the threats and vulnerabilities to which they are exposed[3].

2.2.8. PMI

The PMI prototype is easy to use, because it allows an easy understanding of the information processes, which helps to improve the flaws or vulnerabilities that the information systems have when applying the plans and policies established previously. This prototype is compatible with the Magerit methodology and the Octave prototype, to achieve optimum system performance, successfully controlling the risks that may exist in the information systems for commercial management.

2.2.9. COBIT 2019

It is a reference framework that facilitates the use of information technologies from an investment approach, based on industry standards and best practices. management to provide measures, indicators and processes to take full advantage of the control and implementation of information technologies[2][21].

2.2.10. Risk Matrix

The risk matrix allows us to evaluate the levels of information integrity risks, where a combination of key elements must be used, which are: risks, types of cyber-attacks, impacts and probability of occurrence.

To evaluate the impact of risks and the probability of their occurrence, we use values that are in a range of 1 to 5

Table 6: Impact of risks

Impact level	Punctuation
Mild	1
Low	2
Means, medium	3
High	4
Extreme	5

Table 6 contains the risk impact classification. The chances of a risk occurring are:

Table 7. Probability of Occurrence

Occurrences	Punctuation
Unlikely	1
Probable	2
Very likely	3
Highly probable	4
Extremely Likely	5

Table 7 shows the probability values of certain risks occurring. The criteria of importance of a risk are:

Table 8: Importance of risks

Importance level	Punctuation
Mild	1-5
Low	6-10
Normal	11-15
High	16-20
Critical	20-25

Table 8 contains the index of importance that the risks may have. To find the risk value in our matrix, we are going to use the following formula:

$$VR = PO x I \qquad (4)$$

where:

PO = Probability of Occurrence (number of times that event would   the impact they may have, both qualitative and quantitative).

Table 9. Risk Matrix

Risks	Probability of: Occurrence (PO)	Impact (I)	Risk Value (VR)
Extraction, modification and destruction of confidential information.	4	5	twenty
Inappropriate use of information.	5	5	25
Red Hat and / or Gray Hat attacks.	4	4	16
Information leakage	3	3	9
Network crash	4	3	12
Organization server failures.	3	4	12
Computer virus attacks.	4	4	16
DDoS attacks	4	3	12
Inadequate logical access controls.	two	one	two

In the table 9. The values that are in a range of 1 to 5, do not indicate a security problem. If the values are from 6 to 10, they generate a low importance level. All the values that are in the range of 20 to 25 are considered extremely high risks, to which we must find a solution immediately. It is clarified that the values used in table 9 come from the simulation of a case study of a company X that can be disclosed according to research ethics.

2.3. Methodology to generate results

2.3.1.   Conceptual model

For a security prototype, the following information was taken from the references: phases to obtain the value of a

risk [32], risk categories[6], analysis of the development of security strategies and plans[8].

2.3.2. Security prototype

To propose a security prototype, the following references were taken into account[11],[14]. With these references, a three-phase prototype was analyzed and made to mitigate attacks in business management.

2.3.4. Algorithms

To define the algorithms, the following references were taken into account:[9], [35], [38], [39], [49]. In the algorithm of the security prototype, we demonstrate the phases that are required and carry out the verification by means of a formula that the algorithm is stable.

2.3.4.1. Formula

A formula was determined that with the number of risks and the mitigation capacity of the system can mitigate the attacks, based on tables of security levels in order to optimize the proposed prototype.

2.3.4.2. Simulations

The simulations demonstrated the probability of a security problem occurring and the risk assessment, given five different scenarios, which were defined by the authors.

3. Results

This research attempts to reduce attacks on the cloud that occur daily to steal data from different users.

The following results were obtained:

- Conceptual model to protect business data from attacks.
- Security prototype to mitigate vulnerabilities, threats and risks of information for the control and integration of data in commercial management.
- Algorithm in the flowchart to protect data from risks and attacks.
- Formula to find the probability of a simulation and security problem occurring.
- Risk Analysis and Evaluation

The limitations of the results obtained is that they can be applied in small and medium-sized commercial companies. The results obtained are not oriented at the corporate level. The main advantage is that the five results can be applied independently or in turn all to guarantee the process.

3.1. Conceptual model to protect the cloud against attacks

With this proposed model we can analyze that the security information to mitigate vulnerabilities, threats and risks of the information for the control and integration of data in commercial management are:

In the fig. 3. This model was designed to mitigate risks and protect the data of a business management

organization. We develop a model where we indicate that we will carry out the identification of assets, vulnerabilities, threats and risks, we will also obtain the real mitigation capacity of our prototype and the probability that the risks found will not affect the organization's data.
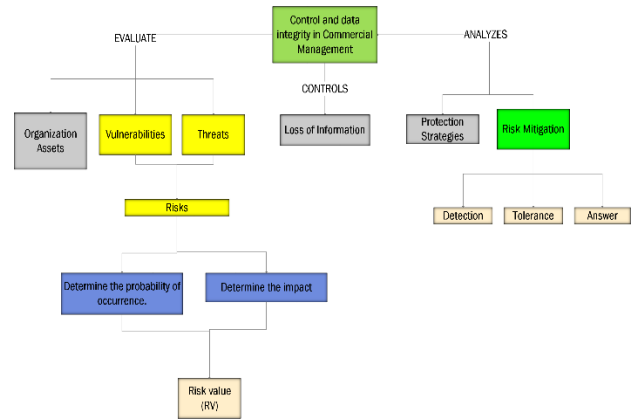
Figure 3: Conceptual model of our proposed protocol

The objective we want to control in the process of finding the value of risks is data loss; the value of the risks will be obtained by determining the probability of occurrence and the impact of each of the risks.

For the calculation of an efficient prototype of the presented conceptual model, the following formula is proposed:

$$x = \frac{\sum_{i=1}^{n}(D+T+R)}{3} \qquad (5)$$

where:

X = Average of the sum of mitigation indicators
D = Mitigation detection (range value 0 - 10)
T = Mitigation tolerance (range value 0 - 10)
R = Mitigation response (range value 0 - 10)

$$CM = \frac{x}{CME} = \frac{x}{10} \qquad (6)$$

Where:

ACM = Actual Mitigation Capacity

CME = Estimated Mitigation Capacity

$$P(R)\% = \frac{ACM^{R}e^{-ACM}}{R!}*100 \qquad (7)$$

where:

P (R) % = Probability that risks affect the system

R = Number of Risks

e = Euler

$$EP = 100 - P(R)\% \qquad (8)$$

where:

EP = Prototype mitigation efficiency

Table 10: Mitigation score

Punctuation	Safe level
80-100	Excellent (E)
50-70	Good (G)
20-40	Regular (R)
0-10	Deficient (D)

Guide to setting measurement values

Example

If we have a system that has a mitigation (Detection = 10, Tolerance = 8, Response 9), in which 9 risks were found.

If we apply the formulas 5, 6, 7 and 8 we have

$$x = \frac{10 + 8 + 9}{3}$$

$$x = 9$$

$$CM = \frac{X}{CME} = \frac{9}{10}$$

$$CM = 0.9$$

$$P(R)\% = \frac{CM^R e^{-CM}}{R!} * 100$$

$$P(R)\% = \frac{(0.9)^9 e^{-0.9}}{9!} * 100$$

$$P(R)\% = 4.34 x 10^{-5}$$

$$EP = 100 - 4.34 x 10^{-5}$$

$$EP = 99.99\% \qquad (9)$$

According to Table 10, our prototype for this scenario shows us that it is optimal.

3.2. Security prototype

It is proposed to have a higher security index, this prototype identifies the vulnerabilities and threats that can generate a risk in the control and integrity of the data, selects mitigation strategies, prepares an action plan, implements and monitors the mitigation strategies implemented.

Mitigation strategies are an important part of data security control, with their help we can reduce the number of information losses, modifications and destruction.

Each section of the prototype is related to security methodologies and prototypes and all these resources to information systems.
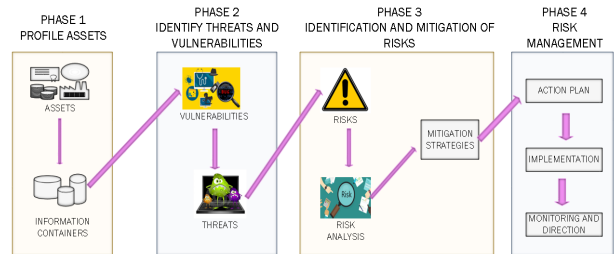
Figure 4: Security prototype

In Figure 4. We find the four phases of our prototype.

First phase:

Here we find the assets that the organization owns and the databases where the organization's data will be stored (information on workers, customers, purchases, sales, etc.).

Second stage:

Vulnerabilities and threats are identified, which give way to information systems risks being generated and which can cause serious security problems.

Third phase:

If there are risks, they must be analyzed and categorized by levels (mild, low, normal, high and critical), in order to implement risk mitigation strategies prioritizing the risks that urgently require attention.

Fourth phase:

Finally, the prototype indicates that an action plan must be generated to carry out the mitigation strategies. Once the action plan is implemented, it must be monitored, to verify that it is being carried out correctly, avoiding loss of information.

3.3. Algorithm in the flowchart to protect data from risks and attacks

The proposed methodology in algorithm and data flow results in the steps that we must take to mitigate vulnerabilities, threats and risks of information for the control and integrity of data in commercial management.

Figure 5. Express the algorithm in a flow diagram, the phases are described below:

Description of the phases:

Phase 1: Profiling assets the assets and information containers owned by the organization must be identified and that can be compromised if a security problem occurs.

Phase 2: Identify threats and vulnerabilities, with the identification of threats and vulnerabilities, we will be able to identify the existing risks in the information systems, since the risks are created thanks to the existence of the vulnerabilities and threats. In the absence of vulnerabilities or threats, the prototype will terminate the control and mitigation processes.

Phase 3: Identify and mitigate risks, the identified risks must have their risk value found, the value of the risks is found by multiplying the probability of occurrence with the impact that each of the risks can generate. Given the value of each risk, they are categorized to know which risks can cause high and critical security problems, the risks that belong to these categories should be solved immediately. The risks are analyzed to be able to select the mitigation strategies, if there are no mitigation strategies, we must create them and re-analyze the risks.
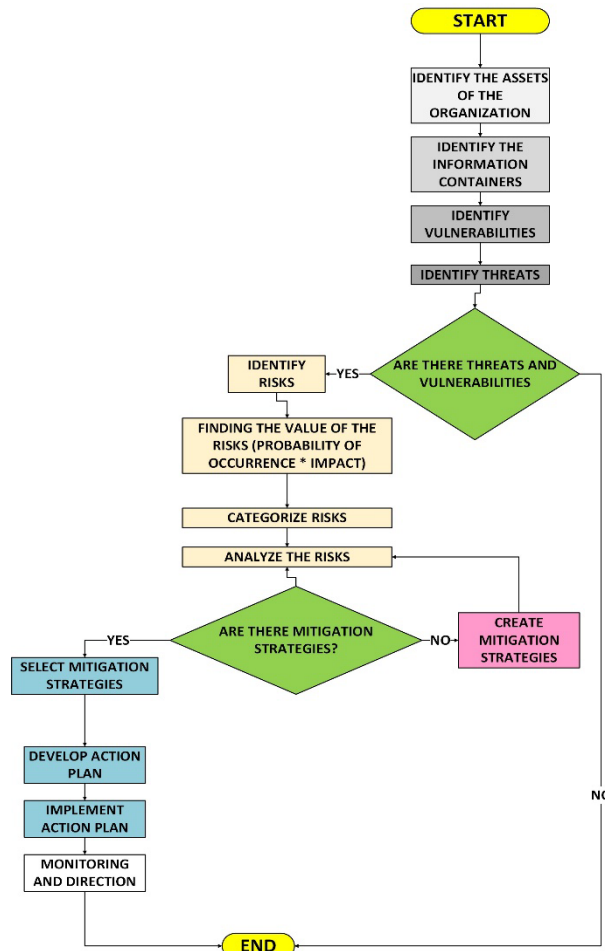
Figure 5: Algorithm of the proposed prototype expressed in a flow diagram

Phase 4: Risk Management, the selected mitigation strategies must be executed and described in the action plan, which will then be implemented and monitored, to verify that security problems do not occur.

Algorithm:

Start
Phase 1: Profile assets
The assets and information containers owned by the organization are identified.
Phase 2: Identify threats and vulnerabilities
Vulnerabilities and threats are identified.
If there are no vulnerabilities and threats, the mitigation process will be terminated.
If there are vulnerabilities and threats, the risks must be identified.
Phase 3: Identification and mitigation of risks.
After identifying the risks, the value of each is found, categorized and analyzed.
Once the risks have been analyzed, we must verify that mitigation strategies exist and are selected.
In the absence of mitigation strategies, strategies must be created.
Phase 4: Risk Management
If mitigation strategies were selected, we can develop an action plan.
This action plan will be implemented and monitored.
End.

We demonstrate with our proposed formulas that the protocol is stable:

$$P_o = \frac{1 - \dfrac{R^*}{R}}{CM} \qquad (10)$$

Finally, we calculate the percentage of the formula used:

$$s = P_o(100\%) \qquad (11)$$

Where:
R = Number of Risks
R * = Number of high and critical risks
Po = Security Level
CM = Mitigation Capacity
s = Percentage of algorithm stability
Example:

If we have a system that has a mitigation (Detection = 10, Tolerance = 8, Response = 9), in which 9 risks were found, of which 4 are of high and critical level, as shown in Table 9.

Table 11: Security algorithm percentage

Punctuation	Safe level
76-100	Excellent
51-75	Optimum
25-50	Regular
0-24	Deficient

We will calculate the percentage of safety of our algorithm using formula 10:

$$P_o = \frac{1 - \frac{4}{9}}{0.9}$$

$$P_o = 0.6173$$

As a last step we calculate the security percentage:

$$s = 0.6173(100\%)$$

$$s = 61.73\%$$

The security percentage is 61.73, according to table 11 our algorithm is optimal to implement it.

Example:

In Figure 6, we can see the percentage of safety of the prototype, the number of risks identified, the number of high risks and the mitigation capacity. For the representation of the simulation, we have 5 scenarios, with different numbers of risks and mitigation capacities. Scenario 2 obtained the highest percentage of safety.
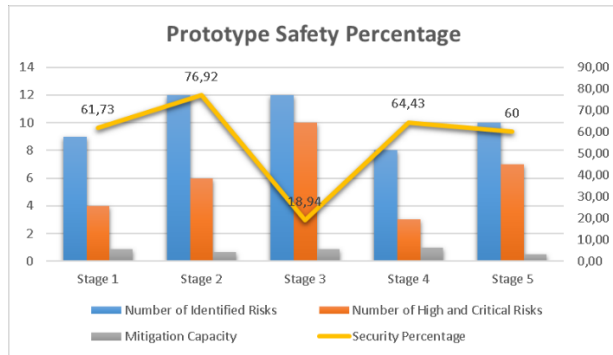
Figure 6: Safety percentage in 5 different scenarios

3.4. Formula to find the probability of a security problem occurring

With the following simulations we can observe the probability that security problems occur due to the number of risks and threats presented in 5 different scenarios:

$$P(n) = [(\#R)^n e^{-\#R}] / n! \qquad (12)$$

where:
P (n) = Probability of a security problem occurring
n = Number of system threats
#R = Number of System Risks

To determine the probability of a security problem occurring in the system, a scenario with 9 risks was performed, and with 12 threats, using Formula 12, a high percentage of 9.48% probability of a security problem occurring was determined. In the system. Figure 8 shows the simulation of five different scenarios using Formula 12 and shows that there is a higher probability of an

information security problem occurring if the threats and risks are high.
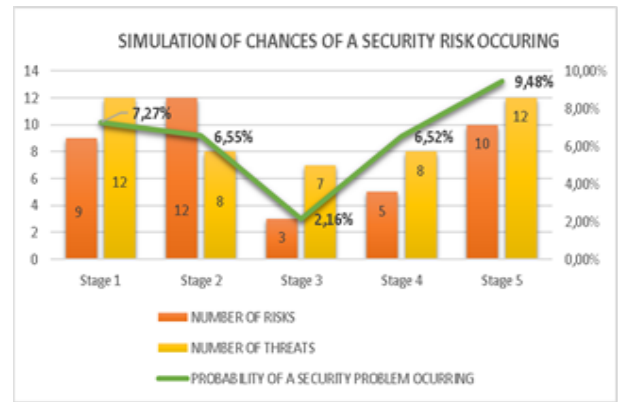
Figure 7: Simulation of the possibilities of a security risk. The simulation is shown in 5 different scenarios

3.5. Risk Analysis and Evaluation

Given the analysis carried out on the methodologies and security models, one of the most important and critical processes refers to the identification and evaluation of risk [14].

Within the existing methodologies and methods for the detection and evaluation of risks, MEHARI[9] and OCTAVE[36] are identified as the powerful methodologies that allow the evaluation and management of risks, with the objective of identifying, categorizing and prioritizing the probability and impact of risks on an asset or process, to determine the rate of security problems that risks can cause.

Risk mitigation capacity is made up of several parameters[35], these parameters are defined on a quantitative scale defined between the values 0-10 in which the value 10 represents the highest value for each indicator.

These numerical parameters are used to calculate the actual mitigation capacity of the system, which defines a simple formula for stable critical analyzes on security problems based on quantitative values, Formula 5 and 6.

Through the use of the risk matrix, we will find the potential risks for the generation of actions that mitigate vulnerabilities, threats and information risks.

4. Discussion

In the analysis we carried out, there were cases of security prototypes that adopted a system similar to the one that we have proposed, a security model based on the Magerit methodology was applied to adapt the mitigation prototype. This made it easier for the system to identify vulnerabilities, threats and risks that could arise in the information systems, to have data security.

The proposed prototype does not define the costs for the implementation of the system; The costs will be according to the size of the company and the place where the proposal is implemented.

In the article[49] algorithms were used to assess risks in a system, in the article[32] the probability of security incidents and the losses caused by security incidents allow us to find the value of the risks, in the article[39] algorithms were used to produce a risk treatment plan, selecting measures to reduce; to hold back; to avoid or transfer risks, in the article[11]. A risk management review and control model were used for information security.

According to the information security models, it is necessary to carry out adequate risk management that allows knowing which are the main vulnerabilities that can affect the organization's information assets and which are the threats that could exploit the vulnerabilities found.

In the simulations we have a security percentage of 76.92%. In the simulations we have that the greater the number of risks and threats, the greater the probability that a security problem will occur.

5. Future Work and Conclusions

In the future, we proposed the application of security prototypes to mitigate vulnerabilities, threats and information risks for public and private organizations with a high rate of cyberattacks.

It was concluded that the security prototype proposed for a commercial information system; It is security system suitable for public and private companies. In the simulation carried out, it was determined that if the number of risks and threats is high, there will be a greater probability that a problem will arise in the security of the system.

According to the mitigation efficiency simulation of the prototype, the efficiency percentage can be high if there is good mitigation capacity in the system.

In the first result, we include a concept map that shows us the mitigation efficiency formula of the prototype. In the second result, we conclude that each phase helps to avoid the loss of information in a commercial management system. In the third result, the algorithm was carried out to verify that our protocol is optimal against the risks that are obtained in a system with the proposed formula that we can verify. In the last result, the simulation showed us the chances of a security problem occurring given the number of threats and risks.

Conflict of Interest

The authors declare no conflict of interest.

Acknowledgment

References

[1] J. Miranda Jiménez, Joan Noheli,Llerena Izquierdo, "Mapeo sistemático de metodologías de Seguridad de la Información para el control de la gestión de riesgos informáticos," Universidad Politécnica Salesiana Sede Guayaquil, 2021.

[2] Y. Supriyadi and C. W. Hardani, "Information system risk scenario using COBIT 5 for risk and NIST SP 800-30 Rev. 1 a case study," in Proceedings - 2018 3rd International Conference on Information Technology, Information Systems and Electrical Engineering, ICITISEE, 287–291, 2018, doi: 10.1109/ICITISEE.2018.8721034.

[3] M. a. Tejena-Macías, "Análisis de riesgos en seguridad de la información," Polo del Conocimiento, **3**(4), 230-238, 2018, doi: 10.23857/pc.v3i4.809.

[4] M. Abomhara and G. M. Køien, "Cyber security and the internet of things: Vulnerabilities, threats, intruders and attacks," J. Cyber Secur. Mobil, **4**(1), 65–88, 2015, doi: 10.13052/jcsm2245-1439.414.

[5] A. N. Kamenskih, M. a. Filippov, and A. a. Yuzhakov, "The Development of Method for Evaluation of Information Security Threats in Critical Systems," in Proceedings of the 2020 IEEE Conference of Russian Young Researchers in Electrical and Electronic Engineering, EIConRus, 333–336, 2020, doi: 10.1109/EIConRus49466.2020.9038960.

[6] A. Alsalamah, "Security risk management in online system," in Proceedings - 2017 5th International Conference on Applied Computing and Information Technology, 2017 4th International Conference on Computational Science/Intelligence and Applied Informatics and 2017 1st International Conference on Big Data, Cloud Compu, 119–124, 2020, doi: 10.1109/ACIT-CSII-BCD.2017.59.

[7] S. M. Carta, S. Consoli, A. S. Podda, D. R. Recupero, and M. M. Stanciu, "Ensembling and Dynamic Asset Selection for Risk-Controlled Statistical Arbitrage," IEEE Access, **9**, 29942–29959, 2021, doi: 10.1109/ACCESS.2021.3059187.

[8] R. Gómez, D. H. Pérez, Y. Donoso, and A. Herrera, "Metodología y gobierno de la gestión de riesgos de tecnologías de la información," Rev. Ing, **1**(31), 109–118, 2010, doi: 10.16924/riua.v0i31.217.

[9] K. D. R. Gaona Vásquez, "Aplicación de la metodología Magerit para el análisis y gestión de riesgos de la seguridad de la información aplicado a la empresa Pesquera e Industrial Bravito S.A. en la ciudad de Machala," Universidad Politécnica Salesiana, 2013.

[10] M. Moyo, H. Abdullah, and R. C. Nienaber, "Information security risk management in small-scale organisations: A case study of secondary schools computerised information systems," in 2013 Information Security for South Africa - Proceedings of the ISSA, 1–6. 2013 doi: 10.1109/ISSA.2013.6641062.

[11] J. Zarei and F. Sadoughi, "Information security risk management for computerized health information systems in hospitals: A case study of Iran," Risk Manag. Healthc. Policy, **9**(1), 75–85, 2016, doi: 10.2147/RMHP.S99908.

[12] X. Li and H. Li, "A Visual Analysis of Research on Information Security Risk by Using CiteSpace," IEEE Access, **6**, 63243–63257, 2018, doi: 10.1109/ACCESS.2018.2873696.

[13] M. Shakibazad and A. J. Rashidi, "New method for assets sensitivity calculation and technical risks assessment in the information systems," IET Inf. Secur, **14**(1), 133–145, 2020, doi: 10.1049/iet-ifs.2018.5390.

[14] F. M. Arévalo and I. P. C. S. a Moscoso, "Agile Methodology for Computer Risk Management," Kill. Técnica, **1**(2) 31–42, 2017, doi: 10.26871/killkana.

[15] A. J. Burns and E. Johnson, "The evolving cyberthreat to privacy," IT Prof, **20**(3), 64–72, 2018, doi: 10.1109/MITP.2018.032501749.

[16] B. Hauer, "Data and information leakage prevention within the scope of information security," IEEE Access, **3**, 2554–2565, 2015, doi: 10.1109/ACCESS.2015.2506185.

[17] H. Chen, D. Bao, H. Gao, and J. Cheng, "A Security evaluation and certification management database based on ISO/IEC standards," in Proceedings - 12th International Conference on Computational Intelligence and Security, 249–253, 2016, doi: 10.1109/CIS.2016.63.

[18] H. Parastvand, O. Bass, M. a. S. Masoum, A. Chapman, and S. Lachowicz, "Cyber-Security Constrained Placement of FACTS Devices in Power Networks from a Novel Topological Perspective," IEEE Access, **8**, 108201–108215, 2020, doi: 10.1109/ACCESS.2020.3001308.

[19] S. Pissanetzky, "On the Future of Information: Reunification, Computability, Adaptation, Cybersecurity, Semantics," IEEE Access, **4**, 1117–1140, 2016, doi: 10.1109/ACCESS.2016.2524403.

[20] S. Walker-Roberts, M. Hammoudeh, and A. Dehghantanha, "A Systematic Review of the Availability and Efficacy of Countermeasures to Internal Threats in Healthcare Critical Infrastructure," IEEE Access, **6**, 25167–25177, 2018, doi: 10.1109/ACCESS.2018.2817560.

[21] R. Rooswati and N. Legowo, "Evaluation of IT Project Management Governance Using Cobit 5 Framework in Financing Company," in Proceedings of 2018 International Conference on Information Management and Technology, ICIMTech, 81–85. 2018, doi: 10.1109/ICIMTech.2018.8528192.

[22] T. Y. T. Y. Lin, "Chinese wall security policies information flows in business cloud," in Proceedings - 2015 IEEE International Conference on Big Data, IEEE Big Data, 1603–1607, 2015, doi: 10.1109/BigData.2015.7363927.

[23] F. Avorgbedor and J. Liu, "Enhancing User Privacy Protection by Enforcing Clark-Wilson Security Model on Facebook," in IEEE International Conference on Electro Information Technology, 155–161. 2020, doi: 10.1109/EIT48999.2020.9208279.

[24] B. Balamurugan, N. G. Shivitha, V. Monisha, and V. Saranya, "A Honey Bee behaviour inspired novel Attribute-based access control using enhanced Bell-Lapadula model in cloud computing," in Proceedings 2015 - IEEE International Conference on Innovation, Information in Computing Technologies, ICIICT, 1–6, 2015, doi: 10.1109/ICIICT.2015.7396064.

[25] M. R. Ogiela and L. Ogiela, "On using cognitive models in cryptography," in Proceedings - International Conference on Advanced Information Networking and Applications, AINA, 1055–1058, 2016, doi: 10.1109/AINA.2016.159.

[26] A. Ahi and A. V. Singh, "Role of Distributed Ledger Technology (DLT) to Enhance Resiliency in Internet of Things (IoT) Ecosystem," in Proceedings - 2019 Amity International Conference on Artificial Intelligence, AICAI, 782–786, 2019. doi: 10.1109/AICAI.2019.8701282.

[27] S. J. Moon, I. H. Park, B. S. Lee, and J. Ju Wook, "A Hyperledger-based P2P Energy Trading Scheme using Cloud Computing with Low Capabillity Devices," in 2019 IEEE International Conference on Smart Cloud (SmartCloud), 190–192, 2019, doi: 10.1109/SmartCloud.2019.00039.

[28] J. S. Suroso, A. Januanto, and A. Retnowardhani, "Risk Management of Debtor Information System at Bank XYZ Using OCTAVE Allegro Method," in 2019 International Conference on Electrical Engineering and Informatics (ICEEI), 261–265, 2019, doi: 10.1109/ICEEI47359.2019.8988890.

[29] L. Kotut and L. a. Wahsheh, "Survey of Cyber Security Challenges and Solutions in Smart Grids," in 2016 Cybersecurity Symposium (CYBERSEC), 32–37, 2016, doi: 10.1109/CYBERSEC.2016.013.

[30] M. Wegerer and S. Tjoa, "Defeating the database adversary using deception - A MySQL database honeypot," Proc. - 2016 Int. Conf. Softw. Secur. Assur. ICSSA, 6–10, 2017, doi: 10.1109/ICSSA.2016.8.

[31] I. V. Anikin, "Information security risks assessment in telecommunication network of the university," 2016 Dyn. Syst. Mech. Mach, 1–4, 2017, doi: 10.1109/Dynamics.2016.7818967.

[32] L. Huang, Y. Shen, G. Zhang, and H. Luo, "Information system security risk assessment based on multidimensional cloud model and the entropy theory," in ICEIEC 2015 - Proceedings of 2015 IEEE 5th International Conference on Electronics Information and Emergency Communication, 11–15, 2015, doi: 10.1109/ICEIEC.2015.7284476.

[33] B. F. Zahra and B. Abdelhamid, "Risk analysis in Internet of Things using EBIOS," in 2017 IEEE 7th Annual Computing and Communication Workshop and Conference (CCWC), 1–7, 2017, doi: 10.1109/CCWC.2017.7868444.

[34] A. Mukhopadhyay, S. Chatterjee, D. Saha, A. Mahanti, and S. K. Sadhukhan, "Cyber-risk decision models: To insure IT or not?," Decis. Support Syst, **56**(1), 11–26, 2013, doi: 10.1016/j.dss.2013.04.004.

[35] J. Porras, S. Pastor, and R. Alvarado, "Modelo de gestión de riesgos de seguridad de la información para PYMES peruanas," Rev. Peru. Comput. y Sist., **1**(1), 47–56, 2018, doi: http://dx.doi.org/10.15381/rpcs.v1i1.14856.

[36] F. Y. H. García and L. M. L. Moreta, "Modelo para Medir la Madurez del Análisis de Riesgo de los Activos de Información en el contexto de las Empresas Navieras," RISTI - Rev. Ibérica Sist. e Tecnol. Informação, **31**, 1–17, 2019, doi: 10.17013/risti.31.1-17.

[37] S. M. T. Toapanta, M. A. P. Sánchez, D. W. B. Valencia, and L. E. M. Gallegos, "An approach of models of information technologies suitable to optimize management in a public organization of Ecuador," in 2019 Third World Conference on Smart Trends in Systems Security and Sustainablity (WorldS4), 207–214, 2019, doi: 10.1109/WorldS4.2019.8904027.

[38] I. C. Satizábal-Echavarría and N. M. Acevedo-Quintana, "MePRiSIA: Risk prevention methodology for academic information systems," Rev. Fac. Ing., **1**(89), 81–101, 2018, doi: 10.17533/UDEA.REDIN.N89A11.

[39] N. Anton and A. Nedelcu, "Security Information and Risk Management Assessment," Appl. Mech. Mater., **809**, 1522–1527, 2015, doi: 10.4028/www.scientific.net/amm.809-810.1522.

[40] S. M. T. Toapanta, I. N. C. Ochoa, R. A. N. Sanchez, and L. E. G. Mafla, "Impact on administrative processes by cyberattacks in a public organization of Ecuador," in Proceedings of the 3rd World Conference on Smart Trends in Systems, Security and Sustainability, WorldS4 2019, 270–274, 2019, doi: 10.1109/WorldS4.2019.8903967.

[41] S. M. Toapanta Toapanta, L. E. Mafla Gallegos, M. J. Chevez Moran, and J. G. Ortiz Rojas, "Analysis of models of security to mitigate the risks, vulnerabilities and threats in a company of services of telecommunications," in 2020 3rd International Conference on Information and Computer Technologies (ICICT), 445–450. 2020, doi: 10.1109/ICICT50521.2020.00077.

[42] Y. Lee, S. Woo, Y. Song, J. Lee, and D. H. Lee, "Practical Vulnerability-Information-Sharing Architecture for Automotive Security-Risk Analysis," IEEE Access, **8**, 120009–120018, 2020, doi: 10.1109/ACCESS.2020.3004661.

[43] M. Mohsin, M. U. Sardar, O. Hasan, and Z. Anwar, "IoTRiskAnalyzer: A Probabilistic Model Checking Based Framework for Formal Risk Analytics of the Internet of Things," IEEE Access, **5**, 5494–5505, 2017, doi: 10.1109/ACCESS.2017.2696031.

[44] J. Webb, A. Ahmad, S. B. Maynard, and G. Shanks, "A situation awareness model for information security risk management," Comput. Secur., **44**. 1–15, 2014, doi: 10.1016/j.cose.2014.04.005.

[45] G. Stergiopoulos, D. Gritzalis, and V. Kouktzoglou, "Using formal distributions for threat likelihood estimation in cloud-enabled IT risk assessment," Comput. Networks, **134**, 23–45, 2018, doi: 10.1016/j.comnet.2018.01.033.

[46] M. Jouini, L. B. A. Rabai, and R. Khedri, "A multidimensional approach towards a quantitative assessment of security threats," Procedia Comput. Sci., **52**(1), 507–514, 2015, doi: 10.1016/j.procs.2015.05.024.

[47] O. T. Arogundade, A. Abayomi-Alli, and S. Misra, "An Ontology-Based Security Risk Management Model for Information Systems," Arab. J. Sci. Eng., **45**(8) 6183–6198, 2020, doi: 10.1007/s13369-020-04524-4.

[48] I. V. Anikin, "Information security risk assessment and management method in computer networks," in 2015 International Siberian Conference on Control and Communications (SIBCON), 1–5, 2015, doi: 10.1109/SIBCON.2015.7146975.

[49] A. Boranbayev, S. Boranbayev, A. Nurusheva, K. Yersakhanov, and Y. Seitkulov, "A Software System for Risk Management of Information Systems∗," in IEEE 12th International Conference on Application of Information and Communication Technologies, AICT 2018 - Proceedings, 1–6, 2018, doi: 10.1109/ICAICT.2018.8747045.

[50] Y. Qi, L. Xiao, and Q. Li, "Information security risk assessment method based on CORAS frame," Proc. - Int. Conf. Comput. Sci. Softw. Eng. CSSE 2008, **3**, 571–574, 2008, doi: 10.1109/CSSE.2008.1001.

[51] B. S. Y. Choo and J. C. L. Goh, "Adapting the ISO31000:2009 enterprise risk management framework using the six sigma approach," IEEE Int. Conf. Ind. Eng. Eng. Manag., 39–43, 2014, doi: 10.1109/IEEM.2014.7058596.

[52] T. Hirakawa, K. Ogura, B. B. Bista, and T. Takata, "A Defense Method against Distributed Slow HTTP DoS Attack," in 2016 19th International Conference on Network-Based Information Systems (NBiS), 152–158, 2016, doi: 10.1109/NBiS.2016.58.

[53] X. Ma, "Research on Black Hat SEO Behaviour Measurement," in 2018 IEEE 3rd Advanced Information Technology, Electronic and Automation Control Conference (IAEAC), 1041–1045, 2018 doi: 10.1109/IAEAC.2018.8577831.

[54] D. Kim, D. Shin, and D. Shin, "Unauthorized Access Point Detection Using Machine Learning Algorithms for Information Protection," in 2018 17th IEEE International Conference On Trust, Security And Privacy In Computing And Communications/ 12th IEEE International Conference On Big Data Science And Engineering (TrustCom/BigDataSE), 1876–1878, 2018 doi: 10.1109/TrustCom/BigDataSE.2018.00284.

Process Mining in Healthcare: A Systematic Literature Review and A Case Study

Fabrizio Striani[*,1], Chiara Colucci[2], Angelo Corallo[1], Roberto Paiano[1], Claudio Pascarelli[1]

[1]University of Salento, Department of Engineering for Innovation, Via per Monteroni, Lecce, 73100, Italy

[2]National Interuniversity Consortium for Informatics, Via Ariosto 25, Roma, 00185, Italy

A R T I C L E I N F O	A B S T R A C T
	Process mining is an innovative technique through which inefficiencies in production systems can be eliminated. This technique has therefore become very important internationally in recent years and is also useful for pursuing the improvement of production systems by extrapolating process knowledge from event logs recorded by information systems. Process mining has easy application in production systems as current business processes are integrated with information systems and this makes data available immediately. This makes the complex nature of industrial operations understandable and, for this reason, process mining could also be used in the healthcare field where cost containment and the quality of service increasing offered to the community has become paramount. The problem is that in this sector, it is much more complex to identify useful data in order to extrapolate the relevant log file. The article aim is to examine the state of the art of the application of process mining in the healthcare sector in order to understand the level of diffusion of these techniques. In the light of this analysis, a case study will then be analysed on the application of process mining techniques in the healthcare sector, and in particular in medical teleconsultation in the field of neuroradiology.

1. Introduction

This paper is an extension of the work originally presented in "Application of Process Mining in Teleconsultation Healthcare: Case study of Puglia Hospital" [1].

Process mining is a recently applied research discipline which combines data mining and computational intelligence on the one hand with process analysis and modelling on the other [2], [3].

Despite the relative youth of this discipline, many techniques and methodologies have been implemented. The most widely used are: Fuzzy and Heuristic Miner. The first algorithm allows the process model to be made simpler, as this technique reduces the model to a desired abstraction threshold and is, therefore, particularly suitable for the extraction of less structured processes with a large amount of conflicting behaviour [4]. The second uses frequencies and parameterisation so that the main behaviour can be recorded in an event log. Considering the dependency measure, it takes into account frequencies and causal dependencies, making it suitable for many real logs [5].

In particular, process mining involves the discovery of processes, the monitoring of compliance through the analysis of deviations (which can be either negative or positive) from best practices and the optimisation of the model based on the deviations found.

Indeed, process mining was born with the aim of extracting knowledge from current information systems (using event logs that can be easily accessed), and through this, to be able to discover, monitor and improve real processes [6]. This technique consists of three phases:

1) discovery (process models are extracted from an event log);
2) conformance checking (or check of any deviation between the model and the log by making a comparison);
3) enhancement (using the information in the logs, improves or extends a process model) [7].

Consequently, the application of these techniques is particularly useful in industrial scenarios where there is the production of complex goods, and, therefore, the analysis of a large amount of information becomes necessary for the development management of new applications.

*Corresponding Author: Fabrizio Striani, fabrizio.striani@unisalento.it

Another natural application field of process mining analysis is healthcare [8], [9]. Several case studies exist in which process mining techniques and tools are applied in this sector [10], [11]. Among these, the oncology and the hospitalisation sector show the maximum number of successful cases [12]. Hospitals, for example, need to focus on managing their processes to have high quality services while reducing costs, especially when patient demand unexpectedly increases (as was the case with the COVID-19 pandemic crisis) [13]-[15]. The biggest problem in the healthcare sector is that the patient care process ("care flow") very often differs even if the patients have a similar diagnosis. The techniques under consideration offer an interesting possibility through which this problem can be solved: process mining has already been used to a very significant extent in service companies and could therefore also be a good solution in the health sector [16], [17].

Another problem is the existence of several systems which store events and data. An intensive care unit, for example, is very often equipped with its own system to store patients' treatments or examinations, while the radiology department has another system to store the entire patient process. It becomes, therefore, crucial that all information is amalgamated in a single source. However, given the great multiplicity of systems involved, which makes data collection complex, process mining techniques could prove very useful as they would allow, starting from the individual events carried out in each division, to obtain the entire process, which could provide an overview that, for example, could ensure good reporting of the examinations performed [18], [19].

In this paper, the first two sections we introduce, explain and give a systematic literature review which evaluates the process mining tools applications in the healthcare scenario. According to its definition, a systematic literature review is "A review of a clearly formulated question that uses systematic and explicit methods to identify, select, and critically appraise relevant research, and to collect and analyse data from the studies that are included in the review. Statistical methods (meta-analysis) may or may not be used to analyse and summarise the results of the included studies" [20].

With this systematic search process, we identify studies addressing a specific research question and we make a systematic presentation and synthesis of the characteristics and outcomes of the research findings. The criteria by which studies are excluded or included are objective, consistently applied and explicitly stated, so that when certain studies are included or excluded from the review, this decision is clear to the readers; or if another researcher decides to use the same criteria, he or she is likely to replicate the same decisions [21].

In the second section we present the Tranfield approach that is used to conduct the systematic literature review, allowing the identification of the most interesting documents in the analysed context. In the third section we show up our case study: an analysis of the log file extracted from the Apulian hospitals' repository. In section 4, we illustrate the use of process mining techniques on the log file (using Disco software [22]) and analyse the results achieved with these techniques. Then, in this section, the AS-IS process is represented with BPMN notation (using the Signavio tool). In the last section, the results of our case study are compared with data related to the Piedmont Region (representing a virtuous Italian region), which are taken from the official source of the Ministry of Health. At this point, we modelled a TO-BE process to optimise the current process.

Finally, there are our conclusions and the references used. Ultimately, our analysis aim is not to investigate new issues but, based on the state of the art, to highlight that Process Mining techniques are useful in healthcare applications. From the above, we can extrapolate the following research question:

"**RQ** - Provided the state of the art obtained from the SLR, and aimed at identifying the scope of application in healthcare, does the use of teleconsultation optimise the performance of the healthcare service in the field of neuroradiology?"
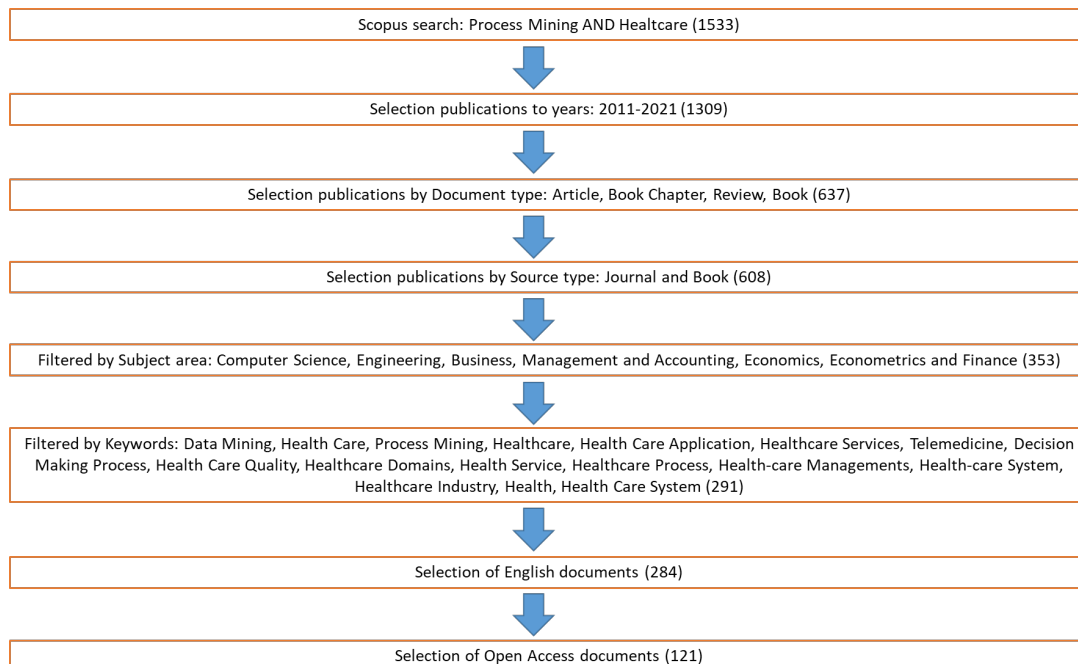
Figure 1: The process of systematic literature review

2. Research Method

Since this is a review article, we will now apply the Tranfield approach to conduct a systematic literature review (SLR), finalised to highlight the usefulness of Process Mining techniques in healthcare applications.

In clinical disciplines, the method theorised by [23] is used to implement a systematic review (SR). We apply the Tranfield approach to develop the "Study Selection" phase of Egger's method, a phase through which the various studies identified are evaluated, so that it is possible to assess whether or not the inclusion criteria are met. The Tranfield approach uses three phases: planning, execution, reporting and dissemination.

In the planning phase, we enter the terms "Process mining" AND "Healthcare" to search for the keywords, abstract and title. Starting to execution, the initial Scopus search, (we are selected the Scopus database to guarantee the review's quality) on the basis of the selected words present in keywords, abstract and title, found a total of 1533 publications. Then, we are limited the analysis to the last 11 years (2011–2021), as our research interest is based on these years, resulting in 1309 publications [21].

By restricting the search to "Article", "Book chapter", "Review", and "Book", we found a total of 637 publications. Considering only the publications in Journals and Books, we identified 608 documents. However, to achieve the aims set initially, we selected only documents included in the fields of Computer Science, Engineering, Business, Management and Accounting, Economics, Econometrics and Finance finding a total of 353 publications.

The selected fields are the one of interest which refer to the case study analysed in the paper. In fact, as mentioned before in the RQ, the aim is to analyse the impact of teleconsultation from a technical point of view (hence the choice of the fields "Computer Science" and "Engineering"), and from a monetary point of view (hence the choice of the fields "Business, Management and Accounting", "Economics, Econometrics and Finance"). At this point, given the important number of articles found, and

considering that the ones of greatest interest would be those incorporating the keywords, we applied a new filter (the keywords selected were: "Data Mining", "Health Care", "Process Mining", "Healthcare", "Health Care Application", "Healthcare Services", "Telemedicine", "Decision Making Process", "Health Care Quality", "Healthcare Domains", "Health Service", "Healthcare Process", "Health-care Managements", "Health-care System", "Healthcare Industry", "Health", "Health Care System"), obtaining 291 publications. After choosing the English language (284), and the Open Access documents, we found 121 documents. Figure 1 shows the SLR process. Finally, we faced the last phase of the Tranfield approach, namely reporting and dissemination.

As we show in Figure 2, the number of publications has increased in the last three years: 14 in 2019, 22 in 2020, 26 in 2021. In the previous years, there was an average of 6 publications, with a marked increase in 2018 (21 publications).

This trend highlights the growing attention to these topics in recent years. In addition, 65 journals published the topics analysed, 11 out of which published two or more articles (59), representing 49% of the total. Analysing the Scopus impact evaluation of sources with most publications, 78% were in the first quartile (which represents the highest quality of the publication magazine); 15% in the second; and only 7% in the third, demonstrating the high standard of the publications, and the level of interest in the subjects (Table 1 and Figure 3) [24], [25].
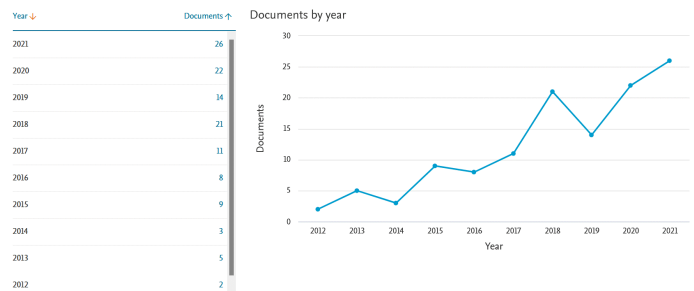
Figure 2 – Documents by year. Source: Scopus

Table 1: Journals with two or more documents published

Source	Documents	Ranking Scopus
"IEEE Access"	21	Q1
"Journal of Biomedical Informatics"	13	Q1
"IEEE Journal of Biomedical and Health Informatics"	4	Q1
"International Journal of Advanced Computer Science and Applications"	4	Q3
Sensors (Switzerland)	4	Q2
Applied Sciences (Switzerland)	3	Q2
Artificial Intelligence in Medicine	2	Q1
Computers Materials and Continua	2	Q1
Expert Systems with Applications	2	Q1
Plos Computational Biology	2	Q1
Sensors	2	Q2
Other	62	
Total	**121**	
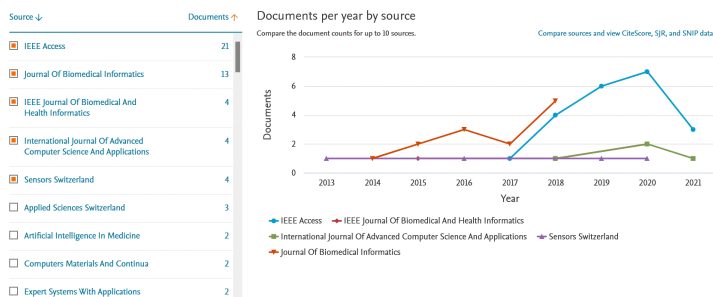
Figure 3: Documents per year by source. Source: Scopus

Moreover, we observed an increase in the number of publications for IEEE Access Journal (Q1) in the years 2018, 2019 and 2020, from 4 in 2018 to 7 in 2020, which again reflects the increasing interest in these themes in recent years.

The Affiliation Identifier allows us to identify and distinguish publications in relation to the reference institutions or organizations. In this case, we noted that the majority of publications comes from the Education area (University, Institute, Laboratory, School, College), followed by other areas: Company, Health Management, Research and Government (Figure 4)
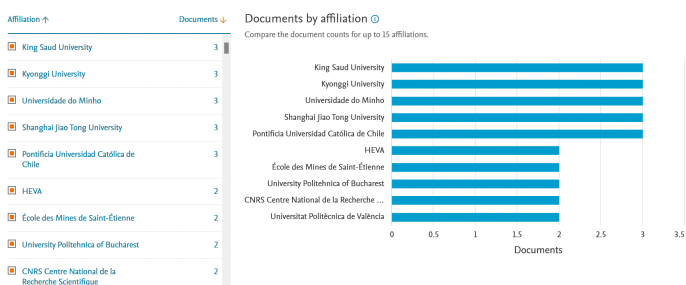
Figure 4: Documents by affiliation. Source: Scopus
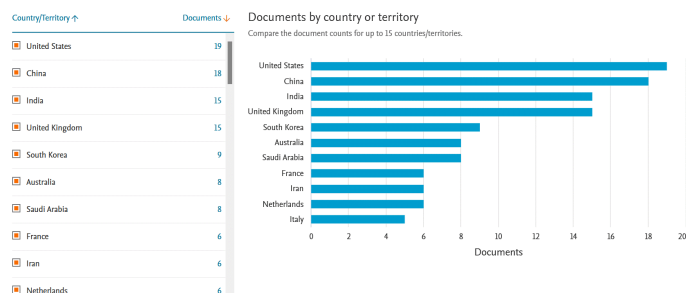
Figure 5: Documents by country or territory. Source: Scopus
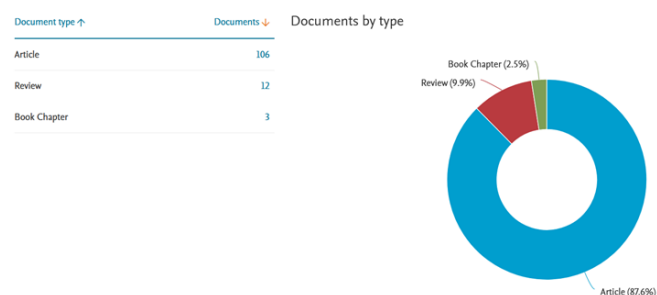
Figure 6: Documents by type. Source: Scopus

Another interesting aspect is the publications on the analysed topics by countries. In particular, most publications were produced in Asian territories (China and Middle East), followed by Europe (United Kingdom, France, Netherlands, Italy), and finally by America (principally United States). This may be further incentive to increase publications in our area (Figure 5).
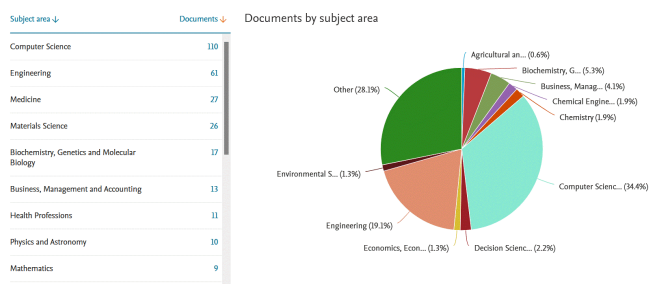
Figure 7: Documents by Subject area (Source: Scopus)

Moreover, as shown in Figure 6, publications consisted mainly of articles (106 – 87,6%), and some reviews (12 – 9,9%). In line with the selected Subject areas for the SLR, the majority of publications were in the Computer Science (110 – 34%) and Engineering (61 – 19%) areas. The areas "Business, Management and Accounting" and "Economics, Econometrics and Finance" counted 13 (4%), and 4 (1%) publications respectively (Figure 7). These findings shows that process mining applied to the healthcare sector has become very useful and relevant [26]. In particular, of the 27 papers about Medicine, the majority (17 – (63%)) concerned research activities in the field of healthcare using innovative approaches, such as: Health Surveillance Software Framework, Time Series Data Mining, Electronic Medical Record Search Engine, Intelligent Personal Health Record. Part of them regarded studies and applications of process mining in the field of neurological pathologies (2 – (7%)), cardiological pathologies (2 – (7%)), and in the radiology sector (2 – (7%)). In the remaining part of this sample, the authors discussed application cases on psychiatric diseases, diabetes and cancer. Since the review process we carried out have not delivered any paper on medical teleconsultation analysis in the neuroradiology field, in this paper we decided to analyse a case study on this subject. This case study is presented in the following section.

3. Case study

Following the considerations in the previous section, in this one we show the case study based on an analysis of process mining about clinical teleconsultation in the neuroradiology domain. We choose the teleconsultation as main topic, since it represents a new and innovative approach to healthcare delivery, also in the light of the pandemic period, therefore representing a very actual topic. Within the scope of this paper, we imagine the process as follows: after the patient is admitted to a medical district, the referring physician requires certain analysis and exams. Once all the necessary documents have been provided, the corresponding doctor sends all the documents (results of tests, images and diagnosis [if expressed]) to the specialist doctor for a second opinion. The specialised doctor returns his/her own diagnosis with the corresponding treatment or further

examinations. At this stage, the patient must undergo the suggested treatment until discharge.

The file log represented in the Table 2 derives from this repository. This log file represents the effective process, knowing that we have anonymised the patient and doctor data. For simplicity, we report only two cases and we add a cost column to the extracted data. The costs presented are the real ones for each activity with the exception of the activity "blood test". For the latter, in fact, we used a flat-rate cost, as a result of ten examinations usually carried out in the medical field of reference, at the cost of 10 euros on average. After acceptance, the patient is assigned to the referring doctor (the corresponding doctor). The physician, after visiting the patient and submitting him or her to the appropriate examinations, analyses the patient's medical history and, if he or she considers it appropriate, may request the specialist support for a second opinion. To request the specialist's support, the physician uses the teleconsultation tool and sends all the documents to the specialised doctor.

When the documentation received has been examined, the specialist can send the diagnosis to the applicant or request further examinations. After the diagnosis has been expressed, the patient must follow the suggested treatment before discharge (patient 1) or is directly discharged if no specific problems occur (patient 2). In next section we will use this log file to obtain the real process.

Table 2: Log file of process

Case id (patient)	Event identification	Timestamp	Activities	Resource	Price (€)
A	1	12/05/2020 h. 08:30	Patient acceptance	Reception	26,40
A	2	14/05/2020 h. 10:30	Referral to the requesting doctor	Support Service	26,51
A	3	17/05/2020 h. 09:30	Visit schedule	Support Service	26,50
A	4	08/06/2020 h. 09:30	Patient official visit	Doctor Silver (Corresponding doctor)	36,16
A	5	10/06/2020 h. 11:00	Angio exam	Doctor Coral	313,19
A	6	11/06/2020 h. 09:30	MRI (Magnetic Resonance Imaging)	Doctor Beige	46,14
A	7	11/06/2020 h. 12:30	Blood analysis	Doctor Blue	80,00
A	8	13/06/2020 h. 10:15	Visit schedule	Support service	26,51
A	9	01/07/2020 h. 15:30	Patient official visit	Doctor Silver	36,15
A	10	04/07/2020 h. 14:00	Request of teleconsultation	Doctor Silver	25,83
A	11	05/07/2020 h. 11:00	Evaluation of the request for consultation	Doctor Golden (Specialised doctor)	41,32
A	12	06/07/2020 h. 12:30	Specialist diagnosis sending	Doctor Golden	33,56
A	13	08/07/2020 h. 13:30	Visit schedule	Support service	26,50
A	14	18/07/2020 h. 15:30	Patient official visit	Doctor Silver	36,17
A	15	29/07/2020 h. 13:15	Radiation therapy I cycle	Doctor Magenta	987,81
A	16	10/08/2020 h. 08:30	Blood analysis	Doctor Blue	80,00
A	17	16/08/2020 h. 10:30	Radiation therapy II cycle	Doctor Magenta	987,80
A	18	18/08/2020 h. 08:30	Blood analysis	Doctor Blue	80,00
A	19	21/08/2020 h. 10:30	Radiation therapy III cycle	Doctor Magenta	987,81
A	20	23/08/2020 h. 08:30	Blood analysis	Doctor Blue	80,00
A	21	25/08/2020 h. 09:15	Visit schedule	Support Service	26,51
A	22	10/09/2020 h. 12:00	Patient official visit	Doctor Silver	36,16
A	23	12/07/2020 h. 09:00	Patient discharge	Reception	26,40
B	24	06/06/2020 h. 10:00	Patient acceptance	Reception	26,40
B	25	10/06/2020 h. 12:15	Referral to the requesting doctor	Support Service	26,51
B	26	12/06/2020 h. 13:00	Visit schedule	Support Service	26,50
B	27	05/07/2020 h. 11:30	Patient official visit	Doctor Brown (Corresponding doctor)	36,16
B	28	08/07/2020 h. 13:30	Eco-doppler exam	Doctor Coral	80,00
B	29	10/07/2020 h. 12:00	Blood analysis	Doctor Blue	80,00
B	30	13/07/2020 h. 13:00	CT (Computed Tomography) scanning	Doctor Blue	56,15
B	31	15/07/2020 h. 12:20	Visit schedule	Support Service	26,50
B	32	28/07/2020 h. 15:00	Patient official visit	Doctor Brown	36,16
B	33	06/08/2020 h. 13:00	Request of teleconsultation	Doctor Brown	25,82
B	34	07/08/2020 h. 07:00	Evaluation of the request for consultation	Doctor Lime (Specialised doctor)	41,32

B	35	09/08/2020 h. 08:15	Sending the request for a new test to the Specialist	Doctor Lime	33,54
B	36	11/08/2020 h. 07:00	Patient communication	Support Service	26,50
B	37	14/08/2020 h. 10:00	PET (Positron Emission Tomography) exam	Doctor Azure	42,21
B	38	16/08/2020 h. 08:40	Visit schedule	Support Service	26,50
B	39	25/08/2020 h. 12:15	Patient official visit	Doctor Brown	36,15
B	40	05/09/2020 h. 09:00	Request of teleconsultation	Doctor Brown	25,82
B	41	06/09/2020 h. 08:15	Evaluation of the request for consultation	Doctor Lime	41,33
B	42	08/09/2020 h. 15:15	Specialist diagnosis sending	Doctor Lime	33,56
B	43	10/09/2020 h. 09:10	Visit schedule	Support Service	26,50
B	44	25/09/2020 h. 17:00	Patient official visit	Doctor Brown	36,17
B	45	26/09/2020 h. 07:30	Patient discharge	Reception	26,40

(Source: own elaborations)
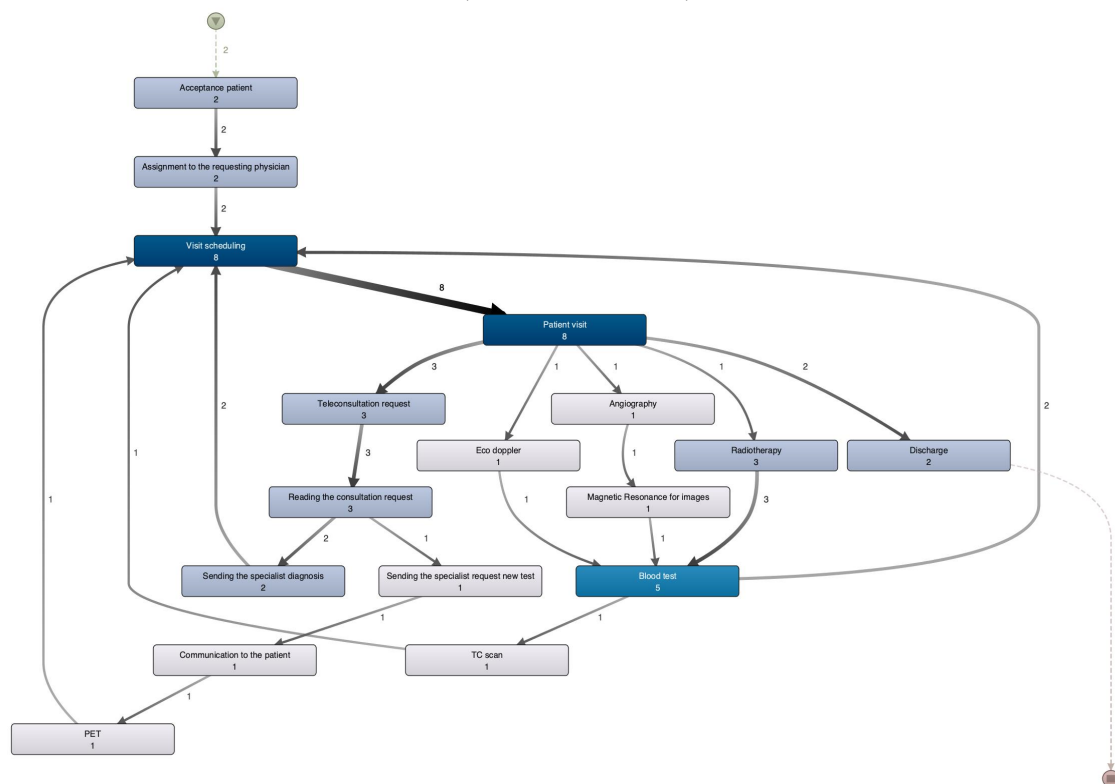
Figure 8: Process discovered (Source: own elaborations)

4. Process mining application and results

In this paragraph, we perform the discovery process as the first step using the Disco software. Elaborating the log file with this software we deliver the process shown in Figure 8.

As we can see, the process obtained from this application does not lead to a good performance. It presents bottlenecks, and even when the teleconsultation tool is used, the case duration is still high.

In particular, the bottlenecks are related to the following resources: Reservation centre (24,44%), Visit scheduling (17,78%), Patient visit (17,78%). Presenting a higher utilisation rate than the other resources, which instead present an underutilised capacity, the above-listed resources led to the entire process slowdown.

Table 3: Statistics for case

Case id	Event	Length	Price	Event price
A	23	118 days	4.073,39	117,10
B	22	104 days 30 minutes	816,22	37,10
Tot.	45		4.889,61	154,20

This aspect is more evident in the following data (Table 3, Table 4 and Table 5).

Now, we use the Business Process Management (BPM) approach in order to model, define, organize and monitor the healthcare processes, analysing and consequently optimising the clinical activities under study [27]. For the graphical representation of process steps, we have adopted the Business Process Model and Notation (BPMN) [28], [29].
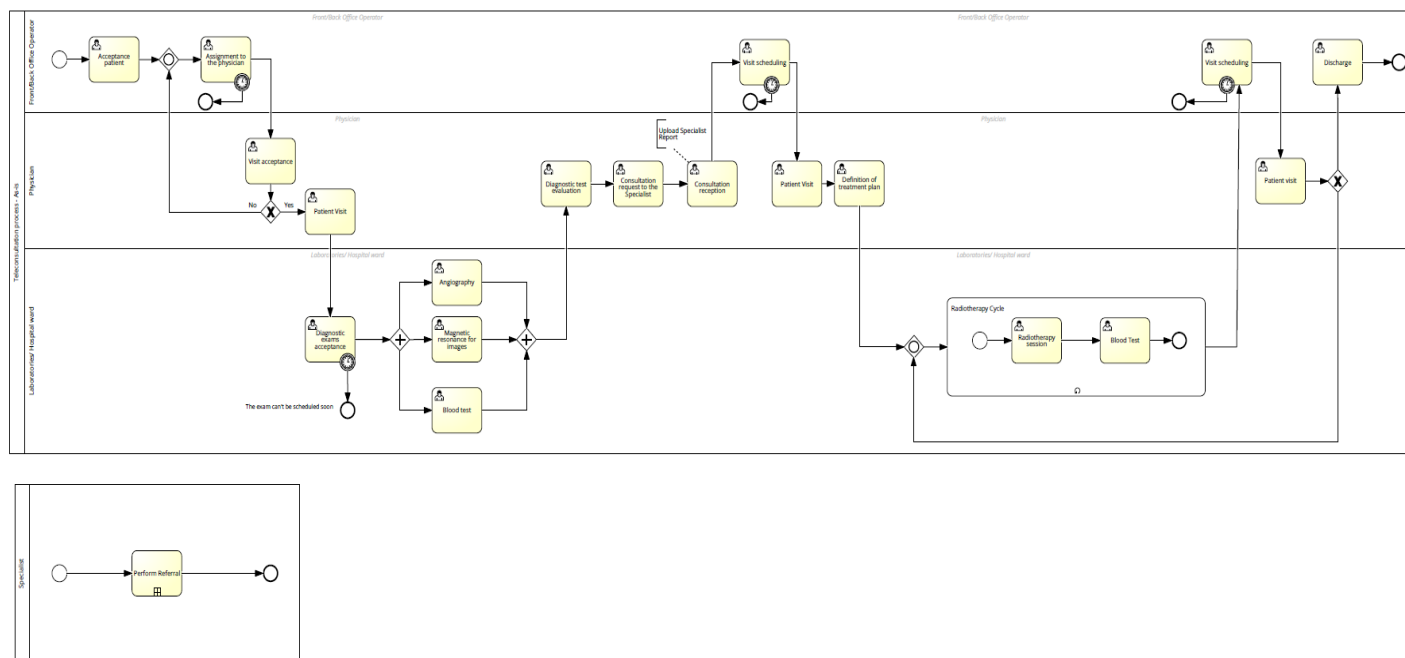
Figure 9: AS-IS process

Table 4: Statistics for activity

n.	Activity	%	Freq.
I	Visit schedule	17,78%	8
II	Patient official visit	17,78%	8
III	Blood analysis	11,11%	5
IV	Request of teleconsultation	6,67%	3
V	Evaluation of the request for consultation	6,67%	3
VI	Radiation therapy	6,67%	3
VII	Patient acceptance	4,44%	2
VIII	Referral to the requesting doctor	4,44%	2
IX	Specialist diagnosis sending	4,44%	2
X	Patient discharge	4,44%	2
XI	Angio exam	2,22%	1
XII	MRI (Magnetic Resonance Imaging)	2,22%	1
XIII	Eco-doppler exam	2,22%	1
XIV	CT (Computed Tomography) scanning	2,22%	1
XV	Sending the request for a new test to the Specialist	2,22%	1
XVI	Patient communication	2,22%	1
XVII	PET (Positron Emission Tomography) exam	2,22%	1
	Tot.	100,00%	45

Table 5: Statistics for resource

n.	Resource	%	Freq.
I	Support Service	24,44%	11
II	Doctor Blue	13,33%	6
III	Doctor Brown	13,33%	6
IV	Doctor Silver	11,11%	5
V	Reception	8,89%	4
VI	Doctor Lime	8,89%	4
VII	Doctor Magenta	6,67%	3
VIII	Doctor Coral	4,44%	2
IX	Doctor Golden	4,44%	2
X	Doctor Beige	2,22%	1
XI	Doctor Azure	2,22%	1
	Tot.	100,00%	45

In particular, the process flow modelled with BPMN notation [30] using Signavio tool is visible in the following figure (Figure 9).

5. Discussion

Starting from the results presented in the previous section, it emerges that our application reveals a fundamentally non-performing process. The analysis actually showed that the process is very slow (almost three months in both cases described), and there are bottlenecks in both resource and activities utilisation.

Then, we match the adopted practices with the best practices implemented in Piedmont, considered a virtuous region. The log file of Piedmont was not available, and therefore we were not possible to perform a compliance between the two processes. From observing data from the Ministry of Health (Table 6), the number of test equipment in Apulia was much lower, and this creates bottlenecks, since many more tests are needed in Apulia than in Piedmont. Furthermore, from the same statistics, we realize that the number of personnel employed in Piedmont was higher than in Apulia, and this affected the unitary personnel performance which, therefore, is higher in Apulia than in Piedmont. This leads to an over-utilisation of the units of work, and consequently bottlenecks also in terms of care pathway duration. These aspects are highlighted in Table 6.

Table 6: Data

Category	Classification	Region	Value
Medical devices number	Angio exam	Region 1	31
		Region 2	12
	MRI (Magnetic Resonance Imaging)	Region 1	33
		Region 2	16
	Eco-doppler exam	Region 1	364
		Region 2	138
	PET (Positron Emission Tomography) exam	Region 1	2
		Region 2	0
	CT (Computed Tomography) scanning	Region 1	80
		Region 2	49
Medical devices performance (per number)	Eco-doppler exam	Region 1	1646,8
		Region 2	2818,2
	CT (Computed Tomography) scanning	Region 1	3960,0
		Region 2	3986,9
	MRI (Magnetic Resonance Imaging)	Region 1	2041,3
		Region 2	2694,4
Age of devices (%)	> 15 years	Region 1	6,5%
		Region 2	18,3%
	10-15 years	Region 1	20,7%
		Region 2	16,6%
	10-7 years	Region 1	13,7%
		Region 2	19,1%
	7-3 years	Region 1	23,5%
		Region 2	18,0%
	< 3 years	Region 1	35,7%
		Region 2	28,0%
Staff workload	Performance per staff unit	Region 1	1362
		Region 2	1647
	Performance by technician	Region 1	2648
		Region 2	3114
	Performance by physician	Region 1	5800
		Region 2	6215
Operating personnel	Facility managers	Region 1	107
		Region 2	60
	Medical managers	Region 1	507
		Region 2	271
	Physical	Region 1	47
		Region 2	12
	Radiology technicians	Region 1	1110
		Region 2	541
	Nurses Professional	Region 1	191
		Region 2	186
	Auxiliaries	Region 1	242
		Region 2	117
	Administrative	Region 1	319
		Region 2	42
	Other personnel	Region 1	92
		Region 2	21

(Note: Piedmont = Region 1, Apulia = Region 2, own elaborations, source: Ministry of Health)
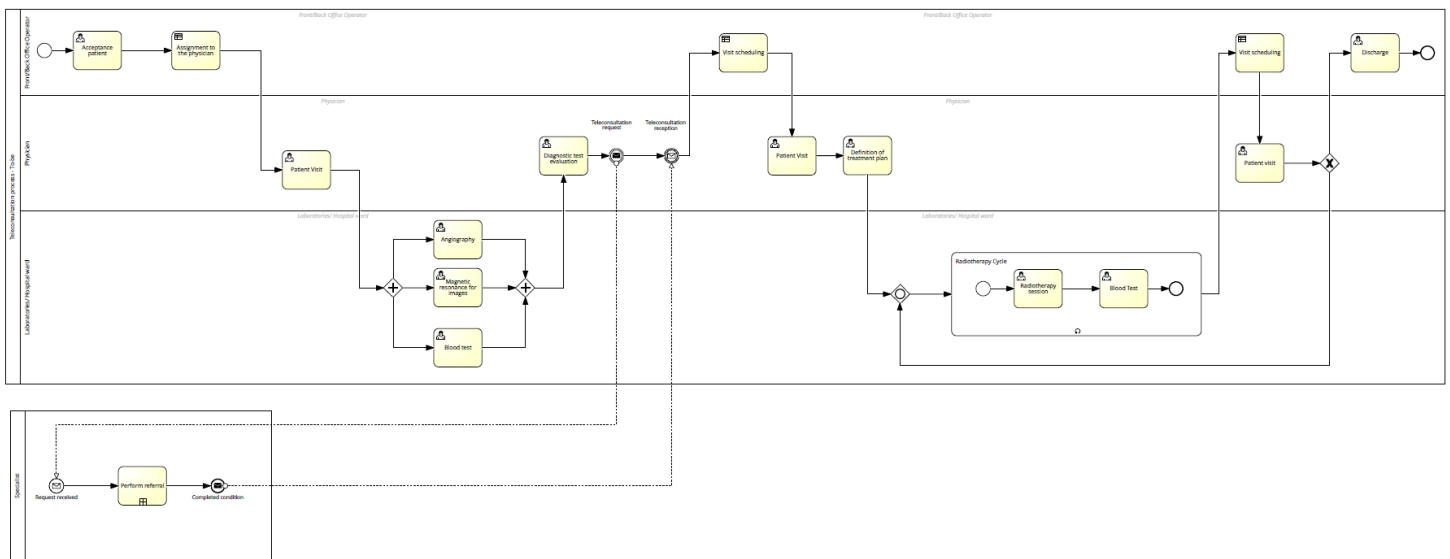
Figure 10: TO-BE process

Given all the problems that we faced in the process, as from the actual application represented by the log file, we designed a new process aimed at improving this process. Everything is represented in Figure 10.

Related to the AS-IS process, we have improved the TO-BE process in terms of time. In fact, in the TO-BE process modelling, the acceptance and scheduling phases of the visit by the doctor rely on certain decision-making procedures well-defined by the system (based on availability and time of doctors).

The TO-BE process included a change in assigning diagnostic examinations to different technicians in order to optimise the use of resources (personnel and healthcare equipment) and waiting times. Furthermore, as far as the teleconsultation is concerned, we have improved the TO-BE process over the AS-IS process. In particular, in the TO-BE process, the teleconsultation is made automatic both in the phase of specialised doctor identification for a second opinion, and in the consultation requesting phase. Even in the case of sending a second opinion, the TO-BE process is more effective, since it uses the same archiving system, which allows the corresponding doctor to examine the diagnosis in a timely manner.

Moreover, with the TO-BE process, we were able to decrease patients waiting duration and to improve the resources utilization, consequently reducing costs and optimising the healthcare service.

6. Conclusions

This paper demonstrates that process mining is a very-often-used technology in business and industrial processes but can also find useful application in the healthcare sector.

In fact, the process mining tools allow to decrease costs, increase employee and customer satisfaction, and to operate more proactively on a daily basis, which is fundamental in the healthcare sector, where it is crucial to improve the services to patients, especially in terms of care duration and cost reduction (primarily on the management side), taking into consideration the considerable financial commitment required by the sector.

However, although (approximate) data are available to create log files, mostly of them are very personal and not-usable. In fact, due to privacy and confidential reasons, hospital organizations are not disposed to grant or share them.

In conclusion, the application of process mining could make available tools finalised to improve the territorial equalisation of the public intervention (expenditure levels homogenization).

In view of the findings above, it would be suitable to use process mining technique in the health sector, and our hope is that this will take place in the future.

References

[1] A. Corallo, M. Lazoi, R. Paiano, F. Striani, "Application of process mining in teleconsultation healthcare: Case study of Puglia hospital. In Proceedings of the 10th International Conference on Information Systems and Technologies", 1-13, 2020, doi: 10.1145/3447568.3448540.

[2] W.V.D. Aalst, A. Adriansyah, A.K.A.D. Medeiros, F. Arcieri, T. Baier, T. Blickle, M. Wynn, "Process mining manifesto. In: International conference on business process management", Springer, Berlin, Heidelberg, 169-194, 2011, doi: 10.1007/978-3-642-28108-2_19.

[3] W. Van der Aalst, "Process Mining: Overview and Opportunities" ACM Trans. Manag. Inf. Syst., **3**, 1–17, 2012, doi: 10.1145/2229156.2229157.

[4] C.W. Günther, W.M.P. Van der Aalst, "Fuzzy Mining – Adaptive Process Simplification Based on Multi-perspective Metrics", Lecture Notes in Computer Science, Springer, Berlin, Heidelberg, **4714**, 2007, doi: 10.1007/978-3-540-75183-0_24.

[5] A. Weijters, W. Van der Aalst, A. de Medeiros, "Process Mining with the Heuristics Miner Algorithm", Technical Report, WP166 Beta Paper Series. Eindhoven University of Technology, Eindhoven, The Netherlands, 2006.

[6] R. Accorsi, Ernesto D, W. Van Der Aalst, "Unleashing operational process mining", 2014, doi: 10.4230/DagRep.3.11.154.

[7] W. Van der Aalst, "Process Mining: Discovery, Conformance and Enhancement of Business Processes", Springer: Berlin, Germany, Heidelberg, Germany, 2011.

[8] G. Geleijnse, H. Aklecha, M. Vroling, R. Verhoeven, F.N. Van Erning, P.A. Vissers, X.A. Verbeek, "Using Process Mining to Evaluate Colon Cancer Guideline Adherence with Cancer Registry Data: a Case Study", 2018.

[9] C. Fernandez-Llatas, B. Valdivieso, V. Traver, J.M. Benedi, "Using Process Mining for Automatic Support of Clinical Pathways Design", In Data Mining in Clinical Medicine, Number 1246, Springer: New York, NY, USA, 79-88, 2015, doi: 10.1007/978-1-4939-1985-7_5.

[10] R. Mans, W. Van der Aalst, R. Vanwersch, "Process Mining in Healthcare", Springer Briefs in Business Process Management, Springer International Publishing, Cham, Germany, 2015.

[11] E. Rojas, J. Munoz-Gama, M. Sepúlveda, D. Capurro, "Process mining in healthcare: A literature review", **61**, 224–236, 2016, doi: 10.1016/j.jbi.2016.04.007.

[12] F. Caron, J. Vanthienen, K. Vanhaecht, E.V. Limbergen, J. de Weerdt, B. Baesens, "Monitoring care processes in the gynecologic oncology department", Comput. Biol. Med., **44**, 88–96, 2014, doi: 10.1016/j.compbiomed.2013.10.015.

[13] V. Tandon, A. Raheja, S. Mishra, K. Garg, C. Dash, S.A. Borkar, S.S. Kale, "Trends in neurosurgical teleconsultation services across the globe during COVID-19 pandemic", World Neurosurgery, **150**, 2021, doi: 10.1016/j.wneu.2021.03.070.

[14] P. Baudier, G. Kondrateva, C. Ammi, V. Chang, F. Schiavone, "Patients' perceptions of teleconsultation during COVID-19: A cross-national study", Technological Forecasting and Social Change, **163**, 120510, 2021, doi: 10.1016/j.techfore.2020.120510.

[15] P. Baudier, G. Kondrateva, C. Ammi, V. Chang, F. Schiavone, "Digital transformation of healthcare during the COVID-19 pandemic: Patients' teleconsultation acceptance and trusting beliefs", Technovation, 102547, 2022, doi: 10.1016/j.technovation.2022.102547.

[16] C. Fernandez-Llatas, J.M. Benedi, J.M. Garcia-Gomez, V. Traver, "Process Mining for Individualized Behavior Modeling Using Wireless Tracking in Nursing Homes", Sensors, **13**, 15434–15451, 2013, doi: 10.3390/s131115434.

[17] R. Mans, H. Schonenberg, G. Leonardi, S. Panzarasa, A. Cavallini, S. Quaglini, W. Van der Aalst, "Process mining techniques: An application to stroke care", Stud. Health Technol. Inf., **136**, 573–578, 2008.

[18] R. Dunkl, K.A. Froschl, W. Grossmann, S. Rinderle-Ma, "Assessing Medical Treatment Compliance Based on Formal Process Modeling", In Information Quality in E-Health, Number 7058 in Lecture Notes in Computer Science, Springer: Berlin, Germany; Heidelberg, Germany, 533–546, 2011, doi: 10.1007/978-3-642-25364-5_37.

[19] A. Vathy-Fogarassy, I. Vassányi, I. Kósa, "Multi-level process mining methodology for exploring disease-specific care processes", 2022, doi: 10.1016/j.jbi.2021.103979.

[20] D. Gough, S. Oliver, J. Thomas, "An introduction to systematic reviews", Sage, 2017.

[21] A. Corallo, M. Lazoi, F. Striani, "Process mining and industrial applications: A systematic literature review", Knowledge and Process Management, **27**(3), 225-233, 2020, doi: 10.1002/kpm.1630 .

[22] Fluxicon Laboratories, Disco, Available online: https://fluxicon.com/disco/

[23] M. Egger, G.D. Smith, D.G. Altman, "Systematic reviews in health care: meta-analysis in context", BMJ Books, London, 2008.

[24] F. Striani, "Green and Blue Economy: Definitions, Challenges and Limits", International Journal of Environmental Sustainability and Green Technologies (IJESGT), **11**(2), 16-33, 2020, doi: 10.4018/IJESGT.2020070102.

[25] T. G. Erdogan, A. Tarhan, "Systematic mapping of process mining studies in healthcare", IEEE, 2018, doi: 10.1109/ACCESS.2018.2831244.

[26] Z. Valero Ramón, "Dynamic risk models for characterising chronic diseases' behaviour using process mining techniques", Doctoral dissertation, Universitat Politècnica de València, 2022, doi: 10.4995/Thesis/10251/181652.

[27] M. Weske, "Business process management architectures - Third edition", Springer, Berlin, Heidelberg, 2019.

[28] D. Bano, J. Michael, B. Rumpe, S. Varga, M. Weske, "Process-aware digital twin cockpit synthesis from event logs", Journal of Computer Languages, 101121, 2022, doi: 10.1016/j.cola.2022.101121.

[29] M. Dumas, M. La Rosa, J. Mendling, H.A. Reijers, "Introduction to business process management", In Fundamentals of business process management, Springer, Berlin, Heidelberg, 1-33, 2018, doi: 10.1007/978-3-662-56509-4_1.

[30] M. Ramos-Merino, L.M. Álvarez-Sabucedo, J. M. Santos-Gago, J. Sanz-Valero, "A BPMN based notation for the representation of workflows in hospital protocols", Journal of medical systems, **42**(10), 1-10, 2018, doi: 10.1007/s10916-018-1034-2.

ASTES

Natural Tsunami Wave Amplitude Reduction by Straits – Seto Inland Sea

Mikhail Lavrentiev[*,1], Andrey Marchuk[1,2], Konstantin Oblaukhov[1], Mikhail Shadrin[1]

[1]*Institute of Automation and Electrometry SB RAS, Novosibirsk, 630090, Russia*

[2]*Institute of Computational Mathematics and Mathematical Geophysics SB RAS, Novosibirsk, 630090, Russia*

A B S T R A C T

Seto Inland Sea is situated between Japanese islands Honshu, Kyushu, and Shikoku. It is separated from the ocean by the Bungo Channel, Kii Channel, and other narrow straits around Shikoku Island. The objective of the article is to draw the attention to the question of how well the coastal population and infrastructure of those locations are protected against a tsunami wave appearing in the area of Nankai through offshore Japan and consequently make informed decision about strengthening the protections if needed. This question is critical because strong underwater earthquakes are expected according to the major earthquake repeatability in this subduction zone. Hence, the influence of strait width and tsunami wave period to the wave amplitude change after passing a strait was studied through the application of numerical modelling. Both models of geometry of computation domain with the flat bottom and the real bathymetry of the area under study were used. Numerical modelling was based on nonlinear shallow water system, commonly used in tsunami related studies. All calculations were made at a personal computer equipped with the hardware code accelerator – FPGA (Field Programmable Gates Array) Calculator, which had been recently introduced by the authors. A series of computational experiments, both with model straits and in the water area around southern part of Japan, have shown that when a tsunami wave passes through the strait, its height is significantly reduced, providing better tsunami safety regulations of the population of the inner seas separated from the ocean by narrow straits. At the same time, longer tsunami waves retain a larger amplitude after passing through the strait compared to shorter ones. Result of the paper consists of numerical study of the influence of narrow straits on the maximal heights of tsunami wave. Qualitative corollaries between length of tsunami and reduction rate of the wave amplitude after passing a strait should help warning services to properly evaluate tsunami danger in water areas separated from tsunami source by a narrow strait.

1. Introduction

This paper is an extension of work originally presented at the conference OCEANS 2021: San Diego – Porto [1].

Tsunami waves, usually created by large underwater earthquakes, are propagated due to the gravity and grow substantially in amplitude as they approach the shore. One of the tasks of a tsunami warning service is to identify coastlines by the level of threat once a tsunami has been confirmed and act accordingly. Namely, it is critical to determine in which areas of the coastline high waves threatening local population and infrastructure are expected and hence evacuation must be announced, and in which areas tsunami damage may be minimal. Observations of tsunamis show that after a wave passes through a narrow strait, its height decreases significantly. Therefore, an area separated by a narrow strait from the open ocean is somewhat protected from tsunami impacts, unless the source of the tsunami is located in that area.

As it's suggested in literature after studies of historical records (see [2]), a major underwater earthquake (following by tsunami wave) is expected at Nankai through offshore Japan. This article evaluates the possible impact of such event to the Seto Inland Sea, bounded by the Honshu, Kyushu, and Shikoku islands of Japan. The bottom relief of the studied water area is given in Figure 1. Tsunami wave can arrive in this water area only through the Bungo

*Corresponding Author: Mikhail Lavrentiev, mmlavrentiev@gmail.com

Channel in the south and Kii Channel in the north. These channels are narrow enough to reduce valuably of the amplitude of tsunami wave. To study numerically this phenomenon, the wave parameters related to the initial seabed displacement at tsunami source of the event, which took place in this area nearly 300 years ago was used but with a rather lower displacement. Such approximation, shown in Figure 2, has been proposed in [2] on the basis of available historical records.
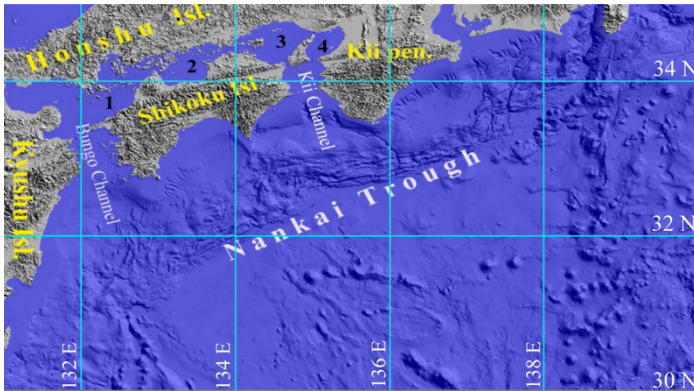

Figure 1: Visualization of the digital bathymetry for the water area under study. Seto Inland Sea surrounded by Shikoku, Honshu and Kyushu Islands is divided in sectors 1 - 4

The goal of the numerical study was to understand the influence of the size of tsunami source to amplitude reduction rate while the wave is passing through a narrow channel. Model tsunami sources considered had time periods from 5 to 15 minutes. Such numbers correspond to sources of an elliptic shape having short axis variation interval between 60 km and 200 km. Note that even trans-oceanic waves with that long period can arrive in the region under the study.
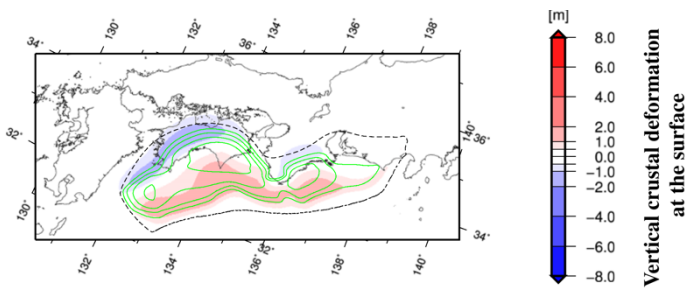
Figure 2: The expected vertical bottom displacement for M_W=8.66 earthquake in Nankai subduction zone [2]

Rest of the paper is arranged as follows. The governing equations (along with the initial shape of the wave) are first introduced and the auxiliary numerical tests concerning straits of model shape are described. In particular, the influence of the strait width and wavelength on the wave amplitude is evaluated. The detected impacts are then confirmed for the real digital bathymetry of the Nankai Through and Seto Inland Sea. The obtained results are then discussed.

2. Design of Numerical Experiments

2.1. Model equations

For numerical modeling of tsunami wave propagation, a nonlinear mathematical shallow water system was chosen without considering external forces (bottom friction, Coriolis force, etc.), except the gravity [3]:

$$\frac{\partial H}{\partial t} + \frac{\partial (uH)}{\partial x} + \frac{\partial (vH)}{\partial y} = 0 \tag{1}$$

$$\frac{\partial u}{\partial t} + u\frac{\partial u}{\partial x} + v\frac{\partial u}{\partial y} + g\frac{\partial H}{\partial x} = g\frac{\partial D}{\partial x} \tag{2}$$

$$\frac{\partial v}{\partial t} + u\frac{\partial v}{\partial x} + v\frac{\partial v}{\partial y} + g\frac{\partial H}{\partial y} = g\frac{\partial D}{\partial y} \tag{3}$$

where $H(x,y,t)=\eta(x,y,t)+D(x,y)$ is the total height of water column, η being the sea surface disturbance (wave height), $D(x,y)$ – depth (which is supposed to be known at all grid points), $u(x,y,t)$ and $v(x,y,t)$ are components of water flow velocity vector, g - acceleration of the gravity. Note that this approximation is widely used for tsunami simulation [4, 5].

2.2. Model Assumptions

The shallow water model (1)-(3) used for numerical modeling of tsunami propagation assumes that the wave length is significantly (at least an order of magnitude) greater than the depth of the water area where the wave is traveling. It follows that the velocity c of tsunami propagation does not depend on its amplitude and is determined only by the water depth by the Lagrange formula [3]: $c = \sqrt{gD}$. Due to the constancy of the tsunami wave period during propagation, its length in the area with constant depth also remains constant. Therefore, in such areas, reasoning in terms of "wave period" and "wave length" is equivalent. In areas with variable depth, such substitution of concepts is incorrect.

2.3. Instrument for Numerical study

In the Method Of Splitting Tsunami (MOST) software package [4,6] (official tsunami modeling instrument of the USA Tsunami Warning Centers) a numerical calculation of shallow water system is based on the splitting method. The system is solved numerically in two steps. During each step the changing of variables only along one space direction is a subject of the study. The essence of the method is that the solution is sought as the result of the variables behavior in the course of the sequential solution of two auxiliary one-dimensional systems. In the present paper a parallel implementation of McCormack's scheme, which has the second order of approximation [7], is used. As the earlier numerical experiments [8] have shown, the proposed software allows finding solutions of the shallow water equation system with the required accuracy. Due to the hardware acceleration, high performance is achieved when using a personal computer [8].

2.4. Auxiliary Numerical Tests

In order to study the process of passage of a long wave through narrow straits and to identify the degree of influence of the strait width and the wave period on the wave parameters beyond the strait, a series of model computational experiments were conducted. In them, the channel (strait) was represented by straight shorelines converging at an angle of 90° until the width of the strait becomes equal to the given "width". After this narrowest point of the strait ("bottle neck"), the shorelines begin to diverge at the same angle 90° (Figure 3).

Computation domain, given in Figure 3, represents a 1000x1000 km square with a constant depth of 1000 m. The two "water reservoirs" having the shape of triangles are connected by a narrow strait with a width of 40 km (as shown in Figure 3) and also 20 km for alternative numerical tests. The dry land, the boundaries of which reflect tsunami waves, is colored in green (Figure 3). The MacCormack difference scheme [7] was realized on FPGA PC board [8] for numerical modeling of tsunami wave propagation. The use of this particular algorithm is not a determining factor in this study. For calculations, any other correct method of solving the shallow water equations could be used, for example, the basic one in MOST software package [4,6].

The initial tsunami wave was generated using boundary conditions on the left boundary of the region, where during the wave period *tp* the vertical displacement of the water surface η and the horizontal velocity components of the water flow were set by the following formulae:

$$\eta = \frac{\eta_0}{2}\left(1 + \cos\left(\frac{t \cdot 2\pi}{tp}\right)\right), \; u = \eta\sqrt{\frac{g}{D}}, \; v=0 \quad (4)$$

here the variable *t* belongs to the interval *0<t<tp*. Period of the tsunami wave is characterized by the quantity *tp*, and η_0 sets the initial wave height of its crest. Such a way for wave generation was developed and tested in [9]. As a result, a tsunami wave is generated at the left boundary, which has a height $\eta_0=1$ m and a period *tp*, moving to the right of this boundary (Figure 3). In numerical calculations, the wave period was set to 300, 600 and 900 seconds. The simulation result is the distribution of tsunami height maxima over the entire computational domain. Figure 3 shows the results of calculations of the wave with a period of 300 seconds through the strait with a width of 40 km at the narrowest point. The height of isolines in Figure 3 (and all other figures, showing results for model straits) are drawn with interval of 5 cm..

"bottle neck", which has a width of 40 km. At the same time, the radiation of wave energy in the right half of the calculation region has a narrow directivity (see Figure 3). To study the effect of wavelength (period), the authors conducted two more computational experiments at the same strait for the passage of the tsunami with a period of 600 and 900 seconds. Figure 4 shows the distribution of maximum heights resulting from the passage of a long wave with a period of 600 sec through the same strait.

Another calculation simulating tsunami passage with the period of 900 sec through the same model strait was also conducted. The results are shown in Figure 5.
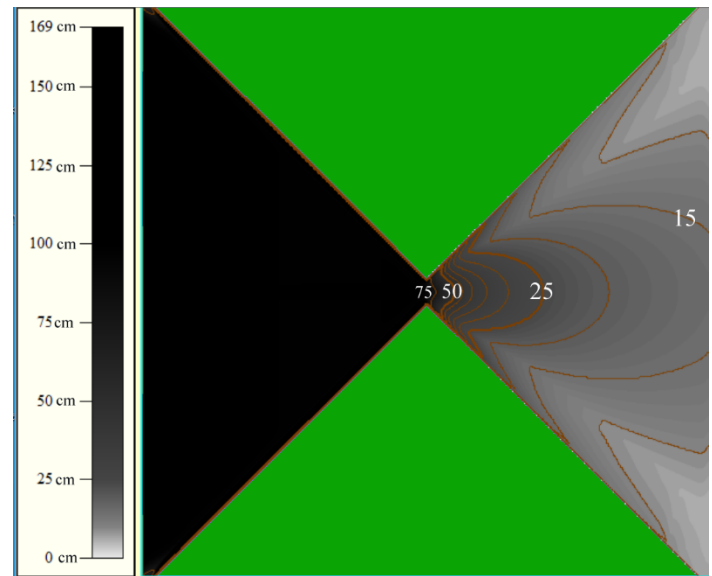
Figure 4: Numerically obtained distribution of the tsunami height maximums. Wave period is 600 sec., strait has 40 km width
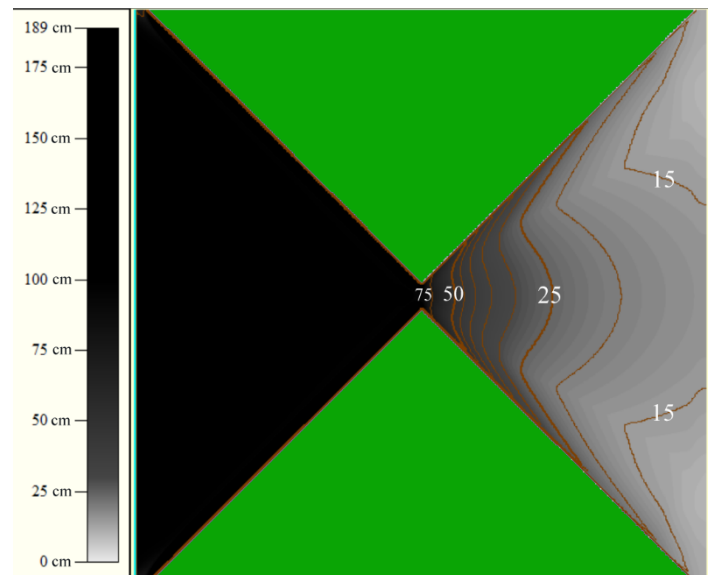
Figure 5: Numerically obtained distribution of the tsunami height maximums. Wave period is 900 sec., strait has 40 km width

Figure 3: Numerically obtained distribution of the tsunami height maximums. Wave period is 300 sec., strait has 40 km width. The entire area is 1000x1000 km square. Interval (in height) between height isolines is equal to 5 cm

Figure 3 shows that the tsunami height, initially equal to 100 cm, begins to decrease quite rapidly just after the passage of the

Figures 3-5 show that, as the length (period) of the tsunami wave passing through the 40-km wide strait increases, the radiation sector of the wave energy expands in the right subarea (after the wave has passed the "bottle neck"). In case of a longer wave, a

slower decrease in the tsunami amplitude is observed with distance from the narrowest point of the strait. In particular, for a wave with a period of 300 seconds, the tsunami height in the center of the right boundary of the computational domain was about 14 cm. For the wave with the period of 600 sec - 16 cm. And for the longest wave (with a period of 900 sec) - 17 cm (Figures 3 – 5). Note that the increased amplitude of the tsunami at the boundaries of the strait is a consequence of the wave reflection from the shore.

During the next series of computational experiments, the width of the narrowest part of the strait was reduced to 20 km, i.e., half as much as in the first series. At the same time, the angle of convergence of the shorelines remained equal to 90°. The parameters and direction of propagation of the generated wave remained the same. Figure 6 shows the distribution of tsunami height maxima with a period of 300 s as it passed through a 20 km wide strait.

Comparison of Figures 3 and 6 shows that the tsunami height decreases significantly faster after the wave passage of the 20-km wide bottle neck compared to the case of the 40-km wide strait.

Figures 7 and 8 show the distribution of maximum tsunami heights when simulating tsunami waves with periods of 600 and 900 sec for the 20 km wide strait.
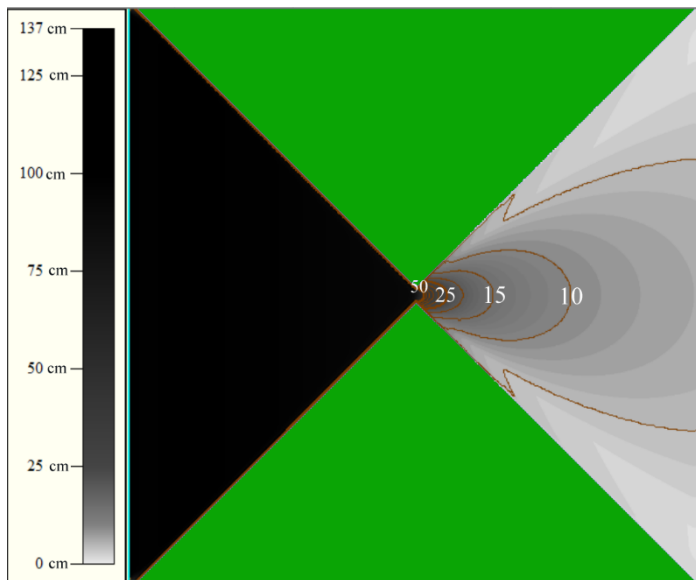
Figure 6: Numerically obtained distribution of the tsunami height maximums. Wave period is 300 sec., strait has 20 km width

Comparing the series of Figures 3-5 with Figures 6-8, when simulating the passage of the wave with the period of 300, 600 and 900 sec through twice as narrow 20 km wide strait, the tsunami heights in the right subarea were expectedly reduced in comparison with the 40 km wide strait. For example, in case of the 40-km wide strait, the height of the wave with the period of 600 seconds in the center of the right boundary of the computational domain equals to 16 cm (Figure 4), while for the 20-km wide strait the height of the initial wave in the same point of the right boundary wave height is detected at 8.5 cm (Figure 7). That is, the height of the wave is almost half as much in the case of a narrower strait. However, when the wave period was increased to 900 sec, this difference decreased and was 17 cm versus 14 cm (Figures 5 and 8).
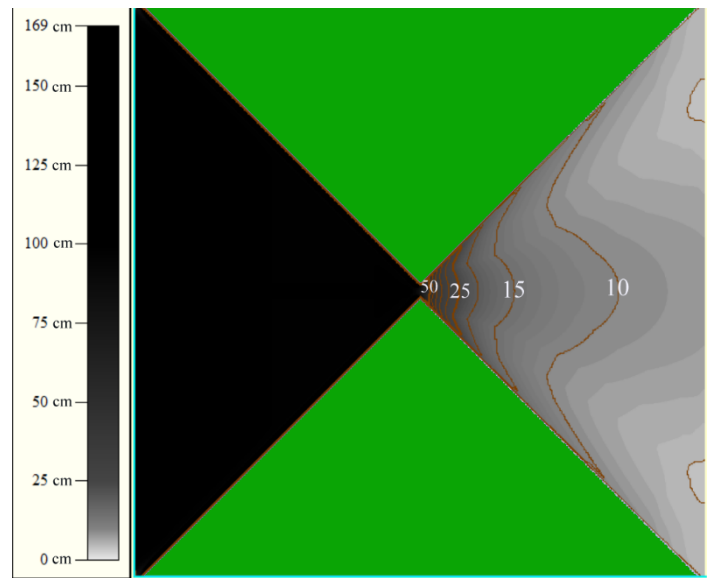
Figure 7: Numerically obtained distribution of the tsunami height maximums. Wave period is 600 sec., strait has 20 km width
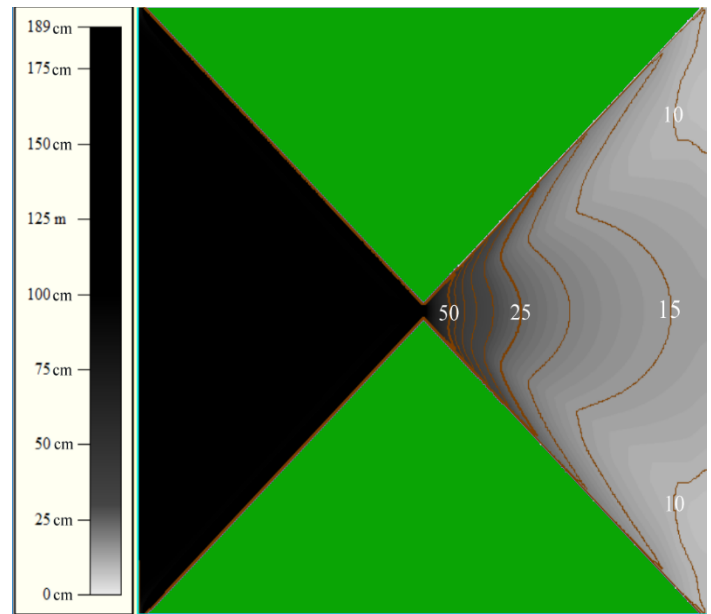
Figure 8: Numerically obtained distribution of the tsunami height maximums. Wave period is 900 sec., strait has 20 km width

3. Numerical Results

3.1. Computational Domain

To investigate the tsunami wave propagation through the straits around Shikoku Island using JODC [10] bathymetric data, a grid bathymetry was prepared, covering the area around the Nankai Trough and Seto Inland Sea from 131° to 140° East Longitude and from 30° up to 35° North Latitude. The depth value array is 3,000 × 2,496 nodes. The spatial grid step in the longitude direction was 0.003 arc degree (282 m), and in the South-North direction the grid step was chosen to be 0.002 arc degree (223 m). Visualization of the computational domain's geography and bathymetry is presented in Figure 1.

3.2. The influence of the tsunami wave period on the wave height in the Seto Inland Sea.

Several numerical tests were conducted to simulate tsunami wave propagation through the narrow strait using real bathymetry. Geographic area around the Shikoku Island (Southward of Japan) was considered. Visualization of this computational domain is given in Figure 1.

The tsunami wave entering through the Bungo Channel and Kii Channel into the Seto Inland Sea was generated using the same boundary conditions (2) on the lower boundary of the computational domain as in the calculations of the wave passing through the straits with the model configuration (cf. Figure 3). Values of flow velocity components must be swapped in the formulae (2).

Similar to numerical tests at the bathymetry model, tsunami waves having periods of 300, 600 and 900 seconds were considered. Initial wave height was 1 m. Numerically obtained tsunami heights maximums around Shikoku Island in case of 600 sec. period wave are shown in Figure 9. The wave was initiated at the lower boundary.
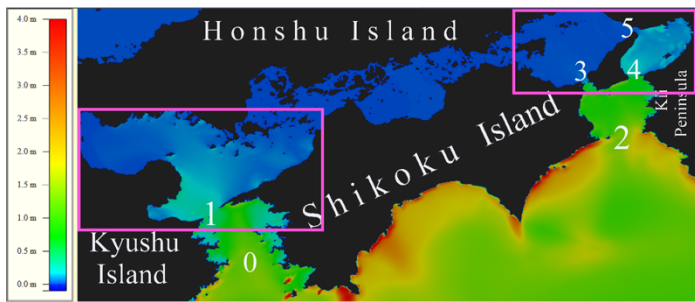
Figure 9: Location and numbering of straits around Shikoku Island. Tsunami wave maxima all around computational area resulted by tsunami modeling of 600 sec. period wave are visualized according to the color legend in the left side of figure

To show the existing narrow straits around Shikoku Island in the considered water area, the white numbers in Figure 9 are used. So, the Bungo Chanel is marked with the number 0. According to numerical experiments, the Kii Channel (having number 2 in Figure 9) has practically no impact on tsunami wave amplitude because it is wide enough. However, the "bottle neck" of the Bungo Channel (indicated by number 1) significantly reduces tsunami height. Numerical results for subareas outlined by pink rectangles (Figure 9) in more detail will be shown later. They contain the straits 1,3,4 and 5.

A series of computational experiments with another tsunami period were carried out in order to study the wavelength influence on the tsunami protection ability of the straits. The influence of the Bungo Chanel on tsunami amplitude is presented in Figure 10 for the 300 sec. period wave.

Numerical results with the same wave period of 300 sec. in the area to the east of Shikoku Island are given in Figure 11. This area, bounded by the pink rectangle in Figure 9, contains the straits number 3-5.

Results of numerical simulation presented in Figures 10 and 11 show high influence of the narrow straits in the Seto Inland Sea on the maximal heights of a tsunami wave. So, the strait 3 (see Figure 9) reduces the wave amplitude by 10 times, while the Straits 1 and 4 – by nearly 4 times. After passing the strait, the wave amplitude is going down because of diffraction and refraction. As a result,

the incoming wave of 1 m amplitude becomes almost negligible (with the height of 1-2 cm) to the north of Shikoku Island behind the straits, which is shown in Figures 10 and 11.
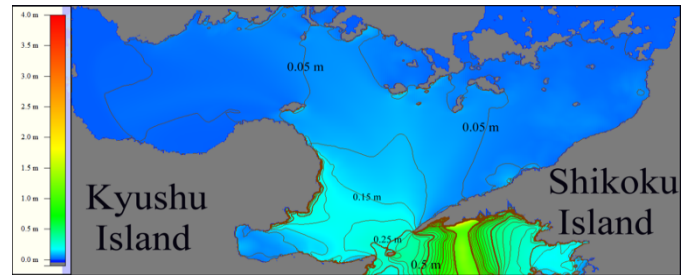
Figure 10: The maximum tsunami heights distribution of the wave having 300 sec period when it passes the Bungo Channel which is indicated by number 1 in Figure 9. Isolines of tsunami height maxima are drawn with an interval of 5 cm
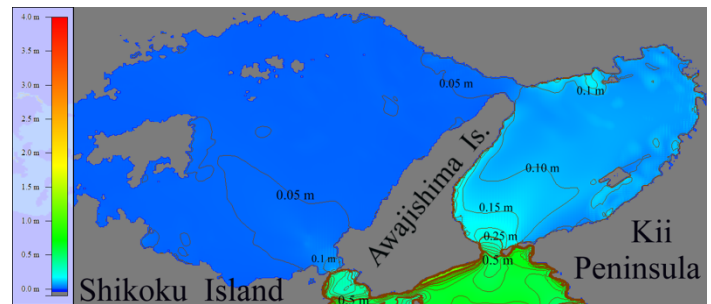
Figure 11: The maximum tsunami heights distribution of the wave having 300 sec period when it passes wide Kii Channel (indicated by number 2 in Figure 9) and narrow straits 3,4 and 5 in the eastern part of Seto Inland Sea

To analyze the dependence of tsunami wave amplitude reduction on the wave period, additional numerical experiments for the Bungo Channel were conducted. The obtained results for the wave periods of 600 and 900 sec. are given in Figures 12 and 13.
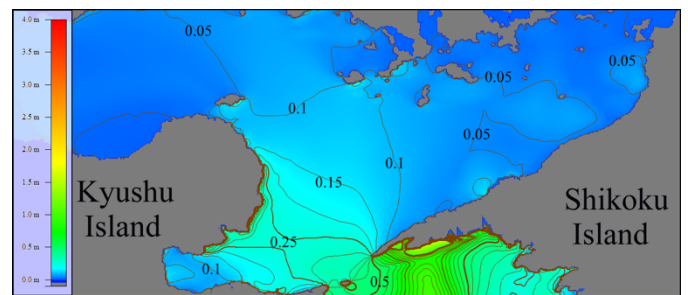
Figure 12: Distribution of tsunami height maxima after the wave having period of 600 sec passed through Bungo Channel. Isolines are drawn with an interval of 5 cm
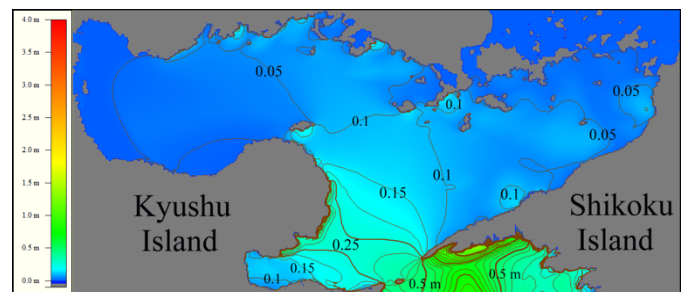
Figure 13: Distribution of tsunami height maxima after the wave having period of 900 sec passed through Bungo Channel

The result of the analysis of the tsunami wave behavior at real bathymetry, shown in Figures 10, 12, 13, is similar to that of the model of numerical experiments, given in Figures 3-8. Namely, the longer is the incoming wave, the larger is the tsunami wave amplitude in the inland sea after the Bungu Channel. The same phenomena are observed for the strait to the right of Shikoku Island studying wave periods of 300, 600 and 900 seconds. Visual results are given in Figures 11, 14 and 15.
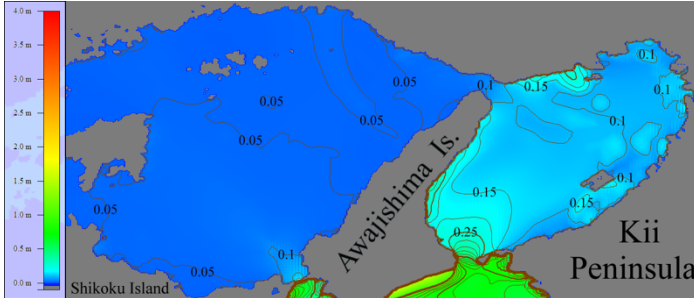
Figure 14: The wave height maxima distribution around Awajishima Island calculated in the course of numerical modeling of tsunami having period 600 sec
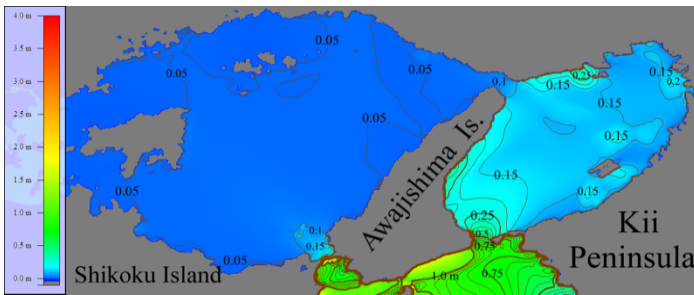
Figure 15: Isolines of the wave height maxima distribution around Awajishima Island calculated in the course of numerical modeling of tsunami having period 900 sec

Considering in detail the water area with the straits number 3, 4 and 5 (Figure 9) one concludes that the rather narrow channels provide better protection against tsunami waves. Indeed, the tsunami height decreases by about three times passing the strait number 4, and by about eight times passing through the strait number 3, Figures 11-15. The inner sea itself, being characterized by a comparatively low depth, reduces tsunami wave amplitude due to diffraction and refraction.

4. Discussion

Numerical calculations for model strait configurations and real straits in the southern part of Japan around Shikoku Island revealed certain patterns of tsunami wave passage through narrow straits. It was found that after passing the narrowest point of the strait, the wave height decreases rapidly in the widening water areas behind the strait due to wave refraction and diffraction. As a result, already in the center of the area, separated from the ocean by the narrow strait, the tsunami height is at an order of magnitude lower than before the wave enters the strait. It is clear from Figures 10-15 that with tsunami heights in front of the narrow straits of the order of 0.5 m to 1 m, the wave heights in the Seto Inland Sea on average are limited by 10 - 15 cm. When the length (period) of the generated wave increases, the maximum heights in the inland waters slightly increase. According to the results of this study, the authors conclude that the population and infrastructure of the Seto Inland Sea coast are sufficiently protected from the impacts of tsunamis generated in the Nankai Trough region. Only in the event of a catastrophic scale with tsunami heights at the entrance to the Straits exceeding 10 m, the population of the coasts of inland waters around Shikoku Island may be severally affected by tsunamis.

5. Conclusion

As a result of a series of numerical calculations of the passage of the tsunami wave with various period through the straits of model configuration, the degree of amplitude reduction after the wave passed the narrowest part of the strait was found. In the same series of numerical experiments, the dependence of the height distribution behind the strait on its width in its narrowest place was studied. The upper limits of tsunami heights in different parts of Seto Inland Sea water area depend on length (period) of the wave coming from Pacific Ocean through the straits around Shikoku Island. The longer the wave period, the higher its amplitude inside this water area. Since narrow straits naturally significantly reduce the height of waves passing through them, tsunamis with a height of more than 1 m can be observed inside Seto Inland Sea only in case of catastrophic events with an extremely large source. Further research on this issue will include model calculations of tsunami behavior in alternative configurations of the straits. Computational experiments simulating the passage of tsunamis through real straits in other places of the Pacific coast will be conducted as well.

Conflict of Interest

The authors declare no conflict of interest.

Acknowledgement

References

[1] M. Lavrentiev, An. Marchuk, K. Oblaukhov, M. Shadrin, "The wavelength influence on tsunami height in Seto Inland Sea," in Global Oceans 2021: San Diego - Porto, In Person & Virtual: September 20-23, 2021, Town and County San Diego, doi: 10.23919/OCEANS44145.2021.9705819.

[2] M. Hyodo, T. Hori, K. Ando, and T. Baba, "The possibility of deeper or shallower extent of the source area of Nankai Trough earthquakes based on the 1707 Hoei tsunami heights along the Pacific and Seto Inland Sea coasts, southwest Japan", Earth, Planets and Space, 66(123), 2014, http://www.earth-planets-space.com/content/66/1/123.

[3] J.J. Stoker, Water Waves. The Mathematical Theory with Applications, Interscience publishers: New York, NY, USA, 1957.

[4] E. Gica, M. Spillane, V. Titov, C. Chamberlin, J. Newman, "Development of the forecast propagation database for NOAA's short-term inundation forecast for tsunamis (SIFT)," *NOAA Technical Memorandum*, 2008. URL: https://nctr.pmel.noaa.gov/Pdf/brochures/sift_Brochure.pdf (accessed on 19 December 2021).

[5] Z. Kowalik, T.S. Murty, Numerical modeling of ocean dynamics, World Scientific, 1993.

[6] V.V. Titov, F.I. Gonzalez, "Implementation and testing of the method of splitting tsunami (MOST) model", NOAA Technical Memorandum ERL PMEL-112, USA, 1977.

[7] R.W. MacCormack, A.J. Paullay, "Computational Efficiency Achieved by Time Splitting of Finite–Difference Operators," in 10th Aerospace Sciences Meeting, San Diego, CA, USA, 17–19 January 1972; AIAA Paper; pp. 72–154.

[8] M.M. Lavrentiev, A.A. Romanenko, K.K. Oblaukhov, An.G. Marchuk, K.F. Lysakov, M.Yu. Shadrin, "FPGA Based Solution for Fast Tsunami Wave Propagation Modeling," in 27th (2017) Int Ocean/Polar Eng Conf, San Francisco, CA, USA, June 25-30, 2017, 924-29.

[9] K. Hayashi, A. Marchuk, A. Vazhenin, "Generating Boundary Conditions for the Calculation of Tsunami Propagation on Nested Grids," Numer. Analys. Appl. 11, 256–267, 2018, https://doi.org/10.1134/S1995423918030060.

[10] J-DOSS|JODC [Electronic resource]. Available online: URL https://jdoss1.jodc.go.jp/vpage/depth500_file.html (accessed 18.07.2022).

Designing the MIMO SDR-based Antenna Array for 5G Telecommunication

Meriem Drissi[1,*], Nabil Benjelloun[2], Philippe Descamps[3], Ali Gharsallah[1]

[1]MER Laboratory, Department of electronics, FST, University Tunis El Manar, 1068, Tunisia

[2]IRSEEM Laboratory, Department of electronics, University Rouen Normandie, Rouen, 76801, France

[3]CNRS Laboratory, Department of electronics, University Caen Normandie, Caen, 14000, France

A B S T R A C T

With the significant spread of 5G telecommunication systems, the demand for high quality of service and better coverage is growing rapidly. Multiple-input–multiple-output is planned to be among the key technologies in 5G telecommunication's field. In this article, a new fully digital 2×2 MIMO testbed is implemented, using USRP B210 and 2 pairs of microstrip antennas with 4 radiation elements. In this implementation we cover the reconfigurability of the USRP combined with MATLAB, providing flexible integration between real-time and software host processing.

1. Introduction

Multiple-input–multiple-output becomes the most challenging technology in the 5G and the upcoming 6G telecommunication applications, given the ability of increasing the quality of communication and the rate of data [1], [2].

Multiple input multiple output (MIMO) has proven to be an important technique for communication systems. This technique benefits by using two or more antennas to transmit and receive data simultaneously, in order to increase the data rate and to provide a better reliability. So, MIMO provides the solution to the challenge [3], [4].

To develop a MIMO system, a microstrip antenna is designed, as well as is widely deployed in telecommunication systems due to its low profile, ease of fabrication and miniature size.

Much research such as [2]-[7] focus mostly on simulations and theorical analysis ignoring the system implementation because of its complexity, power consumption and low cost. the software defined radio has been found to avoid such limitations [1], [3]. More specially, by using SDR flexibility, reconfigurability and Rapid prototyping are covered to support new standards and protocols [8]-[10].

On this issue a new fully digital MIMO 2X2 has been implemented, this prototype is combining pairs of microstrip antennas with 4 radiation elements on both terminals.

For conveying and receive one or more types of wave signals simultaneously, An AM modulation is involved using Simulink and the flexibility, reconfigurability and low cost of USRP B210.

In our testbed, we investigate and profile the characteristics of USRP B210 platform including full steps such, transmission, modulation, spectrum, received signal and demodulation.

The rest of this document is arranged as bellow. Section II describes a comparison between rectangular and circular patch. In Section III, in order to perform the gain and assure circular polarization we moved on antenna array. In Section IV, we introduce an overview of our 2×2 MIMO testbed based on SDR. In Section IV, we define our SISO experimental results while analyzing our results. Even we report our novel model MIMO using AM modulation by studying our system's performance, finally, in section V, we come to end the article.

2. Patch Antenna

2.1. Single element design geometry

The antenna is the first component of the MIMO system. This design uses patch antenna. Considering low profile, ease of

---

*Corresponding Author: Meriem Drissi, drissimeriem1@gmail.com

fabrication, and low cost, patch antennas have proven to be the most frequently antennas [11].

Firstly, we start by a brief comparison between the most common shapes which are rectangular and circular configurations. FR4 epoxy has been chosen. Its relative permittivity is 4.4 [12], in order to provide a balanced comparison.

In fact, both shaped microstrip patch antennas are performed using HFSS. The simulated antennas are resonating at 3.48 GHz.

Starting with the software designed version of rectangular shape which is shown on figure 1, its dimensions are $20 \times 27\ mm^2$.
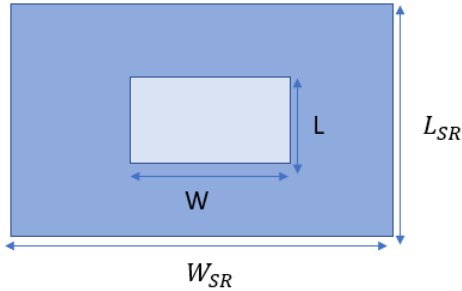
Figure 1: Geometry of the rectangular patch antenna.

In order to determine the microstrip patch antenna's dimensions, the equations below have been used. Based almost entirely on the width and length of the rectangular patch, the design has been conceived [13], [14].

$$W = \frac{c}{2f_r\sqrt{\frac{\epsilon_r+1}{2}}} \quad \text{With} \quad \epsilon_{eff} = \frac{(\epsilon_r+1)}{2} + \frac{(\epsilon_r-1)}{2}\left[1 + 12\frac{h}{W}\right]^{-\frac{1}{2}} \quad (1)$$

$$\text{And} \quad L = \frac{c}{2\times\sqrt{\epsilon_{eff}}\times f_r} - 0.824*h\frac{(\epsilon_{eff}+0.3)(\frac{w}{h}+0.264)}{(\epsilon_{eff}-0.258)(\frac{w}{h}+0.8)} \quad (2)$$

While the figure 2 describes the circular patch's configuration. However, equations [5] and [6] through 2.1 have been used to find out the essential parameter required for the design of this circular patch which is the radius [15].

$$a = \frac{F}{\sqrt{1+\frac{2h}{\Pi\epsilon_r F}\left[\ln\left(\frac{\Pi F}{2h}\right)+1.7726\right]}} \quad \text{with } F = \frac{8.791 X 10^9}{f_r\sqrt{\epsilon_r}} \quad (3)$$
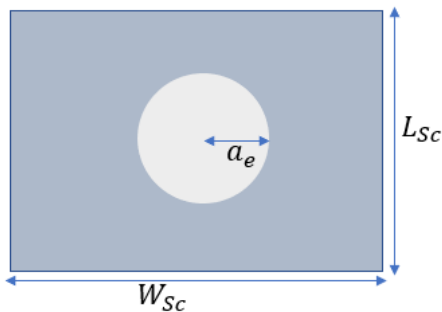
Figure 2: Geometry of circular patch antenna

2.2. Simulations results and discussions

It is clear from the figure below. both the graphs are resonating at the same resonant frequency (3.48GHz). Both shapes present a

good adaptation. In fact, the rectangular patch provides a better result(50dB) by 3dB compared to the circular's return loss(47dB).
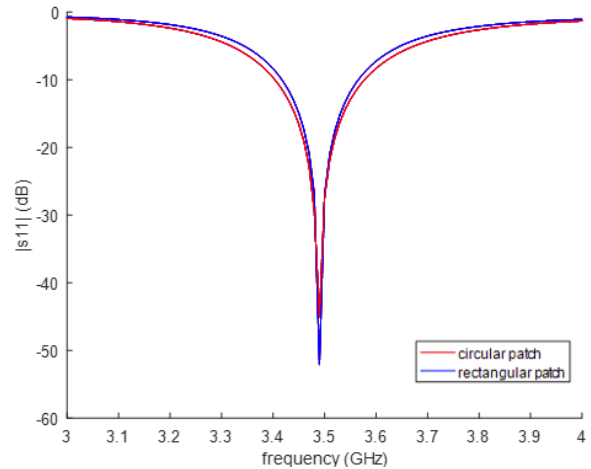
Figure 3: Comparison of return loss for different shapes.
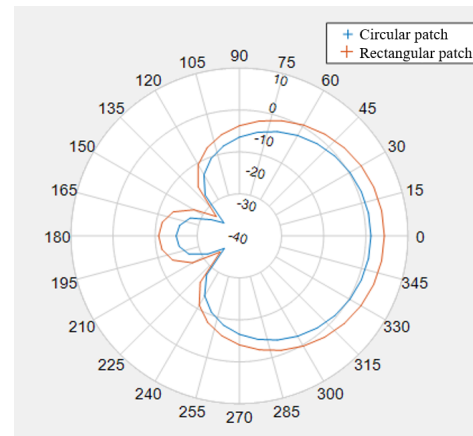
Figure 4: Comparison of 2D radiation pattern for different shapes.

For the antenna suitable for 5G telecommunication systems, a high directivity and a narrow beamwidth are both necessary.

As shown in figure 4, both designs present broadside radiation patterns. Indeed, at 3.48Ghz, the beamwidth shown by the circular patch antenna (90°) is narrower than the rectangular patch (100°). Moreover, the circular patch offers the highest gain value.
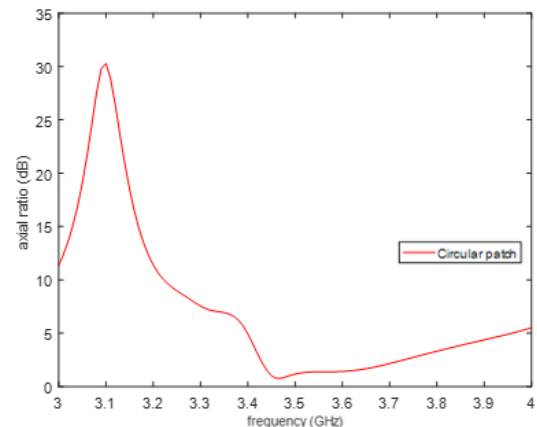
Figure 5: Simulated axial ratio (AR)

A circularly- polarized antenna is defined as having an axial ratio within 3dB at the required frequency [13].

As shown in Figure 5, the axial ratio of the circular configuration presents an axial ratio AR ≤3 dB, with AR bandwidth (less than 3 dB,) is from 3.4 GHz to 3,7 GHz, in fact it reaches 0.7 dB at 3.48 GHz

According to HFSS simulation results, the rectangular shape provides better return loss, whereas the circular shape offers the enhanced gain, the smaller size and the narrower beamwidth.
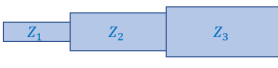
Occasionally, a unique radiation element can meet the needs of the required antenna. But characteristics such beamforming beam steering, and beam scanning are usually achievable when radiation elements are arranged. So, in order to enhance its performance (gain, beamwidth), a compact 4-Element Microstrip antenna array is designed with the most efficient shape.

3. Array antenna

3.1. Antenna prototype

To increase the gain and directivity of the antenna, an antenna array interconnect two pairs of circular shaped antenna which is fed by a corporate-feeding network. It was implemented as the cascade of quarter wave impedance transformers with characteristic impedances $Z_{100}, Z_{70,7}$ and Z_{50} to equally distribute the power [12].

Indeed, to provide a good impedance adaptation, the quarter wave impedance transformers widths are given by the following equation [16].

$$Z_2 = \sqrt{Z_3 \times Z_1}$$

To provide an equal power distribution and to adapt the impedance of patch elements, the quarter wave impedance transformers lines should be tapered.
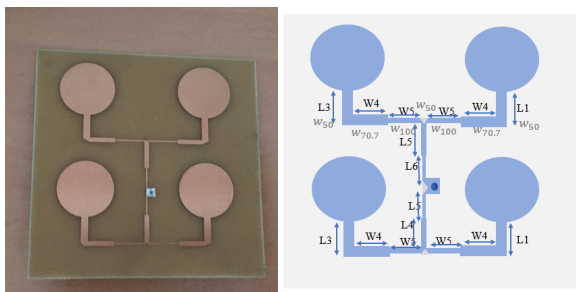
Figure 6: prototype of the proposed antenna array

The figure above describes the geometry of the proposed antenna array. In order to provide reasonable comparison, we kept the same substrate, the same geometry design and feeding network's dimensions [12] with changing the patch's shape. The dimensions of the antenna are illustrated below in millimeters (mm).

3.2. Discussions and results

Figure 7 shows a good agreement between the simulated and measured graphs except minor differences is observed. In fact, both designs deliver the minimum S11 of -30 dB. Indeed, obtain results for the antenna design reveals that the bandwidth of the

fabricated antenna is shifted to 200 MHz different to the simulated bandwidth, it reaches 100MHz.
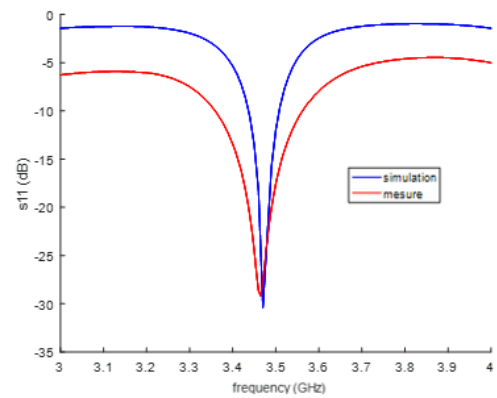
Figure 7: Comparative of simulated and measured S11 plot
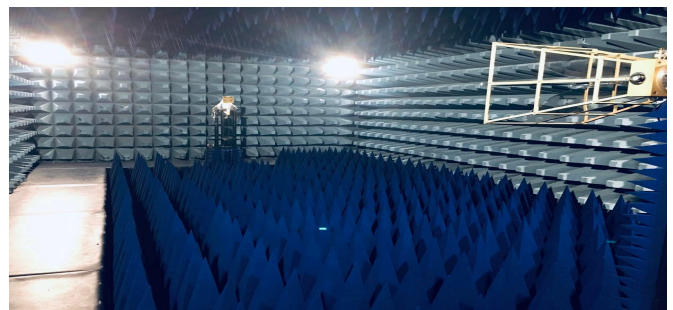
Figure 8: Radiation pattern Measurement

In order to check the electromagnetic field levels emitted by the antenna and to achieve more reproducible measurements, two antennas are fixed in the anechoic chamber. Whereas the first one is the reference antenna which is a QRH18 (QUAD RIDGEDHORN), the other antenna is dedicated to testing antenna in both E-plane and H-plane.
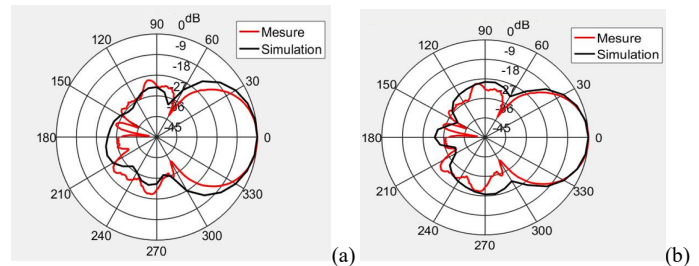
Figure 9: Comparison of the simulated and measured radiation pattern at 3.48GHz; (a) **φ**=90 (b) **φ**=0

The radiation pattern responses for both simulated and measured antenna are shown in figure 9. It can be clearly deduced that the prototype antenna is similar to simulation result. Compared to the single element antenna, the array antenna has the narrower beamwidth. In fact, the antenna array presents a directive radiation pattern. The bandwidth has reached to 40° as predicted in theory. It is also noticed that gain increases as the number of elements goes up. Therefore, the gain is around 5.8114 dB.

Unlike [12] our array antenna with 2 pairs of circular shapes provides a good gain, circular polarization and narrow beamwidth which is suitable for MIMO systems.
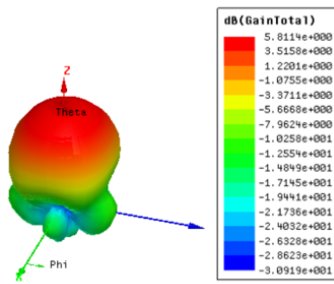
Figure 10: Simulated gain at 3.48GHz.

4. Conception of SISO

The USRP is a radio system conceived for implementation and rapid prototyping systems. [1] Selected because of its flexibility power consumption, low cost compared to other market options, reconfigurability, and high level of customization and high performance [1], [17], the USRP B210 has proven to be among the best choice for our work. Containing an RF front end complete with DACs and ADCs. The SDR attached to computer makes a full SDR system which enables the rest of the signal processing to be within MATLAB/Simulink.

4.1. Experimental setup

For our system prototype, due to the vast variety of supporting platforms, a USRP B210 is used, which provide fully-coherent MIMO 2x2 capability and low cost.

The transmission, reception, and processing of information testbed was performed in IRSEEM laboratory with no supplementary objects between Tx and Rx. The transmitter is located at a distance of around 1m from the receiver. The transmission was done in 3.48 GHz with using the USRP B210 devices which support RF frequencies from 70MHz to 6 GHz frequency. This boards are interconnected to our antennas array prototype via SMA connectors while ensuring a distance of λ/2 between the different Rx and different Rx to provide linear independence between different channels. So, with a carrier of 3.48 GHz, λ is around 85cm, where λ is the wavelength.

On the emission side, we sent a sinusoidal signal of frequency 1Mhz as a data signal to the input of Simulink then with using script of MATLAB via USRP, this data is multiplied by the modulation index, and after adding a constant, the resulting signal is multiplied with a carrier signal of frequency 3.48 GHz.
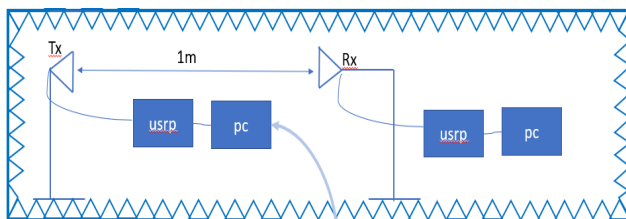
Figure 11: SISO Prototype

To create SDR MIMO applications, USRP B210, host computer and pairs of antenna arrays complete the hardware part of the SDR applications, The host computer is able to configure

the USRP using software (MATLAB/Simulink), it enables users to transmit data using AM Modulation. Since, Simulink supports Universal Hardware Driver, it allows to control several parameters, such sample rate, gain, master clock, central frequency, interpolation factor, decimation factor…

So, first, we implement an AM transmitter based on sink blocks and standard blocks of Simulink to configure gain, center frequency, interpolation, filter and signal data [18] Simulink-USRP B210 enables the user to treat data in real time from USRP B210 and Simulink. Once the signal has been modulated, a spectrum analyzer called Agilent 4404B was interconnected to Tx (output of USRP B210) for displaying a signal in the frequency domain and check transmission problems.

Figure 12: Implementation of SISO

4.2. AM transmitter

This model explains the basic concept/model of amplitude modulation using the USRP board with Simulink, in fact, our antenna array is interconnected to USRP to assure transmission of the signal. The USRP is interfaced also with the pc/ Simulink with an interface called Communications Toolbox supports to transmit and receive RF signals in real time, enabling the use of MATLAB and Simulink to configure radio parameters, design algorithms, generate waveforms and measure and analyze signals.

It is known that to transmit a signal by amplitude modulation, it is necessary to use a carrier at a frequency much higher which is in our case $f_p = 3.48$GHz than the data signal.

The amplitude modulation is done simply by the equation bellow

$$s(t) = A_c \, \mu m(t)\cos{(2\pi f_c t)} + A_c \cos{(2\pi f_c t)} \qquad (4)$$

To build this equation with Simulink, the first part is modelled with Simulink but the second part is done with a block called USRP transmitter which allows to configure the USRP (gain, carrier frequency, interpolation factor).

In our case, we desire transmit a sinusoidal signal with a frequency $f_m = 1MHz$. This signal must be converted into analog form, at the input of the USRP. therefore, the operating frequency of the DAC, or Master Clock Rate must be adjusted, and the interpolation rate operated by the Digital Up Converter above. The following values are possible for these parameters:

* Master Clock Rate: between 5 and 56 MHz

170

* Interpolation: an integer between 1 and 128, an even integer between 128 and 256, an integer divisible by 4 between 256 and 512.

Master clock rate (Hz)= Baseband sample rate Interpolation factor:
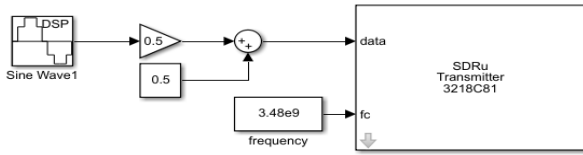
Figure 13: Transmitter model
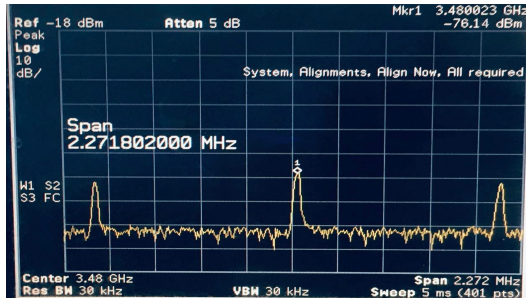
Figure 14: Spectrum

To verify the transmission of this sinusoidal signal, a spectrum analyzer in connected to the output of the USRP B210. When the carrier wave is modulated, both sides of the stable carrier signal sidebands are formed which carry the actual information in the modulation [12]. This can be illustrated by Figure 14 when a strong carrier is on the carrier frequency (3.48Ghz) while the sidebands have a frequency on 3.48Ghz $\pm 1MHZ$.

As expected, the spectrum has the usual presentation: two sidebands are symmetrical on 3.481GHz and 3.479GHz and a powerful carrier signal is in the center. So, the data signal has been successfully transmitted.

4.3. AM Receiver

After finalizing the emission, another patch antenna array 2X2 is used as receiver. For the demodulation part, we use an additional USRP device in order to demodulate the transmitted message using the receiver model.

Next, an overview of the AM demodulator is presented, which starts with the USRP receiver block. Then the demodulated signal can be passed to low-pass filter [17]. In fact, the low-pass filter, is used to remove the high-frequency signals and enable low-frequency signals to pass [15],[17].

As before, the parameters of a block calling SDRu receiver must be programmed in order to recompose the modulating signal. In fact, we have kept the carrier frequency at 3.48. So, we will find two frequencies, the higher frequency will be eliminated by the low pass filter and the other one will allow us to extract the data.
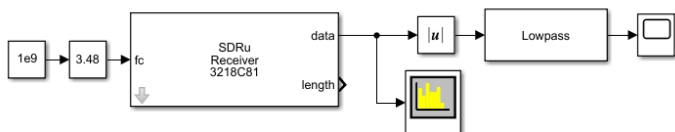
Figure 15: Receiver model
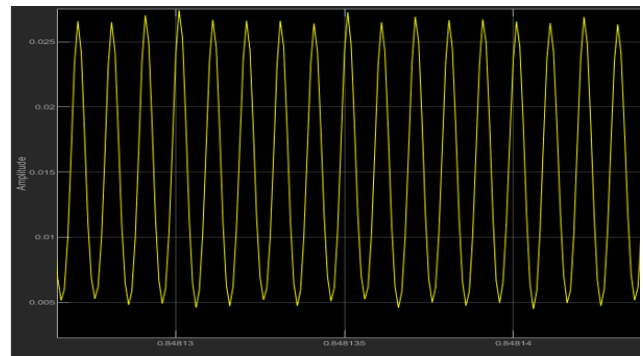
Figure 16: Received signal

The sinusoidal signal has been recuperated but there are fading due to the loss of system.

5. Conception of MIMO 2x2

The USRP B210 board is mainly designed using the following components :

- AD9361 transceiver;
- Xilinx Spartan 6 FPGA;
- The USRP toolbox.

The key component of the first section is the AD9361 transceiver. This block is responsible for using two receive and also two transmit channels for RF front-end processing. The transceiver contains zero-IF-to-RF conversion and feedback, ADC/DAC gain, decimation/interpolation and filtering.

To connect the transceiver to the FPGA a digital data interface is used and to transmit data between them the I\Q way is employed.

The second component describes the Spartan 6 and presents software host processing. It uses both signal channels due to combining 2RX and 2TX chains, so, it is definitely feasible to conceive 2X2 MIMO System based on SDR. For this effect, the user could program a specific modulator/demodulator script. While the final part enables processing
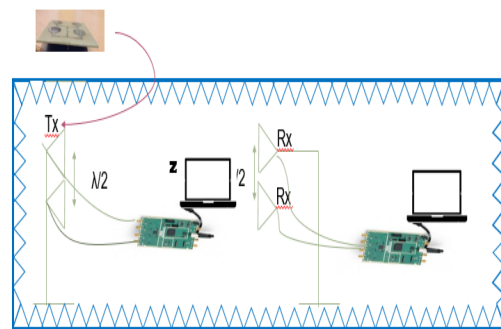
(a)
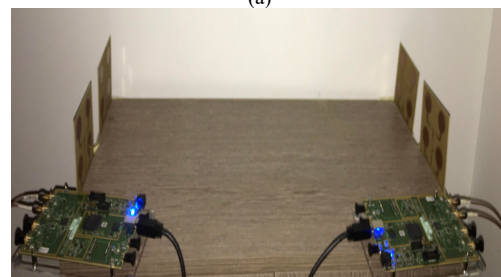
(b)

Figure 17: MIMO 2X2 System (a) illustrative schematic, (b)implementation

As second testbed, we propose a novel Simulink model for coherent 2x2 MIMO, interconnecting each USRP B210 with pairs of antenna array using SMA connectors at both in transmission and reception.

The Full digital MIMO 2x2 system is operating in band C where the digital signal processing is processed on baseband.

5.1. Transmitter

A data matrix received by the SDRu transmitter block will enables the signal waveforms for MIMO mode. Indeed, to use both channels, Channel mapping must be adjusted [1, 2]. And a block called matrix concatenation used as gateway between the block sdru transmitter and the data elements arranged in columns or rows.

The MIMO in this support package receives signals through the RX port and transmits signals through the TX/RX port.
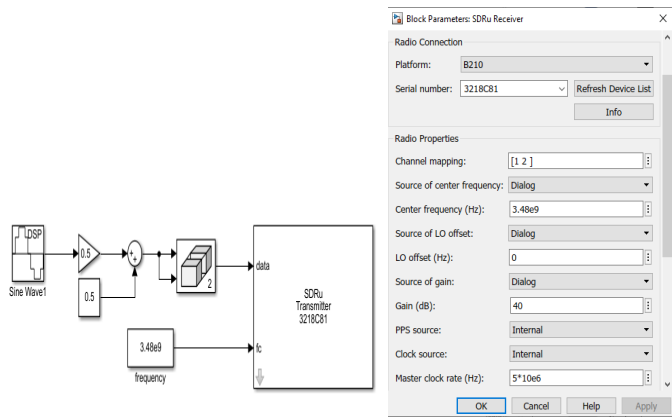
Figure 18: Programming USRP

5.2. AM Receiver

The USRP B210 below describes the hardware implementation framework for MIMO 2x2 model. In fact, for the reception part, the same model of SISO (AM receiver) has been kept, only a slight change with adding a block called select column in order to separate data and to treat each channel separately and simultaneously.
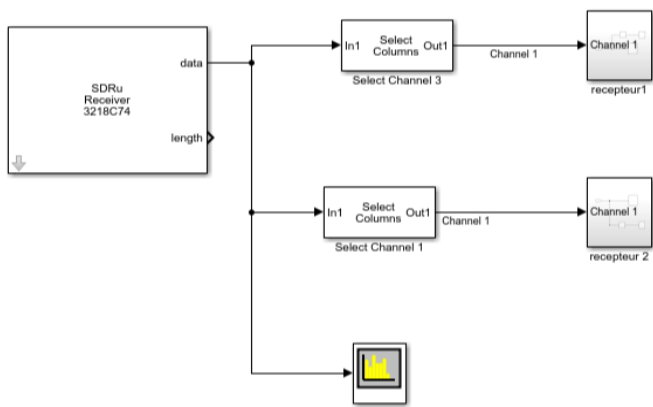
Figure 19: Receiving simultaneously

5.3-Implementation issues

In order to provide synchronization between both Tx antennas array and both Rx antennas array and to achieve interoperability

between cards, The 2 Rx should operate synchronously, we send the sinusoidal signal from the first 2x2 antenna array and the same data from the second prototype antenna. It is very important to adjust the different parameters of both boards in a consistent way such as same center frequency value which is 3.48GHz, master clock, channel mapping, interpolation [16].
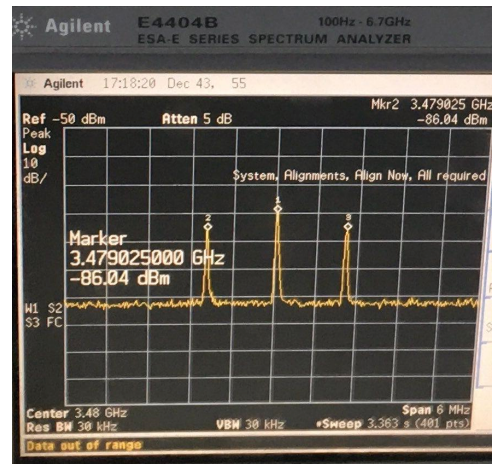
Figure 20: Frequency Spectrum of AM

The spectrum analyzer is connected to the output of the TX/RX port. As before, a strong carrier signal is centered at 3.48GHz, and the two sidebands are symmetrical at 3.481GHZ and 3.479GHz and the information signal is at 1MHz as shown in figure 19. So, MIMO transmission is well adjusted.

The sinusoidal signal with frequency of 1MHz have been usefully recovered. So, MIMO provide better efficiency specially in communications system.

In this work, performance of both MIMO and SISO systems is displayed. In fact, by transmitting the same data over multiple channels, MIMO introduce redundancy and diversity in data transmission that conventional single antenna (SISO) configurations cannot provide. This gives MIMO systems several advantages over conventional SISO configurations such the global throughput can be improved, allowing more quality and quantity data to be sent over the network, and using multiple data flow, problems such as fading caused by lost or dropped data packets can be reduced, this will help to recover all of the resulting data [16].
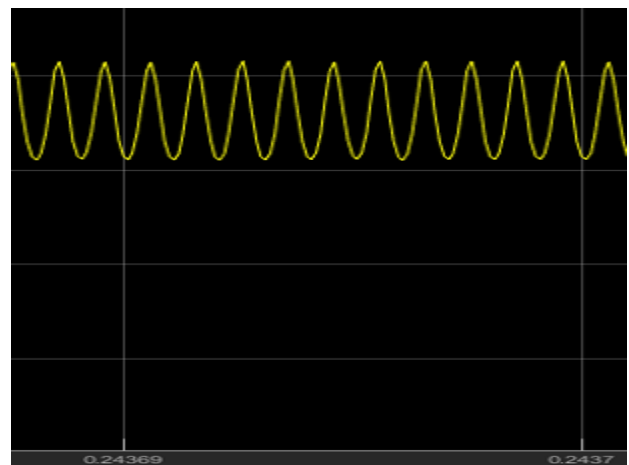
Figure 21: Received signal

6. Conclusion

In this study, a 5G-oriented MIMO prototype system has been designed and implemented equipped with four patch array antenna based on software-defined radios. The model for Amplitude modulation/demodulation has been developed combining USRP and Simulink in both SISO and MIMO Systems, with proving that MIMO is more efficiency than SISO. Moreover, all the analog and digital modules were properly developed and described enabling us to obtain a Full digital 2×2 MIMO system operating in band C. Finally, this system demonstrates great flexibility and scalability to be used in a wide range of applications. In the future MIMO beamforming system is investigated.

References

[1] S.Zhong, H.Feng, P.Zhang, J.Xu , H.Luo, J.Zhang, T.Yuan, L.Huang "Deep Learning Based Antenna Selection for MIMO SDR System," Sensors , 20, 6987, 2020, doi:10.3390/s20236987.

[2] Q. Wang, N. Mu, L. Wang, S. Safavi-Naeini, J. Liu, "5G MIMO conformal microstrip antenna design," Wireless Communications and Mobile Computing. 2017, 1–11, 2017, doi:10.1155/2017/7616825.

[3] S.Zhong, S. H.Feng, P.Zhang, J.Xu, L.Huang, T.Yuan, Y.Huo, "User Oriented Transmit Antenna Selection in Massive Multi-User MIMO SDR Systems," Sensors, 20, 4867, 2020, doi:10.3390/s20174867.

[4] M.Ali and M.Ibrahim, "Design Broadband MIMO Antenna to meet 5G communication systems requirements," in 2021 IEEE 1st International Maghreb Meeting of the Conference on Sciences and Techniques of Automatic Control and Computer Engineering MI-STA, 838-842, 2021,doi: 10.1109/MI-STA52233.2021.9464429.

[5] G.K.D. Prasanna Venkatesan, T.Ranjitha, C. Shimona Neethi, S.Swetha, "Optimisation of mimo antenna for 5G applications," International Journal of Advances in Scientific Research and Engineering (ijasre), 4, 133-139, 2018,doi:10.7324/IJASRE.2018.32642.

[6] R. Gandhiraj, Ranjini Ram, K. P. Soman, "Analog and digital modulation toolkit for software defined radio", Procedia Eng, 30, 1155–1162,2012), doi: 10.1016/j.proeng.2012.01.975.

[7] G. N. Kareem, G. A. Gbotoso, S. O. Omogoye, "MATLAB analysis and Simulink model for amplitude modulation technique", World Journal of Advanced Engineering Technology and Sciences, 2, 21-28, 202, doi: 10.30574/wjaets.2021.2.2.0035.

[8] O.Hiari, R.Mesleh, "A Reconfigurable SDR Transmitter Platform Architecture for Space Modulation MIMOTechniques," IEEE Access, 5, 24214–24228, 2017,doi:10.1109/ACCESS.2017.2761859.

[9] D.M. Molla, H. Badis, L. George, M. Berbineau, "Software Defined Radio Platforms for Wireless Technologies", in IEEE Access, 10, 26203-26229, 2022, doi: 10.1109/ACCESS.2022.3154364

[10] M. Danneberg , I.Gaspar, M.Matthé, D.Zhang, L.Leonel Mendes,G. P. Fettweis,"Implementation of a 2 by 2 GFDM transceiver for robust 5G networks", 2015 International Symposium on Wireless Communication Systems (ISWCS), 236-240,2015,doi: 10.1109/ISWCS.2015.7454336.

[11] T. F. A. Nayna, A. K. M. Baki and F. Ahmed, "Comparative study of rectangular and circular microstrip patch antennas in X band", 2014 International Conference on Electrical Engineering and Information & Communication Technology,1-5, 2014, doi: 10.1109/ICEEICT.2014.6919142

[12] W. Chen, Y. Lin, "Design of 2X2 Microstrip Patch Patch Array Antenna for 5G C-Band Access Point Applications", 2018 IEEE International Workshop on Electromagnetics Applications and Student Innovation Competition (iWEM), 1-2, 2018, doi:10.1109/iWEM.2018.8536673.

[13] M. Drissi, N. Benjelloun, P. Descamps, A. Gharsallah, "Multilayer antenna dedicated to MIMO Beamformig antenna for 5G telecommunication applications", 2021 IEEE Conference on Antenna Measurements & Applications (CAMA) ,183-188, 2021, doi:10.1109/CAMA49227.2021.9703463

[14] C.A. Balanis, "Antenna Theory, Analysis and Design", John Wiley & Sons, New York, 1997.

[15] L.B. Laskov, V. M. Georgieva, "Analysis of Amplitude Modulation and Demodulation in MATLAB Simulink Environment". 2021 56th International Scientific Conference on Information, Communication and Energy Systems and Technologies (ICEST), 223-226, 2021, doi: 10.1109/ICEST52640.2021.9483470

[16] G. Fokin, D. Volgushev, A. Kireev, D. Bulanov and V. Lavrukhin, "Designing the MIMO SDR-based LPD transceiver for long-range robot control applications",2014 6th International Congress on Ultra-Modern Telecommunications and Control Systems and Workshops (ICUMT), 456-461,2014, doi:10.1109/ICUMT.2014.7002144.

[17] C.Gavrila, V.Popescu, M.Alexandru, M. Murroni, C.Sacchi, "An SDR-Based Satellite Gateway for Internet of Remote Things (IoRT) Applications",IEEE Access, 8, 115423-115436, 2020, Doi: 10.1109/ACCESS.2020.3004480.

[18] T.Liuski," AM- ja DSB-modulaatioiden toteuttaminen Simulink-ohjelmistolla USRP- ohjelmistoradioalustalle ,phd thesis, University of Oulu, 2019.

A Structuration View of the South African National Health Insurance Readiness

Nomawethu Tungela, Tiko Iyamu[*]

Department of Informatics and Design, Cape Peninsula University of Technology, Cape Town, +27, South Africa

A R T I C L E   I N F O

A B S T R A C T

The South African government has embarked on the implementation of the National Health Insurance (NHI), to increase access to healthcare and improve service delivery. However, the project has being encountering various challenges, which are not empirically known. The aim of the study is to identify the factors that influence the implementation of the NHI from ICT readiness assessment perspective. Qualitative data was collected from communities and healthcare service providers including government as the legislative body. The duality of structure of structuration theory was used as lens to guide the analysis of the study, from ICT readiness assessment and perspective. From the analysis, four factors, current state, areas of coverage, role of ICT, role of human are found to influence the implementation of the NHI. The originality of the findings lies on the empirical nature of the study.

1. Introduction and Background

Many people in some countries including South Africa have limited access to quality healthcare services [1]. The lack or limited access to healthcare services can be attributed to factors such as exorbitant costs, lack of available or not enough professional healthcare personnel and insufficient healthcare facilities. This leads to inequalities in the use of the healthcare services in many parts of the world [2]. With the increase of inequalities that are faced by the healthcare sector there is a demand for higher accessibility of quality service rendered to the citizens especially in the rural or peri-urban communities. According to [3], peri-urban areas are areas "which have some initial features and functionality of cities but are not yet defined as cities, including the rural–urban interface, small town, township and village". To ensure that these demands are met the World Health Organization (WHO) has made a recommendation for countries to employ the universal health coverage (UHC) [4].

In support and alignment with the UHC, the South African government has introduced the National Health Insurance (NHI), which requires Information and Communication Technology (ICT) in its implementation. The NHI is intended to provide extended access and improved quality of healthcare services across the country. In essence, the NHI system is primarily aimed at bridging the gap between the lower income earners and the middle class by providing equal healthcare services to all citizens [2]. However, how ready the environment is unknown, at least,

from empirical perspective. The term readiness "is related to terms such as 'innovation' and 'adoption' of new technologies" [5]. Assessment is referred to the collection of information on how things are done in an organization [6].

The newness of the NHI requires the South African environment to be ready for its implementation. This is primarily to avoid failure like many other initiatives, which can be a serious catastrophe for the government and the citizens that look forward to its benefits. Over the years, many systems have failed because of factors such as lack of infrastructures [5]. Traditional affiliation and culture of an environment have also been instrumental factors to the success and failure of many systems [7]. From these viewpoints it is essentially important to assess the readiness of a diverse environment like South Africa before critical systems such as the NHI can be implemented, particularly in the rural areas of the country.

The South African NHI makes provision for ease of access to healthcare services irrespective of socio-economic status [8]. Significantly, the NHI is expected to be of benefit. [9] argue that many health fatalities are due to factors such as the waiting period to access healthcare services and insufficient skilled healthcare practitioners. According to [10], private health services are prohibitive, which results to limited access by many citizens. Hence, [11] suggest that benefits of having access to health insurance include reduced cost and ease of access. However, implementation of the NHI requires understanding of its readiness in the South African environment.

[*]Corresponding Author: Tiko Iyamu, connectvilla@yahoo.com

2. Review of literature

This section presents the review of literature focusing on Information and Communication Technology (ICT), healthcare, National Health Insurance (NHI), readiness assessment.

Information and Communication Technology (ICT) has been widely used in the health sector in many different countries. ICT makes it easier and possible for the patients and service providers including government to provide and receive healthcare services [12]. According to [13], there has been a solid development on how ICT is being used in the healthcare sector to improve on service delivery. Through ICT, patients' records are remotely monitored, and medical records are electronically stored [14]. Hence, according to [15], ICT in developing countries has been considered as the principal technology for advancement of quality patient care in healthcare. This is due to its ability to bring change in service delivery especially in the healthcare sector [16].

The use of ICT has seen the birth of many services like e-health which according to [7] are "noticeable on the development of the healthcare sector in developing countries". According to [17], healthcare practitioners can communicate by using their mobile devices such as smart phones to provide healthcare services. In addition, local governments in many countries have made major investment in the ICT infrastructure so that the citizens can receive excellent, efficient healthcare services [18]. Moreover, the innovations that are brought by ICT can bring about change in a way that patients are being diagnosed and monitored [19].

The Universal Health Coverage (UHC) is all about ensuring that all citizens have access to the quality health services they need with minimum contributions [20], which the South African NHI system tries to align with. According to [10], it can also ensure the availability of sufficient resources that are effective. [21] claimed that UHC is only achieved when all citizens of the country receive good health services without financial burden. Furthermore, [22] defined UHC as having equal access of healthcare services amongst all citizens to overcome the differences of the health system. According to [4] "Universal coverage is determined by how much government budget can be allocated to subsidise premiums for poor and low-income families and informal sector workers". To fully achieve the goal of UHC, all citizens of the country should have universal access to the services that are provided by the healthcare.

There is an increasing failure in the implementation of new systems or policies in many organizations including the healthcare sector due to lack of readiness [23]. Various factors such as infrastructure and skill set influences readiness, which should be known and understood before embarking on implementation of new systems [24]. According to [5], readiness assessment is a mechanism for minimising risks and possible failures. Readiness assessment is a tool for supporting service delivery in the healthcare because it identifies the gaps and interventions needed. As stated by [25], readiness assessment is concerned with how the healthcare facilities can deliver basic services at lower standards.

3. Structuration theory

Based on the objectives of the study which concerns factors such as rules, resources, different agents (or agencies), and the relationship between these factors, the structuration theory was selected to underpin the study. Structuration theory, according to [26] is a theory that focuses on social systems with technical enablement. The theory was introduced by Anthony Giddens in 1984 and had since been used in many research fields, including Information Technology (IT) to underpin studies for many years [27]. According to [28], the structuration theory has two main tenets which are (i) structure and (ii) agency, which are the core parts of its duality of structure as shown in Figure 1 below.
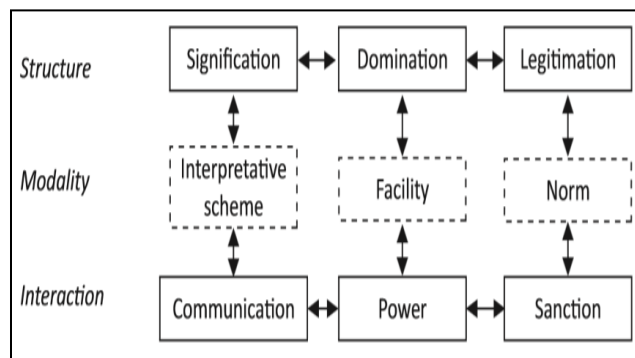
Figure 1: Duality of Structure [27]

According to [29], the structure consists of signification, domination and legitimation. The modality according to [28] consists of the interpretative scheme, facility and norm, and according to [30] the interaction comprises of communication, power and sanction. The author furthermore claims that modality provides the connection between the structure and the interaction of the agencies. Interaction amongst agencies is communicated through the interpretive schemes which are common knowledge that agencies use to interpret events by giving them meaning that demands signification structure [29]. The actions of agencies are made based on the ability to exercise power, using the facilities which are resources to obtain domination structure. The conduct of agencies becomes sanctioned or approved and end-up produces norm which results in the legitimation structure [31].

The structuration theory according to [32] can be used as a lens to enable the researcher to view and interpret data collected. Moreover, [28] claim that the structuration theory has been identified as a theory that is most suitable to interpret the results of the research. According to [29] the structure of the theory is made up of two properties which are rules and resources, and the agency of the theory according to [31] is made up of human and non-human agents. According to [29] the interactions which people make in a social process are constructed from the structures (rules and resources), from which interaction, new rules and resources are formed. The author furthermore claims that this iterative formation of rules and resources by peoples' actions are commonly known as the duality of structure.

4. Research Methodology

We employ the discourse technique to analyze the traces in the views that led to the ideological and believe of individuals and

groups about NHI in South Africa. The discourse approach seeks to identify hegemony and emancipate marginalized individuals and ideas [33]. Using the technique, it allows us to draw from interpretive paradigms [34], meaning we could employ our judgments and subjectivity as explained by [35].

The discourse technique is often applied to analyze within context, to understand the meanings that are associated with object through the process of communication and how it influences mobilization [36]. In the context of this study, the discourse technique allows us to gain insights into how the citizens understand the deployment of NHI in the country, using the radio as a platform to engage and dialogue with citizens. The technique enables tracing of connections between object and subject in a discourse [33].

Table 1: Duality of structure as lens for analysis

#	Level	Duality of structure	Description
1	Macro conversation	Structure	to gain insight on how NHI is understood from social and health contexts in individual's real-life situation. This was structured into attributes, themes, and patterns relevant to the research, from both IT and non-IT related issues.
		Modality	
		Interaction	
2	Micro reflectivity	Structure	Individual's communicative motivation informs the selection of linguistic forms, which influence conversation and meanings associated with the subject (He, 2017). Follows the interplay in the communicative motivation about views on NHI deployment.
		Modality	
		Interaction	
3	Link between the micro and macro components	Structure	Enables reflexivity consideration of how individuals and groups worldviews [35] of the NHI in South Africa. Links the micro and macro views, to reflexively examine our subjective understanding of the views.
		Modality	
		Interaction	

5. Assessing the South African NHI for Readiness

As shown in Table 1, the duality of structure from the perspective of structuration theory is used as a lens, to view the empirical evidence was viewed and answers to the questions were obtained: what is the current state of NHI implementation? presented to answer the question. The duality of structure presented the current state of the implementation of the NHI system in the communities of the country. From the signification structure, the importance of the implementation of the NHI system as the system that promotes access to quality healthcare services for all the citizens of the country. As the South African government communicate regarding this new system the citizens used their stock of knowledge to consider whether what has been communicated was important or not.

In assessing the readiness of the South African NHI for readiness, two fundamental factors were the focus: (1) on macro level, the importance is viewed; and (2) on micro level, the implications of not conducting assessments in the deployment of the concept were examined. Finally, the macro (importance) and micro (implications) were linked, to gain better insight of the current state and factors that influence readiness of the South African NHI, from IT perspective. At the macro level, the following question was used to the determinant: **What is the current state of the implementation of the NHI?** The question, **what are the factors that can enable or constrain the NHI readiness?** was used to examine the influencing factors from a micro level perspective.

5.1. What is the current state of the implementation of the NHI?

From ICT perspective, the current situation leans on two factors, access to health and area of coverage. The factors motivate, at the same time constrain the implementation of the NHI in the country. The factors contribute to the criticality of assessment of the South African NHI before implementation.

Access to healthcare

Currently, there are challenges in accessing healthcare services in the country. The challenges come from both technical and non-technical factors. [37] claim that it is vital to invest in an IT infrastructure to better the health facilities and increase access services in a country. The health sector on its own struggle to improve the quality and access to healthcare services, which negatively affect health of the citizens of the country. According to [20], this has prompted external stakeholders, such as the government and other sectors, to get involved in some countries. According to [38] lack of infrastructure can influence the effectiveness and efficiency of healthcare services delivered to the citizens. [39] assert that encouragement of healthcare personnel and the use of modern technology in healthcare facilities can better the health service delivery.

A successful implementation of the NHI makes it mandatory for the South African government to have a centralised database where patient records can be stored [40]. According to [37] central storage of records assist the health system between different healthcare personnel in different healthcare facilities to respond in real-time. This is because healthcare personnel can retrieve reports on the system through patient history [25]. However, there are many challenges with the current state of healthcare services

and facilities. Two of the predominantly challenges are of technical and non-technical nature.

From the technical perspectives, some of the challenges are security. Security is referred to an act of prohibiting unlicensed users to gain access into an organization's network [41]. Security is also a necessity when medical practitioners share patient data to other service providers [42]. Moreover, [43] assert that data security is needed even when the data is stored. Waiting times are also problematic. The technical challenges heavily contribute to successful implementation of the NHI through healthy readiness assessment [44].

Non-technical factors include availability of skilled healthcare personnel and healthcare infrastructure [25]. This assists the healthcare sector to be able to compare if the existing health resources will be able to stand the requirements to provide the NHI [45]. In India it was found that due to unskilled healthcare personnel the level of incorrect treatment issued was high [44]. Authors continue to claim that the only solution to mitigate the challenges is to continuously check and evaluate new avenues of that specific challenge. Moreover, [46] suggest that to successfully manage the existing challenges, there needs to be continuous planning and management within the healthcare sector.

Area of Coverage

The aim of the NHI is to provide high standard of healthcare services that will be available to all the citizens of the country irrespective of their geographic area [38]. [47] argues that there is still a large gap that exists between the urban and the rural areas of the country in terms of accessing and making use of the healthcare services available. [48] claim that "Expansion of coverage to poor and vulnerable populations often needs strong governmental commitment to give voice to marginalised groups and overcome interest-group politics". This is because in any country that has a united political structure within its government, changes are easily accepted [49].

However, some of the challenges identified in the areas of coverage and access above are not unique to South African. For example, some of the challenges hindered similar programmes to the extent; they were either unsuccessful or terminated in many countries, such as Cyprus [50]. In some countries, there were over expenditure of budget due to implementation challenges [37], which can be attributed to lack of readiness assessment. The USA is an example, where, from inception Obamacare was faced with challenges where citizens were unable to register on its web-based system which left many citizens of the country unable to renew their insurance policies [51]. In Korea, health data have been encrypted so that it can be protected from unauthorised users. In Taiwan all the citizens of the country have been given a unique personal identification, this is to ensure privacy when they access their health information online [37].

5.2. What are the factors that can enable or constrain the NHI readiness?

As revealed from the analysis, primarily, two factors enable and at the same constrain the implementation of the NHI in South Africa. The factors are ICT and humans, which play fundamental roles from both technical and non-technical perspectives. Primarily, the factors require the need to continuously evolute the

technology solutions and, training and development of ICT and healthcare personnel. The factors have the capability to enable and constrain the readiness of the phenomenon. [30] argues that factors enable and at the same time constrain processes and activities in IT projects. Thus, the factors are significant in a sense that it ensures that the various stakeholders adhere to the tasks and processes in the implementation and support of the NHI. Also, factors of influence can happen consciously or unconsciously [27], at both technical and non-technical structural levels during implementation.

Additionally, the factors, ICT and humans enable the integration of healthcare processes with technology solutions of different healthcare facilities, ensuring compatibility. The rationale for this is that the systems will be flexible and accommodate new and old systems when sharing data in an organization. This also ensures the efficiency and the effectiveness of service delivery that is needed in the healthcare sector. Lastly, the factor which is governance and controls plays a big role in the implementation of the NHI. The implication of mismanagement of funds can affect the objective of the organization and can result in the failure of the implementation of the NHI system. With strict policies and accountability this can be minimized.

The Role of ICT

The implementation of the NHI in any government including South Africa, requires the use of ICT as it assists in the improvement of the quality and effectiveness of health service delivery [52]. Daily, the healthcare sector deals with large volumes of data such as sensitive patient information e-Health is defined as the service where the healthcare sector uses ICT to deliver services such as treating patients and monitoring diseases [53]. In addition, [54] suggest that the use of electronic data systems as opposed to the traditional paper-based system can improve the efficiency of medical practitioners.

Many governments around the world including South Africa continuously look at the ways they can use ICT, to better their healthcare services [55]. However, according to [56] healthcare in South Africa is faced with challenges such as poor infrastructure and lack of funds. Another challenge according to [57] is the lack of privacy and security which poses a threat to sensitive healthcare data.

The role of humans

Healthcare personnel are the ones that have an obligation for the implementation of the NHI in South Africa [58]. [59] argue that for the NHI to be successfully implemented in South Africa, the key role players such as medical practitioners in service delivery within the healthcare sector needs to be involved. However, [60] argue that many people around the country including healthcare personnel are not enlightened about the concept of the NHI and that is due to insufficient communication shared so far. On the other hand, [61] suggest that the government and the Department of Health need to take serious measures to have consultation with communities, to spread the word about the NHI system. [62] claim that

requirements such as sufficient human resources need to be achieved simultaneously with the implementation of the NHI.

5.3. Link between importance and implication of implementing the NHI

The macro level allows acknowledgment of how institutional contexts differ in their enabling and constraining influence [63], which makes it useful in classifying the activities and action of the various stakeholders. The macro level helps to maintain inferences at group levels of analysis [64]. Linking the macro and the micro perspectives, is purposely to obtain a comprehensive view [65], on how factors influence and constrain NHI activities at individual and facilities' levels.

Currently, there are challenges in accessing healthcare services in the country. The challenges come from both technical and non-technical factors, which reveal significance and implications in coverage, the role of ICT, and the role of humans. The technical factors include security [66] and data storage [67]. Some of these challenges are contextual, meaning that they must be customized for individual environments. Thus, the same measure cannot be used for two countries, because they often differ in infrastructural, cultural and governmental settings [68], hence, readiness assessment is required.

The NHI system can be successfully implemented in the communities of the country, guided by the influencing factors, to understand the processes and activities better. This includes managing relationship between the factors. Critically, this is intended to guide the interaction between the human-to-human, human-and -technology, and technology-and-technology that are involved in the implementation of the NHI. Through the practical application of the influencing factors, government can become more knowledgeable during and post implementation of the NHI.

6. Conclusion

The influencing factors identified in this study will be of significance to the stakeholders involved in the implementation of the NHI in South Africa, from both technical and non-technical perspectives. The factors are expected to boost the strength and capability of the relevant authorities with knowledgeable power to employ the resources, in implementing the NHI, in providing healthcare services to the community.

The study has been thoroughly carried out following the research methodology as stated in the section above. This includes the use of structuration theory as a lens, which brings rigor to the study. The significance of the study is through the development of the framework which can be of great assistance to the South African government and governments from other countries if followed. The framework can provide guidance on how an ICT system can be implemented for service delivery. The South African government, department of health and other governments from developing countries will benefit from this empirical study in three-fold, theoretically, methodologically and practically. Theoretically as the study will contribute to the existing theory

through the addition to the body of knowledge, methodological based on the philosophies, approaches, methods and techniques that will be followed or employed on the study and practically on the basis that the researcher has developed the framework which will serve as a guide to help governments to better understand processes to be taken before implementation of the new system.

Conflict of Interest

The authors declare no conflict of interest.

Acknowledgment

References

[1] I. Garcia-Subirats, I. Vargas, A.S. Mogollón-Pérez, P. De Paepe, M.R.F. da Silva, J.P. Unger, M.L. Vázquez, "Barriers in access to healthcare in countries with different health systems. A cross-sectional study in municipalities of central Colombia and north-eastern Brazil," Social science & medicine, **106**, 204-213, 2014, doi:10.1016/j.socscimed.2014.01.054.

[2] L. Mhlaba, D. Blaauw, A. Parry, "Is National Health Insurance a viable option for South Africa? Experiences from other countries," AfricaGrowth Agenda, **2016**(10), 8-12, 2016.

[3] L. Tian, B. Ge, Y. Li, "Impacts of state-led and bottom-up urbanization on land use change in the peri-urban areas of Shanghai: Planned growth or uncontrolled sprawl?," Cities, **60**, 476-486, 2016, doi:10.1016/j.cities.2016.01.002.

[4] W.C. Hsiao, S.H. Cheng, W. Yip, "What can be achieved with a single-payer NHI system: The case of Taiwan," Social Science & Medicine, **233**, 265-271, 2019, doi:10.1016/j.socscimed.2016.12.006.

[5] S. Adjorlolo, G. Ellingsen, "Readiness assessment for implementation of electronic patient record in Ghana: a case of university of Ghana hospital," Journal of Health Informatics in Developing Countries, **7**(2), 128-140, 2013.

[6] A.N Hidayanto, M.A. Hasibuan, P.W. Handayani, Y.G. Sucahyo, "Framework for Measuring ERP Implementation Readiness in Small and Medium Enterprise (SME): A Case Study in Software Developer Company," Journal of Computers, **8**(7), 1777-1782, 2013, doi:10.4304/jcp.8.7.1777-1782.

[7] M.R. Hoque, M.F.A. Mazmum, Y. Bao, "e-Health in Bangladesh: current status, challenges, and future direction," The International Technology Management Review, **4**(2), 87-96, 2014, doi:10.2991/itmr.2014.4.2.3.

[8] J. Dixon, E.Y. Tenkorang, I.N. Luginaah, V.Z. Kuuire, G.O. Boateng, "National health insurance scheme enrolment and antenatal care among women in G hana: is there any relationship?," Tropical Medicine & International Health, **19**(1), 98-106, 2014, doi:10.1111/tmi.12223.

[9] A. Mills, "Health care systems in low-and middle-income countries," New England Journal of Medicine, **370**(6), 552-557, 2014, doi:10.1056/NEJMra1110897.

[10] I.A. Odeyemi, "Community-based health insurance programmes and the national health insurance scheme of Nigeria: challenges to uptake and integration," International journal for equity in health, **13**(1), 1-13, 2014, doi:10.1186/1475-9276-13-20.

[11] A. Brugiavini, N. Pace, "Extending health insurance in Ghana: effects of the National Health Insurance Scheme on maternity care," Health economics review, **6**(1), 1-10, 2016, doi:10.1186/s13561-016-0083-9.

[12] D. Haluza, D. Jungwirth, "ICT and the future of health care: aspects of health promotion," International journal of medical informatics, **84**(1), 48-57, 2015, doi:10.1016/j.ijmedinf.2014.09.005.

[13] H.K. Andreassen, L.E. Kjekshus, A. Tjora, "Survival of the project: a case study of ICT innovation in health care," Social Science & Medicine, **132**, 62-69, 2015, doi:10.1016/j.socscimed.2015.03.016.

[14] M.R. Cowie, J. Bax, N. Bruining, J.G. Cleland, F. Koehler, M. Malik, F. Pinto, E. van der Velde, P. Vardas, "e-Health: a position statement of the European Society of Cardiology," European heart journal, **37**(1), 63-66, 2016, doi:10.1093/eurheartj/ehv416.

[15] G. Fitzpatrick, G. Ellingsen, "A review of 25 years of CSCW research in healthcare: contributions, challenges and future agendas," Computer

Supported Cooperative Work (CSCW), **22**(4), 609-665, 2013, doi:10.1007/s10606-012-9168-0.

[16] D. Haluza, D. Jungwirth, "ICT and the future of health care: aspects of pervasive health monitoring," Informatics for Health and Social care, **43**(1), 1-11, 2018, doi:10.1080/17538157.2016.1255215.

[17] A. Solanas, C. Patsakis, M. Conti, I.S. Vlachos, V. Ramos, F. Falcone, O. Postolache, P.A. Pérez-Martínez, R. Di Pietro, D.N. Perrea, et al, "Smart health: A context-aware health paradigm within smart cities," IEEE Communications Magazine, **52**(8), 74-81, 2014, doi:10.1109/MCOM.2014.6871673.

[18] J. Adler-Milstein, N. Sarma, L.R. Woskie, A.K. Jha, "A comparison of how four countries use health IT to support care for people with chronic conditions," Health Affairs, **33**(9), 1559-1566, 2014, doi:10.1377/hlthaff.2014.0424.

[19] C. Hollis, R. Morriss, J. Martin, S. Amani, R. Cotton, M. Denis, S. Lewis, "Technological innovations in mental healthcare: harnessing the digital revolution," The British Journal of Psychiatry, **206**(4), 263-265, 2015, doi:10.1192/bjp.bp.113.142612.

[20] L.O.M. de Andrade, A. Pellegrini Filho, O. Solar, F. Rígoli, L.M. de Salazar, P.C.F. Serrate, K.G. Ribeiro, T.S. Koller, F.N.B. Cruz, R. Atun, "Social determinants of health, universal health coverage, and sustainable development: case studies from Latin American countries," The Lancet, **385**(9975), 1343-1351, 2015, doi:10.1016/S0140-6736(14)61494-X.

[21] D.B. Evans, J. Hsu, T. Boerma, "Universal health coverage and universal access," Bulletin of the World Health Organization, **91**, 546-546A, 2013, doi:10.2471/BLT.13.125450 .

[22] G. Ooms, L.A. Latif, A. Waris, C.E. Brolan, R. Hammonds, E.A. Friedman, M. Mulumba, L. Forman, "Is universal health coverage the practical expression of the right to health care?," BMC International Health and Human Rights, **14**(1), 1-7, 2014, doi:10.1186/1472-698X-14-3.

[23] C.M. Shea, S.R. Jacobs, D.A. Esserman, K. Bruce, B.J. Weiner, "Organizational readiness for implementing change: a psychometric assessment of a new measure," Implementation science, **9**(1), 1-15, 2014, doi:10.1186/1748-5908-9-7.

[24] S. Khoja, H. Durrani, R.E. Scott, A. Sajwani, U. Piryani, "Conceptual framework for development of comprehensive e-health evaluation tool," Telemedicine and e-Health, **19**(1), 48-53, 2013, doi:10.1089/tmj.2012.0073.

[25] K. O'Neill, M. Takane, A. Sheffel, C. Abou-Zahr, T. Boerma, "Monitoring service delivery for universal health coverage: the Service Availability and Readiness Assessment," Bulletin of the World Health Organization, **91**, 923-931, 2013, doi:10.2471/BLT.12.116798.

[26] G. Puron-Cid, "Interdisciplinary application of structuration theory for e-government: A case study of an IT-enabled budget reform," Government Information Quarterly, **30**, S46-S58, 2013, doi:10.1016/j.giq.2012.07.010.

[27] A. Giddens, The constitution of society: Outline of the theory of structuration, University of California Press, 1984.

[28] A.F. Coad, L.G. Glyptis, "Structuration: a position–practice perspective and an illustrative study," Critical Perspectives on Accounting, **25**(2), 142-161, 2014, doi:10.1016/j.cpa.2012.10.002.

[29] C.L.H. Chang, "The interaction of political behaviors in information systems implementation processes–Structuration Theory," Computers in Human Behavior, **33**, 79-91, 2014, doi:10.1016/j.chb.2013.12.029.

[30] T. Iyamu, "Improvising information technology projects through the duality of structure," South African Journal of Information Management, **19**(1), 1-9, 2017, doi:10.4102/sajim.v19i1.797.

[31] H. Englund, J. Gerdin, "Structuration theory in accounting research: Applications and applicability," Critical Perspectives on Accounting, **25**(2), 162-180, 2014, doi:10.1016/j.cpa.2012.10.001.

[32] T. Iyamu, "Underpinning theories: Order of use in information systems research," Journal of Systems and Information Technology, **15**(3), 224-258, 2013, doi:10.1108/JSIT-11-2012-0064.

[33] C. Avgerou, C. Bonina, "Ideologies implicated in IT innovation in government: A critical discourse analysis of Mexico's international trade administration," Information Systems Journal, **30**(1), 70-95, 2020, doi:10.1111/isj.12245.

[34] J.D. Wall, B.C. Stahl, A.F. Salam, "Critical discourse analysis as a review methodology: An empirical example," Communications of the Association for Information Systems, **37**(1), 257-285, 2015, doi:10.17705/1CAIS.03711.

[35] M.D. Myers, H.K. Klein, "A set of principles for conducting critical research in information systems," MIS Quarterly, **35**(1), 17-36, 2011, doi:10.2307/23043487.

[36] F. Shirazi, "Social media and the social movements in the Middle East and North Africa: A critical discourse analysis," Information Technology & People, **26**(1), 28-49, 2013, doi:10.1108/09593841311307123.

[37] T.M. Cheng, "Reflections on the 20th anniversary of Taiwan's single-payer

[38] A. Fusheini, J. Eyles, "Achieving universal health coverage in South Africa through a district health system approach: conflicting ideologies of health care provision," BMC Health Services Research, **16**(1), 1-11, 2016, doi:10.1186/s12913-016-1797-4.

[39] S.R. Mishra, P. Khanal, D.K. Karki, P. Kallestrup, U. Enemark, "National health insurance policy in Nepal: challenges for implementation," Global health action, **8**(1), 28763, 2015, doi:10.3402/gha.v8.28763.

[40] S.O. Hynes, B. Pang, J.A. James, P. Maxwell, M. Salto-Tellez, "Tissue-based next generation sequencing: application in a universal healthcare system," British Journal of Cancer, **116**(5), 553-560, 2017, doi:10.1038/bjc.2016.452.

[41] K. Abouelmehdi, A. Beni-Hessane, H. Khaloufi, "Big healthcare data: preserving security and privacy," Journal of big data, **5**(1), 1-18, 2018, doi:10.1186/s40537-017-0110-7.

[42] A. Mouttham, C. Kuziemsky, D. Langayan, L. Peyton, J. Pereira, "Interoperable support for collaborative, mobile, and accessible health care," Information systems frontiers, **14**(1), 73-85, 2012, doi:10.1007/s10796-011-9296-y.

[43] J.A. Kim, S. Yoon, L.Y. Kim, D.S. Kim, "Towards actualizing the value potential of Korea Health Insurance Review and Assessment (HIRA) data as a resource for health research: strengths, limitations, applications, and strategies for optimal use of HIRA data," Journal of Korean medical science, **32**(5), 718-728, 2017, doi:10.3346/jkms.2017.32.5.718.

[44] C. Bredenkamp, T. Evans, L. Lagrada, J. Langenbrunner, S. Nachuk, T. Palu, "Emerging challenges in implementing universal health coverage in Asia," Social science & medicine, **145**, 243-248, 2015, doi:10.1016/j.socscimed.2015.07.025.

[45] A. Smith, J. Wishnia, D. Strugnell, S. Ranchod, "Human resources for health planning and National Health Insurance: the urgency and the opportunity," South African health review, **2018**(1), 23-31, 2018, doi:10.10520/EJC-14490f63b9.

[46] A. Edward, C. Branchini, I. Aitken, M. Roach, K. Osei-Bonsu, S.H. Arwal, "Toward universal coverage in Afghanistan: a multi-stakeholder assessment of capacity investments in the community health worker system,"Social science & medicine, **145**, 173-183, 2015, doi:10.1016/j.socscimed.2015.06.011.

[47] L. Rispel, "Analysing the progress and fault lines of health sector transformation in South Africa," South African health review, **2016**(1), 17-23, 2016, doi:10.10520/EJC189322.

[48] M.R. Reich, J. Harris, N. Ikegami, A. Maeda, C. Cashin, E.C. Araujo, K. Takemi, T.G. Evans, "Moving towards universal health coverage: lessons from 11 country studies," The Lancet, **387**(10020), p811-816, 2016, doi:10.1016/S0140-6736(15)60002-2.

[49] J. Shiffman, "Political context and health financing reform," Health Systems & Reform, **5**(3), 257-259, 2019, doi:10.1080/23288604.2019.1633894.

[50] A. Polynikis, G. Lavranos, "Cyprus' health system reform: Trials and tribulations," Sağlık Akademisyenleri Dergisi, **5**(1), 1-6, 2018, doi:10.5455/sad.13-1518617280.

[51] T. Rice, L.Y. Unruh, P. Rosenau, A.J. Barnes, R.B. Saltman, E. van Ginneken, "Challenges facing the United States of America in implementing universal coverage," Bulletin of the World Health Organization, **92**, 894-902, 2014, doi:10.2471/BLT.14.141762.

[52] M. Herselman, A. Botha, H. Toivanen, J. Myllyoja, T. Fogwill, R. Alberts, "A digital health innovation ecosystem for South Africa," In 2016 IST-**Africa Week Conference**, 1-11, 2016, doi:10.1109/ISTAFRICA.2016.7530615.

[53] Y.C.J. Li, J.C. Yen, W.T Chiu, W.S. Jian, S. Syed-Abdul, M.H. Hsu, "Building a national electronic medical record exchange system–experiences in Taiwan," Computer methods and programs in biomedicine, **121**(1), 14-20, 2015, doi:10.1016/j.cmpb.2015.04.013.

[54] C.Y. Wright, M. Chersich, A. Mathee, "National Health Insurance and climate change: Planning for South Africa's future," South African Journal of Science, **115**(9-10), 1-3, 2019, doi:10.17159/sajs.20169/5800.

[55] W. Raghupathi, V. Raghupathi, "Big data analytics in healthcare: promise and potential," Health information science and systems, **2**(1), 1-10, 2014, doi:10.1186/2047-2501-2-3.

[56] R. Pankomera, D. Van Greunen, P. Elizabeth, "December. Comparative analysis of the status of ICT usage in healthcare: South Africa, Tanzania, Malawi," In Proceedings of the IASTED A**frican Conference on Health Informatics** (AfricaHI 2014), 2014, doi:10.2316/P.2014.815-021.

[57] T. Mgozi, R. Weeks, "December. The impact of cloud computing on the transformation of healthcare system in South Africa," In 2015 ITU Kaleidoscope: Trust in the Information Society (K-2015), 1-7, 2015,

National Health Insurance System," Health affairs, **34**(3), 502-510, 2015, doi:10.1377/hlthaff.2014.1332.

doi:10.1109/Kaleidoscope.2015.7383636.

[58] S. Mndzebele, M. Matsi, "Perspectives and experiences of healthcare workers on the National Health Insurance at tertiary hospitals in the Limpopo Province, South Africa," PULA: Botswana J Afr Stud, **30**(1), 123-30, 2016.

[59] S. Latiff-Khamissa, P, Naidoo, "Knowledge, awareness and readiness of private sector doctors practising in the Ethekweni and Ugu districts of KwaZulu-Natal province for the implementation of the National Health Insurance," South African Family Practice, **58**(1), 18-23, 2016, doi:10.1080/20786190.2015.1123361.

[60] V.K. Molokomme, E. Seekoe, D.T. Goon, "The perception of professional nurses about the introduction of the National Health Insurance (NHI) in a private hospital in Gauteng, South Africa," The Open Public Health Journal, **11**(1), 234-242, 2018, doi:10.2174/1874944501811010234.

[61] G. Setswe, S. Muyanga, J. Witthuhn, P. Nyasulu, "Public awareness and knowledge of the National Health Insurance in South Africa," Pan African Medical Journal, **22**(1), 19-26, 2015, doi:10.11604/pamj.2015.22.19.6131.

[62] R. Pokharel, P.R. Silwal, "Social health insurance in Nepal: A health system departure toward the universal health coverage," The International journal of health planning and management, **33**(3), 573-580, 2018, doi.org/10.1002/hpm.2530.

[63] J. Van Wijk, C. Zietsma, S. Dorado, F.G. De Bakker, I. Marti, "Social innovation: Integrating micro, meso, and macro level insights from institutional theory," Business & Society, **58**(5), 887-918, 2019, doi:10.1177/0007650318789104.

[64] P.H. Kim, K. Wennberg, G. Croidieu, "Untapped riches of meso-level applications in multilevel entrepreneurship mechanisms," Academy of Management Perspectives, **30**(3), 273-291, 2016, doi:10.5465/amp.2015.0137.

[65] B. Wang, Q. Zhou, "Climate change in the Chinese mind: An overview of public perceptions at macro and micro levels," Wiley Interdisciplinary Reviews: Climate Change, **11**(3), e639, 2020, doi:10.1002/wcc.639.

[66] C. Esposito, A. De Santis, G. Tortora, H. Chang, K.K.R. Choo, "Blockchain: A panacea for healthcare cloud-based data security and privacy?," IEEE Cloud Computing, **5**(1), 31-37, 2018, doi:10.1109/MCC.2018.011791712.

[67] Y. Zhang, M. Qiu, C.W. Tsai, M.M. Hassan, A. Alamri, "Health-CPS: Healthcare cyber-physical system assisted by cloud and big data," IEEE Systems Journal, **11**(1), 88-95, 2015, doi:10.1109/JSYST.2015.2460747.

[68] V. Tangcharoensathien, A. Mills, T. Palu, "Accelerating health equity: the key role of universal health coverage in the Sustainable Development Goals," BMC medicine, **13**(1), 1-5, 2015, doi:10.1186/s12916-015-0342-3.

Birds Images Prediction with Watson Visual Recognition Services from IBM-Cloud and Conventional Neural Network

Fatima-Zahra Elbouni[*,1], Aziza EL Ouaazizi[1,2]

[1] *Laboratory of Engineering Sciences (LSI), Sidi Mohamed Ben Abdallah University, Taza, 1223, Morocco*

[2] *Laboratory of Artificial Intelligence, Data Sciences and Emergent Systems (LIASSE), Sidi Mohamed Ben Abdallah University, Fez, 30013, Morocco*

ARTICLE INFO	ABSTRACT
	Bird watchers and people obsessed with raising and taming birds make a kind of motivation about our subject. It consists of the creation of an Android application called "Birds Images Predictor" which helps users to recognize nearly 210 endemic bird species in the world. The proposed solution compares the performance of the python script, which realizes a convolutional neural network (CNN), and the performance of the cloud-bound mobile application using IBM's visual recognition service to choose the platform one. android form. In the first solution we presented an architecture of a CNN model to predict bird class. While the other solution, which shows its effectiveness, is based on IBM's visual recognition service, we connect the IBM project that contains the training images with our Android Studio project using an API key , and the IBM process classifies the image captured or downloaded from the application and returns the prediction result which indicates the type of bird. Our study highlights three major advantages of the solution using IBM's visual recognition service compared to that of CNN, the first appears in the number of images used in training which is higher compared to the other and the strong distinction between bird types where images and bird positions come together in color. The second advantage is to create a trained model saved on the cloud in order to use it with each prediction the most difficult thing to do locally due to the low processing capacity of smartphones. The last advantage is reflected in the correct prediction with a certainty of 99% unlike the other solution due to the instability of the CNN model.

1 Introduction

This article is an extension of the work originally "Bird Image Recognition and Classification Using IBMCloud's Watson Visual Recognition Services and Conventional Neural Network (CNN)" presented in the conference "International Conference on Electrical Engineering, Communication and Computing (ICECCE) 2021"[1].

Birds are among the living organisms that play an important role in the life cycle of the planet. They have become a center of interest for many people such as ornithologists who are interested in researching different types of birds, curious and passionate people who wish to live closer to them, without forgetting the sanctuaries, associations or large bird stores that are interested in breeding or protecting birds from extinction. These people often need to know certain characteristics of birds such as their diet, family (or gender) and housing in order to provide them with a suitable and comfortable lifestyle. To make it easier for these people, we had the idea to

develop an intelligent bird recognition system.

Science has progressively evolved through several chronological stages. The first phase was based on an experimental paradigm, from the 17th century, which took into account the experiment, the observation of phenomena and the use of this experimentation [2]. The second phase was theoretical, it uses an idea or a hypothesis to explain an observed phenomenon, it is a way of synthesizing the acquired knowledge and inventing new experiments. In fact, there was a dynamic relationship between experimental and theoretical science since one completes the other [3]. Around the year 1995 another paradigm appeared, it is essentially interested in the production, processing and use of information after storage, it is the science of information. This latter one has been developed in an exponential way stimulating the birth of the 4th paradigm of the data oriented science which leads to significant advances in the statistical techniques and machine learning [4].

Machine learning is one of the disciplines of artificial intel-

---

*Corresponding Author: Fatima-Zahra ELBOUNI, Fez-Morocco, +212-616338783 fatimazahra.elbouni@usmba.ac.ma

ligence [5], this notion of intelligence defines two fundamental approaches. The first is the connectionist approach, considers intelligence as a result of all minimalist functions, which are called neurons, by connecting several neurons, which can solve more complex cases and have good results. When we talk about the connectionist approach, we say that it is inductive, we have an input and an output and from the observation we try to understand what it is in order to define one or more rules. On the other hand, there is the symbolic movement of things which affirms that intelligence is only symbols interpreted at a high level. For example when we say "Every Cauchy sequence is a convergent sequence" it means that "If U is a Cauchy sequence, then U is a convergent sequence". This approach is deductive,it deduces the result by applying one or more inference rules on the input, which leads to NP-complete problems due to the exponential complexity of the rule application algorithm.

To achieve our solution, a comparable supervised machine learning model using a convolutional neural network (CNN) [6] has been proposed. The first step is to perform a convolution [7] of raster or tensor image representation of our bird database in order to extract the main features. The second step is to perform the [7] flattening operation on the result of the convolutional layer to have a data format that can be injected into an artificial neural network (ANN). The third step is to train the trained model by back-propagating each ANN layer that are fully connected [8]. In the end, we get a well-trained model that is able to predict the type of a given bird from its image. All the steps mentioned above will be detailed in the third section.

The problem with this method is that the script takes a long time to train the model, updating the network weights each time with the gradient back-propagating algorithm that minimizes the error function, and carrying with small speed CPUs the problem becomes heavier. For this reason, we propose another method for prediction that uses IBM Cloud [9]. In fact, the visual recognition service of IBM Cloud forms the prediction classes once and saves them to exploit them when we need a prediction. This applied technique minimizes the prediction time: we don't need to train the model each time and also it gives the possibility to link the IBM Cloud project with an Android studio project in order to generate an APK installable on an Android OS smart phone, which makes the solution portable and usable.

There are other bird class prediction methods in the literature such as The "Application of Two-level Attention Models in Deep Convolutional Neural Network for Fine-grained Image Classification" [10]. This paper focuses on fine-grained classification by applying visual attention using a deep neural network, It incorporates three types of attention: bottom-up, top-down at the object level and top-down at the part level. All of these attentions are combined to form a domain-specific deep network and then used to enhance aspects of objects and their discriminative features. Bottom-up attention proposes candidate patches, top-down object-level attention selects patches relevant to a certain object, and top-down part-level attention locates discriminative parts. This pipeline provides significant improve ments and achieves the best accuracy under the weakest supervision conditions compared to subsets of the ILSVRC2012 dataset and the CUB200 2011 dataset.

The article "Handcrafted features and late fusion with deep learning for bird sound classification" [11], makes a study on acoustic features, visual features and deep learning for bird sound classification. In order to classify bird caller species a unified model built by combining convolution neural network layers ,convolution layers derives the important features and reduces the dimensionality, then fully connected conventional layers for classification. Based on the experimental results on 14 bird species, this method indicates that the proposed deep learning can achieve an F1 score of 94.36 %, superior to the use of acoustic feature approach which gives a score of 88.97% and the use of visual feature approach which gives a score of 88.87%. To further improve the classification performance, they merged the three approaches: acoustic feature approach, visual feature approach and deep learning approach, to expect a final better score of 95.95%.

The authors of the paper titled "Image based Bird Species Identification using Convolutional Neural Network" [12] have developed a deep learning model to recognize 60 species of birds in order to give the possibility to birders to easily identify the type of birds. The method implements a model to extract information from bird images using the Convolutional Neural Network (CNN) algorithm. The data is gathered from Microsoft's Bing v7 image search API. The classification accuracy rate of CNN on the training set included 80% of data reached 93.19% and the accuracy rate on the test set that included on 20% of data reached just 84.91%. The experimental study was conducted on Windows 10 operating system in Atom Editor with TensorFlow library.

There are other applications on the Play Store such as "Merlin Bird ID" [13] whose purpose is to identify birds using the Photo ID pane which offers a short list of matches between photos taken or imported from photo gallery thanks to patterns trained on thousands of photos of each species. This application covers over 8000 species, has a code size of 25 MB and is trained on images downloaded from the eBird checklists and archived in the Macaulay library. This application can identify species that are currently included in the regional kits that contain the reindeer species in that region.

This article is organized as follows: in the second section we describe the approach adopted for the realization of the solution, in the third section we give a description of the method adopted during recognition, in the fourth section we will give the results obtained then we will devote the fifth section to the discussion and evaluation of the results and the last one to conclude the work and open another research track.

2 Materials and Mrthod

2.1 IBM Watson:

Watson [14] is a cognitive artificial intelligence computer program developed by IBM. It has several sub-services, including Watson Visual Recognition Ref used primarily for visual content recognition and analysis using machine learning. The IBM platform offers choices for managing application interfaces, among which the Android Studio is chosen. After authentication on the IBM Ref Cloud, we create a project as follows:
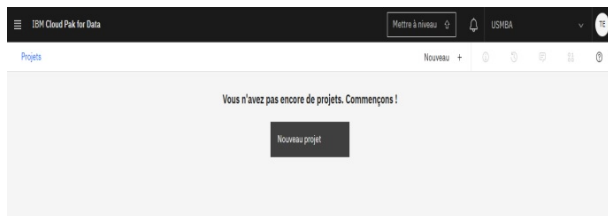
Figure 1: IBM Cloud interface to create new project

The project name and description (optional) must be defined.
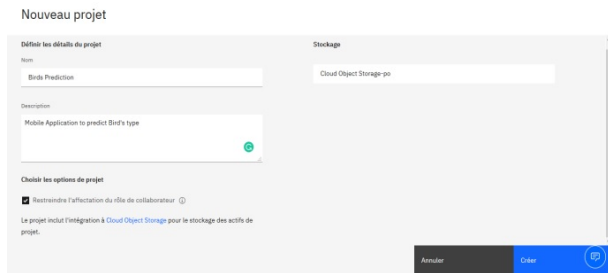
Figure 2: Project information

The next step is to choose the Visual Recognition subsystem of Watson :
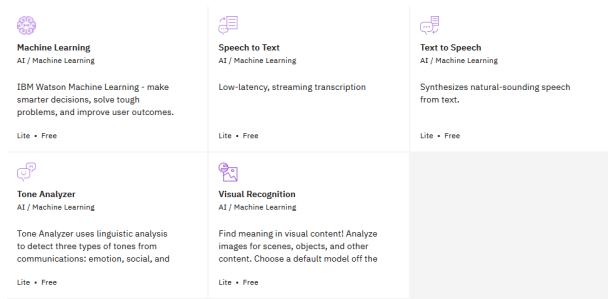
Figure 3: Creation of Visual Recognition Service

The visual recognition service helps to create a registered pattern of bird classes, from a database of images where each class must contain at least 10 different images to facilitate prediction.

On the Kaggle website[15] , a dataset of training images has been uploaded which contains approximately 210 bird types, where each type contains more than 10 images.

2.2 Firebase

To store the different characteristics of each bird, including name, family, diet and housing in addition to other similar images; the external Google "Firebase" database [16] was used.
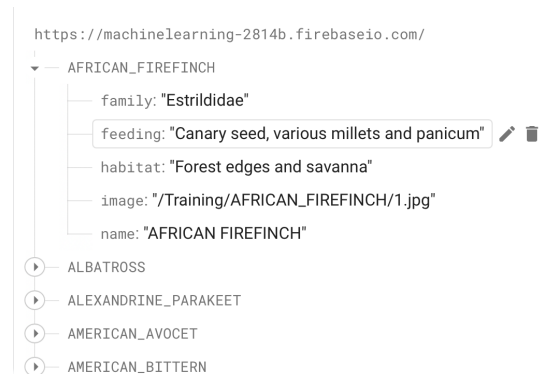
Figure 4: Realtime database of Firebase Storage

3 Recognition Method

Several innovations in various fields of science derive their operating principle from the behavior of the human body, for example fundamental computer science is inspired by the nervous system to develop models of artificial intelligence. The human brain consists of more than 80 billion living cells [17] called "neurons", interconnected with each other to transmit or process chemical or electrical signals. A biological neuron consists of the dendrites (inputs) which are branches that receive information from other neurons, a Soma or cell nucleus that processes the information received from the dendrites, an axon as a cable used by neurons to send information to the output and synapses (outputs) that connects the axon and the other neural dendrites.

By analogy, a formal model has been proposed to be integrated into so-called intelligent systems, which can react almost like humans; named artificial neuron or perceptrons [18]: it is a mathematical function that takes values into account to make a simple calculation and return one or more values as output. The calculation performed by a perceptron is broken down into two phases: a calculation by a linear function(1):

$$f(x_1, x_2..., x_n) = w_1 x_1 + w_2 x_2 + + w_n x_n \tag{1}$$

where the w_i are the weights and the x_i are the input values with $(1 \leq i \leq n)$, followed by an activation function [19] (or transfer function)φ which will decide whether the information will be transmitted to another neuron or not.

There are several activation functions that are chosen according to the type of problem to be solved, such as the Relu function defined by $f(x) = max(0, x)$ and Softmax generally used to solve multi-classification whith single-label problems. Note that we can add an additional weight b_j called bias [20] or error which measures the difference between the expected output value and the estimated output value y_j and the estimated value to have an "affine perceptron".

The juxtaposition of several neurons, grouped by layers, gives the notion of the artificial neural network [6]. Previously, the connectionist approach consists in finding a relation between the input and the output, more formally looking for a function F which connects the input to the output. In real life many types of relationships result in linear or quadratic functions, however there are more complex problems such as predicting the class of a bird which results

in a non-linear function. According to the universal approximation theorem [21], any continuous and bounded function can be approximated by a neural network with n inputs and y_i outputs, possessing a finite number of neurons in a single layer hidden with an activation function and a output whose activation function is linear.

To find the best function F (2) which connects the input to the output

$$F(X_i) \approx Y with (Y = (y_1, y_2, ..., y_m)) \tag{2}$$

It suffices to configure the parameters (the weights $P = (w_1, w_2, ...w_n)$ and the bias b_j) of the network, so that the mide error is minimal. To precisely measure the performance of the approximation, we define a cost function [22]in our case Cross-entropy for categories(3) [23]:

$$E = -y_j \log(\tilde{y}_j) + (1 - y_j) \log(1 - \tilde{y}_j) \tag{3}$$

It sum of E_i the local errors, generally convex and we are looking for its minimum, so we are faced with an optimization problem that can be solved by the method of descent of the gradient [24], the latter assimilates the notion of gradient [24] which is a generalization of the derivation in the case of functions with several variables. The derivation studies the variations of a function and tries to find its extrema; similarly the gradient is a vector which gathers the partial derivations of a function with several variables and which indicates the direction of the greatest slope of the function from a point. The calculation of the gradient vector of the cost function requires the calculation of the partial derivatives of E from those of F by the formula (4):

$$grad f(x_1, ..., x_n) = \begin{pmatrix} \frac{\partial f}{\partial x}(x_1, ..., x_n) \\ . \\ . \\ . \\ \frac{\partial f}{\partial x}(x_1, ..., x_n) \end{pmatrix} \tag{4}$$

Back-propagation [8] is the application of gradient descent on an artificial neural network . Gradient descent is an optimization algorithm used to find the minimum of a function, based on the opposite vector [24] to the gradient vector. To find the minimum error, we start from the initial weights $W_0 = (w_0, w_1, ...)$, the direction of the opposite vector is followed by a step δ, called the learning rate, and we start again from the new weights and stop at the end of a number of iterations fixed in advance or when the error tends to zero; according to the following recurrence formula (5)[8]:

$$P_{k+1} = P_k - \delta \times grad(E_{global}(P_k)) \tag{5}$$

There are three variants of the gradient descent, which is differentiated by the amount of data used in the calculate the gradient of the cost function. If we use the global error E_{global}, we say that there is a classical gradient descent. If we consider at each iteration a single gradient E_i instead of E_{global}, we say that there is a stochastic gradient descent, this technique reduces the amount of calculations, because the calculation of the gradient of E_{global}, involves the calculation of the gradient of each of the E_i, that is to say the partial derivation with respect to each of the weights w_j. If we divide the data into packets of size K. For each packet (called a "batch"), a gradient is calculated and an iteration is performed,

we say that there is a gradient descent in batches (or mini-batches). It is an intermediate method between the descent of the classical gradient (traversing all the data at each iteration) and the descent of the stochastic gradient (which uses only one data at each iteration), at the end of $\frac{N}{K}$ iterations, we have traversed the entire dataset: this is called an epoch.

However, these variations do not always lead to the minimum point, which requires another variation in the learning rate, where δ must be chosen neither too large nor too small: if δ is too large, the P_k points will oscillate around the minimum, but if δ is too small, the P_k points will approach the minimum only after a very long time. For example, it is possible to choose, during training, a fairly large δ_k, then smaller and smaller over the iterations; either by a linear, quadratic or exponential decrease.

The proposed model applies gradient descent Adam [25] stands for Adaptive Momentum Estimation , which is a stochastic gradient descent that combines between two methods Momentum and RMSprop. Momentum [25] is a method that helps to speed up stochastic gradient descent in the appropriate direction and dampen oscillations by adding fractions of previous gradients to the current gradient. RMSprop [25] is based on a decreasing variation of aggressive learning rate.

Algorithm 1: ADAM algorithm

Result: P_t

$m_0 \longleftarrow 0$; *** Initialize the 1ere moment vector

$v_0 \longleftarrow 0$; *** Initialize the 2ere moment vector

$t \longleftarrow 0$; *** Initialize the time step

while P_t *is not convergent* **do**

$\quad t \longleftarrow t + 1$

$\quad grad_t \longleftarrow \nabla f(P_{t-1})$;*** The gradient of the error function at time step t

$\quad m_t \longleftarrow \beta_1 \times m_{t-1} + (1 - \beta_1) \times grad_t$; *** Update first moment biased estimate

$\quad vt_t \longleftarrow \beta_2 \times v_{t-1} + (1 - \beta_2) \times grad_t^2$; *** Update biased raw second moment estimate)

$\quad \hat{m}_t \longleftarrow \frac{m_t}{(1-\beta_1^t)}$; *** First moment estimate corrected for computational bias

$\quad \hat{v}_t \longleftarrow \frac{v_t}{(1-\beta_2^t)}$; *** Second moment estimate corrected for computational bias

$\quad P_t \longleftarrow P_{t-1} - \alpha \times \frac{\hat{m}_t}{(\sqrt{\hat{v}_t}+\epsilon)}$; *** Update settings

end

Our study is focused on a convolutional neural network (CNN) , inspired by the operating principle of the visual lobe of vertebrates. It is a type of artificial neural network suitable for image recognition which is composed of two parts: a convolution part and a classification part corresponds to a classic multilayer model. Convolution [7] is a mathematical method that applies a convolutional product between an array (matrix representation of an image) and a pattern (filter or kernel), frequently used for image processing in order to bring a transformation or derive its main characteristics. This convolutional product [7] can be realized by a neural network with convolution neurons, in which also we apply the gradient descent algorithm to adjust their weights. The result of this convolution forms a feature map. The convolution part also consists of a pooling phase[7], the purpose of which is to reduce the dimensionality which aims to reduce the computational complexity while keeping

the important characteristics of the input image. There are two types of Pooling: max-Pooling and average-Pooling. The first takes the max of each of the sub-matrices (windows) while the second takes the average. The last phase of the convolution part is the flattening phase which converts the feature maps obtained after the Pooling operation into a column vector.

The result column vector will be the input of our artificial neural network which constitutes the second phase of the multilayer model, it is trained using the gradient back-propagation algorithm with two image databases of birds, one for training and another for testing.

A good learning model offers an optimal balance between bias and variance, it simultaneously minimizes these two error quantities, this problem is known as the bias–variance trade-off [20]. On the one hand, a high bias and a low variance cause underlearning[26]: lack of relevant relationships between input/output data; On the other hand, excessive data variance and low bias can lead to overfitting[26], where the model remains too specific to the training data and thus is unable to adapt to new data. To remedy this problem, we use the Dropout technique. Dropout [8] is a technique that temporarily deactivates certain neurons of a layer during training with a given probability, therefore it sets the weights to zero for both evaluation and backpropagation.

Here is a summary diagram of all the steps mentioned above of our adapted version of the RNC (go to the appendix section to see the source code in python):
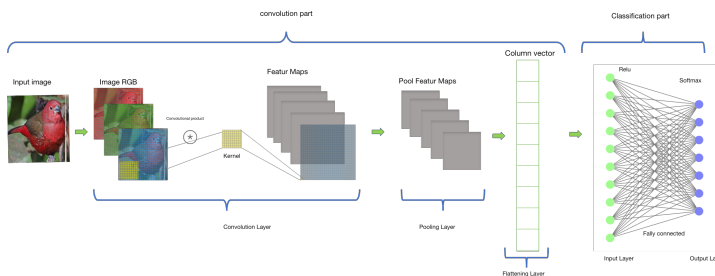
Figure 5: Descriptive schema of the applied convolutional neural network

The problem mentioned in this research is included in the family of image classification problems, so to clearly indicate to which class an image belongs, we need to minimize the gap (2) between each of the images of the input classes (training base) with the images of the same classes of the output (test base), this division of the images into two: test and training, is done to remedy the problem of ias–variance 3. First of all, each RGB image is considered as a matrix of pixels to which convolution 3 is applied to reduce its size and keep only its relevant characteristics in order to transform it into a column vector that we introduce in a Multilayer Perceptron. This operation decreases the computing power required to process the data. The column vector enters the artificial nouron network in which the backpropagation 3 is applied based on the ADAM 3 algorithm, at each iteration of the process and over a series of epochs, the model is able distinguish between dominant features and some low-level features in images and classify them using the Softmax 3 activation function. Here are the essential steps for creating the CNN model:

- Create an image generator for the training data;

- Create an image generator for the training data;

- Upload the training images;

- Create two convolutional layers;

- Create two Pooling layers;

- Create the Flattening Layer;

- Treated the over-learning problem;

- Added a Multilayer Perceptron with one hidden layer and an output layer with 128 neurons which allows the detection of 210 types of birds.

Layer (type)	Output Shape	Param #
conv2d (Conv2D)	(None, 62, 62, 32)	896
conv2d_1 (Conv2D)	(None, 60, 60, 32)	9248
max_pooling2d (MaxPooling2D)	(None, 30, 30, 32)	0
max_pooling2d_1 (MaxPooling2D)	(None, 15, 15, 32)	0
flatten (Flatten)	(None, 7200)	0
dense (Dense)	(None, 128)	921728
dropout (Dropout)	(None, 128)	0
dense_1 (Dense)	(None, 210)	27090

Figure 6: Model architecture summary

4 Experimental Results and Analysis

This study is a comparison between the results of two methods of predicting the class of a bird, such as the python script that implements a convolutional neural network (CNN)[6] and the method of prediction by the IBM Cloud visual recognition service[9].

The first method of the CNN script was trained on 210 bird classes, while the second one offers the possibility to test up to 1010 classes. The latter minimises the error and prediction time, where the prediction reaches a percentage of servitude of 99% and a waiting time of less than 10 seconds. In addition, it offers the possibility to store the trained model in the cloud for later reuse or integration with a solution such as Java, Android Studio or Python. Thus, the process of learning bird images using the CNN method takes enough time for training despite being tested on a small dataset and gives a low prediction accuracy compared to the second method.

The proposed solution integrates the prediction method by IBM Cloud's visual recognition service with an Android Studio project to generate an APK of an Android mobile application.

Here is a table of comparison between CNN model and visual recognition service from IBM Cloud :

Table 1: comparative table between CNN and VRS-IBM

Comparison criterion	CNN	VR-IBM
Number of class	210	1010
Response time	2s	5s
Accuracy	22%	no access
Loss	64%	no access
Model storage	locally	on the cloud
Integration with mobile app	TensorFlow Lite	API

Images show the instability of the CNN model:
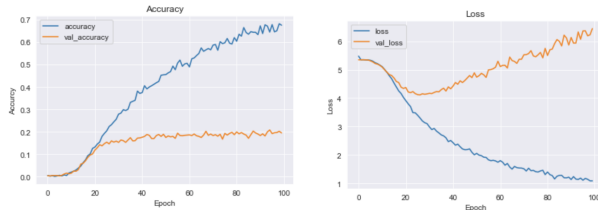
Figure 7: accuracy and loss per epoch graphs

the two graphs above indicate the variation of accuracy and loss over epochs. The first accuracy graph illustrates that the accuracy of the validation increased linearly with the accuracy, but from epoch 18 it fluctuates between values very close and away from the accuracy, this means that the model learns more information at each time; similarly for the loss graph, the validation loss shows that it decreased linearly, but after 18-19 epoch it started to increase. This means that the model tried to store the data. We also notice that the error rate is 64% and the accuracy rate is 22%, which means that the model requires a good adjustment of the hyperparameters to have good results.

The application represents in the first interface "figure 6" a list of bird images, when you press the button of the "eye" icon a detail containing the characteristics (name, family, housing, food) of this race, will be displayed in the form of a table "figure 7" as well as a small gallery of the same race to have more about this race.
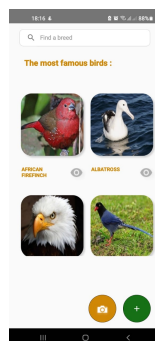
Figure 8: Home interface

Predicting the breed of a bird from its image is done by two options, the first allows you to choose an already captured image saved in the smartphone gallery as indicated by the plus "+" icon in "Figure 6", or by the second method which allows you to capture a new image instantly as illustrated by the camera icon in "Figure 6".
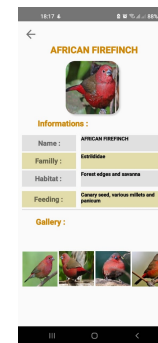
Figure 9: Detail interface

To detail the scenario, once the user uploads or captures an image of a bird, the image will be transmitted to the IBM Cloud Platform through the "ClassifyOptions" object, thereafter the visual recognition service will return the prediction result through the "ClassifiedImages" object in the form of the name of the class to which the bird belongs and the percentage of similarity. After retrieving the name of this bird a query will be sent to the FireBase database with the bird name as parameter in order to receive their characteristics and display them in a table as shown in "Figure 7".

5 Discussion

Our article presents a demonstration of three main results concerning the recognition problem: the first result is the prediction of the class of bird given in the image captured or chosen by the user, this result reflects the correct prediction with certainty 99% unlike the other solution due to CNN model instability. The second result is the presentation of major characteristics of the predicted bird such as its family, its habitat and its food with the display of a small gallery of bird images from the database used, This result illustrates the model's reliability in distinguishing between similar types in the face of the high number of images used in the training phase. The third result is the usability and easy portability of the solution on the phone in the form of an Android mobile application, the solution generates a trained model saved on the cloud in order to use it for each prediction the most difficult thing to be done locally due to the low processing capacity of smartphones. However, our study focuses on 210 classes of endemic bird species to make the exact classification in a targeted and efficient way. The proposed CNN model has been tested on training images, it returns the result with an accuracy of 22%. But due to the visual similarity between bird species, when using a new image, the model sometimes fails to distinguish between two types and ultimately leads to misclassification. On average, testing the data set gives a sensitivity of 64%. Therefore, the visual recognition service of the IBM Cloud method has been adopted to make the prediction of the class of bird species in order to have a simple, fast and efficient result. The latter applies a deep learning algorithm and gives a good numerical precision, which we bet on the success of this project, despite that it does not give access to visualize the model architecture and compare their metrics with that CNN model. have a simple, fast and effective result. The latter applies a deep learning algorithm and gives a good numerical precision, which we bet on the success of this project, de-

spite that it does not give access to visualize the model architecture and compare their metrics with that CNN model. have a simple, fast and effective result. The latter applies a deep learning algorithm and gives a good numerical precision, which we bet on the success of this project, despite that it does not give access to visualize the model architecture and compare their metrics with that CNN model.

In December 2021 the visual recognition service of Watson was obsolete [27], it is replaced by others like the machine learning service and to keep the usability of the application we proposed another solution consists in saving the trained model of the python script, after having improved the setting of the hyper-parameters, in the form of a file with extension "h5" then with this file we will generate another TansorFlow file[28] with extension "tflite" [29]in order to integrate it with the Android studio project by replacing the part of prediction with the services by an image injection on the recorded model.

The "Merlin Bird ID" app [13] is one of the powerful apps in this field of bird species identification, it is released on play store the first time in 2014; it is powered by Visipedia, relies on artificial vision and deep learning, its last update was published in May 2022. It offers other functionality more than the features offered in our image recognition solution. "Merlin Bird ID" contains several pane among them, image recognition photo id pane to identify birds from photos by calling sets of millions of photos contributed by bird watchers in eBird.org at l using other user-provided information such as date and location; it brings together regional kits for example from the United States, Mexico, Central America, from Europe, North Africa and Australia... The Sound Id component is dedicated to audio recognition, it identifies the species from the sound and contains an audio recording library by region. The start pane id who Merlin starts by asking you a few simple questions and then magically gives you a list of birds that best match your description After choosing one you can see more photos, listen to recordings sound and read tips for identification. APK size rating our application is small with 23.64 MB than Merlin of 227 MB, so our study is limited to 210 types compared to the other which has more than 40,000 photos of birds (males, females and juveniles). Finally, Merlin is developed for different languages such as English, Spanish, Portuguese, Hebrew, German, Simplified Chinese and Traditional Chinese unlike our solution which is limited to English language only. The remark that we have noticed as users of this application that always the download and installation of regional kits either in the Photo ID or Sound ID pane fails but is it because of weak connection or technical problem in the application.

The paper "A new mobile application for agricultural pest recognition using deep learning in a cloud computing system" [30] is one of the research topics that exists in the literature in the sense of classification using a mobile application, this paper makes a comparison between the performance of two models, including the convolutional neural network (CNN) with connection hopping and the convolutional neural network without connection hopping. This research focuses on the development of an application that recognises weeds in agricultural areas, such as fields, greenhouses and large farms. The mobile application was developed by Apache Cordova, using Flask Framework to handle the HTTP POST requests sent, the python code executed and hosted in the Cloud on the Python Anywhere environment and Mysql as the database to store all the pest information. So the application is based on Faster R-CNN, it was the result of this study, it gave good results which reached a score of 98.9%, regarding automatic control of pests, about five popular agricultural pests, crops compared to machine learning and deep learning classifiers in previous studies. This study also shows a major advantage in being able to detect pests in similar and complex backgrounds to the images tested. Furthermore, the Faster R-CNN is suitable for real-time identification of agricultural pests in the field, without prior knowledge of the number of objects in the acquired images. Finally, the prediction of the categories and positions of the different agricultural pests are accurately identified.

There is also another achievement in the literature which is based on the visual recognition service of IBM Cloud: "Personal robotic assistants: a proposal based on the intelligent services of the IBM cloud and additive manufacturing"[31], it proposes a robotic assistant as a personalized version of the Otto robot, which relies on additive manufacturing and an intelligent chatbot using IBM Cloud services, which concerns speech and image recognition, in noisy environments. This project uses OpenCV and IBM Cloud's own service for visual recognition, in order to obtain better performance in image recognition both in virtual assistants and in the robotic assistant. So in this discussion we are interested in the image recognition part. The authors use techniques like Gaussian, Image Segmentation, Blur effects, and salt and pepper to add noise to the original images to determine if the machine learning model implemented in the robot (via IBM Watson Cloud) can identify the images. correctly based on 3 levels of acceptance that have only been applied to virtual assistants (telegram and messenger). The result of this article is a combination of precision obtained at the same time in all the assistants.

6   Conclusion

Several projects related to various fields of artificial intelligence exploit image recognition, which makes their success depends on finding the best solution to the recognition problem; our project is the study, realization and development of an Android mobile application named "Birds images predictor" for the classification and recognition of bird images using IBM's cloud visual recognition service which applies a machine learning algorithm more specifically a deep learning algorithm.

The application manages to identify about 210 types of birds from their images captured or chosen by the user, it can be improved by increasing the number of classes of birds, adding other additional options such as the geographical distribution on the map of each of these races. The architecture of the CNN model can also be improved by readjusting its hyperparameters to increase the prediction accuracy and to have a low error rate in order to compare it again with another solution in the same direction.

References

[1] F. Z. ELBouni, T. Elhariri, C. Zouitni, I. BenBahya, H. Elaboui, A. ELOuaazizi, "Bird image recognition and classification using Watson visual recognition services from IBMCloud and Conventional Neural Network," the 3rd International Conference on Electrical, Communication and Computer Engineering, (6), 978–1–6654–3897–1, 2021.

[2] P. Beck, A. Courdent, A. Feriati, P. Hyvon, "Sciences expérimentales et technologie," **79**, 2218945959, 9782218945953, 2012.

[3] M. Michel, A quoi sert l'histoire des sciences?, 2006, ISBN: 978-2-7592-0082-5.

[4] Y. Li, S. Abdallah, "On hyperparameter optimization of machine learning algorithms:Theory and practice," ELSEVIER, **22**, 295–316, 2020.

[5] B. Gilles, F. Jym, "Langage naturel et intelligence artificielle," Hal-Archive, **10**, 1638–1580, 1988.

[6] A. Saad, A. M. Tareq, S. AL-ZAWI, "Understanding of a Convolutional Neural Network," IEEE Access, **6**, 978–1–5386–1949–0, 2017.

[7] S. Dominik, M. Andreas, B. Sven, "Evaluation of Pooling Operations in Convolutional Architectures for Object Recognition," conference, **10**, 164, 53117.

[8] A. Bodin, F. Recher, "Algèbre–Convolution," in Deepmath mathématique simple des réseaux de neurones (pas trop compliqués), Janvier-2021.

[9] IBM, "IBM Cloud," http://www.ibm.com/cloud, 2022.

[10] X. Tianjun, X. Yichong, Y. Kuiyuan, Z. Jiaxing, P. Yuxin, Z. Zheng, "The Application of Two-level Attention Models in Deep Convolutional Neural Network for Fine-grained Image Classification," IEEE Access, **9**, 842–850, 2015.

[11] X. Jie, Z. Mingying, "Handcrafted features and late fusion with deep learning for bird sound classification," IEEE Access, **8**, 75–81, 2019.

[12] R. Satyam, G. Saiaditya, K. Sanu, S. Shidnal, "Image based Bird Species Identification using Convolutional Neural Network," 2278–0181, 2020.

[13] C. University, "Merlin Bird ID," https://merlin.allaboutbirds.org, 2022.

[14] IBM, "Watson Visual Recognition," https://www.ibm.com/no-en/cloud/watson-visual-recognition/pricing, 2022.

[15] Machine, D. Learning, "Kaggle," https://www.kaggle.com/, 2022.

[16] Google, "Firebase," https://firebase.google.com.

[17] S. S. Mader, Biologie humaine, 22 janvier 2010, ISBN: 978-2-8041-2117-4.

[18] C. Touzet, Les réseaux de neurones artificiels, introduction au connexionnisme, Ph.D. thesis, 2016.

[19] E. Chigozie, W. Nwankpa, G. Ijomah Anthony, S. Marshall, "Activation Functions Comparison of Trends in Practice and Research for Deep Learning," **19**, 1811–03378, 2018.

[20] j. Dong, J. Jaeseung, W. Sang, "Prefrontal solution to the bias-variance tradeoff during reinforcement learning," Elsevier, **37**, 37, 110185, 2021.

[21] L. Andrea, S. Fabian, H. Johannes, N. Patrick, "Cybenko's Theorem and the capability of a neural network as function approximator," **32**, 2019.

[22] S. Vézina, "fonction d'erreur," in Le réseau de neurones.

[23] S. Anna, A. Bosman, Engelbrecht, M. Helbig, "Visualising basins of attraction for the cross-entropy and the squared error neural network loss functions," Elsevier, **24**, 113–136, 2020.

[24] A. Frouvelle, "Méthodes de descente de gradient," in Méthodes numériques optimisation, 19 avril 2015".

[25] P. K. Diederik, L. B. Jimmy, "ADAM:A method for stochastic optimization," conference paper, **15**, 2017.

[26] D. Yehuda, M. Vidya, G. B. Richard, "A Farewell to the Bias-Variance Tradeoff? An Overview of the Theory of Overparameterized Machine Learning," Elsevier, **48**, 2021.

[27] IBM, "IBM Documentation," https://www.ibm.com/docs/en/app-connect/containers_cd?topic=SSTTDS_contcd/com.ibm.ace.icp.doc/localconn_ibmwatsonvr.html, 2022.

[28] "TensorFlow," https://www.tensorflow.org/, 2022.

[29] "TensorFlow," https://www.tensorflow.org/lite/guide?hl=fr, 2022.

[30] K. Mohamed Esmail, A. Fahad, S. Albusaymi, A. Sultan, "A new mobile application of agricultural pests recognition using deep learning in cloud computing system," IEEE Access, **10**, 66980–66989, 9 March 2021.

[31] S. Amendan o Murriol, E. Duta n Go, Christian mez Lema-Condo, V. Robles-Bykbaev, "Personal robotic assistants: a proposal based on the intelligent services of the IBM cloud and additive manufacturing," IEEE, (6), 978–1–7281–9365–6, 2020.

A Review of the Role of Information Technology in Brazilian Higher Educational Institutions during Covid-19 Pandemic

Luís Cláudio Dallier Saldanha[*]

Universidade Estácio de Sá, Department of Education, Rio de Janeiro, 20071-001, Brazil

ARTICLE INFO	ABSTRACT
	This paper presents the results of a documentary research on the use of information technology in emergency remote teaching in 66 higher educational institutions in Brazil. The theoretical background of this study is based on the works of Feenberg, Bagglaey, Veloso & Mill, Castañeda & Selwyn and Hodges. The methodological approach consisted of analyzing reports published by YDUQS, an educational holding responsible for managing all the 66 institutions examined in this research. Such analysis aimed at identifying data concerning investments in information technology and its use throughout the Covid-19 pandemic. Results have revealed that investment in information systems as well as technological mediation of academic routines and pedagogical practices paved the way for a rapid response to the crisis triggered by the pandemic and the maintenance of student satisfaction. Nevertheless, the data available within the reports was not enough to draw conclusions on learning management neither on other pedagogical aspects of emergency remote teaching.

1. Introduction

Remote teaching was the educational alternative when in-person pedagogical activities came to a halt with the social distancing imposed by the COVID-19 pandemic during the years of 2020 and 2021.

In Higher Education, the prevalent trend was the adoption of technological solutions based on videoconference platforms and virtual learning environments, in which synchronous communication in online pedagogical activities was predominant with the shift from the four walls of the conventional classroom to digital settings.

Some institutions that already possessed experience with remote or hybrid learning were able to rely on existing digital content, intensive use of technology, technological infrastructure, and more appropriate methodology to promote both real-time classes as well as opportunities for the development of pedagogical activities in virtual environments.

In light of this context, it is fitting to put under scrutiny the implications of these institutions' total dependence on technological mediation so that classes and pedagogical activities could be preserved during the Covid-19 pandemic.

The present research summarizes the analysis of data on the technological mediation of emergency remote teaching in these 66 Brazilian institutions of Higher Education, managed by the same corporate group.

Thus, the results stem from documentary research aimed at examining the educational consequences of information technology within the context of remote learning.

This work was originally presented in the 17th Iberian Conference on Information Systems and Technologies [1]. This introduction is followed by a theoretical background on e-learning and information technology in the field of education, a section on methodological aspects, and, at last, the results of the present research on the investment and on the use of technologies within the higher educational institutions of the YDUQS group.

2. Remote Teaching and Technological Mediation

2.1. Remote Teaching

Expressions such as *remote teaching* (RT)*, emergency remote teaching* (ERT) and emergency remote learning and teaching (ERLT) have become recurrent in contemporary literature to describe online pedagogical activities during the Covid-19 pandemic.

[*]Corresponding Author: Luís Cláudio Dallier Saldanha,
luis.dallier@ensineme.com.br

Initially, in [2] the authors argued that emergency remote teaching (ERT) should not be taken as a byword for online learning or e-learning, while other authors [3] understand remote teaching as equivalent to online learning or e-learning.

The perspective that underscores differences between remote learning and e-learning have prevailed in recent literature on this topic, with only few studies still endorsing their interchangeability. To some extent, the need to set these two concepts apart is, indeed, justified so that the reputation of e-learning is not tainted by the chaos, the improvisation, the frail theoretical background, and the lack of suitable methodologies to cater for students' profiles due to the abrupt adoption of remote learning during the Covid-19 outburst [4].

In addition, their distinctiveness is also be sustained by the fact that private higher educational institutions charge cheaper fees for e-learning, whereas remote learning implicates more costs, with teachers offering synchronous lessons.

In a nutshell, the dissimilarities between remote teaching and e-learning can be described in terms of three major traits of remote teaching: a) the urgent and temporary status of remote learning; b) the transposition of in-person classes into virtual environments; and c) the prevalence of synchronous communication via real time transmission of lectures and video classes.

In turn, e-learning relies on five fundamental prerogatives: a) it must count on didactic and pedagogical frameworks of its own; b) educational contents and activities must be adequately designed; c) pedagogical model and methodologies must cater for students' needs and take their profiles into account; d) students must be familiar with the methodology as well as its technological resources; e) efficient tutoring must supervise and support students' academic performances [5].

In [6] the authors prefer not to set apart the concepts of remote teaching and e-learning based on the assumption that there are more similarities than differences between these two educational modalities. In addition to intrinsic dependence on technology, remote teaching shares other characteristics with e-learning, since in both cases teachers and learners are physically separated and the learning process is mediated by technology.

Furthermore, both modalities may alternate between synchronous and asynchronous communication, virtual environments and videoconference functionalities or application programs. The prevalence of synchronous communication and videoconference platforms in remote teaching would, therefore, consolidate a type of e-learning, instead of an independent educational modality. Due to prolonged social distancing, educational institutions planned remote teaching or a transition to hybrid teaching, developed specific methodologies and contents for these scenarios, in addition to acquiring suitable didactic materials.

Either standing as an independent educational modality or constituting a type of e-learning, remote teaching during the Covid-19 pandemic must be analyzed in light of the many particularities that marked the uniqueness of this period.

2.2. Information Technology and Education

The use of technology for educational purposes is not limited to information systems nor to the era of digital technologies. In a broad sense, technology has been omnipresent in education ever since resources such as chalk, blackboards, books, pens, and pencils were used in the classroom. In other words, technology in the field of education includes far more than computers and mobile digital resources [7]. That is not to deny the huge impact of digital technologies on educational processes, but to acknowledge the longstanding role technology has played in pedagogical mediation over the course of history.

Thus, the use of technology in remote teaching during the Covid-19 pandemic is necessarily intertwined with the broader history of technology in education – and there are many lessons to be learned from such previous experiences.

Many innovations advertised by the EdTechs date back to projects and experiences developed between the 1920s and the 1950s [8].

The infrastructure in information technology (IT) and the use of diverse technological resources have favored not only teaching in situations in which teachers and students are separated by time and space, but also brought forward alternative (and often more interactive) pedagogical practices from which any educational modality can profit.

New digital technologies have become more interactive and user-centered, offering new possibilities within educational settings [9].

In [10] the authors had already identified technological trends focused on ubiquitous and networked experiences with the massification of mobile devices and the further developments of the Web with novel and diversified forms of representation, stimulating environments, and a global IT infrastructure combining decentralization and interoperability.

In this scenario, information technology has become both integrating and pervasive, which explains its ubiquity in the lives of teachers and students as well as the emergence of demands and possibilities regarding its appropriation and use in formal educational contexts.

Information and communication technologies are not solely devoted to the production and the availability of digital contents in different media and languages. In addition to granting access to texts and video classes, these technologies have allowed users to come up with new ways to represent data, concepts, processes and phenomena. Simulations, animations, and games have propelled more meaningful learning experiences. Virtual and augmented realities have also proved efficient in the educational realm.

Moreover, due to recent advances in terms of artificial intelligence, technology has given rise to new forms of pedagogical planning, student-tailored learning experiences, learning management, as well as innovating tools and procedures for assessment.

Therefore, technology has gone far beyond its primary function of guaranteeing remote interaction among teachers and students, surpassing the mere offer of online education to produce new methodological approaches – useful for both in-person as well as remote learning experiences.

Technology has made feasible the mediation or the rise of different forms of communication, interaction and relationship within academic and educational processes.

Thus, it is possible to promote technological mediation within any sort of pedagogical modality, whether in-person or online, even though technologically mediated education has been mostly associated to e-learning. However, this setting has rapidly changed because of the Covid-19 pandemic.

3. Dependence and Resistance to Technology

3.1. Technological dependence

Social distancing during the Covid-19 pandemic imposed technological dependence as the only means of pedagogical mediation for previously in-person Higher Educational courses. Technological dependence was not restricted to the use of digital platforms nor to the videoconferences that suddenly replaced conventional classrooms. In addition to substituting face to face classes with virtual encounters, it was essential to sustain the entire academic routine digitally, making room for other pedagogical activities in the online environment.

At first, part of Brazilian higher educational institutions halted their academic activities for longer periods – some for a few months – which tended to be a more recurrent choice amongst public institutions [11]. Other institutions, mostly private, resumed their academic activities in virtual environments sooner, some improvising more than others. Learning Management Systems (LMS), once confined to e-learning, were adopted as well as applications for videoconference.

Initially, their technological response was most frequently based on platforms or applications responsible for transmitting live-expositive classes, often lacking previous planning and a more careful design process [12]. Services related to academic activities were preserved and especially enhanced by institutions that already counted on online customer service channels, which allowed students to remain in close contact through the use of applications, in addition to providing support and guidance throughout the implementation of remote classes.

So, institutions which had previously invested on a more intensive use of technology in their pedagogical activities and educational services were able to respond more rapidly and more efficiently to the sanitary crisis.

These institutions managed to increase their investments on technology, paving the way for necessary improvements and for the development of information systems capable of handling an increased demand.

Those that lacked prior experiences with technology in face-to-face classes or that did not have online customer services tended to improvise in their attempts to adjust to the crisis, and often resorted to the suspension of pedagogical activities for a few months or even for the entire term.

Such evidence revealed the technological dependence of these higher educational institutions and their need to invest in IT within the contexts of e-learning as well as in-person classes – the latter adapted to hybrid formats due to pandemic restrictions.

3.2. Between resistance and adoption: the technological dilemma

The strong necessity to resort to technology in the field of education during the Covid-19 pandemic heightened tensions: on one hand, it intensified resistance to technology; on the other, it endorsed the unescapable need to adopt it. This dilemma can be described as a conflict that opposed those who saw online education as a natural (and necessary) development of human communication and those who criticized it for automating and mechanizing the learning process.

To fully understand this debate, it is worth analyzing the controversies that marked the rise of distance education mediated digital technologies, especially the pioneering contributions of Andrew Feenberg to philosophy of technology in the United States.

In the early 1980, distance education chiefly relied on printed materials sent to students and on one-way communication via radio, television, and satellite transmission. Back then, Internet was not an option for the general public and electronic mail was still mainly restricted to computing companies and universities developing research on the new technology.

The first program for online education was created when computers were still regarded as devices for data organization and mathematical calculation. Nevertheless, the use of computers in the realm of education helped pave the way for their reinvention as means of communication [13].

While narrating his experiment with online education, in [13] the author describes that the invention of e-learning was aimed at providing a human interface for distance education, which basically consisted of mailing printed didactic materials to learners.

Feenberg's pioneering experiment lasted for about ten years and was initially characterized by difficulties posed by technological limitations of the time: students, for example, had to flawlessly carry out an entire page of commands just to log in the system. It was also necessary to create a new software just to guarantee asynchronous interactions, such as the simple exchange of messages.

In [13] the author distinguished his demonstrations from the increased interests in large-scale distance education in the 1990s, when the financing crisis that hit universities in the United States motivated the adoption of digital technologies and the choice of the Internet to offer and organize online courses. These attempts in the field of online education sought automating learning through the use of the Internet and completely eliminated classroom interactions.

In [13] the author remembers that David Noble, the Marxist historian that denounced the loss of skilled workers to industrial automation, had become the main critic of online education, and joined him in several debates on the vices and virtues of the new system.

The consolidation of online education had to overcome at least two major challenges: the first stemmed from humanist criticism, which basically rejected any sort of electronic mediation in education; the second came from technocrats, looking forward to

completely eliminating the roles of teachers from the educational scenario. What humanist criticism and technocrat approaches to education brought forward was a deterministic understanding of e-learning as either a dehumanizing modality or a profitable business opportunity [13].

Contrary to such deterministic understandings of technology in the educational realm, the instrumentalist approach conceives technology as a neutral tool – either good or bad depending on its use.

Based on this instrumentalist perspective, adopting technology may enhance interaction and the learning experiences itself, mainly in the field of e-learning. The use of technology is seen as unavoidable, after all technology represents innovation and the new forms of communication.

Beyond the pessimistic resistance or the optimistic and unrestrained adoption of technology, it is possible to implement a critical approach that recognizes both the possibilities of expanding and enriching the learning experience as well as the risks of undermining and reducing the educational practices through technological mediation.

Raising critical awareness on the possibilities and shortcomings of technology is crucial within an educational approach mediated by technological resources. Technology should not be understood as an end itself and its uses must be molded in accordance with the objectives of each pedagogical project.

On the other hand, technology should not be seen as the mere means through which an educational objective can be accomplished: technology itself is embedded in its own social, cultural and economic aspects. In other words, technological appropriation demands acknowledging and addressing sociocultural tensions between the educational and the technological realms.

It is essential to recognize the vital influence of the digital technology industry and the big corporations on the molding of educational policies and on the craft of higher educational thought. In [14] the authors argue that this industry has kept on pushing higher educational reforms partially under the guise of necessary help in times of crisis.

Therefore, the data and the indicators related to technology and education should always be read from this critical viewpoint.

4. Method and Analysis of the Results

4.1. Procedures and data obtained

So as to investigate the impact and the results of technological mediation in remote teaching, documentary research was carried out based on data collected by one of the largest higher educational groups in Brazil.

The reports and documents analyzed were: Results Reported 1 T20; Results Reported 3T20; Results Reported 1T21; Results Reported 2T21 & 1S21; YDUQS Ecosystem; and Business Units.

This data was obtained through reports and other documents listing information, indicators as well as operational, academic, and financial analyses of the educational group between 2020 and 2021.

The group identified as YDUQS Participações S.A., a technological holding in the field of education, pulling together a board of trustees comprising 66 higher educational institutions, distributed throughout 52 cities in every state of Brazil. All of them are private institutions characterized according to the Brazilian legislation as non-profit organizations.

The group is listed in the Novo Mercado da B3 (the Brazilian Stock Market) as YDUQ3 and, has also gotten its ADRs (American Depositary Receipts) traded in the North American market under the name YDUQY.

In the beginning of the pandemic, in March 2020, the group comprised 319,000 students in face-to-face courses and 314,000 students in distance education [15].

Since 2018, YDUQS has increased its investments in technology. Nearly half of it was devoted to digital transformation and to enabling technologies.

More than 80% of all procedures related to academic routine and other transactions are carried out digitally aided by applications designed specifically for students and teachers. The application programs are available in any application store and have been rated very positively by their users.

In its digital ecosystem, YDUQS has made remarkable progress in its digital transformation throughout the pandemic and offered services to cater for the demands of the academic community aided by an online model that optimizes students' time and experiences. Besides, YDUQS has also implemented a new virtual classroom (SAVA – Sala de Aula Virtual) for students from online as well as in-person courses.

As part of its digital transformation, two months before the eruption of the pandemic, EnsineMe, the edtech of the group, had already started producing digital content based on pioneering formats and methodologies. Just before the pandemic, YDUQS had started developing and implementing the *Aura* teaching model in its face-to-face graduation courses. Owned by YDUQS itself, this model relies on digital platform, active methodologies and digital contents to support teachers and students in the classroom. Just one year after its implementation, in May 2021, students' approval ratings surpassed 90% according to data collected by an internal survey [16].

In the outset of the pandemic, in the first term of 2020, about 300,000 students from in-person courses migrated to remote teaching with digital classes on the Microsoft Teams platform. Before the Covid-19 outburst, most of these students had already been given access to virtual learning environments with the help of the WebAula platform, where available digital contents and a virtual library complemented their face-to-face learning experiences. The same virtual environment also hosted the online disciplines of in-person graduation courses.

With the pandemic and the implementation of remote teaching, in-person courses were split into two virtual environments: the Teams Platform was used for the transmission of synchronous classes, while the WebAula platform granted access to asynchronous digital contents, such as recorded video classes and other resources.

It took only fifteen days between the suspension of in-person classes and the beginning of remote teaching for graduation courses.

After the first term of 2020, with students from in-person classes studying in entirely virtual environments with remote encounters on the Teams platform, indicators signaled 83% of the students had remained within the institution – a percentage that represented a dropout rate below the expected levels. In the second semester of 2020, in-person courses witnessed a 5.9% decrease in the number of new enrollments, while distance education had a 58% increase [17].

In 2021, in the first term, in-person enrollments recovered and the number of students reached 299,000.

In addition to platforms for remote classes and digital content, students from in-person courses could also rely on the BdQ platform (Banco de Questões), a question database so they could get ready for assessments during the pandemic. The platform had been used previously in face-to-face as well as in remote courses as a source of quizzes and exercises. During 2020, over 4.7 million tests and exercises were done via the BdQ platform.

Furthermore, in the first term of 2021, 43% of the alumni from YDUQS face-to-face courses had access to contents produced in 2020 by the group's edtech, EnsineMe. About 600,000 students from YDUQS from in-person and distance course modalities already had the application program offered by the institution in 2021 [18].

In 2021, YDUQS acquired Qconcursos, an edtech focusing on preparing candidates for admission processes, so that it could progress in providing customized digital learning through adaptative evaluations. Thus, the institutions from the YDUQS group were able to count on various technological resources, as Table I describes.

Table 1: Students Enrolled in Face-to-Face Courses and Digital Platforms

	2020 First term	2021 First term
Students enrolled in face-to-face courses	300,000	299,000
Platforms	Teams WebAula BdQ	Teams WebAula SAVA BdQ
Students' application programs	Minha Estácio	Minha Estácio Meu Ibmec
Teachers' application programs	Estácio docente	Estácio docente Wyden docente Ibmec docente
Edtechs' internal Hub	EnsineMe	EnsineMe QConcursos

	2020 First term	2021 First term
Pedagogical activities in face-to-face courses	Remote classes	Remote classes. In-person practical classes.

Students' evaluation of educational services throughout the pandemic was, indeed, very positive.

Data from an internal survey – carried out by the institution, updated on April 30th 2021, and published in its financial report – reveals a 17-percentage point improvement in terms of the Net Promoter Score (NPS). When compared to results obtained between 2020 and 2021, the NPS presented a record-breaking 21 percentage point increase.

4.2. Analysis of the results

This data reveals that the educational group targeted by this research quickly responded to the challenge of resuming pedagogical activities of in-person courses due to a favorable internal context.

A greater investment in digital transformation had already been set in motion two years before the Covid-19 pandemic, propelling the process of partial digitalization in face-to-face courses, by offering some online and hybrid disciplines.

Such rapid response to the sanitary crisis is also connected to the prior existence of separate application programs for teachers and students. These applications went through several improvements during the pandemic, which helped the institution resume its typical academic routines.

For some students enrolled in face-to-face, communication with the institution, the supervision of the academic programme, and the possibility of studying while connected to mobile devices granted more flexibility to their learning experiences – an advantage priorly restricted to distance education.

For some teachers, submitting information such as students' grades, attendance records, and the content covered within each class became easier once digitalized. Nevertheless, they had to overcome the challenge of transforming remote teaching into a meaningful virtual encounter, not a depleted replica of a classroom.

In the case of YDUQS, the fact teachers from in-person courses could resort to previously acquired knowledge and experiences with digital resources and online environments. Furthermore, teachers' continuing education helped downplay the need to improvise in the transposition of in-person to online classes

Also, the implementation of a new teaching model (the *Aura* model) in face-to-face courses coincided with the beginning of the pandemic, which helped make the replacement of in-person classes smoother.

The support offered by internal EdTechs provided the institution with digital content produced in the pandemic context, furnishing teachers with the tools and resources they needed to assess students' performances in virtual environments.

Most technological solutions were created and managed internally, which explains the development of technological responses that suited the institutions' pedagogical needs and criteria.

The success of this response to the sanitary crisis is clearly reflected in the internal surveys promoted by YDUQS with the students and in the high levels of retention.

The increase of the satisfaction level of students enrolled in face-to-face courses indicates that the institution adopted adequate technological, didactic and pedagogical solutions.

However, the rapid migration from in-person courses to virtual environments in addition to retention indicators and the high levels of students' satisfaction relates to educational management. But the data presented in this report does not deal, for example, with learning management nor with students' academic performance over the course of the pandemic.

Also, this analysis does not cover the effects of large-scale digitalized learning on the relationships between teachers and students, nor amongst students themselves. These other aspects are extremely relevant; after all, the commercial design of educational systems and softwares has increasingly modelled teaching and learning experiences within universities [14]. Therefore, regardless of teachers' pedagogical intentions, softwares used in the educational process can either limit or expand what can be done within the classroom.

5. Conclusion

Based on the theoretical framework presented and on data regarding the implementation of remote teaching in the institutions of the YDUQS group, it is possible to infer that technology operates in both ways, curtailing or favoring communication, interaction and relationships in educational contexts.

A sound technological infrastructure and the use of different digital resources in the field of education before the pandemic created favorable conditions for a more rapid and less improvised response in the process of transposing conventional face-to-face classes to virtual environments.

Technological mediation by itself does not guarantee neither explains the success of the learning experience, since other aspects also play an important role in the educational process.

Despite being both necessary and relevant, this data is not enough to account for all the different aspects of technological mediation of the pedagogical processes during the Covid-19 pandemic in the higher educational institutions of the YDUQS group.

It is necessary to provide further details for this research so that the analysis can go beyond the macro level and look into variables regarding the implementation of remote learning from a micro perspective.

The analysis of data on academic management must be complemented by specific indicators to account for educational challenges of learning through technological mediation during the pandemic, which is certainly a necessary possibility for further investigation on this theme.

Conflict of Interest

The author declares no conflict of interest.

References

[1] L. C. D. Saldanha, "Technological Mediation in Remote Teaching During the Covid-19 Pandemic," 17th Iberian Conference on Information Systems and Technologies (CISTI), 1-7, 2022, doi: 10.23919/CISTI54924.2022.9820052.

[2] C. Hodges, S. Moore, B. Loockee, T. Trust, A. Bond, "The difference between emergency remote teaching and online learning," Educause Review, 27, 2020, Available: https://er.educause.edu/articles/2020/3/the-difference-between-emergency-remote-teaching-and-online-learning.

[3] E. Davis, "What is remote teaching," Top Hat, Glossary, 2020.

[4] J. Baggaley, "Educational distancing," Distance Education, **41**(4), 582-588, 2020, doi: 10.1080/01587919.2020.1821609.

[5] A. Behar, "O ensino remoto emergencial e a educação a distância," Coronavírus, UFRGS, 2020, Available: https://www.ufrgs.br/coronavirus/base/artigo-o-ensino-remoto-emergencial-e-a-educacao-a-distancia/#:~:text=O%20Ensino%20Remoto%20Emergencial%20e%20a%20Educa%C3%A7%C3%A3o%20a%20Dist%C3%A2ncia%20n%C3%A3o,refere%20a%20um%20distanciamento%20geogr%C3%A1fico.

[6] B. Veloso, D. Mill, "Distance Education and Remote Teaching: opposition by the vertex," SciELO Print, 2022, doi: 10.1590/SciELOPreprints.3506.

[7] V. Dusek, Philosophy of Technology: An Introduccion, Blackwell Publishing, 2006.

[8] A. Watters, "Teaching Machines: The History of Peronalized Learning Cambridge, The MIT Press, 2021.

[9] G. Canole, "Bridging the gap between policy and practice: A framework for technological intervention," Journal of e-Learning and Knowledge Society, **6**(1), 13-27, 2010, doi: 10.20368/1971-8829/384.

[10] S. Freitas, G. Canole, "Leaners experiences: How pervasive and integrative tolos influence expectations of study," In R. Sharpe, H, Beetham, S. Freitas (Eds.). Rethinking learning for a digital age: How learners are shaping their own experiences, Routledge, 2010.

[11] L. C. D. Saldanha, "The Discourse of Remote Teaching During the COVID-19 Pandemic," Journal of Higher Education Theory and Practice, [S. l.], **21**(4), 53-63, 2021, doi: 10.33423/jhetp.v21i4.4207.

[12] J. Mattar, A. Loureiro, E. Rodrigues, "Educação online em tempos de pandemia: desafios e oportunidades para professores e alunos," Interacções, **16**(55), 1-5, 2020, doi: 10.25755/int.22001.

[13] A. Feenberg, Tecnologia, modernidade e democracia, MIT Portugal, Inovatec, 2015.

[14] L. Castañeda, N. Selwyn, Reiniciando la universidad: buscando un modelo de universidad en tiempos digitales. Editorial UOC, 2019.

[15] YDUQS, "Divulgação de resultados 1T20," YDUQS Participações S.A., 2020.

[16] YDUQS, "Unidades de negócio," YDUQS Participações S.A., 2022.

[17] YDQUS, "Divulgação de resultados 3T20," YDUQS Participações S.A, 2020.

[18] YDUQS, "Divulgação de resultados 2T21 & 1S21," YDUQS Participações S.A, 2021.

ASTES

Estimating Subjective Appetite based on Cerebral Blood Flow

Lai Kecheng[*], He Qikun, Hu Ning, Fujinami Tsutomu

Creative Society Design Research Area, Japan Advanced Institute of Science and Technology, Nomi City, Japan

A R T I C L E I N F O	A B S T R A C T
	This study aims to develop and validate a biological food preference task that simultaneously evaluates biological responses to visual stimuli of various food states and subjective evaluations of foods and to examine how these biological responses are related to food preference behavior. We recruited seventeen healthy male and female subjects to observe changes in cerebral blood flow related to salivation and the prefrontal cortex region while performing a food preference task related to visual stimuli of various food states. We also examined the relationship between these changes and the subjects' subjective evaluations. The results showed that subjective evaluations of the various states of visual stimuli differed from subjective evaluations of the different food states. Furthermore, comparing the hemodynamic response function of cerebral blood flow to each visual stimulus, we observed a trend of activation of brain activity in the prefrontal and parotid regions during task execution. In addition, correlations were calculated between the subject's subjective evaluation and cerebral blood flow in the prefrontal and parotid regions and between cerebral blood flow in the prefrontal and parotid regions, and significant differences were observed. Our findings demonstrate the potential of combining the evaluation of food in different states with cerebral blood flow indices in biological responses to visual cues of food.

1. Introduction

This paper is an extension of a work originally presented in ICMHI 2021 [1], which used visual stimuli of foods to examine the relationship between salivary responses and appetite. In this study, we developed a food preference task using visual stimuli of various food states rather than visual stimuli of food. We also measured the biological responses with cerebral blood flow in both parotid and prefrontal regions and examined its relationship to the subjects' evaluation of appetite.

The visual appearance of foods may influence the choice of foods. The association between nutrient and energy content of food, as well as pleasant or unpleasant sensations toward food, are paired with different sensory features. Among the various sensory cues, the visual stimulation of food is an important regulator of appetite. When subjects were presented with visual stimuli, a significant difference was found in blood flow in the parotid region between the low-rating and the high-rating groups concerning subjects' appetite [1]. People can predict its characteristics through photos and videos of food, and this action also influences people's eating

behavior. The chemical senses, sight, smell, and taste, play a key role in the sensory effects on appetite, food choice, and intake [2].

Saliva is recognized to have a variety of functions, and it affects oral defense as well as oral and systemic health. Saliva secretion depends on a complex set of factors, including food-related cues, health status, gender, etc.[3,4]. Salivary glands are under the dual control of sympathetic and parasympathetic nerves, and different glands have different salivary characteristics. Sympathetic nervous system activity causes the parotid gland to secrete saliva rich in serum and α-amylase while the parasympathetic nervous system activity causes the submandibular and sublingual glands to produce viscoelastic, mucin-rich saliva [5–7]. Each component of saliva is regulated to perform a particular function. Sensory food cues, such as appearance, fragrance, and taste, may induce a rapid secretion of saliva in the oral cavity, which is called the cephalic phase salivary response [8–11]. Cephalic phase salivary response includes physiological responses to food-related cues such as the thought, fragrance, appearance, and taste of food [12]. Many studies have shown that sensory exposure to various foods increases saliva production.

[*]Corresponding Author: Lai Kecheng, laikecheng199222@gmail.com

Food choice and intake processes consist of various cognitive, sensory, and metabolic components, such as sensory pleasure, metabolic hunger, and knowledge about food[13]. In addition, these non-homeostatic aspects are an important area of research, as cognitive, sensory, and emotional processes often take precedence over food choice decisions in the current food-abundant obesogenic environment [14]. Traditional measures of appetite often use subjective assessment methods that rely on self-report, such as questionnaires or interviews. These subjective assessment methods require cognitive information processing and reasoning by the subject, influenced by factors such as social desirability [13]. However, implicit motivation is difficult to measure, as humans make various daily food decisions. In addition, people's choices and actions regarding food and food cues have characteristics such as motivational processes that we are unaware of, cannot articulate, or do not want to do [13,15]. In recent years, technological advances in biometric systems that measure psychophysiological parameters have made it possible to examine subjective rates of food and the implicit processes involved in food intake [16]. Biometrics, a non-invasive behavioral and physiological measure that may reflect motivation and emotional responses to food, has features that can identify individual characteristics based on biological and physiological properties and is commonly used in food science and consumer science [17].

However, it is still unclear why people respond to foods this way and what psychophysiological processes are possible before and during behavioral responses to food cues. Furthermore, as far as previous studies are concerned, since the number of studies on biometrics is limited, the results are inconsistent, which makes it difficult to compare study results. On the other hand, we believe that biometric measures need to be combined with measures of appetite, as it is necessary to investigate individual motivations and responses behind food choices and intake to promote healthier eating habits.

Therefore, this study aims to develop and test a biological food preference task that simultaneously rates biological responses to visual stimuli of various food states, and subjective evaluations of food. The study then examines how these biological responses are related to food preference behavior. Specifically, differences in biological responses (cerebral blood flow in the prefrontal cortex, salivation) to visual food stimuli under different states of food are rated in a biometric food preference task. Specifically, a database and validation task will be developed using visual stimuli of different states of food. Next, the differences between biological responses to visual stimuli (cerebral blood flow in the prefrontal cortex and parotid region) and the evaluation of foods in response to visual stimuli of foods will be evaluated in a biometric food preference task. Finally, we examine the relationship between biological responses and food preferences.

2. Methodology

2.1. Participants

Seventeen healthy students (5 females, 12 males, aged 25-30) were recruited at Japan Advanced Institute of Science and Technology. Subjects were randomly selected from graduate students who agreed to take part in the study. Before the experiment, all subjects were given a screening session to determine eligibility. A questionnaire survey was conducted on the

subjects' age, gender, and medication status. As a result, all subjects had no evidence of systemic or oral diseases such as periodontal disease, and all were nonsmokers. In addition, participants were selected to be subject if their body mass index (BMI) is within the range of 18.5-25kg/m2 because being overweight or obese tends to impact the secretion of saliva as they secrete more saliva due to food cues[18]. Subjects were excluded if they had dental pathologies or issues chewing and swallowing due to the muscle movement, which could possibly affect their saliva secretion[19,20]. The subjects who volunteered were told they would be watching some photos and videos about ice cream and completing some rating tasks for the experiment. The experimental investigation period was from March 15, 2022 to March 23, 2022. The experiment was conducted on those who had consented to the study after the purpose of the study was explained. On the day of the experiment, participants were instructed not to eat for one hour before the experiment. Drinking water was allowed, but drinks containing sugar were not. Each participant was paid 3,000 yen as an honorarium for his participation in the experiment.

2.2. Data Collection
2.2.1. Experimental Device

In this experiment, two types of experimental devices were used. One was the HOT-2000 device, which can measure cerebral blood flow in the prefrontal cortex, associated with cognitive function, and the other was the WOT-S20 device, which can measure cerebral blood flow in the parotid gland, associated with saliva secretion.
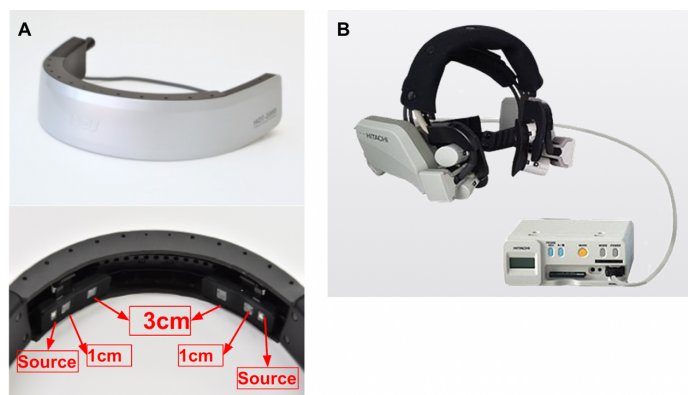
Figure 1: Experimental Devices. A: HOT-2000 device; B: WOT-S20 device.

We measured cerebral blood flow using the HOT-2000. It is a portable brain activity measurement device that can be used in everyday scenarios to simultaneously measure cerebral blood flow change, pulse and head acceleration in real-time [21]. The device used in this study has two Source-Detector (SD) optode pairs. Each optode pair has two optical detectors located at a distance of 1 cm and 3 cm from the light source. The device emits a wavelength of infrared light (about 800 nm) that is easily absorbed by hemoglobin in the blood and the detected light was sampled at a frequency of 10 Hz. The measurement principle is that the infrared light irradiated from the scalp diffuses, and if the area of the brain that is in the path of the light is activated, the amount of light that returns to the detector decreases due to increased blood flow and increased light absorption. The intensity change of the detected light was converted to total-hemoglobin (HbT) on the optical path

of concentration using the modified Beer-Lambert law[22]. The 1cm-SD optode pair is the short separation channel, which provides auxiliary signals from shallow tissues such as the scalp and skull, and we use it to measure what is happening in the scalp and separate brain signals from non-neuronal physiological signals. In contrast, the 3cm-SD optode pair is the long separation channel that reaches the cerebral cortex and reflects blood flow changes associated with neural activity, usually measuring the brain.

We used WOT-S20, a near-infrared optical measuring device for the lateral face (developed by NeU Corporation), to measure cerebral blood flow changes in response to saliva secretion. The WOT-S20 device consists of three components: a headset equipped with a near-infrared light receiving/emitting sensor (one channel each for left and right), a portable control box for wireless data transmission and backup functions, and a measurement controller for real-time display and storage of measurement settings and results [23]. Among them, the source emits infrared light at wavelengths of 705[nm] and 830[nm] to detect hemoglobin changes (Oxy-hemoglobin (HbO), Deoxy-hemoglobin (HbR), Total-hemoglobin (HbT)) in the blood and to capture data at a frequency of 5 Hz. The basic principle of the measurement is that an increase in saliva secretion in the parotid region promotes an increase in blood volume, which decreases the amount of light transmission.

2.2.2. Experimental Materials

For the experimental material, we chose ice cream, a food commonly found in Japanese culture. Four of the most popular ice cream flavors were selected from various commercially available ice cream products and used as experimental materials. The four ice cream flavors selected were matcha, chocolate, strawberry, and vanilla. The ice cream melting process was documented on video by placing each ice cream on a wooden plate and filming the process from hard to wholly melted. Then, we used programming to calculate the area of each state of ice cream during the process from hard to melt. Finally, the ice cream was divided into four states based on the calculated area. In the first stage, only the middle of the ice cream has the characteristic of beginning to melt. In the second stage, the ice cream melts rapidly. In the third stage, the ice cream is still melting, but the melting rate of the ice cream is easing, and finally, in the fourth stage, the general area has not changed much. The fourth stage was a state in which only the middle of the ice cream was melting, although the general area did not change much.
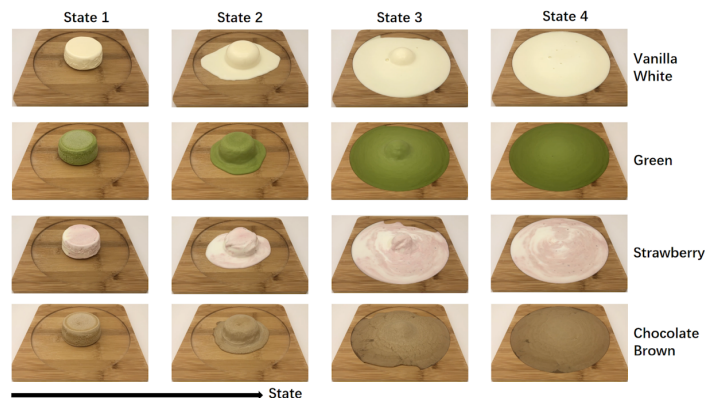
Figure 2: Experimental Material

Then, one representative photo was extracted from each video, and the 16 photos and 16 videos constituted the experimental material database for this experiment.

2.2.3. Experimental Environment

The experimental environment is shown in Figure 3. Figure C on the left shows the subject using the HOT-2000 device and doing the experimental task. Figure D on the right shows the subject wearing the WOT-S20 device and participating in the experiment.
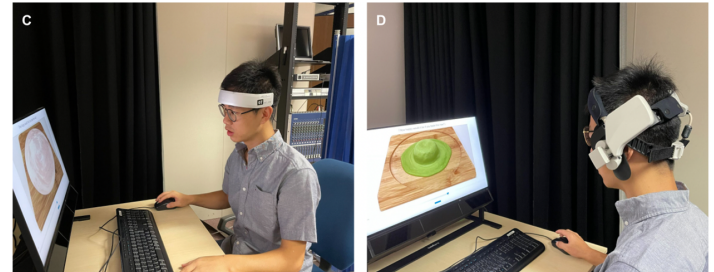
Figure 3: Experimental Environment. C: Experimenting with the HOT-2000 device, D: Experimenting with the WOT-S20 device.

2.2.4. The Flow of the Experiment

According to previous research, the Leeds Food Preference Questionnaire [24]was developed to examine the "liking" and "wanting" components of subjective evaluations of food, which has been reported as a valid method for measuring explicit and implicit aspects of appetite. Moreover, the Leeds Food Preference Questionnaire is a computer task with features that collect ratings, choices, and reaction times to visual food stimuli from different food categories [25].

The task of this study was designed to collect biological responses, including cerebral blood flow in the prefrontal and parotid regions, to food images and video stimuli based on the Leeds Food Preference Questionnaire procedure. A web application was built using JavaScript and HTML for stimulus presentation, and image and video stimuli were presented on the browser. As shown in Figure 2, the visual stimuli of ice cream displayed in the images and video vary in four different states.
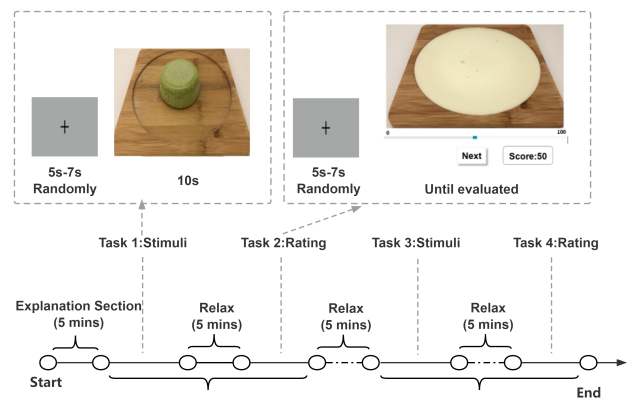
Figure 4: Experimental Procedure

The experimental procedure is illustrated in Figure 4. Participants were instructed to eat one hour before the experiment, and upon arrival at the laboratory, only water was allowed while

the experiment was in progress. After explaining the criteria for participation in the experiment, the purpose, and content of the experiment, and confirming the subjects' eligibility, a preliminary questionnaire was conducted regarding the subjects' age, BMI, frequency of ice cream consumption, and preferences.

As shown in Figure 4, the task is consisted of four parts (Task 1 to Task 4). Task 1 involves passively viewing 16 ice cream pictures on two separate occasions, and Task 2 requires the participants to rate the stimuli presented in Task 1. The specific procedure was that in Task 1, pictures of ice cream were displayed. Then, subjects were allowed to look at them for ten seconds, followed by Task 2, in which subjects were asked to rate them on a scale from 0 to 100 (0 means the lowest degree and 100 means the highest degree of liking and wanting). Then, a new image was presented in Task 1 for ten seconds, and the subject was asked to rate the image presented in Task 1 in Task 2. Thus, sixteen ice cream images were displayed randomly, and subjects were asked to rate them. The subjects were asked to rate each ice cream image using two questions when rating the images. First, they are rated on one food preference component ("How happy would it be if you taste this now?") and then on the other ("How much would you want some of this now?"), in random order. Tasks 3 and 4 followed the same procedure as Tasks 1 and 2. Task 3 consisted of passively viewing 16 ice-cream videos on two separate occasions, and Task 4 evaluated the stimuli of the videos presented in Task 3.

During passive viewing of the images or videos, subjects were presented with the ice cream image or videos for 10 seconds, sufficient to capture the salivary response. After passively viewing each image or video, subjects were asked to rate their feel of "liking" ("How happy would you be if you ate this food now?") or "wanting" ("How much would you like this food now?") explicitly using a 100-point visual analog scale (VAS). In total, 32 passive viewings and ratings were conducted, 16 of which were explicit "liking" ratings and 16 of which were explicit "wanting" ratings. Before each passive viewing, participants were presented with a fixation target[26] with a randomly varying exposure time (5s-7s) to ensure that their gaze was directed to the center of the screen and that participants could not accurately predict the onset of the next stimulus. Before rating, subjects were presented with a fixation target to ensure they were looking at the center of the screen.

2.2.5. fNIRS Data Collection

In this study, we focused on the prefrontal and parotid brain regions. During the experiment, data were collected by measuring each subject's cerebral blood flow data in each task. When measuring cerebral blood flow in the prefrontal cortex, subjects' resting cerebral blood flow was measured for 5 minutes before the experiment. When measuring the cerebral blood flow for resting, subjects were instructed to sit on a chair, close their eyes, and relaxed as much as possible. The cerebral blood flow data of resting for five minutes were used as training data for fNIRS data processing.

2.3. Data Analysis
2.3.1. fNIRS Data Processing (saliva)

The raw data of the cerebral blood flow on saliva includes HbO, HbR, and HbT, where HbT is the sum of HbO and HbR. For the processing of fNIRS data in the parotid region, we first convert the data output from the machine to Shared Near Infrared Spectroscopy Format (SNIRF), developed by the Society for functional Near Infrared Spectroscopy [27]. Then, a general linear model (GLM)[28] was employed for processing the fNIRS data in the parotid region using the open-source HOMER3 toolbox[29] in MATLAB (Mathworks Inc.). The procedure was as follows: Firstly, we used the prune channel function to prune bad or low SNR channels from the measurement list. Next, the raw light intensity signal was converted to optical density. Bandpass filtering was applied to the fNIRS data in the 0-0.5 Hz range. The optical density was then converted to total hemoglobin (HbT) concentration with a default partial path length factor. Finally, a general linear model (GLM) was used to remove whole-body artifacts. The hemodynamic response function (HRF) was estimated using the mean of the long separation channels. A continuous Gaussian function (stdev=1.0, step=1.0) was calculated from rest to speech.

2.3.2. fNIRS Data Processing (PFC)

For the processing of fNIRS data in the prefrontal region, we converted the data to the Shared Near Infrared Spectroscopy Format (SNIRF). Then, the general linear model with temporally embedded canonical correlation analysis (GLM with tCCA)[30] was conducted using the open-source HOMER3 toolbox in MATLAB (Mathworks Inc.). Firstly, the prune channel's function was used to prune bad or low SNR channels from the measurement list. Then we converted the raw optical intensity signal to an optical density. Subsequently, both fNIRS and auxiliary data were conducted the bandpass filtering within 0-0.5 Hz. Then, we converted the optical density to total-hemoglobin (HbT) concentration with default partial path-length factor. Now, to reduce nuisance signals in fNIRS and create optimal regressors, the temporally embedded Canonical Correlation Analysis function was conducted. Finally, a general linear model (GLM) was used to remove the systemic artifacts. The hemodynamic response function (HRF) was estimated using the average of the long separation channels. It was calculated with the consecutive sequence of Gaussian functions (stdev=1.0, step=1.0) from rest to the speech period.

2.3.3. Statistics Analysis

Subjective rating scores for each ice cream were collected during the subject's experiment, and the mean value of each rating score was calculated. After processing the cerebral blood flow data, the mean value and the change of cerebral blood flow signal for each channel were calculated. After confirming the normality of the data, correlations were calculated between subjects' subjective evaluation data and objective fNIRS data.

3. Results

3.1. Results of Ice cream Evaluation

The evaluation results for ice cream are shown in Table1. In addition, photos and videos of ice cream were categorized by state, and the mean value of each rating result was calculated.

Comparing ice cream by state, when subjects were asked how happy they would be if they tasted the ice cream at that moment in response to a photo of ice cream, the mean rating of ice cream in

each state was 56.59 for State 1 and 15.04 for State 2, 9.52 for State 3, and 9.36 for State 4. When subjects were asked how much they would like to eat the ice cream in the picture, the mean rating of ice cream in each state was 63.59 for state 1 and 22.53 for state 2, 8.77 for state 3, and 5.43 for state 4, on the other hand, when subjects were asked how happy they would be if they ate the ice cream in response to a video of ice cream, the mean rating of ice cream in each state was 52.59 for state 1 and 28.22 for state 2, 9.77 for state 3, and 5.89 for state 4, when subjects were asked how much would you like this food now in response to a video of ice cream, the mean rating of ice cream in each state was 56.41 for state 1 and 26.84 for state 2, 8.23 for state 3, and 1.89 for state 4.

Table 1: Rating results for ice cream divided by state□

	State 1			
	State 1	**State 2**	**State 3**	**State 4**
Liking-Photo	56.59	15.04	9.52	9.36
Wanting-Photo	63.59	22.53	8.77	5.43
Liking-Video	52.59	28.22	9.77	5.89
Wanting-Video	56.41	26.84	8.23	1.89

Note: The number in the table is the mean value of the evaluation

3.2. Results of Hemodynamic response function (HRF)

After processing the fNIRS data, the hemodynamic responses of cerebral blood flow in the prefrontal and parotid regions were investigated during the visual stimulation and evaluation of the ice cream. There is a positive correlation between the hemoglobin signal of cerebral blood flow in the parotid region and salivary secretion, meaning that increased cerebral blood flow activity tends to increase saliva secretion. The results of activation in prefrontal and parotid regions by visual stimulation of ice cream in each state are shown in Figure 5 to Figure 7. However, little activation trend was observed in cerebral blood flow in the prefrontal and parotid regions of the subjects to the stimulation of ice cream in State 3, which is not shown in the results.

3.2.1. Results of Hemodynamic response function (HRF) in the parotid region

Figure 5 and Figure 6 shows the results of the brain activation trend observed in the parotid region during the visual stimulation and rating of ice cream. The horizontal axis shows the time course, and the vertical axis shows the average change in cerebral blood flow. The purple dotted line shows the group-averaged mean cerebral blood flow change, and the error bars show the standard error of the group-level mean. In addition, cerebral blood flow activity from -3s to 5s was observed. Time 0 on the horizontal axis represents the stimulation or evaluation start time. Therefore, the mean value of 3s before the start time of stimulation or evaluation was used to estimate the change in cerebral blood flow during 5s from the start time of stimulation or evaluation.

Figure 5 shows the trend of the hemodynamic response function to the stimulation of photos for each ice cream state. According to the results of the hemodynamic response function, when subjects were asked how happy they would be if they tasted

the food in response to a photo of ice cream, we observed a tendency for a stimulation-induced of increase in cerebral blood flow in the left parotid region when subjects were evaluating photos of ice cream in state 1 and state 4, and when they were receiving stimulation of the photo in state 4. Moreover, when subjects were asked how much they would like to eat this food in response to a photo of ice cream, we observed a tendency for cerebral blood flow due to stimulation to increase in the right parotid region when they were receiving stimulation of the ice cream photo in state 1. Furthermore, when they were receiving stimulation of the photo in state 4, an increase of the cerebral blood flow was observed in the left parotid region during the stimulation.
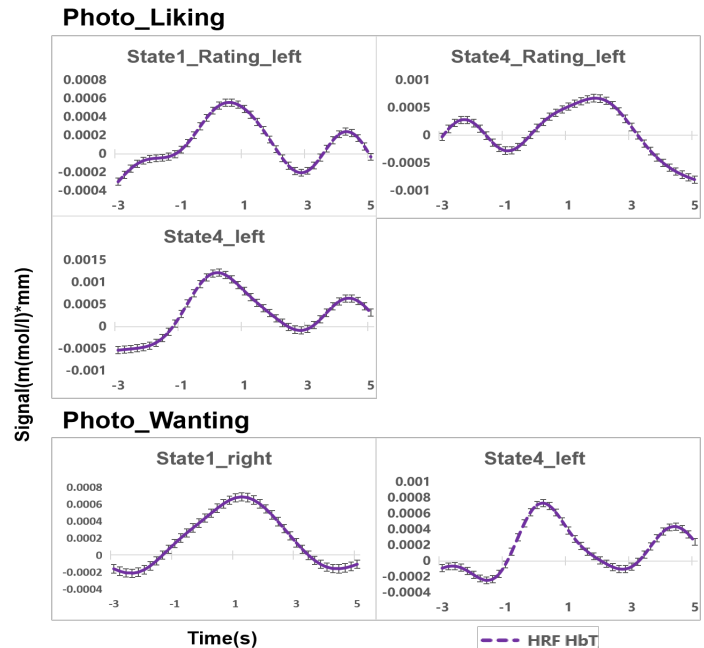
Figure 5: The trend of hemodynamic response function time courses of parotid region to photo stimuli in different states
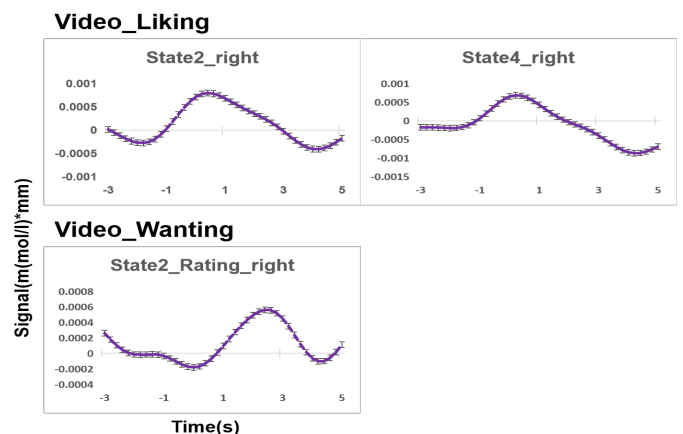
Figure 6: The trend of hemodynamic response function time courses of parotid region to video stimuli in different states.

Figure 6 shows the trend of the hemodynamic response function to the stimulation of videos for each ice cream state. When subjects were asked how happy they would be if they tasted this in response to a video of ice cream, we observed a tendency for a stimulation-induced of increase in cerebral blood flow in the right parotid

region when subjects were evaluating videos of ice cream in state 2 and state 4. Furthermore, when subjects were asked how much they would like to eat this food in response to a video of ice cream, an increase of cerebral blood flow was observed in the right parotid region when subjects were rating videos of ice cream in state 2.

3.2.2 Results of Hemodynamic response function (HRF) in the prefrontal region

Figure 7 shows the results of the observed brain activation trend in the prefrontal cortex during the visual stimulation of ice cream and rating. The horizontal axis shows the time course, and the vertical axis shows the average change in cerebral blood flow. The red solid line shows the group-averaged mean cerebral blood flow change, and the error bars show the standard error of the group-level mean. In addition, cerebral blood flow activity from -2s to 5s was observed. Time 0 on the horizontal axis represents the stimulation or evaluation start time. Therefore, the mean value of 2s before the start time of stimulation or evaluation was used to estimate the change in cerebral blood flow during 5s from the start time of stimulation or evaluation.

According to the results of the hemodynamic response function, when subjects were asked how much they would like to eat this food in response to a photo of ice cream, we observed a tendency for cerebral blood flow due to stimulation to increase in the left prefrontal region when they were receiving stimulation of the ice cream photo in state 2 and state 4. Moreover, when subjects were asked how happy they would be if they tasted the food in response to a video of ice cream, a tendency for cerebral blood flow due to stimulation to increase in the right prefrontal region when they were receiving stimulation of the ice cream photo in state 2. Furthermore, when subjects were asked how much they would like to eat this food in response to a video of ice cream, a tendency for cerebral blood flow to increase was observed in the left prefrontal region when subjects were rating videos of ice cream in state 1.
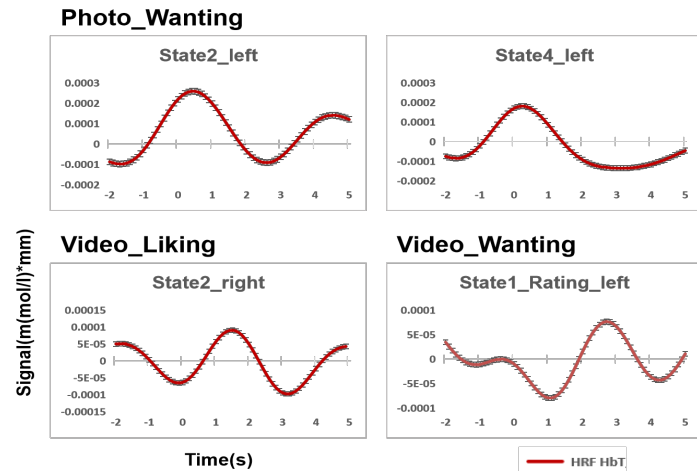
Figure 7: The trend of hemodynamic response function time courses of prefrontal region to photo and video stimuli in different states.

3.3. Results of Correlation

After processing the fNIRS data, the mean value of concentrations of HbR, HbO, and HbT were calculated. Then, the mean values were used to analyze the correlations, and the results are shown in Table2 to Table4. Since there is a positive correlation

between the hemoglobin signal in cerebral blood flow in the parotid region and saliva secretion, a high level of hemoglobin signal in cerebral blood flow in the parotid region means a high level of saliva secretion.

Table 2: Correlation coefficients between subjects' ratings and the signal mean of cerebral

		HbR		HbO		HbT	
		left	right	left	right	left	right
Liking -Photo	stimuli	0.510	0.382	0.821[**]	0.553	0.726[**]	-0.520
	evaluate	0.636	-0.733[**]	-0.601	-0.868[**]	0.177	-0.942[**]
Wanting -Photo	stimuli	-0.878[**]	0.271	0.378	0.991[**]	-0.183	0.571
	evaluate	-0.831[**]	-0.952[**]	-0.350	-0.171	0.820[**]	-0.311
Liking -Video	stimuli	0.957[**]	0.573	0.453	0.070	0.228	-0.598
	evaluate	0.430	0.537	0.778[**]	0.269	0.419	-0.464
Wanting -Video	stimuli	0.076	-0.241	-0.178	-0.349	0.484	-0.174
	evaluate	0.668	0.420	-0.76[**]	0.597	-0.479	0.313

note: **: $p<0.01$
The numbers in the table refer to correlation coefficients.

Table 2 shows the correlation coefficients between subjects' ratings and the change in the signal mean of cerebral blood flow related to saliva were determined separately for each ice cream state. When subjects were asked how happy it would be if they tasted this in response to a photo of ice cream, a strong positive correlation was found between subjects' ratings and HbO ($r = 0.821$) and HbT ($r = 0.726$) on the left side during stimulation. Therefore, it can be said that the mean values of HbO and HbT on the left side tend to increase as the subject's evaluation of the ice cream increases. On the other hand, there was a strong negative correlation between the subject's ratings and the HbR ($r = -0.733$), HbO ($r = -0.868$), and HbT ($r = -0.942$) on the subject's right side while rating the ice cream photos. Thus, it can be concluded that the mean values of HbR, HbO, and HbT on the right side tend to become smaller as the subject's evaluation of the ice cream increases.

When subjects were asked how much they would like this food in response to a photo of ice cream, there was a strong negative correlation between the subject's ratings and HbR ($r = -0.878$) on the left side and a strong positive correlation with HbO ($r = 0.991$) on the right side during stimulation. Thus, it can be concluded that the mean value of HbR on the left side tends to become smaller and the mean value of HbO on the right side tends to become larger as the subject's evaluation of the ice cream increases. On the other hand, when subjects rated the stimulus pictures, there was a strong negative correlation between HbR on the left ($r = -0.831$) and right ($r = -0.952$) sides and a strong positive correlation between HbT ($r = 0.820$) on the left side. Therefore, it can be concluded that the mean values of HbR on the left and right sides become smaller as the subject's evaluation of the ice cream increases, but the mean value of HbT on the left side tends to increase.

When subjects were asked how happy they would be if they tasted this in response to a video of ice cream, a strong positive correlation was found between subjects' ratings and HbR ($r = 0.957$) on the left side during stimulation. Therefore, it can be concluded that the mean values of HbR on the left side tend to increase as the subject's evaluation of the ice cream increases. On

the other hand, there was a strong positive correlation between the subject's ratings and the HbO (r = 0.778) on the subject's left side while rating the ice cream videos. Thus, it can be concluded that the mean values of HbO on the left side tend to become larger as the subject's evaluation of the ice cream increases.

When subjects were asked how much they would like if they could eat it in response to a video of ice cream, no correlation was found between subjects' ratings and subjects' cerebral blood flow during stimulation. However, there was a strong negative correlation between the subject's ratings and the HbO (r = -0.760) on the subject's left side while rating the ice cream videos. Thus, it can be concluded that the mean values of HbO on the left side tend to become smaller as the subject's evaluation of the ice cream increases.

Table 3: Correlation between subjects' ratings and the signal mean of cerebral blood flow in the prefrontal region by state

	Photo_Liking_HbT		Photo_Wanting_HbT		Video_Liking_HbT		Video_Wanting_HbT	
	left	right	left	right	left	right	left	right
stimuli	-0.236	-0.171	-0.137	0.036	0.977**	-0.227	0.118	0.221
evaluate	0.895**	-0.252	-0.888**	-0.193	0.515	0.729**	0.134	0.601

note: **: p<0.01
The numbers in the table refer to correlation coefficients.

Table3 shows the correlation coefficients between subjects' ratings and the change in the signal mean of cerebral blood flow related to cognitive function were determined separately for each ice cream state. When subjects were asked how happy they would be if they tasted this at that moment in response to a photo or video of ice cream, a strong positive correlation was found between subjects' ratings and HbT (r = 0.895) on the left side of the prefrontal cortex while rating the ice cream photos. Moreover, a strong positive correlation was found between subjects' ratings and HbT (r = 0.977) on the left side of the prefrontal cortex during stimulation, and a strong positive correlation was found between subjects' ratings and HbT (r = 0.729) on the right side of the prefrontal cortex while rating the ice cream videos. Thus, it can be said that the higher the subject's evaluation, the larger the mean values of HbT on the left side of the prefrontal cortex tended to be while rating the ice cream photos; the higher the subject's evaluation, the larger the mean values of HbT on the right side of the prefrontal cortex tended to be while rating the ice cream videos, and the larger the mean values of HbT on the left side of the prefrontal cortex tended to be during stimulation of the ice cream videos.

On the other hand, when subjects were asked how much they would like to eat this food in response to a video of ice cream, a strong negative correlation was found between subjects' ratings and HbT (r = -0.888) on the left side of the prefrontal cortex while rating the ice cream photos. Therefore, it can be concluded that the higher the subject's evaluation, the smaller the mean values of HbT on the left side of the prefrontal cortex tended to be while rating the ice cream photos.

Table 4 shows the correlation coefficients between the change in the signal mean of cerebral blood flow related to saliva and the change in the signal mean of cerebral blood flow related to cognitive function were determined separately for each ice cream

state. When subjects were asked how happy they would be if they tasted the food in response to a video of ice cream, a strong positive correlation (r = 0.843) was found between HbT on the right side of the prefrontal cortex and HbT on the right side of the parotid region during stimulation. Thus, it can be concluded that the mean values of HbT on the right side of the parotid region become larger as the the mean values of HbT on the right side of the prefrontal cortex increases.

Table 4: The correlation coefficients of the signal mean change of cerebral blood flow between the parotid and prefrontal regions (By state)

	Photo_Liking_HbT		Photo_Wanting_HbT		Video_Liking_HbT		Video_Wanting_HbT	
	left	right	left	right	left	right	left	right
stimuli	0.110	-0.474	0.541	-0.227	0.409	0.843**	0.681	-0.986**
evaluate	0.450	-0.245	-0.742**	-0.857**	0.569	-0.077	0.323	-0.123

note: **: p<0.01 The numbers in the table refer to correlation coefficients.

On the other hand, when subjects were asked how much they would like this food at that moment in response to a photo of ice cream, a strong negative correlation was found between HbT on the left (r = -0.742) and right (r = -0.857) sides of the parotid region and HbT on the left and right sides of the prefrontal cortex while rating the ice cream photos. Furthermore, when subjects were asked how much they would like this food in response to a video of ice cream, there was a strong negative correlation (r = -0.986) between the HbT on the subject's right side of the parotid region and the HbT on the subject's right side of the prefrontal cortex while rating the ice cream videos. Therefore, it can be concluded that the mean values of HbT on the left and right sides of the parotid region become smaller as the mean values of HbT on the left and right sides of the prefrontal cortex increases, and the mean values of HbT on the right side of the parotid region become smaller as the mean values of HbT on the right side of the prefrontal cortex increases.

3.4. Summary of the results

In this study, to explore the individual motivations behind food choices and how biological responses are related to evaluations of food, we employed an approach for combining biological indicators from prefrontal and parotid regions and examined them in response to visual stimuli of food. We developed and tested a biological food preference task that simultaneously rates biological responses to visual stimuli of various food states and subjective evaluations of food. We also examined how these biological responses are related to food preference behavior. First, the results revealed the differences in subjects' subjective evaluations of the visual stimuli of different states of ice cream. Then, according to the hemodynamic response function of cerebral blood flow during visual stimulation and evaluation, activation was observed in the prefrontal and parotid regions of the brain during the task. Furthermore, we found significant correlations between subjects' subjective evaluation and the mean change in cerebral blood flow in the prefrontal and parotid regions and between the mean change in cerebral blood flow in the prefrontal region and the mean change in cerebral blood flow in the parotid region.

4. Discussion

According to the result of the subjects' subjective evaluations, when the subjects' evaluations were segmented according to the

state of the ice cream, there was a large difference in the subjects' subjective evaluation of each state of the ice cream. In particular, State 1 ice cream had the highest evaluation, and State 4 ice cream had the lowest evaluation. Consequently, when the state of the ice cream changed from hard to completely melted, the subjects' evaluations tended to change from high to low. The visual sense plays an essential role in food selection [2], and some studies have reported that the visual sense of food strongly influences appetite [31–33]. In this study, we controlled the visual changes in food state as cues for visual stimuli of food. During the experimental task, subjects visually process food cues, and along with learned knowledge about the food, there is likely to be a process of evaluating the food as expectations about the food are generated from the visual cues of the food. The fact that there was a significant difference in the evaluation of ice cream by the state is due to the fact that ice cream in a hard state is commonly expected, and as the state of ice cream changes, the subjects tend to feel more uncomfortable with the melting ice cream. Therefore, the subject's evaluation of the ice cream was also lower. Furthermore, many studies have reported that visual changes with aging significantly impact appetite [33–35]. Particularly, appetite is strongly influenced by visual factors such as the state of food [34,35]. In our experiment, the influence of state is significant, which indicated the same results as previous studies.

It has been reported that subjects process visual information about food and that, along with learned knowledge about food, expectations about food are generated from visual cues of food, and various predictive responses can be caused in the body to visual stimuli of food [36]. By detecting changes in oxygen saturation, fNIRS can identify the activation of different brain regions in response to a task or stimulus and has been widely used in many research fields, including cognitive behavior and brain injury[37,38]. The activation of the cerebral cortex causes the concentration of HbT and HbO to increase while the concentration of HbR decrease [39]. In this experiment, biological responses with activation of cerebral blood flow in the prefrontal and parotid regions were observed as predictive responses in the body. Therefore, visual stimulation in different states of food may have led to an increase in cerebral blood flow concentration in the prefrontal and parotid regions. Furthermore, these responses include cognitive and physiological processes [36]. In other words, measuring the different aspects of cognitive and physiological processes may provide insight into facilitating human food selection activities. As the state has an important influence on food selection, in this study, we used a food preference selection task in different states of ice cream. In addition, we asked subjects to rate their liking and wanting to measure brain blood flow responses in prefrontal and parotid regions during the task. Information from the subjects' subjective ratings and cerebral blood flow allowed us to examine how food cues from different states and colors in food categories affect cognitive and physiological processes and how these factors are related.

It was reported that vision is a major factor influencing human food selection[40], visual stimulation of food is an essential regulator of appetite, and visual stimulation of food can activate the reward center of the brain [41]. In this study, we measured the response of cerebral blood flow during passive viewing and evaluation of visual stimuli of food. The results showed that the food evaluation variables differed between each category of

different food states. For example, when subjects were asked how happy they would be if they ate the food in response to a photo of ice cream in different states, a strong negative correlation was observed between the mean change in HbO in the right parotid region and the subject's evaluation. On the other hand, when subjects were asked how much they would like to eat this food in response to a photo of ice cream in different states, a strong positive correlation between the subject's evaluation and the mean change in cerebral blood flow in the left parotid region while rating the pictures detected, but a strong negative correlation with the mean change in cerebral blood flow in the left prefrontal region is observed. Although our results revealed various correlations between subjective evaluation and cerebral blood flow from the approach of food in different stats, the results are inconsistent, and there is currently a limited number of comparable studies on the results of each of the correlations revealed. Some studies demonstrated the differences in biological responses to the taste of different juices[42] and the olfactory cues of smell [43]. In the future, it is conceivable that it may be possible to evoke more cerebral blood flow responses by approaching elements such as the smell and taste of food compared to visual stimuli to food cues.

It was reported that increased cutaneous electrical activity in response to food aversive visual stimuli[42]. Since the materials used in this experiment ranged from normal ice cream shape and state to completely melted ice cream, it is likely that as the ice cream melted, subjects' feelings of liking or disliking each state of ice cream would also change. Similarly, subjects' biological responses to each feeling would change. Based on the results of this experiment, it was found that the subjects' subjective rating scores for each state of ice cream also decreased as the ice cream melted. On the other hand, the characteristics of cerebral blood flow in the prefrontal and parotid regions for each state of ice cream showed that changes in cerebral blood flow did not change with the ice cream state but were somewhat irregular. Furthermore, the characteristics of cerebral blood flow caused by visual stimulation of ice cream revealed differences in cerebral blood flow changes between the left and right parotid brain regions. However, to the best of our knowledge, although the components of saliva secreted by the left and right parotid regions were different, the significance of the differences in cerebral blood flow changes in the left and right parotid regions is still unknown and needs further investigation.

From the hemodynamic response function results and the correlation between the subject's subjective evaluation and cerebral blood flow, it can be inferred that there is more activity in the left hemisphere of the subject's brain. The visual stimuli used in this study led to rational judgments by the subjects, which may have resulted in more activity in the left hemisphere of the brain in the results of this experiment. However, if it is a whole-brain response, then not only visual stimuli but also olfactory and gustatory sensations are essential in the whole-brain response. The appetite examined in this experiment using only visual stimuli is different from the appetite of daily life and is worth improving in the future.

5. Future Works

In the future, we will increase the number of subjects and expand the subjects' age range while investigating whether this

experiment's results can be reproduced. In particular, we will investigate whether visual stimulation can improve appetite and xerostomia in the elderly. We will also examine the response of the brain when visual stimuli are combined with the senses of smell and taste.

References

[1] K.C. Lai, Y.Q. Liu, Q.K. He, M. Yi, T. Fujinami, "Saliva Secretion as Indicator of Appetite," in ICMHI 2021: 2021 5th International Conference on Medical and Health Informatics, Association for Computing Machinery New York NY United States, Kyoto Japan: 249–253, 2021.

[2] S. Boesveldt, K. de Graaf, "The differential role of smell and taste for eating behavior," Perception, **46**(3–4), 307–319, 2017. Doi: 10.1177/03010066166855

[3] M. Levine, "Saliva," Topics in Dental Biochemistry. Springer, Berlin, Heidelberg, 203–230, 2011.

[4] A. M. L. Pedersen, C. E. Sørensen, G. B. Proctor, G. H. Carpenter, "Salivary functions in mastication, taste and textural perception, swallowing and initial digestion," Oral Diseases, **24**(8), 1399–1416, 2018. Doi: 10.1111/odi.12867

[5] G. H. Carpenter, "The secretion, components, and properties of saliva," Annual Review of Food Science and Technology, **4**, 267–276, 2013.

[6] J. R. Stokes, G. A. Davies, "Viscoelasticity of human whole saliva collected after acid and mechanical stimulation," Biorheology , **44**(3), 141–160, 2007.

[7] C. Dawes, A. M.L. Pedersen, A. Villa, J. Ekström, G. B. Proctor, A. Vissink, D. Aframian, R. McGowan, A. Aliko, N. Narayana, Y. W. Sia, R. K. Joshi, S. B. Jensen, A. R. Kerr, A. Wolff, "The functions of human saliva: A review sponsored by the World Workshop on Oral Medicine VI," Archives of Oral Biology, **60**(6), 863–874, 2015, doi: 10.1016/J.ARCHORALBIO.2015.03.004.

[8] R. D. Mattes, "Physiologic Responses to Sensory Stimulation by Food: Nutritional Implications," Journal of the American Dietetic Association, **97**(4), 406–413, 1997, doi:10.1016/S0002-8223(97)00101-6.

[9] P. A.M. Smeets, A. Erkner, C. de Graaf, "Cephalic phase responses and appetite," Nutrition Reviews, **68**(11), 643–655, 2010, doi:10.1111/j.1753-4887.2010.00334.x.

[10] M.A.Zafra, F. Molina, A. Puerto, "The neural/cephalic phase reflexes in the physiology of nutrition," Neuroscience & Biobehavioral Reviews, **30**(7), 1032–1044, 2006, doi:10.1016/J.NEUBIOREV.2006.03.005.

[11] C. SPENCE, "MOUTH-WATERING: THE INFLUENCE OF ENVIRONMENTAL AND COGNITIVE FACTORS ON SALIVATION AND GUSTATORY/FLAVOR PERCEPTION," Journal of Texture Studies, **42**(2), 157–171, 2011, doi: 10.1111/j.1745-4603.2011.00299.x.

[12] M.P. Lasschuijt, M. Mars, C. de Graaf, P.A.M. Smeets, "Endocrine Cephalic Phase Responses to Food Cues: A Systematic Review," Advances in Nutrition, **11**(5), 1364–1383, 2020, doi:10.1093/advances/nmaa059.

[13] R. A. de Wijk He, W. He, M.G. Mensink, R.H. Verhoeven, C. de Graaf, "ANS responses and facial expressions differentiate between the taste of commercial breakfast drinks," PloS One, **9**(4), 2014.

[14] P.C. Lee, J.B. Dixon, "Food for Thought: Reward Mechanisms and Hedonic Overeating in Obesity," Current Obesity Reports, **6**(4), 353–361, 2017, doi:10.1007/s13679-017-0280-9.

[15] H. Münzberg, E. Qualls-Creekmore, S. Yu, C.D. Morrison, H.R. Berthoud, "Hedonics Act in Unison with the Homeostatic System to Unconsciously Control Body Weight," Frontiers in Nutrition, 3, 2016.

[16] C. Gibbons, M. Hopkins, K. Beaulieu, P. Oustric, J.E. Blundell, "Issues in Measuring and Interpreting Human Appetite (Satiety/Satiation) and Its Contribution to Obesity," Current Obesity Reports, **8**(2), 77–87, 2019, doi:10.1007/s13679-019-00340-6.

[17] L. Bell, J. Vogt, C. Willemse, T. Routledge, L.T. Butler, M. Sakaki, "Beyond Self-Report: A Review of Physiological and Neuroscientific Methods to Investigate Consumer Behavior," Frontiers in Psychology, **9**, 2018.

[18] D. Ferriday, J.M. Brunstrom, "'I just can't help myself': effects of food-cue exposure in overweight and lean individuals," International Journal of Obesity, **35**(1), 142–149, 2011, doi:10.1038/ijo.2010.117.

[19] G.H. Carpenter, "The secretion, components, and properties of saliva," Annual Review of Food Science and Technology , **4**, 267–276, 2013.

[20] Y. ILANGAKOON, G.H. CARPENTER, "IS THE MOUTHWATERING SENSATION A TRUE SALIVARY REFLEX?," Journal of Texture Studies, **42**(3), 212–216, 2011, doi:https://doi.org/10.1111/j.1745-4603.2011.00290.x.

[21] Neu co., BRAIN ACTIVITY MEASUREMENT , Dec. 2022.

[22] D.T. Delpy, M. Cope, P. van der Zee, S. Arridge, S. Wray, J. Wyatt, "Estimation of optical pathlength through tissue from direct time of flight measurement," Physics in Medicine & Biology, **33**(12), 1433, 1988, doi:10.1088/0031-9155/33/12/008.

[23] Neu co., WOT-S20, Dec. 2022.

[24] P. Oustric, D. Thivel, M. Dalton, K. Beaulieu, C. Gibbons, M. Hopkins, J. Blundell, G. Finlayson, "Measuring food preference and reward: Application and cross-cultural adaptation of the Leeds Food Preference Questionnaire in human experimental research," Food Quality and Preference, **80**, 103824, 2020, doi:10.1016/J.FOODQUAL.2019.103824.

[25] M. Dalton, G. Finlayson, "Psychobiological examination of liking and wanting for fat and sweet taste in trait binge eating females," Physiology & Behavior, **136**, 128–134, 2014, doi:10.1016/J.PHYSBEH.2014.03.019.

[26] L. Thaler, A.C. Schütz, M.A. Goodale, K.R. Gegenfurtner, "What is the best fixation target? The effect of target shape on stability of fixational eye movements," Vision Research, **76**, 31–42, 2013, doi:10.1016/J.VISRES.2012.10.012.

[27] The Society for functional Near Infrared Spectroscopy, SNIRF, Dec. 2022.

[28] A. von Lühmann, A. Ortega-Martinez, D.A. Boas, M.A. Yücel, "Using the General Linear Model to Improve Performance in fNIRS Single Trial Analysis and Classification: A Perspective.," Frontiers in Human Neuroscience, **14**, 30, 2020, doi:10.3389/fnhum.2020.00030.

[29] T.J. Huppert, S.G. Diamond, M.A. Franceschini, D.A. Boas, "HomER: a review of time-series analysis methods for near-infrared spectroscopy of the brain," Applied Optics, **48**(10), D280–D298, 2009, doi:10.1364/AO.48.00D280.

[30] A. von Lühmann, X. Li, K.R. Müller, D.A. Boas, M.A. Yücel, "Improved physiological noise regression in fNIRS: A multimodal extension of the General Linear Model using temporally embedded Canonical Correlation Analysis," NeuroImage, **208**, 116472, 2020, doi: 10.1016/J.NEUROIMAGE.2019.116472.

[31] K. Tomita, "Effects of the color of Tablecloths on the Sence of Taste," Journal of the Color Science Association of Japan, **28**, 38–39, 2004.(in Japanese)

[32] M. Mitsusada, T. Ohkusa, "Effects of brightness of lighting in room on appetite in elder people," 2019.(in Japanese)

[33] S. Kobayashi, "Appetite for food illuminated with vivid color lights," Architectural Institute of Japan's Journal of Environmental Engineering, **74**(637), 271–276, 2009.(in Japanese)

[34] T. Feiniwa, T. Ueda, A. Hamada, "Research on food distinction and preference through visual sense of the elderly," Journal of the Japanese Society for Culinary Science, **41**(1), 35–41, 2008.(in Japanese)

[35] M. Mitsusada, "Examination of the effects of food morphology on the mental and physical health of elderly people: from autonomic nervous system responses and subjective evaluation," Journal of the Japanese Society for Eating and Swallowing Rehabilitation, **17**(3), 226–232, 2013.(in Japanese)

[36] K.N. Boutelle, M.A. Manzano, D.M. Eichen, "Appetitive traits as targets for weight loss: The role of food cue responsiveness and satiety responsiveness," Physiology & Behavior, **224**, 113018, 2020, doi:10.1016/J.PHYSBEH.2020.113018.

[37] S. Benavides-Varela, D. Gómez, J. Mehler, "Studying neonates' language and memory capacities with functional near-infrared spectroscopy," Frontiers in Psychology, 2, 2011.

[38] H. Obrig, "NIRS in clinical neurology — a 'promising' tool?," NeuroImage, **85**, 535–546, 2014, doi:10.1016/J.NEUROIMAGE.2013.03.045.

[39] T. Ma, H. Lyu, J. Liu, Y. Xia, C. Qian, J. Evans, S. He, "Distinguishing bipolar depression from major depressive disorder using fnirs and deep neural network," Progress In Electromagnetics Research, **169**, 73–86, 2020.

[40] L.N. van der Laan, D.T.D. de Ridder, M.A. Viergever, P.A.M. Smeets, "The first taste is always with the eyes: A meta-analysis on the neural correlates of processing visual food cues," NeuroImage, **55**(1), 296–303, 2011, doi:10.1016/J.NEUROIMAGE.2010.11.055.

[41] L. Nummenmaa, J.K. Hietanen, M.G. Calvo, J. Hyönä, "Food Catches the Eye but Not for Everyone: A BMI–Contingent Attentional Bias in Rapid Detection of Nutriments," PLOS ONE, **6**(5), e19215-, 2011.

[42] L. Danner, S. Haindl, M. Joechl, K. Duerrschmid, "Facial expressions and autonomous nervous system responses elicited by tasting different juices," Food Research International, **64**, 81–90, 2014, doi:10.1016/J.FOODRES.2014.06.003.

[43] W. He, S. Boesveldt, C. de Graaf, R. de Wijk, "Dynamics of autonomic nervous system responses and facial expressions to odors," Frontiers in Psychology, 5, 2014.

Ensemble Extreme Learning Algorithms for Alzheimer's Disease Detection

Vanamala H R[*,1], Samriddha Shukla[1], Vijaya krishna A[2]

[1]*Department of Electronics and Communication Engineering, PES University, Bangalore, India*

[2]*Bosch Global Software Technologies Pvt.Ltd., Bangalore, India*

A R T I C L E I N F O	A B S T R A C T
	Alzheimer's disease has proven to be the major cause of dementia in adults, making its early detection an important research goal. We have used Ensemble ELMs (Extreme Learning Models) on the OASIS (Open Access Series of Imaging Studies) data set for Alzheimer's detection. We have explored various single layered light-weight ELM networks. This is an extension of the conference paper submitted on implementation of various ELMs to study the difference in the timing of execution for classification of Alzheimer's Disease (AD) Data. We have implemented various ensemble ELMs like Ridge, Bagging, Boosting and Negative correlation ELMs and a comparison of their performance on the same data set is provided.

1. Introduction

Advances in healthcare have made significant contributions to the longer survival and healthy lifestyle of human beings. But there are diseases that still pose a daunting challenge to the research community, Alzheimer's Disease (AD) being an important example. AD is a major neuro degenerative disease. The expense of Caring AD patients is quiet high. With the increase in quality of healthcare, the aging population is bound to increase and hence, we will see a greater number of people facing this disease caused by neuro degenerative changes. A treatment that follows an early detection leads to lower severity in the coming times and lowers the risk of damage. The need for having a Computer Aided Diagnosis system (CAD) for early and accurate AD detection and classification is crucial. In the past years, Multi Layer Perceptrons (MLP) have been extensively used for the computer vision analysis on medical images. But the less complex Single Hidden Layer Feed Forward Neural Networks (SLFNs) have been relatively less explored. In this research work, we focus on the SLFNs, taking a step forward in realizing the potential of the ensemble ELM algorithms with the help of iterative error optimization, bagging, boosting and correlation coefficients. This work mainly focuses on evaluation of different Ensemble ELM models and comparison of performance on OASIS imaging data set. Bagging and Boosting ELM gave us good results followed by negative correlation and Incremental ELMs. We have

implemented these methods on Brain MR images unlike the different 2D data sets used in the reference implementations. As a result of the study, we intend to bring forth techniques which shall facilitate clinicians in classifying Alzheimer's experiencing patients from normal individuals in an early stage using MRI imagery.

2. Related work

This paper is an extension of the originally submitted work in the conference "2021 IEEE 4th International Conference on Computing, Power and Communication Technologies (GUCON). [1]

We used Modified Extreme Learning Machine algorithms to study the training computational requirements in comparison to conventional machine learning methods.[2,3] The variations of ELMs used were, Regularized ELM (RELM) and MLPELM [4,5]. Convolution Neural network takes more time for training and the desired accuracy may be difficult to achieve where as ELM is a lightweight SLFN with randomly initialized biases and weights, which when propagated onto the next layer create a Multi-Layer Perceptron without BPA (Back propagation algorithm) with ELM as the backbone of the network, and this network delivers at a faster training speed with similar accuracy rates [6].

In our implementations we had used the ELM algorithm which randomly generates the weights and biases. It tends to have

*Corresponding Author: Vanamala H R, vanamalahr@pes.edu

a good generalizability and all the hidden layers are treated as a whole system. This way, once the feature of the previous hidden layer is extracted, the weights or parameters of the current hidden layer will be fixed and need not be fine-tuned. Therefore, this helps in getting a better accuracy and trains the network faster compared to using MLP with back propagation algorithms. It was observed that Multi Layer Perceptron had the highest accuracy while the training speed was slower, meanwhile, the RELM had lesser accuracy compared to Multi Layer Perceptron but the training speed was faster. There is a trade off between training speed and accuracy [7]-[9].

Lot of research on new approaches with ELMs are done. Dual-tree complex wavelet transforms (DTCWT), Principal Component Analysis(PCA), Linear Discriminant Analysis(LDA), and ELM implementations were used to identify AD conditions. On ADNI dataset, they could get an accuracy of 90%, specificity of 90% and sensitivity of 90% [9]. Another approach where Key Features Screening method based on ELMs (KFS-ELM) was implemented From 920 key functional connections screened from 4005 the accuracy is obtained for detecting AD was 95.33% [10].

Many state-of-the art techniques like Support Vector Machine (SVM), Random Neural Network (RNN), Radial Basis Function Neural Network (RBFNN), Hopfield Neural Network (HNN), Boltzmann Machine (BM), Restricted Boltzmann Machine (RBM), Deep Belief Network (DBN), and other DL methods are compared with ELM implementations like Circular ELM (CELM) and Bootstrap aggregated (B-ELM) and other variants. The observations are that ELMs are faster than these techniques . Many ELM variations are being used and they are comparatively more robust. Implementation is simple and performance in terms of accuracy is also considerably better [11]-[13].

Considering the advantages of ELMs we have incorporated the less utilized ensemble ELMs with necessary modifications on OASIS Brain MR Data set and study the classification performance.

3. Data set

The data set is acquired from the official OASIS repository. The data set used is OASIS-1. The data is made up of 416 subjects with their respective cross-sectional scans from 434 scan sessions. The number of T1-weighted MRI scans varies from 3 to 4 in a single-imaging session. The data acquired is restricted to right-handed individuals of both genders. The number of participants with an age above 60 with diagnosis of AD at various stages is 100.

Every imaging session was stored in its respective directory labeled with its subject ID. The subject ID format is OAS1_xxxx, where 'xxxx' denotes the 4digit ID of a patient(eg: OAS1_0027). All the sessions have been assigned with an ID formatted as OAS1_xxxx_MRy, here y denotes the session number of the participant (eg: OAS1_0034_MR1). A particular session is accompanied by a zip-compressed file with its respective session ID. We have considered totally 1412 images of which 179 Mild Demented, 145 Moderately Demented, 640 Non Demented and 448 Very Mild Demented, from the data set after Preprocessing.

4. Implementation

4.1. Proposed Method

Our objective here is to incorporate the less explored ensemble ELMs with relevant modifications on Brain MR Data and study the classification performance on the OASIS Dataset.

The same Preprocessing steps used in our work earlier [1] are used for processing the images. The steps involved are initially Preprocessing, segmenting and feature extracting leading the vectors into our desired ELM classifier. The sample images and the processed images are shown below in the results section in Figure 2 and Figure 3. Biological implications of AD is that it results in two distinctive abnormalities in the brain, firstly Neuro-fibrillary tangles and secondly senile plaques. A Neuro-fibrillary tangle gets originated in the cytoplasm of neurons in the entorhinal cortex, whereas the plaques found in the neocortex of the brain. Structural changes in the early stages are more dominant in the medial temporal lobe, especially in the entorhinal cortex. With progression of the disease both entorhinal cortex and hippocampus are the indications of the variations observed.

4.1.1. Image Preprocessing

Firstly the unrefined images are denoised and given a level of uniformity. The primary goals are echo reduction, contrast imbalance correction and image resolution rectification. A brain image is primarily comprised of Cerebrospinal Fluid (CSF), White Matter (WM) and Grey Matter (GM). The overview of the situation is that the precision with which the Regions of Interest (RoI) are ascertained among the noise created by the aforementioned features even after threshold removal of skull. We use filtering to make our classification efforts easier as it gets rid of low frequency echoes. A fixed re sizing of 256x256 and grayscale conversions are made. The finalized Preprocessing method chosen upon is median filtering which is a nonlinear method of noise elimination. It functions by iterating through each pixel and substituting each pixel with the median value of the pixels in a certain proximity range all while preserving the edges. It works on the principle of averaging and which effectively eliminates noise and blurring of sharp edges [14].

4.1.2. Image Segmentation

The objective of this process is to segregate the image into non intersecting regions based on similarity indexes. The segmentation technique adopted here is threshold method which relies on normalizing a pixel with respect to its intensity level. It is optimal for object and background separation which comes in handy for skull removal here [15,16].

4.1.3. Feature Extraction

It involves the recreating values by deriving them via consolidation of a large collection of data in order to bring generalization while maintaining its relevance to the task intended in future. Our focus here is texture analysis based on understanding the nature of spatial variation. with the Gray-Level Co-occurrence Matrix (GLCM). We have used the features extracted for earlier algorithms [17]. GLCM is a square matrix representing the frequency count of appearance of a reference pixel with a particular intensity value i with respect to an adjacent

neighbor pixel having an intensity value of j. Therefore, a cell (i,j) represents their cumulative occurrence count. Their separation distance, d is also taken into account for the GLCM function computation along with regional frequency count. Further a matrix consisting of statistical values to increase the descriptive understanding is created [18].

Our earlier implementation was of RELM and MLPELM [19,20]. Further we have worked on the performance of various Ensemble ELMs on Alzheimer's data. Various ELMs with sigmoid , hardlim, gaussian and leaky Relu functions which helps in speeding up of the training for classification and Regression. Incremental Learning and increase in hidden nodes assist in minimizing the error. Multiclass Adaboost ELM (MAELM), Bagging Stepwise ELM and Negative Correlation ELM are suitable for imbalanced data. They are simple, cost effective, supporting many kernels or feature mapping functions for multi class data.Knowing ELMs require lesser time than conventional networks for training from our study performed earlier[1], our objective here is to incorporate the above modifications to ELMs and study the classification performance on the same OASIS Dataset.We also have compared the performance of other state of art techniques like CNNs and SVM. We have studied different Ensemble ELMs like ridge bagging, boosting, (Adaboost ELM)AELM and Negative Correlation ELMs(Incremental ELM) IELM.

4.2. Algorithms

We have implemented different ensemble ELMs and the this section will give the mathematical treatment and the methodology of implementation of these algorithms.

4.2.1. Vanilla ELM (VELM)

ELM for the SLFNs was invented in 2006.The Algorithm 1 represents the basic ELM flow. The Vanilla Extreme Learning Machine network architecture is shown in Figure 1.
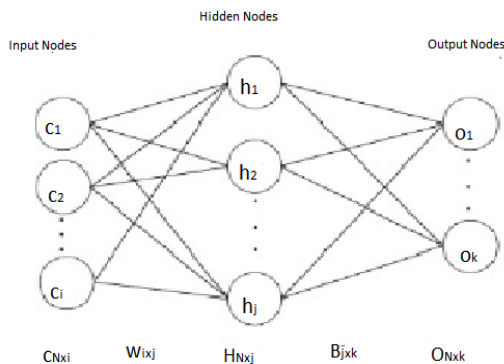
Figure 1: ELM architecture.

Assume N distinct samples (c_r, o_r) where $c_r \in R_i$ and $o_r \in R_k$, r $=1,\ldots,N$. The output hidden layer matrix H is presented as

$$H = \begin{bmatrix} G(w_1, b_1, c_1) & \cdots & G(w_i, b_j, c_1) \\ \vdots & \ddots & \vdots \\ G(w_1, b_1, c_N) & \cdots & G(w_i, b_j, c_N) \end{bmatrix} \quad (1)$$

G(.) gives the activation function, $W_{N \times j} = w_1, \ldots, w_j$ represents the weight matrix between the input layer and the hidden layer and b_r represents the rth hidden node in a particular hidden layer bias. Both of the parameters in an particular layer are randomly initialized [19,20].

Weights B in the output layer are to be adjusted using the Moore–Penrose Generalized Inverse is used to compute the weights B in the between the the hidden layer and output layer

$$B = H\dagger O. \quad (2)$$

here H† denotes the Moore–Penrose inverse of matrix H and

$$O = o_1, \ldots, o_N{}^T \quad (3)$$

Algorithm 1

Consider

Training set T={$(c_r, o_r), c_r \in R_{i,r} \in R_k$, r=1,.., N}

With G• and j representing activation function and the number of hidden nodes respectively

i: Randomly initialize desire parameters (w_r, b_r), r =1,…..j

ii: Compute output hidden layer matrix H

iii: Successively compute matrix B

iv: Resultants are B, W and b

4.2.2. Ridge ELM

Ridrin order added to the robustness of Regularized ELM algorithm by accompanying the matrix B (output hidden layer matrix) with l_2 norm through addition to minimize the matrix B constituents by a certain degree in accordance with Bartwtt's theory which is 'Smaller the weights in the output layer better the generalization performance in case of feed forward neural networks.'[21,22,23] The mathematical model is

$$M_{in} = \frac{1}{2} \sum_{i=1}^{k} \gamma_i^T \gamma_i + \lambda \frac{1}{2} \|B\|^2$$

$$where: \quad y_r = 0_r - \gamma \ , \ \gamma = 1 \ldots k \quad (4)$$

$$B_{jxk} = [\beta_1 ---- \beta_k] \quad (5)$$

$$Y_r = H_{\beta r} \text{ and} \quad (6)$$

$$O_{Nxj} = [o_1 ---- o_j] \quad (7)$$

here λ has a varying range as $\lambda \in (0, \infty)$. In the scenario of the data set being comparatively smaller, we use

$$B = H^T (\frac{I}{H} + HH^T)^{-1} T \quad (8)$$

where as for the latter scenario where N ≫ j, we opt for

$$B = (\frac{1}{\lambda} + H^T H)^{-1} H^T T \qquad (9)$$

here N is the number of training samples and j is the dimension of feature space.

Algorithm 2

Consider

Training set

T=c_r, or, $c_r \in R_i$, or $\in R_k$, r=1,…,N

i: Randomly initialize desire parameters (w_r, b_r), r =1,…..j

ii: Compute output hidden layer matrix H

iii: Successively compute matrix B using Eq.8 or Eq.9

iv: resultants are B, W and b

4.2.3. Bagging ELM Algorithm

Bagging primarily consists of the processes of bootstrapping and aggregation. Bootstrap sampling is adopted to introduce the concept of experts generation which means the further division of training and validation set catered differently by each expert along with the putting back of samples. The models for all experts are trained with the basic algorithm for learning. Bagging uses voting for classification in order to aggregate [24,25,26]. Algorithm 3 explains this bagging technique.[27]

Algorithm 3

Given training set T=c_r, or, $cr \in R_i$, or $\in R_k$, r=1,…N

Learning parameter Φ and E: number of experts

To do: Aggregation of all E experts

Loop in range r = 1:*E*

(i) By bootstrap sample in *D*; get the training and validation set

(ii) train the respective expert with Φ in training set and validation set

End: Resultants are E models of experts

4.2.4. Boosting Ridge ELM

It is an ELM integrated with Boosting Ridge Regression. It consists of two initialization steps where hidden nodes are randomly initialized and the Boosting Ridge ELM chooses bias and input weights randomly. Then, a response matrix is computed for the hidden nodes. Boosting ridge then computes the output weights using boosting ridge regression. Then using feedback based on any output weights being zero, the respective hidden nodes are deleted successive to which bias and input weights matrix update is made .[28,29]The algorithm is as follows:

Algorithm 4:

Given training set T=c_r, or, $cr \in R_i$

i. Randomly initialize input weight w_i and bias bi

ii. Compute hidden layer output matrix

iii. Find output weight $β_{boosting-ridge}$ with the help of boosting ridge regression

$$β = H^T (\frac{I}{C} + WHH^T)^{-1} W^T \qquad (10)$$

iv. Delete the redundant hidden node and do successive updation according to $β_{boosting-ridge}$

v. Adjust the parameter values and number of iterations to get best fit

4.2.5. Negative Correlation ELM

NCELM is made up of i learners, each of which is an ELM, c = 1. . . N, where N is the number of classifiers. The averaged output of a sample x ∈ R

$$p_j(x) = \frac{1}{c}\sum_{c=1}^{C} p_j^{(c)}(x) = \frac{1}{c}\sum_{c=1}^{C} h^{(c)^T}(x)β_j^{(c)} \qquad (11)$$

The end goal is to generalize using minimization of each learner and the using penalization (λ ∈ (0, +∞)), we take care of controlling the diversity which is dynamic to the problem. The minimization can be shown as :

$$Min\ (β_j^i \in R^{DXJ})[(\ ||β_j^{(i)}||^2 + S\ ||H^{(i)}β_j^{(i)} + Y_j||^2 + λ < H^{(i)}β_j^{(i)}, P_j >^2\ )] \qquad (12)$$

Below p_j denotes the ensemble output,

$$P_j = \sum_{c'=1}^{C} H^{(i')} . β_j^{(i')} \qquad (13)$$

Because $β_j^{(c)}$ appears in p_j, the proposed solution for Eq. 12 is to transform the problem in an iterated sequence, with solution of the first iteration $β_j^{(c)}$,(1) for c = 1, . . . , C. The output weight matrices in the rth iteration β (c) j,(r) ,c = 1, . . . , C, for each individual are obtained from the following optimization problem.[30]

The output weight matrices are obtained iteratively with the rth iteration corresponding to $β_j^{(c)}$,(r) ,c = 1, . . . , C, shown as,

$$Min\ (β_{j(r)}^{(c)} \in R^{DXJ})\ (\ ||β_{j,(r)}^{(c)}||^2 + S\ ||H^{(c)}β_{j,(r)}^{(c)} - Y_j||^2 + λ < H^{(c)}β_{j,(r)}^{(c)}, P_{j(r-1)} >^2\ ) \qquad (14)$$

updation of Pj,(r−1) takes place in this manner,

$$P_{j(r-1)} = \frac{1}{c}\sum_{c=1}^{C} H^{(c)} . β_{j(r-1)}^{(c)} \qquad (15)$$

Solution can be obtained for Eqn.14 by deriving it and now by equating to 0.

$$\beta_{j,(r)}^{(c)} = \left(\frac{I}{S} + H^{(c')}H^{(c)} + \frac{\lambda}{S}H^{(c')}P_{j,(r-1)}P'_{j,(r-1)}H^{(c)}\right)^{-1}H^{(c')}Y \tag{16}$$

Iteratively we calculate $(r+1)^{th}$ term and the convergence is assured by the Banach fixed-point theorem.[30]

4.2.6. Incremental ELM

Characteristic of IELM is that the error decreases for every iteration and is dwindled to zero with increase in number of hidden nodes. The trade off is between training time and accuracy as it is no more a one-shot process. The residual error is :

$$\mathbf{E`} = \mathbf{E} - \beta\mathbf{H} \tag{17}$$

To minimize the residual error if we are not satisfied with the minimization magnitude we restart the training of the particular node with new randomly initialized values. [31]

Algorithm 5

Given training set $\{(C, O)\}$, C is a $l \times N$ matrix which is the input of N data sets. O is a $k \times N$ matrix which is the output of N data sets

Step 1: Set the max value J for number of nodes, initial value of residuals ε and set current number of nodes j =0

Step 2: loop until j < J and E > ε :

i. Increment j by 1
ii. Randomly initialize weight ωj and bias bj of the hidden layer neuron hj
iii. Use the activation function $g(c`)$ to calculate the output for the node o_l
   $c` = \omega_j C + b_j$
iv. Find the ouput vector H of hidden layer neurons:
   $H = g(c`)$
v. Calculate β
vi. Re-calculate the residuals error

In the analysis 2D MRI scans were converted to 1D Numpy Arrays and then fed as input to the respective ELMs implemented.The above algorithms were implemented in Python and trained on the OASIS data set considered in our previous study as mentioned earlier. Four class classification is performed and the comparison of the performance is discussed in the results section.

5. Results

In our analyses using the 4 different variations of ELM and Vanilla ELM we predict the stages of the Alzheimer's disease which were non-demented, very mildly demented, mildly demented and moderately demented as indicated in Figure2. The various preprocessing techniques have varying effects which are visible in the Figure 3.
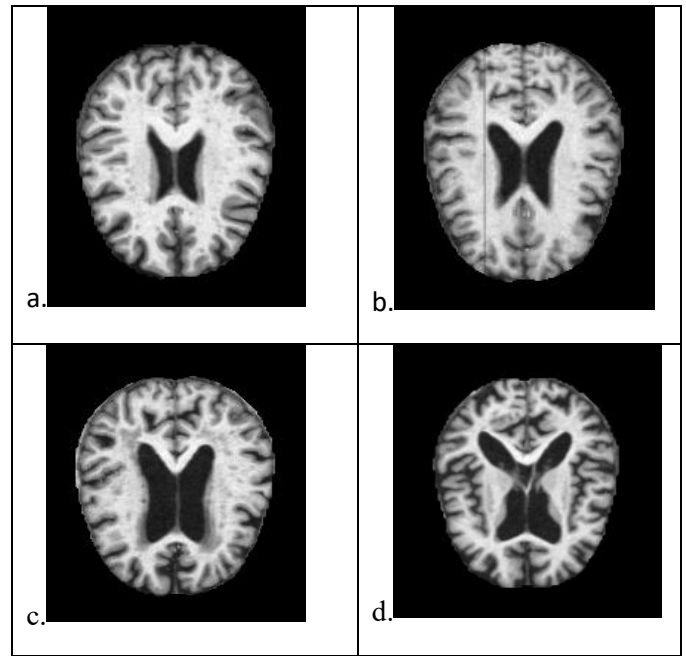
Figure 2: Sample images, a.Non Demented , b.Very Mild Demented , c.Mild Demented , d. Moderate Demented
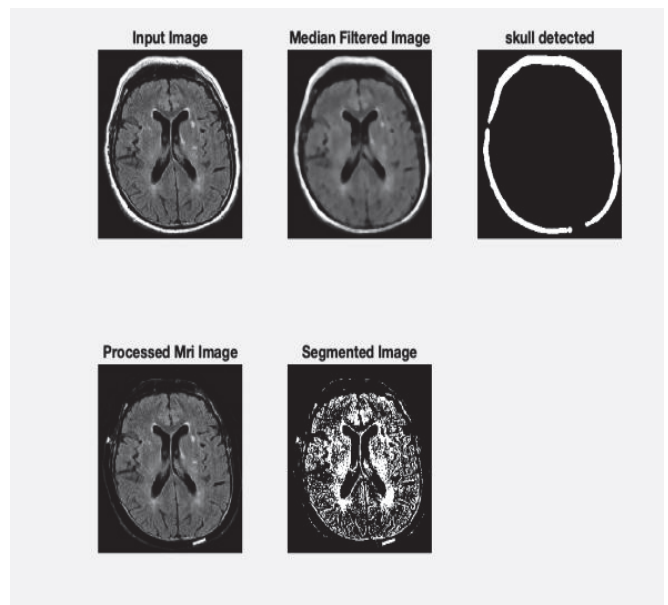
Figure 3: Sample Preprocessed images
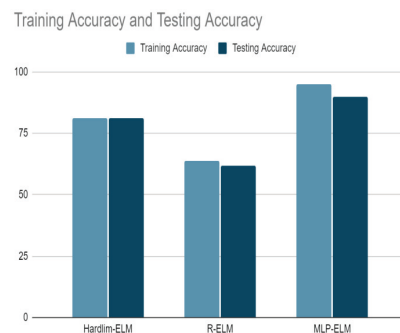
Figure 4: Accuracies of different ELMs implemented

The results obtained for the four class classification of OASIS Data for Hardlim, RELM and MLPELM implemented in the earlier work is shown in Figure4. Timing analysis was done for which MPELM gave us good performance.

The research was focused primarily on implementation of algorithms proposed by earlier researchers and then using the appropriate quantitative initialization parameters associated with them for our Data set.

Table 1 indicates the testing accuracies obtained for different state of art techniques implemented to compare the results with that of the ensemble ELMs.SVM and CNN-LSTM(Long Term Short Term Memory) gave us good results as indicated. With the advantages of ELMs , simple network and faster we find the ELMs more apt. Table 2 shows the comparison of testing accuracy for different activation functions used. Bagging and Boosting gave good results with Sigmoid and Leaky ReLU.

Table 1: Accuracies with our other implementations

Sl. No.	ELM	Testing Accuracy(%) Gaussian	Testing Accuracy (%) Sigmoid	Testing Accuracy(%) Leaky-ReLU
1	Vanilla-ELM	77.05	74.86	71.66
2	Boosting-ELM	88.42	92.32	93.47
3	Incremental-ELM	82.55	82.13	81.09
4	Bagging ELM	98.11	97.63	96%
5	Negative Correlation-ELM	83.49	87.56	84.38

Table 2: Accuracy with other activation functions

l.No.	Model	Testing Accuracy(%)
1	CNN	84.01
2	CNN-LSTM	98.23
3	Decision Tree	81.23
4	SVM	97.41

Table 3: Accuracies of different implemented ELMs

Sl. No.	ELM	Training Accuracy (%) at N=50	Training Accuracy (%) at N=5000	Testing Accuracy (%) at N=5000
1	Vanilla-ELM	53.43	74.86.	72.34
2	Boosting-ELM	62.72	92.32	90.69
3	Incremental-ELM	61.63	82.13	81.23
4	Bagging ELM	63.48	97.63	97.41
5	Negative Correlation-ELM	43.00	87.56	86.03

The bagging and boosting algorithms were tried over with different activation functions which are hardlim, triangular, sigmoid, (with beta=1, used leaky Relu to overcome vanishing gradient problem) and gaussian . We also tuned the negative correlation coefficient in accordance with the bias and the values varied in the order of 10^{-3} to 10^{-4} and the best accuracy was achieved near 6×10^{-3}. We observed that bagging and boosting algorithms took a training time of 18-20 minutes for 5000 nodes in spite of being stepwise whereas the negative correlation ELM took 13 minutes time for training and tuning 500 nodes. The training time of negative correlation ELMs is also dependent on the designated negative correlation coefficient. The incremental ELM algorithm's residual error value acts as a threshold value for stopping which was optimized over multiple epochs for the particular data set. Training and Testing accuracies are shown for Bagging, Boosting , Incremental and NE-ELM in the Figure 5, Figure 6 and Figure 7.
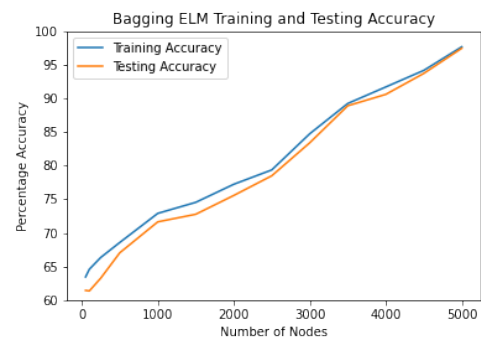
Figure 5: Accuracy of Bagging ELM
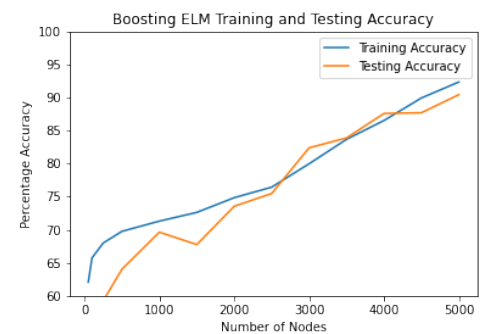
Figure 6: Accuracy of Boosting ELM
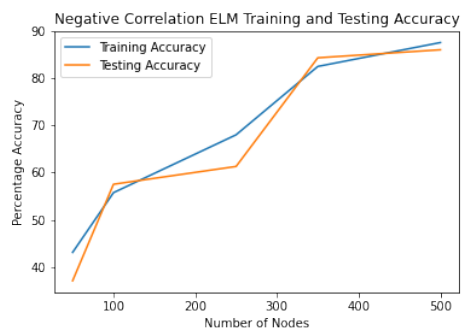
Figure 7: Accuracy of Negative-Correlation ELM

Table 3 indicates Training and testing accuracies obtained for the algorithms implemented. Bagging gave better performance, followed by boosting and NE-ELM for 5000 nodes.

6. Conclusion

We have implemented various ensemble ELMs like Ridge, Bagging, Boosting and Negative correlation ELMs and studied their performance on the OASIS data set. Bagging and Boosting ELM gave us good results followed by negative correlation and Incremental ELMs. These methods are implemented on Brain MR images unlike other 2D data sets used in the reference implementations.

Our approach results in better accuracy and convergence rate. The onset of impact of Alzheimer's disease is delayed if an early diagnosis is made possible which overall helps in prevention of the incurable disease. The regularly used machine learning algorithms such as Import Vector Machine (IVM), Support Vector Machine (SVM) and Radial Basis Functions require iterative training by adjustment of parameters to reduce the error. They are time-intensive and require manual assistance for obtaining the desired accuracy. In our proposed method, we have used the ELM algorithms which rely entirely on random initialization which creates a generalized inductive bias, thus obviating the need for fine-tuning for each layer or node addition.

7. Future Scope

The research on Ensemble ELM networks can be taken forward with the infusion of deep learning kernels such as Convolution ELMs and RNN-ELMs which promise the successful results of dense multi-layered networks without the time indulgence put into fine tuning. If algorithms like RNN-ELM which make use of temporal space weights are used along with Dual-Tree Complex Wavelet Transform (DTCWT) we stand to gain great benefits from the directional sensitivity subsiding shift in variance. It can be implemented and tested on PET (Positron Emission Tomography) Data. Can further work on improving on timing constraints [1].The time required for execution can be optimized.

Conflict of Interest

The authors declare no conflict of interest.

Acknowledgments

References

[1] A. Hari, V. Rajanna, V. A, R. Jain, "An Extreme Learning Machine based Approach to Detect the Alzheimer's Disease," 1–6, 2021, doi:10.1109/GUCON50781.2021.9573589.

[2] R.K. Lama, J. Gwak, J.-S. Park, S.-W. Lee, "Diagnosis of Alzheimer's Disease Based on Structural MRI Images Using a Regularized Extreme Learning Machine and PCA Features," Journal of Healthcare Engineering, **2017**, 5485080, 2017, doi:10.1155/2017/5485080.

[3] K.A. Johnson, N.C. Fox, R.A. Sperling, W.E. Klunk, "Brain imaging in Alzheimer disease," Cold Spring Harb. Perspect. Med., **2**(4), a006213, 2012.

[4] R.N. and G.A. Palimkar Prajyot and Shaw, "Machine Learning Technique to Prognosis Diabetes Disease: Random Forest Classifier Approach," in: Bianchini Monica and Piuri, V. and D. S. and S. R. N., ed., in Advanced Computing and Intelligent Technologies, Springer Singapore, Singapore: 219–244, 2022.

[5] X. Liu, L. Wang, G.-B. Huang, J. Zhang, J. Yin, "Multiple kernel extreme learning machine," Neurocomputing, **149**, 253–264, 2015, doi:https://doi.org/10.1016/j.neucom.2013.09.072.

[6] S. Mandal, V.E. Balas, R.N. Shaw, A. Ghosh, "Prediction Analysis of Idiopathic Pulmonary Fibrosis Progression from OSIC Dataset," in 2020 IEEE International Conference on Computing, Power and Communication Technologies (GUCON), 861–865, 2020, doi:10.1109/GUCON48875.2020.9231239.

[7] G. Huang, G.-B. Huang, S. Song, K. You, "Trends in Extreme Learning Machines: A Review," Neural Networks, **61**, 2014, doi:10.1016/j.neunet.2014.10.001.

[8] S. Suhas, C.R. Venugopal, "MRI image preprocessing and noise removal technique using linear and nonlinear filters," in 2017 International Conference on Electrical, Electronics, Communication, Computer, and Optimization Techniques (ICEECCOT), 1–4, 2017, doi:10.1109/ICEECCOT.2017.8284595.

[9] D. Jha, S. Alam, G.-R. Kwon, "Alzheimer's Disease Detection Using Extreme Learning Machine, Complex Dual Tree Wavelet Principal Coefficients and Linear Discriminant Analysis," Journal of Medical Imaging and Health Informatics, **8**, 881-890(10), 2018.

[10] J. Lu, W. Zeng, L. Zhang, Y. Shi, "A Novel Key Features Screening Method Based on Extreme Learning Machine for Alzheimer's Disease Study," Front Aging Neurosci, **14**, 888575, 2022.

[11] J. Wang, S. Lu, S.-H. Wang, Y.-D. Zhang, "A review on extreme learning machine," Multimedia Tools and Applications, **81**(29), 41611–41660, 2022, doi:10.1007/s11042-021-11007-7.

[12] S. Grueso, R. Viejo-Sobera, "Machine learning methods for predicting progression from mild cognitive impairment to Alzheimer's disease dementia: a systematic review," Alzheimer's Research & Therapy, **13**(1), 162, 2021, doi:10.1186/s13195-021-00900-w.

[13] M. Odusami, R. Maskeliunas, R. Damaseviccius, T. Krilavicius, "Analysis of Features of Alzheimer's Disease: Detection of Early Stage from Functional Brain Changes in Magnetic Resonance Images Using a Finetuned ResNet18 Network," Diagnostics (Basel), **11**(6), 2021.

[14] S. Leandrou, S. Petroudi, P.A. Kyriacou, C.C. Reyes-Aldasoro, C.S. Pattichis, "Quantitative MRI Brain Studies in Mild Cognitive Impairment and Alzheimer's Disease: A Methodological Review," IEEE Rev Biomed Eng, **11**, 97–111, 2018.

[15] G.V.S. Kumar, V.K. .R, "REVIEW ON IMAGE SEGMENTATION TECHNIQUES," International Journal of Scientific Research Engineering & Technology (IJSRET), **3**, 992–997, 2014.

[16] M. Al-amri, D. Kalyankar, D. S.D, "Image segmentation by using edge detection," International Journal on Computer Science and Engineering, **2**, 2010.

[17] D. Tian, "A review on image feature extraction and representation techniques," International Journal of Multimedia and Ubiquitous Engineering, **8**, 385–395, 2013.

[18] T. and S.R.N. and G.A. Sinha Trisha and Chowdhury, "Analysis and Prediction of COVID-19 Confirmed Cases Using Deep Learning Models: A Comparative Study," in: Bianchini Monica and Piuri, V. and D. S. and S. R. N., ed., in Advanced Computing and Intelligent Technologies, Springer Singapore, Singapore: 207–218, 2022.

[19] W. Deng, Q. Zheng, L. Chen, "Regularized Extreme Learning Machine," in 2009 IEEE Symposium on Computational Intelligence and Data Mining, 389–395, 2009, doi:10.1109/CIDM.2009.4938676.

[20] J. Tang, C. Deng, G.-B. Huang, "Extreme Learning Machine for Multilayer Perceptron," IEEE Transactions on Neural Networks and Learning Systems, **27**(4), 809–821, 2016, doi:10.1109/TNNLS.2015.2424995.

[21] R. Yangjun, S. Xiaoguang, S. Huyuan, S. Lijuan, W. Xin, "Boosting ridge extreme learning machine," in 2012 IEEE Symposium on Robotics and Applications (ISRA), 881–884, 2012, doi:10.1109/ISRA.2012.6219332.

[22] B. Jin, Z. Jing, H. Zhao, "Incremental and Decremental Extreme Learning Machine Based on Generalized Inverse," IEEE Access, **5**, 20852–20865, 2017, doi:10.1109/ACCESS.2017.2758645.

[23] G. Feng, G.-B. Huang, Q. Lin, R. Gay, "Error Minimized Extreme Learning Machine With Growth of Hidden Nodes and Incremental Learning," IEEE Transactions on Neural Networks, **20**(8), 1352–1357, 2009, doi:10.1109/TNN.2009.2024147.

[24] Z.X. Chen, H.Y. Zhu, Y.G. Wang, "A modified extreme learning machine with sigmoidal activation functions," Neural Computing and Applications, **22**(3), 541–550, 2013, doi:10.1007/s00521-012-0860-2.

[25] C. Perales-González, "Global convergence of Negative Correlation Extreme Learning Machine," Neural Processing Letters, **53**(3), 2067–2080, 2021, doi:10.1007/s11063-021-10492-z.

[26] P. Khan, Md.F. Kader, S.M.R. Islam, A.B. Rahman, Md.S. Kamal, M.U. Toha, K.-S. Kwak, "Machine Learning and Deep Learning Approaches for Brain Disease Diagnosis: Principles and Recent Advances," IEEE Access, **9**, 37622–37655, 2021, doi:10.1109/ACCESS.2021.3062484.

[27] M. Yang, J. Zhang, H. Lu, J. Jin, "Regularized ELM bagging model for Tropical Cyclone Tracks prediction in South China Sea," Cognitive Systems Research, **65**, 50–59, 2021, doi: 10.1016/j.cogsys.2020.09.005.

[28] A.O.M. Abuassba, D. Zhang, X. Luo, A. Shaheryar, H. Ali, "Improving Classification Performance through an Advanced Ensemble Based Heterogeneous Extreme Learning Machines," Computational Intelligence and Neuroscience, **2017**, 3405463, 2017, doi: 10.1155/2017/3405463.

[29] Y. Jiang, Y. Shen, Y. Liu, W. Liu, "Multiclass AdaBoost ELM and Its Application in LBP Based Face Recognition," Mathematical Problems in Engineering, **2015**, 1–9, 2015, doi:10.1155/2015/918105.

[30] S. Wang, H. Chen, X. Yao, "Negative correlation learning for classification ensembles," in The 2010 International Joint Conference on Neural Networks (IJCNN), 1–8, 2010, doi:10.1109/IJCNN.2010.5596702.

[31] S. Song, M. Wang, Y. Lin, "An improved algorithm for incremental extreme learning machine," Systems Science & Control Engineering, **8**(1), 308–317, 2020, doi:10.1080/21642583.2020.1759156.

ASTES

Emerging Trends in Green Best Practices and the Impact on Government Policy

Emily Holt*, Casey Corrado

The MITRE Corporation, Bedford MA, 01730, USA

A R T I C L E   I N F O

A B S T R A C T

While it is commonly accepted that climate change needs to be addressed to protect both human and environmental health, it is not widely understood what steps need to be taken to accomplish this daunting task. Additionally, there is currently no formal definition of what constitutes a 'green' company or 'green' best practice, despite the rising usage of the term. We found that companies that are considered 'green' have well-documented, quantifiable improvements in their sustainability plans and initiatives. These plans are published yearly in publicly available progress reports. Multi-year goals, with progress mapped from year to year, follow trends in the following areas: reduction in carbon emissions, energy obtained through renewable energy sources, amount of waste diverted from landfills, third-party certifications for buildings, water conservation, increasing 'green' requirements from suppliers, and sustainable fleet management. To address the gap between industry and government practices, and to capitalize on recent interest and investment in 'green', we recommend that all U.S. government agencies formalize and publicly release sustainability policies with quantifiable goals, identify practices to be implemented, and define metrics to measure progress. To effectively develop and implement these plans, we recommend: (1) each agency evaluate their current organization to develop a baseline, (2) define milestones and targets using the baseline as a starting point such that industry standards can be reached, and (3) release a finalized, publicly available sustainability plan.

1. Introduction

The Fourth National Climate Assessment defines climate change as the "changes in average weather conditions that persist over multiple decades or longer" and "encompasses both increases and decreases in temperature, as well as shifts in precipitation, changing risk of certain types of severe weather events, and changes to other features of the climate system" [1]. Over the last decade, climate change has become a central research area with interest and investment across both government and industry. While it is commonly accepted that climate change needs to be addressed to protect both human and environmental health, it is not widely understood what steps need to be taken to accomplish this daunting task. Inconsistencies in sustainability plans and policies between U.S. government and industry showcase the confusion and misunderstanding within the 'green' space. To properly address this issue, the government needs information on what proven and effective 'green' practices exist. With this, various approaches can be unified under a single definition to enact widespread change.

This work expands upon work previously done by the authors, going into a more detailed survey of the exploding popularity of the term 'green' [2]. In this survey, we both demonstrate and evaluate the lack of recognized, concrete definitions or metrics for this term and provide recommendations for action through policy. We will lay out what 'green' practices the U.S. government has already adopted, and, in contrast, what state-of-the-art sustainability practices are being implemented by industry. The authors will analyze the differences between the two groups, using the results as the baseline for developing the set of policy-based recommendations. The guiding research questions we will explore include: who are the industry leaders in the 'green' field; what are the 'green' best practices being utilized by these leaders; and, finally, what quantifiable metrics or features make a company 'green'?

2. Background

2.1. Key Definitions

After assessing the terminology across industry and government, a few key definitions must be articulated to describe

*Corresponding Author: Emily Holt, egholt@mitre.org

'green' best practices. It should be noted that there is no formalized, universally accepted definition for 'green'. Here, 'green' will refer to anything that is accepted to be sustainable or environmentally friendly, including products, practices, technologies, etc. Table 1 below gives an overview of the key terms referenced throughout this paper.

Table 1: Key Definitions in Green Policy

Term	Definition
Green	Anything that is commonly accepted to be sustainable or environmentally friendly
Sustainability	The ability for a community to maintain environmental, health, and economic stability over an extended period. It should be noted that 'green' and sustainable are sometimes used interchangeably in media
Renewable Energy	Energy sources that are derived from sources that are naturally replenishing. These include solar, wind, geothermal, hydropower, and biomass (ex. wood, landfill/biogas, ethanol, biodiesel)
Non-Renewable Energy	Energy sources that once they are depleted, they cannot be replaced. These include petroleum, coal, nuclear, diesel, etc.
Clean Energy	Non-pollutant producing energy sources, including solar, wind, hydropower, geothermal, bioenergy, nuclear, and hydrogen/fuel cells. It should be noted that clean energy sources are not always renewable (ex. nuclear)

2.2. Best Practices

'Green' best practices are a set of actions that can be implemented to improve environmental impact, such as reducing greenhouse gas emissions, minimizing waste, saving water, etc. We observed six main categories of these practices, including renewable energy, sustainable buildings, fleet management, waste reduction, water conservation, and sustainable purchasing. Table 2 below provides a few examples of each category.

Table 2: Overview of Green Best Practices

Best Practice	Example
Renewable Energy	Increasing use of solar, wind, hydropower, and geothermal energy, purchasing of renewable energy credits (RECs)
Sustainable Buildings	Requirements for new constructions to incorporate sustainable design plans, 'green' building certification
Fleet Management	Develop a vehicle fleet with more fuel efficient vehicles, or vehicles that use biofuels/renewable energy
Waste Reduction	Reducing demolition and construction waste, composting, paper reduction, increased recycling
Water Conservation	Installing dual plumbing for incorporating non-potable water sources, reducing landscaping costs, monitoring consumption to better understand use
Sustainable Purchasing	Committing to purchasing recycled, biobased, and other sustainable products

3. Benefits of 'Green' Practices for Government Agencies

In addition to environmental impact, there are many other benefits of implementing 'green' best practices. Some of the key benefits include: cost savings, improved safety and security, and public health. The section below will provide an overview of each of these benefits and how they can impact government agencies.

3.1. Cost Savings

One of the biggest benefits of implementing 'green' practices is the cost-savings, particularly on long term investments. Renewable energy is a great example of substantial cost-savings over time. Many renewable sources, such as solar, wind, or hydropower, do not require fuel costs. Traditional fossil fuel sources, like coal and oil, require not only high material costs, but often involve costly transportation fees as well. The cost of solar photovoltaics (PV) systems has fallen dramatically over the past decade [3] and currently wind is "either competitive with, or less expensive than, coal-generated electricity – and it is a form of Clean Energy. Ongoing cost reduction will soon make wind energy the least expensive source of electricity, perhaps within a decade" [4].

In addition to decreasing energy costs, there are other economic impacts from the implementation of sustainable practices. For example, studies have demonstrated that renewable energy policies within the Rust Belt have the potential to reduce air pollution to such a degree that the savings from improved human health would exceed the costs of the policies by 2030, with more stringent implementation having an even more pronounced cost-savings effect [5]. The decreased energy costs as well as health-related savings makes implementation of 'green' best practices a favorable financial decision for the U.S. government.

3.2. Safety

From a military perspective, safety is a major benefit of 'green' practices. There are direct relationships between increased safety to soldiers through the implementation of these best practices. One example is the use of more energy efficient vehicles. In active war zones, refueling missions are high risk. In Afghanistan, for example, oil refueling operations document one casualty for every 24 field-resupply convoys [6]. More fuel-efficient vehicles not only decrease fossil fuel use and carbon emissions, but can reduce the number of refueling missions required, saving soldiers' lives.

Extending beyond the military, implementing 'green' practices can increase safety for the entire nation. The National Climate Assessment (NCA) report states that "Climate change creates new risks and exacerbates existing vulnerabilities in communities across the United States, presenting growing challenges to human health and safety, quality of life, and the rate of economic growth" and notes that future impacts of climate change are "expected to further disrupt many areas of life, exacerbating existing challenges to prosperity posed by aging and deteriorating infrastructure, stressed ecosystems, and economic inequality" [1]. The report also emphasizes that vulnerable communities, lower-income, historically marginalized, etc., may experience greater impacts [1]. Wide-scale implementation of 'green' practices protects both military and civilian lives.

3.3. Security

'Green' practices are a unique opportunity to fortify national security. Researchers from the National Renewable Energy Lab (NREL) note that "renewable energy can support energy security by adding diversity to an overall electricity generation portfolio…

A more spatially diverse generation and storage energy portfolio can better withstand shocks to the system. With more resources across different geographic areas, such diversity could power infrastructure during disasters, cyberattacks, or other extreme events" [7]. With wider use of these energy sources, there is a decreased dependency on fossil fuels. Disruptions in the supply chain could lead to disastrous effects for both the nation and our military. Transitioning to renewable-energy sources not only addresses supply chain risk but can also increase the physical security of the energy generation process by decreasing reliance on centralized production and subsequent distribution. Many renewable sources can be implemented on-site, such as at military instillations, strengthening the resiliency of the that location's energy supply. The electrical grid is particularly susceptible to attacks, both cyber as well as physical, which could disrupt operation at critical facilities [6]. Localized power on-site using renewable sources decreases these risks and thus greatly improves security.

In addition, climate change is a critical driver of military investment in 'green' practices. Rising sea levels, for example, are a particular concern for the Navy. There is an expected increase in the demand for the Navy's military and humanitarian services in response to the effects of climate change. Both domestic and global bases and ports will be at high risk as sea levels rise and weather patterns become more severe [6]. Slowing the rate of climate change not only gives the Navy and other military branches more time to prepare for these challenges but can also prevent some of these concerns from even becoming a reality.

3.4. Public Health

Implementing these practices will also impact public health through the reduction in greenhouse gas emissions. The National Climate Assessment report notes that the "health and well-being of Americans are already affected by climate change, with the adverse health consequences projected to worsen with additional climate change" due to the effects of "exposures to heat waves, floods, droughts, and other extreme events; vector-, food- and waterborne infectious diseases; changes in the quality and safety of air, food, and water; and stresses to mental health and well-being" [1].

Implementing 'green' practices and enacting sustainability-focused policies has the potential to reduce the risks and impacts from climate-sensitive health outcomes, and researchers project that "additional benefits to health arise from explicitly accounting for climate change risks in infrastructure planning and urban design" [1]. The report claims that "reducing greenhouse gas emissions would benefit the health of Americans in the near and long term" and that "thousands of American lives could be saved and hundreds of billions of dollars in health-related economic benefits gained each year under a pathway of lower greenhouse gas emissions" [1].

4. Methodology

As described above, the benefits of 'green' practices are undeniable, particularly from a government perspective. The goal of this work was to provide an overview of the different definitions of 'green', highlight the emerging trends, and illustrate gaps between government and industry practices. In this process, we illustrate the growing need to set goals, assign priorities, establish regulations, and make investments as well as guidance for where to focus these efforts. This is intended to provide foundational information for implementing green policy, as well as identified resources for where to look for more information when setting or writing future sustainability policies.

The team conducted a survey of 'green' practices and policies across both government and industry. To assess the current state of the government sustainability efforts, the authors reviewed government agency sustainability plans and published 'green' goals, 'green' focused legislation and executive orders (EOs), as well as the timeline of when and how these documents were put into effect. For industry, key players were identified based on a combination of publicly released policies, data, and status on third-party 'green' rankings. The publicly released 'green' initiatives and policies of these companies were then compiled as a list of best practices as well as analyzed for industry-wide trends. The results of these evaluations were then used to identify gaps within current government 'green' efforts. Based on these findings, recommendations were made for what steps the government should take moving forward, as well as what research still needs to be done to properly implement these actions.

4.1. Sustainability Evaluation

While there are plenty of organizations with sustainability practices already in place, it can be challenging to compare different companies to one another. To help with this, several third-party organizations have developed sustainability certifications and rankings to help consumers better understand leaders in industry. These accolades have considerable impact on a company, affecting everything from brand image to product success. Having a high sustainability ranking or 'green' certified products and facilities can attract talent and generate new business. Pew Research studies have shown that adults under 50 believe protecting environment and increasing reliance on renewable energy sources should be a high priority for America's energy policies [8] and adults under 30 place a high priority on protecting the environment [9]. Additionally, both Glassdoor and Forrester Research observe that both job seekers and consumers are gravitating towards companies whose mission and culture align with their values [10] [11]. In addition, as today's consumers become more concerned about the environmental impact of their purchasing decisions, these certifications and rankings can influence purchasing decisions.

4.2. Sustainability Certifications

Sustainability certifications are third-party evaluations that assess the sustainability of a building, business, product, etc. These programs often provide both an assessment of the current sustainability practices or designs in place as well as what steps need to be taken to make further improvements. Additionally, many certifications have varying levels (ex. gold, silver, etc.) that indicate what that particular service has achieved. Table 3 gives an overview of available programs in each of the main certification categories.

Table 3: Sustainability Certification Overview

Category	Certification	Summary
Buildings	LEED	Leadership in Energy and Environmental Design (LEED), certification for buildings based on sustainable design features [12]
	WELL	Building Standard to create buildings and originations with thoughtful and intentional spaces that enhance human health and well-being [13]
	EDGE	Building certification focused on making buildings more resource-efficient [14]
	ParkSmart	Certification program for developing sustainable parking garages [15]
	Energy Star	Certification for products and buildings following standards set by the EPA; Energy Star buildings must save energy, money, and help protect the environment through limited generation of greenhouse gas emissions [16]
	SITES	Sustainability-focused framework for landscape design (reduce water demand, reduce energy consumption, improve air quality, etc.) [17]
	Living Building Challenge Certification	Certification program with a goal to create buildings that generate more energy than they use, capture and treat all water on site, and are built using healthy materials. Several different certifications available: Core Green Building Certification, Zero Energy Certification, and Zero Carbon Certification [18]
	Green Building Initiative	Certification program (Green Globe Certification) designed to allow building owners to select which sustainability features best fit their building and its occupants, creating a custom-tailor approach that helps from the most sustainable outcomes [19]
	BREEAM	Building Research Establishment Environmental Assessment Method (BREEAM); method of assessing, rating, and certifying the sustainability of buildings [20]
Businesses	Green Business Bureau Seal	Online green business certification program using the Green Business Bureau (GBB)'s Eco Assessment tool [21]
	Green America Certified Business	Certification that evaluates companies according to principles of social justice and environmental sustainability [22]
Products/ Materials	Energy Star	Certification for products as well as buildings following standards set by the EPA; products must reach a defined set of criteria, applicable for computers, servers, appliances, heating and cooling systems, electronics, lighting, etc. [16]
	WaterSense	Voluntary partnership program sponsored by the EPA, products and services are certified to use at least 20 percent less water, save energy, and perform as well as or better than regular models [23]
	EPEAT	Certification for electronics; leading ecolabel covering products and services from the electronics sector [24]
	Safer Choice	Certification through the EPA Pollution Prevention which identifies products that are both high performing and contain ingredients that are safer for human health and the environment [25]
	USDA Organic	U.S. certification for foods to be labeled organic according to federal guidelines on soil quality, animal raising practices, pest control, and use of additives [26]
	Fair Trade Certified	Certification evaluating a company's use of equitable trade practices across their supply chain, ensuring fair treatment, prices, and environmental impact [27]
	Green Seal	Green Seal Verification confirms that a raw material, concentrate, formula, or parent roll is proven to meet human and environmental health standards [28]
Other	PEER	Certification for the power and energy sector [29]
	GRESB	Global Real Estate Sustainability Benchmark Certification, assesses the sustainability and ethical impact of real estate and infrastructure [30]
	WasteWise	Program through the EPA to encourage companies to reduce waste, practice environmental stewardship, and incorporate sustainable materials management into their waste-handling processes [31]

4.3. Sustainability Rankings

In addition to various certifications, ranking systems have also come about for the top sustainable companies. The leading classifier is the Global 100, an annual ranking of corporate sustainability performance performed by Corporate Knights (CK). This list is released each January at the World Economic Forum in Davos and is considered the gold standard for sustainability ranking evaluations. For companies to be eligible for the Global 100, they must meet several eligibility requirements. Only publicly listed companies with a gross revenue of a minimum of one billion dollars can be considered. From this initial list, all industries and locations are eligible before screening [32].

CK uses only publicly disclosed data, such as financial filings and sustainability reports, to evaluate 21 different key performance indicators (KPIs) which cover resource management, employee management, clean revenue, and supplier performance. Out of this list, all companies are evaluated on the eight universal KPIs: percentage tax paid, pension fund status, supplier sustainability, women in executive management, women on boards, sustainability pay link score, sanctions deductions, and clean revenue. Other KPIs are considered based on a company's corresponding CK Industry Group. It should be noted that there are automatic disqualifiers such as companies that produce weapons, tobacco, or lobby to block climate change policy [32].

5. Sustainability Policies and Legislation within the United States Government

5.1. Federal Government

Before the early 2020s, the U.S. federal government made minimal steps toward implementing sustainability policy. There was over a decade lull where, for example, no major law regarding sustainability was passed between the mid-2000s through the early 2020s. The Energy Policy Act of 2005 [33] introduced tax incentives and loan guarantees for various energy sources, while the Energy Independence and Security Act of 2007 [34] aimed to move the U.S. toward greater energy independence and security through the increase of clean renewable fuels.

During this lull, only a handful of Executive Orders (EO) and government guidelines were released for implementing sustainable practices. In 2015, a comprehensive document, Planning for Federal Sustainability in the Next Decade [35], was put into effect, outlining the federal government's 10-year plan for implementing more sustainable practices. Following this, several other guidelines were released, including Executive Order 13834, Efficient Federal Operations [36] in 2018 and the Guiding Principles for Sustainable Federal Buildings and Associated Instructions [37] in 2020. EO 13834 "affirms that it is the policy of the United States that agencies meet energy and environmental performance statutory requirements in a manner that increases efficiency, optimizes performance, eliminates unnecessary use of resources, and protects the environment" and that "agencies are tasked to prioritize actions that reduce waste, cut costs, enhance the resilience of federal infrastructure and operations, and enable more effective accomplishment of its mission. Additionally, EO 13834 has been revoked by Executive Order 13990, Protecting Public Health and the Environment and Restoring Science To Tackle the Climate Crisis, which "directs all executive departments and agencies to immediately review and, as appropriate and consistent with applicable law, take action to address the promulgation of federal regulations and other actions during the last 4 years that conflict with these important national objectives, and to immediately commence work to confront the climate crisis" [38].

A major shift in 'green' policy has been seen in the early 2020s, with multiple examples of legislation focused on climate change and sustainability going into effect in just a few short years. This change will be discussed later in this section, but it should be noted that a need still exists to further develop legislation, policy, and regulations to make substantial impact on a 'greener' nation.

5.2. Military Agencies

Many of the benefits of 'green' best practices are valuable to the U.S. military. As discussed above, these practices can help to improve safety for soldiers in the field and increase security of military bases, all while decreasing operational costs. For these reasons, the Department of Defense (DOD) has released yearly Sustainability Reports and Implementation Plans (SRIP), and branches of the military have already identified sustainability as an organization-wide goal. For example, the Navy, Army, Air Force, and National Guard, all have sustainability policies already in place, though these policies largely only reference goals and plans outlined in EOs and the DOD SRIP.

The DOD Sustainability plan released in 2020 identifies four major priorities: energy resilience, water efficiency, sustainable acquisition, and electronics stewardship [39]. When detailing the progress and goals for energy resilience, the report emphasizes goals to reduce energy consumption, while noting that there are goals in place for the DOD "to produce or procure greater than or equal to 25% of the total quantity of facility energy DOD consumes within its facilities during FY 2025 and each fiscal year thereafter from renewable energy sources," but that in 2019, only "6.0% of facility electricity consumption was procured from renewable energy sources" [39]. Although the Department does not have specific water efficiency goals, DOD is successfully using innovative approaches to conserve water, save costs, and assure access to an adequate water supply for mission success [39].

DOD policies and guidance encourage the construction of high performance and sustainable buildings. Policy requires "new construction and major renovations to adhere to the Guiding Principles for Federal Sustainable Buildings" and instructs DOD buildings to obtain "at least the LEED silver level (when cost effective)" [39]. DOD policies also outline quantifiable goals for waste reduction, such as "2% reduction in non-hazardous solid waste generated in FY21 from FY20 40% diverted and 60% sent to treatment and disposal facilities in FY21" [39]. While the report contains quantifiable goals for reducing waste sent to landfills as well as reducing energy consumption and, the report mentions the goal for "continuous improvement" for other 'green' practice adoption goals [39].

In addition to implementing sustainability plans, many military branches have achieved impressive feats in implementing best practices. For example, the Weed Army Community Hospital in Irwin, California has been awarded the LEED Platinum standard, the highest level given. The facility is both carbon neutral and has net zero energy output, meaning that all electricity is generated

onsite from renewable energy sources [40]. While the military is beginning to take steps to make their facilities, fleets, and operations more sustainable, more resources, education, and support is required to make substantial lasting change across the entire organization.

5.3. Environmental Agencies

The leading U.S. government organization focused on the environment is the Environmental Protection Agency (EPA), whose mission is to protect both human health and the environment. In 2018, the EPA published Working Together: FY 2018-2022 U.S. EPA Strategic Plan [41], which gave three goals for accomplishing the above mission. These are outlined in Table 4.

Table 4: EPA FY2018-2022 Strategic Plan Goals Overview [41]

Number	Overview	Description
Goal 1	A cleaner, healthier environment	Deliver a cleaner, safer, and healthier environment for all Americans and future generations by carrying out the Agency's core mission
Goal 2	More effective partnerships	Provide certainty to states, localities, tribal nations, and the regulated community in carrying out shared responsibilities and communicating results to all Americans
Goal 3	Greater certainty, compliance, and effectiveness	Increase certainty, compliance, and effectiveness by applying the rule of law to achieve more efficient and effective agency operations, service delivery, and regulatory relief

In addition to the EPA, the Department of Energy (DOE) does considerable work related to sustainability in the energy sector. The mission of the DOE is to "ensure America's security and prosperity by addressing its energy, environmental, and nuclear challenges through transformative science and technology solutions" [42]. The DOE helps to fund research and development of clean energy technologies, collaborating across industry, academia, and government to produce new and innovative approaches to the energy crisis. Recently, the DOE announced two renewable energy investments, one with the goal to "cut the cost of solar energy by 60% within the next ten years, in addition to nearly $128 million in funding to lower costs, improve performance, and speed the deployment of solar energy technologies" and one with the goal to deploy 30 gigawatts (GW) of offshore wind by 2030 [43]. In addition, the DOE has 17 labs where they operate research topics like climate change. Within the DOE, the Office of Energy Efficiency and Renewable Energy (EERE) focuses specifically on renewable and clean energy.

5.4. Increased Government Sustainability

As stated above, there was minimal investment in 'green' before the early 2020s. No major laws and only few sustainability-focused EOs were implemented over a 15-year period. Beyond just legislation, several climate initiatives were canceled in the late

2010s, such as the Navy's Climate Task Force, and the U.S. officially withdrew from the Paris Climate Agreement in 2020 [44].

Beginning in 2021, however, drastic changes were made across the government that showcased their commitment to creating a more sustainable nation. Not only did the U.S. re-enter the Paris Climate Agreement [45], but many climate change focused EOs were put into place: Executive Order 13990: Protecting Public Health and the Environment and Restoring Science to Tackle the Climate Crisis [38], Executive Order 14008: Tackling the Climate Crisis at Home and Abroad [46], and Executive Order 14013: Rebuilding and Enhancing Programs to Resettle Refugees and Planning for the Impact of Climate Change on Migration [47]. These orders not only established various environmental policies but made a strong statement about the government's stance on the environment moving forward. For example, EO 13990 revoked the permit for the controversial Keystone XL Pipeline [38].

These initiatives grew beyond just EOs and several pieces of legislation focusing on climate change and sustainability have been put into effect. In 2021, the Infrastructure Investment and Jobs Act [48] addressed climate change concerns, specifically on its impact to the transportation system. Furthermore, the Inflation Reduction Act of 2022 [49] marked billions of dollars for climate change and energy research and development, making it the largest U.S. government investment in climate change to date. This trend was seen throughout government activities during 2022. For example, the National Strategy for Advanced Manufacturing [50] stressed the need to invest in sustainable manufacturing to further address the climate crisis.

As a nation, we need to continue this trend and continue to develop further legislation, policy, and regulations to make substantial impact on a 'greener' nation. With this increased investment in sustainability, now is the time to harmonize government 'green' policy to make lasting, impactful changes. By developing sustainability plans and practices like those used by industry, the U.S. can become a leader in the international 'green' space. By actively working on climate change and global warming issues at the national level, the government can influence other nations and make world-wide impact.

6. Industry Sustainability Trends

The observed key players in industry are considered 'green' leaders due to the publicity surrounding their environmental initiatives and publicly available sustainability policies. These yearly sustainability reports contain the company's short and long-term goals, current metrics and measurements, as well as documented progress. This showcases both their sustainability efforts and effort to cultivate the culture of sustainability, in addition to asserting the company's influence in the 'green' space.

6.1. Renewable Energy

All industry leaders investigated in this study place strong emphasis on renewable energy adoption and carbon emission reduction. Google, for example, has achieved carbon neutral-status for the last 12 years and has purchased enough renewable energy to match 100% of their global electricity consumption since 2017 [51]. Similarly, starting in 2018, Apple announced its global facilities (including retail stores, offices, data centers and co-located facilities in 43 countries) are powered with 100%

renewable energy. These renewable energy projects include Apple Park, Apple's headquarters in Cupertino, which is powered by 100% renewable energy. Power comes from multiple sources, including a 17-megawatt onsite rooftop solar installation and four megawatts of biogas fuel cells, all controlled by a microgrid with battery storage [52]. Currently, Starbucks purchases enough renewable energy to power 100% of its company-operated stores in the U.S., Canada, and the U.K. as well as making strategic investments in solar and wind farms [53].

6.2. Circular Economy

The observed industry leaders' sustainability policies also place a strong emphasis on reducing waste through a shift towards a "circular economy", one that benefits businesses, society, and the environment [54]. Google, for example, states that their goal is to "design out waste and pollution", with the aim being to eliminate release of greenhouse gases, the use of toxic and hazardous substances, the pollution of air, land, and water, and landfilling and incineration of waste at the design phase. Their designs aim to maximize product use and reuse: designing for durability, repair, reuse, remanufacturing, and ultimately recycling. Through these more durable and recyclable products, Google seeks to "create demand for recycled materials in order to accelerate the transition to a circular economy" [55]. Similarly, Apple has expanded their refurbished devices program over recent years in their shift towards a "circular economy" mentality. More than 11 million devices were sent by Apple to be refurbished for new users in 2019, a 42% increase from the previous year [53]. While Starbucks does not focus on explicitly implementing the 'circular economy' concept within their business practices, they do set goals to "reduce waste sent to landfills from stores and manufacturing by 50%, driven by a broader shift toward a circular economy" [56].

6.3. Sustainable Buildings

These companies are not only redesigning their products and packaging, but also the buildings that house their operations. By the end of 2019, over 1.4 million square meters (13 million square feet) of Google office facilities had achieved LEED certification [51]. Moving beyond LEED certification, Google is also pursuing the Living Building Challenge (LBC) Materials Petal certification for its facilities, which would certify that every building product on-site has been vetted against the LBC's Red List of worst-in-class chemicals that pose human and environmental health concerns. Similarly, "more than 50 Apple sites have received LEED or BREEAM (Building Research Establishment Environmental Assessment Method) certifications" [53]. Apple facilities feature many 'green' practices such as natural ventilation systems to highly efficient hydronic radiant heating and cooling, smart LED lighting, and high-efficiency water-cooled chillers, low-flow fixtures, and an irrigation system that uses 90% recycled water help to optimize water consumption [53]. Starbucks has similarly built more than 1,600 LEED-certified stores, but intends to go "beyond LEED, expanding the scope and breadth of [their] greener stores commitment with an open-source Greener Stores framework for design, construction and operation" [57].

6.4. Fostering a Sustainable Culture

Industry leaders are changing not only the company's buildings, but also the culture within their organization. For example, Google recognized that "reducing single-use beverages relied on behavior science insights in order to raise the desirability of sustainable and healthy options", and that a broader "culture change also matters" [55]. Similarly, Starbucks provides 'green' education materials and has "14,800 Greener Apron partners" with their goal to "empower 10,000 partners to be sustainability champions by the end of 2020" [57].

6.5. External Sustainable Investments

Companies are also making strategic investments outside of their organization. For example, Google committed to "invest roughly $150M into renewable energy projects in key manufacturing regions" to further reduce carbon emissions. These investments are not limited to just renewables - the company also "requires the highest ethical standards throughout [their] supply chain" and is "working to promote meaningful improvements in the communities in which [they] operate" [58]. Similarly, Apple has made strategic investments in renewable energy technologies. Apple not only runs its facilities on 'green' power (including solar roofs) but has "also convinced 23 companies in its supply chain to sign a pledge to get to 100% renewable energy for the portion of their business relating to Apple products" [59].

Additionally, industry leaders are creating and contributing to funds that will invest in the restoration and protection of forests and natural ecosystems globally. Apple has made several steps in this effort, including creating "a fund in partnership with Conservation International" with the goal to 'help protect and restore the world's forests, wetlands, and grasslands to remove excess carbon from our atmosphere" [53] in addition to working with the Alliance for Water Stewardship, "investing in their work to raise awareness throughout the Asia-Pacific region on this issue, to build tools and training for the AWS certification process, and to increase support for suppliers working to be certified" while encouraging suppliers to pursue AWS certifications [53].

Starbucks has stated a commitment to ethically sourced products [60] marked by their 'Coffee and Farmer Equity (C.A.F.E.) Practices, one of the coffee industry's first set of sustainability standards, verified by third-party experts', which was developed in collaboration with Conservation International (CI), and 'includes over 400,000 coffee farmers in 28 countries that are committed to improving working conditions and spanning more than a million hectares of land committed to sustainable growing practices', recognizing that the 'longevity of the coffee industry is directly linked to the social, economic and environmental conditions of coffee communities' [61]. Starbucks has also invested in reforestation efforts with '40 million trees distributed since 2015' and the goal to provide '100 million coffee trees to farmers by 2025' [57], and links social responsibility to 'green' practices, and notes in their sustainability report that the company sells "99% ethically sourced tea" and have contributed "$46 million invested in farmer loans" [57].

7. Emerging Trends

Across industry, companies are investing in renewable energy to reduce their carbon emissions and transition away from fossil fuels. At a more granular level, companies are implementing 'green' practices in their buildings using new technologies, such as water conservation techniques, natural ventilation systems, and

smart LED lighting. Companies are pursuing LEED certification for their buildings, as well as new, more rigorous certifications. We also observe a focused shift towards a "circular economy" that reuses materials where possible. Each company investigated had a strong focus on employee engagement and fostering a culture that emphasizes sustainable practices. Many of these companies are also exerting their influence on suppliers and making strategic investments (both domestic and abroad) to shape 'green' practice adoption, such as reforestation efforts and renewable energy microgrids.

It should be noted that 'green' work goes beyond industry efforts. Research is being conducted across academia to develop new technologies and practices, as well as identify areas where further 'green' work needs to be done. One example of this is data centers, which have been identified as a major contributor to carbon emissions. These centers contribute exorbitantly to power consumption and their continued growth will be unsustainable such that the energy needed to power these capabilities might be infeasible, contribute greatly to greenhouse gasses, or both. Research is currently being done to assess the state of the art in sustainable computing, as well as identifying and characterizing challenges and potential solutions [62] [63].

8. Conclusions and Research Findings

This work provides an overview of the many different definitions of 'green', in addition to highlighting emerging trends and illustrating the growing gaps between government and industry practices. These findings demonstrate the need to set goals, assign priorities, promulgate regulations, and make investments, as well as guidance for where to focus these efforts. This work is intended to provide foundational information for implementing green policy, as well as identify resources for where to look for more information when creating sustainability policies.

One of the first steps in enacting 'green' practices across the government is to formalize a single definition for the term 'green'. The EOs enacted in 2021 emphasize a need for a "whole-of-government approach to combatting the climate crisis" (which would require coordinated and deliberate approach) as well as a need to "leverage the federal government's footprint and buying power to lead by example" (which would require a consistent example and well understood priorities to follow) [46]. With a formalized definition and articulated 'green' priorities, the combined "whole of government" approach with the federal government's buying power provides unique opportunities to evaluate the national benefits and costs of pursuing more nation-wide transformational 'green' initiatives. Examples of these actions could include incentivizing a large-scale transition to all-electric vehicles and a large-scale shift to a decentralized power grid by using renewable energy based DERs and microgrids.

The phenomenon of "greenwashing," where corporations mislead consumers about their environmental performance or the environmental benefits of a product or service [64], has become increasingly widespread [65] and has eroded consumers and citizens' trust [66]. These incontinences around the term 'green' have created a misunderstanding of the true benefits of implementing more sustainable practices in the government and across the U.S. We recommend the federal government enact a top-down 'green' definition as well as 'green' priorities that will standardize how environmental suitability and planning is approached.

To capture the findings from our survey of 'green' best practices, we provide answers to our original research questions in the following sections.

8.1. What quantifiable metrics or features make a company 'green'?

This work observed that companies considered 'green' have well-documented, quantifiable improvements in their sustainability initiatives. These are published in yearly, publicly available progress reports that often include multi-year goals as well as progress over time. The goals could include reduction in carbon emissions, amount of energy obtained through renewable sources as opposed to traditional fossil fuel sources, amount of waste diverted from landfills compared to previous years and obtaining third-party certifications for sustainable buildings. We also observed quantifiable goals and developments in the areas of fleet management, water conservation techniques, and increasing 'green' requirements for suppliers.

8.2. What are 'green' best practices?

The U.S. government identifies 'green' best practices as practices that improve energy resilience, water efficiency, sustainable acquisition and lifecycle management, and electronics stewardship [39]. As mentioned, the DOD has goals to source greater than 25% of facility energy from renewable energy sources, as well as goals to incorporate innovative approaches to conserve water. DOD policies also prioritize high performance and sustainable buildings that target at least the LEED silver level. DOD policies also outline quantifiable 'green' goals for waste reduction, including quantifiable reduction in waste generated, as well as quantifiable goals for increasing the percentage waste diverted from landfills.

Industry leaders identify 'green' best practices as those that target carbon emissions, focusing on investments in both renewable energy and developing a 'circular economy' business approach. Companies are also implementing more granular 'green' practices such as water conservation techniques (including dual-plumbing systems to leverage non-potable water source where possible), natural air circulation ventilation systems, and smart LED lighting. Additionally, industry leaders emphasize employee engagement and culture shifts to promote a company culture that implements 'green' practices. Many of these companies have also invested in ways to shape 'green' practice adoption outside of their direct organization, such as reforestation efforts and renewable energy microgrids.

As discussed in Section 4.2, third-party certifications help identify 'green' best practices in the areas of sustainable buildings, business values, product manufacturing, and water use. Beyond this, third-party rankings use key performance indicators such as resource management, employee management, clean revenue, and supplier performance to grade companies. Using the well-regarded Corporate Knights method, companies are evaluated on the eight universal KPIs: percentage tax paid, pension fund status, supplier sustainability, women in executive management, women on boards, sustainability pay link score, sanctions deductions, and clean revenue.

8.3. Who are the industry leaders in the 'green' field?

Through our survey, Google, Apple, and Starbucks were identified as viable case studies for 'green' leaders in industry. It should be noted that Disney, IBM, and Dell also appear on sustainability rankings lists but were not used as the primary focus in this investigation [32]. The three chosen companies are not only acknowledged as leading 'green' institutions, but also offer publicly available sustainability reports that could both be reviewed for the purpose of this investigation but can be used as examples for other organizations developing their own plans.

9. Recommendations

To be competitive with industry and international partners, we recommend that all U.S. government agencies formalize and publicly release sustainability policies with (1) quantifiable goals aligned with the major areas industry leaders are targeting, (2) identified 'green' practices the agency plans to implement to meet these goals, and (3) metrics the agency plans to use to measure sustainable progress. As a first step to develop these goals, we recommend each agency evaluate their current organization as a baseline for improvements. The major sustainability areas discussed in this paper (renewable energy use, sustainable building, fleet management, waste reduction, water conservation, and sustainable purchasing) should be included in this investigation. Existing evaluation methods, such as the Corporate Knights ranking procedure, should be used as a guideline during the process. Once the baseline is determined, milestones and targets should be planned such that the government can meet industry standards for sustainable practices (carbon neutral, net-zero to landfill, buildings maintaining LEED certification, etc.). A new EO that standardizes agency green practices across the U.S. government would help catalyze individual agency efforts. Further U.S. government funded research on how 'green' best practices slow climate change and its adverse societal consequences, improve public health, and enhance environmental protection is also recommended.

10. Future Work

While this report outlines the changing landscape of 'green' practices, we recognize that there are a multitude of barriers inhibiting wider-spread adoption of these practices and an evaluation needs to be performed to determine what these barriers are and how to best address them. These barriers include, but are not limited to, the following: perceived cost, conflicting codes and guidelines, and lack of government resources. One of the most widely documented barriers to 'green' practice adoption is the upfront expense for implementation. Additionally, we observed that LEED certification conflicts with certain COVID guidelines, specifically for ventilation.

The next step for this research is to formally investigate these barriers to adoption to propose novel solutions to remove those barriers and enable implementation of 'green' practices and climate mitigation strategies. The authors completed an initial investigation to these barriers specially for solar photovoltaics [67] and are continuing the research.

Conflict of Interest

The authors declare no conflict of interest.

References

[1] Climate Science Special Report: Fourth National Climate Assessment, **I**, Washington, DC, 2017, doi:10.7930/J0J964J6.

[2] E. Holt, C. Corrado, "Emerging Trends in Green Best Practices," in 2021 IEEE International Symposium on Technologies for Homeland Security (HST), IEEE: 1–5, 2021, doi:10.1109/HST53381.2021.9619852.

[3] V. Ramasamy, D. Fledman, U.S. Solar Photovoltaic System and Energy Storage Cost Benchmarks: Q1 2021, 2021.

[4] P. Hawken, Drawdown: The Most Comprehensive Plan Ever Proposed to Reverse Global Warming, Penguin Books, New York, 2017.

[5] E.G. Dimanchev, S. Paltsev, M. Yuan, D. Rothenberg, C.W. Tessum, J.D. Marshall, N.E. Selin, "Health co-benefits of sub-national renewable energy policy in the US," Environmental Research Letters, **14**(8), 085012, 2019, doi:10.1088/1748-9326/ab31d9.

[6] F. Reinhardt, M. Toffel, "Managing Climate Change: Lessons from the U.S. Navy," Harvard Business Review, 102–111, 2017.

[7] S.L. Cox, L. Beshilas, E.L. Hotchkiss, Renewable Energy to Support Energy Security, Golden, CO (United States), 2019, doi:10.2172/1569691.

[8] C. Funk, B. Kennedy, Public Divides Over Environmental Regulation and Energy Policy, 2017.

[9] Pew Research Center, After Seismic Political Shift, Modest Changes in Public's Policy Agenda, 2017.

[10] A. Stansell, Which Workplace Factors Drive Employee Satisfaction Around the World, 2019.

[11] J. Nail, The Power of The Values-Based Consumer - And Of Authentic Brand Values, 2020.

[12] U.S. Green Building Council, LEED Rating System, 2022.

[13] International WELL Building Institute, WELL, 2022.

[14] GBCI, EDGE, 2022.

[15] GBCI, ParkSmart, 2022.

[16] Environmental Protection Agency, Energy Star, United States Department of Energy, 2022.

[17] GBCI, SITES, 2022.

[18] International Living Future Institute, Living Building Challenge Certification, 2022.

[19] Green Building Initiative, Green Building Initiative, 2022.

[20] BRE, BREEAM, 2022.

[21] Clearyst GBB LLC, Green Business Bureau Seal, 2022.

[22] Green America, Green America Certified Business, 2022.

[23] United States Environmental Protection Agency, WaterSense, United States Department of Energy, 2022.

[24] Global Electronics Council, EPEAT, 2022.

[25] United States Environmental Protection Agency, Safer Choice, United States Department of Energy, 2022.

[26] U.S. Department of Agriculture, USDA Organic, 2022.

[27] Fair Trade USA, Fair Trade Certified , 2022.

[28] Green Seal, Green Seal, 2022.

[29] GBCI, PEER, 2022.

[30] GRESB, GRESB, 2022.

[31] Waste & Compliance Management Inc, WasteWise, 2022.

[32] Corporate Knights, The 2020 Global 100: Overview of Corporate Knights Rating Methodology, 2021.

[33] H.R.6 - 109th Congress, The Energy Policy Act of 2005, 2005.

[34] H.R.6 - 110th Congress, Energy Independence and Security Act of 2007, 2007.

[35] D. Trump, Planning for Federal Sustainability In The Next Decade, 2015.

[36] D. Trump, Efficient Federal Operations, 2018.

[37] Environmental Protection Agency, Guiding Principles for Sustainable Federal Buildings and Associated Instructions, 2022.

[38] J. Biden, Executive Order on Protecting Public Health and the Environment and Restoring Science to Tackle the Climate Crisis, 2021.

[39] United States Department of Defense, 2020 Sustainability Report and Implementation Plan, 2020.

[40] J. Morgan, "Army hospital goes above call of duty in sustainable design," Health Facilities Management, 2017.

[41] United States Environmental Protection Agency, Working Together: FY 2018-2022 U.S. EPA Strategic Plan, 2018.

[42] United States Department of Energy, United States Department of Energy, 2022.

[43] United States Department of Energy, Energy Secretary Granholm Announces Ambitious New 30GW Offshore Wind Deployment Target by 2030, United States Department of Energy, 2021.

[44] J. Simkins, "Navy quietly ends climate change task force, reversing Obama initiative," Military Times, 2019.

[45] J. Biden, Paris Climate Agreement, 2021.

[46] J. Biden, Tackling the Climate Crisis at Home and Abroad, 2021.

[47] J. Biden, Rebuilding and Enhancing Programs to Resettle Refugees and Planning for the Impact of Climate Change on Migration , 2021.

[48] H.R.3684 - 117th Congress, Infrastructure Investment and Jobs Acts, 2021.

[49] H.R.5376 - 117th Congress, Inflation Reduction Act of 2022, 2022.

[50] Subcommittee on Advanced Manufacturing, National Strategy for Advanced Manufacturing , 2022.

[51] R. Porat, Google, Our 2020 Environmental Report, 2021.

[52] Apple, Apple now globally powered by 100 percent renewable energy, 2018.

[53] Apple, Environmental Progress Report: Fiscal Year 2019, 2020.

[54] Ellen MacArthur Foundation, The Circular Economy in Detail, Ellen Macarthur Foundation, 2017.

[55] Google, A Circular Google, Google, 2019.

[56] J. Warnick, 5 things to know about Starbucks new environmental sustainability commitment, Starbucks, 2020.

[57] Starbucks, Global Social Impact Report, 2019.

[58] Google, Our Approach to Sustainability , Google, 2019.

[59] M. Sullivan, "Apple Now Runs On 100% Green Energy, And Here's How It Got There," Fast Company, 2018.

[60] Starbucks, 2020 Report: Coffee, 2021.

[61] Starbucks, Making Coffee the World's First Sustainably Sourced Agricultural Product, Starbucks Stories & News, 2015.

[62] S. DeLong, A. Tolk, "Sustainable Computing and Simulation: A Literature Survey," in 2021 Winter Simulation Conference (WSC), IEEE: 1–12, 2021, doi:10.1109/WSC52266.2021.9715447.

[63] C.R. Corrado, S.M. DeLong, E.G. Holt, E.Y. Hua, A. Tolk, "Combining Green Metrics and Digital Twins for Sustainability Planning and Governance of Smart Buildings and Cities," Sustainability, **14**(20), 12988, 2022, doi:10.3390/su142012988.

[64] M.A. Delmas, V.C. Burbano, "The Drivers of Greenwashing," California Management Review, **54**(1), 64–87, 2011, doi:10.1525/cmr.2011.54.1.64.

[65] L.M. Baum, "It's Not Easy Being Green … Or Is It? A Content Analysis of Environmental Claims in Magazine Advertisements from the United States and United Kingdom," Environmental Communication, **6**(4), 423–440, 2012, doi:10.1080/17524032.2012.724022.

[66] M.D.T. de Jong, K.M. Harkink, S. Barth, "Making Green Stuff? Effects of Corporate Greenwashing on Consumers," Journal of Business and Technical Communication, **32**(1), 77–112, 2018, doi:10.1177/1050651917729863.

[67] C. Corrado, E. Holt, L. Schambach, "Barriers to Solar Photovoltaic (PV) Adoption on a National Scale in the United States," in 2022 IEEE 49th Photovoltaics Specialists Conference (PVSC), IEEE: 1110–1117, 2022, doi:10.1109/PVSC48317.2022.9938533.

Operating Systems Vulnerability - An Examination of Windows 10, macOS, and Ubuntu from 2015 to 2021

Jasmin Softić[*], Zanin Vejzović

Faculty of Computer Science, Sarajevo School of Science and Technology, 71000 Sarajevo, Bosnia and Herzegovina

A R T I C L E I N F O	A B S T R A C T
	This study investigated the vulnerabilities of three operating systems: Windows 10, macOS, and Ubuntu. The analysis of secondary data obtained from the CVE and NVD databases for the study period demonstrates varying OS vulnerability. Quantitative assessment of the vulnerability (using the vulnerability score) for the investigated operating systems found consistent results in the security vulnerability of these OS. The correlation of the disclosed vulnerabilities data and the average weighted vulnerability yielded coefficients of -0.3674, -0.4081, and 0.3473 for macOS, Windows 10, and Ubuntu Linux. These results demonstrate windows 10 as having the highest security vulnerability, followed by macOS. Ubuntu Linux had the lowest vulnerability scores. These results were validated by the CVSS distribution of the vulnerability score. The results point to the impact of the popularity of OS on the number of attacks in a given period. OS used by many people tend to attract significant attacks testing their integrity, security, and safety.

1. Introduction & Background

With the advent of big data and analytics, the internet and information systems have become increasingly important for organizations. The growth in the significance of information and computer systems has witnessed increased attacks characterized as malware, virus, or ransomware. Since 2017, cybercriminals have increasingly deployed ransomware to information systems, gained access to files, encrypted them, and demanded millions of dollars from victims for a decryption key. According to [1], ransom demands have increased significantly since 2020. Others also observed cyber-attacks have evolved and are difficult to detect. The success of these attacks points to a continuing vulnerability in information technology systems that attackers can exploit to their advantage. According to the Common Vulnerabilities and Exposures (CVE) (n.d.), a vulnerability refers to "a weakness in the computational logic (e.g., code) found in software and hardware components that, when exploited, results in a negative impact on confidentiality, integrity, or availability." Therefore, operating system (OS) vulnerability can be described as exposures or weaknesses within an OS that allows a cyber-attacker/intruder to undermine the integrity of the OS, or any system installed on it as per [2], [3] and others.

OS vulnerability can either be due to errors in the development process or unpatched or outdated OS that increases the opportunity for security breaches as described in [2] and [4] When coupled with negative user behaviors such as those examined by [5] and others, these vulnerabilities provide attackers with easy access to a system. Outdated software is also a growing cause of vulnerability as it does not take into consideration new updates released as a result of new research or studies indicating their areas of weaknesses [6], though some studies indicate outdated software is difficult to compromise than up to date software [7]. Particularly, attackers have exploited these vulnerabilities to execute Ransom denial of service (RDoS) attacks that have cost individuals and organizations millions of dollars across the world [5], [8]. Besides a denial of service, other vulnerabilities reported by vulnerability databases and vendors include code execution, overflow, exploits, memory corruption, SQL injection, gaining of privileges, HTTP response splitting, file inclusion, XSS, and directory traversal. These vulnerabilities are reported alongside the vulnerability life cycle. Various studies have been conducted on the vulnerability life cycle of software applications and operating systems. They include [9]-[12] studies. While the vulnerability cycle of operating systems is still under exploration, researchers tend to agree that the life cycle is divided into five crucial stages as illustrated in Figure 1. These stages include (a) vulnerability birth or creation (the time when OS weakness is created), (b) vulnerability discovery (the time when OS vulnerability is identified by vendor) (c)

vulnerability disclosure (vendor makes the vulnerability known to the public), (d) patch availability (vendor provides a quick fix to the weakness), and (e) patch installation (the public users of the affected OS install the quick fix solution to address system weakness) [9], [11]. In [3] the author suggested an extra stage described as the "exploit stage" to be inserted between the first and fifth stages indicating that the vulnerability of the system could be exploited before the availability of a patch. They provided a clear demonstration of the vulnerability life cycle as demonstrated in Figure 1.

The time intervals between these stages carry different risks for users for a given system vulnerability. These risks have been given different names. The period between vulnerability discovery or its disclosure to when the patch is installed to fix it is known as the days of risk [3]. The terms black risk, grey risk, and white risk are utilized to describe the awareness of the public regarding vulnerability. Black risk describes the lack of public awareness about the existence of vulnerability in the software or hardware they use.
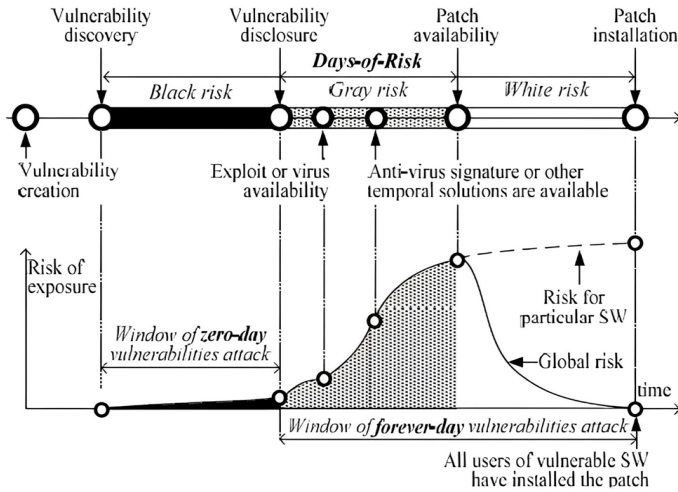
Figure 1: Vulnerability life cycle for software products

While developers and researchers continue to investigate how to address these vulnerabilities, attacks continue to be reported for new product releases by various vendors, indicating the continued existence of errors or weaknesses in the new OS development or evolution of attacks with the ability to overcome OS updates and upgrades. Besides, OS vendors also release patches to their old operating systems to fix vulnerabilities that could be exploited by attackers. Some OS vulnerabilities have been reported, while others have not. For reported vulnerabilities, patches have been released soon before they are exploited. However, for other OS weaknesses, vendors have taken longer to release patches, further exposing users of their products to cyber risks [13]. Enterprise operating systems by major technology companies, including Windows, macOS, Ubuntu, and Google Chrome OS, have been attacked due to their vulnerabilities as discussed by [14], [15] and [16] in their studies. These vulnerabilities have been defined in the literature. However, this study focuses on selected vulnerabilities reviewed in Table 1.

Table 1: OS vulnerabilities

Vulnerability	Definition and Impact of Attack
DoS	An attack meant to shut down OSs, servers, or computing systems making them inaccessible to intended users. DoS attacks can lead to bandwidth depletion or resource depletion [17]
Code Execution	In this type of vulnerability an attacker is able to run an arbitrary code of their choosing with system level privileges on an OS or server that possesses the appropriate weakness. A remote code execution can lead to a denial-of-service attack and sensitive data exposure [18]
Overflow	An overflow is vulnerability in coding errors that attackers can exploit to access systems without authorization. An attacker can manipulates coding errors, altering an application path, and overwrite system memory with this vulnerability [19] ,[20]
Memory Corruption	Entails the altering of OS memory without explicit assignment due to programming errors [21]
Sql Injection	A vulnerability type that allows an attacker to interfere with the queries of applications to their databases, allowing them to access sensitive data [22]
XSS (Cross-site scripting)	This vulnerability makes it possible for attackers to interfere with user interaction with the OS or an application by allowing them to circumvent same origin policy [23],[24]
Directory Traversal	A system weakness that provides an attacker with a means for reading arbitrary files on the server running certain applications. It allows attackers access to sensitive information and data [25]
Http Response Splitting	A web application vulnerability caused by the failure of an application to properly sanitize various input values [26]. Its impacts include web-cache poisoning, XSS attacks, and cross user defacement.
Bypass something	Entails the exploitation of weak OS authentication mechanisms allowing the attacker to access system data [27]
Gain Information	Vulnerabilities that allow attackers to gain information from an operating system
Gain Privileges	OS weaknesses that provide a means for hackers to gain system privileges without proper authentication

A review of the literature by the researcher found limited investigations into the vulnerabilities of popular enterprise operating systems. In [28] conducted a vulnerability assessment of Windows 10 and employed CVE data to test the security of the system. In [29] author examined Linux OS security and how updates can help overcome some of its vulnerabilities. Additionally, in [3] the author examined the vulnerabilities of six

operating systems, including Ubuntu, Red Hat, Windows, macOS, Oracle, and Linux. The study analyzed data from 2012 to 2016. In [3] study is among those that extensively utilized already existing vulnerability data to assess different OSs. However, there are no recent studies examining the vulnerability of the operating systems in the context of increased cyber-attacks and cyber wars between countries before and after COVID-19. The researcher attempts to fill this gap by examining the vulnerability of three popular OSs including Ubuntu, Windows, and macOS. The study focuses on the period 2015 to 2021 to investigate how OS vulnerability has changed over the years amid these cyber wars. The year 2015 is considered because the researcher wants to observe the changes in the subsequent years to understand how vulnerability statistics have changed over the years.

2. Study Objectives

This paper aims to identify changes in operating systems vulnerability over the study period even as cyber wars increase globally to extend literature findings and contribute to the body of knowledge on OS security. To address the research gaps, this study is guided by the following objectives:

- Analyze vulnerabilities that have been disclosed and fixed by respective vendors for the operating systems under study.

- Perform a quantitative comparison of the vulnerability (using the vulnerability score) for different operating systems for the period under study.

- Identify the major vulnerabilities common to the operating systems under examination reported by vendors.

- Identify how OS vulnerabilities have changed over the years (increased or decreased) at the time when significant global attacks (such as ransomware) have been reported.

3. Research Methods

This study employs data from two major databases that aggregate OS statistics to investigate the security vulnerabilities of the selected operating systems. These databases are the Common Vulnerabilities and Exposures System (CVE) and the National Vulnerabilities Database (NVD). CVE (https://cve.mitre.org/) and NVD (https://nvd.nist.gov/) make vulnerability data readily available through their websites. While there are other institutions (such as VNDB and Security Tracker) providing data on the vulnerability of operating systems and other software, the researcher considers CVE and NVD data to be sufficient for this study.

CVE is provided by MITRE Inc., a not-for-profit organization that generates a list of known vulnerabilities and assigns them a CVE-ID. The ID is used for synchronizing with CVE, enabling data exchange. NVD, on the other hand, is provided by the U.S. National Institute of Standards and technology. NVD provides a classification of the severity of the vulnerability and type, which are crucial for this study. The severity of the vulnerability is classified using a CVSS (Common Vulnerability Scoring System) score. Other scoring systems include the Common Platform Enumeration Dictionary (CPE) and the Common Weakness Enumeration Specification (CWE). CWEs are used to classify OS vulnerabilities and provide "a common language of discourse for

discussing, finding, and dealing with causes of software security vulnerability as they are found in code, design, or system architecture",[30].A single vulnerability is represented by a unique CWE. A hierarchical structure is utilized to hold CWEs, enabling multiple levels of abstraction. For example, CWE-311 (missing encryption for sensitive data) is split into CWE-312 (clear-text storage of sensitive information) and CWE-319 (clear-text transmission of sensitive information). The study identifies the most common vulnerabilities facing these OSs using their CWEs. The study examines data from 2015 to 2021, a six-year period. The operating systems to be examined are Windows 10 (by Microsoft Corporation), Mac OS (from Apple Inc.), and Ubuntu (Canonical Ltd.). The vendors for the selected operating systems often issue bulletins about the vulnerabilities in their operating systems. These vendors and their operating systems were chosen because of their popularity among users, suggesting their attractiveness to malicious attackers. It is expected that the higher the number of users for an operating system, the elevated the rate of vulnerability identification and reporting. This ensures the researcher accesses sufficient data for analysis. The study period is chosen to ensure the collected data has an element of reliability by combining vulnerability data for old operating systems and recent operating systems. In [3] the author argued that NVD and CVE vulnerability reports are statistically insufficient for the most recent versions of operating systems. For Microsoft, the operating system under investigation is Windows 10, released on 29 July 2015. For Canonical, vulnerabilities for Ubuntu Linux operating systems are examined. The Apple operating system investigated in this study has undergone several changes in name over the years. Mac OS X data is utilized in this study. Data extracted from these websites are analyzed using Microsoft Excel software to attain the study objectives.

4. Results and Discussions

4.1. Disclosed Vulnerabilities

Table 2 lists these operating systems and the number of vulnerabilities reported from 2015 to 2021. Between 2015 and 2021, the Ubuntu OS [31] reported the highest number of vulnerabilities followed by Windows 10 [32], and macOS [33] came in the third position as illustrated in Table 2.

Table 2: Disclosed cumulative vulnerabilities for the selected Oss

Year	Windows 10	Ubuntu Linux	macOS
2015	57	321	407
2016	172	319	218
2017	262	228	308
2018	258	860	110
2019	448	484	308
2020	807	423	306
2021	485	25	315
Total	**2489**	**2660**	**1972**

Table 3 shows the vulnerabilities reported for the studied OSs. The top five vulnerabilities for the three operating systems are code execution (22.97%), DoS attacks (22.83%), overflow (18.48%), memory corruption (11.25%), and gaining information (9.65%). The code execution vulnerability was highest for macOS followed by Windows 10. DoS vulnerability was highest for Ubuntu while for Windows 10, code execution was the dominant vulnerability.

Table 3: Vulnerability types reported between 2015 and 2021

	Windows 10	Ubuntu	macOS	Total	% Of All
DoS	164	823	639	1626	22.83
Code Execution	514	290	832	1636	22.97
Overflow	161	520	635	1316	18.48
Memory Corruption	49	143	609	801	11.25
Sql Injection	0	2	2	4	0.06
XSS	4	22	8	34	0.48
Directory Traversal	4	30	8	42	0.59
Http Response Splitting	0	3	0	3	0.04
Bypass something	152	122	134	408	5.73
Gain Information	336	155	199	690	9.69
Gain Privileges	205	48	121	374	5.25

Figure 2 shows the disclosed vulnerabilities for the three OSs from 2015 to 2021. The cumulative vulnerabilities for windows 10 have been increasing since 2015, while that for Ubuntu have fluctuated over the years, dropping in 2017 and shooting to the highest in 2018, before dropping further to the lowest for the three OSs.
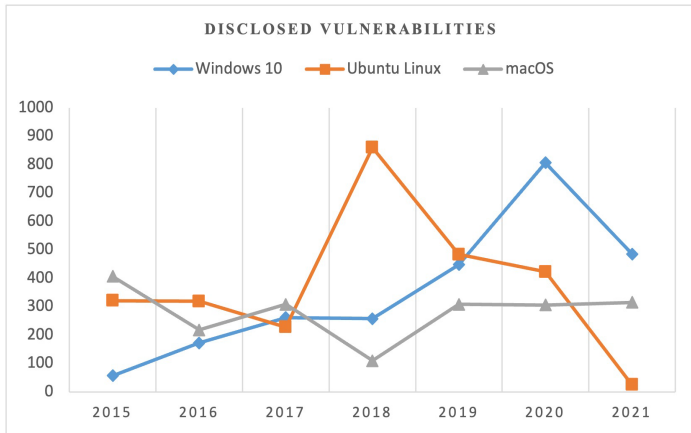
Figure 2: Disclosed vulnerabilities for windows 10, Ubuntu, and macOS (2015 to 2021)

4.2. Vulnerability Scores for Operating Systems – CVSS

Table 4 provides the weighted average vulnerability level for the three operating systems for the study from the CVE databases for the period under study. The weighted average score for each OS was retrieved from the CVE website by searching each year from January to December. Each CVSS score (0-1, 1-2, 2-3…9-10) is assigned the reported number of vulnerabilities and a percentage which are then utilized to compute the weighted average CVSS score. For example, the data for computing the 2015 weighted average for windows 10 can be found in [34]. The process is repeated for the entire period for all the OSs. The average vulnerability score for the study period is computed utilizing a similar approach.

Table 4 and Figure 3 shows the average vulnerability severity level by aggregating common vulnerability scoring system (CVSS) from the CVE database. The figures illustrate macOS to have higher vulnerability scores while Ubuntu has the lowest average for the study period. Vulnerabilities of the Ubuntu Linux are least critical with an average of 6.0 followed by Windows 10 and lastly macOS.

Table 4: Weighted average vulnerability severity for OSs from CVE (CVSS Score)

Year	Windows 10	Ubuntu Linux	macOS
2015	7.6	6.6	7.0
2016	7.5	6.0	7.6
2017	5.4	6.2	7.3
2018	5.8	6.0	7.1
2019	6.9	6.0	7.0
2020	6.2	5.4	6.9
2021	5.7	4.9	6.7
Weighted Average CVSS score	6.2	6.0	7.0
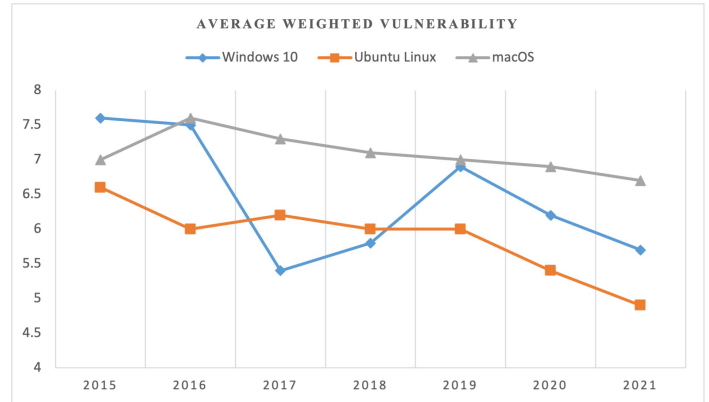
Figure 3: Average weighted vulnerability for the OS

4.3. Disclosed Vulnerability vs Average Weighted Vulnerability

Correlation between disclosed vulnerabilities and average weighted vulnerabilities for the study period yielded coefficient of -0.4081, 0.3473, and -0.3674 for windows, ubuntu, and macOS respectively. The coefficients suggest Ubuntu Linux OS as having the lowest severities while windows has the highest security severities resulting from their vulnerabilities during the study period.

4.4. Vulnerability Severity

The impact of a vulnerability on the integrity, confidentiality, and security of a system is described as vulnerability severity. Vulnerability severity is quantified using the CVSS systems that assigns a score from zero (least severe) to ten (most severe) [35]. A CVSS score is computed from a combination of various metrics including the easiness of exploitation of a vulnerability and its impact (https://www.first.org/cvss/specification-document).

The calculation of the vulnerability severity score utilized in this study is achieved utilizing three metric group – base, temporal, and environmental metrics. The base metric generates a vulnerability score from 0 to 10 and is intrinsic to a vulnerability and does not change. The base score is then modified by scoring environmental and temporal metric. Temporal metrics are those that change over the lifetime of a vulnerability while environmental metric consider the specific environment where the vulnerability exists (www.balbix.com).

NVD uses two ratings of severity scores namely CVSS v2.0 and the CVSS v3.0. Under CVSS v2.0, a range of 0.0 to 3.9 is classified as low, 4.0-6.9 as medium, and 7.0-10.0 (High). In CVSS v3.0, 0.0 denotes no vulnerability, 0.1-3.9 (low), 4.0-6.9 (medium), 7.0-8.9 (High), and 9.0-10.0 (Critical) 35.

Table 4 presents the average severity for the three operating systems for each year and the average for the study period.

Table 5 provides data for the different severity levels for the three operating systems for the study period.

Table 5: Number of vulnerabilities by severity score

Year	OS	Number of vulnerabilities by severity score									
		0-1	1-2	2-3	3-4	4-5	5-6	6-7	7-8	8-9	9-10
2015	Windows 10	0	1	6	0	5	0	7	21	0	17
	Ubuntu	0	3	12	13	60	72	48	88	2	23
	macOS	0	5	22	6	48	52	107	118	3	46
	Total	0	9	40	19	113	124	162	227	5	86
2016	Windows 10	0	3	18	4	18	6	12	54	0	57
	Ubuntu	0	9	22	11	103	61	47	41	0	25
	macOS	0	1	11	2	37	17	30	39	3	78
	Total	0	13	51	17	158	84	89	134	3	160
2017	Windows 10	0	52	36	4	56	7	36	45	2	24
	Ubuntu	0	0	8	2	84	42	39	51	0	2
	macOS	0	0	22	0	62	21	65	44	0	94
	Total	0	52	66	6	202	70	140	140	2	120
2018	Windows 10	0	26	46	4	63	7	29	54	1	28
	Ubuntu	0	9	52	19	295	151	159	164	2	9
	macOS	0	0	9	0	26	9	17	20	0	29
	Total	0	35	107	23	384	167	205	238	3	66
2019	Windows 10	0	3	64	4	97	28	21	111	3	117
	Ubuntu	0	4	25	25	147	100	81	92	1	9
	macOS	0	1	22	2	56	51	71	30	1	74
	Total	0	8	111	31	300	179	173	233	5	200
2020	Windows 10	0	1	104	11	310	16	79	209	1	76
	Ubuntu	0	7	42	25	179	78	55	29	0	8
	macOS	0	1	20	4	73	32	72	34	0	70
	Total	0	9	166	40	562	126	206	272	1	154
2021	Windows 10	0	0	72	9	192	37	97	64	0	14
	Ubuntu	0	1	10	2	4	1	0	7	0	0
	macOS	0	1	18	0	91	25	103	22	2	53
	Total	0	2	100	11	287	63	200	93	2	67
Sum-Total	Windows 10	0	86	346	36	741	101	281	558	7	333
	Ubuntu	0	33	171	97	872	505	429	472	5	76
	macOS	0	9	124	14	393	207	465	307	9	444
	Total	0	128	641	147	2006	813	1175	1337	21	853

Figure 4 shows OS distribution by severity levels. All the OS have the highest quantity of vulnerability at a severity level between 4 and 5. Ubuntu has the lowest critical level severity while macOS has the highest numbers. No operating system has a score between 0 and 1.
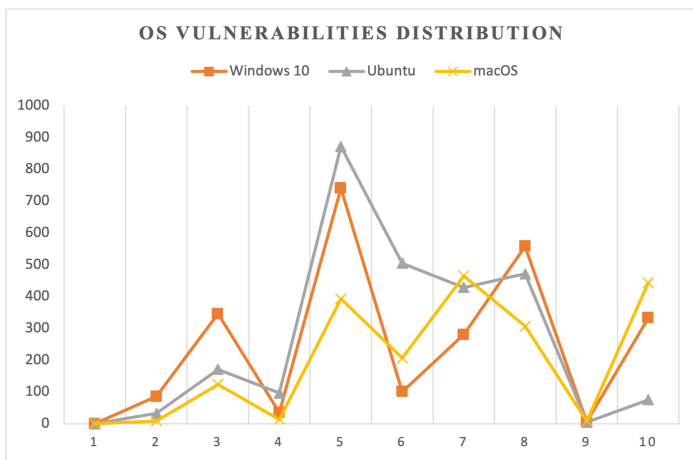

Figure 4: OS vulnerabilities distribution by CVSS severity level

4.5. The Most Common Vulnerabilities

OSs vulnerabilities are classified using the CWE scheme by NVD as proposed by MITRE. The study identified common vulnerabilities as CWE-119, CWE-19, and CWE-20 for macOS and Ubuntu and CWE-119, CWE-19, CWE-20, CWE-281 for Windows 10.

- MITRE Corporation describes CWE-119 as the "improper restriction of operations within the bounds of a memory buffer". The "software performs operations on a memory buffer, but it can read from or write to a memory location that is outside of the intended boundary of the buffer".[36]
- CWE-19 – Weaknesses in the processing of data
- CWE-20 – described as "improper input validation which may result in altered control flow, arbitrary code execution or illegal access to and control of resources"
- CWE-281 – Weakness in the proper presentation of permissions as the software fails to preserve permission or incorrectly preserves it during copying, restoring, or sharing of objects.

5. Discussion and Conclusion

The rise in cyber-attacks in recent years is demonstrated by the findings of this study. Using the operating system vulnerability data from CVE and NVD, this study has shown that operating systems of different versions continue to be attacked and exploited due to their vulnerabilities. However, Windows 10 was attacked more than other OS, demonstrating the impact that a high number of users utilizing a particular OS could have on their long-term security and integrity.

Cybercriminals and attackers exploit these weaknesses to exploit these operating systems to the detriment of the users. Between 2015 and 2021, Ubuntu reported the highest vulnerability (2660), followed by Windows 10 (2489), and lastly macOS (1972). MacOS seems to be most secure of the three operating, but not exempted from further exploitation. The low vulnerability may also suggest low disclosure rates by Apple compared to the other developers. Among the three OSs, code execution was the most common type of vulnerability followed by DoS. Nonetheless, Ubuntu had the lowest vulnerability score while macOS had the highest suggesting that the few vulnerabilities reported for macOS were very serious compared to the many reported for Ubuntu or Windows. The implication of this study is that OS developers and companies need to enhance the security of their products extending findings by [3]. A change in software development processes and practices for disclosing vulnerabilities needs to be effected to enhance the security, confidentiality, and integrity of these systems and, therefore, the user's data. While this study focused on three OS, future work can study more than one OS of different versions using data from multiple sources to develop relationships between vulnerabilities, actual executed exploits, and system safety rating for a given period.

References

[1] D. Palmer, Ransomware demands are growing, but life is getting tougher for malware gangs, ZDNET, 2022.

[2] Kelley Karin, Vulnerability in Security: A Complete Overview, Simplilearn, 2022.

[3] A. Gorbenko, A. Romanovsky, O. Tarasyuk, O. Biloborodov, "From Analyzing Operating System Vulnerabilities to Designing Multiversion Intrusion-Tolerant Architectures," IEEE Transactions on Reliability, **69**(1), 22–39, 2020, doi:10.1109/TR.2019.2897248.

[4] A. Al-Boghdady, K. Wassif, M. El-Ramly, "The Presence, Trends, and Causes of Security Vulnerabilities in Operating Systems of IoT's Low-End Devices," Sensors, **21**(7), 2329, 2021, doi:10.3390/s21072329.

[5] L. Li, W. He, L. Xu, I. Ash, M. Anwar, X. Yuan, "Investigating the impact of cybersecurity policy awareness on employees' cybersecurity behavior," International Journal of Information Management, **45**, 13–24, 2019, doi:10.1016/j.ijinfomgt.2018.10.017.

[6] I. Astaburuaga, A. Lombardi, B. la Torre, C. Hughes, S. Sengupta, "Vulnerability Analysis of AR.Drone 2.0, an Embedded Linux System," in 2019 IEEE 9th Annual Computing and Communication Workshop and Conference (CCWC), IEEE: 0666–0672, 2019, doi:10.1109/CCWC.2019.8666464.

[7] M. Vasek, J. Wadleigh, T. Moore, "Hacking Is Not Random: A Case-Control Study of Webserver-Compromise Risk," IEEE Transactions on Dependable and Secure Computing, **13**(2), 206–219, 2016, doi:10.1109/TDSC.2015.2427847.

[8] L. Tung, FBI warning: This ransomware uses DDoS to threaten victims. Here's what to watch out for, ZDNET, 2022.

[9] L. Bilge, T. Dumitras, "Before we knew it," in Proceedings of the 2012 ACM conference on Computer and communications security - CCS '12, ACM Press, New York, New York, USA: 833, 2012, doi:10.1145/2382196.2382284.

[10] S. Frei, M. May, U. Fiedler, B. Plattner, "Large-scale vulnerability analysis," in Proceedings of the 2006 SIGCOMM workshop on Large-scale attack defense - LSAD '06, ACM Press, New York, New York, USA: 131–138, 2006, doi:10.1145/1162666.1162671.

[11] J. Ruohonen, S. Hyrynsalmi, V. Leppänen, "Software Vulnerability Life Cycles and the Age of Software Products: An Empirical Assertion with Operating System Products," in Conference: Advanced Information Systems Engineering Workshops, 207–218, 2016, doi:10.1007/978-3-319-39564-7_20.

[12] A. Raza, W. Ahmed, "Threat and Vulnerability management life cycle in operating systems. A systematic review," Journal of Multidisciplinary Engineering Science and Technology (JMEST), **9**(1), 2022.

[13] S. Farhang, J. Weidman, M.M. Kamani, J. Grossklags, P. Liu, "Take It or Leave It," in Proceedings of the 34th Annual Computer Security Applications Conference, ACM, New York, NY, USA: 490–504, 2018, doi:10.1145/3274694.3274733.

[14] F. Alharbi, Y. Zhou, F. Qian, Z. Qian, N. Abu-Ghazaleh, "DNS Poisoning of Operating System Caches: Attacks and Mitigations," IEEE Transactions on Dependable and Secure Computing, **19**(4), 2851–2863, 2022, doi:10.1109/TDSC.2022.3142331.

[15] M. Araba Vander-Pallen, P. Addai, S. Isteefanos, T. Khan Mohd, "Survey on Types of Cyber Attacks on Operating System Vulnerabilities since 2018 onwards," in 2022 IEEE World AI IoT Congress (AIIoT), IEEE: 01–07, 2022, doi:10.1109/AIIoT54504.2022.9817246.

[16] F. Alharbi, J. Chang, Y. Zhou, F. Qian, Z. Qian, N. Abu-Ghazaleh, "Collaborative Client-Side DNS Cache Poisoning Attack," in IEEE INFOCOM 2019 - IEEE Conference on Computer Communications, IEEE: 1153–1161, 2019, doi:10.1109/INFOCOM.2019.8737514.

[17] R. v. Deshmukh, K.K. Devadkar, "Understanding DDoS Attack & its Effect in Cloud Environment," Procedia Computer Science, **49**, 202–210, 2015, doi:10.1016/j.procs.2015.04.245.

[18] S.-P. Oriyano, R. Shimonski, Client-Side Attacks Defined, Elsevier: 1–24, 2012, doi:10.1016/B978-1-59-749590-5.00001-8.

[19] C. Cowan, F. Wagle, Calton Pu, S. Beattie, J. Walpole, "Buffer overflows: attacks and defenses for the vulnerability of the decade," in Proceedings DARPA Information Survivability Conference and Exposition. DISCEX'00, IEEE Comput. Soc: 119–129, doi:10.1109/DISCEX.2000.821514.

[20] K.-S. Lhee, S.J. Chapin, "Buffer overflow and format string overflow vulnerabilities," Software: Practice and Experience, **33**(5), 423–460, 2003, doi:10.1002/spe.515.

[21] J. Xu, P. Ning, C. Kil, Y. Zhai, C. Bookholt, "Automatic diagnosis and response to memory corruption vulnerabilities," in Proceedings of the 12th ACM conference on Computer and communications security - CCS '05, ACM Press, New York, New York, USA: 223, 2005, doi:10.1145/1102120.1102151.

[22] M. Junjin, "An Approach for SQL Injection Vulnerability Detection," in 2009 Sixth International Conference on Information Technology: New Generations, IEEE: 1411–1414, 2009, doi:10.1109/ITNG.2009.34.

[23] A. Shrivastava, S. Choudhary, A. Kumar, "XSS vulnerability assessment and prevention in web application," in 2016 2nd International Conference on Next Generation Computing Technologies (NGCT), IEEE: 850–853, 2016, doi:10.1109/NGCT.2016.7877529.

[24] M. Liu, B. Zhang, W. Chen, X. Zhang, "A Survey of Exploitation and Detection Methods of XSS Vulnerabilities," IEEE Access, **7**, 182004–182016, 2019, doi:10.1109/ACCESS.2019.2960449.

[25] M. Flanders, "A Simple and Intuitive Algorithm for Preventing Directory Traversal Attacks," ArXiv, 2019.

[26] D. Kshirsagar, S. Kumar, L. Purohit, "Exploring usage of ontology for HTTP response splitting attack," in 2015 1st International Conference on Next Generation Computing Technologies (NGCT), IEEE: 437–440, 2015, doi:10.1109/NGCT.2015.7375156.

[27] A. Atamli-Reineh, R. Borgaonkar, R.A. Balisane, G. Petracca, A. Martin, "Analysis of Trusted Execution Environment usage in Samsung KNOX," in Proceedings of the 1st Workshop on System Software for Trusted Execution, ACM, New York, NY, USA: 1–6, 2016, doi:10.1145/3007788.3007795.

[28] J. Softic, Z. Vejzovic, "Windows 10 Operating System: Vulnerability Assessment and Exploitation," in 2022 21st International Symposium INFOTEH-JAHORINA (INFOTEH), IEEE: 1–5, 2022, doi:10.1109/INFOTEH53737.2022.9751274.

[29] M.R. Yaswinski, M.M. Chowdhury, M. Jochen, "Linux Security: A Survey," in 2019 IEEE International Conference on Electro Information Technology (EIT), IEEE: 357–362, 2019, doi:10.1109/EIT.2019.8834112.

[30] n.d., NVD Vulnerabilities, NVD, 2022.

[31] n.d. - CVE, Canonical Ubuntu Linux: CVE security vulnerabilities, versions and detailed reports, CVE, 2022.

[32] n.d. - CVE, Microsoft Windows 10: CVE security vulnerabilities, versions and detailed reports, CVE, 2022.

[33] n.d.-CVE, Apple Mac Os X : CVE security vulnerabilities, versions and detailed reports, CVE, 2022.

[34] n.d.-CVE, Computing Weighted average for Windows 10 , CVE, 2022.

[35] n.d.-NVD, NVD Vulnerability Metrics, CVE, 2022.

[36] n.d., Improper Restriction of Operations within the Bounds of a Memory Buffer (4.8), CWE, 2022.

ASTES

Design and Analysis of a Virtual Synchronous Generator Control Scheme to Augment FRT Capability of PMSG-Based Wind Turbine

Heera Jahan Prema[*,1], Md. Rifat Hazari[1,2], Mohammad Abdul Mannan[1,2], Md. Abdur Rahman[1,2]

[1]Department of Electrical and Electronic Engineering, American International University-Bangladesh (AIUB), 408/1, Kuratoli, Khilkhet, Dhaka 1229, Bangladesh

[2]Center for Sustainable Energy Research (CSER), Dr. Anwarul Abedin Institute of Innovation, American International University-Bangladesh (AIUB), 408/1, Kuratoli, Khilkhet, Dhaka 1229, Bangladesh

A R T I C L E I N F O

A B S T R A C T

Massive integration of inverter dominated renewable energy systems (RESs), i.e., wind turbines (WTs), reduces the reliance on conventional alternator-based power stations. The system inertia and damping aspects of the power system were significantly decreased by this extensive integration of inverter-based WT system, which impacts on the fault ride-through (FRT) competence and thus precipitates the frequency instability. Modern grid code instructed to operate the WT system similar like conventional power plants. However, most of the conventional inverter controller failed to fulfil the requirement. To compensate for the issues, an advanced control method of a VSG for variable speed wind turbines with a permanent magnet synchronous generator (VSWT-PMSG) is proposed by this work. The proposed control scheme mimics the behavior of a conventional alternator and includes an active-power frequency control scheme with a governor model accompanied by an automatic voltage regulator (AVR) model, along with a current feedback loop system which enhance the system inertia and consider damping aspects of the system during serious fault conditions, i.e., three line to ground (3LG) fault. The suggested VSG-based inverter controller's functionality has been verified using the simulation model.

1. Introduction

The importance of moving away from fossil fuels to clean, dependable, and affordable RES is a paramount and immediate concern. Furthermore, being an increasingly important source of intermittent renewable energy, the wind energy generation system begins to have huge effects on the power grids nowadays, considering the increased grid penetration of wind farms (WFs) and updated power level of WTs in the energy generation systems. After all, renewable energies are abundant in nature, clean, and safe compared to other energy sources, an ultimate source of green power, and widely accessible. Undoubtedly, one of the most prominent and efficient sources of renewable energy technologies is wind power.

2022 is predicted to be another significant year for wind power developments, specifically for the quickly expanding offshore wind industry, as stated in the Global Wind Report 2022 from the Global Wind Energy Council (GWEC). Globally, 94 GW of wind capacity have been established, including 21 GW offshore, making 2021 the second-best year for the global wind industry. Offshore installation is about to play a bigger role in the leading global wind capacity development. By 2026, the global offshore wind market is anticipated to expand from 21.1 GW in 2021 to 31.4 GW [1].

Among different types of WT systems, PMSG is a popular alternative for installing new WF because of various advantages, including variable speed operation, ability to regulate active and reactive power autonomously, benefit of omitting the gearbox and brush, and inexpensive maintenance [2-3]. However, a massive integration of PMSG-based WT systems in the power grid reduces dependency on traditional units and influences the power system's transient stability.

The new grid code required that the WF work in the same way as traditional units and maintain grid stability during transient states. One of the important criteria of voltage stability is fault ride through (FRT) capability [4].
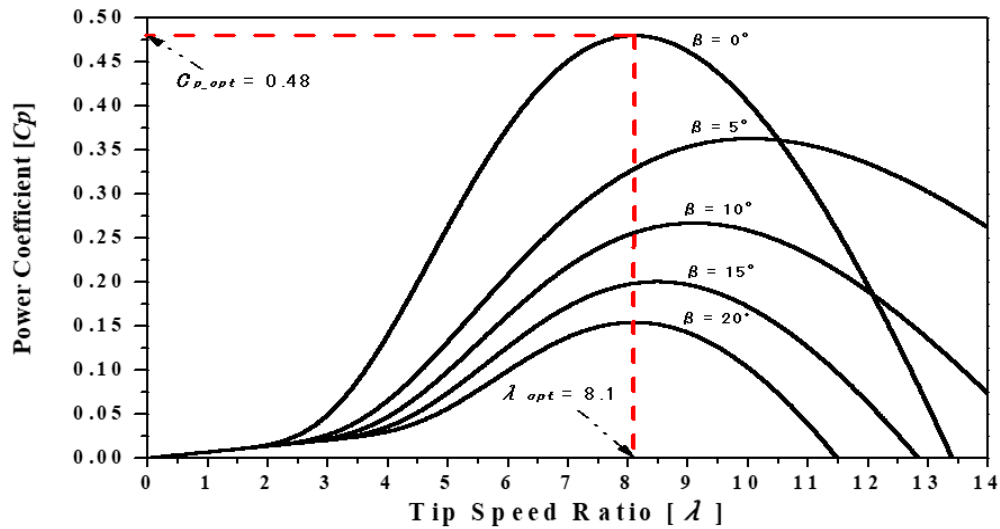
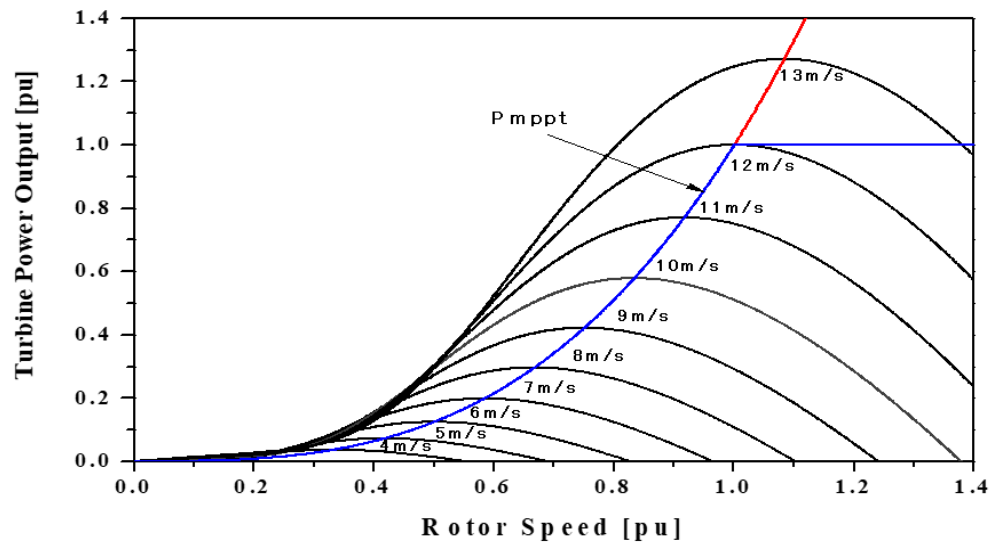Figure 1: C_p vs. λ characteristic curve.

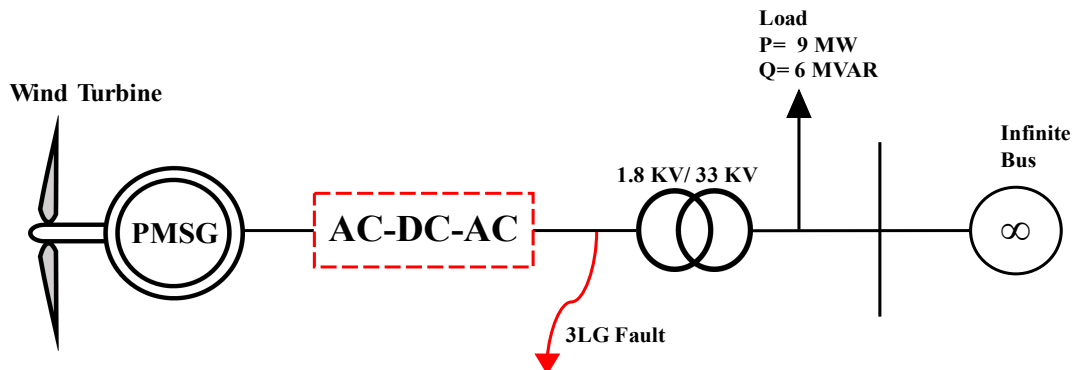Figure 2: Wind generator power response at different wind speed.

Figure 3: Power system model.

Several control mechanisms have been utilized to augment the FRT capability of the PMSG system. For example, well known cascaded control strategy presented in Refs. [5-7]. However, the conventional cascaded control mechanism can't ensure FRT capability properly.

Also, some auxiliary devices, for example, supercapacitors [8], energy storage systems (ESS) [9], static synchronous compensators (STATCOM) [10], unified power flow controllers (UPFC) [11], flywheel energy storage system (FESS) [12] and superconducting magnetic energy storage (SMES) [12] etc., has been applied to augment FRT competence of PMSG system. However, all the auxiliary devices will increase the overall system cost.

Additionally, some inherent control modifications can be made for PMSG to improve the FRT capability. For example, The machine-side converter (MSC) regulates the DC-link voltage and the wind turbine's grid-side converter (GSC) accomplishes the maximum power point tracking (MPPT) in the new control scheme [13].

As a result, the surplus power on the DC-side may be lowered by decreasing the active power generated by the PMSG when the grid-side voltage drops. Thereafter, DC-side voltage stability is simplified. However, in typical conditions, the performance of the control technique mentioned above is erroneous.

In [14], pitch control was used to cut down on the available wind power. The rotor and the DC-link capacitor store the additional power. The GSC also provided the backup for reactive power. The pitch control, on the other hand, is a slow mechanical process that can't respond right away to changes in the system. Also, changing the angle of the pitch too often wears down equipment and shortens the life of the PMSG.

Recently, Researchers are actively concentrating on inverter systems established on VSG principle [15]. In Reference [16] portrayed a basic concept that aims to mimic the properties of a SG while simultaneously providing dampening and inertial support.

Based on the aforementioned contemplations, developing a control scheme based on the VSG technology that enables the PMSG system to improve FRT competency of the system is the main goal of the work. The AVR, damping characteristics, and mechanical governor behavior are all emulated by the suggested inverter control technique for PMSG. With the help of AVR, the proposed VSG system will inject the right amount of reactive power to restore the voltage level.

To assist with the proposed work, the performance of a PMSG-based WF was evaluated in terms of its FRT capabilities, taking into account the 3LG fault, which is the most severe situation. The simulation exhibits the FRT capabilities of the proposed VSG control technique as well as the smooth operation of the PMSG system.

2. Wind Turbine Model

WT power generation relies upon the interaction of the turbine rotor with the wind.

Accessible wind power,

$$P_{wind} = \frac{1}{2}\rho A V_w^3 \tag{1}$$

here, A and V_w are the area used by rotor blades and wind speed, respectively.

In accordance with the Betz law, under an ideal state of affairs, the maximum power that an ideal turbine rotor with an infinite number of blades can produce from wind is 59.26% of the power accessible in the wind.

WTs are restricted to having two or three rotor blades because of underlying and economic contemplations. Thus, how much power they can pull out is nearer to around 50% of the accessible wind power. The Power coefficient C_p represents the ratio of obtainable power to available power.

$$C_p = \frac{Extracted\ power}{Power\ in\ wind} = \frac{P_{rotor}}{P_{wind}} \tag{2}$$

Thus, the extractable power can be written as [17]:

$$P_{wind} = \frac{1}{2}C_p\rho A V_{wind}^3 \tag{3}$$

Finally, the mechanical power output of the turbine is expressed in the following equation:

$$P_w = 0.5\rho\pi R^2 V_w^3 C_p(\lambda,\beta) \tag{4}$$

In this equation, P_w denotes the extracted wind power, $R =$ radius of rotor (m), $C_p =$ Power coefficient, $\rho =$ air density (kg/m^3). Equation of C_p is as follows [5]:

$$C_p(\lambda,\beta) = c_1\left(\frac{c_2}{\lambda_i} - c_3\beta - c_4\right)e^{\frac{-c_5}{\lambda_i}} + c_6\lambda \tag{5}$$

$$\frac{1}{\lambda_i} = \frac{1}{\lambda - 0.08\beta} - \frac{0.035}{\beta^3 + 1} \tag{6}$$

$$\lambda = \frac{\omega_r R}{V_w} \tag{7}$$

$$T_w = \frac{P_w}{w_r'} \tag{8}$$

here, T_w represents the torque of the turbine, $\beta =$ pitch angle (degree), $\omega_r =$ rotor speed (rad/s), c_1 toward $c_6 =$ turbine's characteristic coefficients ($c_1 = 0.5176, c_2 = 116, c_3 = 0.4, c_4 = 5, c_5 = 21, c_6 = 0.0068$) [5,17-18]. λ represents the tip speed ratio.

Figure 1 shows the characteristic graph of C_p vs. λ. The graph is established for a diverse value of β from Equation (5). Here, the optimum value for $\lambda(\lambda_{opt}) = 8.1$, and for the optimal value of $Cp(Cp_{opt}) = 0.48$ [5].

The maximum power point (MPPT) of the PMSG system is displayed in Figure 2 [5].

3. Power System Model

Figure 3 represents a power system model employed to analysis the transient stability of the system. The control strategy and construction of the system are portrayed in the diagram. The system model consists of a WT, a PMSG, a DC/AC, and an AC/DC inverter system. It is a 20 MW system connected to an infinite bus by a 1.8 kV/33 kV transformer. A load of 9 MW and 6 MVAR is attached to the system through the transformer. All the necessary parameters of PMSG system are taken from [19].
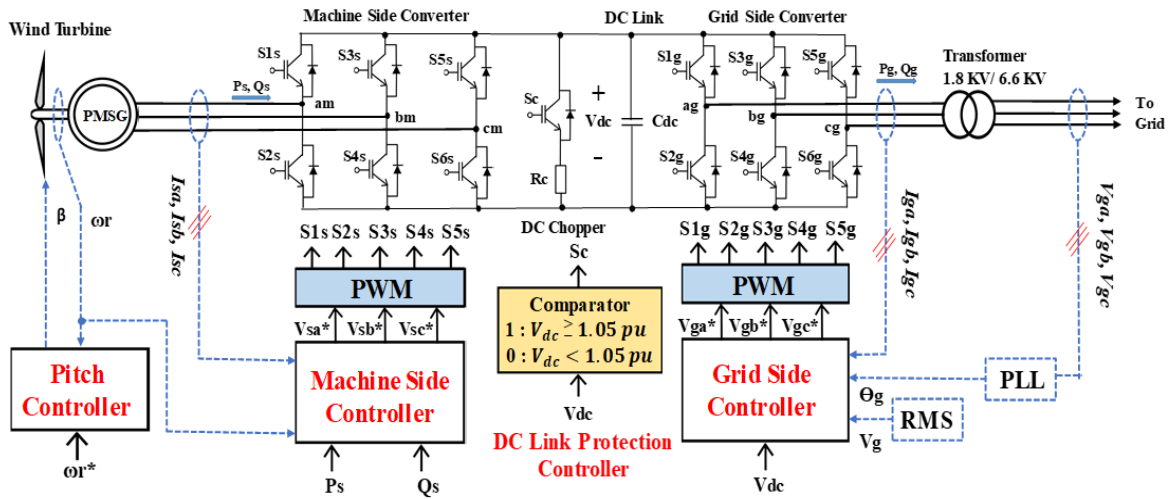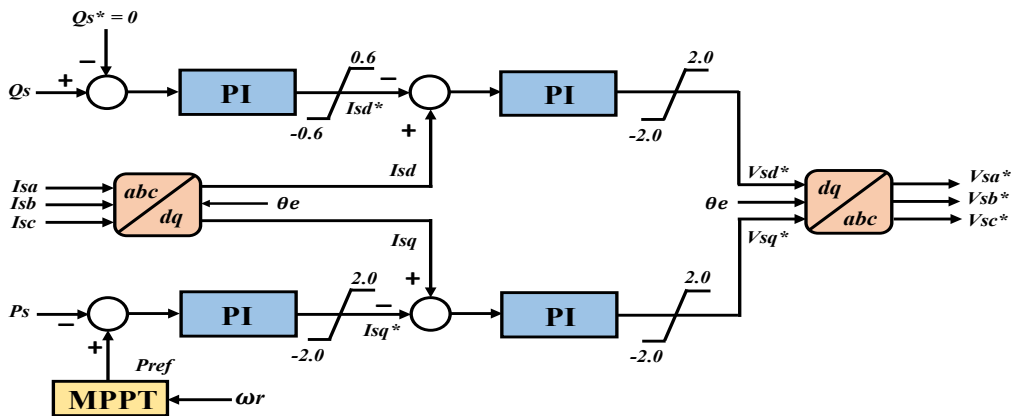
Figure 4: Arrangement of PMSG system.
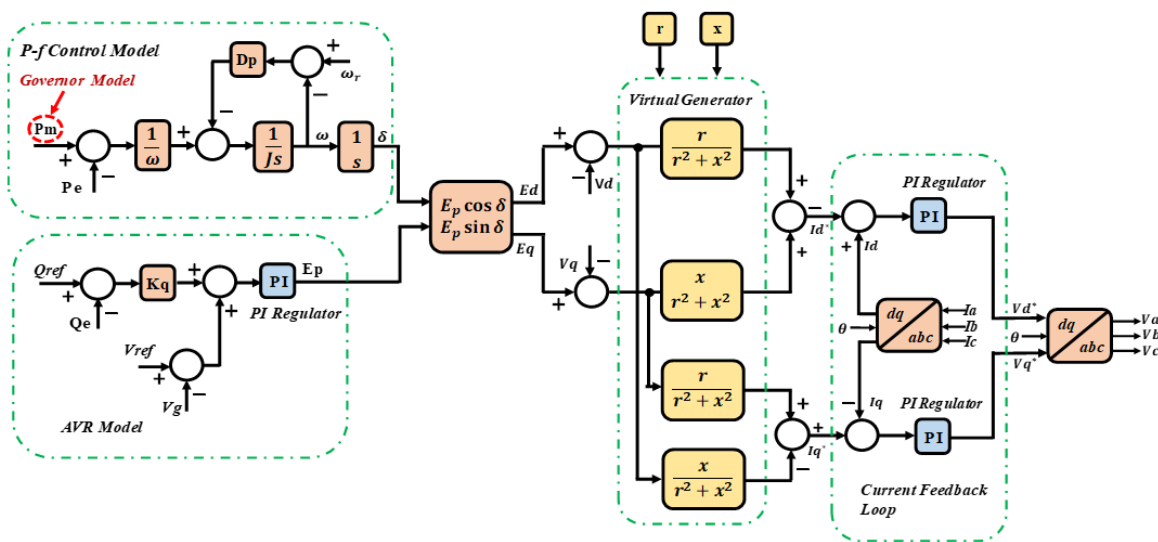

Figure 5: Machine side controller.

Figure 6: Proposed VSG control strategy.

4. PMSG Model and Control System

PMSG is a VSWT generator system furnished with a comprehensive power electronic frontier. Figure 4 portrays the control system and design layout of a PMSG-based VSWT. The total system consists of PMSG, WT with drive train models, pitch angle control system, VSG controlled grid side inverter (GSI), and machine side converter (MSC). Two levels of IGBT are used here to build both the converter circuits used in the system. The MSC and the VSG controller are in charge of controlling the converters. The MSC has a direct link to the stator terminal of PMSG. The GSI system is connected to the grid using step-up transformers. The analysis in this study makes use of the already-available PMSG model from the PSCAD library [20].

The comparator circuit block controls the DC chopper circuit that is included in the DC-link protection controller system. The comparator initiates the DC chopper circuit when the DC-link voltage (V_{dc}) is $\geq$ 1.05 pu and consequently, safeguards the DC-Link system. This system utilizes the PWM strategy, and for both converters, the carrier frequency of 3.0 kHz and the rated V_{dc} of 3.0 kV are chosen [21].

4.1. Machine Side Controller

The MSC converts the entire three-stage, unregulated AC voltage that the PMSG produces into DC voltage. Figure 5 represents the control scheme for the MSC arranged by using four PI controllers. There are two loops in the controller mechanism. The upper loop is employed for reactive power, and the lower loop is responsible for the active power. In the PMSG, the q-axis current (I_{sq}) controls the active power (P_s), and the current of the d-axis (I_{sd}) controls the reactive power (Q_s).

The reference active power (P_{ref}) is determined utilizing the MPPT algorithm. The procedure is narrated in section 3 of this paper. The reference reactive power (Q_s^*) has been set to zero in order to execute the operation regarding the unity power factor [21].

4.2. Proposed VSG Control Strategy

This section briefly portrays the proposed controller of VSG. Figure 6 addresses the generally introduced VSG control procedure. The proposed control framework incorporates a governor model, an AVR model, and a virtual generator model along with a current feedback loop.

4.3. VSG Model

The impedance model for VSG is shown in Figure 7. The armature resistance and the synchronous reactance of the generator are represented by r and x, respectively. The field windings generate an electromotive force which is designated by E_p and δ denotes the load angle between the rotor and the grid.

The voltage of the grid and its prolongation toward axis d and q axis is expressed by V_g, V_d, and V_q respectively. Similarly, I_d^* and I_q^* characterize the armature currents for the axis d and q, respectively and are illustrated in the subsequent equation.

In order to regulate the command regarding the current inverter system, the above-described parameters are occupied.

$$\begin{cases} \begin{bmatrix} I_d^* \\ I_q^* \end{bmatrix} = Y \left\{ \begin{bmatrix} E_d \\ E_q \end{bmatrix} - \begin{bmatrix} V_d \\ V_q \end{bmatrix} \right\} \\ Y = \frac{1}{r^2+x^2} \begin{bmatrix} r & x \\ -x & r \end{bmatrix} \\ \begin{bmatrix} E_d \\ E_q \end{bmatrix} = E_p \begin{bmatrix} \cos \delta \\ \sin \delta \end{bmatrix} \end{cases} \tag{9}$$
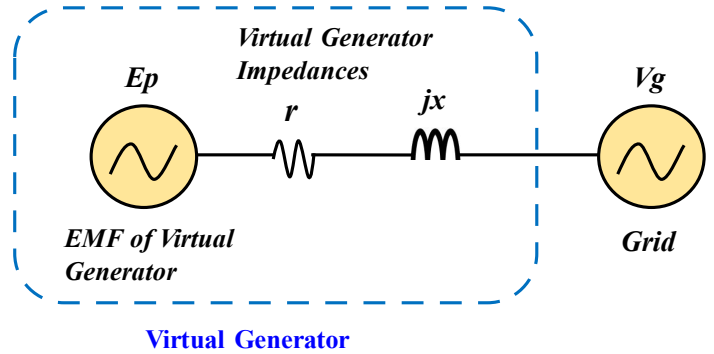
Figure 7: VSG impedance model.

4.4. Active Power-Frequency Control Strategy

The grid frequency can be managed by utilizing the VSG control system. VSG control in the inverter circuit empowers the required control for primary frequency by coordinating a suitable measure of power via inertial feedback. The VSG algorithm obtains the load angle (δ) with the utilization of the swing equation. The swing equation depends on the changes in active power. The equations stated in this section represent the principal contraption of the VSG [22-23].

$$(P_m - P_e)/\omega - D_p(\omega - \omega_r) = J\frac{d\omega}{dt} \tag{10}$$

$$\frac{d\delta}{dt} = \omega \tag{11}$$

Similarly, as a SG, the reference active power and the instantaneous active power are addressed by P_e and P_m successively. Here, the droop constant is represented by D_p, J represents the inertia, angular frequency is represented by ω, and the reference angular frequency by ω_r accordingly. Besides, a governor model is also employed to carry out the task of controlling the input power directive according to frequency alteration. Figure 8 shows the governor model.
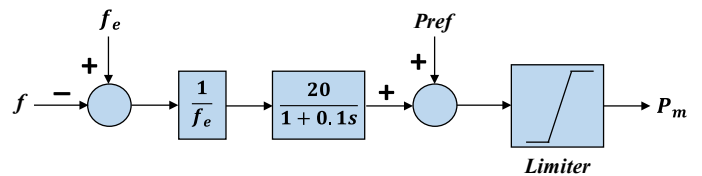
Figure 8: Governor Model.

4.5. AVR Model

By utilizing a fundamental excitation strategy of the SG, the reactive power-voltage regulatory system is possible to plan. Figure 6 portrayed the control strategy. The following equation contemplates the resulting voltage:

$$E_p = \left\{ (Q_{ref} - Q_e)K_q + (V_{ref} - V_g) \right\} \left(K_p + \frac{K_i}{s} \right) \tag{12}$$

Q_{ref} denotes the reference value of reactive power, whereas Q_e stands for the instantaneous reactive power, the reference voltage is expressed by V_{ref}, and the terminal voltage is expressed by Vg, respectively. Kq represents droop control for the reactive power. Kp and Ki, respectively, are used to denote the proportional and integral gains of the PI controller.

4.6. Current Feedback Loop

As depicted in Figure 6, a pair of PI regulators make up the current feedback loop. The mentioned PI regulators remunerate the current of the axis d and q to produce the reference value for d and q axis voltage. The fundamental inclination of the alteration is acquired via the grid network.

5. FRT Requirement for Wind Power Generation

Power quality, reliability, and the electrical grid's stability are just a few of the issues that have arisen owing to the massive incorporation of large-scale wind energy generation facilities into the utility network. The transmission system operators (TSOs) have been urged to update grid codes to accommodate the technical specifications of wind power facilities as a result of this integration [24]. Wind generators having an FRT facility is one of the crucial requirements of WF grid codes which implies that ordinary power production ought to be continued rapidly immediately after the apparent grid voltage has been retrieved after facing disruption in the power production.

FRT prerequisites for the WFs are illustrated in Figure 9 [25]. Suppose there is a voltage dip situation in the system within the predetermined RMS value and the duration of the voltage drop is within the predefined value. In that case, the WFs must stay in operation with the grid. The conditions are illustrated in Figure 9.
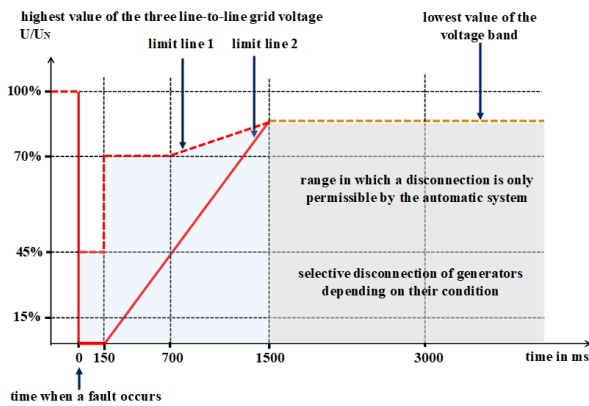
Figure 9: FRT requirement for WF.

Every WT inside the WF hereby remains in operation without any trip on the off chance that the connection point's voltage recuperates the appraised voltage by 90% in 1.5 seconds after the voltage dip situation. This guarantees that wind generation is not interrupted by routinely cleared defects. Utilities also stipulate that wind turbines have voltage stability for set amounts of time and that they must be able to maintain the grid during fault incidents.

6. Simulation Results and Discussions

The power system model presented in Figure 3 was employed to conduct the simulation work utilizing the PSCAD/EMTDC software. As depicted in Figure 3, a 3LG fault is applied near the inverter of the PMSG to investigate the system's transient stability.

The fault happened at 5.0 s, and lasts for 0.05 s. The CB opens at 5.1 s and then closes once more at 6 s based on the supposition that the fault condition has disappeared.

The fault and CB conditions are presented in Figure 10. The total time span of the simulation is considered as 10 s due to transient stability analysis and system frequency is 50 Hz.

Figure 10: 3LG fault conditions.
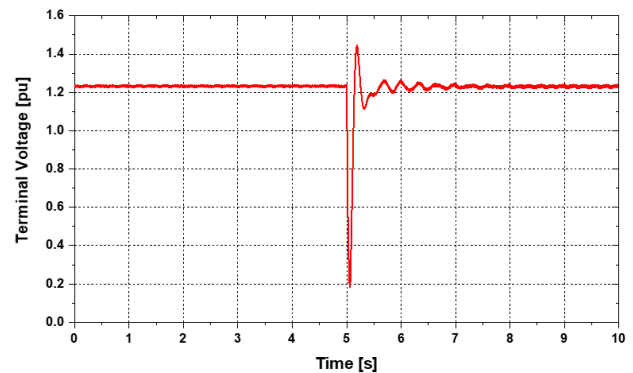
Figure 11: Terminal voltage response.
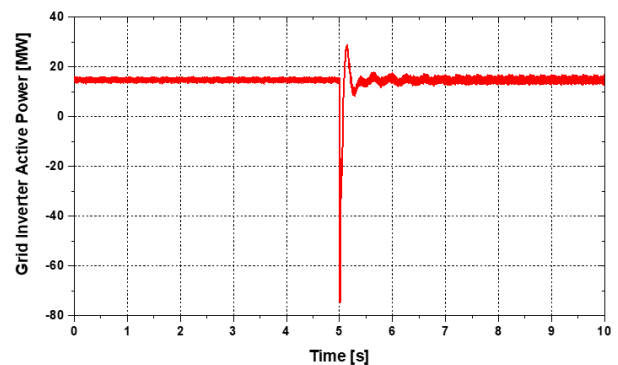
Figure 12: Active power response of grid inverter.

On the assumption that the wind speed wouldn't change for a short while, the applied wind speed to PMSG is maintained constant under rated conditions. Figure 11 through 14 presents the findings from the simulation work. The terminal voltage response of PMSG is illustrated in Figure 11. Initially stable, a voltage dip happened during the fault time. However, the terminal voltage quickly returns to the nominal value after the fault duration and follows the grid code discussed in Section 5. This graph clearly indicates the FRT capability of the proposed VSG control approach.

Figures 12 to 13 show that the PMSG's active and reactive power responses are stable following the fault. Finally, Figure 14 presented the PMSG's rotor speed response. The rotor speed is oscillating more between 5.0 s to 6.0 s. This is because, the severe fault occurs at 5.0 s. Even though, the response is fluctuating during the fault period, the rotor speed is stable after the fault clearance.

Therefore, it may be said that the proposed VSG technique has shown significant effectiveness and efficiency in stabilizing the PMSG system during severe fault periods along with enhancing the FRT capability.
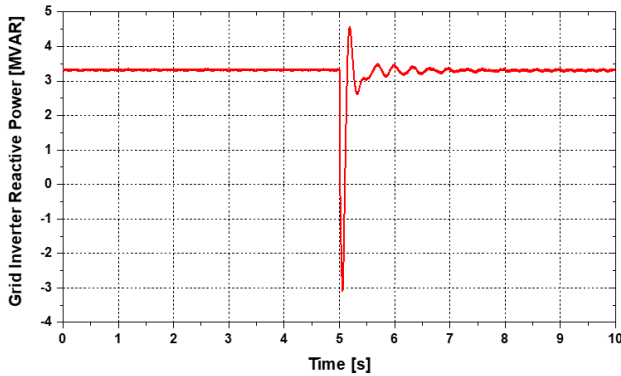
Figure 13: Reactive power response of grid inverter.
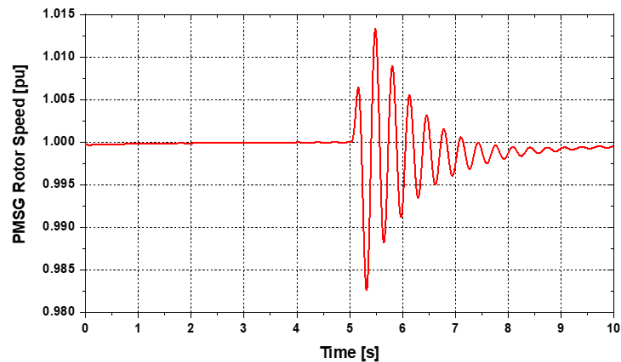
Figure 14: Rotor speed response of PMSG.

7. Conclusion

The most sustainable and renewable source of electricity is still wind. However, the system must be able to sustain voltage dip situations brought on by system faults according to the current WF grid code, which is impossible with a conventional control mechanism but with a VSG control approach. This paper proposes and analyzes a VSG control mechanism for a PMSG-based wind turbine to enhance the system stability and FRT capability of a grid-connected wind energy generation system. All details of the proposed approach, including diagrams along with the related simulation findings, are provided in this paper. According to the simulation results, the system can withstand a severe fault event (3LG fault).

Acknowledgment

References

[1] Global Wind Report 2022, Global Wind Energy Council (GWEC), 2022, (https://gwec.net/global-wind-report-2022/, Accessed on: 30 June, 2022).

[2] Muyeen, S.M., Tamura, J. and Murata, T., Stability Augmentation of a Grid Connected Wind Farm, Springer-Verlag, London, 2009.

[3] L. Zhongyi et al., "Impact Study of PMSG-Based Wind Power Penetration on Power System Transient Stability Using EEAC Theory," Energies, **8**(12), 13419–13441, 2015, doi:10.3390/en81212377.

[4] A. A. MERI, Y. AMARA and C. NICHITA, "Impact of Fault Ride-Through on Wind Turbines Systems Design," in 2018 7th International Conference on Renewable Energy Research and Applications (ICRERA), 567–575, 2018, doi:10.1109/ICRERA.2018.8566910.

[5] M. Rosyadi, A. Umemura, R. Takahashi, J. Tamura, N. Uchiyama, and K. Ide, "Simplified Model of Variable Speed Wind Turbine Generator for Dynamic Simulation Analysis," IEEJ Transactions on Power and Energy, **135**(9), 538–549, 2015, doi:10.1541/ieejpes.135.538.

[6] R. C. Pawaskar and T. B. More, "Improvement in low voltage ride through capability of PMSG based wind energy system," in 2016 International Conference on Global Trends in Signal Processing, Information Computing and Communication (ICGTSPICC), 444–447, 2016, doi:10.1109/ICGTSPICC.2016.7955342.

[7] M. Jahanpour-Dehkordi, S. Vaez-Zadeh and J. Mohammadi, "Development of a Combined Control System to Improve the Performance of a PMSG-Based Wind Energy Conversion System Under Normal and Grid Fault Conditions," IEEE Transactions on Energy Conversion, **34**(3), 1287–1295, Sept. 2019, doi:10.1109/TEC.2019.2912080.

[8] E. Sathya and P. Maruthupandi, "Enhancement of Low Voltage Ride Through Capability for PMSG Based Wind Energy Conversion System With Super Capacitor," in 2018 4th International Conference on Electrical Energy Systems (ICEES), 57–60, 2018, doi:10.1109/ICEES.2018.8443259.

[9] H. Fang, X. Zhang and Y. Wei, "Supercapacitor Energy Storage System based Coordinative Low-Voltage-Ride-Through Control for Wind Energy Conversion System, " in 2021 24th International Conference on Electrical Machines and Systems (ICEMS), 276–280, 2021, doi:10.23919/ICEMS52562.2021.9634199.

[10] Y. Peng et al., "Coordinated Control Strategy of PMSG and Cascaded H-Bridge STATCOM in Dispersed Wind Farm for Suppressing Unbalanced Grid Voltage," IEEE Transactions on Sustainable Energy, **12**(1), 349–359, Jan. 2021, doi:10.1109/TSTE.2020.2995457.

[11] V. Ramachandran, A. S. Perumal, N. Lakshmaiya, P. Paramasivam, and S. Dhanasekaran, "Unified Power Control of Permanent Magnet Synchronous Generator Based Wind Power System with Ancillary Support during Grid Faults," Energies 2022, **15**(19), 7385, doi:10.3390/en15197385.

[12] J. X. Jin, R. H. Yang, R. T. Zhang, Y. J. Fan, Q. Xie, and X. Y. Chen, "Combined low voltage ride through and power smoothing control for DFIG/PMSG hybrid wind energy conversion system employing a SMES-based AC-DC unified power quality conditioner," International Journal of Electrical Power & Energy Systems, **128**, 106733, Jun. 2021, doi:10.1016/j.ijepes.2020.106733.

[13] S. Alepuz, A. Calle, S. Busquets-Monge, S. Kouro and B. Wu, "Use of Stored Energy in PMSG Rotor Inertia for Low-Voltage Ride-Through in Back-to-Back NPC Converter-Based Wind Power Systems," IEEE Transactions on Industrial Electronics, **60**(5), 1787–1796, May 2013, doi:10.1109/TIE.2012.2190954.

[14] Z. Liu, C. Liu and G. Li, "Power coordinated control of wind turbines with permanent magnet synchronous generator for low voltage ride through," in IEEE PES General Meeting | Conference & Exposition, 1–5, 2014, doi:10.1109/PESGM.2014.6939204.

[15] H. Bevrani, T. Ise, and Y. Miura, "Virtual synchronous generators: A survey and new perspectives," International Journal of Electrical Power & Energy Systems, **54**, 244–254, 2014, doi:10.1016/j.ijepes.2013.07.009.

[16] K. Shi, W. Song, P. Xu, R. Liu, Z. Fang, and Y. Ji, "Low-Voltage Ride-Through Control Strategy for a Virtual Synchronous Generator Based on Smooth Switching," IEEE Access, **6**, 2703–2711, 2018, doi:10.1109/ACCESS.2017.2784846.

[17] Singh, Mohit & Santoso, Surya, Dynamic Models for Wind Turbines and Wind Power Plants, Wind Power: Systems Engineering Applications and Design Models, 2011.

[18] Matlab Documentation Center, (http://www.mathworks.co.jp/jp/help/, Accessed on: 20 December, 2016).

[19] Y. Errami, M. Ouassaid, M. Maaroufi, Control of a PMSG based Wind Energy Generation System for Power Maximization and Grid Fault Conditions, Energy Procedia, **42**, 220–229, 2013,

doi:10.1016/j.egypro.2013.11.022.

[20] PSCAD/EMTDC User's Manual (1994), Manitoba HVDC Research Center, Canada.

[21] Y. Hirase, K. Abe, K. Sugimoto, and Y. Shindo, "A grid-connected inverter with virtual synchronous generator model of algebraic type," Electrical Engineering in Japan, Wiley Online Library, **184**(4), 10–21, 2013, doi:10.1002/eej.22428.

[22] J. Meng, Y. Wang, J. Peng, L. Xu, and J. Yin, "Flexible Virtual Synchronous Generator Control for Distributed Generator with Adaptive Inertia," Electric Power Components and Systems, **47**(1-2), 128–140, 2019, doi:10.1080/15325008.2018.1563958.

[23] J. Alipoor, Y. Miura and T. Ise, "Power System Stabilization Using Virtual Synchronous Generator with Alternating Moment of Inertia," IEEE Journal of Emerging and Selected Topics in Power Electronics, **3**(2), 451–458, 2015, doi:10.1109/JESTPE.2014.2362530.

[24] O. P. Mahela, N. Gupta, M. Khosravy and N. Patel, "Comprehensive Overview of Low Voltage Ride Through Methods of Grid Integrated Wind Generator," IEEE Access, **7**, 99299-99326, 2019, doi:10.1109/ACCESS.2019.2930413.

[25] E. ON NETZ GmbH (2006) Grid Connection Regulation for High and Extra High Voltage. E. ON NETZ GmbH, Essen, Germany.

Consideration of Ambiguity in the Analysis Phase of Data Warehouses

Djamila Hammouche[*,1], Karim Atif [2]

[1]Department of computer science, Faculty of exact sciences and informatics, Hassiba Benbouali University, Chlef, 02180, Algeria

[2]Department of computer systems, Faculty of computer science, University of sciences and technology Houari Boumediene, Bab Ezzouar, Algiers, 16111, Algeria

A R T I C L E I N F O	A B S T R A C T
	We are interested in taking into account ambiguity in the analysis phase of data warehouses, using fuzzy logic. We want to offer decision makers the possibility of using natural language in this phase. We created in a previous work the Baccalaureate fuzzy data warehouse which we were able to query with seven natural language terms to which we created seven membership functions. In this work, we present a fuzzy data warehouse for server failures that we created and for which we used the same terms to which we associated seven membership functions too. And, we carried out a comparison at the end of which we concluded that the definition of the values of the membership function differs according to the context of analysis. Our solution is extensible and can be enriched with new natural terms language. The next step is to design a conversational interface that enables a natural language conversation between the decision maker and the fuzzy data warehouse.

1. Introduction

Decision makers need to use natural language in the analysis phase of data warehouses; this allows them to appreciate existing data as they wish. Our field of application is higher education where decision makers need to analyze the failure rate of servers and easily detect the machine that frequently breaks down, the type of failure, the duration in order to be able to make good forecasts.

No machine is 100% reliable. The fault tolerance criterion of the machine is expressed either in average number of hours between failures, or in number of hours of operation before the end of life of the machine. Except this criterion given by the manufacturer, the users of these machines study server failures that occur on a real time basis. It is in this context that our study is written [1].

In this paper, we present the fuzzy server failure data warehouse that we created using Mondrian environment and MDX queries [1].

We are looking for the answer to the questions:

- Which servers have an average failure rate, lowest highest, etc.?

- How to use the terms: medium, high in queries?

The rest of the paper will be organized as follows: We first explain the context of this study, we present an overview of related works, and then we detail the solution based on fuzzy logic and we present the comparative analysis, finally, we finish with conclusion.

2. The study context

The goal of all our work is to show that the use of natural language facilitates the querying of data warehouses. So, we used Fuzzy logic. We defined the membership functions of the predicates that represent the natural language terms most used by analysts. In this context, we have chosen to experiment our solution on two very distinct areas:

- The field of national education to assess the baccalaureate success rate for which we have published the results [2]-[4].
- And the field of server failures to appreciate the server failure rate that we present in this paper.

In this work, we used the same terms to experiment them in the field of server failures and we defined the corresponding membership functions.

3. Related works

In [5]-[8], the author focuses on fuzzy multidimensional data, presenting a solution based on fuzzy logic and using SQL to take

into account imperfect values and vague criteria. ReqFlex is an intuitive user interface to the definition of preferences and the construction of fuzzy queries [9]. Also, the study on the medical data warehouse recording the vital parameters (blood pressure) of patients [10]. In [11], the author adds a new fuzzy layer to the existing model without modifying the data warehouse. Linguistic concepts are integrated for the interpretation of the measurements of the fact table. This separation between the fuzzy concepts and the data warehouse constitutes the strong point of this model. This is the reason why we have retained it in all our work despite the fact that this model has not been tested on a complex system.

4. The solution based on fuzzy logic

There are in classical Boolean logic only two states: TRUE or FALSE. In [12]-[14], the author proposed Fuzzy logic in 1965. This logic makes it possible to express different levels and to describe a phenomenon linguistically, then to represent it by a small number of rules.

A fuzzy term is a natural language word. To model it, we use a trapezoidal function for which characteristic parameters are defined.

4.1. The Fuzzy server failure data warehouse model

We designed the star schema of our data warehouse [15]- [21]. In [1], the model is defined and commented. There is one fact table "FactServerFailure" and four dimension tables: "Dim_Department", "Dim_Section", "Dim_Server" and "Dim_Time".

In fact table "FactServerFailure", there are all the primary keys of all the dimension tables related to the fact table and there is the measurement Failure_rate. It is as the metric to calculate and analyze. It indicates the ratio between the number of failure of a server to the total number of failures of the servers.

Failure_rate=number of server failure*100/total number of server failures.

In the other dimension tables, we find the characteristic attributes of these tables and which constitute axes of analysis such as time, department, etc.

The integration of ambiguous terms is done through two fuzzy meta tables that we call Fuzzy_ct table and Fuzzy_mt table.

Fuzzy Fuzzy_ct table is used to store fuzzy classes associated with linguistic terms (absolutely high, average, absolutely low, etc.) and Fuzzy_mt table is used to store the membership degrees of a value to a fuzzy class and the query result expresses the degree of each failure rate to a fuzzy class. Concrete examples of these degrees of membership are illustrated in the various tables which appear in the section some results.

4.2. The membership functions

We integrated seven fuzzy predicates to qualify the failure rate as absolutely high, rather high, somewhat high, average, somewhat low, rather low and absolutely low and we defined the seven corresponding membership functions.

Table 1: The membership functions

The membership function	Values and intervals
Absolutely high	Y=0 in [0, 7], y=1 in [8, 10] and y=x-7in [7, 8].
Ratherhigh	Y=0 in [0, 6] and [9, 10], y=1 in [7, 8], y=x-6 in [6, 7] and y=-9-x in [8,9].
Somewhathigh	Y=0 in [0, 5] and [9, 10], y=1 in [6,8], y=x-5 in [5, 6] and y=-9-x in [8, 9].
Average	Y=0 in [0, 4] and [7, 10], y=1 in [5,6], y=x-4 in [4, 5] and y=7-x in [6, 7].
Somewhatlow	Y=0 in [0, 6] and [9, 10], y=1 in [7, 8], y=x-6 in [6, 7] and y=-9-x in [8, 9].
Ratherlow	Y=0 in [0, 1] and [5, 10], y=1 in [2, 4], y=x-1 in [1, 2] and y=-x+5 in [4, 5].
Absolutelylow	Y=0 in [3, 10], y=1 in [0, 2] and y=3-x in [2, 3].

4.3. Some results

We present in following some results of the realized system.

In this table appear the servers with their characteristics of the University whose failure rates we have studied since their first commissioning until the year 2020.

Table 2: List of servers studied

Server number	Physical server model	RAM	Storage
1	HP Proliant gen 05	8G	512G
2	HP Proliant gen 05	8G	512G
3	HP Proliant gen 05	8G	512G
4	HP Sauvegarde	8G	512G
5	DELL PowerEdge T300	8G	512G
6	DELL	16G	1.7T
7	HP Z420 Workstation	8G	512G
8	DELL PowerEdge T320	16G	1.7T
9	DELL PowerEdge T320	16G	1.7T
10	DELL PowerEdge T320	16G	1.7T
11	HP Proxy1	12G	900G
12	DELL Proxy2	12G	900G
13	HP server Proliant Gen 10	8G	1T
14	DELL PowerEdge T320	16G	1.7T

In this table appear the servers with failure rates

Table 3: List of servers studied with their failure rates

Server number	Physical server model	Server failure rate
1	HP Proliant gen 05	9.09%
2	HP Proliant gen 05	9.09%
3	HP Proliant gen 05	9.09%
4	HP Sauvegarde	9.09%
5	DELL PowerEdge T300	6.06%

6	DELL	5.05%
7	HP Z420 Workstation	9.09%
8	DELL PowerEdge T320	1.01%
9	DELL PowerEdge T320	5.05%
10	DELL PowerEdge T320	6.06%
11	HP Proxy1	9.09%
12	DELL Proxy2	7.07%
13	HP server Proliant Gen 10	9.09%
14	DELL PowerEdge T320	8.08%

In this table appear the servers that recorded an absolutely high rate of failure. The percentage 9.09% and 8.08% are considered absolutely high failure rates with a total degree of membership (100%) and the percentage 7.07% is considered an absolutely high failure rate with only 07% membership degree. And all the percentages of the other remaining servers are not considered absolutely high failure rates because their membership degree is 0%.

Table 4: Result of query absolutely high

Server number	Server failure rate	Membership degree
1	9.09%	100%
2	9.09%	100%
3	9.09%	100%
4	9.09%	100%
7	9.09%	100%
11	9.09%	100%
13	9.09%	100%
14	8.08%	100%
12	7.07%	07%
05	6.06%	0%
06	5.05	0%
08	1.01%	0%
09	5.05%	0%
10	6.06%	0%

In this table appear the servers that recorded an absolutely low rate of failure. The percentage 1.01% is considered an absolutely low failure rate with a total degree of membership (100%) and all the percentages of the other remaining servers are not considered absolutely low failure rates because their membership degree is 0%.

Table 5: Result of query absolutely low

Server number	Server failure rate	Membership degree
8	1.01%	100%
1	9.09%	0%
2	9.09%	0%
3	9.09%	0%
4	9.09%	0%
5	6.06%	0%
6	5.05%	0%
7	9.09%	0%
9	5.05%	0%
10	6.06%	0%
11	9.09%	0%

12	7.07%	0%
13	9.09%	0%
14	8.08%	0%

4.4. The comparative study

We found that for the same terms the meaning remains the same but the membership functions change significantly. For example, for a very high baccalaureate success rate, the percentage of success is between 90% and 100%, while for server failures the highest rate is around 10% only.

Thus, we have established the following result. The definition of the values of the membership function is closely linked to the field of study. For any natural language term, the term retains its meaning all the time but the definition of the values of the membership function which corresponds to it changes according to the context of study.

We are interested in studying the same terms with other data from similar fields to better frame the definition of values of membership functions and to arrive at a single definition for a field of study. Only multiple experiments will prove it. Also, it is interesting to experiment with these same terms in sub-domains of the same domain like studying the failure rate of computers linked to servers.

Table 6: Results comparison

The membership function	Values in Server failure context	Values in Baccalaureate context[2]
Absolutely high	Y=0 in [0, 7], y=1 in [8, 10] and y=x-7 in [7, 8].	Y=0 in [0.80], y=1 in [90,100] and y=0.1x-8 in [80, 90].
Ratherhigh	Y=0 in [0, 6] and [9, 10], y=1 in [7, 8], y=x-6 in [6, 7] and y=-9-x in [8,9].	Y=0 in [0.70], y=1 in [80, 90], y=0.1x-7 in [70, 80] and y=-0.1x+10 in [90,100].
Somewhathigh	Y=0 in [0, 5] and [9, 10], y=1 in [6, 8], y=x-5 in [5, 6] and y=-9-x in [8,9].	Y=0 in [0.50] and in [90,100], y=1 in [60, 80], y=0.1x-5 in [50, 60] and y=-0.1x+9 in [90,100].
Average	Y=0 in [0, 4] and [7, 10], y=1 in [5,6], y=x-4 in [4, 5] and y=7-x in [6, 7].	Y=0 in [0.40] and in [70,100], y=1 in [50,60], y=0.1x-4 in [40,50] and y=-0.1x+7 in [60,70].
Somewhatlow	Y=0 in [0, 6] and [9, 10], y=1 in [7, 8], y=x-6 in [6, 7] and y=-9-x in [8,9].	Y=0 in [0.30] and in [60,100], y=1 in [40,50], y=0.1x-3 in [30,40] and y=-

		0.1x+6 in [50,60].
Ratherlow	Y=0 in [0, 1] and [5, 10], y=1 in [2, 4], y=x-1 in [1, 2] and y=-x+5 in [4, 5].	Y=0 in [0.10], y=1 in [20,40], y=0.1x-1 in [10,20] and y=-0.1x+5 in [40,50].
Absolutelylow	y=1 in [0, 20].	Y=0 in [0.50] and in [90,100], y=1 in [60,80], y=0.1x-5 in [50,60] and y=-0.1x+9 in [90,100].

5. Conclusion

We presented the context of our study which concerns the two data warehouses, that of the Baccalaureate and that of Server failures. We were interested in the analysis phase of data warehouses where we were able to formulate MDX queries with natural terms using fuzzy logic and we explained some returned results. In this paper, we carried out a comparative analysis between the membership functions defined for each data warehouse and we found that even if the term of the natural language integrated into the model retains all its meaning, but the definition of the membership function which corresponds to it differs from one field of study to another, which has enabled us to affirm that the definition of the values of the membership function is strongly linked to the field of study.

Some perspectives emerge from our work, namely the insertion of new terms and the design of new query methods such as an expert system or a chatbot. Also the experimentation of the models in other establishments of the same domains to better test the defined membership functions.

Conflict of Interest

The authors declare no conflict of interest.

References

[1] D. Hammouche, K.Atif, M.Loukam, "An An expert system for fuzzy server failure data warehouse analysis," ICIST'20, Lecee, Italy, 2020, doi:10.1504/IJDSS.2021.113767.

[2] D. Hammouche, K.Atif, "An extended solution to recommend fuzzy MDX queries for decision makers by a collaborative filtering profile," International Journal of Decision Support Systems **4**(3), 257-270, 2021, doi:10.1504/IJDSS.2021.113767

[3] D. Hammouche, M. Loukam, K.Atif, K.W. Hidouci, "Fuzzy MDX queries for taking into account the ambiguity in querying the Baccalaureate Data warehouse," Control, Decision and Information Technologies (CoDIT), 4th International Conference, Barcelone, 179-183, 2017, doi:10.1109/CoDIT.2017.8102587.

[4] D. Hammouche, L. Metchat, K.Atif, K.W. Hidouci, "A solution to recommend fuzzy MDX queries for decision makers by collaborative filtering profile in baccalaureate Data warehouse," In proceedings of the 2nd Conference on Computing Systems and Applications, Algiers,190-199, 2016.

[5] A. Laurent, S. Gangarski, C. Mar-Sala, "Cooperation between a fuzzy knowledge extraction system and a multidimensional database management system, " Francophone Meetings on Fuzzy Logic and its Applications, La Rochelle, France, Cepaduèce éditions, 325-332, 2000.

[6] A. Laurent, "Fuzzy multidimensional databases," Advanced database days, Agadir, Maroc, Hermès, 107-117, 2001, doi: 10.1007/978-3-642-10663-7-4.

[7] A. Laurent, FUB et FUB MINER: deux systèmes pour la représentation, la manipulation et la fouille de données multidimensionnelles floues, Information Interaction Intelligence, **3**, 37-83, 2003.

[8] C. Favre, A. Laurent,Y. Pitarch.,P. Poncelet, "Représentation graphique des hiérarchies contextuelles : modèle avec satellites," EDA 2011, Clermont Ferrand, Revue des Nouvelles Technologies de l'Information, Vol. B-7, 23-37, 2011, corpus ID:38627526.

[9] G. Smits, O. Pivert et T. Giraults, "ReqFlex: Fuzzy Queries for Everyone,'' In proceedings of the VLDB Endowment, 1206-1209, 2013, doi: 10.14778/2536274.2536277.

[10] Y. Pitarch, A. Laurent, and P. Poncelet," A conceptual model for handling personalized hierarchies in multidimensional databases," In Proceedings of the International Conference on Management of Emergent Digital EcoSystems, France, 107–111, 2009, doi:10.1145/1643823.1643843.

[11] D. Fasel, K.Shahzad "A data warehouse model for integrating fuzzy concepts in meta table structures" 17th ECBS, Oxford, England, 100-109,2010, doi:10.1109/ECBS.2010.18.

[12] D.Dubois, H. Prade, "Using fuzzy sets in flexible querying: Why and how?," In Proc. Workshop on Flexible Query-Answering Systems, 89-103, 1996, corpus ID:33050805.

[13] D. Perez, M. J. Somodevilla, I. H. Pineda. "Fuzzy spatial data warehouse: A multidimensional model," In Eighth Mexican International Conference on Current Trends in Computer Science, 2007, doi: 10.5772/39389.

[14] D. Dubois and H. Prade, Fundamentals of fuzzy sets, **7**, 1-653, 2000, ISBN: 978-1-4615-4429-6.

[15] A.L. Zadeh , "Fuzzy sets," Journal of Information and control, **8**(3), 338-353,1965, doi:10.1016./S0019-9958(65)90241-X .

[16] M. Golfarelli, S. Rizzi., Data Warehouse Design: Modern Principles and Methodologie, Osborne/McGraw-Hill, 2009.

[17] T. Chikawa, M. Hirakawa, "ARES: a relational database with the capability of performing flexible interpretation of queries," In IEEE Transactions on Software Engineering, 624–634, 1986, doi:101109/TSE.1986.6312958.

[18] R. Agrawal., A. Gupta, "Modeling multidimensional databases," In Proceedings. 13th International Conference on Data Engineering, 232–243, 1997, doi:10.1109/ICDE.1997.581777.

[19] R. Bliujute, S. Saltenis, G. Slivinskas, C. Jensen, "Systematic Change Management in Dimensional Data Warehousing," In IIIrd International Baltic Workshop on Databases and Information Systems, Riga, Latvia, 27–41, 1998, corpus ID:10165485.

[20] R. Agrawal, A. Gupta, A. Sarawagi, "Modeling Multidimensional Databases," ICDE'97, 1997, doi:10.1109/ICDE.1997.581777.

[21] C. W. Holsapple, .K.D. Joshi, "Organizational knowledge resources," Decision Support Systems, **31**, 39-54, 2001, doi: 10.1016/S0167-9236(00)00118-4.

Interference-Aware Nodes Deployment of a LoRa-Based Architecture for Smart Agriculture in the Southern Region of Senegal

El Hadji Malick Ndoye[1,*], Ousmane Diallo[1], Nadir Hakem[2], Emmanuel Nicolas Cabral[1]

[1]*Department of Informatics, University of Assane Seck, B. P. 523 Ziguinchor, Senegal*

[2]*Université du Québec en Abitibi Témiscamingue Rouyn-Noranda, Quebec, Canada*

ABSTRACT

In Senegal, agriculture has always been seen as the foundation on which the socioeconomic development of the country rests. However, in the rural world, agriculture remains traditional at a time when the challenges of food self-sufficiency to accompany emergence are launched. In the southern part of Senegal commonly called Casamance, the abundance of rain makes it possible to practice rice cultivation and market gardening research must therefore play a leading role in the introduction of technological innovations, techniques, and decision-support tools to promote productive, competitive, and sustainable agriculture. Therefore, smart agriculture must focus on new solutions for water irrigation, soil quality, and culture monitoring. The emergence of the Internet of Things (IoT) is perceived as a very important lever for successful high-end intelligent agriculture. Indeed, the appearance of increasingly specialized monitoring sensors combined with new wireless communication technologies constitutes good decision-making tools.

The proposal of this paper consists of a new network architecture that can cover a large cultivation area to carry out water irrigation techniques in Casamance. It is, therefore, a question of identifying the best communication technology among new Low-Power, Wide Area Networks (LPWANs) such as Long-Range (LoRa), SigFox, etc which is suited to the environment considered. Also, the choice of the best deployment of sensors for better coverage. The choice of technology must be motivated by the financial costs and the range of transmission. The deployment must fix the optimal distance between the sensors minimizing the interferences according to some parameters specific to the environment. An analytical study is used on the deployment to determine the optimal distance between two gateway nodes to reduce induced interference.

1. Introduction

Today, devices tend to replace humans in their daily work. This induces a permanent interaction between connected devices and humans. Internet of Things (IoT) [1,2] can now be considered one of the most powerful tools for creating, modifying, and sharing countless amounts of information. Indeed, the IoT aims to make objects dialogue with each other and with individuals. It has become an essential means used in many fields such as health [3],[4], agriculture [5], etc. In the case of smart agriculture [6], it is mainly used to modernize the sector. Indeed, the deployment of connected objects allows farmers to have real-time information on the quality of soil, water, plants, etc. So, it offers farmers and producers the opportunity to reduce waste and improve productivity [7–9]. This ranges from the amount of fertilizer used,

and the number of trips made by agricultural vehicles, to more efficient use of resources such as water and electricity.

With new IoT tools, farmers can monitor their field conditions for real-time decision purposes. These decisions can be manual or automated according to the data collected such as humidity, light, temperature, crop health, etc. [10]. Innovations in terms of low consumption and connectivity make it possible to extend the scope of IoT applications for smart agriculture and to deploy connected objects in vast environments with strong constraints. Long Range (LoRa) [11] is a radio communication protocol that constitutes the architecture of the system and which allows low-speed but above all long-range data transmission for all your IoT-connected objects. LoRaWAN (Long Range Wide Area Network) [12] is a communication protocol that works over an LPWAN (Low Power Wide Area Network) network, while LoRa technology is the physical layer of the network. Casamance is a particular region that

stands out from other areas of Senegal due to its enormous edaphic, climatic, hydrographic, and biogeographical potential. The high rainfall combined with very dense vegetation in the region makes it sometimes easier to use LPWAN communication technologies such as LoRa rather than 802.15.4 which is a short-range technology. This paper proposes a new LoRa technology-based network architecture suitable for a smart agriculture solution in the Casamance region of Senegal. The contributions can be divided into two major parts:

- A new LoRa network architecture based on the classical one combines short and long-range LoRa radio links for making it possible to carry out smart agriculture in rural areas, particularly in the southern area of Senegal.

- Evaluation of the proposal is conducted through an analytical study used on the deployment to determine the optimal distance between two gateway nodes to reduce induced interference.

The following presents the rest of the paper. Section 2 presents the context and the motivation, and the state of the art on smart agriculture is presented in section 3. Section 4 focuses on the LoRa networks while section 5 presents the proposed architecture of the network. In section 6, we present an analytical study followed by a discussion. Finally, the paper ends with a conclusion in section 7.

2. The context and motivation

Senegal is located at the most western projection of the African continent into the Atlantic Ocean, at the confluence of Europe, Africa, and the Americas, and a crossroads of major maritime and air routes. The climate is dry tropical and characterized by two seasons: a dry season from November to June and a rainy season from July to October. Three types of vegetation: forest in the south, savanna in the center, and steppe in the north. The southern part called Casamance is the rainiest part of the country. Casamance has a very varied range of soils:

- the tropical ferruginous soils leached with concretion and armor;
- weakly ferritic soils;
- undegraded halomorphic soils;
- and moderately organic hydromorphic soils.

The climate is humid tropical with rainfall above 1200mm which decreases towards the east. It is the wettest part of Senegal (rainfall > 800mm) thanks to the presence of the monsoon flow for more than 8 months and we find 20% arable land in the country. The area benefits from a hydrographic network made up of a set of permanent and seasonal waterways called bolongs. The main one is the Casamance River (350 km).

Basse-Casamance is the administrative region of Ziguinchor and is composed of forest areas and agricultural areas (mainly rice and peanuts). The forest areas are characterized by their density, particularly to the southwest of Oussouye covered with a Guinean vegetation cover made up of large palm groves, thousand-year-old cheese groves, lianas, teak, and giant mango trees. Up to the Gambian border, the forests, often state-owned, are dense and protected. The rice fields largely dominate the agricultural landscape of Basse-Casamance as shown in Figure 1.

Figure 1: Rice fields in Casamance

Casamance is the richest agricultural region in Senegal. Agricultural production is also limited by the lack of large-scale mechanization and the inadequacy of agricultural inputs used.

Today, to win the challenge of large-scale agriculture, it is important to develop new digital tools capable of water irrigation, analyzing soils, proposing the best inputs, or making decisions in the face of warning messages, etc. To achieve this, it is important to make better choices on the sensor equipment. This must be motivated by the transmission range of the sensors, the financial cost, etc. In addition, the criteria for placing the sensors must be well studied to deploy the minimum number of sensor nodes for maximum coverage of the area. Otherwise, it is important to set up a network architecture capable of satisfying coverage and especially monitoring needs. A multi-linear architecture with LoRa radio links seems to be the choice to achieve smart agriculture in the specific case of Casamance. The main goal is to propose an end-to-end wireless LoRa architecture to collect the maximum data for irrigation or soil quality detection use.

3. The state of the art

Today, the world faces many phenomena such as climate change, floods, and threatening bush fires exposing certain particularly African populations to famine. Faced with these threats, it is necessary to find new effective methods to meet the challenges of food self-sufficiency. The democratization of the IoT has enabled digitalization in the field of agriculture. The sector is developing new tools to optimize the management of farms and harvests. This then makes it possible to set up intelligent methods of irrigation and water conservation [7,13–15], to measure the quality of the soil or crops [16,17]. Indeed, data and connected objects allow farmers to improve their productivity through network and data management models. The sensors deployed in agricultural areas are diverse and varied according to the characteristics including range, cost, etc. The sensors deployed in agricultural areas are diverse and varied according to the characteristics including range, cost, etc. Regarding the range, there are several types of 802.15.4 short-range wireless technologies or LPWANs such as LoRa, NB-IoT, SigFox, etc. Consequently, many authors focus on different models of networks for smart agriculture. The SAIoT is a model for smart agriculture described in [18]. The aim goal is to develop a real-time monitoring system for soil properties such as temperature, moisture, etc. The model is composed of three levels: the Farm level, the Server level, and the Client level. It implements also

decision support advisory models for Pest & Disease forewarning, Crop Disease identification using image analysis and SMS (Short Message System) based alerts. Connected objects used to collect information use 802.15.4/Zigbee radio links, which therefore limits the range of the solution to small areas. The authors of the paper [19] present another application of smart farming. It consists of an intelligent irrigation system based on 802.15.4-type sensors. The sensor nodes are deployed in a restricted space of over a hundred meters. LPWAN technologies seem to be best suited to large agricultural areas due to the long transmission range. Studies have recently been conducted in this direction to see the contribution of these wireless technologies in smart agriculture. The paper presented in [20] reviews the most used LPWANs in the case of smart agriculture. It presents the Nb-IoT, Sigfox, and LoRa technologies with the characteristics. NB-IoT is an LPWAN solution based on existing cellular networks. In public mode, the principle of LoRa is similar to Sigfox. Transmitters once positioned in an area covered by the network will send their information directly to the Cloud of the LoRa or Sigfox operator. This requires that each sensor be provisioned with a subscription from the operator to be able to communicate with the Cloud. LoRa technology also offers the possibility of operating in private LoRa mode. This means it is possible to build your own LoRa network using gateways for local coverage. No need for subscriptions with operators in private LoRa mode. This mode of operation of LoRa is very interesting in the case of vast agricultural areas devoid of operator network coverage, in particular, called white areas. This explains why a lot of work in the field of smart agriculture uses solutions based on LoRa. An efficient LoRa-based smart agriculture is presented in [21] for humidity and temperature monitoring uses. In [22], the authors present novel watering management based on sensor nodes using LoRa technology for communication. The solution is designed for the specific case of Vietnam and real-time data management. The model describes three types of nodes. The gateway node performs the core functions of data collection from the nodes via LoRa. Node 1 and sensor node 1 has been designed to act as a relay between node 1 and the gateway Nodes 1 and sensor 2 have been designed to act as a relay between node 1 and the gateway while node 2 monitors the quality of the water coming from the pump. The authors present an architecture composed of LoRa nodes for monitoring roles, a gateway for data collection, and a server for and a server for data analysis and decision-making. They evaluate the architecture in terms of humidity and temperature. Another very important factor in agricultural monitoring is the physical topology of the area. Indeed, it can determine the way to deploy the nodes in the zone. Most agricultural areas in southern Senegal are surrounded by waterways for much of the season. In such a configuration it is easier to carry out a deterministic and linear deployment of the nodes. In addition, given the very large size of these areas, it is necessary to opt for equipment with a long communication range. In this context, linear LoRa networks are more suitable for the considered environments. The advantage of linear wireless networks resides above all in their simplicity of deployment. However, in the specific case of linear LoRa networks, it is important to rethink this deployment taking into account the characteristic parameters of LoRa such as range, data rates, propagation model, etc. Much research on the deployment of nodes in wireless networks has been proposed over the years. Very recently, they have turned to LoRa-type wireless networks. Paper [23] presents a LoRa network of campuses deployed on several sites. It describes a method of deploying LoRa sensors to cover communications. The network covers an area of 20,000 meters.

Because of the scope of LoRa nodes, it would be more interesting to be able to deploy the nodes over a wider area. In paper [24], it is about covering the city of Southampton in the UK using a LoRa network. The deployment method used in this paper focuses on the optimal distance between gateway nodes that can ensure maximum network coverage. The connectivity assessment tested the efficiency of the deployment with the message delivery rate. Interferences if not well managed can negatively impact the deployment of LoRa nodes. In the paper [25], the authors present a modeling of interferences based on a mathematical model. The analysis of parameters such as the SIR or the SNIR provided a clear idea of the impact of the propagation model on interference in LoRa networks. However, the work carried out was done over a radius of 12 km, which is insufficient in the case of vast agricultural areas. An interference study was conducted from an anechoic chamber to give an idea of large-scale deployment. The evaluation of parameters such as the spread factor [26], and the coding rate [27] sets the conditions for deploying nodes. Other works focus on the deployment of LoRa networks based on criteria different from those mentioned so far as in [28]. This paper evaluates the impact of interference on deployment in terms of BER [29] according to various spread factors, coding rates, and bandwidth

As indicated above, the LoRa technology seems to be the most appropriate in the particular case of the Casamance context. Indeed, the transmission range is around 20 km and the possibility of configuring it in private mode makes it possible to cover vast agricultural areas without an operator network. The other advantage of LoRa is the reduction of financial costs. In the following, we review LoRa technology. This is to explain in detail the physical and logical components of the LoRa architecture.

4. An overview of the LoRa technology

Like LPWAN networks, the LoRaWAN network uses a star topology configuration. The architecture of a LoRa network is essentially composed of four components: end devices, gateways, a network server, and an application server. Figure 2 shows these different elements. The end devices are equipped with LoRa modules to allow them to send and receive radio signals and communicate with the gateways. In addition to being able to exchange with the end nodes, the gateways have an interface that allows them to have TCP/IP-based communication with the network server. The network component that has the most work to do is the network server. It allows the administration of the whole network, in other words, it is the conductor. Its role is to route information from the end nodes to the corresponding application servers and to remove redundant packets.
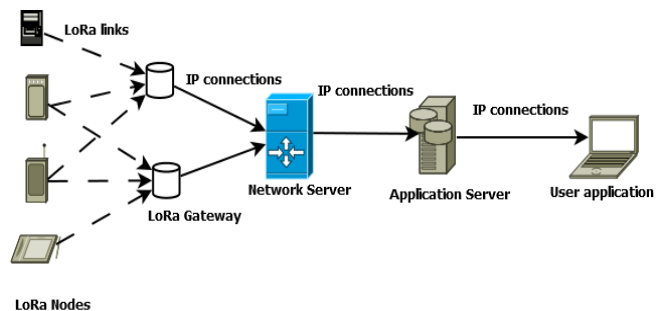

Figure 2: Classic LoRaWAN architecture

4.1 The LoRa physical layer

LoRa is based on spread spectrum modulation which uses the Chirp technique signal in which the frequency increases (up-chirp) or decreases (down-chirp) with time. Spread spectrum is a technique that allows an information signal to be transmitted over a bandwidth several times greater than the minimum bandwidth required. The modulated signals have a constant amplitude with a variable frequency [30]. Spread spectrum modulation reduces energy consumption and increases resistance to interference. In LoRa, signals are modulated in the ISM (Industrial, Scientific, and Medical) frequency band without a license, which varies according to the region (e.g. 868 MHz in Europe, 915 MHz in North America)[30].

The performance of LoRa nodes depends mainly on the following parameters:

The **spreading factor (SF)** is a quantity defined by the ratio between the chip rate and symbol rate. A chip represents pulses of a spread spectrum code and a symbol represents several chips. A chirp contains 2^{SF} bits per symbol. In a LoRaWAN network, the spreading factor is an integer between 7 and 12 [31]. This parameter allows us to vary the transmission range and rate and to send simultaneously on a given channel. A high spreading factor implies a long transmission range and a low data rate (see Table 1).

Table 1: LoRa spreading factor

Spreading factor (for UL at 125 kHz)	Bit rate	Range (Depends on Terrain)	Time on Air (for an 11-bytes payload)
SF10	980 bps	8 km	371 ms
SF9	1760 bps	6 km	185 ms
SF8	3125 bps	4 km	103 ms
SF7	5470 bps	2 km	61 ms

Bandwidth is the difference between the maximum and minimum frequency. High bandwidth values result in high data rates. The transmission time of a symbol (Ts), the spreading factor, and the bandwidth (BW) are related by the following equation :

$$Ts = \frac{2^{sF}}{Bw} \; [8]$$

Coding rate: LoRa uses the FEC (Forward error correction) technique to detect errors in transmitted frames. Extra bits are added in the frame, more precisely at the payload level. In LoRa these extra bits are controlled by the coding rate (CR). The values that the code rate can take are 4/5, 4/6, 4/7, or 4/8 [30].

4.2 The LoRaWAN protocol

LoRaWAN (Long Range Wide Area Network) is an open protocol proposed by LoRa Alliance (the Organization in charge of the promotion of LoRaWAN). It corresponds to the MAC (Medium Access Control) layer of the OSI (Open Systems Interconnection) reference model. LoRaWAN is designed to connect objects equipped with LoRa modules and powered by battery energy to the Internet. A LoRaWAN network consists of LoRa nodes, gateways equipped with LoRa modules, and an interface for connecting to the Internet, a network server, and an

application server. LoRaWAN uses the channel access technique of the ALOHA type [12]. That is, each node in the network can transmit whenever it wishes. According to the LoRaWAN specification [10], Data transmission is performed on multiple channels. Indeed, each device has a maximum of 16 channels that can be preconfigured before a terminal joins a LoRaWAN network. A LoRa frame consists of a preamble, a header, the payload, and an error control field. If the header contains information about the CRC (Cyclic Redundancy Check) and the CR (Coding Rate), the frame is said to be explicit, otherwise, it is implicit.

The LoRaWAN specification defines three modes of operation for end nodes suitable for various IoT applications. Each mode of operation is commonly referred to as a class.

Class A: This is the default class that must be implemented by all end nodes in the LoRaWAN network. In class A, the terminal sends a message to the network server (uplink) through a channel randomly chosen among those configured in the terminal with a data rate, the terminal node opens two reception windows RX1 and RX2 respectively after one second and 2 seconds (default values) following the uplink transmission during which it waits for the server transmission (downlink). If the server does not transmit, then the message is resent. The recommended retransmission limit is eight (8). Due to the short listening window, class A is the most energy efficient.

Class B: Terminals, where class B is enabled, consume more power than those implementing class A because these terminals offer more receive windows. The ping slots are opened at regular time intervals to activate the downlink. They are synchronized through a beacon broadcast in the network to provide the synchronization references. The synchronization time is called BEACON_PERIOD. In addition to these specific features, class B also implements the operating mode of class A.

Class C: Terminals using class C are constantly listening to the channel to receive messages from the network server. In a terminal, class C and class B should not be activated simultaneously. Unlike Class B, which opens only two receive windows, Class C additionally opens an RXC receive window for continuous listening.

As we have already shown, LoRa through its physical and logical components is an ideal candidate for smart agriculture in a country where network coverage is not guaranteed in agricultural areas. Moreover, given the abundance of rainfall and the physical architecture of agricultural areas, it is more judicious to arrange the sensors linearly because of the constraints imposed by the environment. Indeed, arable land is surrounded by waterways. So, for the needs of traceability and economy, it is preferable to deploy them linearly. The works cited above have already shown the interest that researchers have developed in such architecture. It should be noted however that the classical architecture of LoRa as it is presented cannot guarantee good coverage in the particular case of Casamance. The very complex nature of the landscape due to the high rainfall does not guarantee good wired deployment between the gateway nodes and the routers. Indeed, to succeed in such a deployment, specific devices are needed that can protect the cables over long distances, which is likely to be very expensive. The deployment of sensors must take into account several factors such as the extent of the area, the absence of telecommunication operators, and the financial costs. For all these reasons, it is therefore judicious to propose an architecture for deploying sensor

nodes in a linear mode without a wired connection. In other words, the proposed architecture combines LoRa radio links throughout the network with short- and long-range links.

5. The proposed architecture

The contribution of this paper is the implementation of a network architecture based on LoRa for the needs of smart agriculture. Such an architecture must take into account the specific characteristics of the area considered, the financial costs, etc. For all these reasons, the architecture is composed of several types of nodes with different physical characteristics. It is therefore a multi-linear architecture composed of several levels combining short-range and long-range nodes depending on the level as shown in figure 3. The choice of the linear topology is explained for the needs of ease of deployment and location of the nodes, and the complexity of the relief. Indeed, as indicated above, the vegetation in Casamance is very dense and very diversified. Several types of end device nodes can be described according to their role.

- Some sensors measure the rate of wetting on the leaves to anticipate diseases related to leaf humidity and reduce the use of phytosanitary treatments.

- Some sensors measure soil humidity and temperature to control root irrigation and delay the arrival of pests.

- Some measure humidity and air temperature to detect frost, and anticipate the life cycle of insects and diseases.

The end device nodes form the first level and the gateways the second level. Each gateway plays the role of cluster head for all the nodes associated with it. There are mainly two types of links in the network as shown in figure 3:

- Low LoRa links: The Low LoRa links are short-range links, and are used in communications between the nodes of the first level and those of the second level. SF parameters in [7, 8] are used.

- High LoRa links: The high LoRa links are long-range links, and are used in communications between the nodes of the second level in the sink node. SF parameters in this case are in [9, 10, 11].
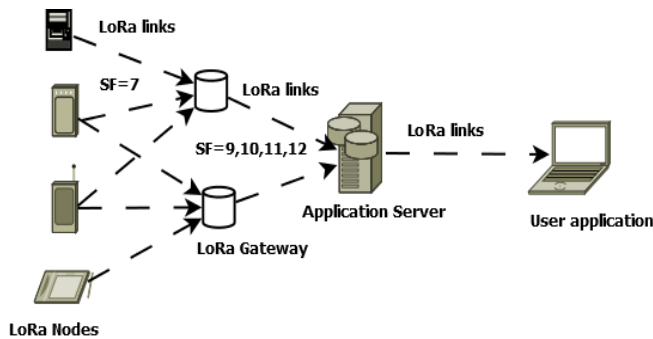
Figure 3: Proposed network architecture

Such architecture faces several challenges. In particular, the challenge of deployment for better optimization of resources such as memories, storage spaces, or computing units. It is well-known that interference in wireless networks can negatively and significantly impact performance. Therefore, in such a network, it is imperative to settle the question of deployment to minimize interference. Figure 4 below gives an illustration of the node's

deployment in a rice field in Casamance. In the following, we present an analytical analysis method to define an optimal deployment of network nodes.
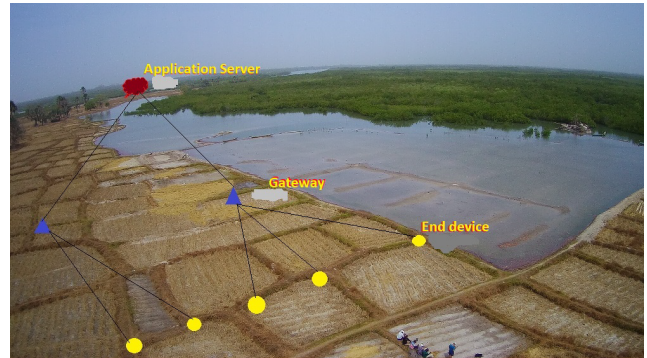
Figure 4: Illustration of node deployment in a rice field

6. Analytical study and discussion

The objective of this study is to define a method for deploying the nodes of the architecture described above. It is therefore a question of defining from certain well-chosen parameters the minimum distance between two gateway nodes which makes it possible to achieve the best deployment. These induce the choice of the spreading factor, the bandwidth, the coding rate, etc. A good interference management policy makes it possible. We can identify the case where there is a risk of interference at the node G_i, interference induced by the activity of the node G_j. We can define the gateway node G_j and the set of nodes j as the interfering nodes for the node G_i. In this condition, an optimal node deployment needs to set a minimum distance between two gateways. In wireless networks, the SIR (Signal-to-Interferences Ratio) [32] is a good indicator of the quality of the received signal. Thus, depending on the desired reception power, it is possible to rely on the SIR to determine the optimal distance between two nodes. In the specific case of this paper, the analysis must determine the optimal distance between two gateways to minimize interference. Indeed, given the proposed architecture, we can consider the gateways as cluster heads. Thus, the distance between the gateway nodes has a significant impact on the deployment.

The cluster i is formed by the gateway G_i which is the cluster head and the set of nodes n_i. In the same way we define cluster j as shown in figure 5. To determine the minimum distance between G_i and G_j, we set:

- T_i: the transmission power of node i
- T_j: the transmission power of node j
- T_G: the transmission power of node G_j
- d_i: the distance between node i and gateway G_i
- d_j: the distance between node j and gateway G_i
- d_{ij}: the distance between gateway i and an interfering gateway
- d: the distance between two adjacent gateways
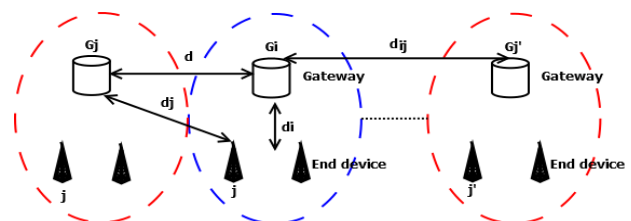
Figure 5: Distance between gateway illustration

The propagation model represents the signal and therefore the interference induced during transmission. To take into account the environmental fluctuations of the medium, Log Normal Shadowing is required in this study because of its random nature. The path loss at an arbitrary distance $d > d_0$ from the transmitter is given by the following equation (1):

$$PL_{dB}(d) = PL_{dB}(d_0) + 10n \, log(\frac{d}{d_0}) \pm X_\sigma \qquad (1)$$

where n is the path loss attenuation factor, $PL_{dB}(d_0)$ is the path loss at a reference distance d_0, and $X\sigma$ is a zero-mean Gaussian distributed random variable. The standard deviation σ is expressed in dB. So, for a given transmission power P_T, the received power is provided by the equation (2):

$$P_{R\sigma} = P_T - PL_{dB}(d) \qquad (2)$$

The received signal at the gateway G_i from node i is the sum of multiple terms: the first, is the desired signal received from node i; the second is the interferences caused by the set of gateways G_j around G_i, the third is the interference generated by all the sets of nodes j associated to the gateways G_j. Let be K' the set of node j associated with a gateway Gj. We can define the SIR [20] as:

$$SIR_{dB} = S(i) - \sum_{j=1}^{x} S(G_j) + \sum_{K' \epsilon G_j} \sum_{k'=1}^{MAX} s(k') \qquad (3)$$

$$S(y) = T_y - PL_{dB}(d_0) - 10 * n * log\left(\frac{d_y}{d_0}\right) \pm X_\sigma(y) \qquad (4)$$

where y can be a gateway or an end device node, x is the number of interfering gateways for the gateway G_i and MAX is the number of nodes associated with a given gateway.

The coexistence of several radio links of different ranges is a particularity of the architecture. Short radio links of 2 km are used at the first level while those of long-range over 4 km are at the second level of the architecture. As shown in figure 3, we note various spreading factors according to the level. Thus, the first level spreading factor is set to 7 while it is in the range {9,10,11} in the second level. Moreover, for the sake of simplicity, it is assumed that a gateway communicates with only one of its nodes at a given time. So, for x interfering gateways, there are x interfering nodes at a specific time. In addition, the transmitting power for the end devices nodes is assumed to be the same value.

So, the *SIR* becomes:

$$SIR_{dB} = S(i) - \sum_{j=1}^{x} S(G_j) - \sum_{j=1}^{x} S(j) \qquad (5)$$

$$SIR_{dB} = T_i - PL_{dB}(d_0) - 10 * n * log\left(\frac{d_i}{d_0}\right) \pm X_\sigma(i) - \sum_{j=1}^{x}(T_G - PL_{dB}(d_0) - 10 * n * log\left(\frac{d_{ij}}{d_0}\right) \pm X_\sigma(Gj)) - \sum_{j=1}^{x}(T_i - PL_{dB}(d_0) - 10 * n * log\left(\frac{d_j}{d_0}\right) \pm X_\sigma(j)) \qquad (6)$$

Environmental fluctuations in the considered area for coverage issues are supposed to be homogeneous. Environmental conditions are known to be very stable in Senegal according to the season. Thus, $X_\sigma(i), X_\sigma(G_j)$, and $X_\sigma(j)$ follow the same Gaussian distributed random variable $N \sim (0, \sigma)$. According to these considerations we have:

$$SIR_{dB} = (2x + 1) * X_\sigma + (1 - x) * T_i + (2x - 1) * PL_{dB}(d_0) \quad (7)$$

$$-x * T_G - 10 * n * log\left(\frac{d_i}{d_0}\right) + 10 * n * \sum_{j=1}^{x} log\left(\frac{d_{ij}}{d_0}\right)$$
$$+10 * n * \sum_{j=1}^{x} log\left(\frac{d_j}{d_0}\right) \qquad (8)$$

We assume that the deployment is deterministic and uniform. Therefore, the relationship between d_{ij} and d is given by the formula (9):

$$d_{ij} = j * d \qquad (9)$$

where j represents the number of interfering gateways for a given gateway i.

In addition, for all the nodes j associated with the same gateway, we can affirm that the distance d_j is almost equivalent to the distance d_{ij}. Thus, from equation (8) we have:

$$SIR_{dB} = (2x + 1) * X_\sigma + (1 - x) * T_i + (2x - 1) * PL_{dB}(d_0)$$
$$-x * T_G - 10 * n * log\left(\frac{d_i}{d_0}\right) + 10 * n * \sum_{j=1}^{x} log\left(\frac{d * j}{d_0}\right)$$
$$+10 * n * \sum_{j=1}^{x} log\left(\frac{d * j}{d_0}\right) \qquad (10)$$

The simplified formula gives:

$$SIR_{dB} = (2x + 1) * X_\sigma + (1 - x) * T_i + (2x - 1) * PL_{dB}(d_0)$$
$$-x * T_G - 10 * n * log\left(\frac{d_i}{d_0}\right) + 20 * n * x * log\frac{d}{d_0}$$
$$+20 * n * log \prod_{j=1}^{x} j \qquad (11)$$

Let be:

$$Z = (2x + 1) * X_\sigma \quad \text{and}$$

$$K = (1 - x) * T_i + (2x - 1) * PL_{dB}(d_0)$$
$$-x * T_G - 10 * n * log\left(\frac{d_i}{d_0}\right) + 20 * n * x * log\frac{d}{d_0}$$
$$+20 * n * log \prod_{j=1}^{x} j \qquad (12)$$

Z is so a gaussian distributed random variable $N \sim (0, (2x + 1) * \sigma^2)$.

Let be

P_{succes} the probability that $SIR \geq SIR_{Thresold}$.

$$P_{succes}[Z + K \geq SIR_{Threshold}] = p \qquad (13)$$

$$\Leftrightarrow P_{succes}[Z \leq SIR_{Threshold} - K] = 1 - p \qquad (14)$$

This is equivalent to:

$$P_{succes}\left[\frac{Z}{\sigma*\sqrt{(2x+1)}} \leq \frac{(SIR_{Threshold}-K)}{\sigma*\sqrt{(2x+1)}}\right] = 1 - p \qquad (15)$$

$$\Leftrightarrow P_{succes}\left[H \leq \frac{(SIR_{Threshold}-K)}{\sigma*\sqrt{2(x+1)}}\right] = 1 - p \qquad (16)$$

where $H = \frac{Z}{\sigma*\sqrt{(2x+1)}}$ is a gaussian random variable $N\sim(0,1)$.

According to the repartition function of $N\sim(0,1)$, it is assuming that:

$$\frac{(SIR_{Threshold}-K)}{\sigma*\sqrt{(2x+1)}} = F^{-1}(1-p) \quad (17)$$

where F^{-1} is the inverse function of F.

We deduce from this equation the value of K.

$$K = SIR_{Threshold} - \sigma*\sqrt{(2x+1)}*F^{-1}(1-p) \quad (18)$$

Finally, the distance between two adjacent gateways is given according to equations (12) and (18):

$$\log d = \left(A + B*x + C*\sqrt{2x+1} + D*log\prod_{j=1}^{x} j\right)\Big/ 20*n*x$$

where:

$$A = SIR_{dB} - T_i + PL_{dB}(d_0) + 10*n*\log\frac{d_i}{d_o}$$

$$B = T_i - 2*PL_{dB}(d_0) + T_G + 20*n*\log d_0$$

$$C = -\sigma*F^{-1}(1-p)$$

$$D = -20*n$$

The mathematical analysis makes it possible to unambiguously determine the optimal deployment of gateway nodes minimizing interference. This allows us to define a reusable deployment pattern to cover a large agricultural area. The choice of pattern takes into account the characteristics of the environment considered as environmental fluctuations due to rainfall, the nature of the soil, etc. The pattern is defined as the set formed by a gateway G_i and the interfering gateway nodes G_j which guarantee a given reception threshold. The minimum distance d as a function of the size of the pattern is proposed in the following.

Evaluation is done according to the conditions described in [33]. It should be noted that in Senegal the work on smart agriculture is currently in a purely experimental phase [34,35]. Therefore, the work does not focus on the propagation model. Hence the choice of parameters for an environment similar to that of Senegal such as in Lebanon's environment. Path loss parameters are shown in Table 2.

Table 2: The path loss parameters

Parameters	Values
T_{ip}	14 dB
T_{Gj}	20 dB
d_i	2000 m
n	4,179
σ	7,2 dB
Reception probability	0.9
$PL_{db}(d_0)$	102,86

It is shown according to the paper [22] that for a spreading factor of 12 and a reception rate of around, the ISR threshold is equal to 6 dB.
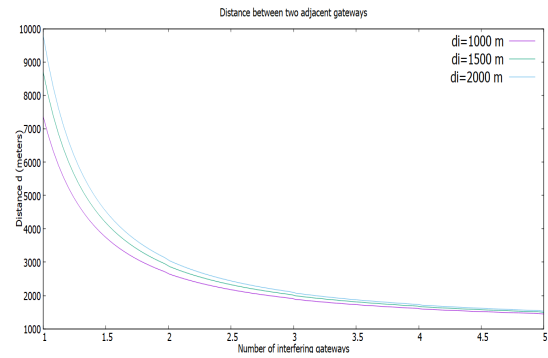
Figure 6: Number of interfering gateways as a function of distance

Figure 6 represents the minimal distance between two adjacent gateways. It shows the influence of the distance between an end device node and its gateway on the deployment. Indeed, it shows the maximum number of interfering gateways for a given distance d_i. The curve shows that the number of interfering gateways is inversely proportional to the distance. Indeed, when the distance is excellent, the interference is less and therefore the interference can be limited to 1 gateway. On the other hand, when the distance is reduced (less than 3000 m), the interferences are very significant. In this case, the number of interferents increases without exceeding a limit of 5. It should also be noted that the minimum distance does not exceed the defined distance d_i.

In the specific case of the rice fields of Casamance, it is preferable to minimize the equipment that makes up the architecture because of the presence of water around the fields. Therefore, it is more advisable to choose the deployment of gateways over long distances (example d = 6Kms).

7. Conclusions and future work

Smart agriculture is seen today as a very important lever for winning the challenge of food self-sufficiency in a world where resources such as water are becoming increasingly scarce. Indeed, the new techniques of irrigation, monitoring of soil quality, of temperature make it possible to improve productivity and maintain cultivable soils. In the particular case of Casamance in Senegal, the practice of smart agriculture must take into account the very dense rainfall in this environment. This implies the choice of the most appropriate sensors and wireless communication technology. Moreover, it is necessary to have an optimal deployment of the sensors to have good coverage of the zone. This induces the study of a network architecture that ensures this purpose.

A new LoRa network architecture based on the classical one is presented in this paper. This architecture combining short and long-range LoRa radio links make it possible to carry out smart agriculture in rural areas, particularly in the southern area of Senegal. It focuses on the specific case of the rice field for irrigation system purposes. An analytical study on the deployment helps us to define a model of deployment of the nodes particularly the gateways. This study is based on factors such as the SIR, the reception probability, the distance between nodes, etc. In future work, we first plan to simulate the network in Omnet++ to confirm the analytical study. This involves conducting a performance study in terms of throughput, end-to-end delay, and energy to analyze the advantages and limits of the model. Then, it is about deploying LoRa sensors and gateways in a real environment.

References

[1] P. Sethi, S.R. Sarangi, "Internet of Things: Architectures, Protocols, and Applications," Journal of Electrical and Computer Engineering, **2017**, 1–25, 2017, doi:10.1155/2017/9324035.

[2] L. Atzori, A. Iera, G. Morabito, "The Internet of Things: A survey," Computer Networks, **54**(15), 2787–2805, 2010, doi:10.1016/j.comnet.2010.05.010.

[3] K.N. Swaroop, K. Chandu, R. Gorrepotu, S. Deb, "A health monitoring system for vital signs using IoT," Internet of Things, **5**, 116–129, 2019, doi:10.1016/j.iot.2019.01.004.

[4] D.S.R. Krishnan, S.C. Gupta, T. Choudhury, "An IoT based Patient Health Monitoring System," in 2018 International Conference on Advances in Computing and Communication Engineering (ICACCE), IEEE: 01–07, 2018, doi:10.1109/ICACCE.2018.8441708.

[5] T.A. Khoa, M.M. Man, T.-Y. Nguyen, V. Nguyen, N.H. Nam, "Smart Agriculture Using IoT Multi-Sensors: A Novel Watering Management System," Journal of Sensor and Actuator Networks, **8**(3), 45, 2019, doi:10.3390/jsan8030045.

[6] M.R.M. Kassim, "IoT Applications in Smart Agriculture: Issues and Challenges," in 2020 IEEE Conference on Open Systems (ICOS), IEEE: 19–24, 2020, doi:10.1109/ICOS50156.2020.9293672.

[7] D. Thakur, Y. Kumar, S. Vijendra, "Smart Irrigation and Intrusions Detection in Agricultural Fields Using I.o.T.," Procedia Computer Science, **167**, 154–162, 2020, doi:10.1016/j.procs.2020.03.193.

[8] D.M. Andeme Bikoro, S. Fosso Wamba, R.M. Etoua, "Effective Contribution of Internet of Things (IoT) in Smart Agriculture: State of Art," Lecture Notes of the Institute for Computer Sciences, Social-Informatics and Telecommunications Engineering, LNICST, **443 LNICST**, 219–233, 2022, doi:10.1007/978-3-031-06374-9_14.

[9] M. Cicioğlu, A. Çalhan, "Smart agriculture with internet of things in cornfields," Computers & Electrical Engineering, **90**, 106982, 2021, doi:10.1016/J.COMPELECENG.2021.106982.

[10] G.S. Nagaraja, A.B. Soppimath, T. Soumya, A. Abhinith, "IoT Based Smart Agriculture Management System," in 2019 4th International Conference on Computational Systems and Information Technology for Sustainable Solution (CSITSS), IEEE: 1–5, 2019, doi:10.1109/CSITSS47250.2019.9031025.

[11] J.P.S. Sundaram, W. Du, Z. Zhao, "A Survey on LoRa Networking: Research Problems, Current Solutions and Open Issues," 2019.

[12] J. Haxhibeqiri, E. de Poorter, I. Moerman, J. Hoebeke, "A Survey of LoRaWAN for IoT: From Technology to Application," Sensors, **18**(11), 3995, 2018, doi:10.3390/s18113995.

[13] E.A. Abioye, M.S.Z. Abidin, M.S.A. Mahmud, S. Buyamin, M.H.I. Ishak, M.K.I.A. Rahman, A.O. Otuoze, P. Onotu, M.S.A. Ramli, "A review on monitoring and advanced control strategies for precision irrigation," Computers and Electronics in Agriculture, **173**, 2020, doi:10.1016/j.compag.2020.105441.

[14] L. García, L. Parra, J.M. Jimenez, J. Lloret, P. Lorenz, "IoT-based smart irrigation systems: An overview on the recent trends on sensors and iot systems for irrigation in precision agriculture," Sensors (Switzerland), **20**(4), 2020, doi:10.3390/S20041042.

[15] R.K. Kodali, M.S. Kuthada, Y.K. Yogi Borra, "LoRa Based Smart Irrigation System," in 2018 4th International Conference on Computing Communication and Automation (ICCCA), IEEE: 1–5, 2018, doi:10.1109/CCAA.2018.8777583.

[16] V. Saiz-Rubio, F. Rovira-Más, "From Smart Farming towards Agriculture 5.0: A Review on Crop Data Management," Agronomy, **10**(2), 207, 2020, doi:10.3390/agronomy10020207.

[17] P. Sumathi, R. Subramanian, V. Karthikeyan, S. Karthik, "Retracted: Soil monitoring and evaluation system using EDL-ASQE: Enhanced deep learning model for IoT smart agriculture network," International Journal of Communication Systems, **34**(11), 2021, doi:10.1002/dac.4859.

[18] K.A. Patil, N.R. Kale, "A model for smart agriculture using IoT," in 2016 International Conference on Global Trends in Signal Processing, Information Computing and Communication (ICGTSPICC), IEEE: 543–545, 2016, doi:10.1109/ICGTSPICC.2016.7955360.

[19] E.M. Hasiri, A. Asniati, M.A. Suryawan, R. Rasmuin, "The Implementation of Smart Farming Application Based on the Microcontroller and Automatic Sprinkler Irrigation System of Agricultural Land," Advances in Science, Technology and Engineering Systems Journal, **5**(2), 174–179, 2020, doi:10.25046/aj050222.

[20] H. Klaina, I.P. Guembe, P. Lopez-Iturri, M.Á. Campo-Bescós, L. Azpilicueta, O. Aghzout, A.V. Alejos, F. Falcone, "Analysis of low power wide area network wireless technologies in smart agriculture for large-scale farm monitoring and tractor communications," Measurement, **187**, 110231, 2022, doi:10.1016/J.MEASUREMENT.2021.110231.

[21] S.J. Suji Prasad, M. Thangatamilan, M. Suresh, H. Panchal, C.A. Rajan, C. Sagana, B. Gunapriya, A. Sharma, T. Panchal, K.K. Sadasivuni, "An efficient LoRa-based smart agriculture management and monitoring system using wireless sensor networks," International Journal of Ambient Energy, 1–4, 2021, doi:10.1080/01430750.2021.1953591.

[22] T.A. Khoa, M.M. Man, T.-Y. Nguyen, V. Nguyen, N.H. Nam, "Smart Agriculture Using IoT Multi-Sensors: A Novel Watering Management System," Journal of Sensor and Actuator Networks, **8**(3), 45, 2019, doi:10.3390/jsan8030045.

[23] G. Ferre, F. Rivet, R. Tajan, E. Kerherve, "Design and Deployment of an IoT Network Based on LoRa," in 2017 27th EAEEIE Annual Conference (EAEEIE), IEEE: 1–5, 2017, doi:10.1109/EAEEIE.2017.8768583.

[24] P.J. Basford, F.M.J. Bulot, M. Apetroaie-Cristea, S.J. Cox, S.J. Ossont, "LoRaWAN for Smart City IoT Deployments: A Long Term Evaluation," Sensors, **20**(3), 648, 2020, doi:10.3390/s20030648.

[25] L. Irio, R. Oliveira, "Modeling the Interference caused to a LoRaWAN Gateway due to Uplink Transmissions," in 2019 Eleventh International Conference on Ubiquitous and Future Networks (ICUFN), IEEE: 336–340, 2019, doi:10.1109/ICUFN.2019.8806142.

[26] B. Reynders, S. Pollin, "Chirp spread spectrum as a modulation technique for long range communication," in 2016 Symposium on Communications and Vehicular Technologies (SCVT), IEEE: 1–5, 2016, doi:10.1109/SCVT.2016.7797659.

[27] G. Baruffa, L. Rugini, V. Mecarelli, L. Germani, F. Frescura, "Coded LoRa Performance in Wireless Channels," in 2019 IEEE 30th Annual International Symposium on Personal, Indoor and Mobile Radio Communications (PIMRC), IEEE: 1–6, 2019, doi:10.1109/PIMRC.2019.8904298.

[28] V.R. Stoynov, V.K. Poulkov, Z. v. Valkova-Jarvis, "Interference Management in LoRaWANs — Overview and Simulation Study," in 2018 Advances in Wireless and Optical Communications (RTUWO), IEEE: 251–256, 2018, doi:10.1109/RTUWO.2018.8587904.

[29] T. Elshabrawy, J. Robert, "Analysis of BER and Coverage Performance of LoRa Modulation under Same Spreading Factor Interference," in 2018 IEEE 29th Annual International Symposium on Personal, Indoor and Mobile Radio Communications (PIMRC), IEEE: 1–6, 2018, doi:10.1109/PIMRC.2018.8581011.

[30] G. Ferre, A. Giremus, "LoRa Physical Layer Principle and Performance Analysis," in 2018 25th IEEE International Conference on Electronics, Circuits and Systems (ICECS), IEEE: 65–68, 2018, doi:10.1109/ICECS.2018.8617880.

[31] J.-T. Lim, Y. Han, "Spreading Factor Allocation for Massive Connectivity in LoRa Systems," IEEE Communications Letters, **22**(4), 800–803, 2018, doi:10.1109/LCOMM.2018.2797274.

[32] G.P. Efthymoglou, P.S. Bithas, A.G. Kanatas, "Exact SNR and SIR analysis in Poisson wireless networks," Electronics Letters, **53**(5), 356–358, 2017, doi:10.1049/el.2016.2378.

[33] R. el Chall, S. Lahoud, M. el Helou, "LoRaWAN Network: Radio Propagation Models and Performance Evaluation in Various Environments in Lebanon," IEEE Internet of Things Journal, **6**(2), 2366–2378, 2019, doi:10.1109/JIOT.2019.2906838.

[34] C.S.M. Babou, B.O. Sane, I. Diane, I. Niang, "Home Edge Computing Architecture for Smart and Sustainable Agriculture and Breeding," in Proceedings of the 2nd International Conference on Networking, Information Systems & Security - NISS19, ACM Press, New York, New York, USA: 1–7, 2019, doi:10.1145/3320326.3320377.

[35] L. Ndiaye, K. Gueye, S. Ouya, "Proposal for an alert and monitoring solution based on the SIP and IoT protocol: the case of agriculture," in The 4th International Conference on Networking, Information Systems amp Security., ACM, New York, NY, USA: 1–6, 2021, doi:10.1145/3454127.3457617.

Optimizing Sensors Locations for Tsunami Warning System

Mikhail Lavrentiev[*,1], Dmitry Kuzakov[1], Andrey Marchuk[1,2]

[1]*Institute of Automation and Electrometry SB RAS, Novosibirsk, 630090, Russia*

[2]*Institute of Computational Mathematics and Mathematical Geophysics SB RAS, Novosibirsk, 630090, Russia*

A B S T R A C T

To reduce the time necessary for determination of tsunami source parameters it is proposed to optimize the location of sensors system and to use only a part of the measured wave profile. Based on computation, it is possible to balance the number of sensors in use and the time period after the earthquake needed to obtain tsunami wave parameters. Numerical experiments show that even a part of the wave period (compared to ¼ of the entire period) provides enough information to get the wave amplitude within the well-known concept of calculation in advance. This is due to the application of Fourier theory in the form of orthogonal decomposition of the measured wave profile. It is important that the proposed algorithm requires only a few seconds using regular personal computer. Using the real depth profile offshore Japan we compute the time required to calculate the wave amplitude (with 10 percent accuracy) in case of one, two and three sensors. Optimization could be performed in terms of minimal time required to get the wave profile. It is also possible to calculate the sensor network design, which provides the maximal time between wave parameters determination and the wave approaching nearest coast. The new feature here observed is that optimal positions of sensors are different if one needs minimizing time to detect tsunami wave or maximazing time it takes the wave to approach the nearest cost after recovering the wave parameters at source. This may require to rearrange decision making at tsunami warning centers.

1. Introduction

This paper is an extension of the work originally presented in the conference OCEANS 2021: San Diego – Porto [1].

As a rule, the numerical modeling modulus of tsunami warning system should contain the following three major parts: wave generation (earthquake magnitude and hypocenter location recalculated in terms of the initial seabed displacement), wave propagation and inundation of the dry land. For example, our reference code, the MOST (Method of Splitting Tsunami) software package (see [2,3]), has all these parts. Alternative codes have similar structure [4,5]. It is natural to use "initial disturbance" at tsunami source as the "input data" to calculate tsunami wave propagation from the source to the coastal area. Displacement of the sea bed (due to the earthquake) could be evaluated on the basis of knowledge of the Earth crust structure and the location of the earthquake epicenter. So, regardless the underlying reasons, in any case the so-obtained initial displacement is nothing but approximation. We propose to use instead the sea surface displacement at tsunami source, obtained by processing the measured profile of the real tsunami wave. These measured data are available due to the rather well-developed system of bottom pressure sensors, located at sea bed around Pacific Ocean, given in Figure 1 from [6].
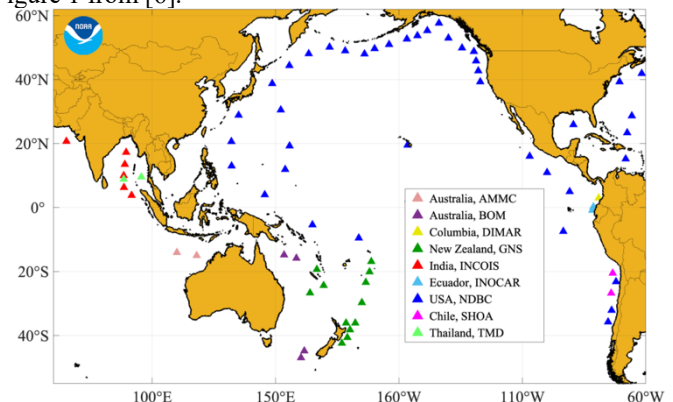

Figure 1. Location of Dart buoys around the Pacific Ocean [6]

In addition, there exist systems of bottom sensors, connected to the dry lend (processing centers) by a cable, for example DONET (Dense Oceanfloor Network system for Earthquakes and Tsunamis) [7] and S-net (Seafloor observation network for earthquakes and tsunamis) [8] being developed in Japan. Figure 2, taken from [8], shows the location of S-net deep-water stations eastward of Honshu Is.
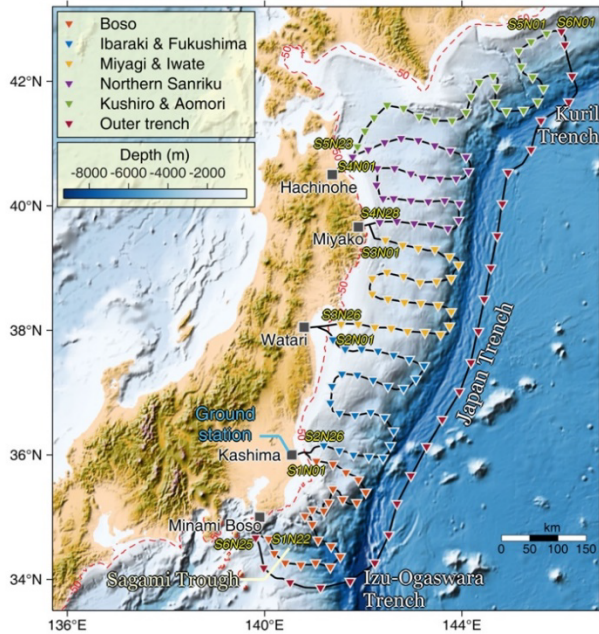

Figure 2. Configuration of the S-net observation system along the Japan trench [8]

In some publications, the optimal positioning of the sensor network refers to the location of sensors that allow detection of a tsunami wave in the shortest time after its occurrence (see, for example, [9] and the references therein). The present article, however, deals with the configuration of a network of deep-water recorders, not for the earliest detection of the tsunami occurrence, but for determining the water surface displacement profile with the required accuracy in the shortest possible time.

In [10] the S-net observation data are used reconstruct the source parameters by the sequential multiple linear regression method.

The original idea of calculation in advance was used in [11]. It consists in introduction of so-called Unit Sources (UnSs). These are nothing but rectangles 50x100 km – typical size of the sea bed displacement in case of 7.5 M earthquake. It is possible to simulate numerically tsunami wave propagation initiated by a given displacement form. Covering the particular subduction zone with such UnSs (along with the typical for this zone shape of the initial sea bed displacement) one can create "in advance" the database of the calculated tsunami wave time series (synthetic mareograms). Suppose that we have a sea bottom pressure sensor (a number of those are installed over the Pacific Ocean) which is able to report the parameters of the tsunami wave passing over in a real time mode. Having such a measured wave profile we now approximate it as a linear combination of several calculated wave profiles, each being initiated by one of the UnSs [12]. In fact, such a database exists and is available for use. System of UnSs covers major subduction zones around Pacific Ocean [13].

As was noted in [14], even a part of the measured wave profile is enough to reconstruct the main tsunami wave parameters within

the calculation in advance strategy. We believe that 10% error is acceptable to decide if a particular wave is dangerous in a given location. Here we show how the necessary time to determine the wave amplitude at source depends of the number of sensors one uses. This is done by the example of three different locations of the "composed" tsunami source within a particular water area offshore Japan.

The rest of this paper is composed as follows. We first describe the "calculation in advance" data inversion strategy. Then the idea of orthogonal decomposition method is given. The method has a very low computational cost and makes it possible to obtain an approximation of tsunami source parameters by using only a part of the measured wave profile. Digital bathymetry offshore the central part of Honshu Island (Japan) is then introduced. Setting up of numerical experiments is then described, including location of model tsunami sources and artificial water level measurement sensors. The obtained numerical results are given in Section 3. Finally, these results are briefly discussed.

2. Setup of Numerical Experiments

2.1. Problem Statement

As part of the general problem of estimating the tsunami hazard in the shortest possible time, let us determine the role of the location of the system of deep-water sensors. We will assume that, at the cost of allowing 10% error in obtained wave amplitude, the source parameters are determined from data from a single sensor, the first one the wave has reached. Moreover, we will use only part of the wave period, which is about 1/4 of this first period (having the positive phase first). The exact value of this NPWP (Necessary Part of Wave Period) is determined automatically, on the basis that the amplitude values practically stop growing as the wave passes over the sensor [14]. Let us consider the ratio of the number of sensors to the time required to determine the approximate values of the wave parameters in the tsunami source.

Following [3], we will assume that the epicenter of the earthquake is located within a certain zone (subduction zone). This assumed zone is covered by 8 rectangles of size 50x100 km - the typical size of the seafloor deformation zone during an earthquake of magnitude M=7.5 (the accepted threshold value of magnitude for the formation of tsunami waves). In each of these rectangles (Unit Sources - UnSs) is placed a perturbation with a shape characteristic of seafloor deformation resulting from earthquakes in this subduction zone. The seafloor deformation during a stronger earthquake will be approximated by a linear combination of four of these UnSs with some coefficients. The problem of determining the source parameters comes down to determining the set of these amplification coefficients.

2.2. Orthogonal Decomposition Method

To elaborate a fast and robust algorithm for the determination of the above amplification coefficients, Fourier series theory was used, as it deals in particular with optimal approximation of a given function with the linear combination of functions being orthogonal and normalized.

Let $f(t)$ be the measured time series of the wave profile (marigram). One can consider the data from DART buoy or nay alternative sensor. By $f_k(t)$, $k=1,...,n$, let us denote the calculated wave profiles, obtained (by direct numerical solutions to the linear or nonlinear shallow water system [15]) at the same point of sensor location. The parameter k means that the source of this wave is

located at the *k*-th UnS having "standard" shape. As was shown numerically, these functions, $f_k(t)$, could be considered linearly independent. To describe better the measured wave, one should determine the coefficients, b_k, for the linear combination of these functions, for which the below difference in L_2 norm is the smallest:

$$\int_0^T \left(\sum_{k=1}^N b_k f_k(t) - f(t)\right)^2 dt \rightarrow min \quad (1)$$

In such a statement the problem of determination of the wave parameters at source is reduced to the one of the optimal approximation of a given function *f(t)* by the linear combination of functions *{f_k(t)}*.

The Fourier series theory states that the coefficients of such optimal approximation (1) are exactly the Fourier coefficients of expansion of *f(t)* in a series with respect to *{f_k(t)}* (see, for example, [16]), provided that the system *{f_k(t)}* is orthogonal and normalized:

$$\left(f_i(t), f_j(t)\right) = \int_{t_0}^T f_i(t) f_j(t) dt = 0, \quad (2)$$

$$\left(f_i(t), f_i(t)\right) = 1. \quad (3)$$

So, the Fourier series theory was used in [17] to design the algorithm to determine coefficients for optimal approximation of the measured tsunami wave. This algorithm, tested in [1,14,18], consists of several stages.

At the first stage the "marigrams" *{f_k(t)}* obtained from the unit sources should be recalculated to meet the requirements (2)-(3).

Then, the function *f(t)* (tsunami wave profile) should be expanded to the Fourier series with respect to recalculated synthetic marigrams. At the last stage the obtained Fourier coefficients are transformed into the sought coefficients in (1).

Note that the described algorithm has a very low computational cost as mostly simple algebraic operations are involved. We consider calculation of integrals (scalar products and L_2 norms as simple operations, too.) During the performed numerical experiments it takes less than a second using regular personal computer.

2.3. Domain for Numerical Study – Bathymetry

All numerical studies were arranged at the water area offshore Kanto Region, central part of the Honshu Island (Japan). JODC database (see [19]) was used to create the gridded bathymetry for the computation area, given in Figure 3. The area under study is bounded in East-West direction by 137.0º and 143.0º East Longitude, and in North-South direction by 32.0º and 37.0º North Latitude. Spatial grid steps are 223 m (East-West direction) and 273 m (North-South direction. Array of computational nodes has size of 2000x2500.

2.4. Description of Numerical Studies Setup

Tsunami sources in subduction zones usually extend along deep-water troughs. In this case, the source is most effectively reconstructed by sensors located in the direction of the short axis of such sources. In the area under consideration the deep-water trench is oriented from North to South (Figure 3), so the possible sources are extended in this direction, and the virtual sensors are located along the meridian, which, in our opinion, allows reconstructing effectively the initial displacement of the water surface using the data of a minimum number of sensors. Along the

northeastern coast of Honshu Island, where S-net sensors are installed (Figure 2), the possible tsunami sources are extended in the direction of Japan Trench, which allows an optimal choice among the already available deep-water recorders. This is not yet possible in the area of the Kanto Peninsula.

We consider offshore water area at the Izu-Bonin subduction zone. Suppose that tsunami sources are expected within the strip covered by eight UnSs (having size 50x100 km each), indicated as white rectangles, see the Figure 1. In total the 100x400 km zone is considered. Simulating a rather strong earthquake, the Composed Sources (CSs) are studied. These are nothing but linear combinations of four neighboring USs with certain amplification coefficients. We choose the following values for the coefficients *(0.7, 0.8, 1.2, 1.3)*. It means that for each of the CS_i, *i=1,2,3*, (indicated in Figure 3) the upper-left UnS has the coefficient *0.7* (in the linear combination, which determines our Composed Source), the lower-left – *0.8*, upper-right – *1.2* and lower-right – *1.3*. The amplitude of sea surface indignation of each of these CS_i does not exceed *+150* cm and its shape is given in Figure 4. Form of such a CS is typical in the area of study. Our task is to determine these amplification coefficients.
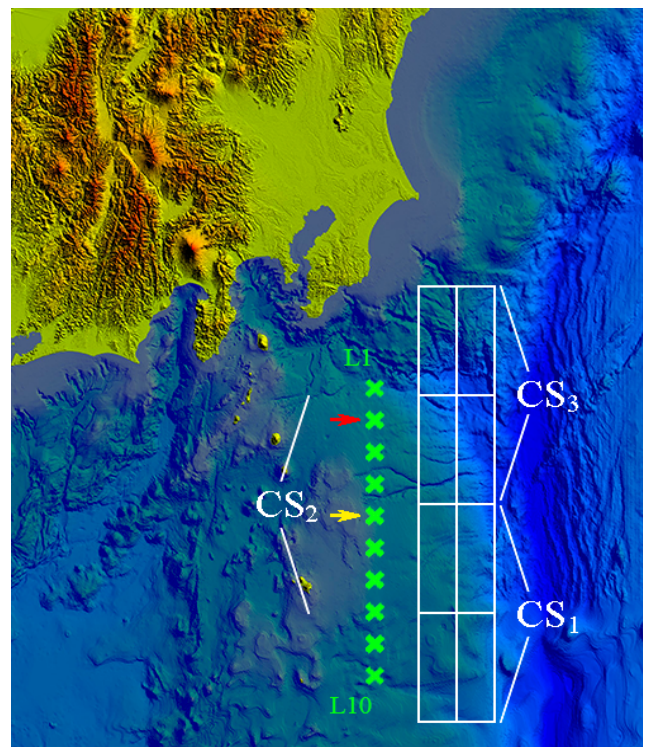
Figure 3: Digital bathymetry of water area under study. Artificial tsunami sources are indicated as CS_i. Green crosses indicate artificial sensors
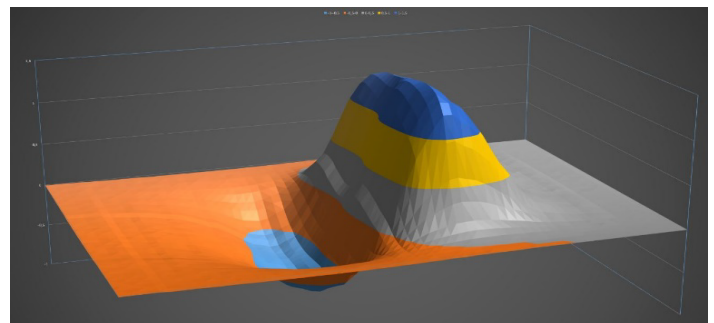
Figure 4: Visualization of CS_i – water level in the artificially composed tsunami source having size 100 x 200 km

A number of virtual tsunami detection sensors are located close to the subduction zone. Exact positions of these 10 "tsunameters" are indicated by green crosses. Numbering is arranged from up (sensor *L1*) to down, the "last one is indicated as *L10*. These "virtual tsunameters" *Li* could coincide with the existing sensors from S-net and DONET, the other could suggest possible positions of DART buoys.

3. Numerical Results

A series of numerical calculations of tsunami propagation from each of the 8 UnSs under consideration was performed to obtain synthetic tsunami profiles, on the basis of which the source parameters recovery algorithm was constructed. For numerical modeling, the MOST algorithm [2,3], which correctly describes tsunami propagation in a sufficiently deep-water area, was used. This method uses difference scheme based on spatial direction splitting difference scheme to approximate the system of nonlinear shallow water differential equations. Calculations can result in wave series at all 10 tsunami recorder locations from each UnS.

A series of computational experiments were carried out to assess the efficiency of reconstructing a composed sources *CSi*, *i=1,2,3*, by using the data from deep-water recorders located at different points in the region. The gridded bathymetry for these calculations is described in Section 2.2, and the field of water surface displacement in the basis (Unit) Source, constructed using the seismic source model in elastic half-space [12], is presented in Figure 5.

Based on the results of numerical modeling of tsunami propagation generated by each of *8* such UnSs, a database of synthetic mareograms (wave time series) at the locations of 10 virtual deep-water detectors (given in Figure 3) was created. Wave series calculated at these virtual tsunameters location were used to reconstruct the source composed of *4* UnSs with different amplification coefficients. To estimate the quality of restoration of composed sources *CSi*, *i=1,2,3,* the results of tsunami modeling generated by each *CSi* at different sensors were used. The time needed for recovery and deviation estimate from the exact wave profile were determined and are presented in the form of tables.
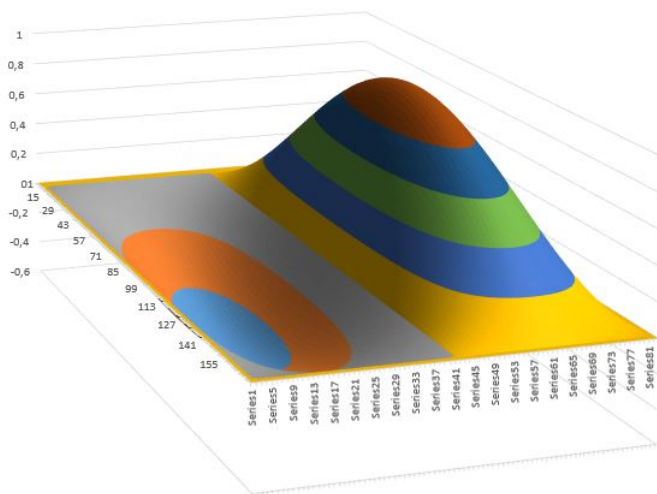
Figure 5. Water surface displacement in the Unit Source having size 50 x 100 km

Results of numerical simulation described in [14] are given in Tables 1-3 below.

The following "critical" time designations are used in the tables:

NPWP – necessary part of the wave profile, measured in seconds, to determine correctly (within 10% error) the coefficients in approximation (1);

T1 (sec) – time moment in which the wave first maximum appears at the given virtual sensor;

T2 (sec) – the time it takes the wave to approach the nearest coast after the moment where the coefficients in (1) are correctly determined.

Table 1: Source CS1 (see Figure 1). Wave travel time to the nearest coast is equal to 1260 sec.

No Rec.	NPWP, sec.	T1, sec	T2, sec
L1	1031	740	229
L2	794	630	466
L3	697	525	563
L4	552	435	708
L5	478	375	782
L6	469	358	791
L7	383	367	877
L8	385	372	875
L9	348	336	912
L10	317	306	943

Table 2: Source CS2 (Figure 1, the middle one). Wave travel time to the nearest coast is equal to 886 sec.

No Rec.	NPWP, sec.	T1, sec	T2, sec
L1	443	343	443
L2	358	285	528
L3	262	266	624
L4	319	303	567
L5	354	340	532
L6	389	373	497
L7	382	368	504
L8	473	366	413
L9	502	391	384
L10	550	443	336

Let us consider three scenarios of a possible tsunami. The combined sources of the form shown in Figure 4 have three possible positions CSi $(i=1,2,3)$, see Figure 3. The analysis of Tables 1-3 shows that if we have only one working sensor at our disposal, it should be placed at point $L5$ (yellow arrow in Figure 1). The guaranteed detection time of the source parameters will be *478* seconds (case of *CS3* source). In the case of any other location of the sensor in at least one scenario under consideration, this time will be longer. However, if we want to have the longest time available before the wave arrives on shore after determining the source parameters, we should choose sensor position *L2* (red arrow in Figure 3). This time will be *466* sec (again for the source *CS3*). With a different location of the sensor, we will find a case where this time will be shorter.

If we have two sensors at our disposal, they must be chosen differently. For the fastest detection time of the source parameters in the "worst" of three cases it will be sensors *L3* and *L10* (shown by yellow arrows in Figure 6), and this time will be *317* seconds (source *CS3*). That is, the addition of one sensor allows reducing the required time by almost 1.5 times. If we want to achieve the longest possible time before the wave arrives on the shore, we should place the sensors at the points *L1* and *L4* (shown by red arrows in Figure 6). This time will be *488* seconds (source *CS1*), which is slightly longer than in the case of one sensor.

Table 3: Source CS3 (the upper one at Figure 1). Wave travel time to the nearest coast is equal to 719 sec.

No Rec.	NPWP, sec.	T1, sec	T2, sec
L1	231	218	488
L2	242	233	477
L3	296	284	423
L4	314	304	405
L5	394	333	325
L6	500	412	219
L7	626	503	93
L8	782	615	0
L9	935	740	0
L10	1049	849	0

For the convenience of further analysis, the data about the optimal location of one and two sensors are collected in Tables 4 and 5.

Table 4: Optimal location of 1 and 2 sensors for fastest determination of source parameters

	Source parameters detected, sec		
	CS1	CS2	CS3
L5	394	354	478
L3+L10	296	262	317

It is clear from Table 4 that by introducing an additional sensor to the monitoring system it is possible to reduce the time for source parameters determination. The "reduction rate" for the necessary time is similar for all considered scenarios CSi, $i=1,2,3$. We may assume that doubling the number of sensors leads to the reduction of time to detect the source parameters compared to 30-40%. Additional numerical experiments are needed to get the exact numbers, which should definitely depend on a particular subduction zone.

Table 5: Optimal location of 1 and 2 sensors to have larger travelling time for the wave to approach nearest dry land after source parameters determination

	Wave travelling time to approach dry land after coefficients determination, sec		
	CS1	CS2	CS3
L2	477	528	466
L1+L4	488	567	708

In case we are interested in time one has after obtaining the source parameters before the wave approaches nearest shore, Table 5 shows, that this time increases after taking into consideration an additional sensor. However, the observed gain is practically negligible for *CS1* scenario and is compared to 40 sec (about 8%) for *CS2* scenario. Note that in these two scenarios we are able to determine source parameters rather fast, see Table 4.

In case of the most unfavorable *CS3* with the largest time required for the source parameters determination, wave traveling time to the nearest dry land increases valuably according to Table 5. This fact leads to a conclusion, that it is far nontrivial to choose the optimality criteria for the monitoring system.

Figure 6: Visualization of the digital bathymetry. Model Composed tsunami sources are indicated as *CSi*. Green crosses indicate artificial sensors

4. Discussion

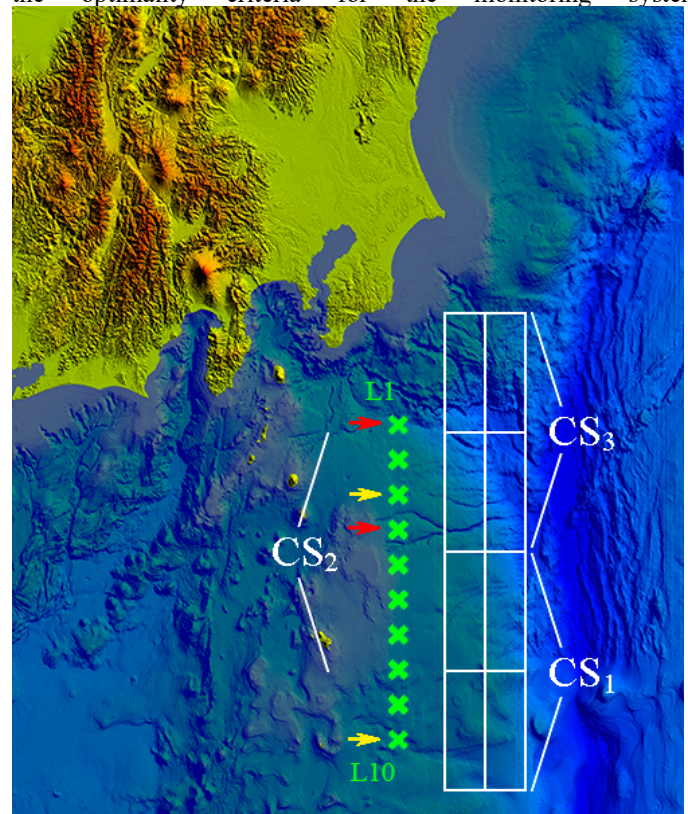Most studies on the organization of the tsunami detection system (location of sensors) to provide data to tsunami warning services have the objective of determining the wave parameters at the source as quickly as possible. By doing so, the distribution of maximum wave heights along the coastline can be predicted more quickly. However, numerical results show that a different location of the sensors would provide more time before the wave arrives at the nearest shore. Considering the fairly densely populated coastline of Japan, this parameter seems to be at least as important as the fastest wave detection. This should be taken into account when planning the location of additional sensors.

The optimal location of the surveillance system can be calculated (not just being randomly suggested) according to the selected criterion. The more sensors are used, the better the value of the selected criterion will be – the source parameters will be determined faster or after determining the source parameters there will be more time until the wave reaches the nearest shore.

Thus, when switching from one to two sensors in the model case under consideration, the time for which the algorithm determines the source parameters decreases from *478* to *317* sec (Table 4), that is, practically one and a half times (source *CS3*). Let us note that in other considered scenarios as well (sources *CS1* and *CS2*) this time decreases from *394* to *296* sec (*1.33* times less time needed) for the *CS1* case and from *354* to *262* sec (*1.35* times less) for the *CS2* source.

For the criterion "maximum time remaining until the wave reaches the nearest shore", this time increases from *466* to *488* sec when an additional sensor is added (Table 4). This is a comparative increase, but for the *CS3* source scenario, the increase in time to analyze and make decisions to evacuate the population is *242* sec (from *466* to *708* sec). This certainly may save lives.

Thus, when designing a monitoring system for tsunami warning centers, it is advisable to choose a criterion for the optimality of the system, taking into account various factors (including the cost of creation) and to optimize the location of sensors.

Conflict of Interest

The authors declare no conflict of interest.

Acknowledgment

References

[1] D. Kuzakov, M. Lavrentiev, An. Marchuk, "Toward the optimization of measurement system for tsunami warning," in 2021 International Conference Global Oceans 2021: San Diego - Porto, In Person Virtual, September 20-23, 2021, Town and County San Diego, doi: 10.23919/OCEANS44145.2021.9705912

[2] V.V. Titov, F.I. Gonzalez, "Implementation and testing of the method of splitting tsunami (MOST) model," in NOAA Technical Memorandum ERL PMEL-112, USA,1977.

[3] E. Gica, M. Spillane, V.V. Titov, C.D. Chamberlin, J.C. Newman, "Development of the forecast propagation database for NOAA's Short-term Inundation Forecast for Tsunamis (SIFT)," in NOAA Tech. Memo. OAR PMEL-139, NTIS: PB2008-109391, 2008.

[4] X. Wang, W.L. Power, COMCOT: A Tsunami Generation Propagation and Run-Up Model, GNS Science, 2011.

[5] A.C. Yalciner, B. Alpar, Y. Altinok, I. Ozbay, F. Imamura, "Tsunamis in the Sea of Marmara: Historical Documents for the Past, Models for Future," Marine Geology, **190**, 445-463, 2002.

[6] DART (Deep-ocean Assessment and Reporting of Tsunamis). Available online: URL http://nctr.pmel.noaa.gov/Dart/ (accessed on 20.07.2022).

[7] DONET system concept. Available online: URL https://www.jamstec.go.jp/donet/e/ (accessed on 31.07.2022).

[8] I.E. Mulia, K. Satake, "Synthetic analysis of the efficacy of the S-net system in tsunami forecasting," Earth Planets Space **73**(36), 2021. https://doi.org/10.1186/s40623-021-01368-6

[9] A. Ferrolino, R. Mendoza, I. Magdalena, J.E. Lope, "Application of particle swarm optimization in optimal placement of tsunami sensors," Peer J Comput. Sci. **6**:e333, 2020. DOI 10.7717/peerj-cs.333

[10] L. Yao, K. Goda, "Hazard and Risk-Based Tsunami Early Warning Algorithms for Ocean Bottom Sensor S-Net System in Tohoku, Japan, Using Sequential Multiple Linear Regression," Geosciences 12.9: 350, 2022.

[11] D.B. Percival, D.W. Denbo, M.C. Eble, E. Gica, H.O. Mofjeld, M.C. Spillane, L. Tang, V.V. Titov, "Extraction of tsunami source coefficients via inversion of DART® buoy data," Nat. Hazards, **58**(1), 567–590, 2011, doi: 10.1007/s11069-010-9688-1.

[12] V.K. Gusiakov, "Residual displacements at elastic halfspace surface," in Conditionally correct problems of mathematical physics of interpretation geophysical surveys, Eds. Computing Center SB RAS, Novosibirsk, 1978, 23-51. (In Russian).

[13] National Data Buoy Center. Available online: URL https://www.ndbc.noaa.gov/obs.shtml (accessed on 20.07.2022).

[14] M. Lavrentiev, D. Kuzakov, An. Marchuk, "Fast Determination of Tsunami Source Parameters," Advances in Science, Technology and Engineering Systems, **4**(6), 61-66, 2019, doi: 10.25046/aj040608

[15] J.J. Stoker, Water Waves. The Mathematical Theory with Applications, Interscience publishers: New York, NY, USA, 1957.

[16] D.R. Kincaid, E.W. Cheney, Numerical analysis: mathematics of scientific computing, **2**, American Mathematical Soc., 2002.

[17] A. Romanenko, P. Tatarintsev, "Algorithm for reconstruction of the initial surface disturbance at the tsunami epicenter", NSU J. of Information Technologies, **11**(1), 113-123, 2013.

[18] D. Kuzakov, M. Lavrentiev, An. Marchuk "Reconstruction of tsunami source by a part of wave time series before the first maximum" Journal of Physics: Conference series, 2019, 1268 012042, p 1-9

[19] J-DOSS|JODC [Electronic resource]: http://jdoss1.jodc.go.jp/vpage/depth500_file.html (accessed 18.07.2022).

ASTES

Transfer and Ensemble Learning in Real-time Accurate Age and Age-group Estimation

Anh-Thu Mai [*,1,2], Duc-Huy Nguyen[1,2], Thanh-Tin Dang[1,3]

[1]*Vietnam National University Ho Chi Minh City (VNU-HCM), Vietnam*

[2]*Training Program of Excellent Engineers in Vietnam (PFIEV), Ho Chi Minh city University of Technology (HCMUT) , Vietnam*

[3]*Faculty of Electrical and Electronics Engineering, Ho Chi Minh city University of Technology (HCMUT), Vietnam*

A R T I C L E I N F O

A B S T R A C T

Aging is considered to be a complex process in almost every species' life, which can be studied at a variety of levels of abstraction as well as in different organs. Not surprisingly, biometric characteristics from facial images play a significant role in predicting human's age. Specifically, automatic age estimation in real-time situation has begun to affirm its position as an essential process in a vast variety of applications. In this paper, two approaches are addressed as solutions for such application: prediction of accurate age and age group by using the two most fundamental techniques in the domain of deep learning – convolutional neural networks (CNNs) and deep neural networks (DNNs). In summary, this work can be split into two main key contributions. By applying a novel hierarchical aggregation built on the base of neural network developed from the training dataset, in the first stage, features extraction, the convolutional activation features are extracted from the captured facial image. As soon as this part is done, the features classification step is performed, in which Softmax Regression (SR) and majority vote classifiers are applied to predict accurate age and age group respectively. The effectiveness of the designed model was showed satisfactorily in the experimental results, which emphasizes the promising of the solution and indicates another direction for future development of algorithms and models in the field of machine learning.

1. Introduction

Automatic age prediction from face images can be employed in a huge number of scenarios, from video surveillance [1], healthcare system, health management and statistics purposes [2], performance of individuals recognition [3], advertisement according to users' age, or even criminal investigations [4]. The problem is the reliability of the results since the acquired images could be in unconstrained conditions because of lighting or pose, or when the photographed individuals do not aware of the cameras' presence. Thanks to the advent of computational approaches, these constraints become less and less stressful for automatic computer vision algorithms. Furthermore, this analysis must be completed in a limited time interval of milliseconds, owing to the fact that it is performed in real time condition. Consequently, it is necessary for the solution of this task to be both fast and accurate.

In order to achieve this goal, first of all, face detection is performed using a tool in real-time computer vision's deep learning based-face detector, OpenCV. Particularly, this method is built mainly on ground of Single Shot Detector (SSD) and ResNet backbone for the purpose of increasing the accuracy and accelerating the estimation process, which could be considered to be a compensation for some acceptable major setbacks such as having unconscious biases in the training set or detecting darker-skinned people less accurately than lighter-skinned ones when comparing with Haar-likes cascades [5] or histogram of oriented gradients (HOG) [6]. After the previous step has been fulfilled, by training with an abundant dataset, an age prediction model is created, thanks to which the features corresponding to each age are extracted using a structure of convolutional neural networks (CNNs). Meanwhile, a binary large object (blob) constructor pre-processes the input images and extracts the face region of interest (ROI) so as to calibrate the convolutional architecture for fast feature embedding (caffe) based model that is utilized in this work.

*Corresponding Author: Anh-Thu Mai, Email: thu.mai.k18@hcmut.edu.vn

Table 1: Outline of Some Outstanding Studies on Age Prediction

Publication	Feature representation	Face database/Database size	Algorithm	Evaluation protocol	Performance/Accuracy
[14]	2D shape, raw pixel values	Private/500	Regression	500 train, 65 test	MAE 4.3
[15]	Anthropometric model	HOIP	Classification	Leave-one-out	CS 57.3%(M), 54.7%(F)
[16]	Ages pattern subspace (AGES)	FG-NET/1002 MORPH	Regression	Train on FG-NET, Test on MORPH	MAE 8.83; CS 70%
[9]	Active appearance model	FG-NET/1002	Hybrid	Leave-one-person-out	MAE 4.97; CS 88%
[17]	BIF	MORPH II/55,132	Regression	50% train, 50% test	MAE 4.2
[11]	Active appearance model, label distribution	FG-NET/1002 MORPH II/55132	Classification	Leave-one-person-out (FG-NET), 10-fold cross-validation	MAE 4.8(FG-NET), 4.8(MORPH II)
[18]	Kullback-Leibler/raw intensities	LFW/150,000 MORPH II/55,132 FG-NET/1002	Classification (CNN)	N/A	MAE 2.8(FG-NET), 2.78(MORPH)

The remaining of this paper is arranged as follow. In the next section, we will briefly review some researches inspiring our work. The architecture of the model will be explained precisely in section 3. The overviewed algorithms and the detailed experimental results will be discussed in section 4 and 5 respectively. The last section provides a summary of this work as well as offers a conclusion and possible future development.

2. Related works

Since the early 2000s, automatic age prediction has drawn researcher's attention in the field of machine learning and has undergone a renewed interest some years later as a consequence of the availability of larger databases having more real-annotated date than in the past. Some noticeable researches are shown in Table 1 to represent the evolution of the methods. Overall, the process of this task involves two main phases: features extraction to pick out particular aging characteristics and features classification to divide these features.

Feature extraction stage. The use of a classifier based on support vector machines (SVMs) and support vector regression (SVR) is widely used in several distinct works, whereas other researchers, who concentrated on achieving a faster and better performance, relied mainly on the combination of textural and local appearance. Facial images analysed by those methods will be capture the variation in shape and intensity. Nevertheless, the applied of deep learning algorithm, especially CNNs and Deep Neural Networks (DNNs) in age estimation has become more and more popular [7][8]. Particularly, the work of using ordinal regression and multiple output CNNs for this task by Niu. has demonstrated superior performance in comparison with other methods, and acts as motivation factor for the development our the deep learning approach.

Pattern classification. It has been proposed, including, among others, to use SVMs and SVR [9], Partial Least Squares (PLS) and Canonical Correlation Analysis (CCA) [10], along with their regularized and kernelized versions, neural networks and their variant of Conditional Probability Neural Network [11]. In multi-task classification issues, Softmax Regression (SR) [12] shows that

it outperforms other methods in terms of performance. A detailed examination on these aging classification approaches has been shown in [13].

3. Deep learning based-face detector

According to the aforementioned technique that is used in this paper, the first step that is performed is face detector using OpenCV. More precisely, the performed face detector is established on a SSD following a ResNet-like features which allow the result to be both faster and more accurate. Besides, this method uses DNNs module barked into OpenCV's library without adjusting parameters and build a lightweight output model. Since the face detection task is much more accurate for lighter-skinned people, we make a decision of calibrating the pre-trained face detector with a dataset of muti-ethnic so as to regain the balance among different skin's colors.

4. Accurate age prediction

Before building the model from pre-trained weights, compiling it with some functions and then training, the facial images from the dataset were pre-processed. Figure 1 shows the overall approach.

4.1. IMDB-WIKI dataset

Among online available database, e.g. MORPH, FG-NET, Kaggle, etc. we chose public celebrities' images from IMDB-WIKI dataset, which offers approximate 0.5 million of images ranging from 0 to 100 years old. The age distribution of this dataset is shown in Figure 2. Furthermore, in this process, several images were randomly ejected so as to each age has the same amount of images. Therefore, about 62,000 images remain for training our CNNs.

4.2. Model's construction using VGG-like pre-trained weights:

In purpose of strengthen the quality of distinguished features, prior to training, a histogram equalization is applied for facial images. This pre-processing stage has claimed its importance from the received results.
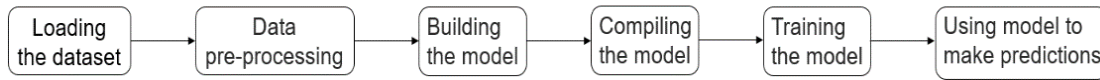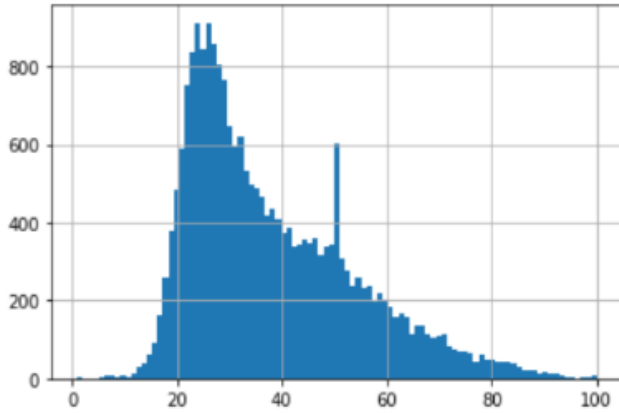
Figure 1: Ensemble process

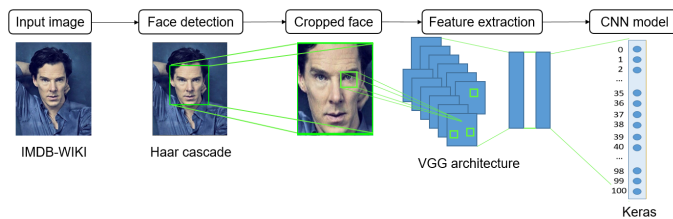Figure 2: Age distribution histogram from the IMDB-WIKI dataset

Figure 3: A general description of our procedure for developing CNN architecture in Keras

In this paper, we use VGG-like pre-trained weights and build our VGG model to deal with the experiments, which grants us the opportunity to fine-tune only the weights of the final layer instead of building and training from the scratch. The essential stage in the compilation process is believed to be selecting the optimizer and loss function. We employ "Adam", i.e. adaptive moment estimation, to adjust the learning rate in the performance of the optimization step. A lower learning rate would result in more accurate weights but in the interim it will stretch the handling time for other weights. Whereas for our loss function and accuracy calculating apparatus for the data use for validating, we utilize Categorical Cross Entropy [19], the foremost common choice for classifying patterns. As specified, transfer learning scheme was applied to train the model to assure that we obtain an output of the overall accurate age combined from 101 layers. Consequently, we might have an outcome with a superior achievement on human face's biometric characteristics.

When processing, an image with a fixed size 224x224 RGB was inputted into this network. The model has five convolutional blocks with a max-pooling at the end of each block. The number of filters are orderly 64, 128, 256, 512 and 512. A block with three dense layers is inserted at the end of the model. The final dense layer acts as a softmax function. This model type used is Sequential which is the most straightforward way to construct such model

layer by layer in Keras, which totally matches with the VGG neural network architecture [20]. The process of building such model's substructure architecture is clearly shown step-by-step in Figure 3.

In order to address a multi-class classification task, as aforementioned, the classifiers that show the finest results are usually a CNN which has SR as the last layer. The previous layers are a combination of Convolutional layers and nonlinear activation functions and pooling. These layers can be considered as a tool to help extract features of the data, the last layer is SR, a transparent but exceptionally effective linear classifier. By this way, we are able to assume that a collection of one-vs-rest classifiers is trained simultaneously, supporting each other, so it will result in better performance than training separately each classifier. The adequacy of CNNs, is that the both models use for feature extraction and classification will be trained together. This classifier allows us to find feasible coefficients which pair with the found feature vector, while the role of the feature extraction model is to fine-tune the coefficients of the convolutional layers in order to receive a linear, consistent feature result in comparison with the classifier in the last layer. We also make a checkpoint to monitor model over iterations and prevent it from overfitting. The iteration which has the least validation loss value will incorporate with the optimum weight coefficients so the validation loss will be monitored and only the best result will be saved.

5. Age-group prediction

5.1. Adience dataset

For age group estimation, Adience benchmark dataset, one of the newest databases which is designed for this kind of task, is used. Over 16000 unconstrained facial images are divided into 8 different age groups: 0-2; 4-6; 8-13; 15-20; 25-32; 38-43; 48-53; 60-.

5.2. Model using Caffe-based

Fistly, the input data images will have to go through a pre-processed phase, in which they will be randomly resized and cropped, subtracted mean values, scaled values with a scaling factor, switched the channel Blue to Red and vice versa by a function from OpenCV. As a result, we achieve a 4-dimensional main matrix with data formatted in batch size, channel, height, and width. The whole detailed process can be seen below in Figure 4.

The pre-trained caffe-based model, which used for detecting ages will go through a calibrating process. In this designed network, the system is built with three convolutional layers, each taken after by a rectified linear unit (ReLU) and followed by a pooling layer. The primary two layers are applied normalization by the local response normalization [21]. Constructed right after these convolutional blocks, a collection of 512 neurons will create a fully-connected layer and there are two such kind of layers.
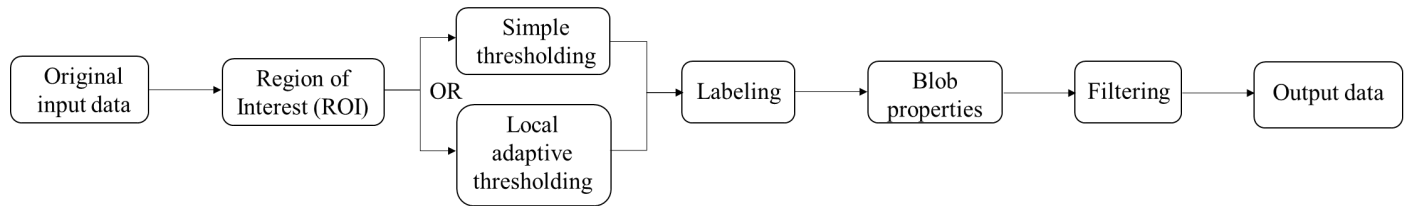
Figure 4: Data pre-processing pipeline

We tested with the method of using the designed model so as to predict age-group for novel faces. In fact, each 256×256 human's facial image will produce an assemblage of four 227×227 which are cropped from each edge as well as another one which takes the center position of the original image as the center. The network is represented by all five of these images in combination with their horizontal reflections, and the final estimation is chosen to be the average value over all of the variants. Nonetheless, there are numerous challenges with the Adience dataset's images, like occlusions or motion blur, which can cause minor misalignments and have a noticeable effect on the accuracy of the calculation. The over-sampling method is designed for this situation. By bypassing the requirement to improve alignment quality and forcusing on immediately supplying the network with many translated versions of the same face, it can correct these misalignments.

5.3. Transfer Learning on VGG Architecture for age-group prediction

In Figure 5, we illustrate our pipline for the proposed architecture that is designed and realized in this work. The convolutional layers are common and follow the pattern of those of VGG16 architecture. The fully connected layers, however are reduced because of our eight target classes. Hence, fc6, fc7 and fc8 has 512, 512 and 8 neurons, respectively.

Transfer learning: The weights of the convolutional network are loaded from VGG model trained on VGG-Face dataset. The model is then fine-tuned. Because there are so few training data, this is a vital procedure. This also provides quicker convergence and reduces overfitting for the model. The network is trained using data from the OUI-Adience Face Image Project. The main steps are outlined in Figure 5, where a pre-trained VGG-Face model based on the two datasets: IMDB-WIKI and VGG-Face CNN descriptor is loaded, froze superfluous weights, and added a customized classifier with pointed layers of trainable parameters to improve the original configuration. This customized classifier is then added to solve the multi-class classification task by training classifier layers on targeting training data, adjusting hyper-parameters, and unfreezing some additional layers if needed.

5.4. Ensemble learning

The next phase involves putting both of the aforementioned models into practice simultaneously under fresh conditions and selecting the superior model by evaluating the outcomes. The category that receives the most votes becomes the main age when classifying an image, which gives the impression that it is an election. As a result, we decide to combine the results using both the weighted majority voting and the soft voting. A summary of the process is shown in Figure 6.
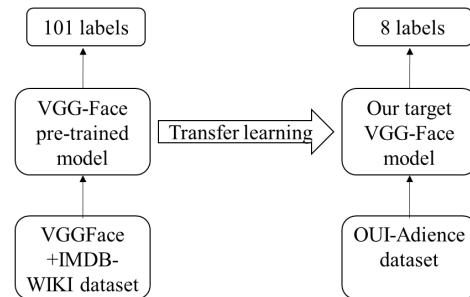
Figure 5: Overview of the Keras-based pipeline for CNN models

6. Overviewed algorithm

6.1. Accurate age prediction algorithm from front view

Because the change of face appearance is less changing and contains more information in frontal view than in profile views with the same rotation in depth, we only construct an age predictor for frontal view with a slight rotation.

When making a prediction from a new face image, the outputs will be a column tensor in which each element corresponds to a class's score. These scores, through softmax, will be normalized into probabilities and softmax classifier has a probabilistic interpretation [22] which will assign the probabilities to each class.

An input x has a probability a_i that it would fall into class i-th. For the age-set problem, y_i is a label, f_j represents the j-th element of the vector of class scores f, which connects the raw image through some rules to the class scores. By combining them, we get the following functions: the softmax function (1) and the cross-entropy loss function (2) [23]:

$$a_i = e^{f_{y_i}} \Big/ \sum_j e^{f_j} \qquad (1)$$

$$L_i = -\log\left(e^{f_{y_i}} \Big/ \sum_j e^{f_j} \right) = -\log\left(a_i \right) \qquad (2)$$

The result of this calculated prediction would be inaccurate and unreliable if we choose the one with highest possibility as the output, as there are a plenty of different classes in this task to estimate accurate age. In order to make this prediction become more reliable, in other words convert this task into a regression classification task, we calculate the probability of each class having an accurate age. By multiplying each output by its corresponding label and computing the sum of those values, we arrive at a summed result. Using the softmax expected value, E, as
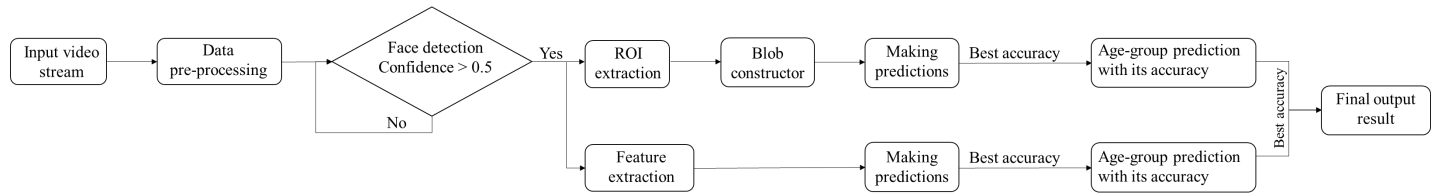
Figure 6: Our overall method

the basis for our apparent age prediction, we calculate the apparent age prediction as follows:

$$E(A) = \sum_{i=0}^{100} y_i a_i \qquad (3)$$

6.2. Majority vote classifiers

Age-group predictions rely primarily on majority votes. In terms of results fusion, among all hard voting and soft voting are the most common schemes.

Hard voting, also known as weighted majority voting, is defined based on the assumption that every image x has the classification C(x) of a model i-th, whose weights w_i, with the total of $w_1,...,w_m$ is equal to 1, C is from an collection of n labels along with I(.) as an indicator function. Each classifier will vote for a class, and the majority class ŷ with most votes [24]:

$$\hat{y} = \arg\max_{j \in n} \sum_{i}^{m} w_i I(C_i(x) = j) \qquad (4)$$

Soft voting, on the other hand, equalizes all classifiers to provide its proper probability for a particular target class. Supposing an image x receive the predicted result ŷ, with m is the number of models and n is the number of classes, then the probability is p_{mn}. The label which possesses the highest sum of weighted probability will represent as the output for this predicting method:

$$\hat{y} = \arg\max_{j \in n} \frac{1}{m} \sum_{i}^{m} p_{ji}(x) \qquad (5)$$

6.3. Real-time application

Face detection is performed by using the Feature Base Approach method. It locates faces by extracting structural features from some facial regions like eyes, nose, mouth etc., which help distinguish between a face and many other objects and then uses them to detect a face. In our paper, we implement a feature-based approach by using OpenCV.

Instead of creating and training the model from scratch, we use one of those trained Haar Cascade models in OpenCV which are available as XML files. In developing this application, we applied our model for real-time situation. Due to the fact that a real-time video stream is an assemblage of images, face detection is then applied for each frame taken by computer. By combining this model with age prediction, we then carry out the estimation step and complete the whole model.

7. Experimental results

In Figure 7 and Figure 8 below, we have illustrated two real-time test cases where each consists of three cases which are Age-group prediction only (left), Accurate age prediction only (center) and Simultaneous age prediction (right): single face and standard condition, and the other, multiple faces and unfavorable condition. Based on this typical case, we discover that our final model gives the most accurate and stable results with the actual age of the sample compared to the two monotone models that we originally built individually. In fact, the efficiency of the age prediction model is its association algorithm, because no matter how good the dataset is, it cannot wipe out all input situations (within the collection ability of our group). Therefore, we choose the optimal development of the algorithm rather than building the perfect dataset from scratch.

7.1. Accurate age prediction

The selective dataset was split into around 16000 train instances and then 6000 or thereabouts test instances. Our final train loss and accuracy were 2.892846 and 0.239473, respectively. Based on 6000 images of the test instances, our target model's mean absolute error (MAE) reaches the value of 4.09 years.

There are some typical scenarios in Table 2 in which we test our modes in real-time conditions and then evaluate their performance. We showed the summary of 50 example cases and each accurate age was tested by 5 different people. The average accuracy is 91.97%, age difference is 2.7 years, with the MAE for age groups under 18, 20-50 and over 60 are 1.2, 2.5 and 5.3, respectively

7.2. Age-group prediction

For the VGG age-group detector, we used a quarter of the dataset for validation and the rest for training. A 100-epoch training process took approximately 6 hours to complete. Its validation and training accuracy are respectively 74.3% and 72.95%. Besides, a one-off accuracy, i.e., the prediction of one more or one less than the actual age group, is 92.11% for this model.

This method outperforms some of the previous studies on age prediction in Table 1 when it comes to performance of a caffe-based age-group detector. A high level of accuracy can be achieved through the oversampling method, which provides an average accuracy of 50.27% with MAE 5.13 age groups and an average one-off accuracy of 84.55%. Furthermore, the display of real-time accuracy with predicted age group also allows us to establish the current stability of the result.
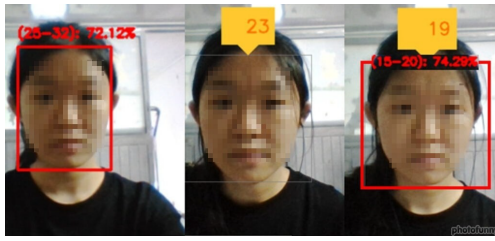
Figure 7: Age-group prediction only (left), Accurate age prediction only (center) and Simultaneous age prediction (right) in single face and standard condition of the 20-year-old girl.
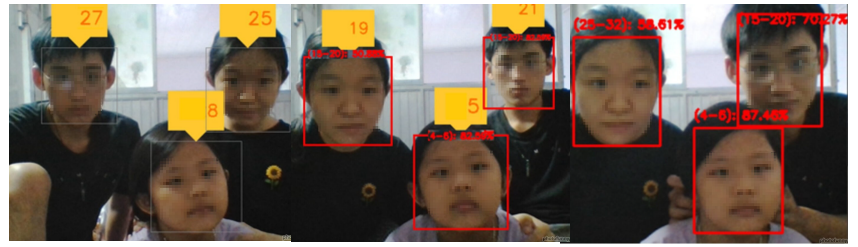
Figure 8: Age-group prediction only (left), Accurate age prediction only (center) and Simutaneous age prediction (right) in multiple faces and unfavorable condition of 3 people whose real age from left to right is 20, 5 and 21.

Table 2: Some Experimental Cases

Age-group test	8-13	8-13	15-20	15-20	25-32	25-32	38-43	38-43	60-	60-
Accurate age test	11	13	16	20	27	30	42	46	65	68
Real age	9,9,7,11, 10	12,12,12, 14, 13	14,16,14, 15,14	20,21,20, 20,20	29,29,30, 25,26	27,27,30, 32,32	37,36,37, 40,38	50,50,47, 51,51	71,71,70, 63,60	76,71,77, 63,72
Condition	Single face, Unfavora-ble	Single face, Standard	Multiple faces, Standard	Single face, Standard	Multiple faces, Standard	Single face, Unfavorable	Multiple faces, Unfavora-ble	Multiple faces, Standard	Multiple faces, Standard	Multiple faces, Unfavora-ble
Age error, accuracy	1.8 83.64%	0.8 93.85%	1.4 91.25%	0.2 99%	2 92.59%	2 93.33%	4.4 90.24%	3.8 91.74%	4.8 92.62%	5.8 91.47%

Table 3: Confusion Matrix of Caffe Model

	0-2	4-6	8-13	15-20	25-32	38-43	48-53	60-
0-2	**0.70**	0.26	0.03	0.00	0.01	0.00	0.00	0.00
4-6	0.15	**0.57**	0.22	0.02	0.03	0.01	0.00	0.00
8-13	0.03	0.17	**0.55**	0.08	0.14	0.02	0.00	0.01
15-20	0.01	0.02	0.15	**0.24**	0.51	0.06	0.01	0.01
25-32	0.01	0.01	0.09	0.11	**0.61**	0.15	0.02	0.01
38-43	0.01	0.01	0.07	0.06	0.46	**0.29**	0.06	0.05
48-53	0.01	0.01	0.06	0.05	0.26	0.34	**0.15**	0.13
60-	0.01	0.01	0.06	0.03	0.11	0.27	0.17	**0.36**

Table 4: Confusion Matrix of VGG Model

	0-2	4-6	8-13	15-20	25-32	38-43	48-53	60-
0-2	**0.86**	0.14	0.00	0.00	0.00	0.00	0.00	0.00
4-6	0.40	**0.83**	0.10	0.00	0.02	0.01	0.00	0.00
8-13	0.00	0.05	**0.76**	0.04	0.13	0.01	0.00	0.00
15-20	0.00	0.01	0.07	**0.33**	0.53	0.05	0.01	0.00
25-32	0.00	0.00	0.01	0.02	**0.79**	0.17	0.01	0.00
38-43	0.00	0.01	0.01	0.00	0.27	**0.64**	0.06	0.01
48-53	0.00	0.01	0.01	0.01	0.07	0.39	**0.40**	0.11
60-	0.00	0.00	0.01	0.00	0.02	0.24	0.30	**0.43**

We attribute the performance of our selective approach to the mutual support of both models. To be more specific, the performance of the caffe-based model for children under 13 is just above average, while VGG-based results are more reliable. But in return, due to confusion with other age groups, the over 60 years old perform less well in terms of efficiency. Moreover, the confusion matrixes in Tables 3 and 4 show that the caffe-based age predictor is heavily biased toward the 25-32 age group. According to the two shown tables, the VGG-Face model estimates age-group labels with greater accuracy than the other, however, the confusion rate (i.e. the difference between the main age label and its adjacent groups) of the caffe-model is smaller than that of the VGG-model in most age groups.

7.3. Comparison between two models

As a result, we find that our age prediction model is slightly influenced by external factors, e.g., real-time lighting conditions and the number of faces within the camera range especially when the boundary overlap of faces occurs. Since our free dataset contains a high number of noisy images, the quality of our prediction fluctuates between some adjacent results. In Table 1, we found that our ensemble method performs better in classification than other methods based on deep neural networks trained on public datasets such as MORPH [14-16] by focusing on the MAE index and the number of divided classes. Furthermore, our method achieved much better results than most deep neural network approaches [15-17], CNN weights are used as feature extractors, while ensemble learning algorithms and majority vote classifiers are applied to generate the most reliable results.

8.   Conclusion

A technique using pre-trained fine-tuned VGG-Face weights and Caffe-based to predict accurate age and age-group was described and developed in this paper. The built model showed satisfying results with an acceptable level of reliability, besides the speed and quality of the performances. Although under some unfavorable conditions the accuracy was not as expected, the model presented promising achievement and indicated the orientation to develop and optimize the algorithm in particular and the whole model in general. The contribution of this paper is to demonstrate a combination of methods that are not overcomplicated but still highly effective. From there we want to show that in addition to investing completely in the dataset, we can take advantage of the strengths of the existing well-performed ones and devote our time to develop and optimize the algorithm.

We intend to put under scrutiny other pre-trained weights as well as datasets and thereby create more ethnically balanced datasets which will be very helpful for more efficient feature extraction in order to evaluate and select the most appropriate model with the best performance. Additionally, a completed model for information collection like face recognition can be developed, is a challenge that authors of this work plan to overcome.

Conflict of Interest

All authors have no conflicts of interest to disclose.

Acknowledgment

References

[1]   A. Dantcheva, P. Elia and A. Ross, "What Else Does Your Biometric Data Reveal? A Survey on Soft Biometrics," IEEE Transactions on Information Forensics and Security, **11**(3), 441-467, 2016, doi: 10.1109/TIFS.2015.2480381.

[2]   Q. Zhang, D. Zhou and X. Zeng, "HeartID: A Multiresolution Convolutional Neural Network for ECG-Based Biometric Human Identification in Smart Health Applications," IEEE Access, 2017, doi: 10.1109/ACCESS.2017.2707460.

[3]   R. D. Labati, A. Genovese, V. Piuri and F. Scotti, "Weight estimation from frame sequences using computational intelligence techniques," IEEE International Conference on Computational Intelligence for Measurement Systems and Applications (CIMSA) Proceedings, 2012, doi: 10.1109/CIMSA.2012.6269603.

[4]   E. Eidinger, R. Enbar and T. Hassner, "Age and Gender Estimation of Unfiltered Faces," IEEE Transactions on Information Forensics and Security, **9**(12), 2170-2179, 2014, doi: 10.1109/TIFS.2014.2359646.

[5]   P. Viola and M. Jones, "Rapid object detection using a boosted cascade of simple features," Proceedings of the 2001 IEEE Computer Society Conference on Computer Vision and Pattern Recognition, doi: 10.1109/CVPR.2001.990517.

[6]   T. Surasak, I. Takahiro, C. Cheng, C. Wang and P. Sheng, "Histogram of oriented gradients for human detection in video," 5th International Conference on Business and Industrial Research (ICBIR), 2018, doi: 10.1109/ICBIR.2018.8391187.

[7]   P. Kruachottikul, N. Cooharojananone, G. Phanomchoeng, T. Chavarnakul, K. Kovitanggoon and D. Trakulwaranont, "Deep learning-based visual defect-inspection system for reinforced concrete bridge substructure: a case of Thailand's department of highways" J Civil Struct Health Monit, 2021, doi: 10.1007/s13349-021-00490-z

[8]   P. Kruachottikul, N. Cooharojananone, G. Phanomchoeng, T. Chavarnakul, K .Kovitanggoon, D. Trakulwaranont, and K. Atchariyachanvanich, "Bridge Sub Structure Defect Inspection Assistance by using Deep Learning," IEEE 10th International Conference on Awareness Science and Technology (iCAST), 2019, doi: 10.1109/ICAwST.2019.8923507.

[9]   G. Guo, Y. Fu, C. R. Dyer and T. S. Huang, "Image-Based Human Age Estimation by Manifold Learning and Locally Adjusted Robust Regression," IEEE Transactions on Image Processing, **17**(7), 1178-1188, 2008, doi: 10.1109/TIP.2008.924280.

[10]   G. Guo and G. Mu, "Simultaneous dimensionality reduction and human age estimation via kernel partial least squares regression," CVPR, 2011, doi: 10.1109/CVPR.2011.5995404.

[11]   X. Geng, C. Yin and Z. -H. Zhou, "Facial Age Estimation by Learning from Label Distributions," IEEE Transactions on Pattern Analysis and Machine Intelligence, **35**(10), 2401-2412, 2013, doi: 10.1109/TPAMI.2013.51.

[12]   F. Li, "Linear classification: Support Vector Machine, Softmax," 2021. [Online]. Available: https://cs231n.github.io/linear-classify/. [Accessed 9 June 2021].

[13]   I. Huerta, C. Fernández, A. Prati, " Facial Age Estimation Through the Fusion of Texture and Local Appearance Descriptors," Computer Vision - ECCV 2014 Workshops, doi: 10.1007/978-3-319-16181-5_51

[14]   A. Lanitis, C. J. Taylor and T. F. Cootes, "Toward automatic simulation of aging effects on face images," IEEE Transactions on Pattern Analysis and Machine Intelligence, **24**(4), 442-455, April 2002, doi: 10.1109/34.993553.

[15]   H. Takimoto, Y. Mitsukura, M. Fukumi, and N. Akamatsu, "Robust gender and age estimation under varying facial pose." Electronics and Communications, 2018, doi: 10.1002/ecj.10125

[16]   X. Geng, Z. -H. Zhou and K. Smith-Miles, "Automatic Age Estimation Based on Facial Aging Patterns," IEEE Transactions on Pattern Analysis and Machine Intelligence, **29**(12), 2234-2240, 2007, doi: 10.1109/TPAMI.2007.70733.

[17]   G. Guo and G. Mu, "Simultaneous dimensionality reduction and human age estimation via kernel partial least squares regression," CVPR, 2011, doi: 10.1109/CVPR.2011.5995404.

[18]   Z Z. Hu, Y. Wen, J. Wang, M. Wang, R. Hong and S. Yan, "Facial Age Estimation With Age Difference," IEEE Transactions on Image Processing, **26**(7), 3087-3097, 2017, doi: 10.1109/TIP.2016.2633868.

[19]   A. Kumar, "Keras – Categorical Cross Entropy Loss Function," 2020. [Online]. Available: https://vitalflux.com/keras-categorical-cross-entropy-loss-function/. [Accessed 2 June 2021].

[20]   Gilbert Tanner, "Introduction to Deep Learning with Keras," 2019. [Online]. Available: https://towardsdatascience.com/introduction-to-deep-learning-with-keras-17c09e4f0eb2. [Accessed 10 June 2021]..

[21]   K. Ricanek and T. Tesafaye, "MORPH: a longitudinal image database of normal adult age-progression," 7th International Conference on Automatic Face and Gesture Recognition (FGR06), 2006, doi: 10.1109/FGR.2006.78.

[22]   "Pandas DataFrame," 2019. [Online]. Available: https://www.geeksforgeeks.org/python-pandas-dataframe/. [Accessed 2 June 2021].

[23]   F.-F. Li, "Linear classification: Support Vector Machine, Softmax,," 2021. [Online]. Available: https://cs231n.github.io/linear-classify/. [Accessed 9 June 2021].

[24]   James, Gareth Michael, "Majority vote classifiers: theory and applications," Stanford University, 1998.

Mobility Intelligence: Machine Learning Methods for Received Signal Strength Indicator-based Passive Outdoor Localization

Fanchen Bao[1], Stepan Mazokha[1], Jason O. Hallstrom[*,1]

[1]*Florida Atlantic University, Institute for Sensing and Embedded Network Systems Engineering (I-SENSE), Boca Raton, FL, 33431, USA*

A R T I C L E   I N F O

A B S T R A C T

Knowledge of pedestrian and vehicle movement patterns can provide valuable insights for city planning. Such knowledge can be acquired via passive outdoor localization of WiFi-enabled devices using measurements of Received Signal Strength Indicator (RSSI) from WiFi probe requests. In this paper, which is an extension of the work initially presented in WiMob 2021, we continue the work on the mobility intelligence system (MobIntel) and study two broad approaches to tackle the problem of RSSI-based passive outdoor localization. One approach concerns multilateration and fingerprinting, both adapted from traditional active localization methods. For fingerprinting, we also show flaws in the previously reported area-under-the-curve method. The second approach uses machine learning, including machine learning-boosted multilateration, reference point classification, and coordinate regression. The localization performance of the two approaches is compared, and the machine learning methods consistently outperform the adapted traditional methods. This indicates that machine learning methods are promising tools for RSSI-based passive outdoor localization.

1   Introduction

City planning initiatives can benefit from insights into mobility patterns of pedestrians and vehicles. Given the prevalence of WiFi-enabled devices carried by individuals and their continuous emission of WiFi probe requests, such mobility patterns can be revealed by localization of the devices based on measurements of WiFi probe requests via the recorded received signal strength indicator (RSSI). **Active** and **passive** localization are the two standard modes of RSSI-based localization [1]. Active localization occurs on the target device with the help of a custom app that may or may not require cooperation (e.g., data exchange); it answers the question "Where am I?" Passive localization occurs without the device's knowledge in an anonymous manner; it answers the question "Where are you?" Due to the apparent difficulty of large-scale mobile app adoption for localization purposes, passive localization is the more realistic choice.

High variability in RSSI measurements due to fading (path-loss), shadowing (temporary obstruction between a sender and a receiver), and interference (overlap of WiFi channels) is a significant challenge in RSSI-based localization [2]. To mitigate RSSI variability, some active localization methods leverage device cooperation to obtain additional location-sensitive information, such as signal angle of arrival [3, 4], round-trip time [5], device orientation [6], and device prior location [7]. However, passive localization cannot benefit from

these methods, as it does not have the luxury of device cooperation.

Other active localization methods achieve good results without device cooperation [8]–[13]. Since the operations of these methods share similarities with passive localization, they might be transferable. However, fundamental differences exist between the two. For instance, missing data are unlikely in active localization because the probing signal is emitted by the access points in large numbers. In passive localization, the probing signal is initiated by the target device in an uncontrolled and sporadic manner. Consequently, the active localization methods may have data requirements unachievable in passive localization.

Previous work has also explored methods tailored to passive localization. However, they typically suit applications on a very small (indoor) or very large scale (entire city), making them inadequate for applications on a medium scale (within the span of a city street) (see Section 2.2 for details).

Therefore, investigation into methods suitable for RSSI-based passive localization in urban areas at the scale of a city street is necessary. The investigation can be divided into two parts. One focuses on the feasibility of adapting the methods used in cooperation-free active localization (hereinafter referred to as "traditional active localization methods") to passive localization; the other focuses on new approaches not fully explored by previous research on passive localization.

To facilitate the investigation, we have developed a privacy-

---

[*]Corresponding Author: Jason O. Hallstrom, Email: jhallstrom@fau.edu

centric mobility intelligence system (MobIntel) consisting of sensors and cloud infrastructure to collect and analyze RSSI measurements from anonymized WiFi probe requests. MobIntel has been tested in downtown West Palm Beach, Florida, to count the number of WiFi-enabled devices in a sensor's visible range and to calculate the percentage of devices that have persisted over time [14].

In this paper, which is an extension of the work initially presented in WiMob 2021 [15], we discuss a significant augmentation to the analytical facilities of MobIntel, exploring methods to conduct passive localization in a controlled environment, with the goal of identifying methods that are performant at the scale of a city street (1.4 km). The specific contributions of the paper include:

1. We conduct a systematic performance evaluation of two adaptations of traditional active localization methods—path-loss-based multilateration and fingerprinting—to support passive localization. We examine performance impacts under varying training and testing data sets, including (1) training and testing on individual RSSI measurements, (2) training and testing on averaged RSSI measurements, and (3) training on averaged, but testing on individual RSSI measurements. We also compare the performance of fingerprinting across three implementation methods, including vector-based Euclidean distance, Gaussian-based area-under-the-curve, and Gaussian-based tail probability.

2. For Gaussian-based fingerprinting in particular, we discover that the previously reported area-under-the-curve method, based on the arithmetic mean of the area-under-the-curve in a Gaussian distribution [7], does not perform well when there is large mismatch between the unknown RSSI measurements and the fingerprint of a reference point. We propose an alternative method, which uses the Gaussian tail probability as the likelihood of the unknown RSSI measurements originating from a particular reference point. We show that our proposed method achieves better localization performance.

3. We carry out a systematic evaluation of the accuracy impact of integrating machine learning algorithms—multi-layer perceptron, support vector machine, and K-nearest neighbors—with traditional active localization methods. We demonstrate that the machine learning-based methods outperform their traditional counterparts, regardless of which model is incorporated, or which training or testing set is used.

This paper is organized as follows. Section 2 provides a brief overview of related work in RSSI-based active and passive localization. Section 3 describes how we adapt the localization method from a traditional active context to a passive context and how we incorporate machine learning methods to boost performance. Section 4 presents details of data collection, including experimental design, hardware configuration, and data collection procedures. Section 5 discusses the preparation of various data sets for analysis. Section 6 reports the localization performance on methods adapted from traditional multilateration and fingerprinting. Section 7 describes the model training process for the machine learning methods and reports their localization performance. Section 8 compares localization performance among the best models of each method

investigated. Finally, Section 9 concludes the paper by presenting limitations and directions for future work.

2 Related Work

Prior work in RSSI-based localization has been conducted in active (localization done on the device) and passive (device has no knowledge of localization) settings. Here, a brief review of related work in both areas is presented. Emphasis is given considering applicability in urban areas.

2.1 Active Localization

Multilateration is a common method for active localization. It involves estimating distances from the target device to all nearby access points (APs) using an RSSI-distance model, and then applying linear least squares regression to pinpoint the device's location based on geometric analysis. Most work in multilateration focuses on building a better or simpler RSSI-distance model. In [12], the authors use the RSSI path-loss model as a base, treat the path-loss exponent as a random variable, and apply maximum likelihood estimation to derive a closed-form distance estimator. In [13], the authors use linear regression to fit RSSI-distance data to a generic path-loss model without estimating the path-loss exponent.

Relying solely on RSSI is usually not sufficient to deliver high accuracy. Thus, some studies incorporate additional location-sensitive information to mitigate RSSI variability and improve model performance. For example, in [5], the authors leverage the newly added fine timing measurement frame in WiFi protocols to compute the RF signal round-trip time between device and AP. Round-trip time is then fused with RSSI using Kalman filter to form a new parameter that provides better distance estimation than RSSI alone.

Other studies, as detailed in the review [4], drop RSSI completely and use signal angle-of-arrival, time-of-arrival, time-difference-of-arrival, and other more consistent measures to estimate device-to-AP distance. These techniques yield higher accuracy than RSSI-based multilateration.

The other commonly used method in active localization is fingerprinting. Fingerprinting has offline and online stages. In the offline stage, a test device roams around a target area surrounded by numerous APs. The APs emit RF signals constantly, which are captured by the test device at various reference points along its path. The RSSI measurements obtained at each reference point form a vector, or fingerprint, which describes the RSSI pattern representative of the reference point in the AP network. Together, the offline RSSI fingerprints form a **radio map** that is used during the online stage to match an unknown vector of RSSI measurements to the most likely reference point.

Much research has focused on the offline stage to improve the quality of fingerprints in the radio map. A common strategy is to incorporate additional location-sensitive information, such as azimuth data collected from a device's magnetometer [6] and a device's prior location and speed data [7, 16], such that an enhanced radio map can be created. These studies have shown that an enhanced radio map yields better localization performance.

One challenge in fingerprinting is the scalability of creating a high quality radio map outdoors. It requires data collection at a large number of reference points and deployment of more APs, both of which are daunting tasks. To resolve these issues, the authors of [17] propose crowdsourcing to build radio maps at large scales. Incentivized volunteers obtain RSSI measurements from public WiFi hotspots and upload the RSSI and GPS data to a server for radio map construction. Their work demonstrates the robustness of crowdsourced data for localization purposes, yet falls short of implementing an actual crowdsourcing solution.

Since passive localization is largely independent of the device, any method requiring additional location-sensitive data from the device cannot be readily adapted. Crowdsourcing might be adaptable because it does not require device cooperation. However, crowdsourcing in passive localization is different from active localization, because the participants are APs instead of mobile devices. In theory, these APs can sniff WiFi probe requests, record their RSSI measurements, and upload the recorded data. Yet, in practice, configuring these APs to serve as crowdsourcing endpoints, which are scattered around private businesses and homes, could be more challenging than simply generating the radio map manually. Thus, crowdsourcing is also not readily applicable to passive localization. In summary, the only methods that are readily adaptable from traditional active localization to passive localization are purely RSSI-based multilateration and fingerprinting.

2.2 Passive Localization

The authors in [18] were the first to propose the concept of device-free passive localization. It is based on the idea that an entity can be detected and tracked in a network of APs that are constantly sending beacons. Due to shadowing effects on the beacon's signal, it is possible to construct a radio map based on RSSI disturbances, and use fingerprinting to localize the entity even if it has no radio frequency capability. In [19], the authors push this idea further by creating a high density AP network, achieving not only localization, but radio tomographic imaging for one or two entities in the AP network. In [20], the authors present device-free localization models based on relevance vector machines and show good performance with single entity tracking in a cluttered environment.

Despite the progress in device-free passive localization, there are two major limitations that preclude its use in an urban environment. First, creating a sufficiently sensitive AP network requires a high density of APs ([19] use 28 APs and [20] use 24 APs, both in a 6 m by 6 m area); this is not scalable to city streets. Second, the number of devices localizable within the AP network is limited because if too many devices are present, the RSSI disturbances would be too chaotic to characterize. This limitation means that the device-free approach cannot handle crowded city streets.

The other approach in passive localization involves the target device emitting a signal spontaneously, such as a WiFi probe request, but without actually communicating with the APs. Probe request sensors are typically deployed at strategic positions to capture and process probe request data. In [21], the authores use this approach to localize static devices in an intersection. A target device is localized to the same position as the sensor that has captured the device's probe request. If multiple sensors detect a device, the position of the sensor receiving the highest RSSI measurements is used. However,

this method has low resolution if the number of sensors deployed is small (i.e., many devices would be localized to the same sensor if that is the only sensor nearby). This can be tolerated if the resolution requirement is low—for instance, at the scale of an entire city, a resolution level of intersections is acceptable—but it is not sufficient to reconstruct movement patterns on a street. One can improve resolution by deploying more sensors at smaller intervals, but this is not scalable.

In [22], the authors also use a qualitative method, but they improve resolution by deploying GPS-enabled mobile sensors carried by volunteers, who roam the monitored area. Since the sensors are mobile, localization is not static. If a mobile sensor and a target device have similar movement patterns, localization resolution can be high. However, if the mobile sensor moves in the opposite direction as the target device, localization resolution is compromised. Another drawback is that continuous human-based monitoring is infeasible over a long period of time. The paper suggests using drones or robots as alternatives, yet the scalability issue remains.

In [1], the authors propose a quantitative method to localize a stationary device using a single mobile sensor, without the need for a radio map. Their method requires the sensor to move either in a straight or right-angled path close to the target device's potential location, taking RSSI measurements from the device's WiFi probe requests at distinct points along the path. Using the RSSI path-loss model, they estimate the distance from the measurement points to the target device. Using these distance measurements, along with the known distance between the consecutive measurement points, they are able to estimate the location of the target device. The advantages of this method include low cost and ease of implementation. However, the method is limited by the requirement that the target device be stationary when the sensor is moving on the data collection path. It also suffers from the scalability issue associated with mobile sensors, if multiple targets are to be localized simultaneously.

Overall, the methods described above for passive localization fall short for the requirements of monitoring mobility patterns on city streets. The device-free methods are appropriate only at small scales, whereas the qualitative methods are only sensitive enough for large scales with low resolution requirements. The methods based on mobile sensors, though capable of delivering higher resolutions, present scalability issues in urban areas. Therefore, to achieve passive localization on city streets, a different approach is needed that leverages device participation (but not cooperation), uses static sensors, and is quantitative in nature.

3 Our Methods

This section describes two general localization approaches that satisfy the abovementioned requirements. The first approach involves adapting traditional active localization methods, including multilateration and fingerprinting. The second leverages machine learning, including machine learning-boosted multilateration, classification of reference points, and regression of reference points' coordinates.

3.1 Multilateration

The concept of multilateration in active localization is described in Section 2.1 and a visual representation is available in [23]. Since

this method is independent of device cooperation, its adaptation to passive localization is straightforward. Instead of using the RSSI measurements obtained by the target device from nearby APs, it relies on RSSI measurements acquired by the sensors from the target device.

The RSSI measurements must be converted to distance values between the target device and each sensor. This can be achieved using the basic RSSI path-loss model shown in (1), where R is the RSSI measurement, d is the distance (non-zero) between the sensor and the target, A is the RSSI measured at a reference distance from the target (e.g., 1 m), and n is the mean, environment-specific path-loss index that describes the speed of signal loss with increasing distance [24]. In a stable environment, A and n are constants. Therefore, the path-loss model can be treated as a negative linear relation between R and $\log(d)$, which can be fitted using linear regression to produce an RSSI path-loss model.

$$R = A - 10n \log(d) \tag{1}$$

After estimating device-to-sensor distances, we use least squares optimization to search for the coordinates $(\hat{x}, \hat{y})$ that minimize the residue in (2). In the equation, d_i is the estimated distance between the target device and the i-th sensor; (x_i, y_i) represents the coordinates of the i-th sensor; and $(\hat{x}, \hat{y})$ represents the estimated coordinates of the target device.

$$\text{Residual} = \sum_{i=1}^{N} \left(d_i - \sqrt{(x_i - \hat{x})^2 + (y_i - \hat{y})^2} \right)^2 \tag{2}$$

3.2 Fingerprinting

The concept of fingerprinting in active localization is described in Section 2.2. Similar to multilateration, the adaptation from active to passive localization only entails changing the manner in which RSSI is obtained, i.e., instead of measuring RSSI on the target device from signals sent by nearby APs, we measure RSSI on the nearby sensors from the signal sent by the target device.

We employ two methods to establish RSSI fingerprints. The first involves *vector-based fingerprinting*. We use RSSI vectors as fingerprints, in which each value is the mean of all RSSI measurements obtained by a specific sensor at a given reference point [11]. For example, given N sensors $S_1, S_2, ..., S_N$ and M reference points $P_1, P_2, ..., P_M$, we denote $R_{ij1}, R_{ij2}, R_{ij3}, ...,$ as the RSSI measurements emitted from reference point P_i ($1 \leq i \leq M$) and captured by sensor S_j ($1 \leq j \leq N$). Let μ_{ij} be the mean of R_{ij1}, $R_{ij2}, R_{ij3}, ...$. The vector-based fingerprint of P_i can be written as $F_i^V = [\mu_{i1}, \mu_{i2}, ..., \mu_{iN}]$.

When a target device generates a vector of RSSI measurements $U = [R'_1, R'_2, ..., R'_N]$ at an unknown location, the penalty of matching U to F_i^V can be approximated by their Euclidean distance. The smaller the distance, the more likely the target device originates from reference point P_i.

The second method is *Gaussian-based fingerprinting*. It uses a set of Gaussian distributions as RSSI fingerprints, where each distribution corresponds to the RSSI measurements obtained by a specific sensor at a given reference point [7]. Extending the example above, *Gaussian-based fingerprinting* computes both the mean (μ_{ij}) and

standard deviation (σ_{ij}) of RSSI measurements collected by sensor S_j with regard to reference point P_i. The Gaussian distribution is expressed in (3).

$$g_{ij}(x) = \frac{1}{\sigma_{ij}\sqrt{2\pi}} e^{-\frac{1}{2}\left(\frac{x-\mu_{ij}}{\sigma_{ij}}\right)^2} \tag{3}$$

Considering a reference point P_i, and N sensors $S_1, S_2, ..., S_N$, P_i's Gaussian-based fingerprint can be expressed as a set of distributions $F_i^G = \{g_{i1}(x), g_{i2}(x), ..., g_{iN}(x)\}$.

Given a set of RSSI measurements $U = [R'_1, R'_2, ..., R'_N]$ from the target device, the penalty of matching U to F_i^G can be estimated in two ways. The first is the area-under-the-curve (AUC) method, proposed by [7]. It computes the AUC (denoted as A_{ij}) for each R'_j under the Gaussian distribution $g_{ij}(x)$, as shown in (4). The penalty of matching U to F_i^G is approximated by the mean of all A_{ij}. The smaller the mean over A_{ij}, the more likely the target device originates from reference point P_i.

$$A_{ij} = \left| \int_{\mu_{ij}}^{R'_j} g_{ij}(x)dx \right| \tag{4}$$

Our initial localization results show that *Gaussian-based fingerprinting* with the AUC method does not perform well, especially when there is significant misalignment between some R'_j and μ_{ij}. This is most likely due to the flaw of the penalty structure in the AUC method (see Section 6.2 for details). To offer a better alternative, we propose the **tail method**, which uses tail probabilities to represent the likelihood that an individual R'_j originates from $g_{ij}(x)$. The product of all such individual likelihoods is the overall likelihood that U matches F_i^G. Concretely, let L_{ij} be a likelihood estimator, which is the smaller of the two AUCs from the cumulative density functions extending from R'_j to either tail of the distribution. Figure 1 illustrates the definition of L_{ij}. In the figure, R'_j is placed in a Gaussian distribution $g_{ij}(x)$, with mean μ_{ij} and standard deviation σ_{ij}. L_{ij} is the AUC from R'_j to the right tail. The larger the value of L_{ij}, or the closer R'_j is to μ_{ij}, the more likely R'_j originates from $g_{ij}(x)$.
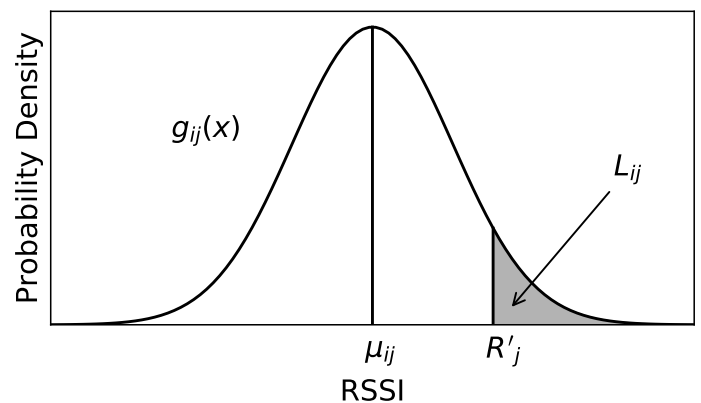

Figure 1: Tail Probability of R'_j in a Gaussian Distribution $g_{ij}(x)$

L_{ij} can be written as (5). The penalty of matching U to F_i^G can be approximated by the product over all L_{ij}, which is then converted to the sum of the negative logarithm of all L_{ij} to facilitate

computation. The smaller the sum, the more likely the target device originates from reference point P_i.

$$L_{ij} = \int_0^{\min(R'_j,\, 2\mu_{ij}-R'_j)} g_{ij}(x)dx \qquad (5)$$

Once the penalty is obtained from the target device to all reference points using either the vector- or Gaussian-based method, K-nearest neighbors is used to find the top k best-match reference points. The exact value of k is determined empirically via a validation set. The average location of the top-k reference points is the predicted location of the target device.

3.3 Machine Learning-boosted Multilateration

We use the RSSI path-loss model in (1) to estimate distance based on RSSI measurement. However, (1) does not capture all the error terms [10]. While it is possible to create more complex path-loss models with add-on error terms, we can train a standard machine learning model to "learn" the relationship between RSSI measurements and distances, with error implicitly included. Machine learning may capture relationships not explicitly described by a physical model. Thus, it is likely that a machine learning model will perform better than the idealized physical model in (1). We use three standard machine learning algorithms—multi-layer perceptron (MLP), support vector machine (SVM), and k-nearest neighbors (K-NN)—to train regression models from RSSI measurements and distance at each sensor. Each model is then used to conduct multilateration, as described in Section 3.1.

3.4 Machine Learning Classification of Reference Points

In fingerprinting, a set of RSSI measurements are passed to a fingerprinting algorithm as inputs, and the most likely reference point is returned as the localization output. This process is similar to a machine learning classification model, where input features are RSSI measurements, and output labels are reference points. The difference between the two is that the former uses pre-specified rules to determine how RSSI measurements match reference points, whereas the matching is "learned" from training data in the latter. We apply the same machine learning algorithms (MLP, SVM, and K-NN) to train classifiers that map a set of RSSI measurements to the best-match reference point.

3.5 Machine Learning Regression of Coordinates

In [9], the authors offer a simple approach to performing active localization. They train a machine learning regressor that takes RSSI measurements and propagation delays of transmitted signals as input, and directly predicts the GPS coordinates of a target device. Despite not having access to the propagation delay data, we can still adapt this approach to passive localization using the RSSI measurements alone. We follow the same setup as in Section 3.4, but instead of training a classifier, we train two regressors that take RSSI measurements as input and predict a reference point's x- and y-coordinate, respectively. With the two regressors, we can directly estimate a target device's location based on the RSSI measurements.

4 Data Collection

To evaluate the passive localization methods discussed in Section 3, RSSI measurements from mock probe requests, along with the coordinates of reference points, were collected in a semi-controlled environment. In the following sections, we present the experimental setup, experimental design, hardware details (sensor and emitter), field preparation, and data collection procedure.

4.1 Experimental Design

Figure 2(A) shows the layout of the testbed. Each cell is a 1 m by 1 m square, making the entire field 15 m by 15 m. Four sensors (red dots) s_1, s_2, s_3, and s_4 are placed at coordinates (0, 15), (15, 15), (0, 0), and (15, 0), respectively. During data collection, an emitter is placed on each data collection point (blue dots) and allowed to send approximately one-thousand mock probe requests. Each contains a Media Access Control (MAC) address that is traceable to a specific data collection point, distinguishable from a genuine probe request, and unique. After a mock probe request is captured by a sensor, the data is uploaded and stored in a database hosted on Amazon Web Services (AWS). Since four sensors are present in the testbed, at most four RSSI measurements are collected per probe request.
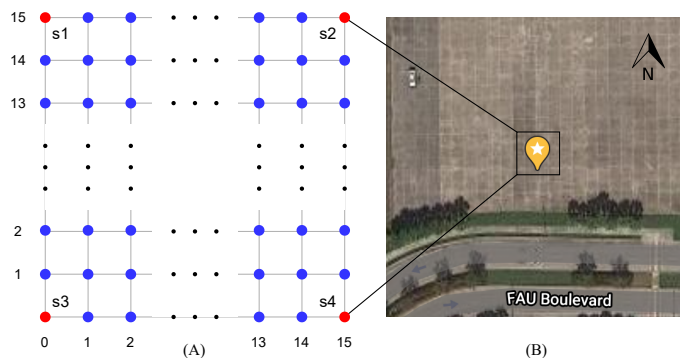
Figure 2: Experimental design and satellite view of the testbed

4.2 Hardware - Sensor

We used the same sensor described in [14]. It captures WiFi probe requests from the environment, removes duplicate MAC addresses at each 30-second window, and uploads aggregated data to AWS. In this paper, we added a new feature to differentiate mock probe requests from genuine probe requests, which allows the sensor to upload mock probe requests to a database dedicated to the experiment. The uploaded data include MAC address, time of capture, and RSSI measurement.

4.3 Hardware - Emitter

We used the same stress testing device described in [14] as the emitter of mock probe requests. It emits WiFi probe requests with a custom MAC address, on a specified channel, at a specified rate.

MAC address customization ensures traceability. The first four letters of the address are synced to the time of emission (timezone EST) in the format "HH:MM". Since the timestamp at each data

collection point is recorded, a time-stamped MAC address encodes the location where the mock probe request was emitted. To ensure mock probe requests are distinguishable from genuine probe requests, the fifth and sixth positions of the address are fixed as "00". A "HH:MM:00" prefix guarantees few, if any, collisions with genuine probe requests. Finally, to ensure that mock probe requests are unique among themselves, the remaining six positions are filled with random hexadecimals. As an example, a mock probe request emitted at 3:04 PM EST would have a MAC address similar to "15:04:00:1A:2B:3C".

The MAC address customization is only traceable at the granularity of one minute. If two mock probe requests are emitted from different data collection points within the same minute of an hour, their locations cannot be distinguished (i.e. the first four letters of their MAC addresses would be identical). To avoid such complications, the emitter remains at each data collection point for at least a full minute before moving to the next. In the experiment, the emitter uses *cronjobs* to send approximately 1,000 mock probe requests in the first 50 seconds of each minute, and zero in the remaining 10.

4.4 Testbed Preparation

An empty outdoor area (GPS: 26.381488, -80.099640) with no nearby obstacles was used as the testbed to avoid complications in RSSI measurement. Figure 2(B) shows an overhead view of the field. Figure 3 provides a detailed view after the 15 m by 15 m grid has been prepared with spray chalk. The southwestern corner is chosen as the origin point of the field, with coordinates $(0, 0)$.
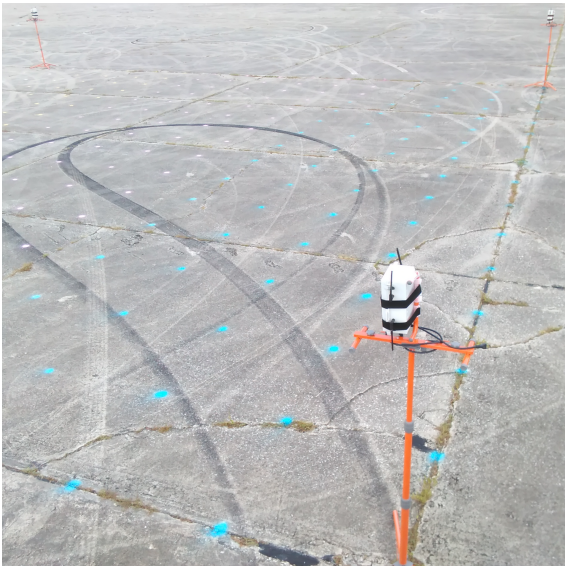
Figure 3: Mounted sensors on the testbed with grid drawn

The sensors were mounted on tripods, with an elevation of approximately 1.8 m above the ground. The four tripods were positioned at s_1, s_2, s_3, and s_4, as illustrated in Figure 2. Three of the tripods are visible in Figure 3.

4.5 Data Collection Procedure

Data are collected by placing the emitter on each data collection point. The emitter is mounted on the same type of tripod as the sensor, but with an elevation of only 1 m. This mimics the height at which a WiFi-enabled device is likely to be carried by a pedestrian. During the first 50 seconds of each minute, the emitter is left alone on the data collection point, without anyone present within the boundaries of the testbed. In the remaining 10 seconds, a researcher enters the field and moves the emitter to the next point. This setup ensures that signal transmissions are not affected by transient obstructions. At each data collection point, the coordinates and the current timestamp are recorded. This procedure is repeated until all data collection points are visited.

Data collection for this manuscript was conducted from 15:00 to 20:00 on 2020-07-16.

5 Data Preparation

The raw probe request data contains 221,553 observations, one per mock probe request. Each observation contains five parameters, corresponding to the RSSI measurement (one per sensor) and timestamp. Observations with missing measurements are discarded. The resulting **cleaned data set** contains 171,537 observations. To further reduce the computation cost of model training, and to balance the number of observations across data collection points, 100 observations are randomly selected from each data collection point to form the **sampled data set**.

The sampled data set is one of the two data sets used in this paper. It contains 25,200 rows and 11 parameters. Each row corresponds to an individual mock probe request. The parameters correspond to four RSSI measurements (R_1 through R_4), coordinates of the data collection points (x and y), distances to each sensor (d_1 to d_4), and unique labels of the data collection points (*label*). Table 1 shows the structure of the sampled data set.

Table 1: Structure of the sampled data set

$R_1...R_4$	x	y	$d_1...d_4$	label
-44 ... -41	0.0	1.0	14.0 ... 15.0	16
-43 ... -41	0.0	2.0	13.0 ... 15.1	32
...	...	...	...	...

The other data set used in this paper is the **mean data set**, derived from the cleaned data set by taking the mean and standard deviation of RSSI measurements from each sensor at each data collection point. The mean data set contains 252 rows and 15 parameters. Each row corresponds to a data collection point. The parameters correspond to four mean RSSI measurements (μ_1 to μ_4), coordinates of the data collection points (x and y), distances to each sensor (d_1 to d_4), four RSSI standard deviations (σ_1 to σ_4), and unique labels of the data collection points (*label*). Table 2 shows the structure of the mean data set.

Table 2: Structure of the mean data set

$\mu_1 \dots \mu_4$	x	y	$d_1 \dots d_4$	$\sigma_1 \dots \sigma_4$	label
-44.3, ..., -42.8	0.0	1.0	14.0 ... 15.0	0.93 ... 1.15	16
-44.1, ..., -40.7	0.0	2.0	13.0 ... 15.1	1.60 ... 0.64	32
...		...	...	...	...	...

After random shuffling, the sampled data set is split into a **sampled training set** (80%, 20,160 observations) and a **sampled testing set** (20%, 5,040 observations) using `scikit-learn` [25]. The mean data set cannot undergo the same splitting procedure due to having only one observation per data collection point. Hence, the entire mean data set is treated as the **mean training set** (252 observations). Finally, the mean and standard deviation of RSSI measurements by each sensor at each data collection point from the sampled testing set form the **mean testing set** (252 observations).

The training sets are used exclusively for model training and validation. In particular, the sampled training set is used in all methods except fingerprinting; the models thus trained are called **sampled models**. The mean training set is used in all methods; the models thus trained are called **mean models**. The difference between sampled and mean models is that the former is tuned using the individual observations in a training set, whereas the latter is tuned by their mean values. It is worth noting that averaging RSSI measurements seems to have both positive and negative impacts on model performance, as it simultaneously reduces random error [2] and training size. It is thus interesting to study how the performance of the mean model compares to that of the sampled model.

All data preparation procedures were conducted using the `pandas` Python library [26]. Figure 4 illustrates the relationships among the derived data sets, where their names, lineage, and shapes (rows × columns) are shown.
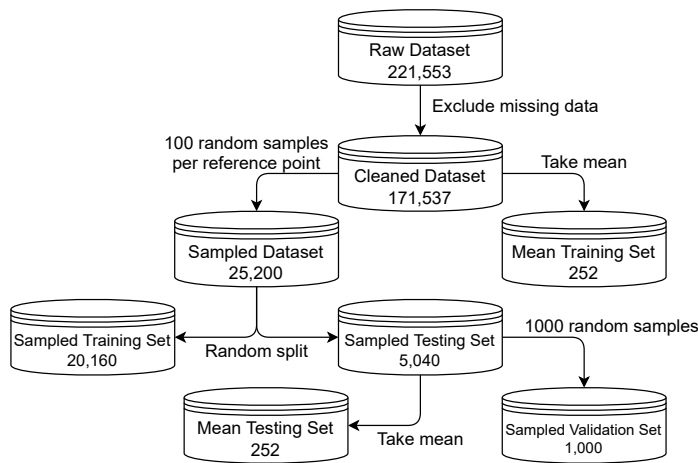

Figure 4: Relationship among all data sets

6 Traditional Methods

In this section, we present the adapted multilateration and fingerprinting methods for passive localization and consider their performance. Here, localization performance is visualized by the cu- mulative distribution function (CDF) curve of localization error. Localization error is defined as the Euclidean distance between the predicted and the true coordinates of a test observation. The larger the area-under-the-curve of a CDF curve of localization error, i.e., the closer the curve gets to the top and left corner, the better the localization performance.

6.1 Multilateration

Two RSSI path-loss models, one using the sampled training set and one using the mean training set, are created by linear regression according to (1) for each sensor. The performance of the two models, evaluated on the sampled testing set, is shown in Table 3. The R^2 score describes the amount of variance explainable by the path-loss model, and the mean absolute error (MAE) describes the error between the estimated and actual distance. Within each sensor, the two models have almost identical performance. This means that averaging RSSI measurements does not alter model performance. Across the models of different sensors, s_4 has the best performance, whereas s_1 has the worst. This may be explained by a consistent source of interference from the northwest corner of the testbed. Since s_1 is closest to the northwest corner, it was affected the most. s_4 is furthest from the interference source, so it was affected the least. However, the validity of this explanation cannot be verified until the same performance pattern repeats over time in future research.

Table 3: Metrics of the path-loss model

Sensor	Sampled		Mean	
	R^2	MAE	R^2	MAE
s_1	0.61	4.62	0.61	4.63
s_2	0.65	4.06	0.65	4.07
s_3	0.61	4.03	0.61	4.03
s_4	0.71	3.44	0.71	3.46

Two multilateration models are generated, one based on the sampled RSSI path-loss model and the other based on the mean RSSI path-loss model. We first convert RSSI measurements to distances, and then pass the distance data to `scipy`'s least squares optimization API to estimate the target device's coordinates [27]. Figure 5(A) demonstrates the localization performance of the traditional multilateration method. The x-axis denotes localization errors, and the y-axis denotes the probability that a model's localization error is smaller or equal to a selected x-axis value. The blue (sampled-sampled), orange (mean-sampled), and green (mean-mean) curves represent the localization performance under three scenarios: the sampled model tested on the sampled testing set, the mean model tested on the sampled testing set, and the mean model tested on the mean testing set, respectively.

The sampled-sampled curve does not show on the figure because it overlaps with the mean-sampled curve. This is expected because the sampled and the mean RSSI path-loss models have similar distance estimation performance. The mean-mean scenario performs slightly better than the other two. However, this is likely an artifact because the mean training and testing sets are very similar. Recall that the cleaned data set is the source of the mean training set, and

the sampled testing set is the source of the mean testing set (Figure 4). Since the sampled testing set is a subset of the cleaned data set, the mean testing set shares information with the mean training set. The similarity between the mean testing and training sets inflates the measured performance of the mean-mean scenario.

6.2 Fingerprinting

The radio map for vector-based fingerprinting is a 252×4 matrix prepared from the mean training set, where each row represents a reference point, and each column represents the mean RSSI measurements from a sensor. As mentioned in Section 3.2, we empirically determine k, the number of top-match reference points that produces the best coordinate estimation. A series of fingerprinting models parameterized with different values of k are used to perform localization on a validation set. The k leading to the least validation error is selected. Usually, the validation set is withheld from the training set. However in fingerprinting, the mean training set, which is also the radio map, has no redundancy to supply a validation set. Therefore, we set aside 1,000 observations from the sampled testing set as the validation set (Figure 4). The observations in the validation set are not included in evaluating model performance. Validation error is defined as the root mean squared localization error, following [11].
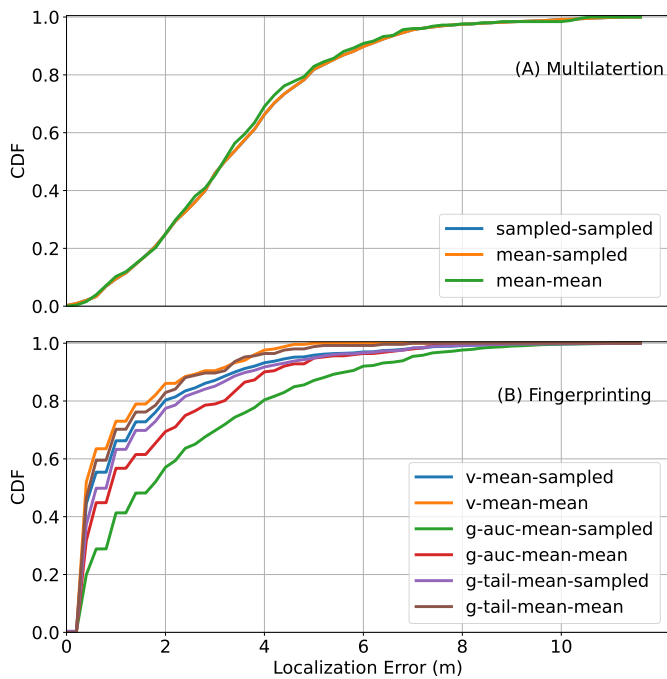

Figure 5: CDF curves of error in traditional methods

We use `scikit-learn`'s K-nearest neighbor API to search for the optimal k. The API is called with default settings, except `algorithm` is set to *brute*, and `n_neighbors` is set to k, which ranges from 1 to 20 for each validation run. For the data sets collected, we find that the validation error reaches its minimum when $k = 2$. Using this k, we evaluate the performance of vector-based fingerprinting; results are shown in Figure 5(B). The axis layout is the same as described earlier. The blue (v-mean-sampled) and

orange (v-mean-mean) curves represent localization performance when vector-based fingerprinting is tested on the sampled (excluding the validation set) and mean testing sets, respectively. Similar to traditional multilateration, the performance of v-mean-mean is better than that of v-mean-sampled. Again, this is most likely an artifact due to information overlap between the mean testing and training sets.

The radio map for Gaussian-based fingerprinting is a 252×4 matrix prepared from the mean training set, where each row represents a reference point, and each column represents the Gaussian distribution, modeled from the mean and standard deviation of the RSSI measurements from the corresponding sensor. We follow the same procedure described above to find the best k, except that in the K-nearest neighbor API, (4) and the mean over A_{ij} are used for the AUC method, whereas (5) and the sum over negative logarithm of L_{ij} are used for the tail method. The result of the search shows that the minimum validation error is reached when $k = 2$ for both the AUC and the tail methods. Figure 5(B) shows the localization performance of Gaussian-based fingerprinting based on the optimal k value. The green (g-auc-mean-sampled) and red (g-auc-mean-mean) curves represent the performance under the AUC method, while the magenta (g-tail-mean-sampled) and brown (g-tail-mean-mean) curves represent the performance under the tail method. Both the g-auc-mean-sampled and g-tail-mean-sampled curves are based on the sampled (excluding the validation set) testing set, whereas both the g-auc-mean-mean and g-tail-mean-mean curves are based on the mean testing sets. The g-auc-mean-mean and g-tail-mean-mean curves again exhibit better performance than the g-auc-mean-sampled and g-tail-mean-sampled curves, respectively, which is likely an artifact.

Comparing performance across all curves (excluding the ones under mean-mean scenario), the vector-based fingerprinting (v-mean-sampled) performs the best. However, its lead over Gaussian-based fingerprinting under the tail method (g-tail-mean-sampled) is very modest.

Comparing the two methods within Gaussian-based fingerprinting, the tail method consistently outperforms the AUC method. This is most likely due to the difference in penalty structure, where the AUC method, unlike the tail method, does not penalize misalignment proportionally to its severity. Figure 6(A) shows an example of how the penalty structure of the AUC method would fail to match a set of unknown RSSI measurements to the most probable fingerprint. In the figure, a Gaussian-based fingerprinting radio map is visualized, which contains two reference points (P_1 and P_2), each fingerprinted by two sensors (S_1 and S_2). The two blue distributions represent the RSSI fingerprint of P_1, denoted by the means $[\mu_{11}, \mu_{12}]$. Similarly, the two orange distributions represent the RSSI fingerprint of P_2, denoted by the means $[\mu_{21}, \mu_{22}]$. For simplicity, all distributions are assumed to have the same standard deviation. The set of unknown RSSI measurements, $U = [R'_1, R'_2]$, are illustrated by two black dashed lines. Finally, the areas-under-the-curve used in the AUC method are labeled as A_{11} and A_{12} for P_1, and A_{21} and A_{22} for P_2.
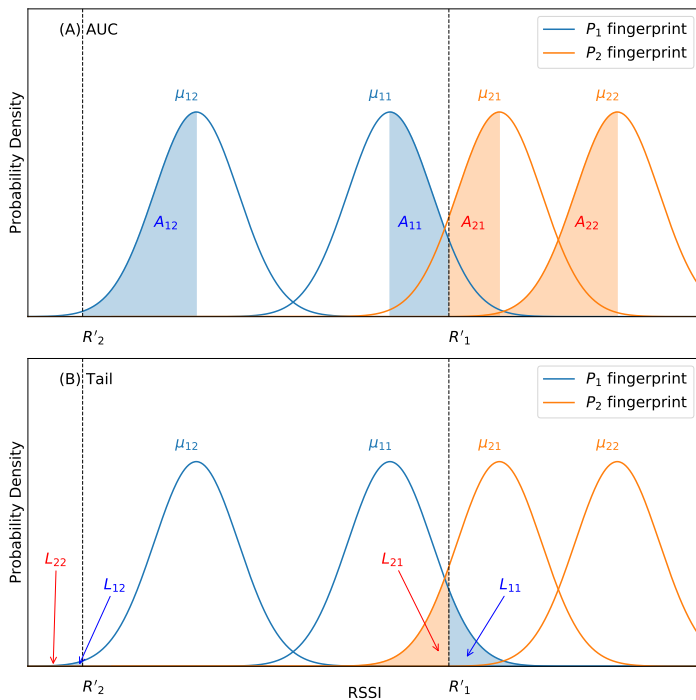
Figure 6: Example of matching under AUC or tail methods

Although it is clear that P_1 is a better match for U than P_2, it is not apparent in Figure 6(A). According to the AUC method described in Section 3.2, the match is selected as the smaller of $A_{11} + A_{12}$ and $A_{21} + A_{22}$. Due to the large misalignment between R'_2 and both μ_{12} and μ_{22}, we have $A_{12} \approx A_{22}$. Thus, the actual comparison is between A_{11} and A_{21}, which does not yield a clear winner at first glance. However, the decision should not have been left to a comparison between A_{11} and A_{21} in the first place. The extreme misalignment between R'_2 and μ_{22} should have already disqualified P_2. The AUC method is unable to recognize this because its penalty structure is inversely proportional to the severity of RSSI misalignment (i.e., the amount of penalty per unit of misalignment decreases as misalignment becomes more severe). R'_2 demonstrates how this penalty structure fails. While it is expected that a match between R'_2 and μ_{22} is penalized much more than a match between R'_2 and μ_{12}, the actual penalty associated with the former (A_{22}) is almost the same as the penalty associated with the latter (A_{12}). Thus, the failure to proportionally penalize misalignment makes the AUC method ill-equipped for Gaussian-based fingerprinting.

On the contrary, Figure 6(B) illustrates that the tail method can readily match U to P_1 as expected. The layout of Figure 6(B) is the same as Figure 6(A), except that the areas-under-the-curve are redefined and labeled as L_{11} and L_{12} for P_1, and L_{21} and L_{22} for P_2. According to the tail method described in Section 3.2, the match is selected as the smaller of $-lg(L_{11}) - lg(L_{12})$ and $-lg(L_{21}) - lg(L_{22})$. While L_{11} and L_{21} remain similar, the difference between L_{12} and L_{22} is large, with L_{22} being virtually 0. As a result, $-lg(L_{11}) - lg(L_{12})$ is easily smaller than $-lg(L_{21}) - lg(L_{22})$, which matches U to P_1. The reasons why the tail method works are two-fold. First, its penalty structure is proportional to the severity of RSSI misalignment, which ensures that larger misalignment receives exponentially more penalty. Second, multiplication of tail probabilities (or the

sum of their negative logarithms) further amplifies the misalignment penalty. In an extreme case, imagine that R'_1 is perfectly aligned with μ_{21} in Figure 6(B), and thus receiving the least amount of penalty. Yet, the severe misalignment between R'_2 and μ_{22} would still overwhelm the overall penalty for P_2 and readily make it a worse match than P_1. Therefore, the tail method is better-suited for Gaussian-based fingerprinting than the traditional AUC method; the difference in their localization performance is thus unsurprising.

7 Machine Learning Methods

Three methods—machine learning-boosted multilateration, machine learning classification of reference points, and machine learning regression of coordinates—are evaluated for RSSI-based passive localization. Each method is approached using three standard machine learning algorithms, MLP, SVM, and K-NN. Each model is trained on sampled and mean training sets to produce sampled and mean models, respectively.

During model training, we conduct two rounds of cross-validation to tune hyperparameters. For the sampled model, standard five-fold cross-validation is used. For the mean model, multi-fold cross-validation is not possible because the mean training set lacks sufficient redundancy. Thus, the same validation set discussed in Section 6.2 is used. In the first round of hyperparameter tuning, a wide range of values are provided, such that an optimal range can be identified for each hyperparameter. In the second round, values within each optimal range are used to find the exact hyperparameter values that minimize cross-validation error.

The finalized hyperparameter values are used to re-train the model, which is then subject to performance evaluation. The outcome of the evaluation is visualized as a CDF curve of the localization error in the same manner as described in Section 6. The sampled model is evaluated on the sampled testing set only, producing a sampled-sampled curve. The mean model is evaluated on both the sampled and mean testing sets, producing mean-sampled and mean-mean curves, respectively. As mentioned before, the validation set is excluded from evaluating the localization performance of the mean models.

All machine learning and hyperparameter tuning algorithms are executed using the corresponding APIs in `scikit-learn`.

7.1 *Machine Learning-boosted Multilateration*

In machine learning-boosted multilateration, the RSSI path-loss model is replaced by a machine learning regressor to estimate distance based on RSSI measurements. The advantage of this approach is that it assumes no prior knowledge of the complex RSSI-distance relationship and conducts regression without the constraints of a physical model.

Table 4: Metrics of machine learning RSSI-distance regressors

| | MLP | | | | SVM | | | | K-NN | | | |
| | Sampled | | Mean | | Sampled | | Mean | | Sampled | | Mean | |
Sensor	R^2	MAE	R^2	MAE	R^2	MAE	R^2	MAE	R^2	MAE	R^2	MAE
s_1	0.53	2.48	0.52	2.50	0.53	2.45	0.53	2.47	0.52	2.48	0.53	2.48
s_2	0.64	2.05	0.64	2.05	0.63	2.05	0.63	2.06	0.63	2.12	0.64	2.07
s_3	0.57	2.39	0.56	2.40	0.56	2.35	0.55	2.36	0.57	2.39	0.56	2.44
s_4	0.68	1.92	0.67	1.93	0.67	1.89	0.66	1.92	0.67	1.89	0.67	1.92
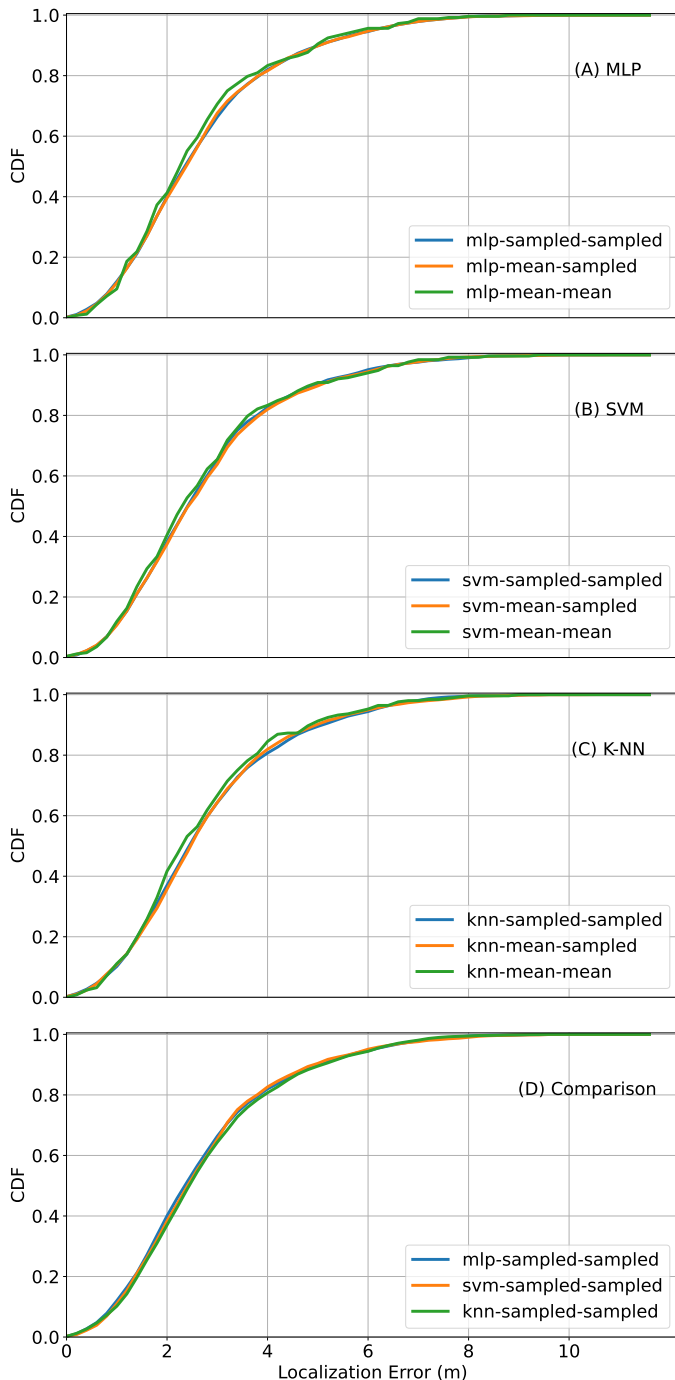
Figure 7: CDF curves of error in machine learning-boosted multilateration

The hyperparameters tuned for the MLP regressor are `hidden_layer_sizes`, `activation`, and `solver`; C, `kernel`, and `gamma` for the SVM regressor; and `n_neighbors`, `weights`, `algorithm`, and `leaf_size` for the K-NN regressor. The maximum number of tuning iterations is 1,000 for the MLP, and 20,000 for the SVM and K-NN regressors.

Table 4 lists the R^2 and MAE values for the machine learning RSSI-distance regressors after two rounds of hyperparameter tuning. Across machine learning algorithms, the sampled and mean models exhibit similar performance. Across sensors, s_4 exhibits the lowest error, whereas s_1 exhibits the highest error. This follows the results from the RSSI path-loss model. Comparing the performance between the machine learning and the RSSI path-loss models, we observe that the former consistently outperforms the latter in terms of MAE.

We use each machine learning RSSI-distance regressor to generate its corresponding multilateration model as described in Section 6.1. Figures 7(A), (B), and (C) demonstrate their localization performance. Across all three machine learning algorithms, the models have similar performance, which is not surprising, given the similar performance in RSSI-distance regression mentioned above. The mean-mean curve performs slightly better, which, as described in Section 6, could be an artifact.

A comparison is also made among the best CDF curves across the three methods (mean-mean curve excluded), as shown in Figure 7(D). There is little difference in localization performance among them.

7.2 Machine Learning Classification of Reference Points

Machine learning classification is an alternative to the traditional fingerprinting method. A trained machine learning classifier takes four RSSI measurements from a target device as input and produces a predicted label as output. The label can be mapped to a reference point, which is considered the estimated location of the target device.

The hyperparameters tuned for the MLP classifier are `hidden_layer_sizes`, `activation`, `solver`, and `alpha`; C, `kernel`, `gamma`, and `decision_function_shape` for the SVM classifier; and `n_neighbors`, `weights`, `algorithm`, and `leaf_size` for the K-NN classifier. The maximum number of tuning iterations is 1,000 for all classifiers.

Table 5: True and adjacent accuracy of machine learning classifiers

Accuracy	MLP		SVM		K-NN	
	Sampled	Mean	Sampled	Mean	Sampled	Mean
True	0.63	0.55	0.70	0.68	0.69	0.68
Adjacent	0.81	0.78	0.84	0.83	0.84	0.80
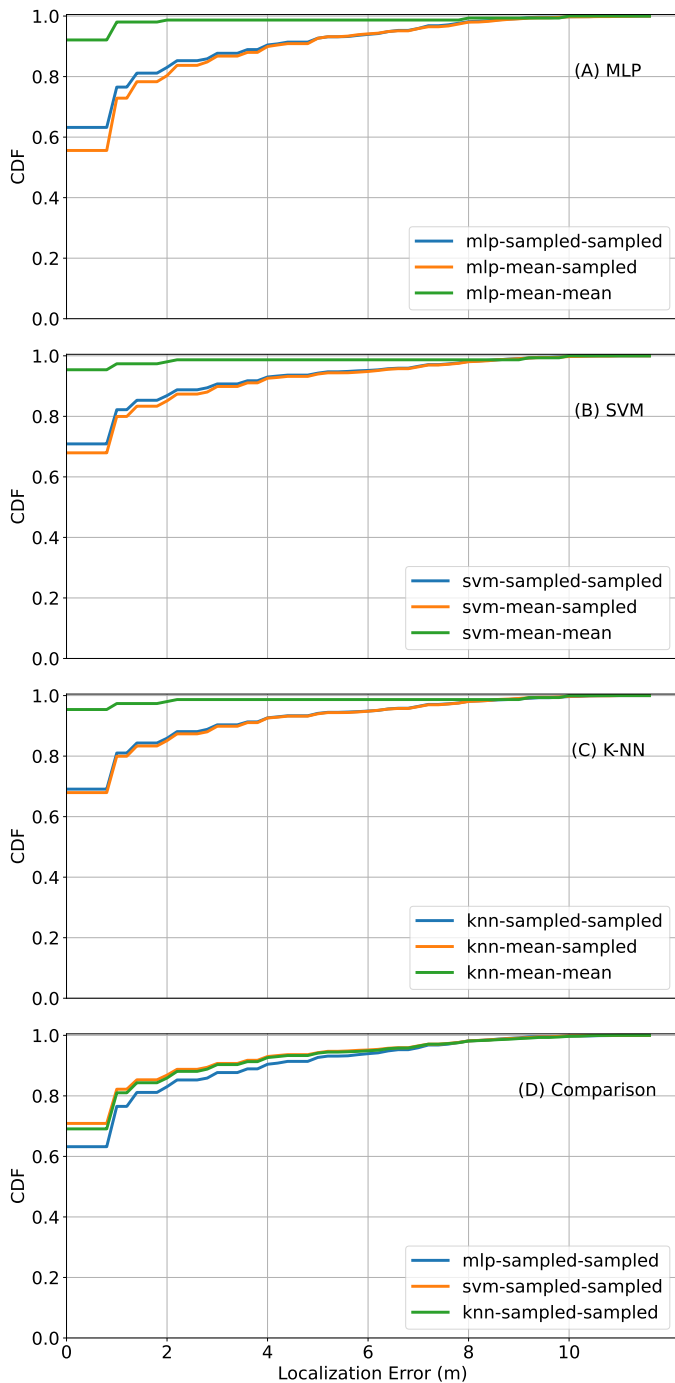
Figure 8: CDF curves of error in machine learning classification

Table 5 lists the true and "adjacent" accuracy of each classifier after two rounds of hyperparameter tuning. True accuracy repre-

sents the proportion of testing observations with correctly predicted labels. *Adjacent* accuracy denotes the proportion of testing observations with predicted labels that either match the true labels or one of the eight surrounding labels. The purpose of including adjacent accuracy is to reveal the degree of inaccuracy when a wrong prediction is made. Due to this intentional leniency, adjacent accuracy is always better than true accuracy. Across machine learning algorithms, the sampled model performs slightly better than the mean model. MLP performs the worst, whereas SVM and K-NN have similar performance.

Figures 8(A), (B), and (C) illustrate the localization performance of all three algorithms. Across machine learning algorithms, the sampled-sampled curve exhibits slightly better performance than the mean-sampled curve, but the mean-mean curve tops them both, with zero meter localization error more than 90% of the time. As discussed earlier, the exceptional performance exhibited by the mean-mean curve is most likely an artifact. However, the exaggeration in classification is much more pronounced than in multilateration. This is due to the way we compute localization errors for classifiers. Since we consider a correct match to a reference point as being equivalent to zero meter localization error, we accumulate many zero-error instances when evaluating the localization performance of classifiers. These zero-error instances inflate the CDF curves. In contrast, multilateration methods never exhibit zero meter localization errors.

We also compare the best CDF curves across the three machine learning algorithms, with the mean-mean curves excluded. Figure 8(D) shows the results, where SVM performs slightly better than the others.

7.3 Machine Learning Regression of Coordinates

Machine learning regression of coordinates trains two RSSI-coordinate regressors based on the x- and y-coordinates, respectively. It allows direct quantitative estimation of a target device's position. Each regressor takes four RSSI measurements from an observation as input and produces a pair of estimated coordinates as output.

The hyperparameters tuned for the MLP regressor are `hidden_layer_sizes`, `activation`, `solver`, and `alpha`; `C`, `kernel`, and `gamma` for the SVM regressor; and `n_neighbors`, `weights`, `algorithm`, and `leaf_size` for the K-NN regressor. The maximum number of iterations is 1,000 for the MLP regressor, and 20,000 for the SVM and KNN regressors.

Table 6: Metrics of machine learning RSSI-coordinate regressors

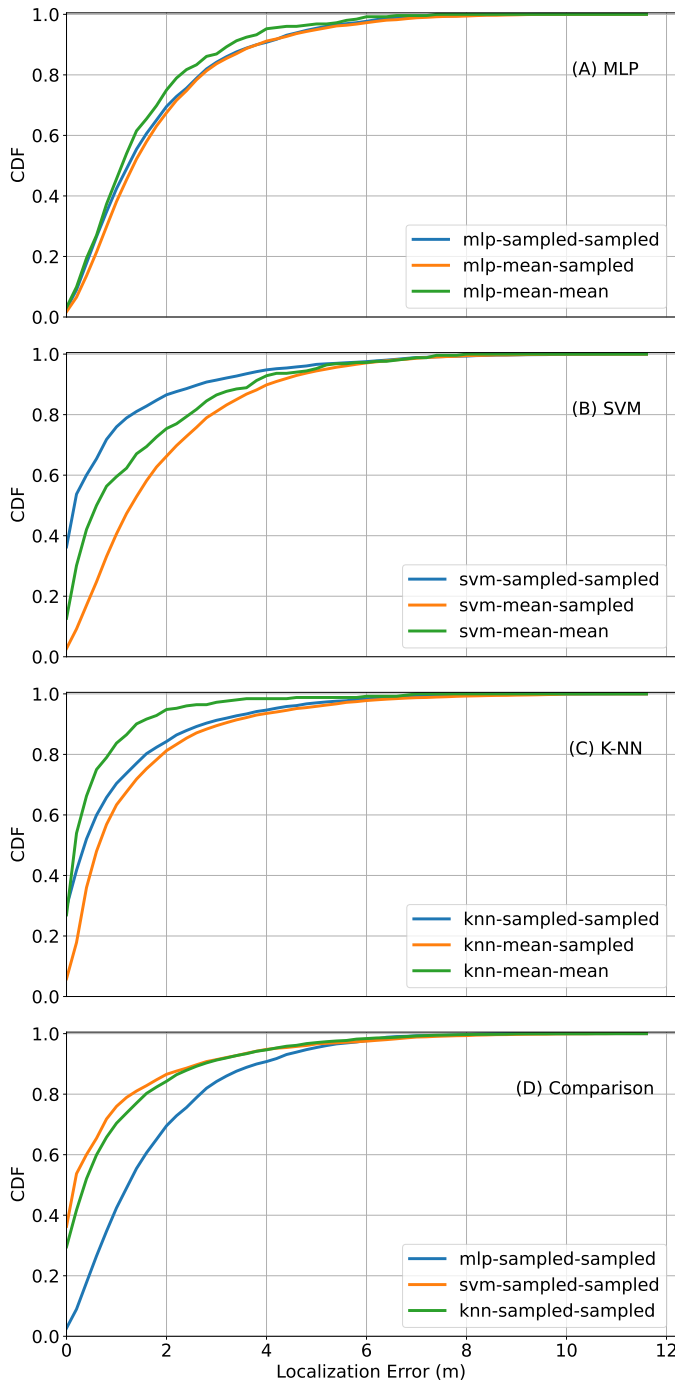| Coordinate	MLP				SVM				K-NN			
	Sampled		Mean		Sampled		Mean		Sampled		Mean	
	R^2	MAE	R^2	MAE	R^2	MAE	R^2	MAE	R^2	MAE	R^2	MAE
x	0.84	1.24	0.83	1.30	0.91	0.71	0.82	1.29	0.91	0.71	0.88	0.97
y	0.86	1.16	0.85	1.24	0.90	0.74	0.85	1.21	0.91	0.71	0.90	0.80

Figure 9: CDF of error with machine learning RSSI-coordinate regression

Table 6 lists the R^2 and MAE values for the machine learning

RSSI-coordinate regressors after two rounds of hyperparameter tuning. Across all regressors, the sampled model has better regression performance than the mean model, which is likely due to the difference in training size. However, it is worth noting that the difference in training set size does not affect the performance of the RSSI-distance regressors (Section 7.1). A possible explanation of why the RSSI-coordinate regressor is more sensitive to training set size is that it is a more complex model (four features as input) than the RSSI-distance regressor (one feature as input). Across algorithms, the sampled models of SVM and K-NN perform slightly better than that of MLP, while the mean model of K-NN outperforms that of MLP and SVM. Between the two coordinates, y-coordinates generally have lower estimation error than x-coordinates. We speculate that this is the result of how our testbed is prepared, where there is more measuring variability in the x- versus y-axis.

Figures 9(A), (B), and (C) summarize the localization performance of all three algorithms. Within MLP and K-NN, the sampled-sampled curve performs slightly better than the mean-sampled curve, but the mean-mean curve outperforms both. This aligns with our earlier hypothesis that indicates performance exaggeration in the mean-mean curve. However, in the SVM models, the situation is surprisingly reversed. The sampled-sampled curve shows better performance than the exaggerated mean-mean curve. This is most likely due to the superior RSSI-coordinate regression performance of the SVM sampled model compared to the SVM mean model.

We then compare the performance of the best CDF curves across the three machine learning algorithms (excluding the mean-mean curves), as shown in Figure 9(D). The results show that the sampled-sampled SVM model performs the best.

8 Royal Rumble

To find the best-performing model overall, we juxtapose the best model within each method (excluding the mean-mean curves) in the same plot. If multiple models show equally good performance within a particular method, a model is arbitrarily selected. The result is shown in Figure 10. The axes are the same as before. The blue curve corresponds to the best performant model in traditional multilateration (sampled-sampled); the orange curve corresponds to the best in traditional fingerprinting (v-mean-sampled); the green curve corresponds to the best in machine learning-boosted multilateration (mlp-sampled-sampled); the red curve corresponds to the best in machine learning classification of reference points (svm-sampled-smapled); and the purple curve corresponds to the best in machine learning regression of coordinates (svm-sampled-sampled). Several observations can be made.

First, the best machine learning models outperform the best

traditional models. Specifically, machine learning-boosted multilateration performs better than its traditional counterpart. Similarly, machine learning classification performs better than traditional fingerprinting. This is not surprising because machine learning methods can train regressors and classifiers based on RSSI measurements without the constraints imposed by an underlying physical model. It allows them to capture patterns that might be ignored in the traditional methods.
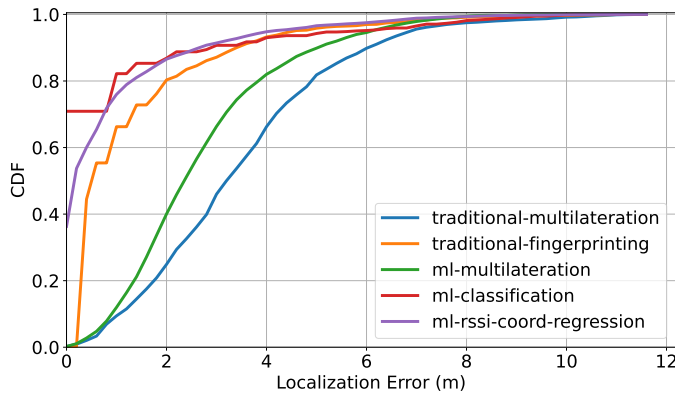

Figure 10: The best CDF curves of error among all methods

Second, the best non-multilateration models outperform the best multilateration models by a wide margin. This is most likely due to the nature of the multilateration methods, where two rounds of estimation are involved: RSSI to distance and distance to coordinates. Since each round of estimation incurs error, the multilateration methods accumulate more error than the other methods, where only one round of estimation is involved.

Third, except for fingerprinting, where there is no sampled-sampled option, all of the CDF curves used for comparison in Figure 10 are sampled-sampled curves. In other words, given the same sampled testing set, the sampled models either outperform or perform as well as the mean models for all methods. This result answers the question raised at the close of Section 5: The benefit of reduced random error in the mean training set does not outweigh the costs of reducing the size of the training set.

Finally, for a localization model to function at the scale of a city street, its error must be below a certain threshold. Ideally, the error should be small enough to tell whether a target device has moved from one business to another. Based on this reasoning, the best machine learning classifier (svm-sampled-sampled), the best machine learning RSSI-coordinate regressor (svm-sampled-sampled), and the best traditional fingerprinting (v-sampled-sampled) are the best candidates, as they all exhibit above 90% probability of having four meters or less localization error. However, future research must examine their spatial robustness (e.g., does the model work outside the testbed?) and temporal robustness (e.g., does the model work on data collected a week or a month later?).

9 Conclusion

In this paper, we have systematically evaluated the localization performance of several RSSI-based passive localization methods using data collected in a semi-controlled, obstruction-free outdoor environment. The methods include two adaptations of traditional active localization methods (multilateration and fingerprinting) and three machine learning methods (machine learning-boosted multilateration, machine learning classification of reference points, and machine learning regression of coordinates). The results show that the machine learning methods perform better than the traditional methods. Further, the SVM sampled model in the classification-based approach, the SVM sampled model in the RSSI-coordinate regression-based approach, and the traditional fingerprinting approach seem to have sufficiently good performance to be considered for use in real-world mobility monitoring. However, several limitations in formulating and evaluating these methods must be addressed and improved upon in future research.

First, all the models in this paper are trained and tested on data collected in a five-hour window on the same day. In practice, we have documented and verified that RSSI measured under identical emitter, sensor, and visible environmental conditions exhibits temporal variability [28]. Thus, a localization model must possess temporal robustness such that the time of data collection is irrelevant to its performance. Further, the exceptional performance of the mean-mean curves in almost all models appears to be an artifact due to the information overlap between the mean testing and training sets. It will be interesting to see whether the mean-mean curves remain exceptional when the mean testing set comes from data collected during a different session. Future research will pursue this evaluation.

In addition, the data used in this paper were collected in a near-ideal environment, free of obstructions and adverse weather events. We have yet to include samples with missing data in the analysis (e.g., three instead of four RSSI measurements in a sample). However, signal noise and incomplete data are inevitable in practice. Thus, future research will investigate how model performance deteriorates when data are collected with missing features (e.g., not all sensors capture a probe request), under unfavorable weather conditions (e.g., rain), in the presence of obstructions (e.g., walls, people), or with interference from other devices.

Relatedly, all the models trained in this paper are based on data collected by exactly four sensors. This presents a scalability issue, in which the addition or removal of a few sensors could require model re-training. Since scaling sensor deployments up and down is not uncommon, future research will focus on generating models resistant or adaptable to small changes in sensor availability.

References

[1] L. Sun, S. Chen, Z. Zheng, L. Xu, "Mobile Device Passive Localization Based on IEEE 802.11 Probe Request Frames," Mobile Information Systems, **2017**, 1–10, 2017, doi:10.1155/2017/7821585.

[2] W. Xue, W. Qiu, X. Hua, K. Yu, "Improved Wi-Fi RSSI Measurement for Indoor Localization," IEEE Sensors Journal, **17**(7), 2224–2230, 2017, doi: 10.1109/JSEN.2017.2660522, conference Name: IEEE Sensors Journal.

[3] K. K. Mamidi, K. P. V., "ALTAR: Area-based Localization Techniques using AoA and RSS measures for Wireless Sensor Networks," in 2019 International Conference on contemporary Computing and Informatics (IC3I), 160–168, 2019, doi:10.1109/IC3I46837.2019.9055582.

[4] X. Li, Z. D. Deng, L. T. Rauchenstein, T. J. Carlson, "Contributed Review: Source-localization algorithms and applications using time of arrival and time difference of arrival measurements," Review of Scientific Instruments, **87**(4), 041502, 2016, doi:10.1063/1.4947001, publisher: American Institute of Physics.

[5] G. Guo, R. Chen, F. Ye, X. Peng, Z. Liu, Y. Pan, "Indoor Smartphone Localization: A Hybrid WiFi RTT-RSS Ranging Approach," IEEE Access, **7**, 176767–176781, 2019, doi:10.1109/ACCESS.2019.2957753, conference Name: IEEE Access.

[6] N.-S. Duong, T.-M. Dinh, "Indoor Localization with lightweight RSS Fingerprint using BLE iBeacon on iOS platform," in 2019 19th International Symposium on Communications and Information Technologies (ISCIT), 91–95, 2019, doi:10.1109/ISCIT.2019.8905160, iSSN: 2643-6175.

[7] C.-H. Lin, L.-H. Chen, H.-K. Wu, M.-H. Jin, G.-H. Chen, J. L. Garcia Gomez, C.-F. Chou, "An Indoor Positioning Algorithm Based on Fingerprint and Mobility Prediction in RSS Fluctuation-Prone WLANs," IEEE Transactions on Systems, Man, and Cybernetics: Systems, 1–11, 2019, doi: 10.1109/TSMC.2019.2917955, conference Name: IEEE Transactions on Systems, Man, and Cybernetics: Systems.

[8] J. Wang, J. Luo, S. J. Pan, A. Sun, "Learning-Based Outdoor Localization Exploiting Crowd-Labeled WiFi Hotspots," IEEE Transactions on Mobile Computing, **18**(4), 896–909, 2019, doi:10.1109/TMC.2018.2849416, conference Name: IEEE Transactions on Mobile Computing.

[9] L. L. Oliveira, L. A. Oliveira, G. W. A. Silva, R. D. A. Timoteo, D. C. Cunha, "An RSS-based regression model for user equipment location in cellular networks using machine learning," Wireless Networks, **25**(8), 4839–4848, 2019, doi:10.1007/s11276-018-1774-4.

[10] Z. He, Y. Li, L. Pei, R. Chen, N. El-Sheimy, "Calibrating Multi-Channel RSS Observations for Localization Using Gaussian Process," IEEE Wireless Communications Letters, **8**(4), 1116–1119, 2019, doi:10.1109/LWC.2019.2908397, conference Name: IEEE Wireless Communications Letters.

[11] S. Yiu, M. Dashti, H. Claussen, F. Perez-Cruz, "Wireless RSSI fingerprinting localization," Signal Processing, **131**, 235–244, 2017, doi:10.1016/j.sigpro.2016.07.005.

[12] R. Sari, H. Zayyani, "RSS Localization Using Unknown Statistical Path Loss Exponent Model," IEEE Communications Letters, **22**(9), 1830–1833, 2018, doi:10.1109/LCOMM.2018.2849963, conference Name: IEEE Communications Letters.

[13] S. Sadowski, P. Spachos, "RSSI-Based Indoor Localization With the Internet of Things," IEEE Access, **6**, 30149–30161, 2018, doi:10.1109/ACCESS.2018.2843325, conference Name: IEEE Access.

[14] S. Mazokha, F. Bao, J. Zhai, J. Hallstrom, "MobIntel: Sensing and Analytics Infrastructure for Urban Mobility Intelligence," in 2020 IEEE International Conference on Smart Computing (SMARTCOMP) (SMARTCOMP 2020), Bologna, Italy, Italy, 2020.

[15] F. Bao, S. Mazokha, J. O. Hallstrom, "MobIntel: Passive Outdoor Localization via RSSI and Machine Learning," in 2021 17th International Conference on Wireless and Mobile Computing, Networking and Communications (WiMob), 247–252, 2021, doi:10.1109/WiMob52687.2021.9606338.

[16] D. Alshamaa, F. Mourad-Chehade, P. Honeine, "Mobility-based Tracking Using WiFi RSS in Indoor Wireless Sensor Networks," in 2018 9th IFIP International Conference on New Technologies, Mobility and Security (NTMS), 1–5, 2018, doi:10.1109/NTMS.2018.8328704, iSSN: 2157-4960.

[17] H. Du, C. Zhang, Q. Ye, W. Xu, P. L. Kibenge, K. Yao, "A hybrid outdoor localization scheme with high-position accuracy and low-power consumption," EURASIP Journal on Wireless Communications and Networking, **2018**(1), 4, 2018, doi:10.1186/s13638-017-1010-4.

[18] M. Youssef, M. Mah, A. Agrawala, "Challenges: device-free passive localization for wireless environments," in Proceedings of the 13th annual ACM international conference on Mobile computing and networking, MobiCom '07, 222–229, Association for Computing Machinery, New York, NY, USA, 2007, doi:10.1145/1287853.1287880.

[19] J. Wilson, N. Patwari, "Radio Tomographic Imaging with Wireless Networks," IEEE Transactions on Mobile Computing, **9**(5), 621–632, 2010, doi: 10.1109/TMC.2009.174, conference Name: IEEE Transactions on Mobile Computing.

[20] G.-l. Wang, X.-b. Hong, X.-m. Guo, Y. Fang, "A Data-Driven Three-Dimensional RSS Model for Device-Free Localization and Tracking," in 2019 IEEE 21st International Conference on High Performance Computing and Communications; IEEE 17th International Conference on Smart City; IEEE 5th International Conference on Data Science and Systems (HPCC/SmartCity/DSS), 1705–1713, 2019, doi:10.1109/HPCC/SmartCity/DSS.2019.00233.

[21] A. Guillen-Perez, M.-D. Cano, "Counting and locating people in outdoor environments: a comparative experimental study using WiFi-based passive methods," ITM Web of Conferences, **24**, 01010, 2019, doi:10.1051/itmconf/20192401010, publisher: EDP Sciences.

[22] T. Kulshrestha, D. Saxena, R. Niyogi, J. Cao, "Real-Time Crowd Monitoring Using Seamless Indoor-Outdoor Localization," IEEE Transactions on Mobile Computing, **19**(3), 664–679, 2020, doi:10.1109/TMC.2019.2897561, conference Name: IEEE Transactions on Mobile Computing.

[23] J. Du, C. Yuan, M. Yue, T. Ma, "A Novel Localization Algorithm Based on RSSI and Multilateration for Indoor Environments," Electronics, **11**(2), 2022, doi:10.3390/electronics11020289.

[24] F. Shang, W. Su, Q. Wang, H. Gao, Q. Fu, "A Location Estimation Algorithm Based on RSSI Vector Similarity Degree," International Journal of Distributed Sensor Networks, **10**(8), 371350, 2014, doi:10.1155/2014/371350, publisher: SAGE Publications.

[25] F. Pedregosa, G. Varoquaux, A. Gramfort, V. Michel, B. Thirion, O. Grisel, M. Blondel, P. Prettenhofer, R. Weiss, V. Dubourg, J. Vanderplas, A. Passos, D. Cournapeau, M. Brucher, M. Perrot, E. Duchesnay, "Scikit-learn: Machine Learning in Python," Journal of Machine Learning Research, **12**, 2825–2830, 2011.

[26] Wes McKinney, "Data Structures for Statistical Computing in Python," in Stéfan van der Walt, Jarrod Millman, editors, Proceedings of the 9th Python in Science Conference, 56 – 61, 2010, doi:10.25080/Majora-92bf1922-00a.

[27] P. Virtanen, R. Gommers, T. E. Oliphant, M. Haberland, T. Reddy, D. Cournapeau, E. Burovski, P. Peterson, W. Weckesser, J. Bright, S. J. van der Walt, M. Brett, J. Wilson, K. Jarrod Millman, N. Mayorov, A. R. J. Nelson, E. Jones, R. Kern, E. Larson, C. Carey, İ. Polat, Y. Feng, E. W. Moore, J. Vand erPlas, D. Laxalde, J. Perktold, R. Cimrman, I. Henriksen, E. A. Quintero, C. R. Harris, A. M. Archibald, A. H. Ribeiro, F. Pedregosa, P. van Mulbregt, S. . . Contributors, "SciPy 1.0: Fundamental Algorithms for Scientific Computing in Python," Nature Methods, **17**, 261–272, 2020, doi: https://doi.org/10.1038/s41592-019-0686-2.

[28] S. J. Pan, V. W. Zheng, Q. Yang, D. H. Hu, "Transfer Learning for WiFi-based Indoor Localization," AAAI Conference on Artificial Intelligence, 6, 2008.

Technical Aspects and Social Science Expertise to Support Safe and Secure Handling of Autonomous Railway Systems

Clemens Gnauer[*,1], Andrea Prochazka[1], Elke Szalai[2], Sebastian Chlup[3], Anton Fraunschiel[4]

[1]*Forschung Burgenland, Research Area for Sustainable Innovation, Eisenstadt, 7000, Austria*

[2]*University of Applied Sciences Burgenland, Social Studies, Eisenstadt, 7000, Austria*

[3]*Austrian Institute of Technology, Digital Safety and Security, Institute, Vienna, 1210 , Austria*

[4]*IQSoft GmbH, Vienna, 1120, Austria*

A R T I C L E I N F O

A B S T R A C T

In recent years the development of autonomous vehicles has increased tremendously and a variety of methodologies had been applied to make them more safe and secure. This work shows a multilevel approach combining Failure Mode, Effects and Criticality Analysis of an autonomous railway system with sociological and technical aspects to support safe operations and human-machine interactions in the field of autonomous railway systems. This approach includes all relevant technical components, as well as the assessment of measures for a safety process based on the Failure Mode, Effects and Criticality Analysis. We applied the Persona-Roberta model to assess safety aspects at the interface between humans and machines and applied both results to establish training materials. The results provide answers to questions about the avoidance of technical errors, discussions on security and safety aspects and shows organizational development tools for accident prevention. In the future the created knowledge will be used to improve trust in digital solutions and Cyber-Physical Systems.

1 Introduction

This paper is an extension of work originally presented in 2021 at the 5th International Conference on System Reliability and Safety (ICSRS) [1]. In the paper entitled "Knowledge Based Training Derived from Risk Evaluation Concerning Failure Mode, Effects and Criticality Analysis in Autonomous Railway Systems" the following four topics have been discussed:

- Railway vehicles, autonomous systems, safety & security, risk mitigation

- Development of a component meta-model (Figure 1)

- Risk evaluation with Failure Mode Effects and Criticality Analysis (FMECA)
  focused on technical and social aspects and the combination of these aspects to find solutions for minimizing risks

- Finding a solution to the issues of interaction between autonomous systems, Cyber- Physical Systems (CPS) and humans (Persona–Roberta model)

In thier work [2] looked at a meta-model that would assist the development of Cyber-Physical Systems (CPS) which are to be used to manage and control autonomous train systems on auxiliary railway lines in a safe and secure manner. In doing so, they discovered that most meta-models do not meet the particular requirements of the railway domain, particularly when focusing on the integration of the combination between safety and security issues. Our meta-model, which was developed in response to these findings, incorporates a wide range of particular technological and sociocultural factors as well as their interoperability. It serves as the foundation for the study described in this publication . In the extension for this article, the authors would like to discuss aspects of the research process in the interaction between CPS and people working at an operating site regarding safety and security aspects. This also concerns tools for developing trust and trustworthiness in technology and CPS. Therefore, we developed training materials for different target groups, which are working with and within these systems in different positions. For that, it is important to understand, which person has tacit knowledge and can decide actions and which person can only operate along a guideline.

The authors have been conducting research on the topic of au-

---

[*]Corresponding Author: Clemens Gnauer, Campus 1, A-7000 Eisenstadt, 0043577055471 & clemens.gnauer@forschung-burgenland.at

tonomous rail-bound vehicles on branch lines in Linz, Austria for over a total of 18 months. The overall project duration of the research project in which the presented research had been conducted was three years from August 2019- January 2021. Through direct access to the practical use of the planned autonomous system, safety aspects have been comprehensively discussed in the project. The authors overall objective is to connect social, technical and legal issues in an integrative way to achieve greater safety and security for humans and machines in autonomous systems.

Based on the data and research reports on technology acceptance and social issues in technology social research, a mixed methods approach was chosen, which helps to illuminate the research object with different methods according to the grounded theory [3]. Mixed methods research is often used in the behavioural, health, and social sciences, especially in multidisciplinary settings and complex situational or societal research. This approach is chosen when data is to be collected using different methods. These can be quantitative and qualitative methods, but they are not used side by side or in parallel, but triangulated to produce results. In the present research project, this approach was the right one, as the research question asks for social and technical aspects and interdisciplinary cooperation was used. Therefore, desk research methods were used to evaluate existing literature along categories of technical and social aspects. Based on the results, discussions were held with experts to generate information for the development of the Persona-Roberta model indicators. Furthermore, with this basis, the existing FMECA was extended to include social aspects. The aim of all these steps was to extend the error correction measures on the technical side to include social correction measures. These are the training materials developed from these steps, which in turn were fed from the tacit knowledge of the people responsible for the operation. In this way, a knowledge cycle was created to move from person-controlled rail-based operation to safe autonomous operation.

Doing this we set the following research objectives:

- Implementing social aspects to support the technical development of an autonomous railway system

- Extension of FMECA with design thinking methods

- Development of training concepts and materials to ensure safe and secure operation for humans and machines interacting with rail-bond vehicles

The rest of the paper is structured as follows. In section 2, relevant related scientific literature on the subjects of autonomous railway vehicles, FMECA and training materials and the Persona-Roberta model are presented. The next section 3 presents all objects used in the FMECA, failure mitigation and improvement opportunities in detail, followed by section 4, where training materials derived from the FMECA are presented. In the conclusion, a summary of the research is given and further research is presented.

2 Related Works

2.1 Autonomous Railway Vehicles

Recent technological improvements have led to more focus on the sector of autonomous vehicles. A variety of technologies are con-

tributing to the progress of projects and research in this fields. When considering autonomous driving, roughly three parts, scene recognition, path planning and vehicle control are required [4]. While the first demands localization, object-detection and object-tracking algorithms, the second uses motion and mission planning. The latter makes use of the motion planner and uses path following. All these components use algorithms to aid and enable autonomous driving for vehicles. Regarding the railway sector, a variety of projects have targeted different aspects of autonomous driving for trains and railway vehicles, such as self-driving trains, autonomous train systems and others. Technologies such as the Internet of Things (IoT), AI, Dedicated Short-Range Communication (DSRC) and Positive Train Control (PTC) all enhance the autonomy of railway vehicles. Various work in the field of autonomous railway vehicles have been done in academia already. Speed scheduling for autonomous railway vehicle control systems has been researched using a variety of algorithms such as Neural Network [5], Neuro-Fuzzy systems [6], fuzzy interference system [7]. They propose the need for a secure and safe operation of trains enabled by an AI supported system.

Autonomous railway vehicles can be classified based on four Grades of Automation (GoA) [8]. GoA 1 describes controlled manual operations where the driver manually drives the train, opens passenger doors, etc. and is supported by a safety system, the Automatic Train Protection (ATP). GoA 2 includes automatic braking and change of rail tracks, etc. but is still dependent upon a driver. GoA 3 represents trains that operate autonomously but need a driver to attend the train, be onboard and take control in case of an emergency. GoA 4, however, are fully autonomous trains without a driver present. A lot of progress has been done in recent years regarding fully autonomous train systems. Rio Tinto, for examples, uses fully automated trains for its iron-ore freights in Pilbara, Australia. The system, called AutoHaul, operates 50 automated and unmanned trains on a 1500 km railroad, reducing time and costs [9].

In a recent work by [10], autonomous maintenance technologies for localisation and navigation have been presented. Respective technologies, such as on-board sensors, like Inertia Measurement Unit (IMU), tachometers, satellite-based position systems and cameras are used to identify the exact location, speed and other factors regarding the trains. In a further step, these technologies can be used for autonomous movement and driving of a train, as expressed by [11], for monitoring passengers and goods as well as trains and other systems. These advancements and technologies, however, bring up further issues regarding safety of humans, passengers in particular, and other objects involved that are interacting in one way or the other with an automated/driverless railway vehicle or corresponding control system. These factors need to be addressed appropriately.

2.2 Failure Mode Effects and Criticality Analysis

The Failure Mode and Effects Analysis (FMEA) is a formalized method that enables the identification of possible failures of components of an overall system and their further classification based on root causes, failure modes and estimation of risk [12]. Therefore, errors are identified for specific objects of a system and technical effects for this error are described as well as possible reasons for the respective errors. In this article, we present results from a special form, the Failure Mode Effects and Criticality Analysis

(FMECA)that additionally includes a Criticality Analysis. This is represented in the risk priority number (RPN) assigned to each risk for each failure. The RPN is calculated by multiplying severity, occurrence and detection rates for each failure [13], [14].

When looking at scientific research in the field, FMECA has been applied in various areas of railroad systems. For example, in [15] author conducted an FMECA assessment for heating, ventilation and air conditioning (HVAC) systems of transportation railway systems. They identified the main criticalities and in a further step applied a new analytical method to identify a threshold risk value. In their study, [16] used an FMECA on the passenger door systems of railroad rolling stock. Additionally, they looked at inexpensive and reliable criteria in that context and developed a mileage-based preventive maintenance program to lessen failure recurrence.

To find an optimum FMECA process and methodology for railroad systems, [17] have done a structured evaluation of various FMEA approaches. As a result, they contrasted the approaches and traits of the FMECA standards MIL-1629a, SAE-J1739, and IEC-60812 for use in the automotive, electronics, and military industries, respectively. They discovered that each was deficient in certain components necessary for a comprehensive approach to FMECA for train systems, and, as a result they combined elements of failure modes (SAE-J1739), maintenance analysis (MIL-1629a), and localization of impacts (IEC-60812). These examples demonstrate that research in this area is ongoing, however it appears that there are no studies that examine the social implications of risk reduction and error correction in FMECA. This gave us even more motivation to pursue improved FMECA research in the railway industry and incorporating social measures for error correction.

2.3 Training materials and the Persona-Roberta Model

The chosen models of error analysis (FMECA) and the developed Persona–Roberta model make it clear that it is relevant and important to seriously work on these levels in order to create meaningful error correction measures, but also training and work documents for the executing employees.

It is known from models of technology assessment that an awareness of the possible consequences of a technical implementation, but also of a human action, must be comprehensively created. These models are complemented by technology acceptance approaches that help to convey assessment processes or develop teaching tools for the people concerned. Acceptance is the subject of numerous scientific studies. One of the best-known models for explaining acceptance is the Technology Acceptance Model (TAM) [18]. This model describes the acceptance of new technology in IT. Technology interacts strongly with the product, the application of knowledge and with the development of a product. Both terms structure technology developments and the access of people to these developments. This approach is the basis for the further development of the Persona-Roberta model chosen in the research project, because as the error analysis and the development of the error correction measures (FMECA) show, in addition to technical knowledge, it also - or above all - requires trust in the new technology.

Knowledge about acceptance requires knowledge about the attitudes of the counterpart and in order to make these visible, the aforementioned model of Persona(s) was chosen. Interactions between people and technology (human-machine) require an exact understanding of precisely these interactions. For this purpose, the Persona(s) model can be extended to the Robertas, which makes interfaces and interactions between these two systems visible. In the present use case - in the case of self-propelled rail-bound vehicles in connection with industrial production, this existing knowledge of the employees must be recognised, used and further developed in order to ensure safe - in the sense of error- and accident-free - operations. In the research project, established models were further developed and combined by the various disciplines represented in order to find customised solutions. The combination of FMECA theory, TAM-models and the Persona–Roberta model allowed the derivation of proposals for the development of communication tools and training materials for the staff concerned.

"In the future, there will be a co-existence between humans and machines. ( ) The relationship (...) will therefore be crucial for the experience" [19]. This pattern is also about trust in the machine (sensors, camera, IoT, ...) , about knowing how it works and about the impact of the interaction with his Persona as an expert for autonomous railways. The development of the Persona(s) supported the research process and made it possible to draw on the generated ideas of possible expectations and fears. This is important, because one result of fear could be errors or wrong reactions in the event of a malfunction, which must be avoided. For this reason, the Persona model was expanded and shows in detail the possible interactions between human and machines. The development was based on the Persona-Robona model in [20] and makes it possible to describe and understand relationships between the systems that are responsible for a smooth process. At the same time, required knowledge modules, expertise and communication requirements become visible, which can subsequently be addressed through training measures [20].

3 Results of Failure Mode Effects and Criticality Analysis

In this section, the FMECA objects identified in the research project [1] are presented and their respective RPNs and technical, as well as socio-technical error corrective measures are displayed.

The research concentrated on auxiliary railway lines, while especially focusing on aspects of security and safety related to this form of railway transportation. In this matter, the authors present the autonomous railway vehicle as an exemplary extract from the proposed autonomous railway system. Figure 1 shows the components of the respective component of an autonomous railway vehicle. For each component of the meta-model the conducted FMECA is presented, including technological as well as socio-technical error correction measures.

3.1 Camera

When it comes to retrieving information about surroundings, cameras represent one of the most common technologies. They represent a component that is comparatively cheap but has a significant impact on the perception of the surroundings. In this sense we are not talking about a simple camera but a component capable of

processing image data in order to detect and identify potential obstacles such moving humans or static objects. In combination with other components a camera can contribute to the decision making within an automated vehicle and therefore, has a vital impact on the safety[21].
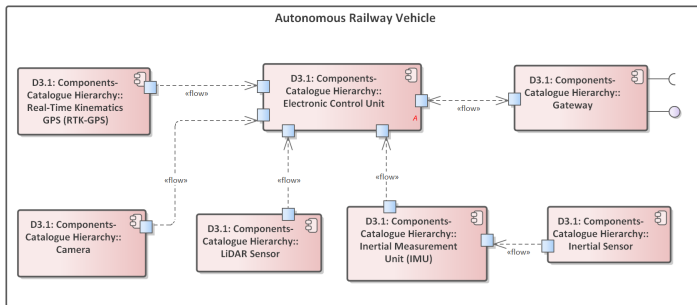

Figure 1: Subcomponents of the autonomous railway vehicle as a component of the meta-model

current (respectively planned state) object Camera			
possible errors	defect on the camera and/or the lense	unclean lense	error in the power connection
possible technical effects	obstacles are not recognized (by Persona or Roberta depending on what needs to be done)	pictures are not displayed correctly (Persona - doesn't recognize that the camera is the reason for the failure)	no action possibilities in case of missing pictures
possible error reasons	object falls down / accident	deposit on the lens	power cable damaged
estimation of the potential danger as well as possible measures for error prevention			
occurrence (O)	6	7	3
severity (S)	10	8	10
detection (D)	4	1	6
risk priority number (RPN)	240	56	180
technical error correction measure	protect camera or lens	cleaning the lens, self-cleaning lens, second camera	install power cable alternatively, redundant power supply
socio-technical error correction measure	interaction between Roberta and Persona	at the Persona level: schedule regular cleaning / "cleaning plan"	check the cable sheathing for visible damage

Figure 2: Camera object from FMECA

For a graphical depiction of the result of the FMECA for the object camera see Figure 2. When we connect the camera component to the FMECA, we identified the following possible errors: a defect on the camera itself, an unclean lens or an error in the power connection. The possible technical effects of the error defect on the camera itself are, firstly, that obstacles are not recognized, secondly, pictures are not displayed correctly, or lastly, that there are no action possibilities in case of missing pictures. Possible reasons for the above-mentioned errors are accidents caused by fallen objects, deposits on the lens or damages on the power cables. Regarding the estimation of the potential danger as well as possible measures for error prevention, we evaluate the error possibilities with the metrics occurrence (O), severity (S) and detection (D). For each of them we developed a metric corresponding to the potential occurrences of errors, as well as to the risk of severity and detection in several rounds based on the respective expert knowledge of the entire project team.

The RPN determined was assigned to three categories with the help of an ABC analysis. The first category is reserved for RPNs between 0 and 299, where the risk is assessed as low and will be accepted. The second category is for RPNs between 300 and 749, where the risk is assessed as medium and, thus, taking measures to omit the failure mode is recommended. The third category is for RPN from 750 to the maximum possible RPN of 1000, the risk is assessed as high and, thus, assessed that an action is necessary, since on this level people could be in danger [1]. Doing this we receive the RPN for each scenario. In the shown case of the camera, we receive the RPN 240 for "obstacles are not recognized" caused by a "defect on the camera itself", the RPN 56 for "pictures are not displayed correctly" caused by an "unclean lens" and the RPN 180 for "no action possibilities in case of missing pictures" caused by an "error in the power connection". For the high-risk areas identified in this way, troubleshooting measures will be developed in a separate next step. For all possible errors listed in the FMECA, measures have also been taken to reduce the cause of errors within the system. These measures are divided into technical and sociological measures [1]. For the technical corrective measure, we determine tasks to protect the camera and/or lens to eliminate the possibility of a defect of the camera or lens. To avoid the possible errors induced by unclean lenses we can clean the lens and/or use self-cleaning lenses and/or a built-in redundancy by using a second camera. To avoid an error in the power connection we focus on the opportunities of alternative ways and areas for the installation, as well as a safer installation of the power chords and/or implementing a redundant power supply. As socio-technical corrective measures we determine the following actions to increase the safety level of the object camera. Continuous interaction between Persona(s) and Roberta(s) to detect possible defects on the camera and/or lens as soon as possible.

3.2 Real Time Kinematics Global Positioning System

Global Navigation Satellite Systems (GNSS) offer various ways of positioning solutions. One of which is standalone Global Positioning System (GPS). It utilizes signals retrieved from a radio link to calculate the current position [22]. However, standalone GPS provides an accuracy of only 2-5 metres [23] and therefore does not represent the up-to-date best solution when it comes to automating vehicles. Consequently, other solutions to determine the position more accurately were invented. With Differential GPS (D-GPS) a more precise position can be calculated. By adding a reference station whose position is known, an additional stationary point can be added to the calculation [24]. Thus, the moving object receives information from the satellites as well as the reference station which enables a precision of 0.3-0.8 meters [23]. The currently most advanced version of GNSS based position detection is Real Time Kinematics (RTK). They are based on the same principles as D-GPS but involve sophisticated computations and formulas during the course of processing the data. With RTK accuracies of 1-5 centimetres can be achieved [23].

For a graphical depiction of the result of the FMECA for the object Real Time Kinematics Global Positioning System see Figure 3. When we connect the Real Time Kinematics RTK-GPS component to the FMECA, we identified the following possible errors: a loss of the power connection to the RTK-GPS and a loss of the possibility

to connect to the reference station.

current (respectively planned state) object Real Time Kinematics RTK-GPS		
possible errors	lost power connection to the RTK-GPS	connection to reference station not possible
possible technical effects	unknown position of the autonomous vehicle	incorrectly displayed position of the autonomous vehicle
possible error reasons	damaged power cable mechanical damage by a person	RTK-GPS damaged, reference station damaged
estimation of the potential danger as well as possible measures for error prevention		
occurrence (O)	3	4
severity (S)	8	6
detection (D)	4	6
risk priority number (RPN)	96	144
technical error correction measure	install power cable alternatively	regular inspection intervals with checklists for the stations
socio-technical error correction measure	check the cable sheathing for visible damage	regularly check compliance with the inspection plan

Figure 3: RTK object from FMECA

The possible technical effects of the error loss of the power connection are, firstly, that the position of the autonomous vehicle is unknown and, secondly, incorrectly displayed positions of the autonomous vehicle. Possible reasons for the above-mentioned errors are damages on the power cables and/or damages on the reference station. Regarding the estimation of the potential danger as well as possible measures for error prevention we evaluate the error possibilities with the metrics occurrence (O), severity (S) and detection (D). For each of them we developed a metric corresponding to the potential occurrences of errors as well as to the risk of severity and detection. Doing this we received the RPN 96 for damages on the power cables and the RPN 144 for damages on the reference station.

3.3 Light Detection and Ranging Sensor

In the past Light Detection and Ranging (LiDAR) was utilized in areas such as measuring ground topography, vegetation canopies or predicting forest stand structures [25]. Nowadays the application field of LiDAR has adapted towards automation and autonomous vehicles. With LiDAR one can measure the distance to targets which might be potential obstacles. This is done by directing a laser onto surfaces within the environment and measure the time-of-flight, i.e. the time needed for the reflected light to return to the light source [26]. Moreover, the change in wavelength is considered. This way, the environment can be scanned and a digital representation of the surroundings is generated. Especially, when thinking about autonomous systems such as robots, vehicles or railway vehicles it becomes apparent that static information and manual measurements are not sufficient, as an up-to-date representation of the current surrounding of the automated entity is required. Therefore, LiDAR takes care of remote sensing in terms of obstacle detection by scanning the environment for autonomous vehicles and other objects and plays an essential role in automatically navigating through a given path.

current (respectively planned state) object Lidar Sensor						
possible errors	obstacle is overlooked	broken sensor	lost power connection to the Lidar Sensor	distance measurement does not work	EMERGENCY STOP sensors trigger at the wrong time, although there is no danger	EMERGENCY STOP sensors are not triggered in the event of danger	positioning at the parking position, blast furnace or steel mill does not work at the wrong time
possible technical effects	crash with obstacle	values are not forwarded or forwarded incorrectly	no response from Lidar Sensor	crash with obstacle	availability is limited - autonomous operation is difficult	Danger to persons and damage to property possible	end of journey unclear
possible error reasons	speed measurement faulty	broken sensor	damaged power cable mechanical damage by a person	unclean sensor	sensors parameterised too sensitively or environmental influences	Sensors incorrectly parameterized or environmental influences	positioning sensors failed
estimation of the potential danger as well as possible measures for error prevention						
occurrence (O)	2	6	4	7	8	9	4
severity (S)	10	7	4	9	4	10	3
detection (D)	8	7	3	4	3	9	6
risk priority number (RPN)	160	294	48	252	96	810	72
technical error correction measure	compare speed measurement using GPS data	plausibility check, comparison with other sensors	install power cable alternatively, redundant power supply	install sensor alternatively. Install self-cleaning for LIDAR (e.g. ultrasound)	use certified systems or carry out certification, redundancy	use certified systems, redundancy	for important positions install 2 sensors
socio-technical error correction measure	persona must not intervene	set limit values and training measure on this table / knowledge	check the cable sheathing for visible damage	clean sensors at regular intervals	train the operating people	train the operating people	integrate regular test intervals

Figure 4: LiDAR object from FMECA

For a graphical depiction of the result of the FMECA for the object Light Detection and Ranging Sensor see Figure 4. When we connect the Lidar Sensor to the FMECA, we identify the following possible errors: obstacle is overlooked, broken sensor, lost power connection to the LiDAR sensor, distance measurement does not work, EMERGENCY STOP sensors trigger at the wrong time, although there is no danger, EMERGENCY STOP sensors are not triggered in the event of danger and positioning at the parking position, blast furnace or steel mill does not work at the wrong time. The possible technical effects of these errors are: crash with obstacle, Sensor values are not forwarded or forwarded incorrectly, no response from LiDAR sensor, crash with obstacle, availability is limited and ,thus, autonomous operation is difficult, danger to persons and damage to property possible and end of journey unclear. Regarding the estimation of the potential danger as well as possible measures for error prevention we evaluate the error possibilities with the metrics occurrence (O), severity (S) and detection (D). For each of them we developed a metric corresponding to the potential occurrences of errors as well as to the risk of severity and detection. Doing this we received the RPNs from left to right RPN 160, RPN 294, RPN 48, RPN 252, RPN 96, RPN 810 and RPN 72. For the technical corrective measures, we determine tasks to protect the LiDAR Sensor. To avoid the "possible error obstacle is overlooked" we compare speed measurement using GPS data, plausibility checks and comparison with other sensors to avoid broken sensors and a safer installation of the power connections to avoid errors in the power connection to the LiDAR Sensor. To avoid "the possible error distance measurement does not work" we install sensors alternatively and/or install self-cleaning capabilities for the LiDAR unit (e.g. ultrasound). To avoid "EMERGENCY STOP sensors trigger at the wrong time, although there is no danger" as well as "EMERGENCY STOP sensors are not triggered in the event of danger", we use certified systems and/or carry out certification, redundancy and avoid that "positioning at the parking position, blast furnace or steel mill does not work at the wrong time" we install two separate LiDAR sensors for important positions. As socio-technical corrective measures we determine the following actions to increase the safety level of the system Lidar Sensor. In case of "obstacle is overlooked" the Persona(s) must not intervene, in case of "broken sensor" limiting values should be set and training measure on this

table / knowledge, in case of "lost power connection to the LiDAR Sensor" one has to check the cable sheathing for visible damage. In case of "distance measurement does not work" the sensors must be cleaned at regular intervals. In case of "EMERGENCY STOP sensors trigger at the wrong time, although there is no danger" and "EMERGENCY STOP sensors are not triggered in the event of danger" a measure is to train the operating people and in case of "positioning at the parking position, blast furnace or steel mill does not work at the wrong time" regular test intervals should be integrated.

3.4 Inertial Measurement Unit (IMU)

Inertial Measurement Units (IMU) are utilized in a variety of today's technical systems. Most commonly, IMUs are applied in the automotive and aerospace sector. But even smartphones rely on the technology to measure velocity, acceleration, rotation and gravitational force [27]. An IMU relies mainly on two types of sensors. An accelerometer capable of measuring the inertial acceleration and a gyroscope aimed at detecting the angular rotation. Alongside a given starting location e.g. retrieved via D-GPS or Real Time Kinematics GPS an IMU can give information about a vehicle's position and even orientation. For this, linear and angular acceleration measurements are used to improve the precision of the location determination. Some newer IMUs even integrate a magnetometer to further boost the gyroscope measurements [28] , [29]. Moreover, IMUs in contrast to cameras, LiDARs or other sensing components need no exposure to the outside and can be mounted at any part of the vehicle and are not affected by outside conditions. [29]. Consequently, they can aid in a precise localization of an autonomous railway vehicle, especially in areas where other types of sensors reach their limits e.g. in tunnels where the GPS signal is lost.

current (respectively planned state) object Inertial Measurement Unit IMU				
possible errors	broken sensor	input is incorrectly processed/At the Persona level: identification of submitter/At the Roberta level: check state of interaction	output is incorrectly processed/At the Persona level: identification of submitter/At the Roberta level: check state of interaction	error in the power connection
possible technical effects	values are not forwarded or forwarded incorrectly	precision is not given	wrong information in the output	no action possibilities in the IMU
possible error reasons	sensors incorrectly calibrated At the Persona level: identify who calibrated the sensor	wrong input	wrong output	damaged power cable machanical damage by a person
estimation of the potential danger as well as possible measures for error prevention				
occurrence (O)	6	2	2	3
severity (S)	4	4	4	4
detection (D)	3	8	8	4
risk priority number (RPN)	72	64	64	48
technical error correction measure	calibration monitoring	testdrive before first use	testdrive before first use	install power cable alternatively, redundant power supply
socio-technical error correction measure	define table of values for calibration and develop training measure on this table/knowledge	define error table - when is it wrong?, Train the Personas	set up error correction measures using Robertas; At the personal level: knowledge of recognizing and adapting faulty programs	check the cable sheathing for visible damage

Figure 5: Inertial Measurement Unit object from FMECA

For a graphical depiction of the result of the FMECA for the object Inertial Measurement Unit see Figure 5. When we connect the Inertial Measurement Unit IMU to the FMECA, we identified the following errors: "broken sensor", "incorrectly proceeded input", "incorrectly proceeded output" and "errors in the power connection". The possible technical effects of the error "broken sensor" are that values are not forwarded or forwarded incorrectly. The technical

effect of the error "incorrectly proceeded input" is that the needed precision is not given. The technical effect of the error "incorrectly proceeded output" is that wrong information is used for further actions and the technical effect for "error in the power connection" is that there is no action possible for the IMU. Possible reasons for the above-mentioned errors are: incorrectly calibrated sensors, wrong inputs, wrong outputs and damages on the power cable. Regarding the estimation of the potential danger as well as possible measures for error prevention we evaluate the error possibilities with the metrics occurrence (O), severity (S) and detection (D). For each of them we developed a metric corresponding to the potential occurrences of errors as well as to the risk of severity and detection. Doing this we received the RPNs from left to right in Figure 5 RPN 72, RPN 64, RPN 64 and RPN 48. As technical corrective measures we determine tasks to protect the IMU to eliminate the possibility of failure. In this case we determine the calibration of the monitors to avoid broken sensors, test drives before first usage, to avoid incorrect inputs as well as incorrect outputs and alternative ways for the installation, as well as a safer installation of the power connections. As socio-technical corrective measures we determine the following actions to increase the safety level of the system IMU. To avoid errors in the calibration we define "table of values for calibration and develop training measure on this table/knowledge". To avoid incorrect inputs, we identified the measure "define error table and train the Persona(s)". To avoid incorrect outputs, we set up error correction measures using Robertas. At the Persona level we train the knowledge of recognizing and adapting faulty programs and to avoid errors in the power connection, we implement continuous cable sheathing checking.

3.5 Inertial Sensor

For a graphical depiction of the result of the FMECA for the object Inertial Sensor see Figure 6. When we connect the Inertial Sensor to the FMECA, we identified the following possible errors: "no data output", "a broken sensor", "incorrect values", "errors in the power connection".

current (respectively planned state) object Inertial Sensor				
possible errors	no data output	broken sensor	incorrect values	lost power connection to the Inertial Sensor
possible technical effects	data won't be forwarded	values are not forwarded or forwarded incorrectly	incorrect values are passed on	no response from Internal Sensor
possible error reasons	damaged power cable machanical damage by a person	broken sensor	sensors incorrectly calibrated	damaged power cable machanical damage by a person
estimation of the potential danger as well as possible measures for error prevention				
occurrence (O)	3	6	4	4
severity (S)	4	4	6	4
detection (D)	4	3	5	3
risk priority number (RPN)	48	72	120	48
technical error correction measure	install power cable alternatively, redundant power supply	plausibility check, comparison with other sensors	implement regular intervals for calibration	install power cable alternatively, redundant power supply
socio-technical error correction measure	check the cable sheathing for visible damage	set limit values and training measure on this table / knowledge	train personas to an acceptable range of values	knowing where which power cables are, which measures must be taken to start emergency supply - training measure

Figure 6: Inertial Sensor object from FMECA

The possible technical effects of the error "no data output" is that data won't be forwarded. The technical effect of the error "broken sensor" is that values are not forwarded or forwarded incorrectly. The technical effect of the error "incorrect values" is that incorrect values are passed on and the technical effect of an error in the power

connection is that there is no response from the Inertial Sensor. Possible reasons for the above-mentioned errors are damages in the cables, broken sensors, incorrectly calibrated sensors, and damages on the power cable. Regarding the estimation of the potential danger as well as possible measures for error prevention we evaluate the error possibilities with the metrics occurrence (O), severity (S) and detection (D). For each of them we developed a metric corresponding to the potential occurrences of errors as well as to the risk of severity and detection. Doing this we received the RPNs from left to right in Figure 6 RPN 48, RPN 72, RPN 120 and RPN 48. As the technical corrective measure, we determine tasks to protect the Inertial Sensor to eliminate the possibility of failure. In this case we determine an alternative installation of the cables to avoid the error of "no data output", plausibility checks and comparison with other sensors to avoid "broken sensor". To avoid "incorrect values", we implement regular intervals for calibration and to avoid errors in the power connection we implement a safer installation of the power connections. As socio-technical corrective measures we determine the following actions to increase the safety level of the system Inertial Sensor. To avoid errors in the power connection we implement continuous cable sheathing checking. To avoid errors caused by a broken sensor we set limits of values and develop training measures on this table/knowledge. To avoid incorrect values, we define an acceptable range of values and train the Persona(s). To avoid errors in the power connection we implement trainings to identify and know the exact locations of power cables and which measures must be taken to start emergency power supply.

3.6 Gateway

A Gateway or network gateway is used to establish communication between networks. It represents a hardware component capable of addressing a host potentially unknown to the user and enables the exchange of data with various other components. In our use case, we require a gateway for the automated railway vehicle to communicate with the infrastructure, provide information as well as receive information in terms of controls and reactions. Gateways find multiple applications in networking and in the area of IoT [30], [31].

current (respectively planned state) object Gateway			
possible errors	data will not be transmitted	disruption in the data transmission	lost power connection to the Gateway
possible technical effects	movement command is not executed	data records are not accepted	no response from Gateway
possible error reasons	data line interrupted	data timestamps faulty	damaged power cable mechanical damage by a person
estimation of the potential danger as well as possible measures for error prevention			
occurrence (O)	5	5	3
severity (S)	4	2	4
detection (D)	7	9	3
risk priority number (RPN)	140	90	36
technical error correction measure	query to the ECU if data flow is available	timestamp sanity-check	Install power cable alternatively, redundant power supply
socio-technical error correction measure	at the Persona level: train how to recognize that data line is broken and requiers response	sensor/signal if timestamp is incorrect/training to pay attention to this	check the cable sheathing for visible damage

Figure 7: Gateway object from FMECA

For a graphical depiction of the result of the FMECA for the object Gateway see Figure 7. When we connect the Gateway to the FMECA, we identified the following possible errors: "data will not be transmitted", "distribution in the data transmission", "errors in

the power connection". The possible technical effects of the error "data will not be transmitted" are that movement commands are not executed. The technical effects of a distribution in the data transmission are that data records are not accepted and the technical effect of an error in the power connection is that that there is no response from the Gateway. Possible reasons for the above-mentioned errors are interruptions in the data line, faulty data timestamps and damages on the power cables. Regarding the estimation of the potential danger as well as possible measures for error prevention we evaluate the error possibilities with the metrics occurrence (O), severity (S) and detection (D). For each of them we developed a metric corresponding to the potential occurrences of errors as well as to the risk of severity and detection. Doing this we received the RPNs from left to right in Figure 7 of RPN 140, RPN 90 and RPN 36. As the technical corrective measure, we determine tasks to protect the Gateway to eliminate the possibility of failure. To avoid the possible error that data will not be transmitted, we implement a query to the ECU if data flow is available. To avoid a distribution in the data transmission, we implement timestamp sanity checks and to avoid errors in the power connection we implement continuous cable sheathing checking. As socio-technical corrective measures we determine the following actions to increase the safety level of the system Gateway. To avoid errors that data will not be transmitted we train the employees on how to recognize that data lines are broken and require a response. To avoid a distribution in the data transmission we implement alerts that show when timestamps are incorrect and train the employees to pay attention to these alerts. To avoid errors in the power connection, we implement continuous cable sheathing checking.

3.7 Electronic Control Unit

For a graphical depiction of the result of the FMECA for the object camera see Figure 8. When we connect the Electronic Control Unit (ECU) to the FMECA, we identified as possible errors a mechanical damage, a big in the control software, a software update error, and errors in the power connection.

current (respectively planned state) object Electronic Control Unit ECU			
possible errors	mechanical damage	bug in the control software	software update error	lost power connection to the ECU
possible technical effects	broken ECU	crashed ECU	control function of the ECU is not fulfilled	no response from ECU
possible error reasons	solder joints loosened, damaged by thermal effects (e.g. flying sparks, liquid steel)	incorrect input validation (e.g. readings from sensors outside the expected range)	software-update	damaged power cable machanical damage by a person
estimation of the potential danger as well as possible measures for error prevention				
occurrence (O)	3	4	4	3
severity (S)	9	7	9	8
detection (D)	6	6	7	5
risk priority number (RPN)	162	168	252	120
technical error correction measure	chenage position, use covers	defensive programming, intensive testing (fuzzing, random, etc.)	functional check after software updates with the staggered-update-system	install power cable alternatively, redundant power supply
socio-technical error correction measure	at the persona level: Detect mechanical damage and damage in the solderings, initiate repair	training for the software developers, integration of acceptance procedures	at the persona level: event-related controls	check the cable sheathing for visible damage

Figure 8: Electronic Control Unit object from FMECA

The possible technical effects of the error mechanical damage are broken ECU. The technical effect of the error bug in the control software is a crashed ECU. The technical effect of a software update error is that the ECU cannot fulfil their control function and the technical effect of an error in the power connection is that there is no

response from the ECU. Possible reasons for the above-mentioned errors are loosened solder joints, incorrect input validations, wrong software updates and damages on the power cable. Regarding the estimation of the potential danger as well as possible measures for error prevention we evaluate the error possibilities with the metrics occurrence (O), severity (S) and detection (D). For each of them we developed a metric corresponding to the potential occurrences of errors as well as to the risk of severity and detection. Doing this we received the RPNs from left to right RPN 162, RPN 168, RPN 252 and RPN 120. For the technical corrective measure, we determine tasks to protect the ECU to eliminate the possibility of failure. In this case we determine a safer installation for the ECU and/or the usage of covers, defensive programming and intensive testing, a functional check after software updates with the staggered-update-system and a safer installation of the power connections. As socio-technical corrective measures we determine the following actions to increase the safety level of the system ECU. To avoid errors in the calibration we define table of values for calibration and develop training measures on this table/knowledge. To avoid mechanical damages, we define scheduled controlling and train the Persona(s). To avoid a crashed ECU, we implement trainings for the software developers and integrate of acceptance procedures. To avoid software update errors, we implement event-related controls at the Persona level and to avoid errors in the power connection we implement continuous cable sheathing checking.

3.8 *Combining multiple sensor data for safety autonomous driving*

In the previous chapter multiple sensor types were pointed out. Cameras, RTK GPS , LiDAR and IMUs were picked as an example to clarify the need of different types of sensors for localization and obstacle detection. Especially, in autonomous/automated (railway) vehicles sensors represent a vital factor when it comes to perceiving surroundings and position detection. From a safety perspective there must also be a redundancy within these components in case of failure. The components must be either present multiple times or another component can take over in terms of failure. However, this also requires ways to identify failures, on the one hand, and to be able to correct them, on the other hand. Therefore, data from multiple sensors must be combined in order to enable thorough decision making. This is also called sensor fusion [32]. With sensor fusion data from multiple sensors can be analysed and incorporated. In our case information is exchanged with the infrastructure over a gateway. Thus, yielding additional data for the sensor fusion to compute. Moreover, discrepancies between sensors can be identified and corrected. This way, information from contradicting data sources can be identified and data from various sources enables precise decision making.

4 Development of training materials

4.1 *Persona-Roberta model*

The interaction between humans and machines is illustrated by the Persona-Roberta model in Figure 9). It shows, what interactions there are between the systems that have to work together in automated operation and do flawlessly so as not to put anyone in danger. On one side are Personas that act as a model and in the analysis of the possible social factors that can act in the cooperation. These include social categories that characterise a person, an employee, such as his or her age and language, but also his or her professional experience or position in the company. All these factors have an influence on their actions and their understanding of the overall system, but also on their willingness to learn and develop, which is necessary as technical and organisational systems evolve. On the other hand, the Roberta model helps to understand which different technical systems are used, which knowledge is required to operate and understand them and which errors can also occur. This knowledge about the technical processes and systems is necessary to recognise errors and to prevent them before they cause damage. In this field of the model, we have to link it with the FMECA to find solutions for a safe operation at any time. These insights help to connect the measures for error elimination with concrete human knowledge and to take appropriate measures. Critical errors can only be eliminated on a conditional technical basis with suggestions in FMECA. This modelled mapping can be used for the development of error correction measures related to the FMECA as well as for the development of training measures. These should make particular reference to the interfaces and interactions between these systems and design training measures accordingly.
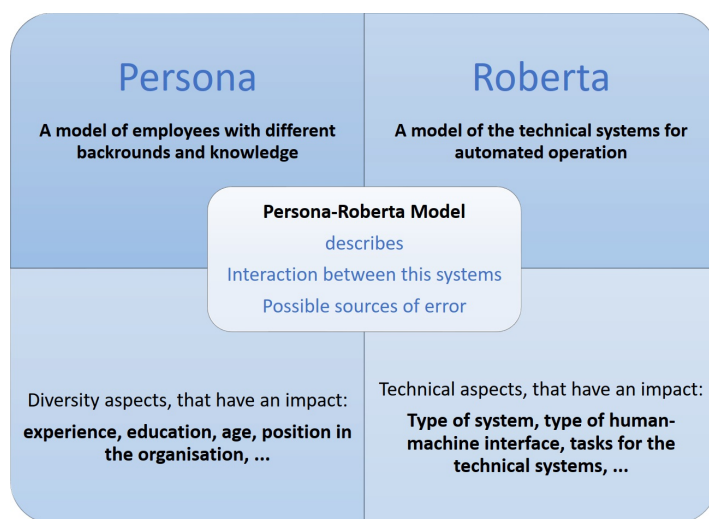

Figure 9: Persona-Roberta model

4.2 *On-the-job training*

Based the theoretical groundwork presented in Section 2 and expert discussions with the industry partners, a training concept was developed that empowers people to gain confidence in the machine and to make the right decisions based on their experience. For the development of the first draft of the training concept, learning theory principles and organisational learning as well as the generated error correction measures from the FMECA were used. Thus, a sound safety concept is a basis of the training concept that helps to comply with safety standards. Furthermore, responsibilities are clearly addressed to persons who bring in existing experience, but

who can also be trained specifically for new requirements.

In order to be able to develop training measures as precisely as possible, it needs:

- Document analysis of work instructions

- Overview of safety guidelines

- Analysis of current training folders

- Interviews or participatory observations

It is also clear that in system-theoretical adult education or systemic-constructivist didactics, no lectures and conversions [33] should happen, but to put self-direction and the learning of the individual person as knowledge carrier in the centre. This is also about the possibility of co-developing training measures [34].

It can also be recommended that training should include a mix of formal and informal teaching steps and that "learning on-the-job" should be established. In any case, any documents produced should be continuously revised in order to incorporate technical changes / further developments, but also to bring new teaching methods and knowledge of the knowledge bearers into training documents. Building on the knowledge management approach to learning organisations, the following initial concept of training or planned documentation was developed. In [35], the author have bridged organisational development and organisational learning with the field of enterprises as For-Profit-Organisations and their highly structured and determined process for learning environments. In [36], the author calls for the necessity of addressing formal and informal power as an aspect of advanced internal trainings, which also seems relevant when addressing possible resistance to new technologies by employees. In [37], the author points out that the organisational identity of an enterprise is also relevant – in our case a self-reference as "innovative", "participative", "learning organisation" or "modern". Research in this area has shown that up to now, the full potential of informal learning processes and tacit knowledge of employees, as well as participative methods have not been tapped by internal trainings.

Identify people who have knowledge and those who need to be trained and create appropriate materials. These have the focus of stimulating learning, learning to solve complex problems together and presenting them through simple language and symbols. On-the-job trainings for employees should be designed in a way that they address their specific worries, needs, state of knowledge and enable them to participate within the design process and to bring in their ideas to reduce risk factors – including oral and written didactic methods as well as thinking-out-loud processes to gain access to implicit and tacit knowledge. Elderly workers or users are often seen as digital migrants and a tackle for implementing new technologies. However, we call for applying ethnographical observations of experienced operators to sustain and involve treasure trove of their experience in the development of new technologies. Thus, a modern understanding of innovation which allows modifications during the process is vital. Technical methods like FMECA should be combined with sociological methods like Design Thinking. For the training settings, management tools are also presented to create an understanding of plan-do-check-act [38].

4.3 Tools and settings for developing the trainings and materials

How do people learn in organisations?

One important point is to use existing tacit knowledge of experienced employees and to take it seriously. There are different tools from knowledge management to capture this knowledge. Helpful are: Expert discussions, how-to listens, but also concepts such as micro-articles, which help to prepare knowledge clearly for other people [39]. The selection of interviewees is based on the identified Persona(s) and the concrete contact persons derived from them as well as the work areas identified in the FMECA. Narrative interviews are conducted with these people to help capture their experiences and knowledge of the processes and activities. In this way, it becomes clear which activities and actions are currently being carried out and what changes will occur as a result of automated operation. After this acidity the development of basic materials and trainings settings can start. This should be linked with the results of the FMECA to include possible dangerous situations and solutions to solve it.

In general it is important to define and communicate for update intervals, responsible persons and admins, including an annual training plan. This plan must be communicated by the management and the technical experts of the industry partner. All these steps must be linked to the time requirements for updates and many more. In the training documents, documents are continuously developed and simple training settings are set.

The following framework conditions are planned in the research project: The focus is on knowledge in the organisation and a transfer of knowledge. Documents and a handbook will be developed for the training courses with knowledge carriers, which can be continuously developed and adapted to the current technical requirements. The focus of the developed documents will be on using simple language and clear symbols in order to be able to communicate the complex process of self-driving operation to all persons equally. Furthermore, it will be addressed that not all persons need to know everything, but are comprehensively and well trained in their fields of work.

The following learning concepts are used for this purpose: Self-directed learning [40], as this concept considers the individual's own learning speed and prior knowledge. Basic documents on paper but also on videos are provided and simple tests to check knowledge. In addition to self-directed learning, this teaching concept also allows individual parts of the documents / videos to be easily expanded or exchanged. "The benefits of self-directed learning can be described in an effective manner in terms of the types of learners it develops. The self-directed learners demonstrate a greater awareness in terms of responsibilities." [40] Beside the self-directed learning concept, a peer-learning concept will be used. In the practice settings, learners practice in tandems. In particular, documentation sheets are filled in and reflected on as examples. Focus on the presentation and explanation of all components and their connections, as well as the possible errors. It is also planned to engage specially trained persons (admins), which are responsible for an overview on the whole content and new requirements. The goal of all measures is to train responsibility through learning theoretical expansion! For this purpose, a review and adaptation of all created documents is required at least every 12 months when changing the sensor or increasing

knowledge in real operation. Furthermore, it must also be a matter of discussing planning with staff and checking for understanding. This can happen with small online tests that the person has to do or by independently handling a possible error correction action. This can be documented by the training management with the help of an internship or observation sheet and any retraining can be proposed. In this way, the entire team can develop further.

For the development of initial materials and didactic concepts for in-company training in relation to new work processes through automated rail-bound driving on the premises, the basic work was used in order to make custom-fit proposals from a socio-scientific-technical point of view. These are, as shown: FMECA - Persona-Roberta model - Building blocks of knowledge management - Foundations of organisational learning.
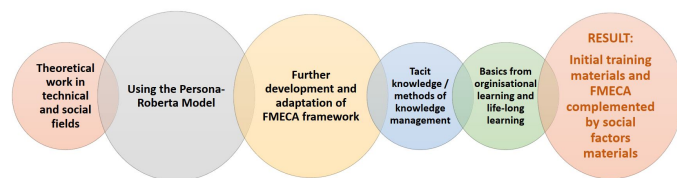

Figure 10: Combination of tools for training material development

As Figure 10 illustrates, there is no simple implementation guide, but there are many tools and methods that can be used to ensure smooth and flawless operation of autonomous rail-bound vehicles in the industry. The tools shown can be used to further develop and use them according to one's own requirements. This is achieved through the cooperation of different disciplines that contribute their technical and social expertise.

These tools and methods were supplemented by the basics of adult education and e-learning, since parts of the planned further education are to function online and with the concept of self-directed learning in the future. All documents are to be developed and reviewed in consultation with the Human Resources, Technical Development and Hazard Management departments. It will also be clearly worked out who is responsible for the final design of all documents and course units, who is responsible for the individual training parts, who adapts and modernises them accordingly if something changes in the sequence of events. It can be assumed that this technology will continue to develop and, therefore, documents, as well as tools and concepts, must be constantly updated. These aspects point to the future and also show the challenges of future research work. It is clear that concepts of adult education and a managing diversity concept [41] should be taken as a basis. People with their knowledge and social characteristics are thus perceived in their entirety as a relevant resource and integrated into knowledge processes. This also closes the circle to knowledge management, which had been used in the research project in particular to raise the explicit knowledge of the employees. How do adults learn? There is no one-size-fits-all answer, but there are frameworks that help to design one's own learning environment in order to be able to communicate new technologies that bring about changes in work processes. The needs of adults, which can motivate them to learn, must be as precisely as possible and relate them to the respective needs (qualification profiles, etc.) [42]

If we combine these starting points with the aspects of organisational learning, managing diversity theory and knowledge management that have already been worked out, they provide sufficient orientation for the selection of didactic methods and the targeted preparation of content and learning materials. Once again, reference should be made to the diversity of learners in an industrial company and to the requirements of clear languages, unambiguous images and small snippets of information that will make it possible to organise the interaction between man and machine with the most well-founded knowledge possible in a safe and error-free manner. A regular evaluation of the success of the training courses with regard to possible incidents complements the overall approach of integrating social and socio-scientific aspects into technical training.

5 Conclusion and further research

The proposed set of tools and models can contribute to more appropriate training materials for humans interacting with machines, in the area of autonomous railway vehicles. Especially, the extended FMECA participates and provides a holistic approach to what a railway operating system should look like and shows which requirements, influences and interfaces must be considered. Additionally, it is an effective technique to spot security as well as safety concerns at a point where planned systems and human actors interact at the very beginning of the design process. However, the descriptions of the subcomponents of the component autonomous railway vehicle in section 3, indicates a strong relationship between the technical and sociological error correction measures. Regarding the estimation of the potential danger as well as possible measures for error prevention we evaluated the error possibilities with the metrics occurrence (O), severity (S) and detection (D). For each of them, a metric was developed that is corresponding to the potential occurrences of errors as well as to the risk of severity and detection in several rounds based on the knowledge of the entire project team. A multitude of tools and models are then implemented to identify and develop adequate training materials. These are based on theoretical work in technical and social fields, the Persona-Roberta model, as a model focusing on interaction between humans and machines, tacit knowledge and methods of knowledge management as well as basics of organisational and life-long learning. We propose that together these tools will help and enhance developing more adequate training materials for the autonomous railway sector. In a further step, these materials should then be generated based on the proceedings that have been described and applied to a genuine context of an autonomous railway system.

The novelty of the research and the article lies in the combination of the different research methods and models, which complement each other and combine technical and social issues. It is well known from knowledge management and organizational development that the introduction of new technical processes that bring innovation to operations and processes requires knowledge about the people who will be affected by them. Therefore, research questions such as "What makes an organizational culture that produces technical and social innovations?" but also "How does the use of the tacit knowledge of the employees succeed?" For that the research team used methods from organizational learning including aspects of

safety and security and of knowledge management. To stick social and technical aspects together the method of "personas" from design thinking processes was extended with the technical aspects – "Roberta". Furthermore, the model of [43] for organizational learning was included.

In the research projects as well as in this article, it could be shown that it is relevant and important to be aware of technical expert knowledge. And besides there must also be knowledge about social factors and social negotiation processes in an organisation, which have an effect on the introduction and operation of new technical systems. It can be stated that interdisciplinary cooperation can deepen the processing of the interaction between machines and humans. The use and further development of known instruments such as the FMECA and models such as the Persona-Roberta model enables a structured derivation of possible training measures and contents. The existing knowledge of (long-term) employees must be used as a basis in order to be able to integrate informal experiential knowledge specifically into the selection of the learning setting and the preparation of the materials. Existing hazard plans in the organisations and technical knowledge complement the development and help to establish safe operations. In summary, it can be said that this contribution shows where research and development must go in the future, in order to further develop autonomous rail-bound driving on company premises, both technically and socially. The presented research results have already been implmented in teachings in a variety of departments at the University of Applied Scienes Burgenland. And the research partners further suggest on implementing the results in upcoming research projects in the field of autonomous railway systems and others with focus on sustainable nationwide mobilty. We further suggest that the implementation of social aspects can aid in developing such a system and support the further mitigation of failures by applying and developing adequate training materials.

Conflict of Interest The authors declare no conflict of interest.

References

[1] C. Gnauer, A. Prochazka, E. Szalai, S. Chlup, S. Luimpöck, A. Fraunschiel, C. Schmittner, "Knowledge Based Training Derived from Risk Evaluation Concerning Failure Mode, Effects and Criticality Analysis in Autonomous Railway Systems," in 2021 5th International Conference on System Reliability and Safety (ICSRS), 47–52, 2021, doi:10.1109/ICSRS53853.2021.9660726.

[2] D. Hofbauer, C. Schmittner, M. Brandstetter, M. Tauber, "Autonomous CPS Mobility Securely Designed," in 2019 IEEE 20th International Symposium on "A World of Wireless, Mobile and Multimedia Networks" (WoWMoM), 1–6, 2019, doi:10.1109/WoWMoM.2019.8793050.

[3] D. Walker, F. Myrick, "Grounded theory: An exploration of process and procedure," Qualitative health research, **16**(4), 547–559, 2006, doi:doi:10.1177/1049732305285972.

[4] S. Kato, E. Takeuchi, Y. Ishiguro, Y. Ninomiya, K. Takeda, T. Hamada, "An open approach to autonomous vehicles," IEEE Micro, **35**(6), 60–68, 2015.

[5] N. Anwar, M. S. Khan, K. Ahmed, A. Ahmad, A. Athar, "Speed scheduling of autonomous railway vehicle control system using ANN," International Journal of Scientific & Engineering Research, **2**(6), 1–6, 2011.

[6] A. Ahmad, M. S. Khan, K. Ahmed, N. Anwar, A. Athar, "Speed Scheduling of Autonomous Railway Vehicle Control System using Neuro-Fuzzy System," International Journal of Scientific and Engineering Research, **2**(6), 272–277, 2011.

[7] A. Ahmad, M. S. Khan, K. Ahmed, N. Anwar, U. Farooq, "FIS Based Speed Scheduling System of Autonomous Railway Vehicle," International Journal of Scientific and Engineering Research, **2**(6), 299–304, 2011.

[8] P. Singh, M. A. Dulebenets, J. Pasha, E. D. S. Gonzalez, Y.-Y. Lau, R. Kampmann, "Deployment of autonomous trains in rail transportation: Current trends and existing challenges," IEEE Access, **9**, 91427–91461, 2021.

[9] "Rise of the machines: Rio Tinto breaks new ground with AutoHaul," 2019.

[10] M. Rahimi, H. Liu, I. D. Cardenas, A. Starr, A. Hall, R. Anderson, "A Review on Technologies for Localisation and Navigation in Autonomous Railway Maintenance Systems," Sensors, **22**(11), 2022, doi:10.3390/s22114185.

[11] R. Lagay, G. M. Adell, "The autonomous train: A game changer for the railways industry," in 2018 16th international conference on intelligent transportation systems telecommunications (ITST), 1–5, IEEE, 2018, doi:10.1109/ITST.2018.8566728.

[12] M. Shafiee, F. Dinmohammadi, "An FMEA-based risk assessment approach for wind turbine systems: a comparative study of onshore and offshore," Energies, **7**(2), 619–642, 2014, doi:10.3390/en7020619.

[13] L. S. Lipol, J. Haq, "Risk analysis method: FMEA/FMECA in the organizations," International Journal of Basic & Applied Sciences, **11**(5), 74–82, 2011.

[14] J. Singh, S. Singh, A. Singh, "Distribution transformer failure modes, effects and criticality analysis (FMECA)," Engineering Failure Analysis, **99**, 180–191, 2019, doi:https://doi.org/10.1016/j.engfailanal.2019.02.014.

[15] M. Catelani, L. Ciani, D. Galar, G. Guidi, S. Matucci, G. Patrizi, "FMECA assessment for railway safety-critical systems investigating a new risk threshold method," IEEE Access, **9**, 86243–86253, 2021, doi:10.1109/ACCESS.2021.3088948.

[16] F. Dinmohammadi, B. Alkali, M. Shafiee, C. Bérenguer, A. Labib, "Risk evaluation of railway rolling stock failures using FMECA technique: a case study of passenger door system," Urban Rail Transit, **2**(3), 128–145, 2016, doi:10.1007/s40864-016-0043-z.

[17] J. Kim, H. Jeong, J. Park, "Development of the FMECA process and analysis methodology for railroad systems," International Journal of Automotive Technology, **10**(6), 753–759, 2009.

[18] F. D. Davis, "Perceived usefulness, perceived ease of use, and user acceptance of information technology," MIS quarterly, 319–340, 1989, doi:10.2307/249008.

[19] M. Lewrick, P. Link, L. Leifer, N. Langensand, Das Design Thinking Playbook: mit traditionellen, aktuellen und zukünftigen Erfolgsfaktoren, Vahlen, 2018.

[20] M. Lewrick, P. Link, L. Leifer, A. Schmidt, Das Design Thinking Toolbook: Die besten Werkzeuge & Methoden, Franz Vahlen, 2019.

[21] D. J. Yeong, G. Velasco-Hernandez, J. Barry, J. Walsh, "Sensor and Sensor Fusion Technology in Autonomous Vehicles: A Review," Sensors, **21**(6), 2021, doi:10.3390/s21062140.

[22] Y. Feng, J. Wang, "GPS RTK Performance Characteristics and Analysis," Journal of Global Positioning Systems, **7**, 2008, doi:10.5081/jgps.7.1.1.

[23] "What is the Difference Between RTK & DGPS?" 2019.

[24] F. Van Diggelen, "GPS and GPS+ GLONASS RTK," in Proceedings of the 10th International Technical Meeting of the Satellite Division of The Institute of Navigation (ION GPS 1997), 139–144, 1997.

[25] N. Mehendale, S. Neoge, "Review on Lidar Technology," 2020, doi:10.2139/ssrn.3604309.

[26] M. A. Lefsky, W. B. Cohen, G. G. Parker, D. J. Harding, "Lidar Remote Sensing for Ecosystem Studies: Lidar, an emerging remote sensing technology that directly measures the three-dimensional distribution of plant canopies, can accurately estimate vegetation structural attributes and should be of particular interest to forest, landscape, and global ecologists," BioScience, **52**(1), 19–30, 2002, doi:10.1641/0006-3568(2002)052[0019:LRSFES]2.0.CO;2.

[27] "What is IMU?" 2021.

[28] N. Ahmad, R. A. R. Ghazilla, N. M. Khairi, V. Kasi, "Reviews on Various Inertial Measurement Unit (IMU) Sensor Applications," International Journal of Signal Processing Systems, 256–262, 2013, doi:10.12720/ijsps.1.2.256-262.

[29] "Inertial Measurement Units for Localisation and Navigation of Autonomous Vehicles," 2019.

[30] C. P. Kruger, A. M. Abu-Mahfouz, G. P. Hancke, "Rapid prototyping of a wireless sensor network gateway for the internet of things using off-the-shelf components," in 2015 IEEE International Conference on Industrial Technology (ICIT), 1926–1931, IEEE, 2015, doi:10.1109/ICIT.2015.7125378.

[31] R. He, B. Ai, G. Wang, K. Guan, Z. Zhong, A. F. Molisch, C. Briso-Rodriguez, C. P. Oestges, "High-speed railway communications: From GSM-R to LTE-R," Ieee vehIcular technology magazIne, **11**(3), 49–58, 2016, doi:10.1109/MVT.2016.2564446.

[32] S. Ataei, A. Aghakouchak, M. Marefat, S. Mohammadzadeh, "Sensor fusion of a railway bridge load test using neural networks," Expert Systems with Applications, **29**(3), 678–683, 2005, doi:https://doi.org/10.1016/j.eswa.2005.04.038.

[33] R. Arnold, H. Siebert, "Konstruktivistische Erwachsenenbildung. Von der Deutung zur Konstruktion der Wirklichkeit. Baltmannsweiler," 2003.

[34] S. Nolda, Einführung in die Theorie der Erwachsenenbildung, WBG Darmstadt, 2012.

[35] N. Engel, S. Koch, "Betrieb als Gegenstand und Ort organisationspädagogischer Forschung und Praxis," in Handbuch Organisationspädagogik, 793–804, Springer, 2018, doi:10.1007/978-3-658-07512-5_77.

[36] P. Faulstich, Strategien der betrieblichen Weiterbildung: Kompetenz und Organisation, Vahlen, 1998, doi:10.1007/s11618-000-0016-5.

[37] S. Kirchner, "Organisationsidentität und Unsicherheit," in Organisation und Unsicherheit, 69–85, Springer, 2015, doi:10.1007/978-3-531-19237-6.

[38] S. M. Weber, M. Göhlich, A. Schröer, H. Macha, C. Fahrenwald, "Organisation und Partizipation–interdisziplinäre Verhältnisbestimmungen und organisationspädagogische Perspektiven," in Organisation und Partizipation, 9–28, Springer, 2013, doi:10.1007/978-3-658-00450-7_1.

[39] A. Mittelmann, Werkzeugkasten Wissensmanagement, BoD–Books on Demand, 2011.

[40] R. Kapur, "Significance of Self-Directed Learning," 2019.

[41] L. Gardenswartz, A. Rowe, Managing diversity: A complete desk reference and planning guide, McGraw Hill Professional, 1998.

[42] B. Dewe, K. Feistel, Betriebliche Weiterbildung Materialien in didaktischer und bildungsökonomischer Perspektive, Franz Steiner Verlag, 2013.

[43] G. Probst, S. Raub, K. Romhardt, Bausteine des Wissensmanagements, 25–33, Gabler Verlag, Wiesbaden, 2003, doi:10.1007/978-3-322-94790-1_3.